Mass Spectrometry of Nucleic Acid Noncovalent Complexes

Eric Largy, Alexander König, Anirban Ghosh, Debasmita Ghosh, Sanae Benabou, Frédéric Rosu, Valérie Gabelica

Mass Spectrometry of Nucleic Acid Non-Covalent Complexes

Eric Largy,[1] Alexander König,[1] Anirban Ghosh,[1] Debasmita Ghosh,[1] Sanae Benabou,[1] Frédéric Rosu,[2] Valérie Gabelica[1]*

[1] Univ. Bordeaux, CNRS, INSERM, ARNA, UMR 5320, U1212, IECB, F-33600 Pessac, France

[2] Univ. Bordeaux, CNRS, INSERM, IECB, UMS 3033, F-33600 Pessac, France

Abstract

Nucleic acids have been among the first targets for antitumor drugs and antibiotics, and with the unveiling of new biological roles in regulation of gene expression, specific DNA and RNA structures have become very attractive targets, especially when the corresponding proteins are undruggable. Biophysical assays to test target structure and ligand binding stoichiometry, affinity, specificity and binding modes are part of the drug development pipeline. Mass spectrometry offers unique advantages as a biophysical method due to its ability to distinguish each stoichiometry present in a mixture. In addition, advanced mass spectrometry approaches (reactive probing, fragmentation techniques, ion mobility spectrometry, ion spectroscopy) provide more detailed information on the complexes. Here we review the fundamentals of mass spectrometry and all its particularities when studying non-covalent nucleic acid structures, and then review what has been learned thanks to mass spectrometry on nucleic acid structures, self-assemblies (e.g., duplexes or G-quadruplexes), and their complexes with ligands.

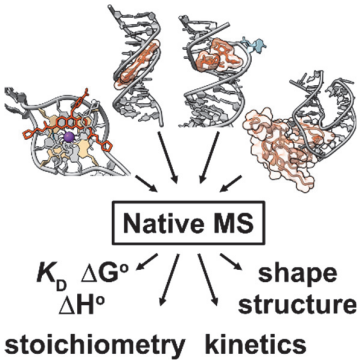

Table of contents

1. Introduction

Nucleic acid complexes are at the crossroads between chemistry and biology. On the one hand, nucleic acids are essential players in the central dogma of molecular biology: our DNA contains the blueprint of the genetic information. It can be replicated for cell division, and transcribed into pieces of RNA that either have their own function, or are themselves the blueprint for translation into proteins. Consequently, small molecules that target natural nucleic acids can have pharmacological interest, the best known being as anticancer therapeutics[1,2] or antibiotics.[3,4] On the other hand, nucleic acids and derivatives can be chemically synthesized, and form structures or supramolecular assemblies that can adopt a variety of functions: molecular recognition,[5] catalysis,[6] switches,[7] therapeutics,[8]… Their assemblies can be complex and beautiful.[9,10]

To characterize non-covalent complexes, mass spectrometry has the unique advantage of providing an assumption-free determination of the stoichiometries present in the sample, while the peak intensities inform on the relative abundance of each species in solution. Furthermore, advanced mass spectrometry method can be exploited to further characterize the complexes in the gas phase, e.g., their kinetic stability, reactivity, shape, or spectroscopic properties. But as in all measurement sciences, a key question is the extent to which the molecular system could be perturbed by the measurement itself. Mass spectrometry is carried out in the gas phase, and on ions. Ionization and desolvation will inevitably affect the complexes: the hydrophobic (water exclusion) effect can't exist in the gas phase, specific interactions with water will be lost, while electrostatic interactions are magnified by the lower dielectric constant of vacuum. So, the key question is not whether the structure will be different in the gas phase compared to in solution but rather: To what extent? Does it matter for the question at hand? Can we tailor better experiments depending on the question? Depending on the system?

In section 2, we will describe the structures of nucleic acids and their complexes, focusing on the types of non-covalent forces at stake in solution. This will allow us to better reflect on how these forces will be altered upon transfer from the solution to the gas phase. This section will also allow mass spectrometrists to learn the basics of nucleic acid structures and follow the discussion of the specific results. Researchers with a good command of nucleic acids complexes can directly switch to section 3, where we will describe all mass spectrometry approaches that can be used to study non-covalent complexes and have been applied to nucleic acids. This section will introduce each approach and its fundamental principles, so that readers with no prior knowledge of native mass spectrometry can also follow how information is obtained for various nucleic acid complexes. Finally, section 4 will gather case studies on non-covalent interactions in nucleic acids, studied by mass spectrometry. We comprehensively gathered the literature on MS studies of intramolecular oligonucleotide folding, and intermolecular complexes between nucleic acid structures and ligands (cations, small molecules, peptides, proteins…). We however restricted the bibliography to articles using native mass spectrometry (not, for example, papers describing solution affinity capture with mass spectrometry readout). We also left aside the literature where the nucleic acid had no secondary or tertiary structure (lone nucleobases, or unstructured single strands). Finally, in the vast literature on protein-nucleic acid complexes, we include here only the references where the complex was studied from the nucleic acid side of the coin. The readers may find complementary information in the following past reviews on nucleic acid studies by native mass spectrometry,[11–19] and more general reviews on either supramolecular mass spectrometry[20,21] or nucleic acids.[22,23]

2. Non-covalent interactions in nucleic acids

Nucleic acids come in all shapes and sizes. Although they normally fold into right-handed, antiparallel double helices following well-known base pairing rules, both DNA and RNA can adopt a wide range of alternative structures.[24] Many of these structures are involved in biological processes with therapeutic potential,[25,26] and can be used themselves as therapeutic agents,[27,28,28] molecular probes,[29,30] and nanotechnology building blocks.[31–33] Moreover, numerous modified nucleobases and backbones have been discovered or designed over the years,[28,29,34–37] increasing the chemical and structural space of nucleic acids. In this section, we introduce canonical and non-canonical chemical structures, from primary to tertiary structure, and lay out the necessary background to understand the noncovalent driving forces involved in nucleic acid folding and interactions with cations, small molecules, or other partners.

2.1 Primary structure: DNA, RNA and other backbones

2.1.1 Canonical nucleic acids

Nucleic acids are polymers of nucleotide monophosphates, composed of a nitrogenous heterocyclic base, a pentose, and a phosphate group. The phosphates and sugars form the backbone of nucleic acids. Nucleic acid strands are therefore polyanions in solution (except at very acidic pH, and for some modified backbones such as PNA). In natural nucleic acids, the sugar is either a D-ribose for ribonucleic acids (RNA) or a 2'-deoxy-D-ribose for deoxyribonucleic acids (DNA), locked into a furanose cyclic conformation (Chart 1A). Each sugar is linked to a base by a C1'-N9 (purines) or C1'-N1 (pyrimidines) N-glycosidic bond. The combination of a base and a sugar is called nucleoside. By convention, deoxyribonucleotides are abbreviated dN (where N is the nucleotide's single-letter code), and ribonucleotides rN.

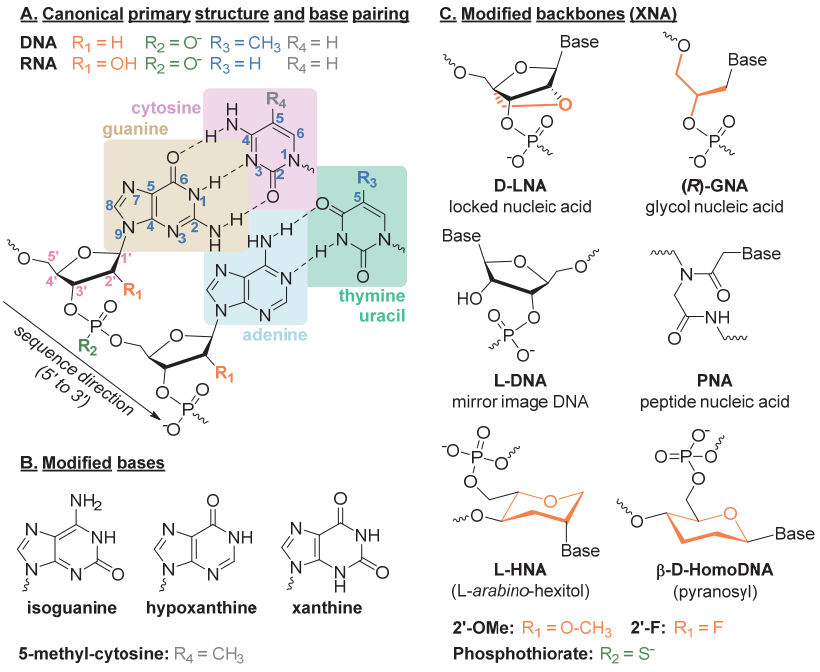

Chart 1. Primary structure and Watson-Crick base pairing of canonical nucleic acids (sugar numbering in pink, nucleobase numbering in blue). B. Modified nucleobases and C. modified backbones of particular interest in this review.

The unmodified, natural DNA bases are adenine (single-letter code: A; nucleoside name: deoxyadenosine/dA) and guanine (G; deoxyguanosine/dG), which are purines, and cytosine (C; deoxycytidine/dC) and thymine (T; thymidine/dT), which are pyrimidines. In RNA, uracil (U; uridine/rU)

substitutes thymine, from which it only differs by the absence of a methyl group. Canonically, guanines associate with cytosines with three Watson-Crick H-bonds, and adenines are complementary to thymines and uracils through the formation of two H-bonds.

In this review, most cited studies involve relatively short nucleic acid strands called oligonucleotides. By convention, oligonucleotide sequences are given in the 5'-to-3' direction, following the sugar numbering convention presented in Chart 1A. An oligonucleotide containing *n* nucleotides is called *n*-mer. Oligonucleotide sequences can be written using the *d* and *r* prefixes used to denote deoxyribo- and ribonucleotides, and repeated nucleotides can be noted once with the number of repetitions annotated as a subscript. For instance, $dGA_3G(AT)_3GC$ refers to a 13-mer DNA oligonucleotide whose complete sequence in the 5' to 3' direction is GAAAGATATATGC.

2.1.2 Modified nucleic acids

Besides the naturally occurring DNA and RNA primary structures presented above, a large number of modified backbones and bases exist. Such modifications can occur naturally on bases, e.g. because of their chemical reactivity (hydrolysis, oxidation, non-enzymatic methylation),[37] or for epigenetic gene expression regulation.[34] A large range of synthetic modifications have also been designed.[28,29,35,36] These additional types of nucleic acids are called XNA for xenobiotic nucleic acids. XNA can be used for applications such as aptamer selection and optimization,[38,39] increasing thermal stability, nuclease resistance and bioavailability,[27,40] secondary structure tuning, stabilization and probing,[41] crosslinking,[42] improved antisense binding and triplex formation,[26,43–45] or the creation of orthogonal genomes.[27,35] The following sections present modified nucleic acids that have been studied by mass spectrometry.

2.1.2.1 Modified bases

Isoguanine (or 2-hydroxyadenine) is a naturally-occurring base that is the result of adenine oxidation, specifically hydroxylation of the position 2. Its structure resembles that of guanine where the amino and carbonyl group are transposed (Chart 1B). It can base-pair with thymines and cytosines,[46] and form cation-mediated pentads.[47]

Hypoxanthine and xanthine are naturally-occurring purine bases, whose structures differ from guanine at the position 2.[48] Specifically, hypoxanthine lacks the H-bond donor amino group, and xanthine substitutes it by an acceptor carbonyl (Chart 1B). Their nucleoside names are inosine (I) and xanthosine (X).

5-methylcytosine (5mC) is an abundant and important DNA modification. The addition of a methyl group in position 5 (the same that constitutes the difference between T and U) does not alter its base-pairing capabilities compared to cytosine (Chart 1B).[49]

2.1.2.2 Modified phosphodiester linkage and sugar moieties

L-nucleic acids are mirror image of natural D-nucleic acids (Chart 1C), with whom they share physico-chemical and base pairing properties, but form left-handed rather than right-handed helices.[50] Unlike the synthetic analogs presented thereafter, which can bind to complementary DNA or RNA with both Watson-Crick and Hoogsteen motifs, **L-DNA** cannot form stable duplexes with D-DNA in physiological conditions (regardless of sequence complementarity).[51,52] They can be used as aptamers for their high biostability and low immunogenicity properties,[53] or as molecular tags.[54,55] They can be targeted selectively (vs. D-DNA) by small molecules.[56]

A common and minimal type of nucleic acid modifications is the substitution of the (deoxy)ribose 2' position. For instance, **2'-OMe RNA** (Chart 1C) sequences, first reported in 1959,[57] have an improved resistance to nucleases and altered sensitivity towards other enzymes.[58,59] The modification does not

impact the sugar puckering and base pairing of nucleotides, and therefore 2'-OMe oligonucleotides form stable duplex with complementary sequences (modified or not).[58,60–62] Substitution of **phosphorothioate** moieties for the phosphate linkage is another example of a simple modification providing nuclease resistance.[63] Although this modification is minimal, it generates a chiral center that may affect the oligonucleotide properties, for instance the stability of the duplexes formed.[64]

Peptide nucleic acids (**PNA**) are nucleic acid variants whose achiral backbone is constituted by *N*-(2-aminoethyl)-glycine units linked by peptide bonds, with the bases attached by a methylene carbonyl linkage (Chart 1C). PNAs were designed to be homomorphous to DNA with respect to the number of backbone bonds and distance between, with the aim to bind double stranded DNA (dsDNA) in the major groove (see section 2.2.2).[65] Importantly, in the context of mass spectrometry, the PNA backbone is neutral (bases may still be charged at non-physiological pH). This allows for stronger binding to natural nucleic acids.[66,67] PNAs are most notably used in antisense, anti- and pro-gene, and anti-microRNA therapies,[30,68] gene editing,[68,69] and biosensing.[30,70]

Locked nucleic acids (**LNA**) are synthetic analogs of DNA that feature a bicyclic β-D-2'-*O*-4'-C-methylene ribofuranose sugar (Chart 1C). LNA-containing DNA oligonucleotide form more stable duplexes with DNA or RNA than unmodified strands, and LNA:LNA duplexes are exceptionally stable.[71–73] These properties have been leveraged for therapeutic and biosensing applications.[70,74,75] Glycol nucleic acids (**GNA**) are simplified nucleic acid analogues that rely on an acyclic propylene glycol backbone (Chart 1C), while preserving hybridization properties by Watson-Crick base pairing for both the *R*- and *S*-enantiomers (but only with a complementary strand of same chirality).[76–78] They were introduced fairly recently to streamline the synthesis of artificial nucleic-acids for e.g. nanotechnology applications.[76] A variety of 6-membered-ring nucleotides have been reported, including α- and β-**Homo-DNA**, p-RNA, CeNA, CNA, ANA, p-ara-NA, and **HNA**.[79] Among these, Hexitol (1',5'-anhydro-D-*arabino*-hexitol) nucleic acids (D-HNA) form HNA:HNA duplexes with good thermal stability, and can hybridize with complementary RNA oligonucleotides as well.[80–82]

2.2 Secondary structures

In nucleic acids, the definition of secondary, tertiary and quaternary structure is blurrier than in the case of proteins. Here, we will define "secondary structures" as structures formed by the contiguous stacking of hydrogen-bonded bases, independently of whether these structures may form intramolecularly or with several strands. The term "tertiary structure" will be reserved to structures formed intramolecularly by the interactions between distinct secondary structures as building blocks. The term "quaternary structures" will not be used in this review and we will speak about "complexes".

2.2.1 Duplexes

2.2.1.1 A, B, and Z forms

Nucleic acids can form three major forms of double stranded helices: the A-helix, B-helix, and Z-helix. All three are made of two strands intertwined in opposite 5'-to-3' directions, with the sugar and phosphate groups sitting on the outside, their bases associated internally by Watson-Crick H-bonds and stacked to their intra-strand neighbors (see section 2.3.1).[83] Base pairing is possible between complementary bases, but may also take place when bases are mismatched and by alternative binding modes (see section 2.2.1.2). Self-complementary oligonucleotides, called palindromic sequences, can form an intermolecular duplex with a second identical oligonucleotide (see all three double-stranded structures in Figure 1), or fold intramolecularly into a hairpin (see section 2.2.1.3).

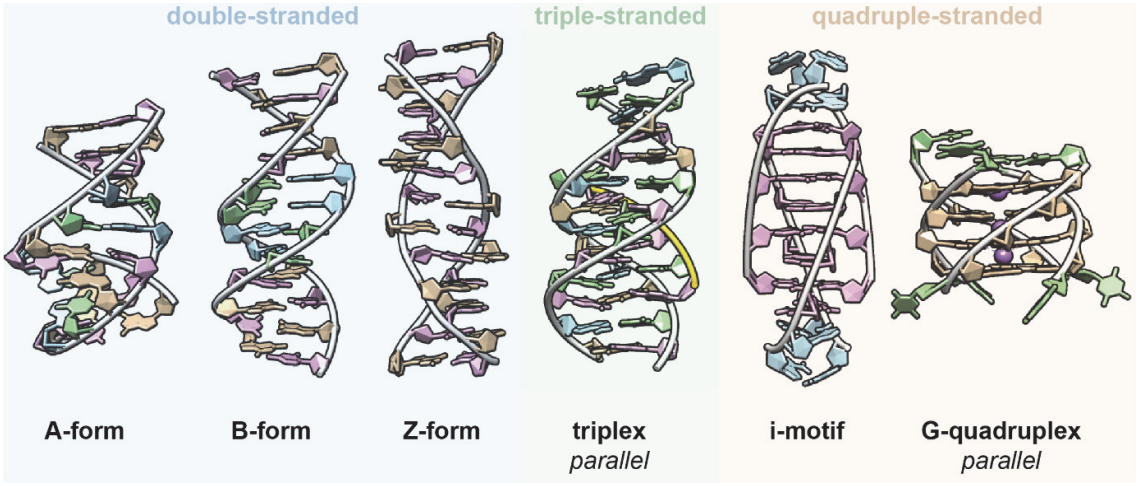

Figure 1. Comparison of the major canonical and non-canonical secondary structures of nucleic acids. Left: duplexes formed by the association of two DNA strands adopting the right-handed A-form dCCGTACGTACGG, PDB: 117D[84]; X-ray diffraction), B-form dCGCGAATTCGCG, PDB: 9BNA[85]; X-ray diffraction), or left-handed Z-form dCGCGCGCGCGCG, PDB: 4OCB[86]; X-ray diffraction). Middle: Triplex formed by the binding of a DNA hexamer dCTCTCT, gold; parallel base pairing) into the major groove of dsDNA truncated to a dodecamer dCTGAGAGACGTA + complementary sequence, PDB: 1BWG;[87] solution NMR). Right: i-motif (PDB: 1YBL;[88] solution NMR) and G-quadruplex (PDB: 2O4F;[89] X-ray diffraction) formed by the association of four identical dAACCCC or dTGGGGT strands, respectively. All the structures (excluding the TFO from the triplex) contain 24 nucleotides and are scaled identically. Adenosines are colored in blue, cytidines in pink, guanosines in tan, thymidines in green, phosphodiester backbone in white, and sodium in purple.

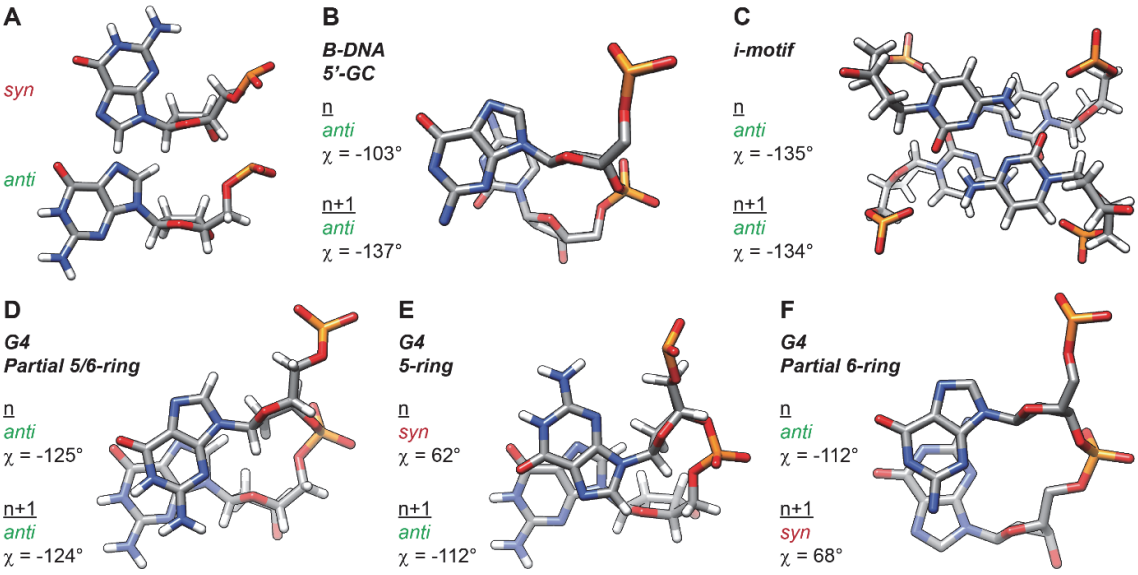

Figure 2. A. The syn and anti configurations of nucleosides (here guanosines), indicating the position of the base relative to the glycosidic bond angle. B—F. Stacking between a guanine and a cytosine in a B-DNA (B; extracted from 9BNA[85]), four cytosines in an i-motif (C; 1YBL[88]), two guanines from successive G-quartets with anti/anti (D; 2O3M[90]), syn/anti (E; 2JPZ[91]) and anti/syn (F; 1JPQ[92]) steps. Nucleosides n are on top, n+1 at the bottom. Glycosidic torsion angles χ are defined by the O4'-C1'-N9-C4 atoms for purines, and O4'-C1'-N1-C2 for pyrimidines.

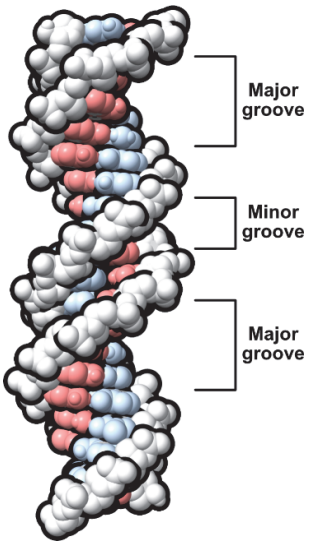

Figure 3. Minor and major grooves in a B-helix

Both the A- and B-helices are right handed, whereas the Z-helix is left-handed.[24,83,93] The B-helix has a width of 20 Å with a helical twist of around 36° per base pair, that is 10 base pairs (bp) per helical turn, and sugar moieties in the C2' endo conformation (Figure 1).[24,83] The bases are in *anti* conformation, stacked over the axis, almost exactly perpendicular to it, with a vertical rise between two consecutive bp of 3.38 Å (Figure *2*A,B).[24] Two distinct grooves, namely the major and minor grooves, are defined by the surface between the sugars-phosphodiester backbones (Figure 3). Grooves provide surfaces for not only protein but also synthetic small molecule binding (see section 2.5.1). In physiological conditions, DNA:DNA duplexes favor the B-helix conformation.

The sugars in the A-helix are in a C3' endo conformation, which leads to closer 5' and 3' carbons, in turn resulting in a smaller rise (2.54 Å), slightly wider helix with a smaller helical twist (32.7°, ~ 11 bp per turn), and base pairs twisted, tilted and displaced away from the helix axis.[24,83,94] This leads to shallower and wider minor grooves, and deeper and narrower major grooves.[24] RNA duplexes are constrained in this conformation because the 2'-OH (absent in DNA) precludes the adoption of the C2' endo sugar puckering. RNA:DNA duplexes (formed during transcription and replication) also favor the A-form. Although DNA has also been observed in the A form, it is in many cases due to the crystallization conditions.[24]

Z-DNA can be formed by alternating GC repeats, particularly in cases where DNA is negatively supercoiled, and in high salt conditions.[24,83,95,96] The repeating unit is the dinucleotide, in which the guanosine and cytosine residues have distinctly different conformations. Guanosines are in *syn* conformation, with a C3' endo sugar puckering, whereas cytidines maintain the C2' endo, *anti* conformation found in B-DNA.[83,93] The rise of a dinucleotide unit is 7.25 Å, corresponding to an average rise of 3.6 Å per nucleotide, slightly larger than in B-DNA.[24] The helical twist (~30° on average, 12 bp per turn) is smaller than is A- and B-DNA, as is the width (18 Å).[24,83] Phosphates adopt a zig-zagging backbone with a virtually inexistent major groove, but a deep and narrow minor groove.[24,83,93]

2.2.1.2 Non-canonical base pairing

2.2.1.2.1 Mismatches

Mismatch nucleotides (or mispairs) are pairs of nucleotides within dsDNA that do not follow the classical Watson-Crick base pairing (Chart 2A). Mismatches can occur naturally during replication or

homologous recombination,[97] following the hydrolysis of cytosine into uracil (yielding a G·U mismatch),[37] or be caused by external factors such as mutagenic molecules or ionizing radiations.[97,98] The efficiency of enzymatic mismatch repair depends on the nature of the mismatched pair (and neighboring canonical pairs), and deficiencies in mismatch repair is associated with many cancers.[97]

There are eight possible mispairs for natural DNA bases, for which the nearest-neighbor thermodynamic parameters have been determined, yielding the following trend of decreasing stabilities: G·G > G·T ≥ A·G > T·T ≥ A·A > C·T ≥ A·C ≥ C·C.[99–104] Generally, mismatches are destabilized compared to canonical base pairs.[104,105] Single or even double mismatches do not significantly alter the overall helix shape of double-stranded DNA, and they are usually well stacked in the helix (Figure 4A).[105–109] Still, they may produce local structure alterations (e.g. minor groove dimensions) and destabilization (increase in breathing frequency), in a sequence-dependent manner.[105,106] Some mismatches can yield different base-pairing motifs in equilibrium, for instance T·T (Chart 2A).[109] A particular case of mismatch yielding a fundamentally different secondary structure is C·C$^+$ (actually a hemi-protonated C-H$^+$-C base pair) which is the building block of the quadruple-stranded i-motif structure (see section 2.2.4).

There is a large number of mismatches in RNA.[110] Among these, G·U is prevalent, presents a stability close to those of canonical base pairs, and is nearly isomorphic to them (Chart 2A).[111,112] In fact, G·U base pairs are not considered as a mismatch in part of the literature, and are sometimes referred to as wobble pairs.[110,113]

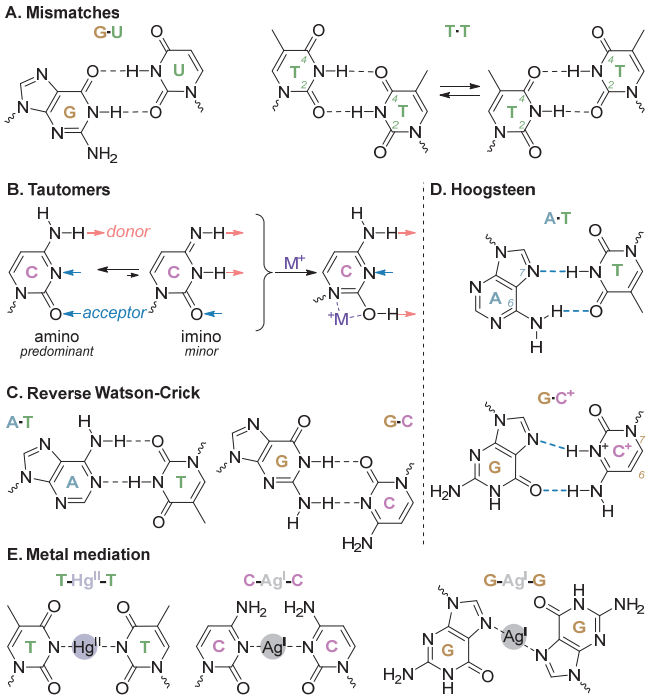

Chart 2. Non-canonical hydrogen-bonding pattern and base pairing. A. Example of wobble base pairing observed in G·U[112] and T·T[109] mismatches. B. Example of three tautomers of cytosine, wherein the predominant amino tautomer can form Watson-Crick base pairs with guanine (see also Chart 1), the imino tautomer presents an altered H-bonding pattern. Tautomers can be favored by binding to metals, and be produced during electrospray ionization.[114] C. Reverse Watson-Crick and D. Hoogsteen base pairs typically found in parallel duplex and parallel triplex structures, respectively (see also Figure 5). E. metal mediated base pairs, where bases behave as monodentate ligands without engaging in H-bonding.

2.2.1.2.2 Abasic sites

An abasic site is a nucleotide lacking its base. Such depurination or depyrimidination result from the hydrolytic cleavage of the glycosidic bond, leaving only the (deoxy)ribose moiety in the DNA or RNA strand.[115,116] This can occur with high frequency naturally, via different mechanisms, or exogenously (e.g. after alkylation by small molecules, UV irradiation).[115,117,118] Like mismatches, these defects can be repaired,[119,120] and are involved in many biological processes.[115] Duplex DNA containing a single abasic site remains in the B configuration, with an increased flexibility, and sequence-dependent localized alterations.[121–125] In particular, pyrimidines facing an abasic site tend to flip out of the helix, whereas purines can remain intrahelical, thus preserving π-stacking interactions.[124–126] The presence of an abasic site significantly decreases the melting temperature of duplex DNA (by about 10°C), to an extent that depends on the facing base and neighboring base pairs (GC pairs provide more stability).[127,128]

2.2.1.2.3 Tautomers

DNA bases are subjects to tautomerism, a chemical equilibrium between at least two species differing by the location of a hydrogen atom (Chart 2B). Generally speaking, tautomerism equilibria are regulated by various factors, including the pK_a of the labile proton, the solvent polarity, and the temperature.[129,130] The preferred tautomers are those classically depicted in canonical base pairs. The formation of a non-dominant tautomer can significantly alter the hydrogen bonding—and therefore base pairing—capabilities of nucleobases. Consequently, tautomers are frequently involved in mismatches and other non-canonical pairing. Such tautomers can be promoted by metal cations (including alkali cations).[129,131] Importantly within the context of mass spectrometry, tautomers of isolated bases can coexist in the gas-phase, and be produced during ionization.[114,132]

2.2.1.2.4 Reverse Watson-Crick and Hoogsteen pairs

Reverse Watson-Crick pairing associates the traditional pairs (A-T and G-C), but with a different relative orientation that is typically encountered in parallel duplexes (see 2.2.1.4) (Chart 2C).[133,134] Hoogsteen pairing is another variation of base pairing in which the major groove face of purine bases is involved in H-bonding (with the N7 acting as an acceptor; Chart 2D).[135] This type of association is possible at neutral pH for A·T, as observed in parallel triplexes (see Figure 5A; section 2.2.2). G·C$^+$ Hoogsteen pairs are also observed in parallel triplexes, provided the pH is sufficiently acidic.[136,137] The most famous instance of Hoogsteen pairing is probably the G-quartet, in which each of the four guanines are H-bonding with their Hoogsteen face to the Watson-Crick face of another guanine (see Figure 6, section 2.2.3). Reverse Hoogsteen base pairing, in which the thymine is flipped along the glycosidic bond, can also be achieved in A·T pairs, e.g. in antiparallel triplexes (Figure 5B).

2.2.1.2.5 Metal-mediated base pairs

Natural nucleotides can form metal-mediated base pairs.[138] In this context, mismatched nucleotides can be hybridized with high stability, which can be leveraged for supramolecular chemistry and DNA-based nanotechnology applications.[138,139] An early example is the T-Hg^{II}-T base pairs, in which two thymines bind one mercury cation by their deprotonated N3, with a linear coordination geometry (Chart 2E, Figure 4B).[140,141] Similarly, two cytosine N3's or guanine N7's (on the Hoogsteen face) can coordinate a silver cation to produce stable C-Ag^{I}-C and G-Ag^{I}-G base pairs, respectively (Figure 4C).[142–144] A duplex can contain several consecutive metal-mediated base pairs, with the metal ions able to engage in metal-metal bonds, and promote non-canonical helices.[145,146] Many modified bases have also been designed to form metal-mediated base pairs including imidazole,[146] thiopyrimidine,[147] and pyrrolo-dC[148] derivatives.

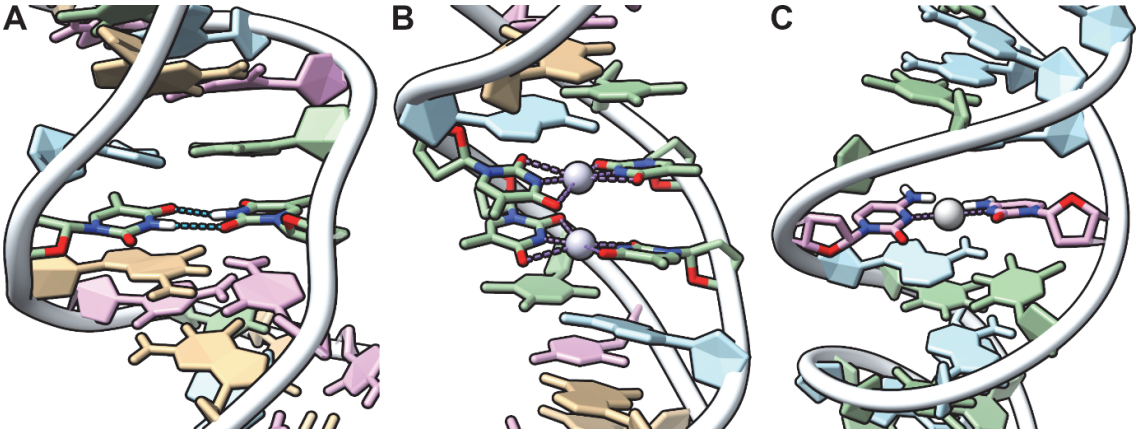

Figure 4. Non-canonical hydrogen-bonding pattern and base pairing in dsDNA: A. T·T mismatch (PDB: 2LL9;[108] solution NMR), B. two consecutive T-Hg^{II}-T base pairs (PDB: 4L24[141]; X-ray diffraction), and C. C-Ag^{I}-C base pair (PDB: 2RVP;[144] solution NMR). Phophodiester backbone in white, guanosines in tan, adenosines in blue, thymidine in green, cytosines in pink, Hg and Ag atoms as grey spheres. Non-canonical base pairs have colored heteroatoms (oxygen: red, nitrogen: blue, hydrogen: white), H-bonds in blue, and metal coordination bonds in purple.

2.2.1.3 Hairpins

Hairpins, also called stem-loops, are essentially intramolecular double-stranded nucleic acids. They consist of a double stranded stem and a single-stranded loop bridging them. In RNA, they are the most common secondary structural elements. They can guide folding, and play a central role in protein binding and gene regulation.[149–151] DNA and RNA stems differ by the type of helix they adopt (B and A, respectively).

Both the loop size and composition influence hairpin stability.[104,149,152–157] In RNA, short loops are favored both thermodynamically and kinetically.[158] Stabilizing interactions may occur in the loop itself, such as base stacking, intra-loop base pairing, inter-loop contacts (for longer sequences), and cation binding.[156,159] As a result, the hairpin stability can vary dramatically as a function of the loop sequence (for a constant length).[152,157] Additionally, naturally occurring hairpins often contain mismatches and bulges (i.e. unpaired nucleotides) that have destabilizing effects.[155] Classically, such structures are favored by higher counter-ion concentrations (in particular with Mg^{2+}) to overcome the coulombic repulsion between phosphates.[149,159,160]

Palindromic sequences can fold into hairpins by sacrificing some base pairs to form the loop, to an extent depending on the sequence.[152,161] The hairpin is generally favored over the corresponding bimolecular duplex by lower strand concentration and ionic strength,[162–164] and higher temperatures (too high temperatures yielding a random coil).[152,163] The interconversion between hairpins and intermolecular duplexes is usually a slow process,[152,153] which may be of importance when preparing samples for mass spectrometry analysis. The thermodynamics of hairpin formation and intermolecular duplex hybridization can be simulated using the Mfold and DINAMelt web servers, hosted at http://www.unafold.org/, and available in the UNAFOLD software package.[165–167]

2.2.1.4 Parallel-stranded duplexes

Parallel-stranded duplexes are right-handed double helices in which the two strands are oriented in the same 5'-to-3' direction through reverse Watson–Crick A-T and G-C base pairing (Chart 2C).[133,134,168–170] Such structures can form under normal solution conditions, particularly by A-T rich sequences, but are thermodynamically disfavored compared to antiparallel dsDNA.[171] They can also be promoted by metal-mediated base pairs.[145]

2.2.2 Triplexes

Triple-stranded nucleic acids (triplexes), first observed in the fifties,[172,173] consist of the association of a third strand (called TFO for triplex-forming oligonucleotide) by pairing a purine-rich strand in the major groove of a duplex (Figure 1 and Figure 5). Triplexes have been studied for their biological functions (*e.g.* gene expression regulation, genomic instability),[44,174,175] therapeutic potential (*e.g.* gene targeting and modification, nucleic acid-protein binding inhibition),[43–45,136] and nanotechnology applications (*e.g.* catalysis, hydrogels, switches, sensing, drug release).[31,32]

Strand association in a triplex can be intramolecular, forming the so-called H-DNA,[174,176,176,177] or intermolecular by binding of a DNA TFO to dsDNA, or an RNA TFO to dsDNA or dsRNA.[44,136,175,178] PNA forms very stable triplexes with dsDNA, but it occurs via binding of two PNA oligonucleotides to one DNA strand while displacing the complementary strand.[43,65] Chemically modified oligonucleotides (PNA, LNA, 2'-OMe RNA, phosphothiorates, phosphoramidates) have been exploited as TFOs.[44,45,69]

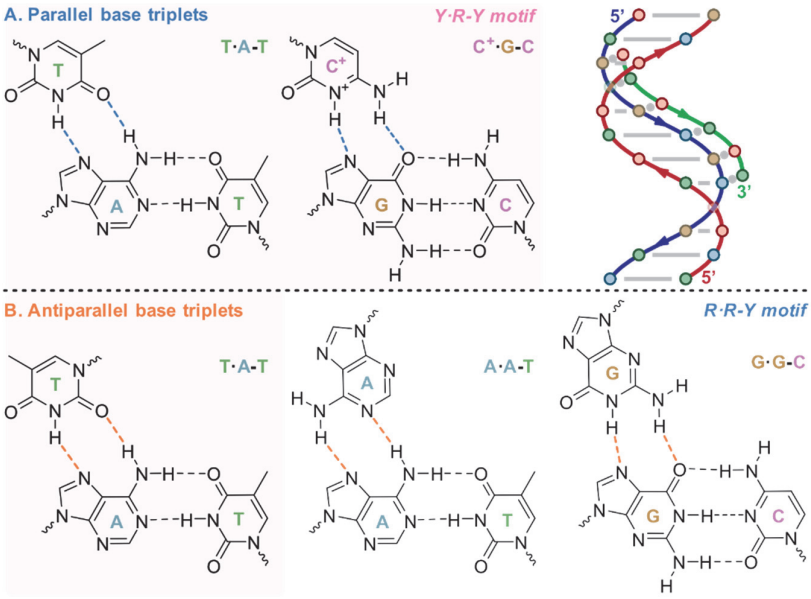

Figure 5. Base triplets typically found in A. parallel and B. antiparallel triplexes. Hoogsteen and reverse Hoogsteen H-bonds are shown in blue and orange, respectively. Top-right: parallel triplex formed by the binding of one strand (green) within the major groove of dsDNA (blue and red).

The nucleotides from the TFO can base pair the purine-rich strand in a parallel direction *via* Hoogsteen base pairing, typically a pyrimidine (Y) binding the purine (R) from a canonical Watson-Crick base pair (R-Y), e.g. T•A-T and C^+•G-C (Figure *5*A).[179] The association can also be antiparallel *via* reverse-Hoogsteen base pairing, often a purine-rich TFO forming mostly R·R-Y motifs (e.g. G•G-C, A•A-T), or Y·R-Y motifs (e.g. T•A-T) (Figure *5*B).[180]

Parallel triplexes with C^+•G-C base pairs are favored in acidic conditions, wherein the N3 from TFO cytosines may protonate ($pK_a \sim 4.5$).[136,137] The formation of antiparallel triplexes are not pH-dependent but may be inhibited by monovalent cations (particularly potassium) that may favor the folding of G-rich strands into G-quadruplexes (see below).[181,182] Triplexes are more stable when binding uninterrupted long stretches of purines, although they can still form in presence of pyrimidines on the purine-rich strand.[183–185] Finally, triplex formation is very dependent on the ionic strength, and requires relatively high amounts of monovalent cations, or smaller amounts of Mg^{2+}.[186]

2.2.3 G-Quadruplexes

G-quadruplexes (G4) are quadruple-stranded nucleic acid helices, formed by one (intramolecular), two (bimolecular) or four (tetramolecular) nucleic acid strands rich in guanines and preferably poor in cytosines.[187,188] They can be obtained from both natural and artificial (e.g. PNA[189], L-DNA[190]) nucleic acids. G4s from natural DNA or RNA are most often right-handed quadruple helices, and only a few sequences form left-handed G4s (called Z-G4).[191] G4s are involved in a number of critical biological processes (at both the DNA and RNA levels) making them promising therapeutic targets (e.g. gene regulation, telomerase inhibition, DNA damage).[192–195] They are sometimes formed by aptamers,[196] and can be used in nanotechnology.[33]

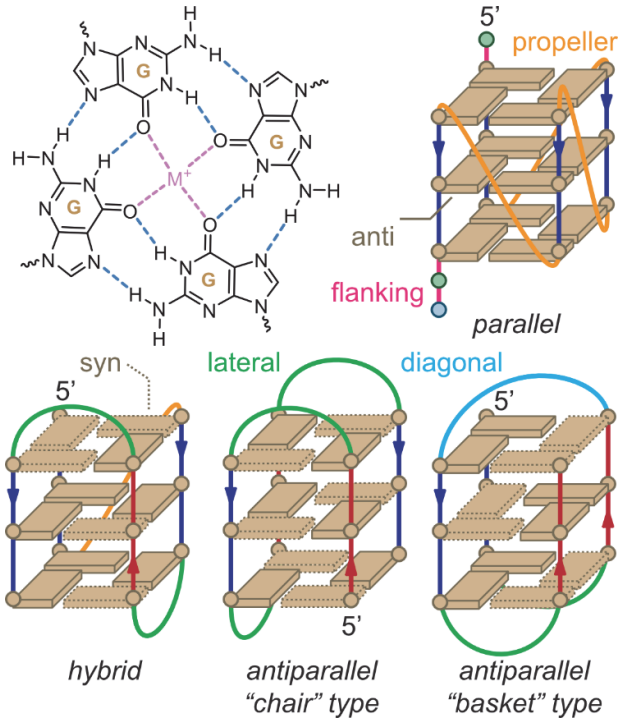

Figure 6. G-quartet (top left) and the four main tolopogies of G-quadruplexes

G4s are formed by a core of at least two stacked G-quartets (also called G-tetrads) (Figure 1 and Figure 6). A G-quartet is composed of four guanines associated by eight hydrogen bonds on both their Watson-Crick and Hoogsteen faces. A metal cation (typically K^+ or Na^+) is coordinated by the O6 of eight guanines belonging to two consecutively stacked G-quartets.[197] Consequently, a G-quadruplex containing *n* G-quartets generally coordinates *n*-1 cations, as confirmed by mass spectrometry.[198–200] The ionic radius greatly influences a cation's tendency to form G-quadruplexes (see further discussion in section 2.3.2.2.2).

In a G4, the guanines involved in G-quartets constitute G-tracts. The nucleotides from the 5'- and 3'-termini positioned before the first or after the last G-quartets are called flanking sequences (Figure 6). Loops linking G-tracts can adopt different geometries, mainly the propeller (connecting guanines from adjacent G-tracts but opposite quartets), lateral (adjacent G-tracts and same quartet), and diagonal (diagonally opposed G-tracts and same quartet).[201] G-quadruplexes are particularly polymorphic; some sequences may adopt distinct conformations, sometimes co-existing in equilibrium.[202,203] Both the flanking and loop residues can favor specific conformers by forming base pairs with other flanking or loop residues, and stacking on external G-quartets.[204–206] As a rule of thumb, sequences with shorter loops tend to adopt a propeller geometry and yield more stable G4s than those with long loops.[207]

The topology of G4s is usually defined by the relative orientations of the G-tracts and/or of the guanine stacking. It is parallel when all tracts are in the same direction (all guanines are homo-stacked in *anti*), antiparallel when two strands are oriented in the opposite direction to the two others (hetero-stacking of *syn* and *anti* guanines), and hybrid when one strand lies in the opposite direction to the three others (mix of homo- and hetero-stacking) (Figure 6).[201] The antiparallel topologies where the opposite-direction strands are laterally ("chair" type, all loops are lateral) or diagonally ("basket" type, one diagonal loop) opposed are not equivalent. The hybrid topology name was introduced late (2006),[208] and therefore a large portion of the earlier literature only discusses the parallel and antiparallel topologies.[96]

2.2.4 i-motifs

At slightly acidic pH, oligonucleotides (DNA, RNA, PNA) containing several cytosine tracts (C-tract) can fold into another type of quadruple-stranded structure called i-motif.[209–211] i-motifs have emerged fairly recently,[209] and interest in these structures is currently high with evidences that some sequences or experimental conditions allow them to fold at neutral pH,[212–214] in fixed-cell nuclei,[215] and in artificial construct introduced in living mammalian cells.[216] They also have been touted for nanotechnological applications, in particular for their pH sensitivity.[33,217]

An i-motif is made of two head-to-tail-oriented parallel duplexes intercalated into one another, themselves composed of two C-H$^+$-C hemi-protonated base pairs (Figure 1 and Figure 7), in *anti* configuration (Figure 2C). The resulting right-handed quadruple helix has both a small vertical rise (6.2 Å between two covalently linked residues, that is 3.1 Å between intercalated base pairs) and twist (12—20°), and contains two narrow minor grooves and two wide major grooves.[218] As a results, there are short distances between phosphates.

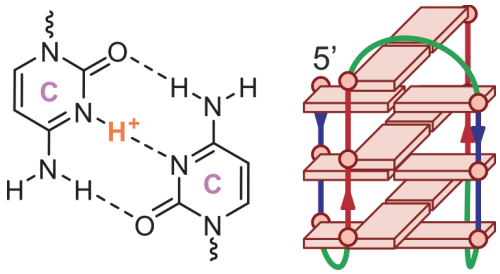

Figure 7. C-H$^+$-C base pair (left) and example of intramolecular i-motif structure (right).

Similarly to G4s, i-motifs can be formed by a single oligonucleotide containing four C-tracts,[219–221] two (hairpin) oligonucleotides containing two C-tracts,[222] or four oligonucleotides (usually identical) carrying a single C-tract.[223] A given sequence can form i-motifs of different strand stoichiometries.[161,224] An intramolecular i-motif contains three loops spread asymmetrically (one on the termini side, two on the other side). Furthermore, two conformations called 5'E and 3'E are theoretically possible, in which the outermost base pair contains the 5' residue or 3' residue, respectively.[225] Typically, a sequence complementary to a G4-forming sequence is a good candidate for i-motif formation (in which case both structures are competing with the canonical duplex),[217] for instance in human telomeres.[220,221,226]

The stability of i-motifs is dependent on the solution pH; most often slightly acidic conditions are favored to form the C-H$^+$-C base pairs, given that isolated cytosines have a pK_a of around 4.5.[221,227] The stability is also influenced by the sequence, and in particular the C-tract length,[212,228] loop length and composition.[229–232] Contrary to G-quadruplexes, i-motifs remain mostly unaffected by the nature of

cations. Other external factors such as molecular crowding (which favors the i-motif vs. unfolded or dsDNA, but are not MS compatible) and small molecule ligands can also influence their formation.[213]

2.3 Non-covalent interaction involved in nucleic acid folding

2.3.1 Base pairing and base stacking

Nucleic acids secondary structures are stabilized by an ensemble of non-covalent interactions. Among these, base stacking (along the helix axis) and pairing (orthogonal to the helix axis) are the two main contributors.[233] Others factors might contribute significantly in specific cases, for instance cation binding to G4s,[197] or sugar-sugar interactions in i-motifs.[234]

Base pairing is achieved by H-bonding, except in a few specific instances (e.g. metal-mediated base pairs, section 2.2.1.2.5). The donor and acceptor groups, and the number of H-bonds, depend on the primary and secondary structure. Canonical base pairs have 3 (G-C) and 2 (A-T/U) H-bonds on their Watson-Crick faces (Chart 1), but other pairings are possible (e.g. reverse Watson-Crick, Hoogsteen; Chart 2), potentially within non-canonical motifs (e.g. triplets, quartets; Figure 5, Figure 6, and Figure 7). Watson-Crick H-bonds typically have lengths in the 2.75—2.95 Å range; this varies depending on the measurement method but is consistent overall, and is not significantly dependent on cation binding.[24,235–237] *In silico*, H-bonds provide interaction enthalpies of around 25—30 kcal/mol to G-C and 13—17 kcal/mol to A-T base pairs, that is 7—10 kcal/mol per H-bond, depending on the computational method.[24,235–238] Similar contributions are obtained for quartets of guanines, i.e. ~79 kcal/mol or ~10 kcal/mol per bond.[239] i-motifs, which suffer from poor stacking, are stabilized by around 40 kcal/mol per C-H^+-C base pair.[240] In aqueous media, H-bond formation between bases is disfavored enthalpically (disruption of H-bonds to water) and entropically (loss of translation and rotation freedom) contributions, but the driving force is stacking (if a sufficient number of base pairs form).[238,241,242]

Base stacking stabilizes nucleic acids structure by π-π interactions (dispersion and electrostatic interactions) arising from the face-to-face overlap of neighboring (aromatic) bases, to an extent depending on several factors pertaining to the primary (nature of the bases) and secondary structures (extent of the juxtaposition) (Figure 2B—F).[241,242] Quantification of base stacking energy by computational methods is challenging and can be very dependent on the choice of functional and basis set. The highest level of theory should be employed.[235,238,242,243] The mean rise between stacked base pairs in B-helix is 3.38 Å. Base stacking is favored by non-polar interactions, therefore (9-membered double-ring) purines provide more stabilization than (6-membered single-ring) pyrimidines.[244] Secondary structures dictate the nature of base stacking motifs (e.g. base pairs, triplets, quartets). Within these, the stacking parameters (rise, slide, shift, tilt) influence the extent of stacking energy.[245,246]

2.3.2 Role of cations

In mass spectrometry, ammonium cations and their derivatives are more widespread, while in biophysics using NaCl is more common. Yet potassium cations predominate in cells (orders of magnitude of free cations: 100 mM K^+, 10 mM Na^+, 1 mM Mg^{2+}), while sodium dominates in extracellular media (5 mM K^+, 150 mM Na^+, 1 mM Mg^{2+}).[247,248] Nucleic acids are polyanions; they are therefore expected to bind cations to minimize phosphate-phosphate electrostatic repulsions and achieve folding.[249] The nature and concentration of cations therefore influences the structure, stability, and binding of nucleic acids.[247,250–252]

Here we will distinguish site-bound (specific) cations from diffuse (or non-specific) cations as two extremes of a continuum (Figure 8).[253] Specific cations have a discrete stoichiometry, and may lose some of their coordinated water molecules to produce inner sphere complexes with nucleic

acids.[159,197,247,254,255] A prime example is the G-quartet coordination of K^+ in G4s.[197] Non-specific cations are delocalized around the nucleic acids structure, have non-complete occupancy, and can retain their hydration shell.[159,247,254,255] Electrostatic screening of phosphate groups typically occurs through diffuse (non-specific) cation binding, but this contribution is very important for the thermodynamic stability of any specific nucleic acid structure.

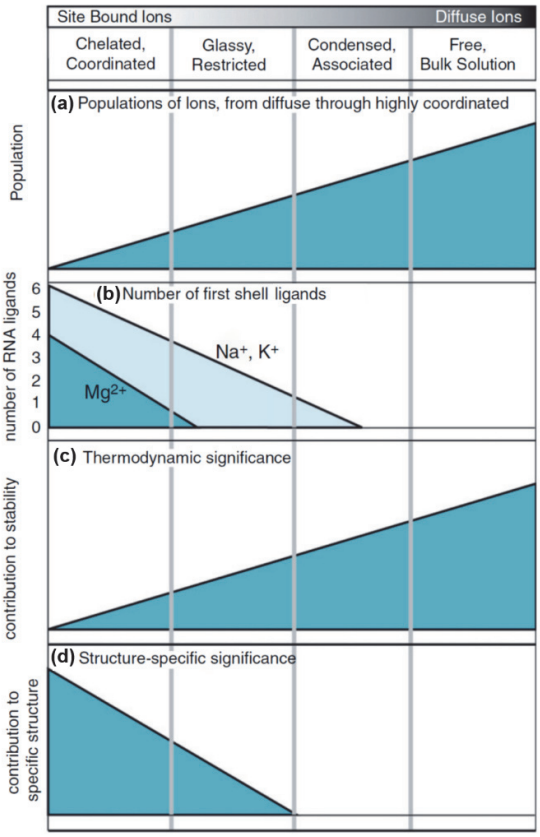

Figure 8. Schematic illustration of parameters describing nucleic acid-cation interactions. (A) The population of diffuse cations is much greater than the population of site-bound cations. (B) Diffuse ions are not directly coordinated. The number of first shell ligands contributed by nucleic acids to Na^+ or K^+ can generally vary from zero to six. In G-quadruplexes, monovalent cations are coordinated by up to eight first shell ligands. The number of first shell ligands contributed by RNA to Mg^{2+} can vary from zero to four. (C) As the number of first shell ligands increases, the thermodynamic significance of cation association decreases, primarily because the number of cations with first shell ligands is relatively small. (D) The specific structural significance of a cation increases with the number of first shell ligands. Figure adapted with permission from Ref. 253. Copyright 2012 Elsevier.

A further distinction can be made with regard to the degree of covalency of nucleic acids-cation binding. The binding of hard acids such as Na^+ or K^+ tends to be electrostatic, and favors oxygen over nitrogen. Therefore they mainly bind O-rich phosphate groups (non-specifically) and base pairs and quartets oxygens,[256,257] but can still bind bases' nitrogen to some extent.[247,258] The binding of soft acids, however, has a more covalent character, and favors nitrogen over oxygen atoms, therefore promoting the interaction with nucleobases nitrogens. This is the case in metal-mediated base pairs, for instance Hg^{2+} binds thymines' deprotonated N3,[140,141] and Ag^+ binds cytosines' N3 and guanines' N7 (see Chart 2 and Figure 4, and section 2.2.1.2.5).[142–144]

2.3.2.1 Nonspecific cations and the effect of ionic strength

Increasing the ionic strength ($I = \frac{1}{2}\sum_i C_i z_i^2$ where for all ions i, C_i is the cation concentration and z_i the ion charge) usually stabilizes secondary structures, thanks to an enhanced screening of phosphates' charges.[259–261] Notorious counterexamples are the neutral PNA:PNA duplexes, PNA:DNA duplexes,[262] and i-motifs.[227,263] Maintaining a constant ionic strength with different cation compositions does not necessarily yield an identical charge screening, in particular when changing the ratio of monovalent to divalent cations.[249] This is likely due to the contribution of condensed or associated cations. For example, Mg^{2+} is more efficient at stabilizing duplexes.[249,254,264] Hairpin loops and RNA tertiary structures are also stabilized more effectively by Mg^{2+} than Na^+.[160,265]

The stability of canonical double helices increases when monovalent cations (e.g. Li^+, Na^+, K^+) or Mg^{2+} are added.[254] However, large salt concentrations ($\gtrsim$ 1 M) lead to dsDNA (including hairpins) destabilization.[260,266–269] In the case of self-complementary DNA sequences, although an increase of ionic strength favors hairpin loops formation,[160] the equilibrium is displaced towards the corresponding intermolecular duplex at high cation concentrations.[162–164] Stabilization of dsDNA is only weakly dependent of small alkali cations;[261,270] in particular, K^+ and Na^+ yield very similar stabilities.[254,259,267] Ammonium, a mass spectrometry favorite, also stabilizes dsDNA, hairpins and tRNA, usually to an extent that is close to that of sodium.[261,271–273] Larger tetraalkylammonium cations are less stabilizing because their alkyl groups are bulky, presumably because they cannot approach the backbone as closely in the double helix conformation (but can for random coils).[261] Trimethylammonium cation (TMA^+) also used in mass spectrometry could enter the grooves and interacts with the nucleobase as well as the phosphate groups. However the penetration in the grooves is not significant and TMA^+ act more as an electrostatic phosphate shielding.[274]

Triplex DNA formation (stability, association/dissociation rates) is strongly dependent on ionic strength; it requires relatively high monovalent cation concentrations, or lower Mg^{2+} concentrations, to allow the hybridization of three negatively-charged chains.[179,186,275,275–279] The ionic strength dependence decreases with larger C^+·G-C contents.[186] Triplexes are also stabilized by ammonium (somewhat better than Na^+),[280] and polyamines such as spermine.[182,275,281]

2.3.2.2 Specific cations

2.3.2.2.1 Double-stranded structures

Although monovalent cation binding to dsDNA is generally considered diffuse, there are some evidences of more sequence-specific cation binding sites. For example, K^+ favors the major groove of GC-rich sequences, whereas Na^+ or NH_4^+ favor minor grooves an AT-rich regions.[247,271,282] Mg^{2+} also has a stark preference for G-C vs. A-T base pairs, and can form inner-sphere complexes in the former case only.[255]

RNA folding requires monovalent cations to form its secondary structural elements, mostly for charge screening, as described above. Mg^{2+} is then sometimes involved to assemble these elements into their tertiary structure. This is the case of some kissing loops, but not all. For instance, the RNA dimerization initiation sites (DIS) of HIV-1 subtype A binds an hydrated Mg^{2+} cation in the dimerization site through the Hoogsteen face of two guanosines and the O4 of two uridines (Figure 9A).[283] By contrast, the subtype B, in which these two uridines are replaced by cytidines, does not display this specific binding site and does not require Mg^{2+} for efficient dimerization. Note that a recent analysis deduced that only 15% of Mg^{2+} binding sites identified in RNA X-ray structure should be considered as thrustworty.[284]

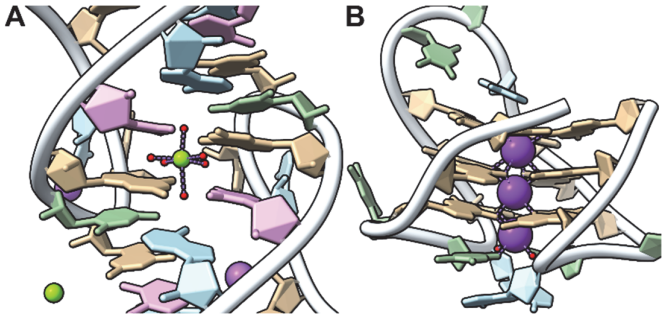

Figure 9. A. Dimerization site of the HIV-1 DIS subtype A (crystal structure, PDB: 2B8S,[283] zoomed on 5'-rAGGUGCACA). An Mg^{2+} cation (green sphere; water oxygen in red) is specifically bound by the Hoogsteen face of two G276 (tan) and the O4 of two U275 (light green). Note the other Mg^{2+} and Na^{+} (purple sphere) cations more diffusely bound. B. Three-tetrad G4 formed by a bromo-substituted human telomeric sequence (crystal structure, PDB: 6JKN,[285] $dG_3T_2AG^{Br}GGT_2AG_3T_2AG^{Br}GG$. Two K^{+} are coordinated by two quartets each, a third is coordinated by one quartet and two loop thymines (two water molecules complete the octa-coordination).

2.3.2.2.2 Cation binding to G-quadruplexes

Although G-quadruplex folding requires a sufficiently high ionic strength to shield the electrostatic repulsion of phosphates, this is not sufficient. G4 folding is indeed driven by the specific coordination of cations by the G-quartets.[197] Consequently, when the ionic strength is set only by cations that are not well coordinated by G-quartets (e.g. Li^{+}, Mg^{2+}, Cs^{+}, trimethylammonium),[286] the folding is not favored.[197,203]

Specific cation coordination is ensured by the O6 of guanines involved in G-quartets, creating an ion channel (Figure 6, Figure 9B). The ionic radius greatly influences a cation's tendency to bind within G-quadruplexes. If the cation is too big, the coordination in-between G-quartets is sterically hindered.[198] If the cation is too small, it cannot coordinate with a sufficient amount of guanines' O6 to form a G-quadruplex. Moreover, when the ionic radius decreases, the dehydration enthalpy increases, which creates an additional thermodynamic and kinetic barrier for the cation to enter the G-quadruplex.[287] Typically, K^{+} and, to a lower extent, Na^{+} are used for their physiological relevance and ability to promote G4 folding. Other cations are used, and the consensus stabilization trend is $Sr^{2+} > Ba^{2+} > K^{+} > Ca^{2+} > NH_4^{+}$, Na^{+}, $Rb^{+} > Mg^{2+} > Li^{+} \geq Cs^{+}$.[203,288–291] The ionic radius of ammonium, $r(^{VIII}NH_4^{+})$ = 1.54 Å,[292] more closely resembles that of K^{+} (1.51 Å) than of Na^{+} (1.18 Å).[293] Although the trend above is verified most of the time, the difference of thermal stability in presence of different cations depends strongly on the sequence.[207]

The topology of quadruplexes is also strongly dependent on cation coordination. Notoriously, the structure of the human telomeric sequence has a strong dependence on the cation nature.[203,226,294] For instance, the 22-mer $dA(G_3T_2A)_3G_3$ adopts a single antiparallel topology in sodium conditions (PDB: 143D),[295] and a mixture of topologies (hybrid and antiparallel) in potassium-containing solutions.[199,296] Small sequence changes can alter the cation-dependency, e.g. the 24-mer $dTT(G_3T_2A)_3G_3A$ adopts a single hybrid conformation in potassium solutions (PDB: 2GKU).[297] A change in specific cation concentration (at constant ionic strength) can also lead to changes in conformations.[200] For instance, some sequences form 3-tetrad G4s in presence of 100 mM KCl, and a 2-tetrad antiparallel G4 with 1 mM KCl (ionic strength adjusted with LiCl or trimethylammonium acetate).[199,203] Cations coordinated within a G4 can exchange with the bulk medium.[298–300] Consequently, it is possible to displace one cation by another.[203,208,301]

2.4 Tertiary structures

The tertiary structure of nucleic acids is defined as the tridimensional structures incorporating several secondary structure elements. In DNA, the overall tridimensional shape mediates the binding of proteins.[302] In RNA, tertiary structures are the results of interactions between secondary structure elements (helices, loops, bulges), possibly mediated by ions, without much distortion of these elements.[110,158,159] Coaxial helix stacking, forming a more stable pseudo-contiguous helix, is prevalent in RNA tertiary structures.[303] Other motifs such as triplexes, kissing complexes, and pseudoknots can occur by interdomain (often non-canonical) hydrogen bonding. Some RNA molecules (e.g. ribozymes) require such compact structures to be functional.[304]

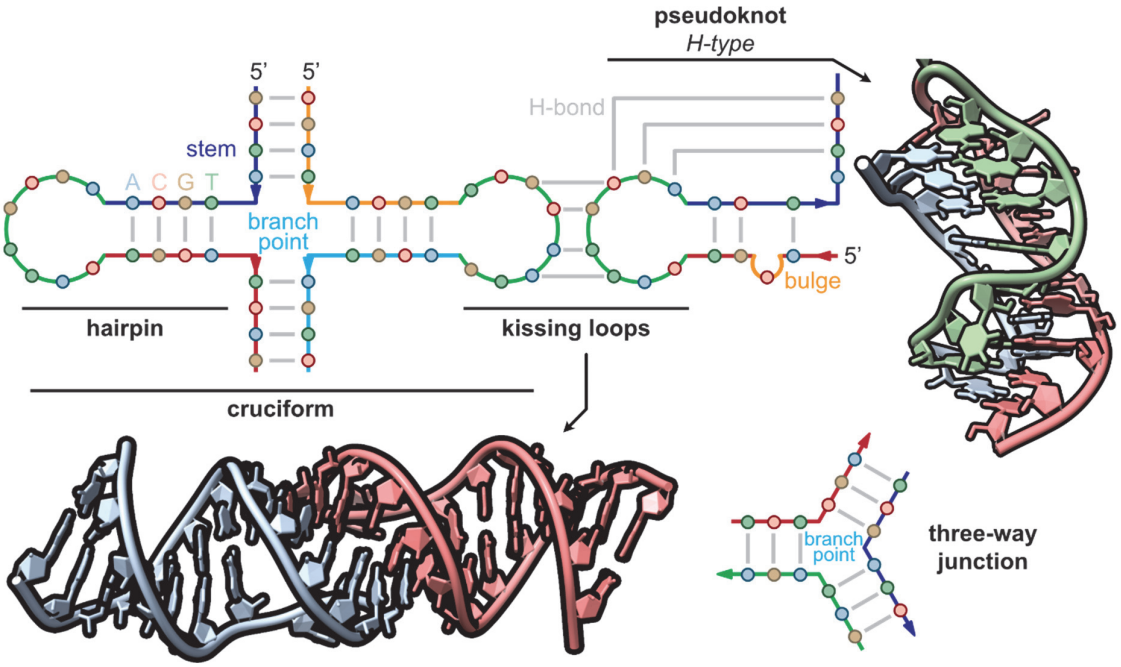

Figure 10. Hairpins are formed by a double-stranded stem closed by a single-stranded loop. Hairpins can form within duplex DNA, and form cruciform if a hairpin is present on both strands. In RNA, hairpin loops can base pair intramolecularly to form a pseudoknot, and two loops can base pair to form a kissing complex. Three strands can hybridize into three duplexes that converge into a branch point (that can contain unpaired nucleotides), forming a three-way junction.

Three-way junctions (TWJ) are structures resulting from the convergence of three duplexes towards a branch point, forming a tridimensional Y-shaped structure devoid of helix-helix stacking (Figure 10).[305,306] **Cruciform** DNA is obtained by the extrusion into hairpins of two auto-complementary regions, from opposite strands of a duplex (Figure 10). It therefore contains two stems, two loops, and a branch point at the extrusion site.[307,308] It is favored *in vivo* by negatively supercoiled DNA, in which double-strand opening is facilitated.

Kissing complexes (or hairpin loop–loop complexes) are formed by base-pairing of two sequence-complementary hairpin loops, which can be stabilized by binding Mg^{2+} (Figure 9, Figure 10).[309] When this interaction is intramolecular, such complexes are also pseudoknots. **Pseudoknots** are intramolecular structural elements found in RNA that participates in many key biological processes, in particular virus replication.[310,311] They are formed by single-stranded hairpin (H), loop (L), bulge (B), interior (I) or multibranched (M) loop regions base pairing with another single-stranded (and complementary) region of the same chain (Figure 10).[311] The latter can also be part of a secondary structure element; for instance two hairpin loop can base-pair to form an H-H pseudoknot (akin to an intramolecular kissing loop). **RNA triplexes** are frequently found in pseudoknots and other RNA

structures.[44] RNA can form major-groove triplexes similarly to DNA (except that U substitute T), in particular when containing many U·A-U triplets and in presence of Mg^{2+}.[44] Additionally, "A-minor" minor-groove triplexes are present in many large structured RNA, although they are not stable in isolation.[44]

2.5 Targeting nucleic acids with organic ligands

2.5.1 Duplex ligands

Small molecules can interact with dsDNA by intercalation between base pairs or groove binding, although non-specific, electrostatic, external binding to the polyanionic backbone can also occur (with e.g. cationic porphyrins).[312–315] Less often, covalent binding to nucleobases (metal coordination, cross-linking) is involved. Although out of the scope of this review, it may occur concomitantly to non-covalent binding and will therefore be discussed in this context only.[316,317]

2.5.1.1 Intercalation

Intercalating ligands usually contain an aromatic, planar polyheterocyclic core, often fused, with a size similar to that of a base pair (Chart 3).[312] Cationic porphyrins such as TMPyP4 and TMPyP3 can end-stack on dsDNA when adopting a planar configuration, that is when the free rotating *meso* *N*-methylpyridyl groups are in the same plane as the tetrapyrrole core.[313]

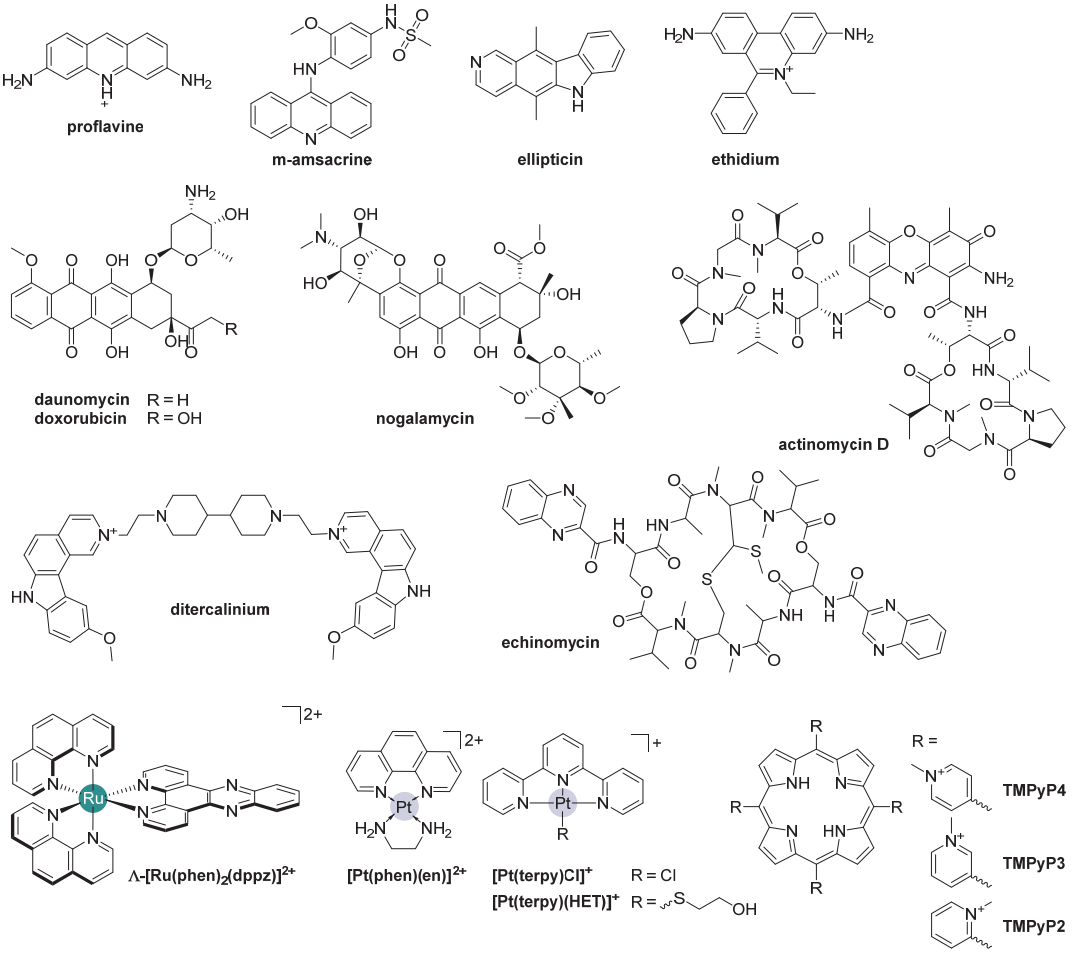

Chart 3. dsDNA intercalators

For intercalation to occur, the duplex is partially unwound—which is energetically unfavorable—to form a binding site between two consecutive base pairs, allowing the ligand to intercalate parallel to the base-pair planes (Figure 11A—D).[318] Intercalation often leads to left-handed helix unwinding, lengthening (by ~ 3.4 Å per ligand), and stiffening, to a degree that depends on the ligand.[312,314,319,320] This step is an entropically favorable hydrophobic transfer process of a non-polar molecule from the polar bulk medium to the inner helix.[318] The binding of cationic ligands also benefits from the entropically favorable release of counter-anions, in line with the polyelectrolyte theory.[252,314,318,321] Following this step, several non-covalent interactions contribute to the overall binding free energy, including H-bonding, specific electrostatic bonds, polarization forces and van der Waals dispersion interactions.[312,318,322] This is favored if the ligand is more polarized (often by heteroatoms, e.g. nitrogen) and electron-deficient (e.g. presence of a positive charge as in proflavine and ethidium; Chart 3).[312] The binding of an additional ligand to a neighboring site is strongly disfavored or, in other words, binding can only occur every other base-pair.[312,323–325] This may be a consequence of the structural constraints forced on the backbone by the first binding event.[312,326]

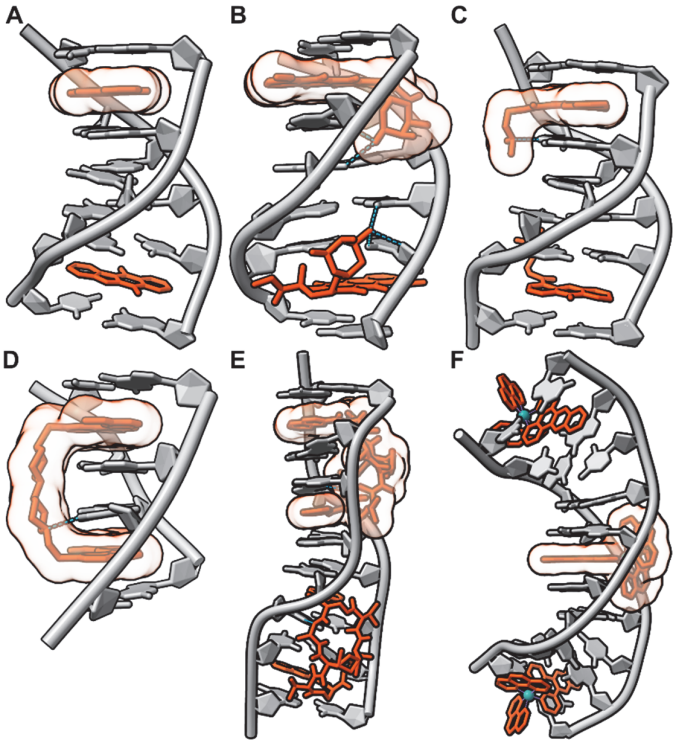

Figure 11. Duplex DNA intercalation: A. ellipticine, a pure intercalator (dCGATCG, X-ray diffraction, PDB: 1Z3F),[327] B. doxorubicine, an intercalator with ancillary groups providing additional interactions in the minor groove (dCGATCG, X-ray diffraction, PDB: 1P20),[328] C. 9-amino-DACA, an acridine derivative with a dimethylamino-capped side chain H-bonding a guanine N7 in the major groove (dCGTACG, X-ray diffraction, PDB: 465D),[329] D. ditercalinium bis-intercalated via the major groove of dCGCG and H-bonding a guanine's N7 (X-ray diffraction, PDB: 1D32),[330] E. echinomycin bis-intercalated into CG steps of the self-complementary and significantly unwound dGCGTACGC, via the minor groove (X-ray diffraction, PDB: 1PFE),[331] and F. the Λ-[Ru(phen)$_2$(dppz)]$^{2+}$ complex fully intercalated in an TA step (central binding site), and semi-intercalated into GG/CC steps (extremity binding sites; dCCGGTACCGG, X-ray diffraction, PDB: 3U38).[332] DNA is shown in grey, ligands in orange. Some cations have been hidden for the sake of clarity.

Classical "pure" intercalators, such as ethidium, ellipticine, or acridine derivatives (e.g., proflavine) have no substituents, have weak (for 5'-pyrimidine-purine steps) to no binding selectivity, and do not interfere with the nucleobase hydrogen bonding (Figure 11A).[312,314,315,333] Increased specificity can be achieved – often in natural products – by ancillary groups such as side chains, sugars, and peptide units, which usually bind within the minor grooves by van der Waals interactions, and by establishing

hydrogen bonds with neighboring bases (e.g. actinomycin, doxorubicin; Figure 11B).[328,334] Synthetic ligands have also been designed to provide additional interactions in the major groove (where proteins usually bind), for instance some acridine derivatives (Figure 11C).[329,335,336] Some intercalators can interact in both the major and minor grooves, and have slower association and dissociation kinetics than classical intercalators.[108,314,337]

Bis-intercalators can also provide enhanced selectivities, in addition to enhanced affinities. For instance, the antibiotic depsipeptide echinomycin bis-intercalates preferentially to four-nucleotide stretches with a central GC step (Figure 11E).[331,338,339] Bis-intercalators can bind *via* the minor groove, as in the case of echinomycin, or the major groove like ditercalinium (an ellipticine dimer; Figure 11D).[330] Generally, bis-intercalators yield roughly twice the unwinding per ligand than mono-intercalators.[312] For instance, echinomycin and ditercalinum cause a much larger unwinding (49° and 36°; Figure 11D,E) than ethidium bromide (26°), or ellipticine (22°; Figure 11A).[327,330,331,338–340]

Transition metal complexes containing aromatic ligands can interact with DNA through a pure intercalative mode (if the metal is relatively inert), or by both intercalation and covalent binding.[316,319,341,342] The so-called bimodal metal complexes first intercalate into dsDNA, then covalently bind to nucleobases. For instance, the chloride of complexes such as $[Pt(terpy)Cl]^+$, are hydrolysed, eventually leading to base coordination.[316,342] When such hydrolysis is not possible, as in $[Pt(terpy)(HET)]^+$, only intercalation occurs.[342–344] In intercalative binding, the metal cations provide positive charges to the aromatic moieties that π-stack with nucleobases. Typical aromatic ligands include terpyridines (terpy), phenantrolines (phen) and dipyridophenazine (dppz) (Chart 3).[341–343] The most used transition metals for intercalation are platinum (II) and ruthenium (II and III), but many others have been used (e.g. rhodium, copper, nickel, zinc, palladium or gold).[342] There can be several metal cations in each binder (multinuclear complexes), and there can be multiple stacking moieties to achieve bisintercalation.[342] Thanks to their structural rigidity and well-defined symmetry, metal complexes with fairly simple organic ligands can achieve sequence-selective binding.[341,342,344,345] The nature and geometry around the metal is also a determinant of nucleic acid binding.[313,332,342,346,347]

2.5.1.2 Minor groove binding

B-DNA contains two grooves, called minor and major, that differ in size, shape, hydration, and electrostatic potential in a sequence-specific manner (Figure 3).[348] They also present different H-bonding donor and acceptor groups along the edges of nucleobases (Figure 12A). A relatively diverse set of molecules, typically positively charged polyheterocycles, bind reversibly into the minor grooves of dsDNA, which is narrower than the major groove, and is surrounded by the phosphodiester backbone. Unlike intercalators, the heterocycles are linked rather than fused; the resulting rotational freedom allows the ligands to fit the helicity of the target.[312,314,349] Examples of minor groove binders include DAPI, Hoechst 33258, distamycin, and netropsin (Chart 4). Compared to intercalation, groove-binding generally offers superior sequence specificity, high affinities, and generally lower toxicity and mutagenicity.[349]

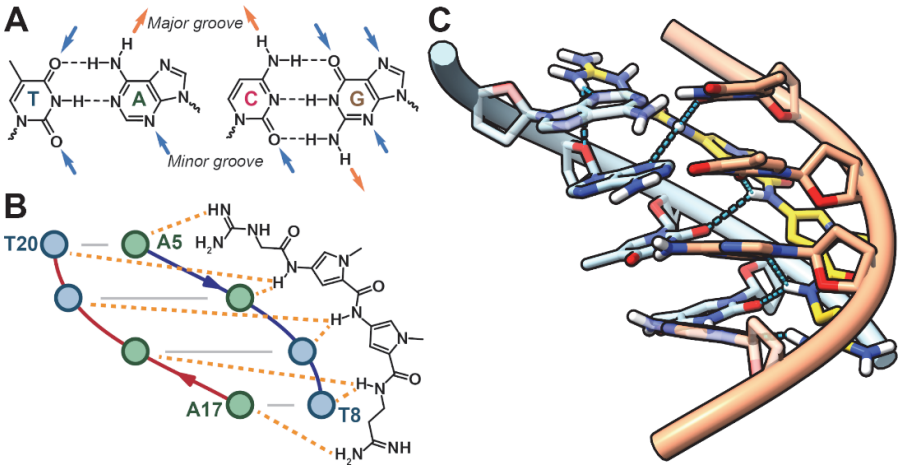

Figure 12. H-bonding opportunities in dsDNA grooves. A. Donor and acceptor groups on the edge of base pairs, highlighted with orange and blue arrows, respectively, B. Schematic of the H-bonding interactions between netropsin and adenine N3 or thymine O2 atoms on the floor of the AATT minor groove of dCGCGAATT^{Br}CGCG. Figure adapted with permission from Ref. 350 Copyright 1985 Elsevier. C. corresponding X-ray diffraction structure (full structure shown in Figure 13G; PDB: 6BNA[350]).

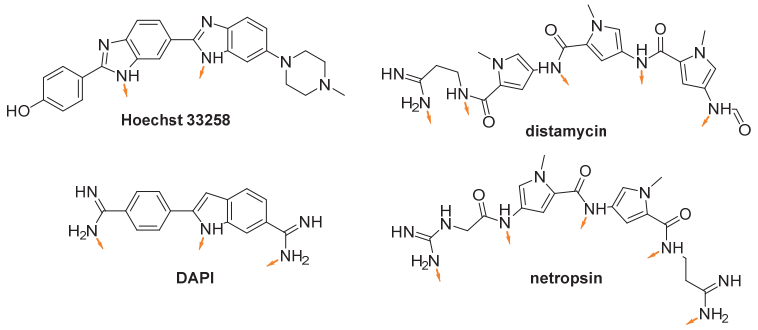

Chart 4. dsDNA minor groove binders

Groove binders interact with their aromatic moieties parallel to the DNA backbone, generating van der Waals contacts with non-polar atoms of the backbone, and their binding is therefore also largely hydrophobic in nature.[314,349] Indeed, upon hydrophobic transfer of the ligand from the bulk medium into the minor groove, the structured spine of water is released from the minor groove, while the ligand may also release water and counter-ions.[318,351,352] In the case of Hoechst 33258, these favorable entropic contributions are larger than the cost from the loss of rotational and translational freedom, and constitute the driving force in terms of binding free energy.[351]

Additionally, ligands may establish H-bonds through their heterocycles or side chains, with the N3 of A and G and the O2 of C and T acting as acceptors (Figure 12).[314,349] The position of the latter changes with the sequence, groove shape and curvature, hence providing the ground for sequence specificity.[349] The gain of H-bonds is counter-balanced by the loss of H-bonds from displaced water molecules, and thus contribute little to the binding free energy.[351] Minor groove binding is therefore generally entropically driven, the enthalpic contributions being in fact sometimes unfavorable.[351] Molecular interactions remain important to tune the sequence-selectivity of minor groove binders, because different DNA sequences provide distinct binding sites with specific H-bonding opportunities.[318,351] Hence, the binding of some ligands, for instance netropsin, is enthalpically exothermic for some sequences but not others, depending on the relative contributions of specific H-bonding, van der Waals interactions, and overall hydration of the free DNA and ligands.[318,349,352,353]

Unlike intercalators, minor groove binders usually favor AT-rich regions, and do not alter dsDNA structures significantly (Figure 13A).[312,314,318,350,354] Stretches of consecutive AT base pairs produce narrower grooves, allowing for a deep and tight binding of heterocyclic compounds.[349] Minor-groove binding in GC-rich grooves is disfavored because i) they are wider, which decreases van der Waals contacts, ii) the H-bond between guanines' N2 and cytosines' O2 lying in the minor groove sterically hinders binding, and iii) AT regions have a more negative electrostatic potential, which is favorable for the binding of positively charged molecules.[314,349,355,356] Accordingly, interruption of AT stretches by a GC base pair can lead to a large decrease of the equilibrium binding constant of classical minor groove ligands, although this can be overcome or even leveraged with adequate molecular designs.[349,357,358] This is sometimes accompanied by ligand dimerization within the groove, hence forming 2:1 ligand:DNA complexes (Figure 13B).

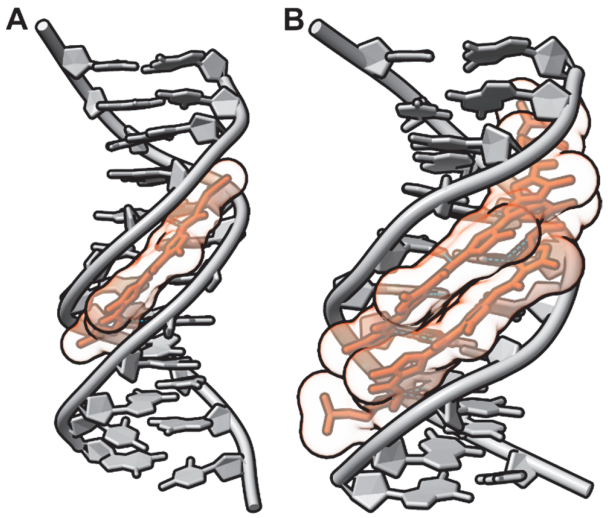

Figure 13. Duplex DNA minor groove binding: A. Netropsin fitting tightly into an AT-rich groove and establishing specific H-bonds without unwinding nor elongating the double helix (dCGCGAATT^{Br}CGCG, X-ray diffraction, PDB: 6BNA),[350] and B. GC-rich wider minor groove binding by antiparallel side-by-side pairing of two four-ring pyrrole-imidazole polyamides establishing an extensive network of hydrogen bonds (dCCAGG^{Br}CCTGG, X-ray diffraction, PDB: 365D).[358] DNA is shown in grey, ligands in orange. Some cations have been hidden for the sake of clarity.

Transition metal complexes can electrostatically bind in dsDNA grooves without helix perturbation, sometimes even if the organic ligand appears better adapted to intercalation (e.g. $[Ru(bpy)_3]^{2+}$, $[Ru(terpy)_3]^{2+}$).[359] Metal complexes can also target the major groove.[360,361] TMPyP4 porphyrin derivatives coordinating Mn^{3+}, Fe^{3+}, Co^{3+} and Zn^{2+} with axially bound ligands bind to dsDNA grooves, contrary to their square-planar counterparts (see above).[313,346,347] In absence of metal coordination, non-planar positively charged porphyrins like TMPyP2 (Chart 3), in which the *meso* substituents cannot freely rotate, can bind in the minor grooves of AT-rich dsDNA as well.[313]

Bimodal minor groove and covalent binding can also be achieved, for instance by conjugating a coordinating metal center (e.g. cisplatin) to a classical minor groove binder such as distamycin or netropsin.[362] Combilexins constitute another class of bimodal ligands, obtained by conjugation of a sequence-specific minor-groove binding moiety with an intercalator further stabilizing the complex.[363–365]

2.5.1.3 Major groove binding

Methyl green and a number of natural products and derivatives are among the few small molecules targeting the major groove of DNA.[366,367] Among these, some aminoglycoside antibiotics like neomycin, which are primarily known to bind RNA (see section 2.5.5.1), are able to bind the narrower

major grooves of GC-rich, A-form dsDNA, and even induce the B-to-A form transition.[367,368] Some bis-intercalators such as ditercalinium bind *via* the major groove and unwind significantly the helix as expected from a dual intercalative binding.[330] Note also that triplex formation is a particular case of major groove binding: TFOs of various nature (DNA, RNA, PNA, LNA, 2'-OMe RNA, phosphothiorates, phosphoramidates) bind in the major groove of dsDNA or dsRNA to form triplex structures (see section 2.2.2).[44,45,69,136,175,178]

The major groove is historically considered to be the usual recognition site for proteins. It is sterically more accessible than the minor groove (it is wide enough to accommodate α-helices), and the arrangement of H-bonding donor and acceptor groups is unique for each base pair (GC, CG, TA, AT), which constitutes a sequence-specific recognition platform.[369–371] α-helices can also bind to minor grooves, as can β-sheets (Figure 14C,D).[370] H-bonding is also possible in the minor groove (Figure 14B,D), although without distinguishing between AT and TA base pairs .[370,372] In either major or minor groove binding, hydrophobic contacts with bases can occur, and many H-bonds are formed with the backbone and not the bases, contributing less to the sequence specificity.[370,373]

Although this direct base readout has been evidenced in most DNA-protein complexes, the conformation of DNA (global and local shape readout, e.g. helix bending and base pair kinking, respectively),[374,375] and electrostatics (phosphate repulsion/neutralization)[376] can also influence protein binding energetics and specificity (see for instance the bending of the TATA element upon protein binding; Figure 14C).[370,372,373] Changes in DNA conformation may be necessary for H-bonding to take place, resulting in a so-called indirect readout.[370] Complexes where DNA is highly deformed have unfavorable formation enthalpy and favorable formation entropy, whereas the reverse is true when the DNA conformation remains mostly unchanged.[373]

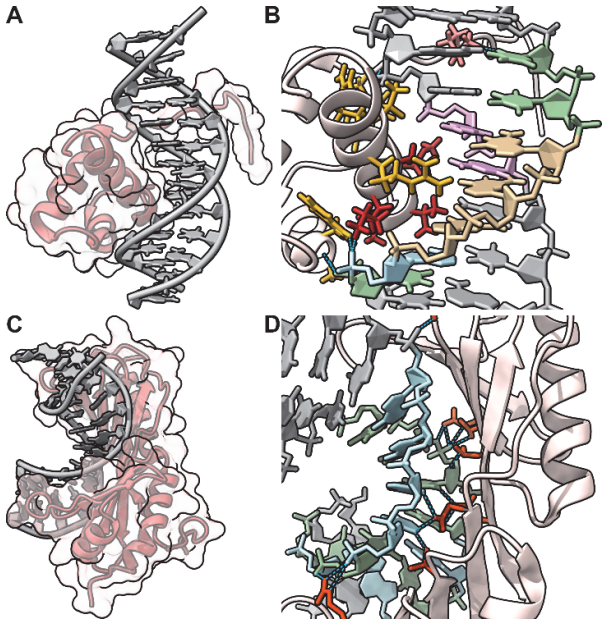

Figure 14. DNA complex with proteins. A and B. Complex between double-stranded human telomeric DNA (grey) and Trf2 (orange) ($dGT_2AG_3T_2AG_3/dC_3TA_2C_3TA_2C$, solution NMR, PDB: 1VFC).[377] The Lys447 (pink) from the N-terminal arm interacts with the T9 (green) in the minor groove, and the third α-helix specifically binds the T3AGGG7 sequence in the major groove: Ala484 and Val485 make hydrophobic contacts with T3, Lys488 with G5, and Val485, Met486 and Asp489 make contacts with two Cs pairing with G6 and G7 (amino acids side chains in red, G in tan, A in light blue, C in purple, T in green). Trp450, Trp470, Ala471, Lys488, Arg490, Arg492, and Thr493 (yellow) make additional non-specific hydrophobic, electrostatic, and H-bonding (blue) interactions with sugars and phosphate groups. C and D. The TATA box-binding protein (orange) interacts with the minor groove of the adenovirus major late promoter TATA box (AdMLP; grey), establishing a number of H-bonds with the A/T-rich core sequence (dGCTATAAAAGGGCA/dTGCCCTTTTATAGC, X-ray diffraction, PDB: 1QNE).[372]

2.5.2 Triplex ligands

Triplex ligands are mostly classical dsDNA intercalators (e.g. acridine,[378] proflavine,[378] ellipticine,[378] ethidium bromide,[378–380] benzo[*e*]pyridoindole derivatives[381,382]) and compounds with aromatic cores intercalating between the base triplets, generally favoring AT-rich sequences, and sometimes decorated with cationic side chains located in the minor groove contributing favorably to the binding free energy.[383–388] More triplex-specific ligands arose from the rational design of naphthylquinoline LS-8 and derivatives, whose unfused and torsionally-flexible aromatic moieties match the crescent shaped, propeller-twisted base triplets (Chart 5).[382,383,386,389,390] Positive charges (permanent or arising from *in situ* protonation) in the aromatic core are also desirable to balance the large negative charge density found in triplexes.[383,386,389,390] Crescent-shaped, but fused, intercalators such as benzoquinoquinoxaline (BQQ) derivatives can also selectively bind triplex DNA.[387,391–393]

Some dsDNA minor groove binders can interact with triplex DNA and DNA/RNA hybrids but favor dsDNA binding (e.g. DAPI,[378,380] distamycin,[394] Hoechst 33258,[395] netropsin[378,380,396,397]) and in fact often destabilize the triplex. Aminoglycoside antibiotics, in particular neomycin (Chart 7), bind more specifically to the Watson-Hoogsteen triplex grooves (the wider section of the TFO-bound major groove, also called major-major groove[386]), without altering the stability of dsDNA.[388,398,399]

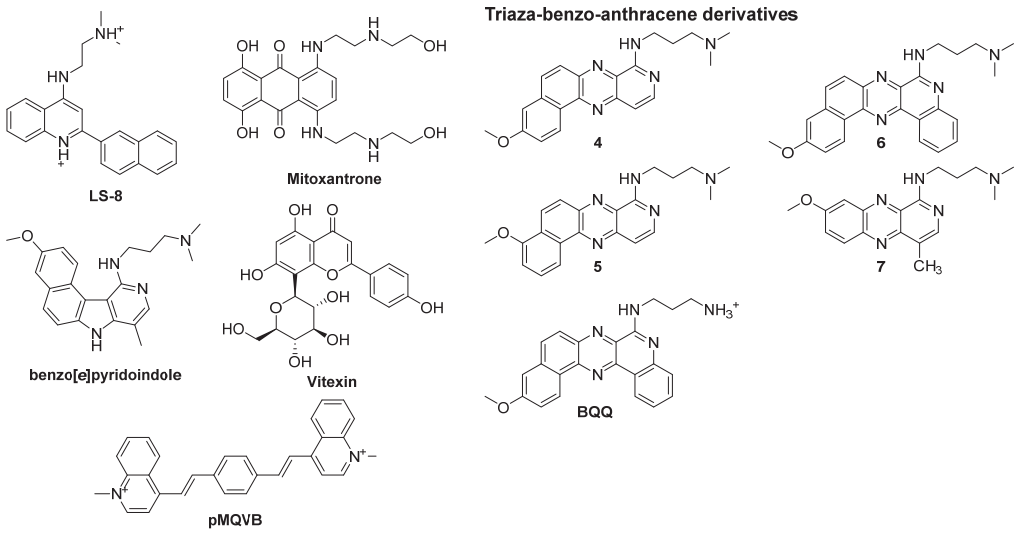

Chart 5. Triplex ligands

2.5.3 G-quadruplex ligands

In most cases, small molecules bind to G4s by stacking over the external quartets. Such ligands share structural features with dsDNA intercalators, *i.e.* a fused aromatic core promoting π-π stacking with the G-quartets, often decorated with side chains. (Chart 6).[400–402] Accordingly, numerous dsDNA intercalators also bind G4s. Positive charges favor electrostatic interactions, and can be provided by *in situ* protonation of side-chain amines (e.g. BRACO-19, PIPER, pyridostatin),[403–405] *N*-methylation of heterocycles (e.g. PhenDC3, RHPS4, TMPyP4),[313,403,406] or transition metals (e.g. Cu-ttpy, Pt-tripod).[407–410]

The design of the first generations of G4 ligands has consequently been heavily inspired by dsDNA intercalators. Given the difference in size and shape between G-quartets and base-pairs, increased affinity and specificity can rely on an increase of the aromatic surface to optimize its overlap with the G-quartets. An early example is RHPS4 (Chart 6).[403] Phen-DC3, with a high affinity and selectivity

against dsDNA, is a good example of rational optimization of the aromatic core size and shape (Chart 6).[406] Its overlap over G-quartets was later confirmed by solution NMR (Figure 15A).[411] The addition of protonable side chains, and the optimization of their nature and length, can also favorably contribute to the binding, modulate selectivity, and provide enhanced water solubility.[412–417] A seminal example is BRACO-19, a 3,6,9-trisubstituted acridine (Chart 6; compare with proflavine in Chart 3) whose side-chain pyrrolidines provide favorable hydrophobic interactions with the sides of the grooves, while the 9-anilino substituent lies snugly in a third groove (Figure 15B).[403,412,418] Analogues with longer chains have lower affinities, probably because the pyrrolidines extend too far out of the grooves.[412] Similarly, pyridostatin is a derivative of 360A in which three side chains have been added, and the quinolines are no longer *N*-methylated (Chart 6).[405]

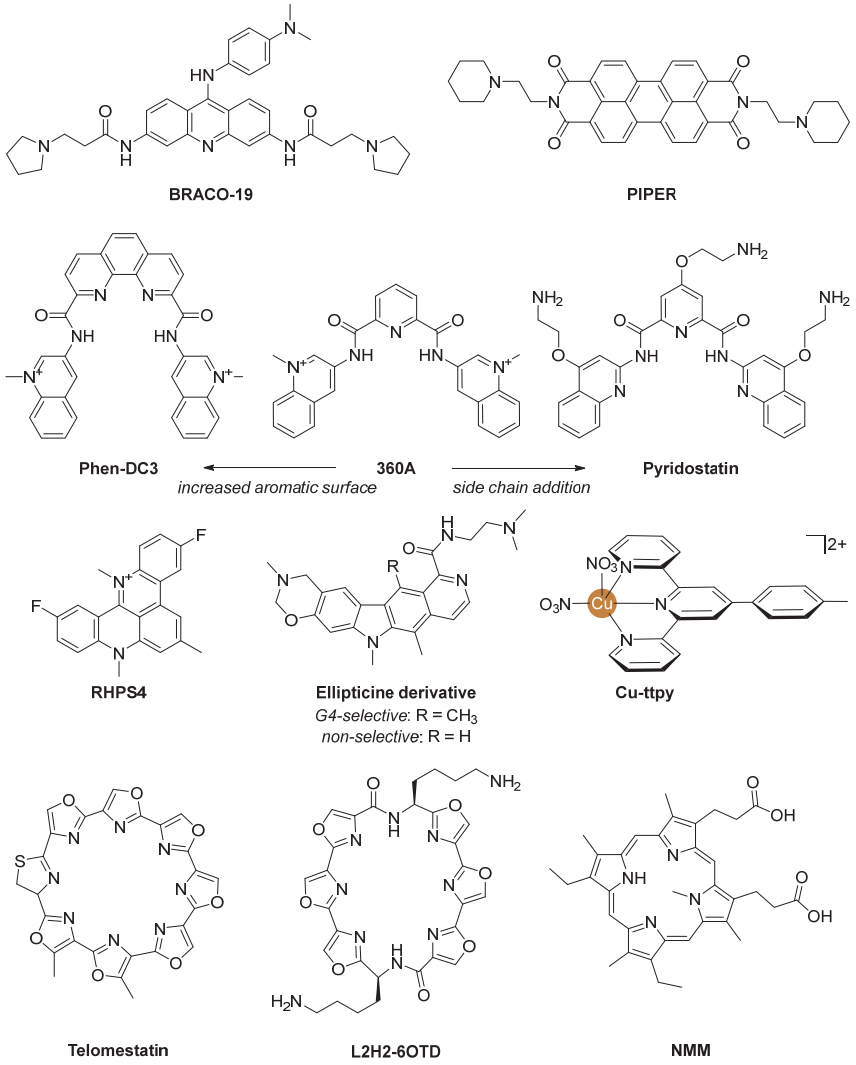

Chart 6. G-quadruplex ligands

Another approach to increase the G4 selectivity of end-stackers is to prevent dsDNA intercalation with off-plane substituents. For instance, the well-known dsDNA intercalator ellipticine can be converted into selective G4 binders by addition of sterically-clashing alkyl groups and side chains disrupting the ligand's planarity (Chart 6).[419] In the same vein, apical ligands in transition metal complexes can be a source of increased selectivity (e.g. Cu-ttpy).[420]

Numerous metal (e.g. Pt(II), Pd(II), Cu(II), Ni(II), Ru(II), Zn(II)) complexes with aromatic ligands (e.g. salphens, terpyridines, phenantrolines) bind G4s.[400,407–409] The metal withdraws some of the electron density from the aromatic ligands, increasing their stacking ability, and can act as an additional cation in the central ionic channel from G4s.[407,409] Metal cations can be conjugated to classical stackers, and there can be several metal cations for a single ligand, in which case the metal ions may interact with several grooves and loops (e.g. Pt-tripod, Figure 15C).[410]

Macrocyclic scaffolds made of unfused heterocycles (e.g. 6OTD derivatives; Chart 6), inspired by telomestatin, a neutral natural compound with a great selectivity for G4s, are attractive for their lack of dsDNA affinity. Their shape and size are similar to those of G-quartets (Figure 15D).[421–424]

Another family of macrocyclic G4 ligands are cationic porphyrins.[313,425,426] The archetype of this family, TMPyP4 (Chart 3), stacks over G-quartets thanks to their similar sizes,[313,425,426] but with little to no selectivity over dsDNA.[427–430] Other external binding modes of higher ligand:DNA stoichiometry and much lower affinity have been evidenced but are not well characterized.[313,431,432] The selectivity of cationic porphyrin for G4 DNA is improved by increasing the bulkiness of the *meso* substituents, preventing dsDNA intercalation and groove binding.[313,430] Metal coordination can improve their binding affinity, by decreasing the electron density of the porphyrin.[313] Generally, cationic porphyrins do not display any particular selectivity for individual G4 conformers.[313] An exception is the negatively-charged porphyrin *N*-methylmesoporphyrin IX (NMM; Chart 6), which favors parallel G4 over other topologies and dsDNA (with which charge repulsion is greater).[433–436]

The important structural polymorphism of G4s opens avenues to achieve sequence-specific targeting of nucleic acids, but to date few ligands have the ability to significantly discriminate different conformers. In that regard, external stacking alone appears limited because it targets a structural feature, the G-quartets, shared by all G4s. The ability to also bind to loops, grooves and flanking sequence residues, which may be more unique to a given conformer, is therefore desirable. Side chains of adequate length and nature may help in that regard (see above). By analogy with dsDNA, higher specificities may be reached by the use of groove-binding ligands, but examples are scarce, and difficult to corroborate.[402] Unfused polyheterocycles like TOxaPy, resembling dsDNA minor-groove binders or non-macrocyclic telomestatin, bind preferentially to antiparallel G4s over other topologies, and not to dsDNA.[437,438] This selectivity was tentatively attributed to groove binding. Distamycin dimerizes into the grooves of $d(TG_4T)_4$, a binding mode sometimes visible in larger minor grooves of dsDNA (Compare Figure 15E and Figure 13B), but is obviously not G4-selective.[439] This lack of selectivity has been observed for another ligand for which groove binding was proposed.[440]

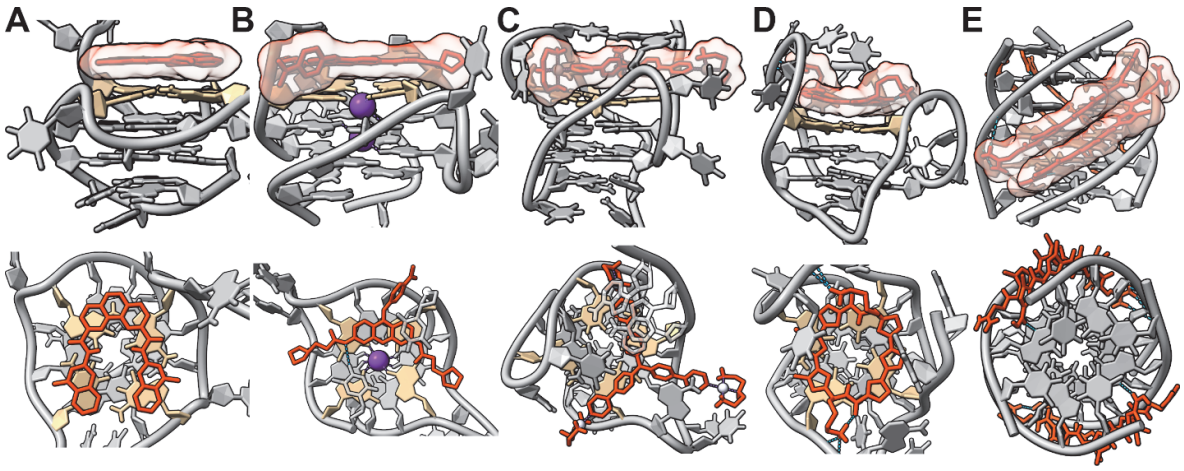

Figure 15. G4 DNA binding by small molecules. A. Phen-DC3 stacking on a parallel c-myc G4 (dTGAG$_3$TG$_2$TGAG$_3$TG$_4$A$_2$G$_2$, solution NMR, PDB: 2MGN),[411] B. BRACO-19 stacking on a bimolecular parallel human telomeric G4 (dTAG$_3$T$_2$AG$_3$T, X-ray diffraction, PDB: 3CE5),[418] C. Trinuclear Pt(II) Pt-tripod complex stacking on a hybrid human telomeric G4 (dA$_3$G$_3$T$_2$AG$_3$T$_2$AG$_3$T$_2$AG$_3$A$_2$, solution NMR, PDB: 5Z80),[410] D. Telomestatin-derivative L2H2-6OTD stacking on a hybrid human telomeric G4 (dT$_2$G$_3$T$_2$AG$_3$T$_2$AG$_3$T$_2$AG$_3$A, solution NMR, PDB: 2MB3),[422] and E. four distamycin molecules binding as dimers in two grooves of a parallel tetramolecular G4 ((dTG$_4$T)$_4$, solution NMR, PDB: 2JT7). Ligands are colored in orange, potassium in purple, and the targeted external G-quartets in tan.

2.5.4 i-motif ligands

Compared to ds- and G4-DNA, small molecules targeting i-motif structures are few, and the determinants of binding are still not well known.[441] Many are in fact dsDNA intercalators, G4 stackers, or derivative thereof, which turn out to bind to i-motifs as well.[441–444] Accordingly, most reported i-motif ligands (e.g. TMPyP4, thioflavin T, thiazole orange, crystal violet, BisA, Phen-DC3, BRACO-19, mitoxantrone, [Ru(bpy)$_2$(dppz)]$^{2+}$) are not selective against ds- and/or G4-DNA, and often disfavor i-motif binding.[441–444] Additionally, some (BRACO-19, mitoxantrone, Phen-DC3) may unfold i-motifs by interacting preferentially with the unfolded conformers.[443,444] Specific recognition of the hemi-protonated C-H$^+$-C base pairs themselves with negatively-charged ligands has been proposed, with the negative charge also preventing interactions with ds- and G4-DNA.[445]

2.5.5 RNA binders

2.5.5.1 Small molecule ligands

RNA adopts a large variety of secondary and tertiary structures. These can be bound and sometimes altered by small molecules, eventually modulating their functions, similar to small molecule occupancy of protein binding pockets.[446–448] Many natural and synthetic antibiotics (e.g. macrolides, aminoglycosides, chloramphenicol, tetracyclines, oxazoladinones) target bacterial ribosomal RNA (rRNA).[446,448–453] Additionally, a growing number of synthetic small molecules binding various other targets (non-coding RNAs, messenger RNA, viral RNA, riboswitches, splicing RNAs) have been designed or discovered by screening of chemical libraries, as reviewed elsewhere.[446–448,452–456]

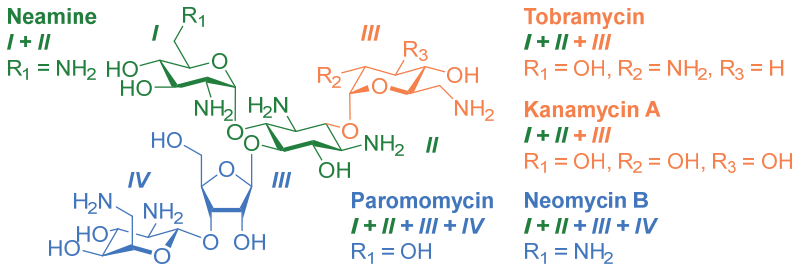

Chart 7. Structure of some rRNA-binding aminoglycosides.

The bacterial ribosome is historically the most studied RNA target, which is reflected in the mass spectrometry literature; we will therefore focus here on the binding of aminoglycosides to rRNA. Aminoglycosides are potent bactericidal small molecules (e.g. neomycin, paromomycin, tobramycin, and kanamycin; Chart 7) binding the A-site of the decoding region of bacterial 16S rRNA.[446,448–453] The A-site possesses an opened form, wherein two adenines are flipped out of the helix when binding a cognate tRNA, resulting in correct peptide synthesis.[457] Aminoglycosides bind within the major groove of the stem-loop-structured A-site through an extensive network of H-bonds, sometimes mediated by water molecules (Figure 16A,B).[458] A number of these H-bonds are conserved across aminoglycosides, which also adopt very similar conformations.[458] In particular, the sugar ring **I** stacks on a guanine and forms two H-bonds with the Watson–Crick face of an adenine (Figure 16B).[458]

The A-site subdomain can fold and function autonomously from the rest of the RNA molecule, which allows carrying out binding experiments with comparatively short oligonucleotide analytes.[459,460]

2.5.5.2 Protein-RNA recognition

Numerous and structurally diverse RNA-binding proteins (RBPs) interact dynamically with ss- and ds-RNA, with sometimes significant rearrangements in both RNA and protein.[461–464] These interactions are not fully understood but typically mediated by (i) H-bonds and van der Waals interactions between proteins (mostly side chains, and mostly by Arg, Lys, Asn and Ser) and the nucleobases (U and G more frequently than A and C), ribose 2'OH, and phosphodiester backbone of RNA (0.5–4.5 kcal/mol per bond),[461,462,465–467] (ii) hydrophobic interactions between RNA bases and hydrophobic side chains (1—2 kcal/mol per interaction),[461,462] (iii) π interactions between nucleobases and aromatic (Trp, His, Phe, and Tyr) or acyclic (Arg, Glu, and Asp) π-containing amino acids (2—6 kcal/mol per interaction), with a preference for stacking arrangements,[461,462,468] and (iv) electrostatic attraction between positively-charged patches on protein surfaces and polyanionic RNA (Figure 16C,D).[462]

Compared to DNA, RNA nucleotides are less involved in base-pairing and present an additional ribose 2'-OH, which constitutes additional interaction opportunities.[461,467] RBPs cannot always surround their target the way DNA-binding proteins often do because of the large range of structural elements forming RNA tertiary structures (compare Figure 16 and Figure 14).[461] Some RPBs can also bind DNA, although not necessarily by the same binding mode.[469,470]

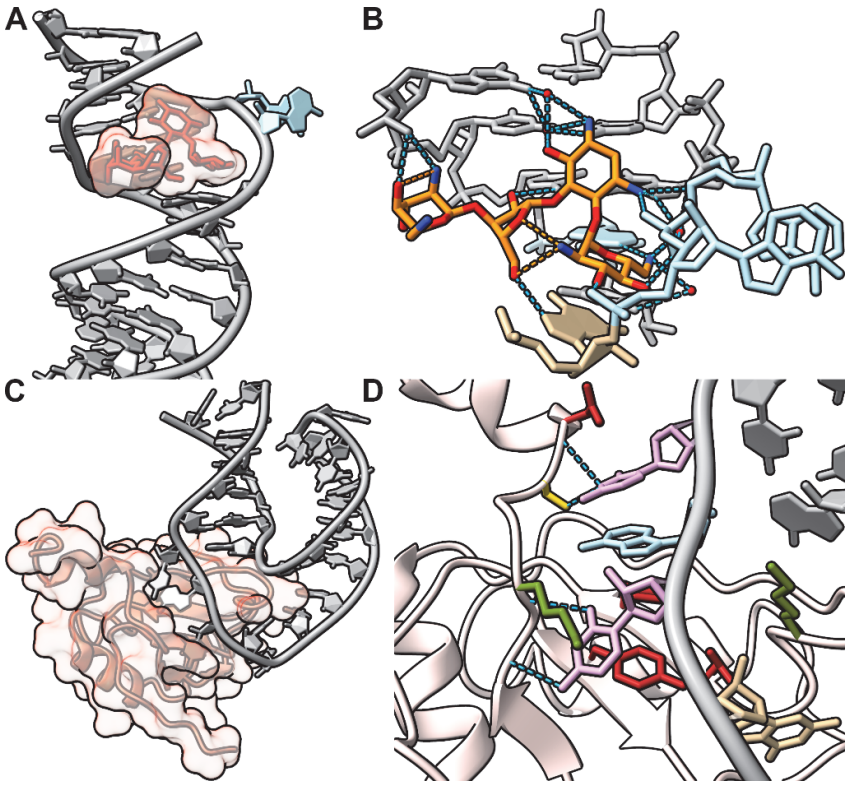

Figure 16. RNA complexes with small molecules and proteins. A: neomycin B (orange) binds in the major groove of the 16S rRNA A-site (grey, flipped out adenines in light blue) by B. stacking of the ring I to a guanine (tan), pseudo base pairing to an adenine (light blue) and establishing an extensive network of hydrogen bonds (blue) with the bases, phosphodiester backbone and water (rCGCGUCACAC$_2$G$_2$UGA$_2$GUCGC, X-ray diffraction, PDB: 2ET4).[458] C and D (zoomed): complex between the human U1A protein and the polyadenylation inhibition element (PIE) RNA contains examples of hydrogen bonding between nucleotides and amino-acid side chains (OH of Ser90, yellow with the O2 of C45, purple) or backbone (Asp91 with C45, Lys87 and Tyr85 with C43, purple), stacking (all stacking amino acids in red: Phe55 and Asp91 with A44, blue, and C45, purple; Gln53 with G42, tan; Tyr12 with C43, purple), and electrostatic (Lys49 and Lys87, green) interactions (r(G$_2$CAGAGUC$_2$U$_2$CG$_3$ACAU$_2$GCAC$_2$UGC$_2$), solution NMR, PDB: 1AUD).[471]

3. Mass spectrometry methods

3.1 Direct detection of intact complexes

3.1.1 Ionization of intact complexes

3.1.1.1 Electrospray ionization (ESI)

3.1.1.1.1 Mechanism of ESI

Electrospray ionization (ESI)[472] is the most widely used method to transfer intact analyte ions from solution to the gas phase for mass spectrometry analysis. The process by which analytes in solution become ions in the gas phase can be decomposed in three steps:[473] (1) production of the charged droplet at the capillary tip (Figure 17A), (2) successive cycles of shrinkage and asymmetric fission of the charged droplets due to solvent evaporation and Coulomb repulsion (Figure 17B), and (3) formation of gas phase ions from charged droplets (Figure 18).

The solution is infused through a metal capillary, which is held at a few kilovolts.[474] With the electric field, the solution at the capillary tip deforms into a Taylor cone that emits a fine mist of droplets. As the droplets evaporate, their charge density increases until the Rayleigh limit is reached.[475] At this point, the Coulombic repulsive forces become equal to the surface tension of the liquid (Equation (1)),

$$q = 8\pi(\varepsilon_0 \gamma R^3)^{1/2} \quad (1)$$

where R is the droplet radius, q is the charge, ε_0 is the permittivity of vacuum and γ is the surface tension of the solvent. At droplet radii below the Rayleigh limit, asymmetric droplet fission occurs: the parent droplet typically produces ~20 offspring droplets, which carry away 2% of the mass and 15% of the charge of the parent droplet.[476] Figure 17B shows the droplet evolution at the Rayleigh limit. This type of fission is known as 'jet fission'. The succession of evaporation and asymmetric fission of the droplet depends on the initial size and charge of the droplets produced by electrospray. In standard electrospray, the initial droplets have radii in the micrometer range, while in nanoelectrospray the droplets are one order of magnitude smaller (further discussion in section 3.1.1.2.1).[477]

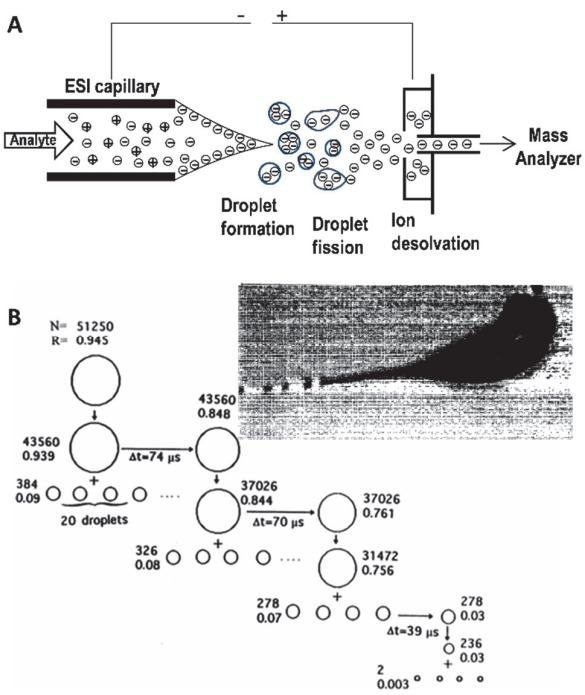

Figure 17. A. An ESI source working in negative ion mode. Figure adapted from Ref. 474. Copyright 2013 American Chemical Society. B. Droplet evolution at the Rayleigh limit. R corresponds to the radius of droplet in micrometers, N is the number of elementary charges, and Δt (μs) is the time required for droplet shrinkage to reach the next fission. Figure adapted with permission from Ref. 475. Copyright 2000 Wiley. At constant total charge, solvent evaporation increases the Coulomb repulsion. This results in droplet jet fission. Droplet jet fission is shown at the top right. Figure reproduced with permission from Ref. 476. Copyright 1994 AIP.

The last step—the formation of gas-phase ions—can follow three different mechanisms (Figure 18): the ion evaporation mechanism (IEM), the charge residue mechanism (CRM) or the chain ejection mechanism (CEM):[475]

- Low molecular weight species are believed to be transferred to the gas phase by the IEM (Figure 18A).[478] In this mechanism, ions evaporate from the droplet surface by carrying away only a thin solvation shell. The IEM limiting case requires high electrostatic energy, yet a droplet size larger than the analyte residue and larger than the Rayleigh limit. If the latter is reached first, ion evaporation can still occur: the field strength at the surface of the droplet becomes high enough to assist the desorption of solvated ions from the surface.[479] The physics involved is the same for such IEM and for the asymmetric droplet fission; the main difference is the size and charge of the offspring droplet.
- Large globular analytes (e.g., native proteins) are released into the gas phase via the CRM (Figure 18B).[480] In this mechanism, droplets containing only one large analyte shrink due to the solvent evaporation. The solvent shell disappears and the charge carriers are transferred to the analyte (cation or anion adduction, protonation or deprotonation). During shrinkage, the radius of the nanodroplet containing the large analyte must remain larger or equal to the Rayleigh limit. If it becomes smaller, the charge density of the droplet can decrease by IEM ejection of small ions and solvated protons.[481,482] CRM is often contrasted with IEM, but the main difference between the two phenomena is the size of the analyte and thus of the solvent shell that surrounds it.
- Finally, disordered organic polymers or unfolded proteins undergo ESI via the CEM (Figure 18C).[474] In this mechanism, when the conformation is extended and flexible, and when

hydrophobic groups become exposed to the solvent, the molecule migrates on the droplet surface, like a surfactant. Another requisite for the CEM is that charges can be transferred to the molecule with sufficient density. The analyte is extruded from the droplet surface to the gas phase, one charge at a time. We can also see analogies between the CEM, IEM and droplet fission. One the one hand, the CEM can be viewed as a series of IEM events, where the charges are tethered on the molecule like beads on the string.[483] On the other hand, the CEM can be viewed as an asymmetric fission of the droplet, wherein a macromolecular chain is trapped in the filament produced from the parent droplet.

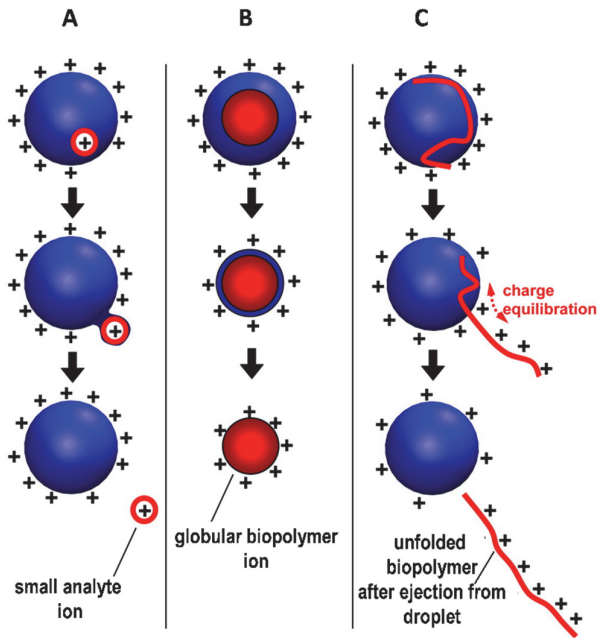

Figure 18. Different mechanisms involved in ESI. A. IEM showing the process of desorption of a small ion from the surface of a charged droplet. B. CRM showing the release of large globular protein into the gas phase. C. CEM showing the process of ejection of an unfolded protein from droplet surface. Figure adapted from Ref. 474. Copyright 2012 American Chemical Society.

3.1.1.1.2 Equilibrium partitioning effects on signal relative intensities

The relative intensities of the ions in an ESI mass spectrum do not always reflect the relative concentrations of the corresponding analytes in solution. Tang and Kebarle[484] interpreted this observation as an evidence for the IEM: the surface activity of the analyte plays a role because the ions evaporate from the surface of the droplet. In 1997, Enke proposed the equilibrium partitioning model to account for the concentration dependence of analyte response.[485] In this model, the effect is a consequence of the asymmetric droplet fission and not of the final ion production mechanism. Indeed, small offspring droplets are emitted from the surface of the parent droplet, and will thus be enriched in surface-active compounds.[486] Because the charges are located on the surface of the droplet, to become detectable ions the analytes must be present at the droplet surface, which is considered as a phase separated from the neutral droplet interior. If ion partitioning between these two phases is sufficiently rapid, one can define an equilibrium constant between the surface and the interior of the droplet.

At low concentration, the surface is not saturated and all ions can freely access the surface. At high concentration, the surface is saturated, the different analytes compete to access the surface, and the different response will highly depend on the respective partitioning constants. In nanoelectrospray,

droplets are initially smaller and undergo fewer cycles of asymmetric fission before the ions are produced. Consequently, the ion relative intensities often better reflect the solution concentration ratios.[487]

3.1.1.1.3 Why is it recommended to use the negative ion mode for nucleic acids native mass spectrometry?

Most of the literature in biomolecular mass spectrometry is focused on proteins ionized in the positive ion mode. However, nucleic acids carry an excess of negative charges in physiological conditions on the phosphate groups, while the bases are mostly neutral at physiological pH. Consequently, nucleic acid analysis is usually more sensitive in negative ion mode. Few groups have studied the ionization of nucleic acid complexes in both polarities.[488–490] For non-covalent complexes, the use of positive mode was problematic.[489] For example, complexes with intercalating agents could not be detected in positive mode, although they exist in solution and are detected in negative mode. Complexes with minor groove binders could be observed in positive mode but their relative intensity did not reflect their abundance in solution. The difference is a consequence of the nature of the charge carriers. In negative mode, the charge carriers in the sprayed ions are the phosphate groups, like in solution. However, not all phosphate groups remain negatively charged, as many are neutralized by counter-ions. In contrast, to produce multiply charged positive ions, the phosphate groups are all neutralized and in addition, some nucleobases must be protonated as well. As a result, the network of native non-covalent bonds is more likely to be perturbed in positive ions than in the negative ions.

3.1.1.1.4 Charge state distributions

Electrospray ionization of biomolecules results in multiply charge states.[491] For oligonucleotides, the charge state distribution (CSD) in negative mode depends on the ammonium ion concentration in solution.[492] Oligonucleotide solutions sprayed at low ionic strength show broad CSD and higher charge states. A higher ionic strength neutralizes a higher proportion of phosphate groups, and thus favors lower charge states and a narrower CSD (Figure 19). The extent of charging can also be manipulated by adding organic bases to the electrosprayed solution.[493] Additives with higher gas-phase basicity (the $-\Delta G°$ associated with the reaction $B + H^+ \rightarrow BH^+$ in the gas phase) result in a higher density of negative charges being accommodated on the biomolecule, independently of the solution pH.

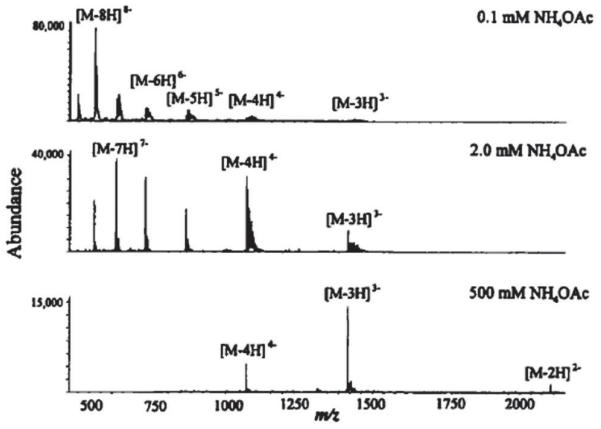

Figure 19. Charge state distribution for a 10 µM solution of an oligonucleotide dGAGACTGCCAAGCG as a function of solution ammonium ion concentration. Figure reproduced from Ref. 492. Copyright 1997 American Chemical Society.

Iavarone and co-workers discovered that the addition of m-nitrobenzyl alcohol (m-NBA) to the sprayed solution increases the charging when the original solution has a lower surface tension than m-NBA.[494] This phenomenon, called "supercharging", must necessarily occur in an intermediate regime between the bulk solution and the pure gas-phase reactivity, i.e. in the charged droplet/air interface.[495] Less volatile supercharging agents concentrate in the evaporating charged droplets. Those with weak basicity can increase the charge in positive mode by increasing protonation of analyte basic sites in the interface. Some supercharging additives work in both modes, and this was attributed to enhanced ion pairing in the presence of these highly polar molecules.[495]

There are few examples of supercharging studies on nucleic acid complexes.[488,496,497] Chingin and co-workers induced the supercharging effect on oligonucleotide single strands and duplexes either with m-NBA or by elevating the temperature of the ESI capillary.[488] More extensive analyte charging with lower degree of denaturation was observed with m-NBA. The supercharging effect was attributed to a decrease of ionic strength during the ESI process, without analyte denaturation. The results support that the supercharging phenomenon involves a direct interaction between a biopolymer and supercharging reagent occurring in evaporating ESI droplets.

3.1.1.1.5 ESI of nucleic acids in the negative ion mode: the known and the unknown

In the negative mode, the droplets carry an excess of negative charges. For a simple model of nucleic acids in ammonium acetate, the charged droplet surface thus contains fewer ammonium ions than the sum of acetate ions and phosphate groups. Figure 20 shows such hypothetical negatively charged droplet. Let's examine the three possible ionization mechanisms.

- The IEM is unlikely to occur for nucleic acids, given their size. However, small negative ions from the electrolyte might evaporate, and currently the ion evaporation propensity of small anions is not yet documented.
- The CRM, however, is realistic in native MS of nucleic acids: they are folded and expose most of their (hydrophilic) charged phosphate groups to the solvent while the hydrophobic parts are buried. They will thus tend to stay in the center of water droplets. The CRM is the desired outcome in native MS, because if the solvent shell is preserved longer, the native set of non-covalent interactions is more likely to be preserved.
- The CEM can become realistic for denatured nucleic acids in the negative mode. The CEM requires that the nucleic acids move towards the surface. Nucleobases are not overly hydrophobic, so denaturation should not play a big role in changing the surface affinity (although that is not quantitatively documented to date). However, denaturation is necessary for the oligonucleotide to be ejected as a chain. Moreover, the CEM will be more favored in negative mode because the nucleic acids can serve as primary negative charge carriers on the droplet surface, while in the positive mode the nucleic acid would occupy the second layer at the surface behind positive ions.[489] The chain ejection requires a sufficient charge density to provide sufficient electric extraction energy. In the negative mode, many phosphate groups are available, and it is possible that in the positive mode, the same charge density cannot be reached by base protonation. This may explain why charging beyond 4-5 charges per ~20-mer was never observed in the positive ion mode,[490] even in presence of supercharging additives.[488]

The competition between the CRM and the CEM for a given unfolded oligonucleotide depends on the ionic strength.[263] Lowering the ionic strength increased the fraction of the analytes borrowing the CEM and ending up at high charge states. This was attributed to a competition between the nucleic acid and the acetate ions from the electrolyte for the charged surface. The remaining unknowns are the

quantitative elements that would allow to tune the ionization mechanism and the final charge states. Further work is also required to firmly establish whether supercharging occurs via increasing the charges conferred through the CRM ("native supercharging") or via increasing the fraction of ions borrowing the CEM.

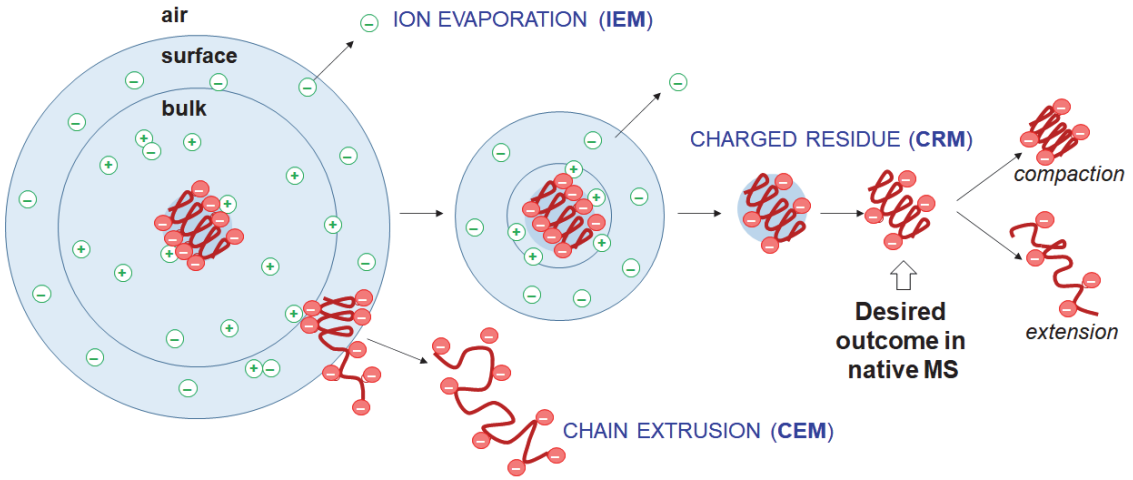

Figure 20. Summary of current understanding of nucleic acid electrospray mechanisms. Red helix: a large, pre-charged analyte, is folded in the bulk solution. Cations and anions are shown in green (there is an excess of anions at the droplet surface in the negative mode). Small electrolyte ions are released from the droplet by IEM. Longer chains, sitting at the droplet surface, can be ejected by CEM. Analytes that stay in the center of the droplet until complete desolvation and declustering are ionized by CRM.

3.1.1.1.6 Tricks of the trade

Nucleic acids require sufficient ionic strength to overcome phosphate-phosphate repulsion and fold (i-motifs are the only exception: they are more stable at low ionic strength). Mammalian cells typically contain 139 mM K^+, 12 mM Na^+ and 0.8 mM Mg^{2+}.[498] Unfortunately, such conditions are typically incompatible with electrospray. Alkali or alkaline-earth metals binds well to oxygen atoms and forms adducts, which are "non-volatile": they cannot be removed by increasing the internal energy of the system. In contrast, ammonium (NH_4^+) is volatile: when the internal energy of the system is increased, a proton can be transferred from ammonium to the biomolecule, releasing NH_3 (Scheme 1).

Scheme 1. Ion adduction mechanism with non-volatile Na+, and phosphate protonation by volatile NH_4^+.

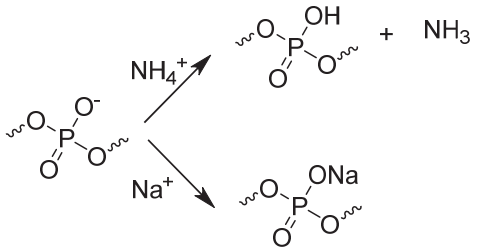

Ammonium acetate is thus frequently used in native mass spectrometry, and its concentration is chosen according to the desired ionic strength (150 mM NH_4OAc mimics the physiological ionic strength). Ammonium acetate is however not a pH buffer.[499] In some instances, trimethylammonium acetate (TMAA) was used to study the interaction of K^+ ions with G-quadruplexes.[198,200] The size of the trimethylammonium cation is larger than the space between G-quartets. This favors the binding of K^+ ions between G-quartets. Another bulky volatile electrolyte is triethylammonium acetate (TEAA).[500–502] This favors the formation of less non-specific adduct of sodium and potassium.[501] Alkylamines are

extensively used as ion-pairing agent for the analysis of oligonucleotides by LC-MS because they enhance the ionization and minimize adduction (further discussed in section 3.1.2.1).[503]

The ionization efficiency also depends on the chemical composition of the solution.[504] For example, hexafluoroisopropanol (HFIP) was used to enhance the signal of G-quadruplexes.[505] Another common practice to increase electrospray yields is to add organic co-solvents to the aqueous ammonium acetate, for example 20%,[506] 25%,[507] or 50% methanol,[508] or 10%[509,510] to 20%[505] isopropanol just before spraying. Acetonitrile can also boost ion currents.[511] This can was explained with the solvent viscosity and surface tension, that affect the evaporation process.

However, it must be remembered that organic co-solvents can affect the solution phase equilibria. For example, organic co-solvents often stabilize G-quadruplexes and accelerate their formation, as shown by ESI-MS[512–514] and other solution spectroscopic methods.[515,516] This may be desirable in some cases, but when the aim is to mimic physiological aqueous solutions, no co-solvents should be used.

3.1.1.2 Variants of ESI

Here we focus on sources that have been used for nucleic acid non-covalent complexes.

3.1.1.2.1 nanoESI

A variant of ESI, nanoelectrospray (nanoESI) was introduced by Wilm and Mann in 1996.[517] Nanospray capillaries were made by pulling capillary to a fine tip, resulting in a smaller spraying orifice diameter and a flow rate of 20 nL/min.[518] This helps to streamline the desolvation process by forming smaller initial droplets than the ESI droplets. Pure nanoESI does not require the presence of solvent pumps and inlet valves.

Adduct formation to oligonucleotides depends on the nanospray diameter size (Figure 21).[519] Non-volatile salt adducts could be suppressed by using smaller capillaries. Generally, volatile ammonium acetate is used for the analysis but nanoESI could be used when the presence of nonvolatile salts is required. nanoESI was exploited in a few native MS studies on oligonucleotides.[520,521] However, nanoESI spectra depend on capillary position, shape of the capillary tip (which can be difficult to reproduce). Thus, reproducing the relative intensities of the complexes in the mass spectra remains an art,[522] and electrospray in ammonium acetate is often preferred for its robustness.

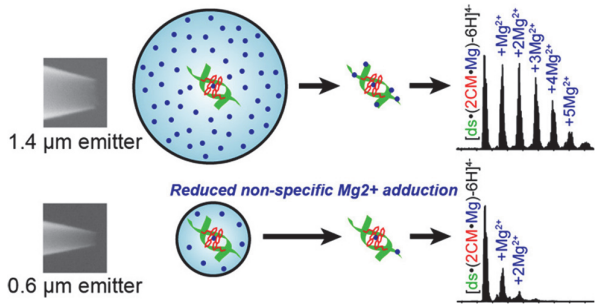

Figure 21. Comparison of MS spectra of double-stranded DNA generated from different capillary emitter (micrometer and submicrometer-size). nanoESI (bottom panel) produces a spectrum with reduced non-specific adduct. Figure reproduced from Ref. 519. Copyright 2018 American Chemical Society.

3.1.1.2.2 Laser spray ionization

Laser spray ionization mass spectrometry, developed by Hiraoka *et al.*,[523,524] has been used to characterize the stability of noncovalent complexes.[525] Akashi and co-workers have used the technique to probe the intrinsic stability of double-stranded DNA sequences and their binding affinities with various drugs in the solution phase. Dissociation curves as a function of laser power were plotted for each dsDNA or each complex. The laser power $E_{50\%}$ corresponds to the 50%

dissociation of each dsDNA or each complex. $E_{50\%}$ was compared with its melting temperature (T_m), which was determined by UV spectroscopy. The authors have also reported the relative solution binding affinities (K_D) of dsDNA-ligand complexes by laser spray mass spectrometry. Binding affinities of protein-mutant DNA complexes in solution were investigated as well.[526]

3.1.1.2.3 Cold spray ionization

Investigation of non-covalent complexes having low thermal stability can be difficult by conventional ESI. Cold-spray ionization (CSI), which operates at low temperature (ca −80°C to 10°C), allows one to characterize a wider variety of oligodeoxynucleotide complexes.[527,528] CSI allowed to detect multiply charged molecular ions with many solvent molecules attached. Very unstable DNA duplexes, triple- and quadruple-stranded oligodeoxynucleotides have been analyzed by this ionization technique.[527] Figure 22 shows the CSI and ESI mass spectra of a triple helical DNA $T_{25}•A_{25}$-T_{25} in negative mode.

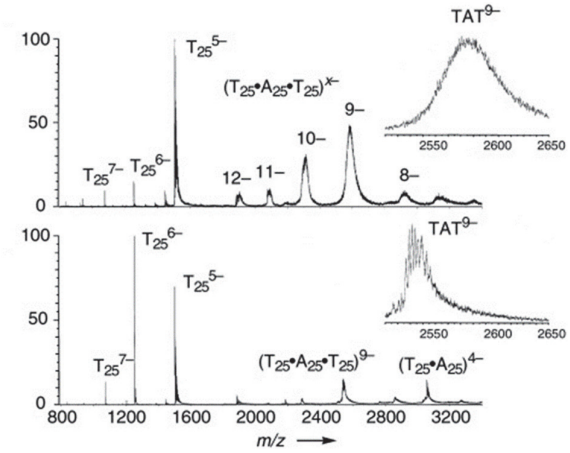

Figure 22. CSI (top panel) and ESI (bottom panel) mass spectra of T25·A25-T25 in negative mode. Figure reproduced with permission from Ref. 527. Copyright 2003 Wiley.

3.1.1.3 MALDI

Matrix-assisted laser desorption/ionization (MALDI) has been used for the analysis of different organic molecules, biomolecules like nucleic acids, proteins, peptides and their non-covalent complexes.[529–531] MALDI involves mixing of the analyte with a matrix, and deposition on a metal plate. A pulsed laser irradiates the sample to cause ablation and desorption. The molecules are ionized by protonation or deprotonation in the hot plume of ablated gases, and the ions are transferred to the mass spectrometer.[532]

Matrices mixed with ammonium salts are generally used for the detection of oligonucleotides. 2,5-dihydroxybenzoic acid (DHB) and 2,3,4-trihydroxyacetophenone (2,3,4-THAP), 3-hydroxypicolinic acid (3-HPA), 2,4,6-trihydroxyacetophenone (2,4,6-THAP), and 6-aza-2-thiothymine (ATT) were used as matrices for oligonucleotide non-covalent complexes.[530,533] The ammonium salts enhance the protonation and deprotonation of oligonucleotides and help suppressing the alkali-ion adducts.[534] Additives such as methylene blue, spermine, β-MSH, or ammonium citrate were also used to stabilize the duplexes by MALDI-MS.[531,533,535,536]

Yet the detection of native non-covalent complexes of oligonucleotides by MALDI-MS suffers some limitations. The weak non-covalent interactions of duplexes can be destroyed during the crystallization or desorption processes. However, complexes between negatively charged oligonucleotides and positively charged binders (drugs or ligands) can be very well preserved by MALDI-MS. Electrostatic interactions between the negatively charged phosphate groups of nucleic

acids and the basic side chains of the arginine and lysine residues can provide stability to the non-covalent complexes.[530,537–539]

3.1.1.4 LILBID

Laser-induced liquid bead ion desorption, LILBID, was introduced in 1996.[540,541] LILBID was claimed to have superior salt tolerance, and to be softer than ESI or MALDI because it produces lower charge states.[542,543] With LILBID, oligonucleotides solvated in micro-droplets of aqueous buffer are brought into the gas phase by laser ablation at 3 µm. During the desorption process, variation of the laser energy affects the degree of complex dissociation. The sensitivity and softness of LILBID allowed to detect single- and double-stranded oligonucleotide and noncovalent oligonucleotide-protein complexes.[542,544–546] Even large macromolecular complex like 50S ribosome of thermus thermophilus can be analyzed by this method.[545] The binding affinity of noncovalent complexes in solution was calculated from the LILBID laser dissociation curves.[544]

3.1.2 Non-denaturing chromatography coupling

Liquid chromatography (LC) and capillary electrophoresis (to a lower extent) are routinely coupled to mass spectrometry for the analysis of compounds ranging from small molecules to large biomacromolecules and polymers. In the field of biomolecular analysis, and in particular in the case of oligonucleotides, this is most often performed under denaturing conditions as a mean of online desalting.[547,548] Despite their potential, non-denaturing approaches remain rare as they present many challenges, particularly the choice of mobile phases that offer a good compromise between separation power, MS signal intensity, and the ability to preserve non-covalent interactions. If the latter is critical, for instance to quantitatively monitor binding equilibria, direct infusion should be favored.

3.1.2.1 Ion-pairing reversed-phase LC

The most used method for oligonucleotide quantitation and characterization is ion-pairing reversed-phase LC (IP-RP-LC) coupled to ESI-MS.[547,549,550] RP-LC is conducted with non-polar stationary phases, polar mobile phases (usually a mixture of water and methanol or acetonitrile), and analytes elute in order of decreasing polarity. Oligonucleotides are not well retained on non-polar phases, hence the need for ion-pairing (IP) agents, typically alkylammonium salts (*e.g.* triethylammonium acetate). IPs contain lipophilic cations that interact with the oligonucleotides to produce neutral pairs of increased hydrophobicity that are more retained by the stationary phase and less prone to cation adduction, but have a suppression effects on the MS signal.[504,551,552,503,553] Weak acidic modifiers are used to adjust the mobile phase pH, achieve better chromatographic peaks, and as a source of protons for the electrochemical reduction reaction occurring in negative ESI (increasing the MS signal, in particular for lower charge states), but can also compete for ionization with oligonucleotides.[504,554] Fluorinated alcohols (e.g. hexafluoroisopropanol: HFIP), which are volatile enough to be depleted early from the droplets, have been generally favored.[551,552,555,556]

Native structures can modify the retention times in IP-RP-LC,[551,557] but examples of native IP-RP-LC/MS analysis of non-covalent complexes remain scarce. In fact, most studies explicitly favor denaturing conditions because they provide higher MS signals and more efficient LC separations.[558,559] Operating under non-denaturing conditions may require the use of additives not compatible with MS (e.g. non-volatile salts), low column temperatures, and the careful optimization of the IP and weak acid modifiers. For instance, it is more difficult to achieve satisfying peak separation performances while obtaining a good ESI-MS signal with non-denatured siRNA duplex species than with denatured single strands.[560–562] For this particular example, an optimized combination of hexylamine and HFIP allows the separation and MS identification of all major duplex variants.[560] Hexylammonium acetate (HAA, 25 mM, pH 7.0) was also proposed as a cost-effective alternative to HFIP-based mobile phases for

routine RNA duplex non-denaturing LC/MS analysis.[563] Some fluorinated alcohols are more efficient to transfer structured oligonucleotides into the gas phase than others, both in terms of signal intensity and preservation of secondary structures. For instance, nonafluoro-tert-butyl alcohol (NFTB) suppresses the signal of hairpin-forming oligonucleotides but preserves their conformations when used with octylamine, in particular for the more stable secondary structures.[556]

Hyphenation to IP-RP-LC conditions increases the risk of disrupting non-covalent interactions, and should be restricted to qualitative studies, as illustrated by the work of D'Alonzo *et al*. on the formation of duplexes by HNA oligonucleotides.[564] In this study, different retention times were observed for the single strands and their corresponding duplexes, but also between different duplexes. For instance, two LC peaks were observed for the monomer and homo-duplex forms of β-D-homo-DNA-A_{13}, an artificial 13-mer oligonucleotide in which deoxyribose moieties are substituted by pyranoses (Figure 23A and Chart 1 and section 2.1.2.2). In presence of L-HNA-T_{13} (a 13-mer oligonucleotide made of hexitol nucleic acid; another type of 6-membered-sugar nucleosides; see Chart 1 and section 2.1.2.2), the hetero-duplex elutes later than the homo-duplex, which is not visible anymore (Figure 23B). Importantly, duplexes are probably not quantitatively preserved during the analyses, and the observed amount can depend on their gas-phase stability as well. Native MS also requires ion transfer soft conditions, and the reader should critically evaluate whether the reported conditions are indeed soft enough (see section 3.1.3).

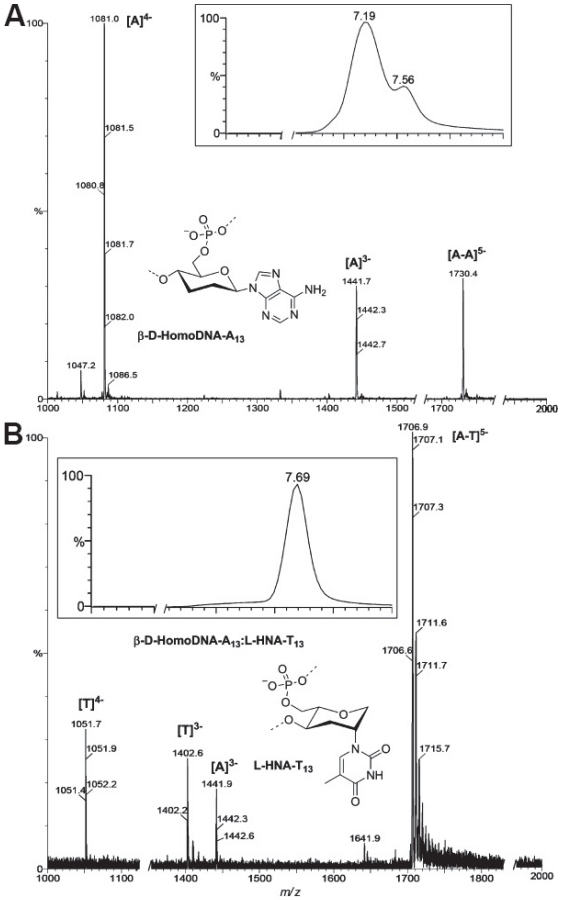

Figure 23. LC-MS profiles of the β-D-homo-DNA-A_{13} oligonucleotide in absence (A) and presence (B) of the L-HNA-T_{13} oligonucleotide (both chemical structures only show a single nucleotide from these 13-mer sequences). Analysis of 100 µM oligonucleotide samples in a mobile phase made of H_2O containing HCO_2NH_4 (1 M), N,N-dimethylaminobutane/HFIP and acetonitrile, on a C18 PepMap 0.5x15 mm column (Dionex) coupled to an orthogonal acceleration/time-of-flight mass

spectrometer (Q-Tof-2, Micromass, Manchester, UK) in negative ion mode. Figure adapted with permission from Ref. 564. Copyright 2009 Wiley.

Hydrophilic interaction liquid chromatography (HILIC) uses a polar stationary phase and a relatively non-polar mobile phase in which (buffered) water is the strong solvent. Analytes are partitioned between a layer of water formed on the stationary phase and the bulk mobile phase enriched in organic solvent (often acetonitrile), and elute by order of increasing polarity. Recently, non-denaturing HILIC/MS of DNA and RNA oligonucleotides was reported for the first time.[565] The impacts of column temperature and mobile phases additives on both chromatographic separation and MS response were evaluated.

3.1.2.2 Non-denaturing capillary electrophoresis coupling

Capillary electrophoresis (CE) is routinely used to study a wide range of analytes including nucleic acids and their complexes.[566–570] CE is based on the differential migration of analytes in an electrophoretic solution contained in a capillary under the influence of an electric field.[566] It offers better resolutions and peak shapes from smaller amounts of sample compared to conventional liquid chromatography.[547]

The separation typically relies on a non-equilibrium mechanism depending on the particular method used.[571] In capillary zone electrophoresis (CZE, or free solution capillary electrophoresis, FSCE), wherein the capillary is entirely filled with a background electrolyte (BGE) as carrier, the analytes mobility is related to their charge and size. Nucleic acids bound to small molecules or proteins are readily separated by this method.[568] Alternatively, capillary gel electrophoresis (CGE) separates nucleic acids by their size and conformation (smaller analytes migrate faster than longer ones) by sieving through a gel.[566,572,573] Denaturing conditions are favored when the separation efficiency is important, because they allow the separation of ssDNA with increased resolutions compared to the corresponding dsDNA molecules.[566,574] Non-denaturing conditions result in mobility shifts for changes as small as a single nucleotide in ssDNA (but not dsDNA), due to conformational changes.[566] Non-denaturing CE also allows separating DNA complexed by small molecules or proteins, and estimating binding constants and thermodynamic parameters of complex formation.[575–580]

Combining the advantages of CE to MS (mostly ESI, but MALDI and ICP were also used) is attractive but remains challenging, in particular the coupling of the separation voltage with that of the MS source, and the significant dilution of the CE effluent in co-axial sheath liquid interfaces.[571,581] Compared to IP-RP-LC, the low flow rates of CE and the absence of ion-pairing agents are beneficial to improve MS ionization.[571] Fundamental and instrumental aspects of the electrospray and nanospray processes with different CE interfaces have been reviewed elsewhere.[581,582]

A few examples of non-denaturing CE of nucleic acids coupled to MS show a potential for in-depth characterization of non-covalent complexes. Przybylski and coworkers have implemented an affinity capillary electrophoresis separation, in which the ligand is added in increasing concentrations to the BGE, coupled to an ESI ion-trap mass spectrometer, to provide the stoichiometry, micro and macroscopic dissociation constants, binding cooperativity, and free energy data of ss- and dsDNA non-covalent complexes with various (poly)cationic β-cyclodextrins.[583] The Berezovski group coupled on-line kinetic capillary electrophoresis with ion mobility and mass spectrometry to study fast conformational dynamics of DNA G4s in solution (cation-binding affinity, folding- and unfolding-rate constants).[584]

3.1.3 Optimizing ion transfer

At the late stages of electrospray, the ions are transferred to the gas phase with a solvation shell and electrolytes still attached (mainly cations attached to the nucleic acid polyanions). The signal is thus

spread on multiple adducts, and this is detrimental to mass accuracy and sensitivity. It is necessary to transfer additional internal energy to the ions in order to get rid of the nonspecifically bound solvent, additives and electrolytes. However, if the goal is to analyze intact non-covalent complexes, the native non-covalent bonds (those that are present in solution and responsible for the specific structure adopted) must be maintained. Thus, in native MS, the instrument tuning is a trade-off between maintaining the specific interactions while disrupting the nonspecific ones.

The internal energy transferred to the ions depends on all collisional activation events the ions encountered during their journey to the analyzer, i.e. in the source, in all transfer optics and all analyzers preceding the analyzer of interest. The readers interested in the relationship between collisional activation and ion internal energy can consult useful reviews.[585–587] For nucleic acids, Griffey et al. showed in 2000 that series of ammonium adducts (but not water adducts) could be clearly distinguished on 16S RNA ions.[588] Their group at Ibis Therapeutics established automated drug-RNA screening methods, wherein the automatic tuning of the spectrometer relied on this ammonium adduct distribution. Maintaining visible ammonium adducts ensures that complexes of the same size and charge maintained by a single hydrogen bond will be detectable.[588] In 2010, a protocol describes a similar tuning procedure, wherein a [12-bp duplex DNA]$^{5-}$ was used for tuning: first a rough tuning to maintain the duplex, then a fine tuning so that the intensity of the first ammonium adduct is 20-30% of that of the naked ion.[589]

In latter work on DNA G-quadruplexes, we found that even softer tuning was required to maintain the three specific ammonium adducts inside the bimolecular G-quadruplex $[(dG_4T_4G_4)_2 \bullet (NH_4^+)_3]^{5-}$,[300] and to date we use this complex to tune our spectrometers when the softest conditions are required for nucleic acid complexes in the negative mode. Figure 24 shows the best results obtained on three very different mass spectrometers.[590] Although the 3-NH_4^+ adduct is maximized, the three distributions differ. In particular, the distribution on panel B shows both additional adducts (up to 5-NH_4^+) and fewer adducts (0-NH_4^+), illustrating that the ion population can be characterized by a broad internal energy distribution: a fraction of the ions received high amounts of internal energy and lost all their NH_4^+ ions, while a fraction received low amounts of internal energy and preserved three inter-quartet ammonium ions and even additional ones.

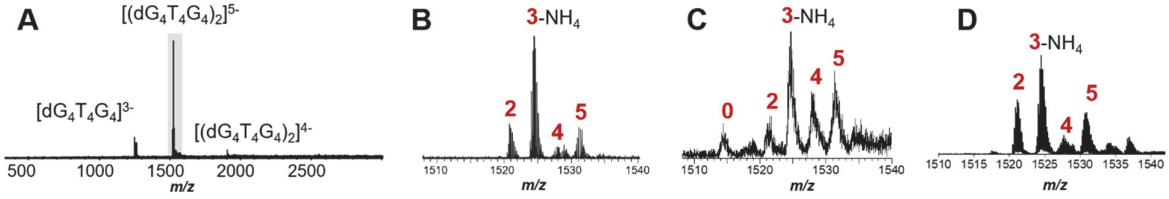

Figure 24. Influence of instrument choice and tuning on ammonium ion preservation in $[(dG_4T_4G_4)_2]^{5-}$. The number of preserved ammonium ions is written in red. (A) Representative full scan mass spectrum and (B-D) zooms on the 5- charge state in softest conditions on (B) a Solarix 9.4 T ESI-Q-FTICRMS (Bruker Daltonics, Bremen, Germany),[300] (C) a Q-TOF Ultima Global ESI-Q-TOFMS (Waters, Manchester, UK) [300] and (D) a 6560 IMS-Q-TOF with the drift tube operated in nitrogen.[590] Figure adapted with permission from Ref. 300, Copyright 2013 American Chemical Society (panels B and C), and from Ref. 590, Copyright 2018 American Chemical Society (panel D).

3.1.4 Quantitation of the solution binding affinities

3.1.4.1 Quantitative comparisons

In pharmacology, the potency of a drug is evaluated by its ability to affect a biochemical process. The potency is linked to the fraction of target that is captured in a bound state. It is thus relevant to compare ligand activity for a given target by comparing the fraction of bound target at a given total target concentration and total ligand concentration. In ESI-MS, the potency of a ligand (*L*) towards a

nucleic acid target (*NA*) can be quickly assessed by comparing the signal intensities of unbound *NA* (NA_{free}) and *NA* bound to ligands (*NA*·$L_{1...n}$). The fraction of NA bound ($f_{NA_{bound}}$) is given by:

$$f_{NA_{bound}} = 1 - f_{NA_{free}} = \frac{\sum_{i=1}^{n} I_{(NA \cdot L_i)}}{\sum_{i=0}^{n} I_{(NA \cdot L_i)}} \quad (2)$$

Equation (2) assumes that the response factor of the NA does not change upon ligand binding. When comparing ligands, in case the responses of the complexes change compared to the free DNA, what matters is that all complexes respond in a similar way independently of the ligand. $f_{NA_{bound}}$ can be used for ligand screening (section 4.5).[13,591–599] When exclusively 1:1 complexes are formed, plots of $f_{NA_{bound}}$ as a function of total added ligand ($[L]_{total}$) can be used to determine apparent K_D values.[600–605] Note that the condition of exclusive 1:1 complexes was not met in each paper.

Ranking ligands using Equation (3) however masks the effects of the stoichiometries of bound ligand. Imagine mixtures containing $[NA]_{tot} = [L]_{tot}$, two ligands giving $f_{NA_{bound}} = 0.5$, the difference being that ligand 1 forms a 1:1 complex and ligand 2 forms a 2:1 (L:NA) complex. Based on $f_{NA_{bound}}$ both ligands appear equally potent, but the amount of bound ligand is twice higher for ligand 2 compared to ligand 1. If the experiment had been carried out at higher $[L]_{tot}$, ligand 2 would have appeared more potent. For this reason, some authors rather choose to compare the concentration of bound ligand when doing ligand screening, using:[317,382,599]

$$[L]_{bound} = [NA]_{tot} \cdot \frac{\sum_{i=1}^{n} i \cdot I_{(NA \cdot L_i)}}{\sum_{i=0}^{n} I_{(NA \cdot L_i)}} \quad (3)$$

Finally, when comparing ligand binding to different targets, the total amount of bound ligand *per target* does not reflect directly the affinity *per binding site* if the number of binding sites differs (for example, when comparing a duplex with 12 base pairs with a G-quadruplex with 4 G-quartets. Thus, in some papers, the concentration of bound ligand was calculated per monomeric unit (Watson-Crick base pair, triplet of base, G-quartet) for the sake of comparison with solution phase spectroscopic techniques (equilibrium dialysis methods with UV or fluorescence quantification).[599,606,607] However, it must be noted that the number of binding sites per target is an assumption that can influence the comparative results.

3.1.4.2 Determining equilibrium association constants K_A values

3.1.4.2.1 Single-spectrum determination vs. titration experiments

The definite advantage of native MS is that it is possible to detect and quantify each stoichiometry. This gives access to each consecutive solution-phase equilibrium association constant defined in Equation (4), for the chemical equilibrium defined in Eq. (5):

$$K_{A_j} = \frac{1}{K_{D_n}} = \frac{[NA \cdot L_j]}{[NA \cdot L_{j-1}][L]_{free}} \quad (4)$$

$$NA \cdot L_{j-1} + L \rightleftharpoons NA \cdot L_j \quad (5)$$

Determining a K_A value from a single mass spectrum requires two assumptions: (1) equal response factors for the different (free and bound) forms of the nucleic acid, and (2) that the complexes do not dissociate upon transfer from the solution to the gas phase.

The concentration of each nucleic acid form is obtained using:

$$[NA \cdot L_j] = [NA]_{tot} \cdot \frac{I_{(NA \cdot L_j)}}{\sum_{i=0}^{n} I_{(NA \cdot L_i)}} \quad (6)$$

And the concentration of free ligand is obtained using

$$[L]_{free} = [L]_{total} - [L]_{bound} \quad (7)$$

$[L]_{bound}$ is given in Equation (3).

Here intensities can comprise every charge and adduct state (Equation (8)), or can be calculated on selected charge states or adducts. A commonly used procedure is to use the most abundant charge state and the zero-adduct peak. All procedures are correct as long as they are properly documented.

$$I_{(NA \cdot L_j)} = \sum_{z} \sum_{a} I_{(NA \cdot L_j \cdot adduct_a)^{z-}} \quad (8)$$

Several papers have used K_A values determined using single mass spectra to sort ligands based on their affinities.[13,489,591,608–612] Based on the relative magnitude of the successive equililbrium association constants, cooperative binding phenomena can be deduced.[13]

ESI-MS titration, where mass spectra are gathered at different ligand:NA ratios may reveal stoichiometries that are not detectable at one selected concentration. A titration curve features the concentration of ligand added on the x-axis and the concentration of free nucleic acid and/or complexes on the y-axis. An example is shown in Figure 25.

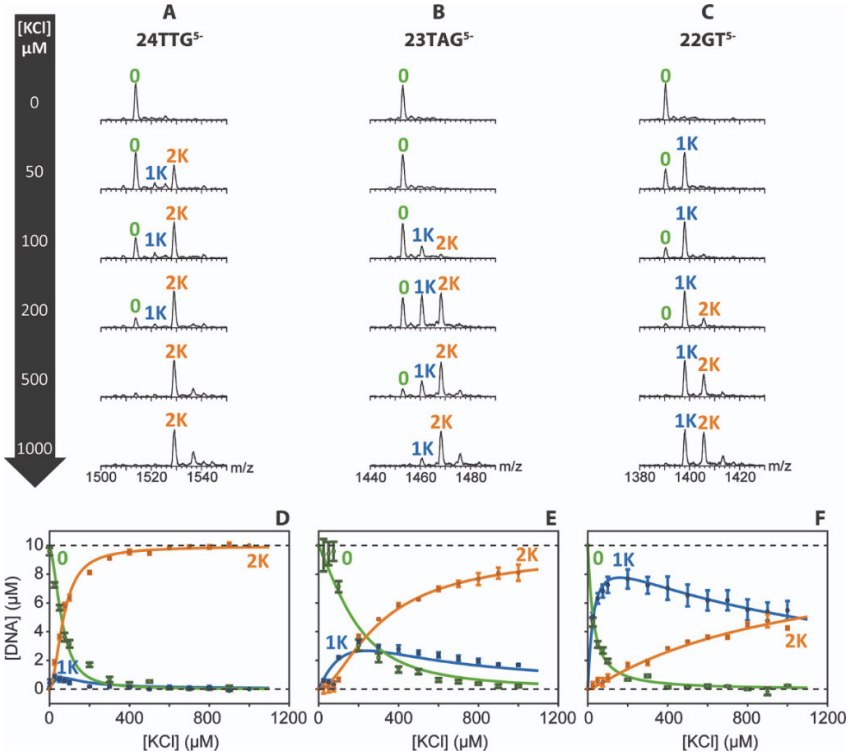

Figure 25. ESI-MS titration experiments of K^+ binding to three different G-quadruplex forming sequences containing the human telomeric motif (24TTG: dTT(G_3T_2A)$_3G_3A$, 23TAG: dTA(G_3T_2A)$_3G_3$, 22GT: d(G_3T_2A)$_3G_3T$). The K_{D1} and K_{D2} were determined through dynamic fitting of the titration data with the mass balance equations. Due to the difference in m/z ratios, K_{D1} and K_{D2} may be calculated independently from one another. Figure reproduced with permission from Ref. 199. Copyright 2016 Oxford Academic.

The individual K_D values are then obtained from numerical fitting of the titration curves, for example using the program DYNAFIT.[613,614] One approach involves plotting the concentrations of all ligand-oligonucleotide species with the mass balance equations as fitting functions.[199,203,615–617] Some authors also linearize the mass balance equations and obtain K_D values by means of linear regression using Scatchard plots,[618] but details about multiple stoichiometries, which are precisely the added value of MS, are masked with this procedure.[611,612] Another approach to determine the apparent dissociation constants is to plot $f_{NA_{bound}}$ as a function of the ligand concentration and using nonlinear curve fitting (Equation (9)).[600–605,619] This approach is valid only for 1:1 stoichiometries. One example of such a titration curve is shown in Figure 26. Other equations using the same approximate mathematical approach have been presented for one ligand vs. two binding sites and two ligands vs. one binding site.[600] In summary, if multiple stoichiometries are revealed by mass spectrometry, only numerical fitting can extract individual equilibrium constants, because analytical derivations become too complex.

$$f_{NA_{bound}} = \frac{([NA]_{tot} + [L]_{tot} + K_D) - \sqrt{([NA]_{tot} + [L]_{tot} + K_D)^2 - 4[NA]_{tot}[L]_{tot}}}{2[NA]_{tot}} \quad (9)$$

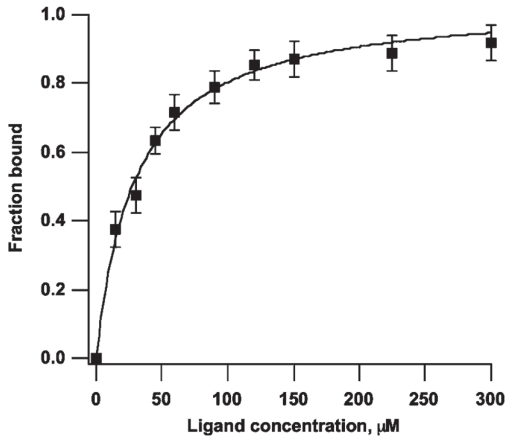

Figure 26. ESI-MS titration curve of a peptide binding to hairpin-RNA, forming a 1:1 complex. Each point shows the mean average of three independent experiments. The K_D value (29 μM) was determined using nonlinear regressing with Equation (9). Figure adapted from Ref. 601. Copyright 2009 American Chemical Society.

3.1.4.2.2 Removing the nonspecific adducts contribution

When high ligand concentrations have to be used for a binding experiment, the risk of observing nonspecific adducts increases. This is particularly acute when determining the K_D values of cation binding to oligonucleotides with titrations up to 1 mM cation added: the ESI-MS spectra will have an overlay of specifically bound cations and nonspecific cation adducts. To obtain the correct values of [*NA*] and [*NA·L*], the contribution of nonspecific adducts must be subtracted before calculating K_D values. As "specific" binding is defined in a context of well-defined binding site (e.g., the coordination between two G-quartets). The key is to design the proper control experiment. The usual approach is to carry out a separate series of experiments with a control sequence that is similar to the target sequence.[199,203,287,615] Attempts to mathematically predict the fraction of nonspecific adducts has been reported, based on the assumption that nonspecific binding is characterized by numerous equivalent sites.[620]

3.1.4.2.3 Taking the difference in response factors into account

The assumption that signal intensities in native MS reflect the solution abundances is valid if the response factors of the bound and unbound species are equal. The response factor mostly depends on (1) the efficiency of ion production in ESI, (2) the ion transmission efficiency, and (3) the possible activation/dissociation in the mass spectrometer. Section 3.1.3 comments on the latter. According to the equilibrium partitioning model (see 3.1.1.1.2), the ionization efficiency is related to a difference of exposure of hydrophilic/hydrophobic groups.[621] For nucleic acids, the phosphate groups are negatively charged and screened by counter-ions in solution. The grooves are also filled with solvent and cations. The global ionization efficiency thus also depends on the ease of declustering of the nucleic acids (removal of the solvent and counterion shell), which will change as a function of the structure (duplex vs. quadruplex) and topology (parallel G-quadruplexes tend to decluster better). Therefore, any change in size, conformation or charge state distribution on the molecular surface induced by the ligand may cause a change in response factor.[13,622]

Early reports outline ESI-MS titration methodologies for the simultaneous determination of response factors and K_D values of DNA duplex formation[623] and DNA duplex complexation.[622] A more universal method for the determination of response factors has been introduced, based on the mass balance equation and the comparison of all intensities with that of an internal standard of fixed concentration, which (1) is chemically similar to the analyte and (2) interacts neither with the oligonucleotide nor with the ligand so that its abundance remains constant throughout the titration. For nucleic acids, the short oligonucleotide dT_6 is often used. A set of linear equations is obtained, and one thus needs at least as many titration points as unknown response factors. If more titration points are recorded, then the matrix pseudoinverse can find the best response factors.[624]

3.1.4.3 Comparison with other biophysical methods

Few papers have compared the K_A (or K_D) values determined by ESI-MS for nucleic acid complexes with those determined with other biophysical methods,[609,610,619,625] and even fewer compared the values determined for the exact same target and solution composition.[609,625] A study on duplex complexes with minor groove binders showed a systematic underestimation of the affinities by ESI-MS compared to fluorescence titration, possibly ascribed to a difference in solution composition (presence of 20% methanol in ESI-MS). However, the trends in relative binding affinities were very well reflected. ESI-MS revealed the presence of minor 2:1 complexes, which allowed to select the correct fitting equation for the fluorescence titration.[609]

The revelation of stoichiometry by ESI-MS was critical for the interpretation of the fluorescence titration of thioflavin T (ThT) to G-quadruplex DNA, which would have been incorrectly interpreted with a 1:1 model (Figure 27).[625] Other papers compared the trends in relative fraction of ligand bound obtained with ESI-MS with those obtained by equilibrium dialysis, and obtained a good correlation between the trends.[599,606,607] ESI-MS derived quantities were also used to reconstruct the individual circular dichroism spectra of each cation-bound stoichiometry of a G-quadruplex.[199]

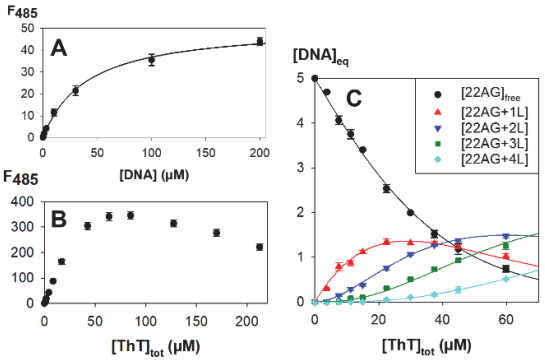

Figure 27. Comparison between fluorescence titration and MS titration for the G-quadruplex 22AG with ThT in NH_4OAc (adapted from the data of [625]). Fluorescence was measured at 485 nm in relative units (F_{485} = 1 before the titration). (A) Fluorescence titration curve of ThT by DNA, which fits well with a 1:1 binding model. (B) Fluorescence titration of DNA by ThT reveals additional phenomena at high ligand concentration. (C) Results of ESI-MS titration of 5 μM 22AG with ThT, revealing up to four ligands bound per 22AG molecule. Error bars represent standard error of triplicate measurements. Figure adapted from Ref. 625. Copyright 2013 American Chemical Society.

3.1.5 Time-resolved native mass spectrometry

The folding of nucleic acids can be particularly slow. This is due to the many possibilities of non-native—yet strong—electrostatic interactions that can trap the nucleic acids in misfolded conformations.[626,627] When the time constant of nucleic acid folding or self-assembly is several minutes or longer, the kinetics can be monitored on-line by mass spectrometry after manual mixing. This simple protocol was applied to monitor duplex formation between the (G-rich) telomeric G-quadruplex and its complementary strand, and how a G-quadruplex specific ligand slowed the process.[628] Response factor correction can be applied to improve the quantitative determination of the rates.[624] Tetramolecular G-quadruplex formation upon cation addition was also monitored, and mass spectrometry revealed kinetically trapped species based on the stoichiometry (pentamers, slipped-stranded structures with fewer cations than the final structure).[512] Octamer formation was also studied over several hours' time scale.[629,630] Even intramolecular folding can take minutes to hours, as exemplified by potassium-induced G-quadruplex formation.[199] For monitoring faster intermolecular reactions, a variety of on-line mixing devices can be used.[631] A recent example demonstrated a temperature-jump setup, where folding or unfolding of nucleic acids was triggered by a brutal change of temperature.[632]

The specific folding mechanisms of nucleic acids have several implications for the design of native mass spectrometry experiments. Even when one wants to study nucleic acid complexes in equilibrium, it is important that the sample preparation protocol allows for the equilibrium to be reached. Also, to make it possible to reproduce the results, it is important to document the complete sample preparation protocol (combination of concentrations, temperature, and time frames). Finally, MS-monitored kinetics experiments revealed that the kinetics of G-quadruplex formation can change by orders of magnitude when adding organic co-solvents.[512–514] These observations led our group to totally abandon methanol addition to electrospray samples when our goal was to mimic physiological (water-only) conditions.

3.1.6 Temperature-resolved native mass spectrometry

By default, equilibria or kinetics are studied at the room's temperature, but one can construct devices to control the temperature of the electrospray solution, down to the emitter, for temperature-resolved experiments. A variety of home-made designs have been proposed,[633–635] and some have been applied to nucleic acids studies.[636–638,632,639]

3.2 Gas-phase probing of non-covalent interactions

Gas-phase probing takes advantage of MS-based separation to enable interrogating each stoichiometry. However, when the ultimate information of interest is the non-covalent structure in solution, the disadvantage of gas-phase probing is that the structure may have changed upon transfer from the solution to the gas phase (for example, solvent exclusion driving forces are absent, while ionic interactions will be reinforced in vacuo) or during ion transfer to the probing region (section 3.1.3). Also, the probing method itself should not perturb the network of non-covalent interactions.

3.2.1 Fragmentation

Fragmentation methods typically require increasing the internal energy of the ions, and are more likely to alter the non-covalent bond network. Thus, their interpretation to deduce information on non-covalent interactions in solution is delicate. We will first describe how fragmentation can be induced, and the main types of fragments of oligonucleotide backbones.

3.2.1.1 Nucleic acid fragmentation techniques

The fragments are annotated with McLuckey's nomenclature[640] (Figure 28) and a review gives a very useful primer on oligonucleotide fragmentation.[641] *a*, *b*, *c* and *d* fragments contain the 5'-end of the sequence, while *w, x, y* and *z* fragments contain the 3'-end. Base loss is also frequent, and more favored if the base is unpaired.[642] Finally, internal fragments consist of the central part of an oligonucleotide that fragmented twice.

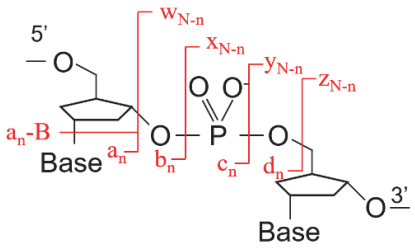

Figure 28. Fragmentation nomenclature for oligonucleotide backbones. N is the total number of bases and n is the number of bases on the 5'-side of the fragmentation site.

3.2.1.1.1 Fragmentation of closed-shell species

Electrospray, MALDI and LILBID all produce closed-shell ions from the solution. At room temperature, such ions can survive several minutes without fragmenting. Fragmentation requires increasing the internal energy of the ions, which means increasing their vibrational energy (populating higher vibrational energy levels than at room temperature). Vibrational energy can be conferred by direct infrared radiation absorption in vibrational energy levels (the energy is quickly redistributed evenly among vibrational energy levels), or by inelastic collisions with a neutral gas.[585] The latter method is most often called collision-induced dissociation (CID). To fragment large ions such as non-covalent complexes discussed herein, multiple collisions are necessary to obtain sufficient internal energy. For example, in Fourier transform ion cyclotron resonance (FT-ICR) mass spectrometers, sustained off-resonance irradiation CID (SORI-CID) is a method for slow internal energy build-up in ICR cells.

Dissociation in a mass spectrometer is irreversible. This is an important concept, because the extent of gas-phase dissociation reflects the dissociation *kinetics*, *not* a dissociation *equilibrium*. Throughout the review, we will speak about *gas phase kinetic stabilities* when ranking the complexes that are the best preserved in the gas-phase. Several theories relating the dissociation rates to the internal energy exist, the best known being the Rice-Rampsberger-Kassel-Marcus (RRKM) theory.[643] A simplified form is the RRK equation, with *k(E)* the reaction rate as a function of the internal energy

$$k(E) = \nu_s \left(\frac{E - E_0}{E}\right)^{3N-7} \quad (10)$$

where E_0 is the difference between the zero-point energy of the transition state and that of the reactant, ν_s is a frequency factor (probability of the reaction to occur, for example to take into account multiple channels giving the same fragment), and N is the number of atoms in the molecule (larger molecules have more numerous vibrational degrees of freedom on which the energy can redistribute instead of being funneled in the reaction channel of threshold E_0.

Note that a population of ions has a distribution of internal energies, which is hard to determine on most instruments, so that it's in practice difficult to infer E_0 from dissociation rates. Most experimental papers instead show breakdown curves, which are plots of the relative intensity of intact parent ion and/or of some fragments as a function of an instrumental parameter correlated with ion internal energy. Many factors influence the type and abundance of the fragments: the nature of the gas, the gas pressure, the relative speed of the ions as they traverse the gas, and the time allowed for fragmentation. Non-mass spectrometry experts must remember that different instruments can give different results. Infrared multiple photon dissociation (IRMPD)[644] is caused by direct absorption of infrared photons. Again, multiple photons are necessary for large ions such as considered here. IRMPD gives the same fragmentation pattern as CID because both result in vibrational energy increase, but differences can arise depending on the speed of internal energy increase, and on whether collisions also occur during infrared irradiation.

Collisions can be activating (collisional activation) or deactivating (collisional cooling). Similarly, infrared photons can be absorbed and re-emitted. For physical chemistry, an interesting particular case is when the energy exchange is much faster than the dissociation, because this rapid energy exchange results in a Boltzmann internal energy distribution. In low-pressure ion cyclotron resonance cells, the ions acquire the internal temperature of the cell walls by exchange of blackbody infrared radiation, and the dissociation method is called BIRD (blackbody infrared radiation dissociation). If ions are stored and remain static in high-pressure regions, the collisions with the gas ensure that the ion internal temperature is that of the chamber walls. The advantage of this configuration is that the dissociation rate can be measured as a function of the wall temperature to obtain the activation energy E_a and the pre-exponential factor A (Equation (11)). E_a gives access to the activation enthalpy of the dissociation $\Delta H^{\ddagger}_{diss}$.[645]

$$k_{obs}(T) = A.exp\left(\frac{-E_a}{kT}\right) \quad (11)$$

The activation energies and pre-exponential factors have been determined on nucleic acids for the base loss channel,[646] and for the strand separation of short duplexes.[647]

3.2.1.1.2 Radical-based fragmentation

Typically, radical ions are less kinetically stable than their corresponding closed-shell ions, and sequence coverage is more extensive from radicals. A variety of methods, often with the acronym "ExD" (Electron *something* Dissociation) exist to create and fragment these radicals, either in one step or in two steps (radical formation then its vibrational activation to cause dissociation).

In proteins, creating radicals by electron capture dissociation (ECD) or electron transfer dissociation (ETD) is widely used in top-down sequencing from multiply charged cations. ECD[648,649] and ETD[650] have been applied to oligonucleotides as well. However, nucleic acids are best ionized as multiply charged anions, and radicals are therefore more easily accessed by electron detachment. It can be caused by (1) interactions with (16—20 eV) electrons; the method is called EDD[651,652] (electron detachment

dissociation), (2) electron transfer from a radical anion; the method is called nETD[653,654] (negative ion electron transfer dissociation), or (3) irradiation by ultraviolet photons; the method is called EPD[655] (electron photodetachment dissociation). nETD and EPD typically require the re-activation of the radicals, while fragments can be produced by EDD in one step, although further activation can help.[656]

3.2.1.2 Competition between backbone fragmentation and dissociation of non-covalent nucleic acid complexes

In solution, non-covalent interactions are typically weaker than covalent bonds. This is not necessarily the case in the gas phase, for two reasons. First, as said above, in the gas phase one has to think in terms of dissociation rates or kinetic stabilities. Second, the magnitude of all electrostatic interactions changes in the gas phase ($\varepsilon_0 = 1$) compared to in solution ($\varepsilon_{H_2O} = 78$ at 25°C, and $\varepsilon = 8$ inside nucleic acids[657]). All attractive electrostatic forces are thus higher in the gas phase, to the point that salt bridges can typically not break at activation energies sufficient to break the phosphate backbone.[539,658] Coulomb repulsion between like charges is also enhanced in the gas phase, and thus the energy required to break bonds or dissociate a complex depends on the charges of the partners. Consequently, a complex between two strands can dissociate into their constitutive strands at high charge state, while it fragments by covalent bond breakage resulting in neutral base loss at low charge state.

Favoring backbone fragmentation in non-covalent complexes can be exploited to map binding sites,[509,659,660] or intramolecular interaction intefaces.[656] For some complexes stabilized by salt bridges, this can be achieved by fragmentation of closed-shell species. However, for some less kinetically stable complexes, it may be advantageous to weaken the covalent bonds by using radical-based fragmentation. On the other hand, favoring the dissociation of the complex over backbone fragmentation is necessary to deduce information about the strength of molecular interactions at the binding interface from the dissociation kinetics, as explained in the following section.

3.2.1.3 Gas-phase probing of intrinsic molecular interactions

Knowing the extent to which various non-covalent forces contribute to the binding free energy in solution helps bridging structure and thermodynamics.[661] Using the assumption that the variables can be separated, different contributions to the free energy of complex formation can be parsed in a sum of terms. Chaires proposed the following decomposition for nucleic acid-ligand complex formation:[318]

$$\Delta G^{\circ}_{obs} = \Delta G^{\circ}_{conf} + \Delta G^{\circ}_{t+r} + \Delta G^{\circ}_{hyd} + \Delta G^{\circ}_{pe} + \Delta G^{\circ}_{mol} \quad (12)$$

ΔG°_{obs} is the experimentally observed binding free energy, estimated from the equilibrium association constant ($\Delta G^{\circ}_{obs} = -RTlnK$), ΔG°_{conf} is the free energy contribution from conformational changes upon complex formation and can be estimated by modeling if the structures are known, ΔG°_{t+r} is the energy cost resulting from losses in translational and rotational degrees of freedom upon complex formation and is calculated classically. ΔG°_{hyd} is the free energy for the hydrophobic contribution, calculated from the difference in solvent accessible surface area between the complex and its separated partners. ΔG°_{pe} is the polyelectrolyte contribution to the binding free energy, arising from the release of condensed counterions from DNA upon complex formation; it is deduced from the ionic strength dependence of ΔG°_{obs}.

Finally, ΔG°_{mol} is the free energy contribution from the formation of noncovalent molecular interactions between the drug and the DNA. These molecular interactions include hydrogen bond formation, van der Waals interactions and electrostatic interactions. Based on solution experiments, ΔG°_{mol} is deduced by difference. It can also be theoretically calculated based on a structural model. The contribution of a specific chemical group can be probed by mutation analysis. Thus, the ΔG°_{mol}

contribution is the most difficult to obtain from solution experiment. However, gas-phase experiments are ideal to probe the intrinsic contribution of molecular interactions: the hydrophobic and polyelectrolyte contributions are absent, the conformational and *t+r* contribution would translate in an entropy term, while the molecular interactions would translate in an enthalpy term.

However, if the aim is to use gas-phase dissociation experiments to rank the molecular interactions, the following notions must be kept in mind for the interpretation:

- Dissociation experiments probe the dissociation kinetics (see 3.2.1.1.1), and thus probe a "kinetic stability" not a "thermodynamic stability". $\Delta H_{diss}^{\ddagger}$ can however be close to ΔH_{diss}° for the direct detachment of a neutral ligand. In case of dissociation between charged partners, the Coulomb repulsion will affect $\Delta H_{diss}^{\ddagger}$. The kinetic stability of complexes of different charge states z cannot be compared.
- The RRK equation (10) also reminds us to compare only complexes of similar size (N).
- The ranking of kinetic stabilities will match the ranking of $\Delta H_{diss}^{\ddagger}$ only if the pre-exponential factors are identical. This requires that at least the dissociation pathways are identical.

3.2.2 Gas-phase reactivity

Besides fragmentation and dissociation and electron attachment or detachment, other types of reactivities can be investigated in the gas phase through ion/ion reactions or ion/molecule reactions. Most such techniques were explored for proteins, but seldom for nucleic acids. We will highlight here the basic principles and cite the instances of application to nucleic acid non-covalent complexes, noting that there is ample room for further exploration.

The best-known ion/molecule reaction is gas-phase hydrogen/deuterium exchange, wherein an ion is left to react in a chamber containing deuterated solvent vapors.[662,663] The replacement of labile hydrogens by deuterons is detectable by the mass shift. Accessibility of the exchange site to the solvent vapor is required, but the relay mechanism also states that the proximity of other sites is necessary,[664] and consequently neither the most extended nor the most compact conformations are those that exchange the fastest.[665] Gas-phase HDX has been applied to study the conformation of small oligonucleotides,[666,667] and nucleic acid higher-order structures (base pair formation[668,669] and G-quadruplex formation[670,671]), but the relay mechanism and consequent absence of direct correlation between exchange rates and folding has hampered the adoption of gas-phase HDX to characterize unknown structures.

Another type of ion/molecule reaction is gas-phase proton transfer.[672] Proton transfer can be used to manipulate charge state distributions by reducing the charges[673–675] Proton transfer depends on the ion conformation because it depends on the intramolecular electrostatic interactions.[672,676] This aspect has, however, not been exploited for nucleic acid higher-order structure characterization. Yet one contribution noted apparent electron autodetachment from trapped oligonucleotides containing base pairs,[677] but the mass resolution does not allow to conclude whether the phenomenon was actually electron detachment or simply proton transfer.

Ion/ion reactions can also be explored, and reactivity spans e.g. proton transfer, electron transfer (ETD and nETD are particular cases), ion attachment, and ion transfer.[678] The McLuckey group pioneered this technique, applied it to oligonucleotides,[679,680] culminating in the exploitation of ion/ion proton transfer to simplify MS/MS spectra of intact large (although non-folded) tRNAs.[681] Turner *et al.* demonstrated a very interesting application of ion/ion reactions of folded nucleic acid polyanions and negatively charged chelators in order to clean up the nucleic acid spectra from sodium and magnesium adducts.[682]

3.2.3 Ion Mobility Spectrometry (IMS)

3.2.3.1 Determination of collision cross sections

Ion mobility spectrometry is the gas-phase counterpart of electrophoresis: the ions are dragged in a gas (helium, nitrogen,…) under the influence of an electric field E (Figure 29) and because of the friction (collisions) with the gas, the drift velocity v_d of the ions comes to an apparent steady state.[683–685] For biomolecule studies, ion mobility analyzers are most often coupled to mass analyzers, and one obtains *m/z*-resolved mobility information (the technique is then called ion mobility mass spectrometry—IM-MS).[686]

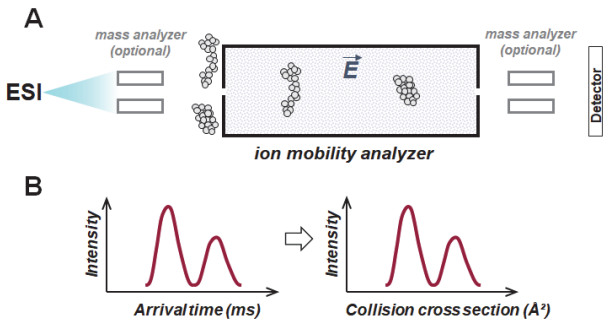

Figure 29. A) Schematics of an ion mobility spectrometer, here with a drift tube analyzer. The most compact ions travel faster and reach the detector earlier than the more extended ions (assuming they have the same mass and charge). B) A typical ion mobility spectrum: ion counts as a function of the time elapsed between the pulsing in the mobility analyzer and the detector. The arrival time distributions can be converted into collision cross section distributions.

The ion's mobility K is the proportionality constant between v_d and E.

$$v_d = K \cdot E \tag{13}$$

The mobility K depends on properties of the ion-gas pair, namely the gas's nature, temperature and mass, and the ion's mass and a factor called the momentum transfer collision integral Ω (often called the collision cross section—CCS) which depends on the ion's size, shape and ion-gas interaction potentials (which is thus also dependent on the gas nature). K also depends on the magnitude of the electric field, but to interpret K in terms of ion shape one must remain in the low-field limit (purely elastic collisions of low relative velocity compared to the gas thermal velocity). The CCS (Ω) is related to the mobility K by Equation (14).

$$\Omega = \frac{3}{16}\sqrt{\frac{2\pi}{\mu k_B T}}\frac{ze}{N_0\left(\frac{p}{p_0}\cdot\frac{T_0}{T}\right)K} \tag{14}$$

μ is the reduced mass of the ion-gas pair, $\mu = m_i m_g/(m_i + m_g)$, where m_i is the mass of the ion and m_g is the mass of the gas, k_B is the Boltzmann constant (1.381×10^{-23} J.K^{-1}), N_0 is Loschmidt's number (2.687×10^{25} m^{-3}), i.e. the gas number density at standard pressure p_0 = 1 atm and standard temperature T_0 = 273.15 K. Ω has the dimensions of a surface, and is often reported in Å².

The mobility K can be determined directly in a drift tube ion mobility spectrometer (DTIMS), wherein E, T, p and v_d are readily accessible. Other instruments such as travelling wave ion mobility spectrometers (TWIMS)[687] or trapped ion mobility spectrometers (TIMS)[688] must be calibrated against DTIMS values because their electric fields and gas flows make it more difficult to access the primary values.[686] The calibration of TWIMS is often done in the CCS domain, using ${}^{DT}\Omega_{He}$ values (Ω determined in a drift tube in helium) even if the TWIMS operates mainly with nitrogen in the IMS.[689] The

annotation to convey this is: ${}^{TW}\Omega_{N_2 \rightarrow He}$. Note that calibrated values may depend on the choice of the calibrants, on the quality of the ${}^{DT}\Omega_{He}$ values of the calibrant, and on the calibration procedure.[686]

Table 1 lists CCS values reported to date (1997-2020) for oligonucleotides and nucleic acid higher-order structures (nucleic acid-ligand complexes are not included). Note however that the data can be more complex than a single value per ion ensemble. For example, multiple peaks can be clearly distinguished and the CCS can be determined for each peak. In some instances, peaks can be broader than the instrument factor, indicating an ensemble of non-interconverting conformations, but it can be hard to extract individual peaks even with fitting algorithms. To convey that information, publications often include CCS distributions reconstructed from the measurables.[690] Finally, the entire internal energy history of the ions (from the source to the ion mobility analyzer) can influence the gas-phase conformation in the IMS analyzer. Note that some isomerization reactions (in particular, opening driven by Coulomb repulsion) are irreversible and subject to the same principles as fragmentation reactions (see section 3.2.1.1), while others are reversible (the reaction can proceed both ways). However, if an ion population undergoes fast reversible isomerization inside the IMS analyzer (compared to the time scale of the measurement), the entire population will drift with the same average velocity and there will be only one narrow peak.[691] A single narrow peak can thus mean either the presence of one rigid structure, or of one fast-interconverting ensemble, while a broad peak indicates several conformations that do not (fully) interconvert on the time scale of the mobility measurement.

Table 1. Ion mobility spectrometry literature on oligonucleotide structures, with collision cross section values or CCS distributions.

Ion	#nt	Presumed structure	Conditions	*z*	CCS (Å²)	Ref.
dTGT	3	Single strand	$^{DT}\Omega_{He}$	-1	196	[692]
dGTT	3	Single strand	$^{DT}\Omega_{He}$	-1	194	[692]
dTTG	3	Single strand	$^{DT}\Omega_{He}$	-1	195	[692]
dA_6	6	Single strand	$^{DT}\Omega_{He}$	-2→-4	*CCSD*[b]	[693]
dG_6	6	Single strand	$^{DT}\Omega_{He}$	-2→-4	CCSD[b]	[693]
dC_6	6	Single strand	$^{DT}\Omega_{He}$	-2→-4	*CCSD*[b]	[693]
dT_6	6	Single strand	$^{DT}\Omega_{He}$	-2 -3 -4	306 334 399	[690]
dT_8	8	Single strand	$^{DT}\Omega_{He}$	-2 -3 -5	360 386 523	[690]
dT_{10}	10	Single strand	$^{DT}\Omega_{He}$	-2 -3 -4 -5 -6	447 446 537 627 641	[694]
dT_{12}	12	Single strand	$^{DT}\Omega_{He}$	-3 -5 -7	487 682 768	[690]
dT_{16}	16	Single strand	$^{DT}\Omega_{He}$	-5 -7 -9	732 957 1012	[690]
dT_{20}	20	Single strand	$^{DT}\Omega_{He}$	-6 -9 -11	914 1216 1255	[690]
dT_{24}	24	Single strand	$^{DT}\Omega_{He}$	-7 -10 -13	1106 1430 1501	[690]
dGCGAAGC	7	Hairpin	$^{TW}\Omega_{N_2 \rightarrow He}$	-2 -3 -4	324 375 472	[695]

dTGCGATACTCATCGCA	16	Hairpin	$^{DT}\Omega_{He}$	-4 -5 -6 -7	622 718 811 909	696
dGCGATTTCTGACCGCTTTTTTGT	23	Hairpin or pseudoknot	$^{DT}\Omega_{He}$	-6 -7 -8 -9	902 1009 1122 1219	696
rGGAGCCUGGGAGCUCC	16	Hairpin	$^{DT}\Omega_{He}$	-4	552	697
rGGUCGGUCCCAGACGAC	17	Hairpin	$^{DT}\Omega_{He}$	-4	590	697
rGGCAACGGAUGGUUCGUUGCC	22	Hairpin	$^{DT}\Omega_{He}$	-5	695	697
rGCACCGAACCAUCCGGUGC	19	Hairpin	$^{DT}\Omega_{He}$	-4	607	697
rGGCAACGGAUGGUUCGUUGCC•rGCACCGAACCAUCCGGUGC	40	Kissing complex	$^{DT}\Omega_{He}$	-7	1055	697
rGGAGCCUGGGAGCUCC•rGGUCGGUCCCAGACGAC	35	Kissing complex	$^{DT}\Omega_{He}$	-6	986	697
$[d(CG)_2]_2$•Na^+	8	Duplex	$^{DT}\Omega_{He}$	-3	352	698
$[d(CG)_3]_2$	12	Duplex	$^{DT}\Omega_{He}$	-3	430	698
$[d(CG)_4]_2$	16	Duplex	$^{DT}\Omega_{He}$	-3 -4 -5	508 530 586	145
$[d(CG)_4]_2$•Na^+	16	Duplex	$^{DT}\Omega_{He}$	-4	536, 667	698
$[d(CG)_5]_2$	20	Duplex	$^{DT}\Omega_{He}$	-4 -5 -5	626 646 718	145 145 698
$[d(CG)_6]_2$	24	Duplex	$^{DT}\Omega_{He}$	-4 -5 -6	705 725 793	145 145 145
$[d(CG)_7]_2$	28	Duplex	$^{DT}\Omega_{He}$	-5 -6 -7 -9	823 861 990 1013	145 145 145 698
$[d(CG)_7]_2$•NH_4^+	28	Duplex	$^{DT}\Omega_{He}$	-7	1006	698
$[d(CG)_9]_2$•NH_4^+	36	Duplex	$^{DT}\Omega_{He}$	-9	1265	698

$[d(CG)_9]_2$	36	Duplex	${}^{DT}\Omega_{He}$	-5 -6 -7 -8 -9 -9 -11	1014 1037 1077 1167 1253 1268 1272	145 145 145 145 145 698,699 698
$[d(CG)_{11}]_2$	44	Duplex	${}^{DT}\Omega_{He}$	-6 -7 -8 -9 -11	1005 1037 1328 1432 1403, 1558	145 145 145 145 699
$[d(CG)_{13}]_2$	52	Duplex	${}^{DT}\Omega_{He}$	-7 -8 -9 -13	1136 1180 1471 1763	145 145 145 699
$[d(CG)_{15}]_2$	60	Duplex	${}^{DT}\Omega_{He}$	-8 -9 -15	1262 1563 1948, 2249	145 145 699
$d(GA)_5$•$d(TC)_5$	20	Duplex	${}^{DT}\Omega_{He}$	-5	741	700
dCGCGGGCCCG•compl[a]	20	Duplex	${}^{DT}\Omega_{He}$	-4 -5	622 655	701
$[dCGTAAATTTACG]_2$	24	Duplex	${}^{DT}\Omega_{He}$	-4 -5 -6 -6	709 760, 750[c] 823, 916 835,[c] 922[c]	701
$[dCGCGAATTCGCG]_2$	24	Duplex	${}^{DT}\Omega_{He}$	-4 -5 -6 -7	697 735, 803, 777[c] 788, 876, 881[c] 1012[c]	701
$[dCGCGGGCCCGCG]_2$	24	Duplex	${}^{DT}\Omega_{He}$	-4 -5 -6 -7	706 730, 726[c] 784, 824[c] 941[c]	701

$[rCGCGAAUUCGCG]_2$	24	Duplex	${}^{DT}\Omega_{He}$	-4 -5	695 733	[701]
$[rCGCGGGCCCGCG]_2$	24	Duplex	${}^{DT}\Omega_{He}$	-4 -5	696 737	[701]
dTAATACGACTTAAC•compl[a]	28	Duplex	${}^{DT}\Omega_{He}$	-5 -6 -7	822 873, 923[c] 1041[c]	[701]
dCCTACTCGTTACCTTCTT•compl[a]	36	Duplex	${}^{DT}\Omega_{He}$	-5 -6 -7 -8 -9	935 983, 970,[c] 1088[c] 1046,[c] 1192[c] 1193[c], 1297[c] 1398[c]	[701]
dCCTACTCGTTACCTTCTTCTGA•compl[a]	44	Duplex	${}^{DT}\Omega_{He}$	-6 -7 -7 -8 -8 -9	1078, 1085[c] 1112, 1202 1110[c], 1275[c] 1338 1198,[c] 1387[c] 1514[c]	[701]
$[dCGCGAATTCGCGCGCGAATTCGCG]_2$	48	Duplex	${}^{DT}\Omega_{He}$	-6 -7	1119 1148, 1293	[701]
$[dCGCGGGCCCGCGCGCGGGCCCGCG]_2$	48	Duplex	${}^{DT}\Omega_{He}$	-6 -7	1106, 1249 1142, 1336	[701]
$[rCGCGAAUUCGCGCGCGAAUUCGCG]_2$	48	Duplex	${}^{DT}\Omega_{He}$	-7 -8	1300 1386	[701]
$[rCGCGGGCCCGCGCGCGGGCCCGCG]_2$	48	Duplex	${}^{DT}\Omega_{He}$	-7	1162, 1331	[701]
dCCTACTCGTTACCTTCTTCTGATA•compl[a]	48	Duplex	${}^{DT}\Omega_{He}$	-6 -7 -8 -9 -10	1126, 1127[c] 1160 1166,[c] 1308[c] 1225,[c] 1456[c] 1332,[c] 1568[c] 1694[c]	[701]
dCCTACTCGTTACCTTCTTCTGATACTGTTTAA•compl[a]	64	Duplex	${}^{DT}\Omega_{He}$	-7 -8 -9 -10	1367, 1368[c] 1410, 1416[c] 1467[c] 1619,[c] 1944[c]	[701]

[dCGCGAATTCGCGCGCGGGCCCGCGCGCGAAATTTCGCG]$_2$	72	Duplex	$^{DT}\Omega_{He}$	-8 -9	1490 1540	[701]
[dCGCGGGCCCGCGCGCGGGCCCGCGCGCGGGCCCGCG]$_2$	72	Duplex	$^{DT}\Omega_{He}$	-8 -9	1449 1526, 1811	[701]
[rCGCGGGCCCGCGCGCGGGCCCGCGCGCGGGCCCGCG]$_2$	72	Duplex	$^{DT}\Omega_{He}$	-8 -9	1488 1523, 1856	[701]
[rCGCGAATTCGCGCGCGGGCCCGCGCGCGAAATTTCGCG]$_2$	72	Duplex	$^{DT}\Omega_{He}$	-8 -9	1729, 1833,	[701]
dCCTACTCGTTTACCTTTCTTTCTGACTTTCCCTCTTTCTT•compl[a]	72	Duplex	$^{DT}\Omega_{He}$	-8 -9 -10 -11	1495, 1503[c] 1556, 1554[c] 1516,[c] 1881[c] 2180[c]	[701]
dTATATTAAATATGCGGCG•compl[a]	36	Duplex	$^{TW}\Omega_{N_2\rightarrow He}$	-7	1071, 1195	[702]
dTATATTAAAGCCGCGGCG•compl[a]	36	Duplex	$^{TW}\Omega_{N_2\rightarrow He}$	-7	1088, 1181	[702]
dTATATTCGCGCCGCGGCG•compl[a]	36	Duplex	$^{TW}\Omega_{N_2\rightarrow He}$	-7	1117	[702]
dATTTAACGGCCGAATTTA•compl[a]	36	Duplex	$^{TW}\Omega_{N_2\rightarrow He}$	-7	1083, 1160	[702]
dATTTACCGGCCGCCTTTA•compl[a]	36	Duplex	$^{TW}\Omega_{N_2\rightarrow He}$	-7	1104	[702]
dATTGCCCGGCCGCCGTTA•compl[a]	36	Duplex	$^{TW}\Omega_{N_2\rightarrow He}$	-7	1103	[702]
dCCGTTAAATAAATATGCC•compl[a]	36	Duplex	$^{TW}\Omega_{N_2\rightarrow He}$	-7	1105, 1195	[702]
dCCGCTAAATAAATGCGCC•compl[a]	36	Duplex	$^{TW}\Omega_{N_2\rightarrow He}$	-7	1069, 1160	[702]
dCCGCGGAATAAAGGCGCC•compl[a]	36	Duplex	$^{TW}\Omega_{N_2\rightarrow He}$	-7	1047, 1133	[702]
dGCGCCGCGGCGCGGCCCG•compl[a]	36	Duplex	$^{TW}\Omega_{N_2\rightarrow He}$	-7	1067	[702]
[dCAGTGATCGCGATCACTG]$_2$	36	Duplex	$^{DT}\Omega_{He}$	-9	1227, 1319	[699]
[dCAGTCACGGATTCGAATCCGTGACTG]$_2$	52	Duplex	$^{DT}\Omega_{He}$	-13 -15	1776, 2020 1784, 2031	[699]
[dGACCTAGATTCGAATCTAGGTC]$_2$	44	Duplex	$^{DT}\Omega_{He}$	-11 -13	1529 1542	[699]
dAGAAAATTATTGTCTGGCATAGTGCAACAG•compl[a]	60	Duplex	$^{DT}\Omega_{He}$	-15	2203, 2406	[699]
[dCCATAATTTACC]$_2$	24	Duplex	$^{TIMS}\Omega_{N_2}$	-4 +4	752, 814 843, 898	[703]
[dCCTATTAAATCC]$_2$	24	Duplex	$^{TIMS}\Omega_{N_2}$	-4 +4	745, 809 846, 903	[703]
dCCATAATTTACC•dCCTATTAAATCC	24	Duplex	$^{TIMS}\Omega_{N_2}$	-4 +4	753, 811 849, 908	[703]
dCCGGCCGGATACGCGCGCG•dCGCGCGCGATACCGGCCGG	40	Cruciform	$^{DT}\Omega_{He}$	-11	1485, 1653	[696]

$d(TC^+)_6$-$d(GA)_6$•$(TC)_6$	36	Triplex	${}^{TW}\Omega_{N_2 \rightarrow He}$	-6 -7 -8	970 1020 1180	704
$d(TC^+)_9$-$d(GA)_9$•$(TC)_9$	54	Triplex	${}^{TW}\Omega_{N_2 \rightarrow He}$	-7 -8 -9	1340 1420 1500	704
$d(TCC)_6$-$d(GAA)_6$•$d(TCC)_6$	54	Triplex	${}^{DT}\Omega_{He}$	+7 +8	1611 1695	705
$[d(TCC)_6$-$d(GAA)_6$•$d(TCC)_6]_2$	108	Triplex Dimer	${}^{DT}\Omega_{He}$	+10 +11	2338 2597	705
$d(TCC)_9$-$d(GAA)_9$•$d(TCC)_9$	81	Triplex	${}^{DT}\Omega_{He}$	+8 +9 +10	2326 2586 2700	705
$d(TCC)_{12}$-$d(GAA)_{12}$•$d(TCC)_{12}$	108	Triplex	${}^{DT}\Omega_{He}$	+10 +11	2927 2932	705
$[(dTGGGGT)_4$•$(NH_4^+)_3]$	24	G-quadruplex	${}^{DT}\Omega_{He}$ ${}^{DT}\Omega_{N_2}$	-4 -5 -5 -5	736 788 775 1010	690 690,706 700,707 706
$[(dGGGGTTTTGGGG)_2$•$(NH_4^+)_3]$	24	G-quadruplex	${}^{TW}\Omega_{N_2 \rightarrow He}$	-4 -5 -6	802 802 803	300
$[(dGGGGTTTGGGG)_2$•$(NH_4^+)_3]$	22	G-quadruplex	${}^{TW}\Omega_{N_2 \rightarrow He}$	-4 -5 -6	740 747 753	300
$[(dGGGTTTTGGGG)_2$•$(NH_4^+)_2]$	24	G-quadruplex	${}^{TW}\Omega_{N_2 \rightarrow He}$	-4 -5 -6	740 747 762	300
$[dGGGG(TTTTGGGG)_3$•$(NH_4^+)_3]$	28	G-quadruplex	${}^{TW}\Omega_{N_2 \rightarrow He}$	-5 -6 -7	897 915 941	300

[dGGTTGGTGTGGTTGG•NH_4^+]	15	G-quadruplex	$^{TW}\Omega_{N_2 \rightarrow He}$	-3 -4 -5	566 583 625	300
[$(dTTAGGG)_4$•$(NH_4^+)_2$]	24	G-quadruplex	$^{DT}\Omega_{He}$	-5	805	707
[$d(TTAGGG)_2]_2$	24	G-quadruplex	$^{DT}\Omega_{He}$	-5	790, 838	707
$dGGG(TTAGGG)_3$	21	G-quadruplex	$^{DT}\Omega_{He}$	-4 -5	688 718	708
$d(TTAGGG)_4$	24	G-quadruplex	$^{DT}\Omega_{He}$	-5 -6 -7 -8	789 805 950, 1041 1054	707
$d(TTAGGG)_4$, $dTT(GGGTTA)_3GGGA$, $d(TTAGGG)_4TT$ $r(UUAGGG)_4$, $rUU(GGGUUA)_3GGGA$, $r(UUAGGG)_4UU$	24, 26	G-quadruplex	$^{DT}\Omega_{He}$	-4→-6	CCSD[b]	709
$d(TTAGGG)_6$	36	G-quadruplex	$^{DT}\Omega_{He}$	-5 -6 -7 -8	989 1010 1074,[d] 1232 1405	707,708
$d(TTAGGG)_8$, $dTT(GGGTTA)_7GGGA$, $d(TTAGGG)_8TT$ $r(UUAGGG)_8$, $rUU(GGGUUA)_7GGGA$, $r(UUAGGG)_8UU$	48, 50	G-quadruplex (2 subunits)	$^{DT}\Omega_{He}$	-6→-8	CCSD[b]	709
dGAGGGTGGGGAGGGTGGGGAAG	22	G-quadruplex	$^{DT}\Omega_{He}$	-4 -5	701 696, 757[d]	708
$[(dGAGGGTGGGGAGGGTGGGGAAG)]_2$	44	G-quadruplex (2 subunits)	$^{DT}\Omega_{He}$	-7 -8 -9	1098 1113 1313	710
dTGGGGAGGGTGGGGAGGGTGGGGAAGG	27	G-quadruplex	$^{DT}\Omega_{He}$	-5 -6 -7	810 846,[d] 949 1080	708
14 G-rich sequences	18→26	Single strand (0 K^+) or G-quadruplex (2 K^+)	$^{DT}\Omega_{He}$	-5	CCSD[b]	200
$d(CCCTAA)_3CCC$, pH = 7.5	21	Single strand	$^{DT}\Omega_{He}$	-4 -5 -6 -7 -8 -9	641 671 740 984 1063 1111	263

$d(CCCTAA)_3CCC$, pH = 5.5	21	i-motif	$^{DT}\Omega_{He}$	-3→-11 -4 -5 -6 -7 -8 -9	CCSD[b] 630 654 717 983 1042 1106	711 263
$d(CCCTAA)_3CCC$	21	i-motif	$^{TIMS}\Omega_{N_2}$	-3 -4 -5 -6 -7 -8 -9 +3 +4 +5	821 863 917 1023, 1190 1111, 1234, 1314, 1360 1335, 1362, 1394, 1436 1462, 1482 1548 800 846 922	490
$d(TAACTC)_5$, pH = 5.5	30	Single strand	$^{DT}\Omega_{He}$	-5 -6 -7 -8 -9 -10	842 883 928 1275 1393 1504	263
$d(TAACCC)_5$, pH = 5.5	30	i-motif	$^{DT}\Omega_{He}$	-5 -6 -7 -8 -9 -10	820 850 907 1009 1145 1217	263

[a] Complementary sequence to form a Watson-Crick antiparallel duplex

[b] Collision cross section distribution

[c] Sulfolane was used as supercharging agent

[d] Favored if 2 NH_4^+ ions bound and in soft pre-IMS conditions

3.2.3.2 Structural interpretation of collision cross sections

A CCS value alone does not inform on the structure, but comparing CCS values for systems of the same size (name number of nucleobases) can reveal which ion ensembles have more compact (low CCS) or more extended (high CCS) conformations. Table 1 shows that the CCS generally increases with the charge state. This is due to Coulomb repulsion: the compactness of the structure depends on the balance between attractive forces (by order of strength: attraction between opposite charges, hydrogen bonds, dipolar interactions and van der Waals interactions) and repulsive forces (Coulomb repulsion between like charges). Performing ion mobility spectrometry in native conditions requires minimizing the charge-dependent and internal energy-dependent rearrangements,[712] while preserving the native network of non-covalent interactions. CCS measurements help testing at what charge states unfolding starts to occur.[713]

In addition to this relative (compact/extended) assignment, one can analyze how the CCS increases with the number of monomeric units (*n*) for families of (presumably) structures of similar shape, to deduce the shape of the series. For example, the CCS of spherical ions would grow proportionally to $n^{2/3}$ while the CCS of rod-shaped ions would grow proportionally to n.[714] Other shapes have been discussed elsewhere.[715–717] For example, in the case of duplex nucleic acids, a linear growth with the number of base pairs is expected if the solution structure is preserved in the gas phase. As will be further discussed in section 4.3.1.6, the experimental values reveal a more complex behavior.

Finally, one can test structural hypotheses by (i) creating 3D molecular models, (ii) calculating their theoretical Ω, and comparing these theoretical values with the experimental ones. Step (i) is critical and far from trivial. Most CCS calculations need atomic coordinates. The starting coordinates can either be created from scratch based on an original structural hypothesis, or taken from pre-existing coordinates (e.g., from the Nucleic Acid Database[718,719] if one wishes to test whether a given NMR-derived or crystal structure is preserved in the gas phase). The structures need to be at least relaxed, or better, optimized, in the gas phase. The choice of computational chemistry approaches is vast, with tradeoffs between accuracy and speed. Typically, force fields molecular mechanics is fast but not parameterized for the gas phase, while *ab initio* quantum chemistry approaches are accurate in the gas phase but computationally demanding. Semi-empirical calculations and DFT calculations stand in-between, with an accuracy highly depending on the choice of the parameterization or functional, respectively. Beyond mere relaxation of the atom position into gas-phase realistic structures, one may also take into account through molecular dynamics (MD) that the IM measurement is performed at non-zero temperature, and thus that atomic coordinates fluctuate. Finally, one may model rearrangements possibly occurring prior to the IM measurement depending on the ion internal energy.

In structural studies of nucleic acids by ion mobility spectrometry, the approaches have evolved over the years thanks to increased computer power. In the early 2000's the Bowers group used molecular mechanics minimization for di- and tri-nucleotides,[692,720] and later 2-ns force field MD on larger structures.[708] The Fabris group explored coarse grained MD to model larger structures with standard computers.[721] The Orozco and Gabelica groups exploited the Barcelona Supercomputing Center to explore multiple replica and longer force field MD runs (e.g., 30 µs on a 36-nt triplex,[704] multiple µs replica exchange molecular dynamics on 24-nt duplexes,[701] multiple µs MD on RNA kissing complexes,[697] 250 µs on a 7-nt hairpin[695]), but although the calculated CCS values match the experimental ones, the hydrogen bonding patterns are mostly disrupted in the gas phase,[701,704,722,723] except for G-quadruplexes.[706,724] Furthermore, the same group used 20-ps Car-Parrinello MD were carried out to evidence proton transfer events between phosphate groups,[695] a phenomenon that cannot be modeled by force field MD. Recently, our group started using DFT (M06-2X functional[725])

and semiempirical (PM7[726]) calculations on duplexes, and found that base pairing and base stacking interactions can be preserved in structures having CCS matching well with experimental values.[145,701] In our most recent work, we used 1 ps MD at the semiempirical (PM7) level, starting from PDB coordinates, to confirm preservation of the topology of some G-quadruplexes by IMS.[190,727]

The calculation of CCS values from the models is not trivial either.[728] Several physical models exist, the most widely used being, by order of accuracy and computational expense, the projection approximation (PA), the exact hard spheres scattering (EHSS),[729] and the trajectory model (TM).[730] The projection superposition approximation (PSA)[731] is a variant of PA considering that atoms are not hard spheres, and that structures with concave surface will have a higher momentum transfer collision integral than predicted by simple projections. Several computer programs, each with their algorithms, are available to implement these models. Finally, the parameterization can differ among computer programs, or can be set by the user. Each of these choices will potentially influence the Ω value obtained. The nature of the gas is important: at room temperature, helium-ion collisions typically have a hard spheres character, and using EHSS is appropriate, while nitrogen-ion collisions should better be described by the trajectory model. The latter is harder to parameterize, especially in nitrogen. Most groups therefore used ${}^{\mathrm{DT}}\Omega_{He}$ or ${}^{\mathrm{TW}}\Omega_{N_2 \rightarrow He}$ values when structural interpretation is sought. For nucleic acids, the Bowers group used EHSS and TM in the Mobcal package. We showed that for the typical size range of interest for nucleic acid-drug complexes (~24-nt), EHSS calculations with Siu *et al*.'s revised parameters[732] or TM with the original Mobcal parameters were appropriate.[706] To interpret ${}^{\mathrm{TIMS}}\Omega_{N_2}$ values, the Fernandez-Lima group[490,703] used the projection superposition approximation (PSA) model and the IMoS[733,734] package, which contains a diffusive hard spheres scattering model (DHSS).

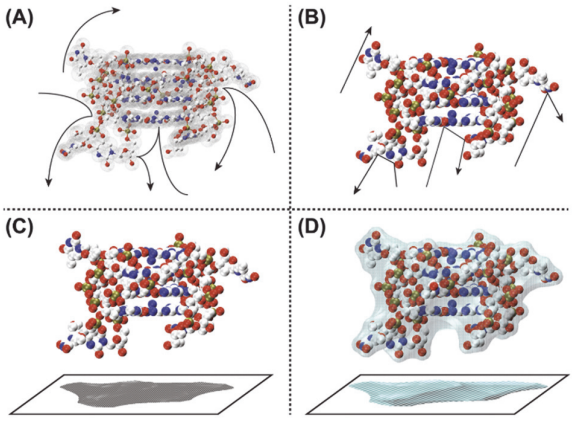

Figure 30. Illustration of the ion-gas interactions taken into account in three theoretical models for collision cross section calculation. A) The trajectory model (TM) calculates the momentum transfer collision integral by considering long-range interaction potentials between the ion and the gas. These interaction potentials can be attractive or repulsive, and their magnitude depends on the temperature. B) The exact hard spheres scattering (EHSS) model calculates the momentum transfer collision integral by assuming that the ion and gas collide as hard spheres. C) The projection approximation (PA) model calculates the collision cross section as a projection of the ion on a surface, averaged on all possible orientations, assuming an all-or-none interaction. D) The projection superposition approximation (PSA) is a projection approximation wherein the ion's atoms are considered as 'soft' spheres, accounting for the collective size effect by superimposition of all atomic contributions, and the resulting value is scaled by a shape factor ρ, which takes into account the shape effects by assessing the molecule's concavities. Figure reproduced with permission from Ref. 706. Copyright 2015 Wiley.

3.2.4 Ion spectroscopy

In solution biophysics, vibrational spectroscopy is used to obtain information on the biomolecule's conformation, whereas electronic spectroscopy (UV-vis absorption spectroscopy, or electronic circular dichroism spectroscopy) provides information on the chromophore's environment. For nucleic acid higher-order structures, vibrational spectroscopy informs on the hydrogen bonding status of various functional groups, while electronic spectroscopy provides information on base stacking. Both spectroscopic methods are interpreted thanks to quantum chemistry, because resonant absorption of electromagnetic radiation at *specific* wavelengths is due to the fact that energy levels are quantized (Figure 31).

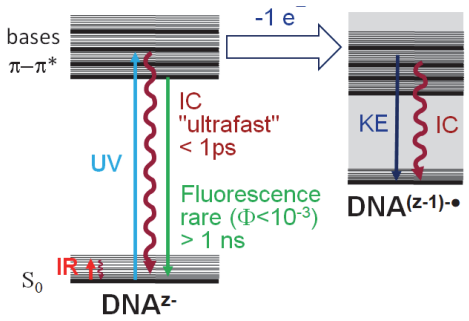

Figure 31. Schematic energy levels involved in UV (electronic) spectroscopy, IR (vibrational) spectroscopy and photoelectron spectroscopy. Thick lines are electronic energy levels and thin lines are vibrational energy levels. IR absorption results in intramolecular vibrational energy redistribution among several degrees of freedom. UV absorption can result in (i) total internal conversion into vibrational energy at the ground state, (ii) fluorescence, (iii) reaction directly from the electronic excited state, as depicted here with electron detachment. The system ends up on the potential energy surfaces of the product (here the DNA radical with one fewer charge). In this particular case, the kinetic energy of the electron (KE) can also inform us on electron binding energy (difference of energy between $DNA^{(z-1)\bullet-}$ and DNA^{z-}) and excited states of the radical.

Ion spectroscopy consists in interrogating ions trapped inside a mass spectrometer with a wavelength-tunable laser.[735] However, absorption spectroscopy is not possible on trapped ions, because the ions are too few and the photons are too many. Instead, one uses action spectroscopy: laser resonant absorption causes an action (typically, fragmentation or electron detachment), which efficiency is monitored as a function of the wavelength.

Fluorescence after UV excitation of the bases is a rare event, but other fluorophores (ligands, modified bases, covalently grafted fluorophores) can be investigated in their specific wavelength range. Fluorescence measurements in the gas phase have been demonstrated for proteins,[736,737] and applied to nucleic acids[738] with grafted a fluorophore and a quencher to measure the Fluorescence Resonant Energy Transfer (FRET), which indicates the fluorophore-quencher distance. The intrinsic gas-phase fluorescence of several DNA ligands has also been reported.[739–741] Finally, with a well-chosen quencher, FRET can also result in a fragmentation. This kind of experiment, coined "action-FRET",[742,743] has not yet been applied to nucleic acids.

The action yield Y for each product ion is determined as follows:

$$Y_{product} = \frac{I_{product}}{I_{total}} \tag{15}$$

$I_{product}$ is the integrated peak area of the product ion in the mass spectrum, and I_{total} is the total area (precursor ion plus all products).

3.2.4.1 Vibrational action spectroscopy

Wavelength-tunable Infrared lasers can be interfaced with mass spectrometers to study electrosprayed ions at room temperature. When large ions such as nucleic acid complexes are activated and the action is fragmentation, multiple photons are required in order to accumulate sufficient internal energy and cause fragmentation: this is IRMPD spectroscopy.[644,744,745] Single-photon vibrational action spectroscopy requires pump-probe (dual-laser) schemes, or cold ion tagging to have a low-threshold dissociation channel; however the use of such schemes was not published to date for nucleic acid non-covalent complexes. IRMPD spectroscopy is typically interpreted using quantum chemical calculations of the vibrational energy levels of candidate structures. An example of application to study the conformation of a mononucleotide is shown in Figure 32.[746] Numerous studies were devoted to IRMPD spectroscopy of nucleobases, nucleosides and mononucleotides. However, in the context of nucleic acid higher-order structures, IRMPD spectroscopy has to date only been applied to study the conformation of 6-mer oligonucleotides,[693] DNA duplexes,[747] guanine tetrads,[748] G-quadruplexes,[749] and i-motifs.[711] Mostly the base C=O and NH_2 absorption region (1400-1900 cm^{-1}) has been investigated, and for high photon fluxes this requires using a free electron laser,[750] coupled on trapping mass spectrometer only available at few facilities. This limits the use of IRMPD spectroscopy.

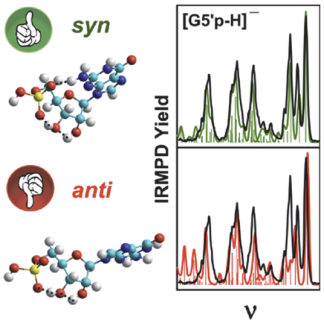

Figure 32. Black: experimental IRMPD action spectrum recorded on deprotonated guanosine-5'-monophosphate. Green: calculated IR spectrum for the syn *conformation. Red: calculated IR spectrum for the* anti *conformation. All bands match for the* syn *conformation, whereas one band is not matching for the* anti *conformation. Figure reproduced from Ref. 746. Copyright 2013 American Chemical Society.*

3.2.4.2 Electronic action spectroscopy

As outlined in Figure 31, the two main types of action following electronic excitation are fragmentation and (for polyanions) electron detachment. If fragmentation results from internal conversion, multiple photons may be required. In contrast, electron detachment is usually a single-photon process.[751] To reconstruct the action spectra, the action efficiencies are normalized by a factor proportional to the number of photons to obtain the relative efficiency (RE) of each action (ePD = electron photodetachment, fragm = fragmentation):

$$RE_{ePD} = Y_{ePD}/(\lambda * E_{trans}) \quad (16)$$

$$RE_{fragm} = Y_{fragm}/(\lambda * E_{trans}) \quad (17)$$

This linear normalization is appropriate for electron photodetachment, which is a single-photon process, while it is arbitrary for fragmentation, which is likely a multiple-photon process. The action spectra can differ according to the action. In particular, excitation of purine bases (around 260 nm), and especially guanines, favors electron photodetachment (Figure 33).[693,751] Electron photodetachment action spectroscopy has been exploited to obtain electronic spectra of proteins[752] and nucleic acid higher-order structures, among which DNA duplexes[753] and G-quadruplexes,[693,753] each compared with their respective single strands. Small changes in spectral shape were observed. However, changes in internal Coulomb repulsion can alter electron binding energies, as revealed by

photoelectron spectroscopy,[754,755] and this can in turn subtly alter action spectral shape.[693] Therefore, like in solution,[756,757] gas-phase electronic spectra in the base absorption band is not very informative on nucleic acid higher-order structure. In solution biophysics, electronic circular dichroism (the difference of absorption between left- and right-circularly polarized light) gives much better signatures of the base stacking.[758]

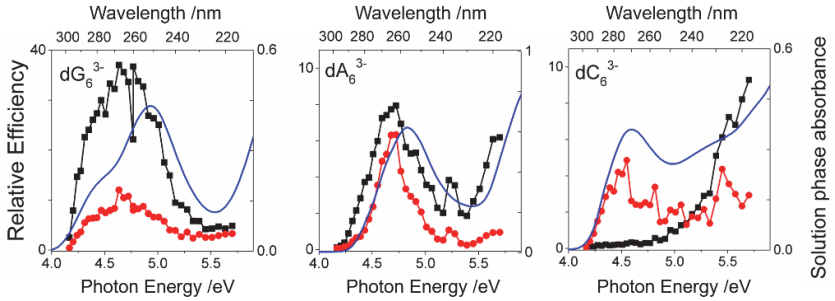

Figure 33. Electronic (UV) action spectra of oligonucleotides. Red circles: fragmentation relative efficiency; Black squares: electron photodetachment relative efficiency as a function of wavelength (top axis) or photon energy (bottom axis). Blue: solution absorption spectra. The results illustrate that the preferred action depends on the base nature. Figure adapted with permission from Ref. 693. Copyright 2019 RSC Publishing.

The first mass-resolved electronic circular dichroism spectra of nucleic acids have been recently published.[190] The CD of a nucleic acids ions of a given *m/z* ratio is measured by irradiation with a single laser pulse of selected wavelength with controlled circular polarization and pulse energy. The polarization state is changed by rotating a quarter-wave plate. The average value of the relative electron detachment yield for left circularly polarized light (LCP) and right-handed circularly polarized light (RCP) is calculated and CD is expressed as an asymmetry factor (Equation (18)). The method was applied to distinguish different G-quadruplex and G-duplex topologies (Figure 34).

$$g_{ePD} = \frac{\Delta ePD}{\overline{ePD}} = 2\left(\frac{\overline{Y_{ePD}^{LCP}} - \overline{Y_{ePD}^{RCP}}}{\overline{Y_{ePD}^{LCP}} + \overline{Y_{ePD}^{RCP}}}\right) \quad (18)$$

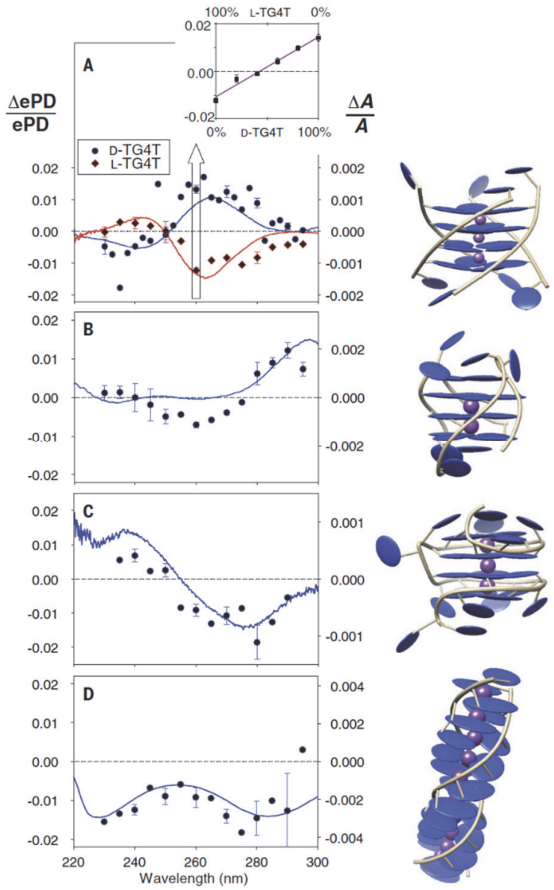

Figure 34. Gas-phase circular dichroism spectra (ΔePD/ePD) compared to the equivalent solution-phase spectra (ΔA/A). Symbols and lines denote gas-phase and solution-phase CD data, respectively. (A) TG4T: natural right-handed D-$[(dTGGGGT)_4•(NH_4^+)_3]^{5-}$ (blue) and its mirror image L-$[(dTGGGGT)_4•(NH_4^+)_3]^{5-}$ (red). Inset: Gas-phase CD measured at 260 nm for $[(dTGGGGT)_4•(NH_4^+)_3]^{5-}$ ions prepared from 5 μM solutions with varying ratios of D-TG4T and L-TG4T. Error bars show the 95% confidence interval calculated from the standard error (three replicas, except at 260 nm with five replicas). (B to D) Gas-phase and solution-phase CD spectra for the antiparallel G-quadruplex $[d(GGGTTA)_2GGGTTTGGG•(K^+)_2]^{5-}$ (B), the left-handed G-quadruplex $[dT(GGT)_4TG(TGG)_3TGTT•(NH_4^+)_3]^{6-}$ (C), and the G-duplex $[(dG_{11})_2•(Ag^+)_{11}]^{5-}$ (D). The illustrations showing helicity were generated using Chimera from Protein Data Bank coordinates (entries 2O4F, 5YEY, 6GZ6, and 4JRD), respectively. Figure reproduced with permission from Ref. 190. Copyright 2020 AAAS.

3.3 Solution probing with mass spectrometry readout

Native MS provides a direct readout of binding stoichiometries and is well suited to determine binding affinities (see section 3.1.4). Obtaining structural information is more challenging, and usually requires additional analysis steps in the gas phase (see section 3.2) or in solution. In this section, we describe methods based on solution reactivity revealed by mass spectrometry. We limit the discussion to methods providing structural insights; MS-based proteomics workflows for the high-throughput identification of nucleic-acid binding proteins are discussed elsewhere.[759–761]

Solution probing is performed under non-denaturing conditions, but the MS readout needs not, which can be advantageous in terms of sensitivity. Here what matters is that the initial chemical modifications do not induce conformational changes in the target structure that could lead to modifications of initially unexposed sites. Also, the kinetics of the labeling reaction matters: sparsely populated ensembles can be kinetically trapped on the labeling time scale, giving an inaccurate representation of the conformational landscape.[762] The use of multiple probes and orthogonal methods is thus recommended to interpret the results and obtain a more complete picture.[763–770]

Operating under native conditions in both solution and gas phases can still be beneficial, for example to sort out the labeled complexes according to their stoichiometries[771] or ion mobilities.

3.3.1 Chemical probing

Chemical probing relies on a reaction with the biomolecule in solution, which rate is structure-dependent. Chemical probes can be classified based on the information they provide (here we only list probes that have been used for nucleic acids and in combination with MS):[772]

1. Solvent accessibility probes, usually hydroxyl radicals (•OH; A), which cleave nucleic acid backbones independently of the nature of the nucleotides.
2. Base-selective probes that specifically form stable covalent adducts with one or several bases, and are usually inhibited by base pairing and/or stacking and/or binding by ligands (Scheme 2B).
    - Potassium permanganate $KMnO_4$ and glyoxal to probe ds- and G4 DNA;
    - Dimethylsulfate (DMS), 1-cyclohexyl-3-(2-morpholinoethyl)carbodiimide metho-*p*-toluenesulfonate (CMCT), and β-ethoxy-α-ketobutyraldehyde (kethoxal, KT) to probe RNA;
    - Mercury(II), which coordinates thymines in T·T mismatches.[773]
3. Spatial-selective probes, using bifunctional cross-linking reagents (short to long range) or UV-induced crosslinking ("zero" distance) (Scheme 2D).
4. Local nucleotide flexibility/dynamics probing, using reagents sensitive to secondary and tertiary structures, and potentially labeling all nucleotides (Scheme 2C).
    - Hydroxyl-selective electrophiles reacting 2'-OH RNA groups of flexible nucleotides to form a 2'-*O*-adduct that are then analyzed by primer extension (SHAPE).
    - Isotopic exchange of nucleobases with deuterium, using deuterium oxide (D_2O), which is sensitive to the H-bonding status of nucleobase H-bond donor groups.

Scheme 2. Examples of chemical probes and their reactivity with their substrates.

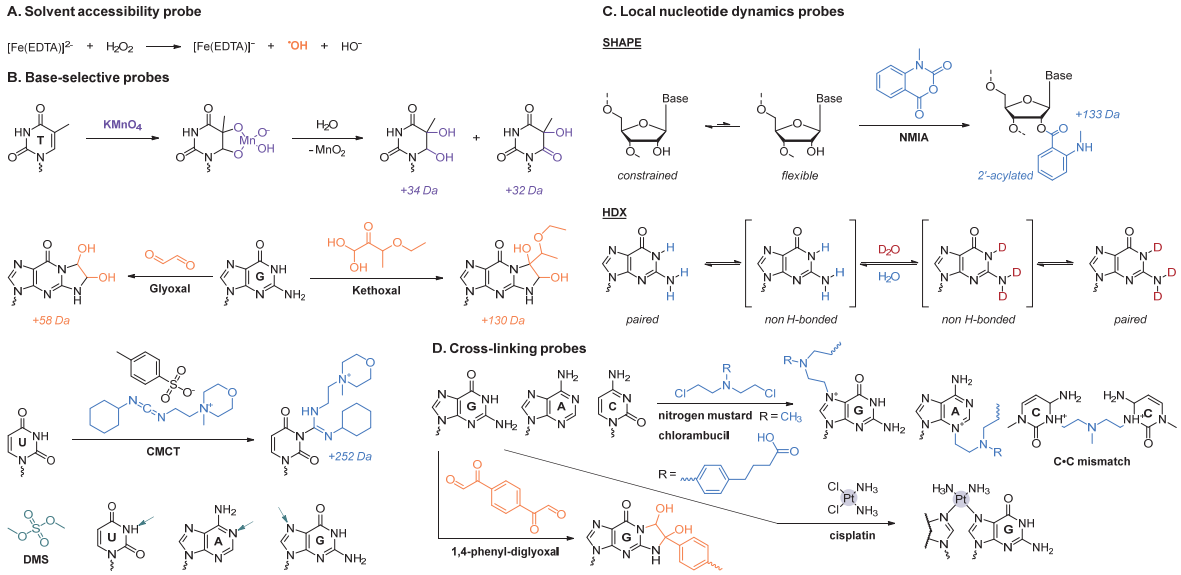

3.3.1.1 Solvent accessibility probes

Hydroxyl radicals (•OH) are widely used for the footprinting of nucleic acid structures, by abstracting solvent accessible hydrogen atoms from the backbone (deoxy)ribose sugars, eventually causing strand cleavage.[774–777] •OH reactivity is directed by the solvent accessibility of residues, but is independent of

the nucleotide sequence.[774–776] It can therefore yield quantitative thermodynamic and kinetic data on the structure, and dynamics of nucleic acids, with single-nucleotide resolution.[774–776] Hydroxyl radicals can be generated by the Fenton reaction of Fe(II)–EDTA with hydrogen peroxide (Scheme 2A), water radiolysis, and hydrogen peroxide photolysis.[762,774–776,778] Usually, the ^{32}P or fluorescently-labelled cleavage products are separated with high-resolution denaturing gels or chromatographic techniques.[774–776] Although the radical footprinting of proteins and their complexes with nucleic acids can be analyzed by mass spectrometry,[778,779] there is to our knowledge no example of MS analysis of the nucleic acids themselves.

3.3.1.2 Base-selective probing

3.3.1.2.1 DNA probing with potassium permanganate and glyoxal

Potassium permanganate is a potent, cheap and relatively safe oxidant, used since the 1960s to oxidize DNA bases.[780–782] It selectively reacts with the double bond of thymines (or uracyl, although slightly slower), and to a lower extent cytosines, without altering the rest of the structure.[782,783] It is very reactive in presence of unstacked nucleotides, but relatively inert with canonically-folded DNA.[782] Consequently, it can probe single-stranded regions (e.g. in hairpins) and conformational changes induced by the binding of small molecules (e.g. echinomycin bis-intercalation[784]) or proteins (e.g. RecBCD unwinding of dsDNA in ssDNA[785]).

When carried out at neutral pH, the reaction produces a mixture of diol and α-hydroxylketone (Scheme 2B). Traditionally, the sites of oxidation of radiolabeled analytes are cleaved by piperidine heat treatment, then sequenced by polyacrylamide gel electrophoresis.[784,785] However, Mazzitelli and Brodbelt leveraged the mass shifts (+34 Da for the diol) to determine the extent of DNA oxidation by ESI-MS.[783] The oxidation sites were localized by CID and IRMPD. Strand separation is prevalent in CID, and therefore a second activation stage was necessary. The method revealed differences in oxidation between ss- and dsDNA, between dsDNA bound by different intercalators and groove binders, and was used to determine ligand binding sites.

Brodbelt and coworkers complemented the $KMnO_4$ oxidation monitored with ESI-MS with glyoxal probing.[769,786] Glyoxal is a highly reactive dialdehyde that alters both nucleic acids and proteins.[787] Glyoxal preferably reacts with unpaired guanines,[769,786] yielding an additional fused five-membered ring bearing two hydroxyl groups on the Watson-Crick face (N1 and N2 atoms; Scheme 2B).[787–789] Glyoxal can also react with low efficiency with cytosines.[769] The secondary structure of both ds- and G4-DNA is lost in the reversed-phased clean-up step,[786] although the glyoxal reaction itself may contribute to denaturation.[769]

The mass shift (+58 Da) is readily distinguishable from sodium adducts by ESI-MS, but long reaction times may still yield cluttered spectra.[769] The extent of structural alteration by ligand binding can be quantified by ESI-MS analysis if some guanines become more or less available for glyoxal adduction.[769,786] The localization of glyoxal adducts is not possible using CID because the main channels are glyoxal loss, dehydration of the adducted strands, and loss of native and adducted guanine bases, none of which being informative.[786] IRMPD produces *a*, *b* and *w* adducted fragment ions, mostly located adjacently to guanines.[786] No apparent preference for specific guanines was found for the reaction of glyoxal with ligand-bound G-quadruplexes.

3.3.1.2.2 RNA probing with DMS, CMCT, and kethoxal

DMS, CMCT, and kethoxal are used for probing RNA structures and interactions because their base specificity is complementary (Scheme 2B). DMS methylates the N7 of guanines that are not involved in base stacking, tertiary interactions or ligand binding .[763,780,790,791] DMS also reacts with the N1 of adenines and to a lower extent the N3 of cytidines, when these positions are not involved in base-

pairing.[763,780,790,791] CMCT reacts preferentially with the N3 of uridines not involved in base-pairing (mass shift: +252 Da),[790] and kethoxal, like glyoxal, with the N1 and N2 of unpaired guanines (mass shift: +130 Da).[791]

Traditionally, the reaction products are analyzed by gel electrophoresis.[763,792] However, the mass shifts caused by these chemicals can be more quickly and accurately detected by mass spectrometry from little material, which was been exploited by the Fabris group and others (Figure 35).[763–768,793] Mass spectrometry also allows to multiplex the use of chemical probes.[765,766]

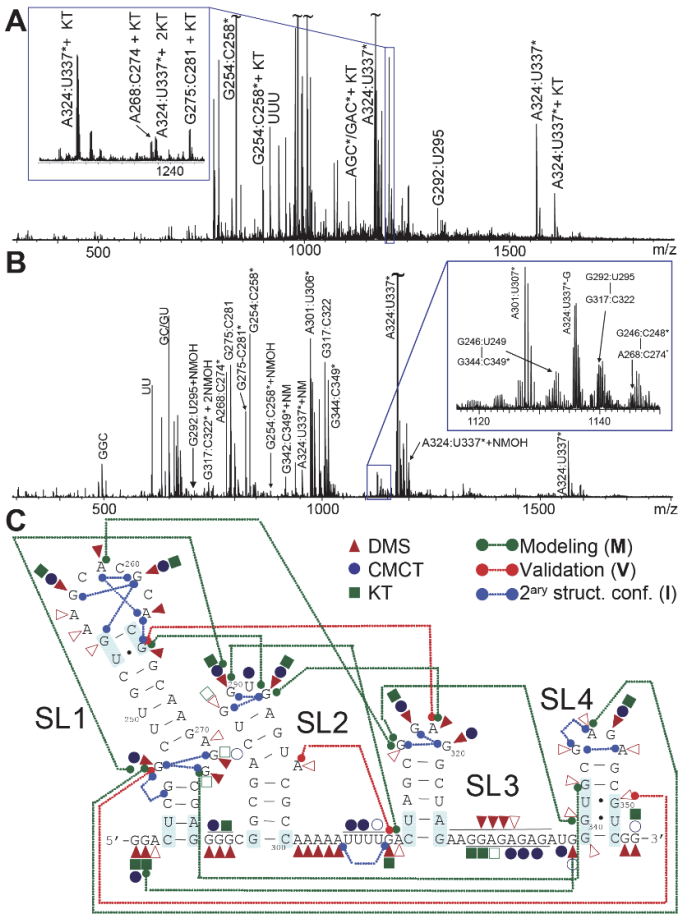

Figure 35. A, B: ESI-FTICR mass spectra of RNase A digestion products obtained from full-length HIV-1 packaging signal (Ψ-RNA) probed with A) kethoxal (KT) and B) nitrogen mustard (NM; cross-linked products are connected by a bar). C. Map summarizing the probing of Ψ-RNA by DMS (red triangles), CMCT (blue circles), KT (green squares), and nucleotides bridged by NM (dashed lines; non-exhaustive, and colored by use: modeling, validation, or secondary structure confirmation). Adapted with permission from Ref. 768. Copyright 2008 National Academy of Sciences

Large RNA molecules can be analyzed with a bottom-up approach, by digestion with ribonuclease A (RNase A) or T_1 (RNase T_1) in ammonium-based buffers.[763,765,766,768] The MS readout also offers the possibility to detect possible overalkylation and structural distortion that may inhibit the nucleases' activity.[764]

Mass spectrometric analysis is generally performed in the negative ion mode by direct infusion of sample solutions containing ammonium acetate[763–766,768] In case of ambiguity on the location of chemical modifications on the digests, tandem MS can be employed. Fabris and coworkers have carried out CID on mass-selected precursor ions up to 6 kDa on an FT-ICR instrument to obtain sequence-specific fragment ions.[763,764,768] Unlike other probes, kethoxal adducts are not sufficiently

stable under classical CID conditions to allow proper localization.[764] Specialized software may be necessary for data reduction and interpretation of complex spectra produced by large analytes.[762,764,765]

3.3.1.3 Cross-linking

Crosslinking consists in covalently linking two biopolymer side chains that are in close proximity, in order to identify the binding interfaces in complexes and multi-subunit assemblies, with the help of dedicated software (in particular for sequence assignment; not discussed herein).[761,762,794,795] In essence, crosslinking replaces non-covalent interactions with covalent bonds; the resulting complexes thus become resistant to denaturing separation and characterization methods commonly used in bottom-up workflows. Crosslinking of nucleic acids to other nucleic acids or proteins is achieved either by UV irradiation (UV crosslinking) or using bifunctional reagents (chemical crosslinking).

3.3.1.3.1 UV crosslinking

UV-induced crosslinking provides information on secondary and tertiary structure of nucleic acids (particularly RNA), the identify of bound proteins and their binding sites .[761,795,796] It relies on the intrinsic reactivity of nucleobases (uracil being the most reactive). Upon excitation at 254 nm with a UV lamp or laser, nucleobases can form a covalent bond with spatially close bases or amino acids, without the significant structural changes that could arise from the use chemical crosslinkers.[761,795] All amino-acids can potentially be crosslinked, but with large differences in reactivity depending on both their nature and that of the nucleotides.[797–799] UV irradiation also yields protein-protein crosslinks, which have been discussed elsewhere.[800–806,795]

Typical methods employed to analyzed the crosslinked complexes are SDS-PAGE, western blotting, immunoprecipitation, and mass spectrometry.[761] Identification of the crosslinking sites is typically performed after enzymatically cleaving the nucleic acids (with e.g. RNase A and/or T_1,[807–823] benzonase,[810,820,824] nuclease P1,[824] DNase I[825]) and proteins (with e.g. trypsin and/or chymotrypsin,[807,810–830] Glu-C and/or Lys-C,[808,809,824,825,827,828] proteinase K,[825,826,831] pronase[827]). This bottom-up approach generates a mixture of conjugated species with characteristic masses and fragmentation patterns that can be identified and sequenced by LC-MS(/MS) (Figure 36A).[761,795]

UV-crosslinking suffers from inherently low yields, which is problematic for MS identification, and subsequent MS/MS sequencing.[761] This critical issue can be partially addressed using isolation and enrichment steps (e.g. denaturing reversed phase or size-exclusion,[807–809,816–819,821–824,829,831,832] immobilized metal affinity chromatography,[807,816,826,831] and TiO_2 chromatography[810,812–815,820–822,824]), the use of UV-induced chemical crosslinker,[823] or by site-specific or random introduction of photo-reactive base analogues (6-thio-G, 4-thio-U, 5-iodo-U, 5-bromo-U).[812,829] In the latter case, the labeled nucleotides are specifically activated at higher wavelengths (312 nm and 365 nm for halogeno- and thio-nucleotides, respectively), which also eliminates potential substrate photocleavage and oxidation issues.[761]

MS analysis of peptide-containing fragments is usually performed in positive ion mode, although the negatively-charged oligonucleotide components decrease the ionization efficiency.[761] In the case of long oligonucleotides, it may in fact be beneficial to switch to the negative ion mode.[807] Initial methods were carried out with MALDI-MS,[807–811,816,818,819,826,827,831–834] but LC-ESI-MS is now the method of choice because of it provides improved sensitivity and sequence information.[812–817,820–824,829,830]

MS/MS is useful to obtain the oligonucleotide and peptide sequences: post-source decay (PSD) or CID on MALDI instruments and CID or HCD on ESI instruments have been performed.[807,810,816–818,822–824,828,829,831] Regrettably, long oligonucleotides tend to suppress peptide fragment ions.[761] This can be

addressed by oligonucleotide enzymatic or chemical (e.g. HF,[826] formic acid[828]) cleavage into smaller strands or even mononucleotides.[761,795] However, this non-specific cleavage into very small fragments comes at the cost of losing the nucleic acid sequence context.[795]

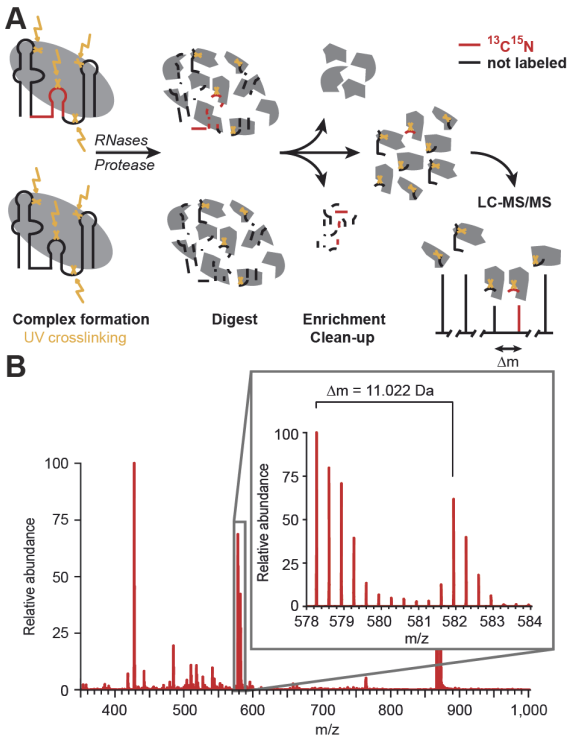

Figure 36. A. Typical workflow of RNA:protein UV-crosslinking, involving nucleases and protease digestion, enrichment, and LC-MS/MS analysis of the fragments. In CLIR-MS/MS, the nucleic acid is $^{13}C,^{15}N$-labeled segmentally to unambiguously assign crosslinks to a nucleic acid region (an example of labeled stem-loop segment is shown in red). B. Typical isotope pattern observed in CLIR-MS/MS arising from the 50% isotope labeling of uracil. Figure adapted with permission from Ref. 820. Copyright 2017 Springer Nature.

To reestablish this context, isotopic-labeling approaches have been proposed. Lelyveld *et al*. have developed a site-specific stable-isotope (^{18}O; mass shift: +2 Da) labeling approach to pinpoint the nucleotide involved at a crosslinking site.[828] This was applied to identify which of two uridines from a stem-loop crosslinks to the Lin28A protein, using CID to confirm the position and identity of the observed peptide-nucleotide species. High-resolution MS is required to confidently assign the relatively small mass shift that overlaps the natural isotopic distribution. The risk of ^{18}O exchange with the bulk medium can be mitigated by performing the digestion at lower temperature.

Dorn and colleagues have used segmental isotope labeling of RNA in a method coined CLIR-MS/MS (CrossLinking of segmentally Isotope labeled RNA and tandem Mass Spectrometry).[820] The method involves mixing equimolar ratios of unlabeled and fully $^{13}C,^{15}N$-labeled RNA so that the crosslinked RNA-protein complexes appear as doublets separated by a mass shift equal to the label mass (e.g. 11.022 Da for rU; Figure 36B). To identify binding regions, the labeling is segmented: several analytes are prepared with only one region labeled, so that the whole sequence is covered across several experiments. As a result, crosslinks presenting the doublet pattern during MS analysis can only belong to a labeled region.

3.3.1.3.2 Chemical crosslinking

Chemical crosslinking using bifunctional molecules overcomes the relatively low crosslinking yields of UV crosslinking.[794] Cross-linking reagents consist of two reactive groups, connected by a spacer arm,

which covalently link residues in close proximity. Schilling *et al*. have proposed a nomenclature for peptide crosslinks depending on the outcome: *type 0* for dead-end crosslinks (only one reactive group has reacted with a biopolymer, *i.e.* the crosslink has failed), *type 1* for internal crosslinks, and *type 2* for intermolecular crosslinks (needed to analyze intermolecular complexes).[835] Mass spectrometry is an effective method to identify chemically-crosslinked components; it is routinely used to decipher protein-protein interactions (reviewed elsewhere[795,803–806]), with only few studies dedicated to nucleic acid complexes.[794] The (relatively fewer) crosslinkers available for nucleic acid crosslinking include psoralens, 2-haloethylamines, platinum complexes, epoxides, alkylsulfonates, and some photo-activatable compounds.[766,767,794,823,836]

The nature of the reactive group can be tuned to crosslink specific residues, and the length of the linker can be varied to provide different sets of distance constraints.[794] Among 2-haloethylamines, nitrogen mustard (NM; mass shift: 83 Da) and chlorambucil (CHB; mass shift: 231 Da) preferentially react with guanine N7, adenine N3, and cytosine N3 (in that order of preference), establishing covalent bonds between residues 6—12 Å apart, which is compatible with the generation of type 1 crosslink across hairpin loops or type 2 crosslinks at RNA:RNA interaction surfaces (Figure 35).[766–768] Conversely, cisplatin (which also favors guanine N7, and to a lower extent adenine N7;[18,837] mass shift: 226 Da, distance: 3.2 Å) mainly crosslinks immediately contiguous purines in single- and double-stranded regions.[767] 1,4-phenyl-diglyoxal reacts with guanine N1 and N2 and is more rigid than NM (mass shift: 190 Da, distance: 7—8 Å).[768] Dithiothreitol (DTT; mass shift: 152 Da, distance ~ 10 Å) can produce crosslinks between uracil and proteins by irradiation at 254 nm, as in classical UV crosslinking, but in much higher yields and specifically with cysteines.[823]

Crosslinked analytes can be analyzed under non-denaturing conditions, but this is neither usual nor necessarily desirable. A recent example is the ESI-MS analysis (in the positive mode) of transplatin crosslinks between dsDNA and the DNA binding domain of the Forkhead box protein O4 (FOXO4-DBD).[836] Under native conditions, the complexes are preserved (whether the dsDNA is crosslinked to FOXO4-DBD or not), meaning that it is not possible to discriminate between intra- and intermolecular crosslinks, their elemental composition being effectively identical. Mildly denaturing conditions that disrupt the complexes devoid of type 2 crosslinks were therefore favored.

Both bottom-up workflows, where the analytes are digested with nucleases—and proteases if a protein is complexed—before (LC-)MS(/MS) analysis,[766,768,836,838] and top-down strategies, where the analytes are fragmented in the gas-phase,[767,768] have been employed.[794] In bottom-up workflows, digestions can be performed in ammonium acetate, which is MS compatible and provides a near-neutral pH preventing the degradation of RNA.[794] Crosslinking site down to the atomic level can sometimes be determined: Rojsitthisak *et al*. evidenced by CID on enzymatically-digested fragments that NM crosslinks C·C mismatches by bridging the cytosines' N3 position.[839] However, more fragile crosslinkers such as bikethoxal are significantly cleaved off even in gentle activation conditions, complicating the interpretation of the results.[767] Similarly, in a study where dsDNA was crosslinked to a protein using transplatin, fragmentation of Pt-base bonds occurred instead of backbone cleavage, preventing sequencing.[836] In addition, base loss is promoted by covalent conjugation, particularly in the case of purine N7.[794]

3.3.1.4 Local nucleotide flexibility/dynamics probing

3.3.1.4.1 SHAPE and SHAMS

SHAPE (Selective 2'-Hydroxyl Acylation analyzed by Primer Extension) is a method designed to analyze the structure and interactions of RNA at the nucleotide level, and is the most common application of 2'-OH acylation reactions.[840–842] SHAPE uses electrophile small-molecules that react preferentially with

the 2′-OH group of nucleotides to form a 2′-*O*-adduct, with the reactivity being highly sensitive to nucleotide conformations.[840–844] Flexible nucleotides (*i.e.* not or weakly base-paired, not involved in tertiary interactions) visit multiple conformations, few of which increase the nucleophilic reactivity of the 2′-OH group.[840–844] As a result, the reactivity is roughly inversely proportional to the probability of a canonical base pair being formed,[843,845] with little dependence on the nature of nucleotides.[846] The position of the 2′-*O*-adducts is determined from the complementary DNA extension products obtained by primer extension with reverse transcriptase, which stops one nucleotide prior to an acylated nucleotide.[840] The relative reactivities of nucleotides are determined by capillary or gel electrophoresis,[840] providing a quantitative measurement of local dynamics of all four nucleotides in a single experiment.[844,846]

Turner *et al*. devised the SHAMS method, in which the chemical modifications are directly detected and located through their mass increment by tandem MS (Figure 37),[770] similarly to the approach developed for base-specific chemical probes.[763–765] The classical acylating agent *N*-methylisatoic anhydride (NMIA; mass shift: 133 Da) was used.[770] NMIA forms bulky 2′-*O*-adducts, therefore the reaction is unlikely to occur on nucleotides embedded in folded helical structures or bound by small molecules and proteins. The method was applied to an RNA/DNA duplex hybrid, which was denatured at 80°C after reaction to facilitate data analysis.[770] Direct MS monitoring of the number of modified sites helps optimizing the probe:analyte ratio to avoid distortion or unfolding of the analyte (Figure 37A—C). The phosphates, carrying the charges, remain unaffected by the probe, meaning that the MS signal intensities should reflect solution-phase abundances. The location of the NMIA-adducted sites was determined by CID of mass-selected ions with an FTICR spectrometer (Figure 37D). Given that the adducts are located on the 2′-O or RNA, the *d*-H_2O series cannot undergo the loss of H_2O and therefore is observed as a *c* series, together with the *y* series ions.

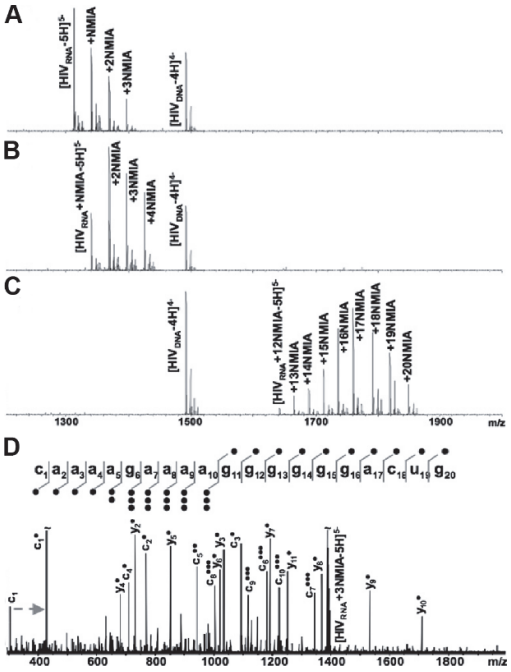

Figure 37. A—C: NanoESI mass spectra of HIV-1 polypurine tract (PPT) RNA/DNA hybrid after reaction with a 10-fold (A; partially modified), 50-fold (B; mostly modified), and 100-fold (C; fully modified) NMIA excess for 50 min at 37°C. The DNA strand remains unmodified in all cases (no 2′-OH groups). D: CID spectrum of the triply modified RNA substrate in the 5- charge state. Only the modified fragments are labeled, except c1 to highlight the mass increment (grey arrow). The number of NMIA adducts is shown with •. Figure adapted with permission from Ref. 770. CC 2009 RNA Society.

3.3.1.4.1 Solution HDX-native MS

Hydrogen-deuterium exchange coupled to mass spectrometry is now a well-established method for the analysis of protein structures and dynamics.[778,847–851] It relies on measuring exchange rates of backbone amide hydrogens in a deuterium-rich solution (mass shift: 1.00628 Da), because these rates are heavily dependent on hydrogen-bonding and solvent accessibility.

Nucleic acids can also undergo HDX reactions, both in the gas-phase (see section 3.2.2) and in-solution. In the latter case, the exchange is usually monitored by NMR.[41,852] Recently, in-solution HDX of DNA oligonucleotides was coupled to native MS readout.[771] In DNA, the exchangeable sites are the imino and amino protons of nucleobases, meaning that (i) HDX is strongly inhibited by base-pairing, (ii) the probing operates at the nucleotide level, and (iii) it is potentially amenable to other backbone chemistry (e.g. PNA[189,211]) and modified nucleobases. Under the soft-source conditions of this study, the phosphates neutralized during the ESI process are fully back-exchanged, while nucleobases retain their shifted isotopic composition. As a result, the exchange rates depend strongly on the secondary structure of DNA but not on the charge state of the detected ions, nor on the presence of non-specific adducts. The MS measurement is both accurate and precise on a wide time scale. Direct infusion of manually-mixed exchanging solutions was used for minute-to-days measurements, while second-scale events were monitored using a continuous-flow setup (Figure 38). Coupling to native MS was used to access individual exchange rates of mass-resolved non-covalent complexes (see section 4.4.2.4).

Among the chemical probing methods described in this chapter, HDX is the least likely to be disruptive of nucleic acids structures and the only one with explicitly native MS readout. It does not require digestion, quenching, and chromatographic separation steps, found routinely in bottom-up HDX/MS of proteins and in most of the other chemical probing techniques described herein.

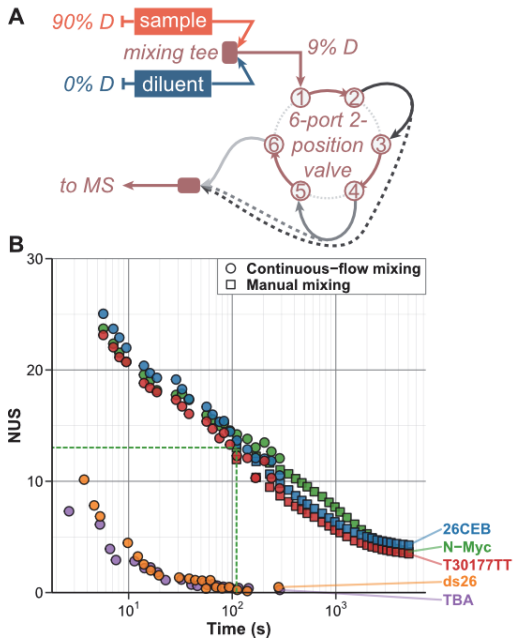

Figure 38. A. Continuous-flow HDX/MS setup to monitor of fast exchanging sites (1—300 s), making use of a 6-port, 2-position valve to easily cycle through capillary sizes (shades of grey; dashed lines illustrate direct coupling of a capillary to the MS source to shorten the mixing time). In this setup, oligonucleotides exchange in the D-to-H direction (90% to 9% D) B. Exchange kinetics of five oligonucleotides acquired by continuous-flow (circles) and manual mixing (squares) native HDX/MS. 26CEB, N-Myc, and T30177TT are 3-tetrad G4s, TBA is a 2-tetrad G4, and ds26 forms a canonical B-helix. Figure adapted from Ref. 771. Copyright 2020 American Chemical Society.

3.3.2 Enzymatic probing

In the bottom-up approaches described above, nucleotide-specific nucleases (e.g. RNase A and T1) are usually employed. Conversely, some nucleases cleave the phosphodiester backbone of nucleic acids adopting a particular conformation, and can therefore be used to map secondary structures. Subsequent sequencing typically requires conversion of the cleaved fragments into complementary DNA, or to perform primer extension for sequencing purpose.[853] ESI-MS is well suited to analyze these digested strands, without the need for labeling or additional experimental steps. van den Heuvel *et al.* monitored the hydrolysis of DNA in real time with an ESI-TOF instrument in positive ion mode, detecting both the DNA fragments and transient DNA:protein complexes.[854]

Scalabrin *et al*. explored the use of the mung bean (MB) and V1 nucleases that cleave ss- and dsDNA, respectively, in combination with a top-down MS readout.[853] Both nucleases were able to cleave an RNA hairpin in ammonium acetate solutions, producing relatively large and redundant fragments compared to the nucleotide-specific nucleases sometimes used in chemical probing. However, shorter fragments may have altered or more dynamic structures, leading to a decrease of cleavage specificity. This was partially mitigated by increasing the ammonium acetate concentration and adding MS-compatible amounts of Mg^{2+}. The identity of the analytes was determined based on their mass, corroborated by tandem MS, taking advantage of the redundancy of cleavage to minimize ambiguities.

4. Mass spectrometry studies of nucleic acid non-covalent complexes

4.1 Nucleobase self-assembly

4.1.1 Magic number clusters

The concept of magic number clusters is to compare all possible stoichiometries for a cation cluster with *m* nucleobases attached. In the case of unspecific clustering, the ESI-MS signal distribution among all clusters ($M_xB_2^{x+}$ to $M_xB_m^{x+}$) follows the Poisson distribution.[855,856] However, in the event of meta-clusters formation (such as a G-quartet), a specific stoichiometry prevails over unspecific adducts. Therefore, if the signal intensity for one stoichiometry is significantly higher in comparison to its neighbors, it is considered a magic number cluster. A numerical approach to characterize magic number clusters is presented by the magic number factor:[857]

$$magic\ number\ factor = \frac{I_m^2}{I_{m-1} \cdot I_{m+1}} > n \qquad (19)$$

The differentiation among magic number clusters and non-magic number clusters can be made based on the arbitrary limit *n*, which is defined in accordance with the experimental conditions/results. For clusters that have neighbors with zero abundancy, the magic number factor cannot be calculated (even though by definition they are still magic number clusters). The presence of magic number clusters can mean that the given stoichiometry was 1) particularly abundant in solution 2) particularly resistant to collisions in the gas phase or 3) both. Thus, using magic cluster numbers to infer solution-phase abundances must always be done in experimental conditions that minimize collision-induced dissociation.

4.1.1.1 Clusters of guanine derivatives

As discussed in section 2.2.3, guanine is able to form G-quartets. The formation of these G-quartet clusters has been characterized for guanine (G),[858–862] desoxyguanosine (dG),[863–866] guanosine (rG),[860,863,867] 9-ethylguanine (9eG)[748,860,868,869] as well as other semi-synthetic guanine derivatives.[869–877] Metallic cations (M) are essential for the self-assembly of guanines. The addition of a K^+-binding cryptand (working in a similar fashion as a commonly used crown ether) causes the highly abundant ESI-MS signal of one specific G-cluster to disappear and break down into monomers.[870] Owing to their non-covalent nature, G-clusters are very diverse.

4.1.1.1.1 Stoichiometry and structure

Various cation/guanine stoichiometries have been observed in ESI-MS experiments, including: MG_2,[859–865,867–869] MG_3[859,860,863–868] and MG_6[863,864,866,867] (if not further specified, the notation "G" refers to any guanine derivative). The formation of these clusters is non-specific, which has been confirmed by 1) ESI-MS spectra showing that these adducts display low relative abundancies compared to other (specific) adducts[748,859,863,869] 2) CID experiments reporting the loss of guanine even at low collision energies[860,867] and 3) IMS-MS verifying the globular conformation of an MG_6 cluster.[864]

However, the most common phenomenon is the formation of G4-clusters with one (MG_4), two 7(MG_8), three (M_2G_{12}) and four quartets (M_3G_{16}) (Figure 39). The specificity of these G4-clusters is confirmed by their high ESI-MS relative abundance in comparison to other stoichiometries, making them magic number clusters. The quadruplex structure has been verified in IMS-MS by comparing the experimental collision cross sections (CCS) to theoretically calculated CCS values.[864] The IMS-MS data also revealed that not all the identified G-quadruplexes follow the "magic number" stoichiometries. Instead, they formed adducts with additional desoxyguanosine bases and ammonium ions, such as

$(NH_4)_2(dG)_{11}^{2+}$, $(NH_4)_3(dG)_{12}^{3+}$, $(NH_4)_3(dG)_{18}^{3+}$ or $(NH_4)_4(dG)_{22}^{4+}$. Finally, $(NH_4)_4(dG)_{24}^{4+}$ forms 6 layers of G-quartets stacked on top of each other. The 4 ammonium ions are located between the two top and bottom layers, leaving the two middle G-quartets without any cation stabilization.[864]

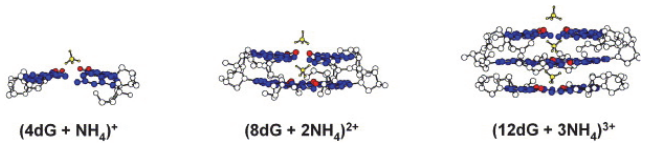

Figure 39. Theoretical structures of the NH_4^+ mediated G4-clusters MG_4, MG_8 and M_2G_{12}. The latter two are modeled with an additional NH_4^+ ion outside the G4-cluster. Figure adapted from Ref. 864. Copyright 2005 American Chemical Society.

IRMPD spectra on the one-quartet system NaG_4^+ confirm that the sodium cation is located at the center of a non-planar G-quartet, which can rapidly interconvert between two populations.[748,858] The inclusion of the cation depends on its ionic radius (see below). According to SORI-CID experiments on alkaline earth metals, the MG_4^+ cluster is most kinetically stable in the presence of Li^+ or Na^+. Only sufficiently small cations may actually fit inside the G-quartet.[748] In the case of multi-quartet clusters the ratio of cations to G-quartet indicates that one cation associates with two G-quartets, suggesting that the cations must be located in-between the G-quartets.

4.1.1.1.2 Influence of the cation

The cation's radius and charge influence the G4-cluster formation. As indicated previously, the MG_4^+ cluster is most stable when the cation is small enough to fit inside the G-quartet. Competitive ESI-MS assays[863,868] and CID fragmentation experiments[748] on alkaline metals were used to establish the relative stability of the MG_4^+ cluster for each cation, the resulting order being $Na^+ > Li^+ > K^+ > Rb^+/Cs^+$ (Figure 40). However, smaller cations are less prone to form multi-quartet G4-clusters. LiG_8^+ could not be detected in ESI-MS.[863,869] The sodiated G-quadruplexes NaG_8^+,[863,869,873] $Na_2G_{12}^{2+}$ [869,875] and $Na_3G_{16}^{3+}$ [865,869,875] have been detected, but ESI-MS titration experiments on the $Na_3G_{16}^{3+}$ cluster demonstrated that sodium is gradually displaced with increasing concentrations of potassium.[875]

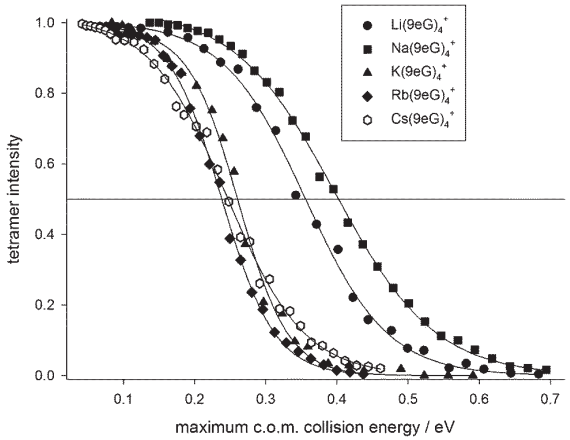

Figure 40. Gas-phase dissociation curves of alkaline metal MG_4^+ clusters as a function of the center of mass energy, assessed by SORI-CID. Figure reproduced with permission from Ref. 748. Copyright 2015 RSC Publishing.

In contrast, larger cations, such as K^+, NH_4^+ and Rb^+ form multi-quartet clusters with significant relative abundancies in ESI-MS.[748,864,868,873,875–877] Divalent alkaline earth metals predominantly form MG_8^{2+}-clusters, but no assemblies with more than two G-quartets.[866,867,872,874,877] The MG_8^{2+}-clusters of different divalent cations were compared in terms of their in-solution affinity through competitive ESI-MS assays[866,872], as well as their kinetic gas-phase stability through CID experiments[866], Both methodologies give the same relative ranking: $Sr^{2+} > Ba^{2+} > Pb^{2+} > Ca^{2+} >> Mg^{2+}$. For lanthanide cations,

the most abundant species are MG_8^{3+} and MG_{12}^{3+}, the latter being unique to trivalent cations, where one cation coordinates three G-quartets. The cations giving the more relative abundance of the MG_8^{3+} cluster is ranked: $Tm^{3+} > Dy^{3+} > Tb^{3+} > Eu^{3+} > La^{3+}$.[871]

4.1.1.1.3 Influence of the nucleotide backbone

The cluster formation of nucleobases, nucleosides and nucleotides has been compared.[863,867–869] K^+-mediated multi-quartet clusters (KG_8^+, $K_2G_{12}^{2+}$, $K_3G_{16}^{3+}$) were only formed with the nucleoside/nucleotide, but not the bare nucleobase. Consequently, the sugar moiety facilitates the stacking process of G-quartets, although its exact involvement in the formation of G-quadruplexes in solution cannot be elucidated solely from mass spectra.[868,869] The clusters $Na_2(dG)_3(rG)_5^{2+}$ and $Na_2(dG)_5(rG)_3^{2+}$ have the same CID fragmentation pattern, implying that the 2'-ribose hydroxyl group is not involved in G-quadruplex formation.[863] On the contrary, the G-quartet species $Ca_2(rG)_4^{2+}$ and the globular cluster $Ca_2(rG)_6^{2+}$ had different fragmentation patterns. At low collision energies the unspecific cluster lost guanine units, whereas low-energy fragmentation of the G4-cluster occurred on the sugar moiety. From these results one can derive that the nucleotide backbone does not stabilize the gas-phase structure of G4-clusters.[867]

4.1.1.1.4 Other metaclusters

Xanthine (X), which is a derivate of guanine, forms KX_4^+ and KX_8^+ clusters of significant intensity in ESI-MS spectra, when compared to other stoichiometries.[859] Hypoxanthine, which possesses no substituent in the 2-position, does not form any G4-type clusters with K^+, Mg^{2+}, Ca^{2+}, Sr^{2+} or Ba^{2+}, that could be observed in ESI-MS spectra.[859,878,879] On the contrary, 9-methylhypoxanthine does form quartets with alkaline metal ions.[879] This comparison of guanine derivates underlines the importance of H-donor/acceptor groups for the formation of specific nucleobase self-assemblies. Iso-guanine (isoG) is an isomer of guanine in which the $-NH_2$ group and the C=O group have swapped positions. The rearrangement of the Hoogsten-binding groups changes the bonding angle, which results in the formation of isoG-pentads, in place of G-quartets (Figure 41). The formation of the clusters $Li(isoG)_5^+$, $Li(isoG)_{10}^+$ and $K(isoG)_{10}^+$, involving methylated isoguanine, has been reported in ESI-MS spectra.[870,880] Finally, when guanine was modified with chalconyl-groups, irradiating the G-quadruplex with UV light makes the side-chains undergo a [2+2]-Diels-Alder reaction, creating a covalent link between different G-quartets of $K_3G_{16}^{3+}$. This reaction only occurred when the G-units were assembled into G4-clusters.[876]

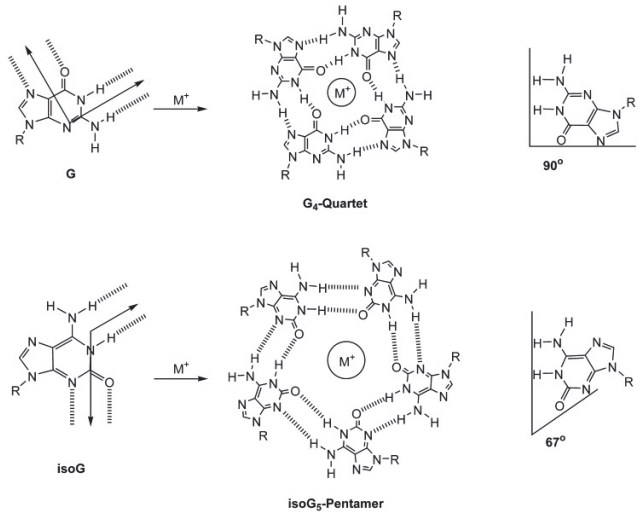

Figure 41. Different H-bonding geometries resulting in different magic number stoichiometries for guanine (top) and iso-guanine (bottom). Figure reproduced with permission from Ref. 880. Copyright 2004 Wiley.

4.1.1.2 Clusters of other canonical nucleobases

In addition to the previously introduced G4-clusters, magic number clusters of other nucleobases have been identified by ESI-MS. An overview is presented in Table 2. Unlike guanine, adenine does not form magic number clusters.[862,863] In the case of pyrimidines, the behavior of cytosine and thymine/uracil differs significantly. The cytidine trimer[863] and a cytosine tetramer[856] are magic number clusters, however the structure of a C-based meta-cluster could not be assessed through ESI-MS spectra. Thymine and uracil can also form planar H-bonded associates around a central cation. The size of the cluster depends on the size of the cation. The magic number clusters observed constitute of LiT_3^+/LiU_3^+, NaT_4^+/NaU_4^+ and MT_5^+/MU_5^+ (M = K, Rb, Cs, NH_4), as depicted in Figure 42.[861,862,881–884]

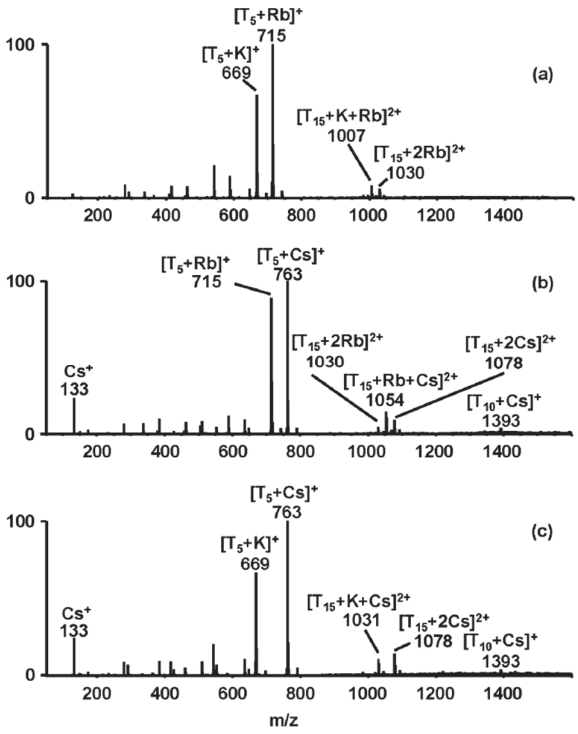

Figure 42. Competition between cations. ESI-MS spectra of 600 µM thymine with a) 200 µM KCl and 200 µM RbCl b) 200 µM RbCl and 200 µM CsCl c) 200 µM KCl and 200 µM CsCl. The stoichiometry of the most abundant species depends on the size of the cation. Figure reproduced with permission from Ref. 881. Copyright 2011 Wiley.

The magic number stoichiometries for thymine and uracil are often multiples of five, hinting at the formation of a T_5/U_5-meta-cluster. The clusters $M_2T_{15}^{2+}$ (M = K, Rb, Cs) mainly lose entire T_5-units when fragmented in a CID setup.[881] Based on the signal intensities in the corresponding ESI-MS spectra, the stabilizing effect of the cation on T-pentads was ranked in the order $Cs^+ \approx Rb^+ > K^+$.[881,885] However, although similar magic number clusters with lithium (LiT_{10}^+, LiU_{10}^+, $Li_2U_{20}^{2+}$) and sodium (NaT_{10}^+, NaU_{10}^+, NaT_{20}^+) formed under ESI-MS conditions, the CID fragmentation patterns of these clusters displayed statistically distributed losses of T/U-units.[881,882,886] ESI-MS of cluster of methylated and thionated pyrimidine bases has been performed in an attempt to determine which functional groups partake in the H-bonding network of the MU_5^+ assemblies.[885]

Thymine and uracil also form magic number clusters with Ca(II), i.e. CaB_6^{2+}, CaB_{10}^{2+}, CaB_{12}^{2+} and CaB_{14}^{2+}. MS^2 and MS^3 experiments concluded that these clusters have similar fragmentation patterns (with CaB_6^{2+} always being the smallest fragment) and they must therefore belong to the same type of meta-cluster. The structure of this meta-cluster has yet to be characterized.[855,856] The clusters below CaU_6^{2+} i.e. CaU_n^{2+} (*n* = 2-5) dissociate through sequential losses of either neutral or protonated uracil units.[887]

Table 2. Magic number clusters, as observed in ESI-MS

	G[748,858,859,861–869,871–876,878,880]	**A**[862,863]	**C**[856,862,863]	**T**[856,861–863,881,884,885]	**U**[855,856,862,863,882,885,886]
Li^+	LiG_4^+, $Li(dG)_4^+$	(none)	$Li(rC)_3^+$, $Li_2C_{15}^{2+}$	LiT_3^+ LiT_7^+ LiT_{10}^+ $Li_2T_{14}^{2+}$	LiU_3^+ LiU_{10}^+ $Li_2U_{20}^{2+}$
Na^+	NaG_4^+ $Na(dG)_4^+$, $Na(rG)_4^+$ $Na(dG)_8^+$, $Na(rG)_8^+$ $Na_2(dG)_{12}^{2+}$, $Na_2(rG)_{12}^{2+}$ $Na_3(dG)_{16}^{3+}$, $Na_3(rG)_{16}^{3+}$	(none)	$Na(rC)_3^+$	$Na(dT)_3^+$ NaT_4^+ NaT_7^+ NaT_{10}^+ NaT_{20}^+	NaU_4^+ NaU_7^+ NaU_{10}^+ NaU_{16}^+
K^+	KG_4^+, $K(dG)_4^+$, $K(rG)_4^+$ KG_8^+, $K(dG)_8^+$, $K(rG)_8^+$ $K_2(dG)_{12}^{2+}$, $K_2(rG)_{12}^{2+}$ $K_3(dG)_{16}^{3+}$, $K_3(rG)_{16}^{3+}$	(none)	(none)	$K(dT)_3^+$ KT_5^+ KT_{10}^+ KT_7^+ $K_2T_{15}^{2+}$	KU_5^+ KU_{10}^+ $K_2U_{15}^{2+}$
NH_4^+	$NH_4(dG)_4^+$ $NH_4(dG)_8^+$, $(NH_4)_2(dG)_{12}^{2+}$, $(NH_4)_3(dG)_{16}^{3+}$	(none)	(none)	$NH_4T_5^+$ $NH_4T_{10}^+$ $(NH_4)_2T_{15}^{2+}$	$NH_4U_5^+$ $NH_4U_{10}^+$ $(NH_4)_2(rU)_{12}^{2+}$ $(NH4)_2U_{15}^{2+}$
Rb^+	RbG_4^+	(none)	(none)	RbT_5^+ RbT_{10}^+ $Rb_2T_{15}^{2+}$	(none)
Cs^+	CsG_4^+, $Cs(rG)_4^+$, $Cs_2(dG)_{12}^{2+}$, $Cs_2(rG)_{12}^{2+}$	(none)	(none)	CsT_5^+ CsT_{10}^+ $Cs_2T_{15}^{2+}$	CsU_5^+
Ca^{2+}	$Ca_2(rG)_4^{2+}$ $Ca(dG)_8^{2+}$, $Ca(rG)_8^{2+}$	(none)	CaC_4^{2+}	CaT_6^{2+} CaT_{10}^{2+} CaT_{12}^{2+} CaT_{14}^{2+}	CaU_6^{2+}, CaU_8^{2+} CaU_{10}^{2+}, CaU_{12}^{2+} CaU_{14}^{2+}, CaU_{18}^{2+} CaU_{24}^{2+}

4.1.2 *d*-metal-cation assemblies

Apart from G4-clusters with lead (see 4.2.2.2), ESI-MS spectra confirm the formation of complexes between pyrimidine nucleobases/nucleosides and the d-metal cations Pb^{2+},[888–890] Cu^{2+},[891,892] and Mn^{2+}/Zn^{2+}.[893] Instead of being viewed as nucleobase clusters, these complexes can be better understood as organometallic complexes with the nucleobases acting as ligands. A potential method to determine the cation binding site on pyrimidines is $^{15}N/^{13}C$ isotope-labelled MS/MS. However, this methodology has only been carried out on protonated pyrimidine bases.[891]

Mn^{2+} and Zn^{2+} lead to different adduct stoichiometries than Mg^{2+} and Ca^{2+}. The most abundant adducts are $Mn(rC)_3^{2+}$ and $Zn(rC)_2^{2+}$, which coincide with the preferred coordination numbers of Mn^{2+} and Zn^{2+}, being 6 and 4, respectively. These coordination numbers allude to cytosine acting as a bidental ligand.[893] Cu^{2+} can oxidize uracil, as indicated by the presence of the species $[Cu(U\text{-}H)]^+$ in the ESI-MS spectrum. $[CuU_2 - H]^+$ has also been identified.[891] Pb^{2+} forms complexes with uracil, thymine and cytosine. MS/MS experiments identified the loss of a $[PbNCO]^+$ group, meaning that lead(II) ions most likely target an NCO-group, forming a bidental complex.[888,890] The protonation of cytosine causes a reduced intensity of Pb-C-complexes when compared with the less proton affine bases thymine and uracil.[890] Clusters of guanine with Cd^{2+} that have been identified by ESI-MS include CdG_n^{2+} (n = 2-8),

$Cd(rG)_n^{2+}$ (n = 2-8) and $Cd(9eG)_n^{2+}$ (n = 2-8). However, there were no "magical" intensities for the CdG_4^{2+} and the CdG_8^{2+} stoichiometries, and the formation of G4-clusters could not be verified.[860]

4.1.3 Protonated nucleobase assemblies

Clusters of canonical nucleobases with their protonated forms (pH < 3) have been reported by ESI-MS.[861–863] For all nucleobases, except cytosine, the base peak is the single-base species $[B + H]^+$. However, in the ESI-MS spectra of protonated cytosine nucleosides, the base peaks are the dimeric species $[dC_2 + H]^+$ and $[rC_2 + H]^+$.[863,894]

Yang and Rodgers studied the effect of base methylation and of the sugar moiety on the base pairing energy (BPE) of hemiprotonated base pairs, using threshold CID in a guided ion beam tandem mass spectrometer that ensures proper quantitation of the ion internal energies (Figure 43).[895] Excellent agreement between calculated and experimental energies suggest that the base pair models of Figure 43 are correct. Methylation affects the N3 proton affinity of the cytosine, which is correlated with the base polarizability. The proton affinity of cytosine has been also been determined elsewhere (1011 ± 9 kJ/mol).[896] These C-H^+-C type associations form the structural basis of i-motif assemblies, which are discussed in sections 4.3.4 and 4.4.3.

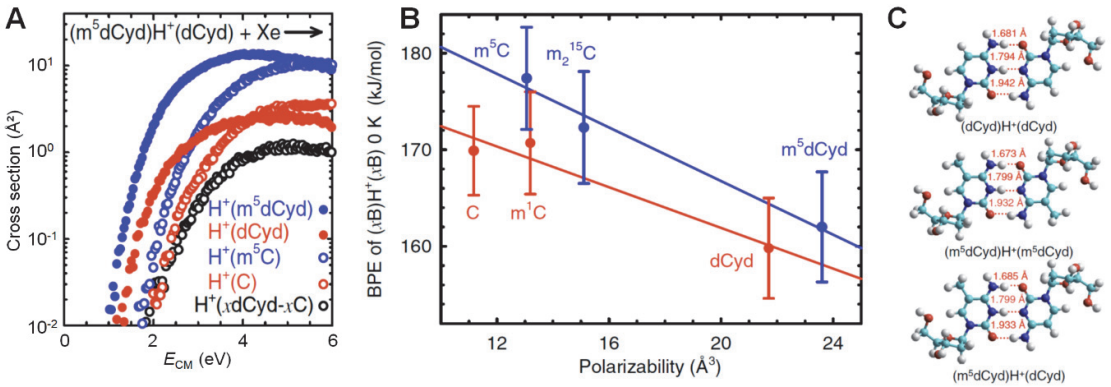

Figure 43. Effect of base methylation on the base pairing energy. A) Threshold CID results: reaction cross section as a function of the center-of-mass collision energy (E_{CM}). B) Base pairing energy (BPE) correlates with the polarizability of the bases. C) B3LYP/6-31G optimized geometries of the ground-state conformations of the $(dCyd)H^+(dCyd)$, $(m^5dCyd)H^+(m^5dCyd)$, and $(m^5dCyd)H^+(dCyd)$ protonated nucleoside base pairs. Figure adapted from Ref. 895. Copyright 2015 American Chemical Society.*

4.2 Cation binding to oligonucleotides

4.2.1 Monovalent cations

4.2.1.1 Ammonium

Mass spectrometry studies on the specific interaction between ammonium cations and oligonucleotides exclusively appear in the context of G4 systems. ESI-MS is a powerful tool to assess the stoichiometry of the complexes formed by NH_4^+ with monomolecular G-quadruplexes[198,300,608,897–900], bimolecular G-quadruplexes[300,513,514,898,901,902], tetramolecular quadruplexes[190,512,671,700,898,903,904] and other higher-order structures[512,629,710].

Ammonia loss is a common occurrence when analyzing NH_4^+-DNA adducts in mass spectrometry. Consequently, the energy uptake during the gas-phase transfer may give cause to a systematic bias against sensitive adducts within the distribution of ammonium adducts as observed in ESI-MS spectra. NH_4^+-stabilized G-quadruplexes have been preserved with increasing internal energy uptake within an ESI-IMS-MS setup, showing that specifically bound ammonium ions are more protected from ammonia loss than unspecific adducts. Nonetheless, even specifically bound NH_4^+ ions are susceptible to ammonia loss in less stable systems such as bimolecular and tetramolecular G-quadruplexes (see section 3.1.3). Thus, specifically retained NH_4^+ ions can be understood with the concept of magic number clusters: to be retained, they must have been present in solution but also must have been retained better than the nonspecific adducts in the gas phase. Such resilient ammonium adducts have a high signal intensity when compared to other stoichiometries, similar to magic number clusters, indicating the formation of G-quadruplexes. For every *n* specific NH_4^+ there are *n*+1 G-quartet (see section 4.3.3.2.1). Since the number of NH_4^+ ions corresponds to different m/z ratios, the stoichiometry of a G-quadruplex can be directly inferred from ESI-MS data.[190,300,512–514,629,671,898,899,901,903,904]

The fact that specifically retained NH_4^+ ions are indeed located in the G-quadruplex stem was probed by IMS. The loss of one single ammonium ion in a multi-quartet bimolecular G-quadruplex caused a significant change in its CCS value, indicating that in multi-quartet systems all cations are essential for maintaining the G-quadruplex structure. In further perspective, the possibility of utilizing such ammonium adducts, which would be considered 'fragile' in ESI-MS conditions, to confirm that any given experimental setup is applicable for native MS has been discussed.[300,513]

The influence of solvent on the formation of NH_4^+ mediated G-quadruplexes has been analyzed.[512–514] Two methods to confirm that the NH_4^+ ions are specifically bound inside the G-quadruplex have been introduced, which are 1) observing a significant difference in collision cross sections via IMS, given that G-quadruplex formation changes the conformation of the oligonucleotide strand[300,513] and 2) comparing K^+ and NH_4^+ in HDX-MS. In the case of specific binding, the number of gas-phase H/D exchanges remains constant, since the NH_4^+ protons are not interacting with the solvent.[671] The addition of less polar cosolvents accelerates the formation of multimolecular G-quadruplexes with ammonium and thus stabilizes them.[512–514]

4.2.1.2 Sodium

Sodium adducts of oligonucleotide strands have been reported mostly in ESI-MS on single-strands,[256,519,623,682,905–910] G-quadruplexes[203,616,670,911] and other high-order structures,[710,912,913] but also in MALDI-TOF MS.[912,914,915] Comparative studies on single-strand, duplex and triplex systems deduced a direct correlation between the number of phosphate groups and the number of sodium ions attached to the system.[912] Similarly, the number of sodium adducts on single strand DNA increases proportionally with the sequence length.[915] In great excess of sodium (e.g. 3 µM RNA vs. 40 mM NaCl) the highest number of possible sodium adducts in negative ESI-MS is equal to the number of

phosphate groups on the oligonucleotide strand.[519,912] Analysis of ssDNA in positive ESI-MS is possible, but requires adduct formation with the nucleobases.[519,912] CID fragmentation studies on single-stranded DNA found that Na^+ adducts are located at the center of the strand, whereas negative charges were located at the terminal ends.[907] The sodiation of a phosphate group changes the fragmentation pattern of ssDNA in CID. When no cations are present, base loss is a common fragmentation mechanism for all nucleobases except thymine. But in the presence of Na^+, pyrimidine bases become susceptible to base loss, whereas strand cleavage becomes more common for purine bases.[909]

Similar ESI-MS experiments with G-rich sequences highlight that Na^+ ions do promote the formation of G-quadruplexes.[203,616,670,911] ESI-MS titration experiments on the thrombin binding aptamer (TBA) concluded that the specificity of Na^+ ions binding to G-quartets vs. negatively charged phosphate groups is relatively low.[616,670] IRMPD was also used to localize Na^+ on the TBA sequence.[616] In similar experiments on polymorphic G4-sequences, Na^+ ions inside the G-quadruplex are susceptible to being replaced by competing cations, if they are present in solution, most notably K^+.[203,911]

4.2.1.3 Potassium

Potassium forms adducts with ssDNA where it presumably associates with the negatively charged phosphate groups located at the DNA backbone.[616,906] Potassium is also well-known for promoting the formation of more stable G-quadruplexes than other cations. Numerous studies have analyzed K^+-mediated G-quadruplexes of the thrombin binding aptamer (TBA),[616,670,880] various telomeric sequences[190,198–200,505,660,710,916] or other G4-forming sequences.[200,203,911,917,918]

The number of G-quartets in a G-quadruplex can be directly inferred from the number of associated K^+ cations, since they are a structural component of the G-quadruplex.[190,197–200,203,505,616,660,670,911,917,918] The same approach was used for NH_4^+ specific adducts, but K^+ has the advantage of not being labile upon collisional activation of negatively charged ions. Methodologies to confirm that the K^+ binding is indeed specific (inter-quartet) include 1) a comparative assay with multiple sequences that vary in G-richness[670] 2) using a G-rich sequence that does not form a G-quadruplex as a control in order to subtract unspecific adducts[198,199,916] or 3) monitoring the change of H/D-exchange rates by in-solution HDX-MS, given that specific cation binding induces a conformational change in the DNA strand.[771]

In the case of three-quartet quadruplexes, the separation of adduct states by *m/z* ratio also enables the determination of equilibrium dissociation constants K_D for both the 1:1 (K_{D1}) and the 2:1 (K_{D2}) complex. The equilibrium constants of various K^+-stabilized G4-quadruplexes have been determined by ESI-MS titration (Figure 44) after removal of the contribution of nonspecific adducts (see section 3.1.4.2.2).[197,199,203,616] ESI-MS titration experiments visualize and quantify the concentration-dependent shifts to different adduct states,[199,203,918] as well as cation exchange.[198,203,911] Potassium forms very stable quadruplexes, and can displace sodium[203,911] and ammonium[198] from preformed structures. Divalent cations such as lead[670,880,917], strontium[620,670,880] and barium[670,880] were also used for competition experiments.

Sections 4.3.3 and 4.4.2 provide more extensive discussion what was learned on G-quadruplex structures thanks to advanced mass spectrometry methods.

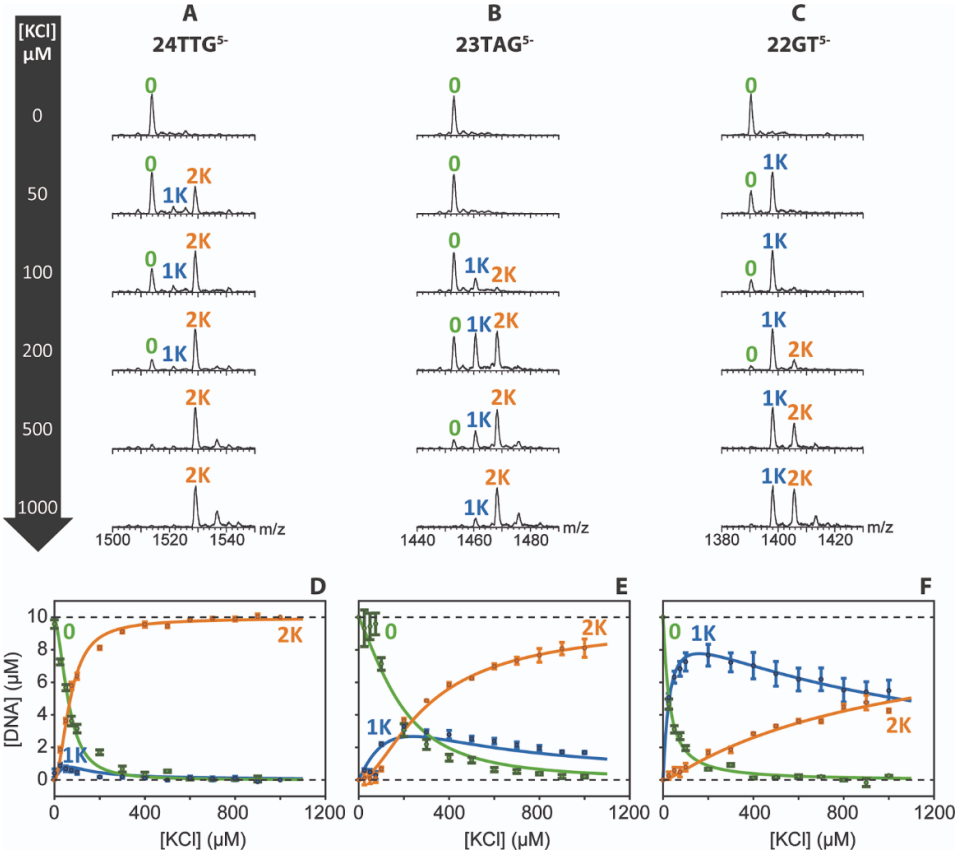

Figure 44. ESI-MS titration experiments of K^+ binding to G-quadruplex forming sequences. Due to the different m/z ratios, the K_{D1} and K_{D2} values may be determined independent from one another. Figure reproduced with permission from Ref. 199. Copyright 2016 Oxford Academic.

4.2.1.4 Other alkaline metals

Comprehensive studies of the alkaline metals Li^+, Na^+, K^+, Rb^+ and Cs^+ binding to DNA have been carried out in ESI-MS conditions. All alkaline metals form cation adducts where they most likely bind to the negatively charged phosphate groups located at the DNA backbone.[203,616,670,906,909,919] Na^+ and K^+ promote the formation of G-quadruplexes, whereas Li^+, Rb^+ and Cs^+ do not, which is presumably related to their respective ionic radii.[203,616,670,906]

4.2.1.5 Silver

Ag^+ cations can disrupt entirely Watson-Crick DNA duplexes, as demonstrated on the ESI-MS spectra of dG_{11}/dC_{11} and dA_{11}/dT_{11} duplexes, where after the addition of silver(I) cations no more duplex strand could be detected (Figure 45).[143] Apart from binding to single-stranded DNA, Ag^+ cations promote the association of C-Ag^I-C mismatches[142,143,145,920–922], G-Ag^I-G mismatches[143,145,921], and, to a lesser extent, A-T dimers[143]. The promotion of T-T- or A-A-mismatches by Ag^+ cations has not been observed in ESI-MS.[143]

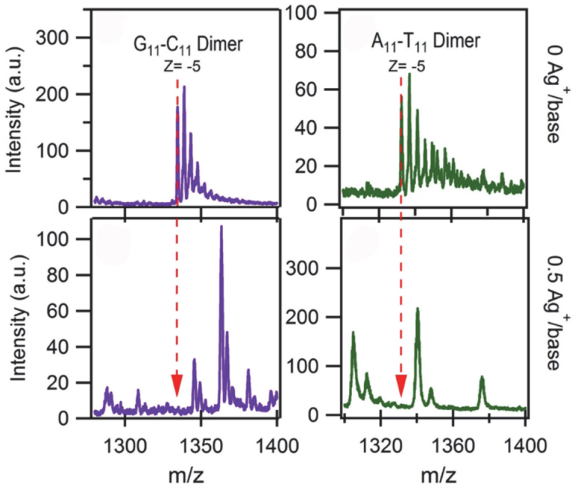

Figure 45. Disruption of Watson-Crick duplexes after the addition of 0.5 equivalents Ag^+ per base, as observed in ESI-MS. Figure adapted with permission from Ref. 143. Copyright 2015 Springer Nature.

The 1:1 stoichiometry for Ag^+ and C-Ag^I-C pairs in dsDNA has been confirmed by ESI-MS experiments.[142,143,145,920] Moreover, thiopyrimidine bases[147] as well as pyrrolo-cytosine bases[148] are capable of binding two equivalents of Ag^+, forming C-Ag_2-C pairs. ESI-MS titration experiments with duplex DNA containing a various mismatches showed that Ag^+ cations specifically target C:C mismatches[920] Ag^+-mediated C-C mismatches form stable DNA duplexes with polycytosine DNA strands[143,145] as well as G-rich DNA sequences[922].

As evidenced by ESI-MS spectra, guanine-rich strands associate into G-Ag^I-G type duplexes, similar to cytosine.[143,145,921] Furthermore, adding Ag^+ ions to preformed $(dTG_nT)_4$ tetramolecular G-quadruplexes induced a structural conversion into an Ag^+-mediated G-duplex, which demonstrates the capability of Ag^+ ions to disrupt the formation of very stable G-quadruplexes. Structural information about these G-duplexes was gained through IMS-MS. The results imply that Ag^+-mediated G-duplexes are linear and less flexible than their polycytosine counterparts.[145]

4.2.2 Divalent cations

4.2.2.1 Alkaline earth metals

Comparative studies among the alkaline earth metals Mg^{2+}, Ca^{2+}, Sr^{2+} and Ba^{2+} have been conducted by ESI-MS on the thrombin binding aptamer (TBA), a 15-mer DNA with forms a two-quartet G-quadruplex.[287,670] The equilibrium association constants of the 1:1 and 2:1 cation/TBA complexes were determined by ESI-MS titration (Figure 46). The K_{A1} values for Sr^{2+} and Ba^{2+} exceed the ones for Mg^{2+} and Ca^{2+} by a factor of 1000. Based on these results, Sr^{2+} and Ba^{2+} both form stable G-quadruplexes.[287] HDX-MS experiments performed on TBA found that when Sr^{2+} is added, less H/D exchanges occur within the same timeframe, revealing that Sr^{2+} binding to TBA changes its topology into a more compact structure, which confirms the formation of a G-quadruplex.[670] The binding stoichiometry of Sr^{2+} to telomeric G-quadruplexes has also been determined with ESI-MS.[923] The equilibrium dissociation constants of the cations Sr^{2+} and K^+ binding to TBA have been determined by ESI-MS titration (240 nM and 5000 nM respectively).[620] Through temperature-dependent ESI-MS titration experiments, the binding enthalpy of the Sr^{2+}-TBA complex was determined to be -17 kcal/mol.[620]

Mg^{2+} and Ca^{2+} do not help forming stable G-quadruplexes, which is attributed to their small ionic radii and comparatively high dehydration free energy. However, they are known to electrostatically interact with the negatively charged phosphate groups located at the DNA backbone.[287,519,670,906,908,909,919] An ESI-MS study of duplexes shows that Mg^{2+} forms adducts with Watson-Crick duplexes, whereas Ba^{2+}

does not.[924] This further implicates that Mg^{2+} and Ca^{2+} interact with the phosphate groups, whereas Sr^{2+} and Ba^{2+} have a stronger affinity towards the nucleobases, most notably guanine.[203,924] A comprehensive CID study points out that Ba^{2+}, Sr^{2+} as well as Ca^{2+} alter the fragmentation behavior of ssDNA (at high and low charge states) significantly more than alkaline or transition metal cations.[919] These results give the notion that alkaline earth metals induce some changes in the gas-phase structure of oligonucleotide strands.

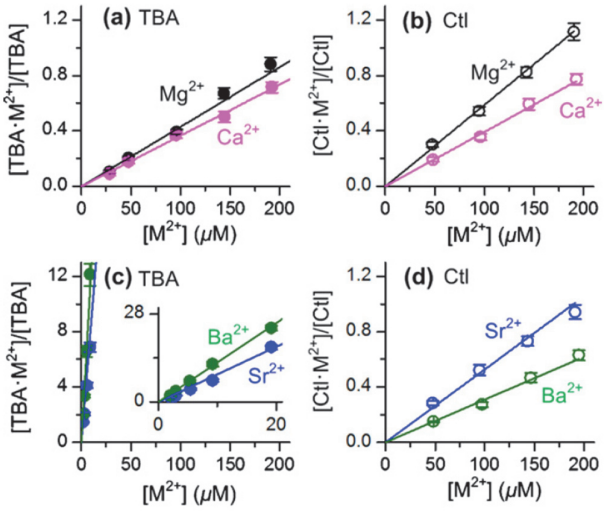

Figure 46. Binding of alkaline earth metal ions to (a,c) the TBA sequence dGGTTGGTGTGGTTTGG and (b,d) the control (Ctl) sequence dAATTAATGTAATTAA, which does not form a G-quadruplex. (a,b) Mg^{2+} and Ca^{2+} bind similarly to both sequences, while (c,d) Ba^{2+} and Sr^{2+} bind much better to the TBA sequence, suggesting a specific, inter-quartet interaction. Figure adapted with permission from Ref. 287. Copyright 2012 Elsevier.

Since volatile salts are preferable when working in ESI-MS conditions, Mg^{2+} is occasionally replaced by NH_4^+.[596,606,704,705,925–930] Mg^{2+} is nevertheless often required to form tertiary RNA structures, including RNA duplexes,[931] RNA kissing complexes (section 4.3.5),[697,931] and RNA aptamers (section 4.5.5).[932] This has been confirmed through ESI-IMS-MS experiments, where the addition of Mg^{2+} has induced a change in the CCS distribution towards more compact (i.e. folded) structures.[931,932] The necessity of Mg^{2+} ions to maintain tertiary RNA structures was further demonstrated in a nanoESI-MS experiment, where an RNA-enzyme complex could no longer be observed after Mg^{2+} ions were extracted from the complex by adding a chelating agent to the analyte solution.[682]

4.2.2.2 Lead

Pb^{2+} promotes the formation of two-quartet G-quadruplexes in G-rich sequences. The 1:1 stoichiometry was confirmed utilizing ESI-MS.[913,917,933] Competition experiments have been carried out with sodium[913], potassium[917] and strontium/barium[670]. Competition between Pb^{2+} and K^+ has been observed in time-resolved ESI-MS, where one cation may replace the other. In the same experiment, Pb^{2+}-K^+-G4 intermediates have been detected. It is implied that the G-quadruplexes formed with Pb^{2+} are more stable than those with Na^+ and K^+.

4.2.2.3 Transition metals

The interactions of transition metals with nucleic acids have been probed by mass spectrometry for Fe^{2+},[915,934–938] Ni^{2+},[256,910,919,934,939–941] Cu^{2+},[934,936,937,939–942] Zn^{2+},[910,934,935,937,939] Hg^{2+},[773,919,939,942–944] and Ce^{3+}.[937] Summarizing trends across cations shows that light metals, in particular alkaline and alkaline earth metals, favor electrostatic interactions. On the other hand, heavy metals, in particular transition metals, are more lenient towards covalent bonding. IMS-MS studies on Watson-Crick duplexes implicate that hardness/softness of metal ions as Lewis acids is a factor that contributes to a cation

favoring electrostatic/covalent binding.[256] Transition metals have a tendency to intercalate into duplex structures, promoting the formation of non-canonical base pairs. ESI-MS experiments confirmed that Ni^{2+} and Cu^{2+} may intercalate into DNA duplexes, but the binding mechanism remains unknown.[941] CID-MS confirmed that transition metals dianions alter the fragmentation path of 6-mer dsDNA. While the regular duplex (charge state 3-) mainly dissociates through ejection of nucleobase anions, dsDNA adducts with $Mn^{2+}/Fe^{2+}/Co^{2+}/Ni^{2+}/Cu^{2+}/Zn^{2+}$ (charge state 3-) have strand separation as their main fragmentation path.[934] This indicates that the presence of transition metal cations destabilizes the Watson-Crick duplex structure. On the contrary, these transition metal cations increase the gas-phase stability of singe-stranded ODN's, increasing the V_{50}- values (the collision voltage at which 50% of the complex has dissociated) of various 6-mer strands by about 2-fold.[910] This effect may be caused by divalent cations creating non-covalent cross-links between two phosphate groups and/or nucleobases.[910]

The promotion of non-canonical base pairings is most known for the cations Ag^{+} and Hg^{2+}. Mercury promotes T-Hg^{II}-T base pairings which has been demonstrated in various ESI-MS experiments (one example is shown in Figure 47) on duplex DNA,[773,944] synthetic duplex DNA,[942] singular polythymine strands,[773,943] and even G-quadruplexes.[945] Hg^{2+} does not disrupt the formation of G-quadruplexes, but instead targets thymines located in the loop sections,[945] where it most likely binds to the amine groups.[773] Experiments with thiothymines bear the same results.[147]

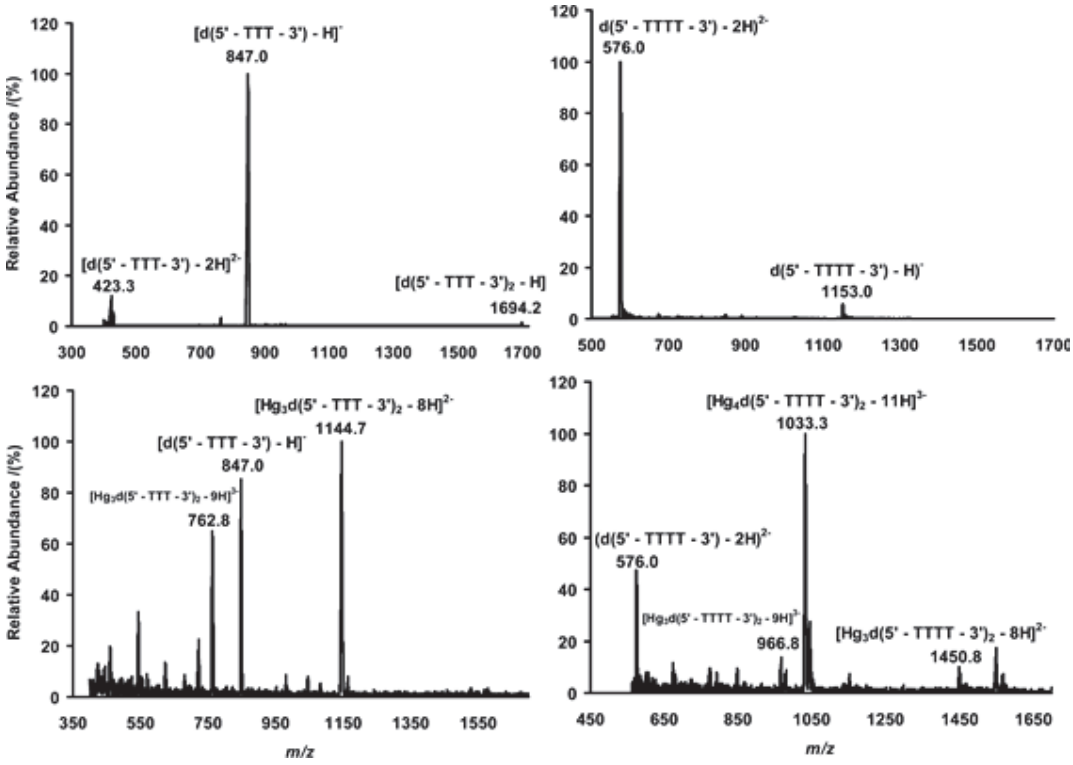

Figure 47. ESI-MS spectra of 20 µM DNA before and after adding 0.5 equivalents of Hg^{2+} per base. Figure reproduced from Ref. 773. Copyright 2010 American Chemical Society.

ESI-MS experiments reported Mn^{2+} adducts of aptameric DNA.[946] Mn^{2+} does not form specific interaction with G-quadruplex DNA.[670] According to similar experiments with chemically modified DNA the cations Co^{2+}, Ni^{2+}, Cu^{2+} and Zn^{2+} do not compete with Na^{+} in the formation of a tetramolecular G-quadruplex, indicating that they do not promote the formation of G-quadruplexes.[939] Zn^{2+} and Fe^{2+} form adducts with ssDNA, where they bind to phosphate groups at the oligonucleotide backbone, as

evidenced by CID fragmentation experiments.[935] In MALDI conditions, Zn^{2+} and Fe^{2+} may also target the nucleobases. Fragmentation experiments indicate a particular affinity towards guanine.[937] Ni^{2+} [940] and Mn^{2+} [946] mediate DNA-ligand interactions and integrate into the ligand-DNA-complex. Finally, uranyl ions (UO_2^{2+}) form adducts on the phosphate group of single-stranded DNA, as confirmed by ESI-MS/MS spectra.[908]

4.2.3 Trivalent cations

Adducts of 5-mer DNA with Fe^{3+} ions have been reported in ESI-MS. CID experiments on these Fe^{3+} adducts conclude that Fe^{3+} binds to phosphate groups. The presence of Fe^{3+} ions may stabilize the nucleotide backbone, as the main fragmentation pathway consists of nucleobase losses and no Fe^{3+} adducts of small fragments are observed.[935]

4.3 Multi-stranded assemblies

4.3.1 Double helices

4.3.1.1 MALDI-MS studies

Bahr et al. reported the detection and relative quantification of siRNA double strands by MALDI-MS under soft conditions and after denaturation with formic acid.[536] Using single strand RNA as internal standard, the relative intensities of duplex RNA were correlated with melting temperature and the number of GC base pairs in solution, indicating that MALDI-MS can be used as a method to determine the relative stability of double strands.

Determination of duplex DNA sequence and characterization of it structure was enabled by combining exonuclease III enzymatic digestion and MALDI-MS.[947] Thanks to the enzyme's high specificity for double strand in presence of divalent metal cation (such as Mn^{2+} to promote it activity), rapid and direct sequencing of 30-bp dsDNA was possible. MALDI-MS was also used to identified single-nucleotide polymorphism in duplex sequences by using DNA polymerase,[948–950] to detected the reduced cross-link structures in DNA duplex coming from reaction of an abasic site[951] and to analyzed the products coming from the hydrolysis of DNA duplex containing a site-specific G·U mismatch by uracil-DNA glycosylase[952]. The double-stranded DNA structure was also detected in the gas-phase by MALDI-MS in nonacidic matrices. Sudha *et al.* found a correlation between the duplex to monomer relative intensities with the amount of GC base pairs and melting temperature.[535] However, because of its greater softness compared to MALDI-MS and the fact it works directly from dilute solutions, ESI-MS is the most used technique to detect the formation of duplex structure.[953]

4.3.1.2 Detection by ESI

The earliest reports on detecting intact DNA duplexes by ESI-MS date back to the early days of native mass spectrometry.[954–958] Rodrigues *et al*. studied the noncovalent interaction between two complementary RNA sequences by microESI-MS.[959] The results showed the formation of RNA duplex in water from equimolar mixture of RNA oligonucleotides as well as the formation of ternary complexes.

Barylyuk *et al.* reported an interesting model system to study monomer-dimer equilibria by ESI-MS titration.[623] Seven 10-mers oligonucleotides were designed to be self-complementary DNA with same mass, chemical composition, and size but different sequences to avoid different ion transmission, different ionization efficiencies and different detection efficiencies in ESI-MS. The results showed that the K_D values determined by ESI-MS titration were lower than those determined in solution by isothermal calorimetry titration, due to a higher electrospray response factor of double strands relative to single strands.

Native chromatography coupled to sensitive ESI-MS was also used to study the formation of double helix structures.[560–562,564] The use of hexafluoroisopropanol/triethylamine ion-pairing buffer with a methanol gradient was able to separate single-stranded oligonucleotide components from the duplex. This method was capable of characterizing and separating duplex structure from non-duplex variants.[560] The results showed that the double helix was metabolized mostly from one end. LC-MS was also used to detect hetero-chiral complexes in duplex with 1',5'-Anhhydro-L-Hexitol nucleic acid (L-HNA).[564]

4.3.1.3 Fragmentation and dissociation channels

Dissociation of duplex DNA was extensively studied by fragmentation techniques such as CID. In addition to noncovalent dissociation of the duplex into single strands, other covalent bond fragmentation channels were observed. The dissociation of duplex DNA is a multistep unzipping

process. During unzipping, base loss occurs preferentially at terminal base pairs and this can induce the backbone fragmentation of one of the single strands (DS-frag in Figure 48A). The base loss can also be followed by unzipping to produce the regular single-strand fragments. The dissociation pathways of DNA duplex was studied by applying different collision regimes in a hexapole collision cell (fast activation) or in a quadrupole ion trap (slow activation).[960] In slow activation, base loss and strand fragmentation is favored, while in fast activation duplex dissociation into single strands is favored. This means that base loss has a low energy threshold and a rate constant $k(E)$ increasing less steeply with energy (Figure 48b), while the noncovalent dissociation is an entropy-favored process and thus the rate constant increases more steeply with energy (Figure 48B).

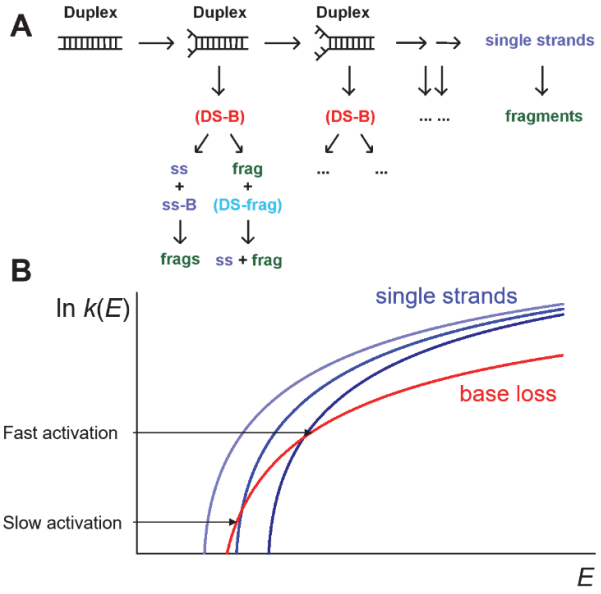

Figure 48. (A) Fragmentation channels of duplex DNA. Each partially unzipped state can undergo base loss and subsequent fragmentation. The detection of pieces of duplex with a missing fragment (DS-frag) led to conclude to a multi-step unzipping mechanism. (B) Dependence of unimolecular reaction rate constants for neutral base loss (red) and noncovalent dissociation of the duplex to single strands (blue) on the internal energy. In slow heating conditions, the reaction times are longer and the k(E) sampled are lower; this favors the base loss channel. In fast heating conditions, the reaction time is shorter and one must reach higher k(E); this favors dissociation of the duplex into single strands. Figure adapted from Ref. 960. Copyright 2002 American Chemical Society.

Griffey *et al.* reported the first study on the formation of DNA-RNA duplex by ESI-MS and MS/MS.[642] The authors detected and located the base pairs mismatches in 14-mer duplexes by monitoring base loss at low activation energy. The results showed that duplexes with A·C base pair mismatch displayed selective cleavage of A nucleobase and duplexes with C·C mismatches presented selective fragmentation for C nucleobase.

Madsen *et al.* studied the charge partitioning of DNA duplexes upon dissociation into the two constituent single strands by CID in ion trap mass spectrometer.[961] The factors affecting the asymmetric charge partitioning are duplex size, precursor charge state, GC base composition, and internal energy deposition. High charge states of large duplexes exhibited higher degrees of asymmetric dissociation than low charge states of small duplexes. The duplexes with high number of GC base pairs showed less symmetric charge partitioning than TA rich duplexes. The high collisional energy drives more asymmetric dissociation. 15-mer DNA-DNA duplexes and DNA-LNA hybrid duplexes were investigated by ESI-MS and CID.[962] The results demonstrated that the backbone nature can have strong effects on the dissociation of DNA duplexes. Similarly, a study on tricyclo-DNA conjugates, which are more rigid than the natural counterparts, shows a higher propensity for base

loss, which was attributed to changes in the activation entropy (pre-exponential factor) in the rigidified duplexes.[963] Burmistrova *et al.* showed by IMS that (18-bp)$^{7-}$ duplex rearrangements could occur at collision energies below those required for base loss or strand dissociation.[702] The dynamics of conformational changes of DNA duplexes in the gas phase was also studied by gas-phase FRET.[677,738] Danell *et al.* observed intermediate state of unzipping 14-mer duplex corresponding to weak binding. Together, these results suggest that in natural duplexes, rearrangements occur before total strand separation, and that modification altering these rearrangements potentially change the pre-exponential factor of Eq. (11), making it impossible to infer changes in threshold energies based solely on the extent of CID fragmentation.

Gabelica *et al.* studied the effect of irradiating 12-mer duplexes with a UV laser on electron photodetachment dissociation (EPD).[964] The results showed that the electron photodetachment efficiency depends on the number of guanines in the sequence and it is optimum near 266 nm. The combination of EPD followed by CID on the produced radical anions of single strand DNA^{3-} induced extensive fragmentation including neutral base loss, w, d, a• and z• series. In contrast, only neutral loses were detected for duplex and hairpin DNA at moderate collision energy of charge state 4-, suggesting that EPD could be used to probe higher-order structures of DNA and the kind of base pairing can prevents the loss of fragments. Similar results were obtained on hairpins (see section 4.4.1), and interpreted as base pairing preventing separation of the fragments.

4.3.1.4 Gas-phase kinetic stability

The kinetic stability of duplexes was studied, using different ways to increase the ion internal energy. In 1997, Schnier and co-authors studied the dissociation kinetics of 4-mer and 7-mer DNA duplexes by BIRD (section 3.2.1.1.1).[647] The reaction channels were cleavage of the noncovalent bonds to generate the single strands and cleavage of covalent bonds to produce base loss. The correlation of activation energies for the dissociation into single strands suggests that the Watson-Crick base pairing is conserved in the gas-phase. Gabelica *et al.* compared the kinetic stability of 16-mer duplexes in solution-phase and gas-phase by ion trap CID and by increasing the temperature of a source heated capillary,[965] and also found a good correlation between gas-phase kinetic stability and the fraction of GC base pairs. In a later study, they found that the hexapole-collision-cell MS/MS fragmentation yields of 16-mer DNA duplexes, with the same fraction of GC base pairs but different sequences, still correlate with ΔH_{diss} in solution.[966] These results suggest that both hydrogen bonding and base stacking interactions are conserved in the gas phase.

Similar to DNA duplexes, the gas-phase stability of RNA duplexes was also studied using ESI-MS and CID.[967] Yang *et al.* compared the kinetic stability of 16-mer and 12-mer RNA duplexes in gas and solution phases. In contrast to the solution phase, the results showed that duplexes with tandem mismatches G·A base pairs were more stable than the ones with Watson-Crick base pairs in the gas phase, indicating that hydrogen bonding can have a higher contribution than base stacking in the gas phase. In addition, MS/MS was able to differentiate between the stability of tandem- and single-mismatched duplexes. This type of comparison is more sensitive in the gas phase than in solution. Pan *et al.* reported a systematic ESI-MS and CID study of 9-mer DNA duplexes differing by the central base pair only, which was either a match or a mismatch.[968] The results showed correlation between (1) the solution stabilities, (2) the relative ion abundances in the ESI-MS spectra, and (3) the gas-phase kinetic stabilities upon CID.

4.3.1.5 Ion spectroscopy

Rosu *et al.* reported the UV spectroscopy of isolated ions of electrosprayed 12-mer DNA duplexes.[753] The results showed clear differences in UV spectra of duplex and single strands, with a red shift in the [duplex]$^{5-}$ compared to the [single strand]$^{3-}$, suggesting an effect of base stacking (however, a later

study cautioned that the charge distribution can also cause apparent shifts).[693] Hydrogen bonding was investigated using IRMPD spectroscopy.[747] A remarkable difference is observed in the spectrum of the GC-only duplex (Figure 49d) compared to its single strands (Figure 49c), with a specific band around 1680 cm^{-1} that is compatible with Watson-Crick GC base pairing. However, the AT-only duplex spectrum (Figure 49b) was similar to those of the constituting single strands (Figure 49a). Thus, although the presence of AT base pairs in the gas phase could not be confirmed, the presence of GC base pairs is attested, and this suffices to explain the influence of the fraction of GC base pairs on gas-phase kinetic stabilities.

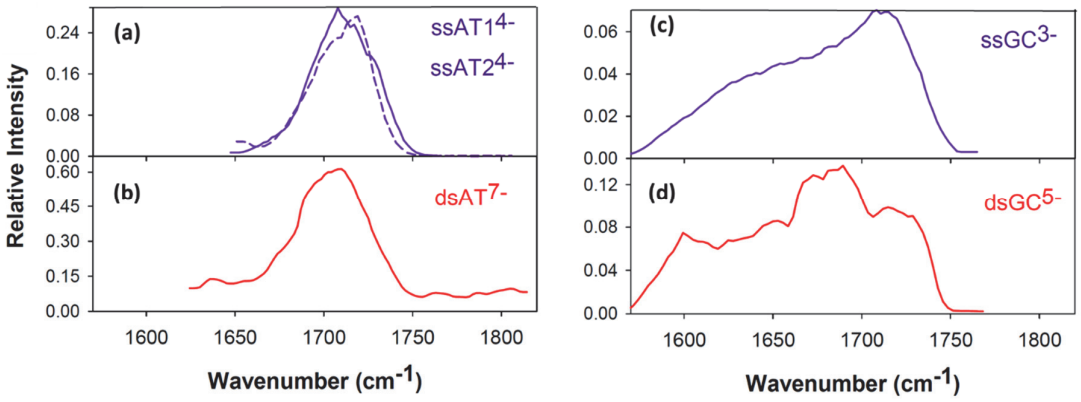

Figure 49. IRMPD spectroscopy of electrosprayed, multiply deprotonated DNA single strands and duplexes: (a) AT-only single strands ssAT14^{-} (sequence: dAAATTATAATATTAAA) and ssAT$_2^{4-}$ (sequence: dTTTAATATTATAATTT); (b) duplex dsAT^{7-} constituted by ssAT$_1$ and ssAT$_2$; (c) GC-only single strand ssGC^{3-} (sequence: dCGCGGGCCCGCG); (d) self-complementary duplex dsGC^{5-} (same sequence). Figure adapted with permission from Ref. 747. Copyright 2014 Springer.

4.3.1.6 Ion mobility spectrometry and molecular modeling

Dissociation studies thus suggest that both base pairing and base stacking is preserved in the gas phase. As soon as 2003, Rueda *et al.* reported the first molecular dynamics modeling of a [12-bp]$^{5-}$ duplex DNA in the gas phase.[722] This study also introduced the concept of modeling localized charges (choosing which phosphate groups are neutralized in the modeled system) or delocalized charges (spreading the charge by giving the proper fractional charge to each phosphate group). In all cases, the dimer is preserved even at high temperature, but the shape of the structure is rather distorted (Figure 50A), although GC base pairs are preserved.

Ion mobility spectrometry has the advantage of probing directly the shape of gas-phase structural ensembles, through measurements of their collision cross sections. Gidden studied the gas phase conformation of a series of poly(CG)$_n$ duplexes from 4 to 26 base pairs by ESI-IMS-MS and MD.[698,699] Based on the CCS measured for relatively high charge states (z/nt = 0.25, z being the absolute charge and nt the number of nucleotides) and CCS calculated on structures obtained with short unrestrained MD modeling, they concluded that short helices (up to 18-bp) adopt an A-helix form and longer a B-helix form (typical models are shown in Figure 50B). However, different results were obtained on DNA or RNA duplex structures sprayed from 150 mM aqueous NH_4OAc. In those conditions, lower average charge states are produced and the corresponding CCS values are much smaller (up to 30%) than predicted by unrestrained MD.[701] This confusing situation led some authors to propose scaling their CCS calibration method to match with the calculated CCS,[969] and others to scale their calculated CCS by a factor of 0.65 to match with the experiments (in that case, to assign antiparallel vs. parallel duplexes).[703]

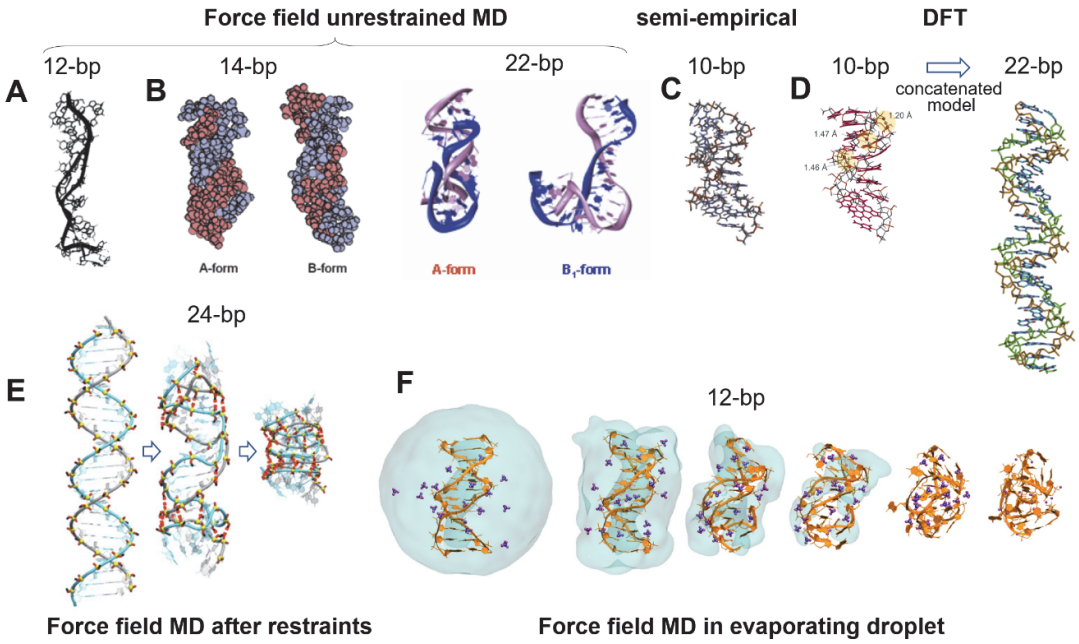

Figure 50. Retrospective of molecular modeling of charged duplex DNA in the gas phase. A) 250 ns force field MD on 12-bp $(dCGCGAATTCGCG)_2^{5-}$. Figure adapted from Ref. 722. Copyright 2003 American Chemical Society. B) 2-ns force field MD on $[d(CG)_7]_2^{7-}$ and $[d(CG)_{11}]_2^{11-}$ starting from a canonical A-helix or B-helix. Figures adapted from 698, Copyright 2004 American Chemical Society, and Ref. 699, Copyright 2007 American Chemical Society. C) Semi-empirical (PM7) optimization of $[d(CG)_5]_2^{4-}$, and D) DFT (M06-2X ,4-31G(d)) optimization of of $[d(CG)_5]_2^{4-}$, showing hydrogen bond formation between phosphate groups across the minor groove, and concatenated model that served to obtain the DFT trend line in Figure 51. Figures adapted from Ref. 701, Copyright 2017 American Chemical Society, and Ref. 145, Copyright 2018 American Chemical Society. E) Hypothetical model of a B-helix zipped by H-bonds across both the minor and major groove, thanks to restraints then force field MD, and F) compaction of $(dCGCGAATTCGCG)_2^{5-}$ modeled by force field MD in an evaporating charged water droplet containing the duplex^{22-} and 17 NH_4^+ ions. The last step of the modeling consisted of placing the protons on their nearest phosphate group and continuing the unrestrained MD on the gas-phase duplex. Figures adapted from Ref. 701. Copyright 2017 American Chemical Society.

Figure 51 displays experimental CCS values (Table 1), recorded in helium for duplexes (DNA and RNA) containing only CG base pairs (black data) or mixed sequences (red data), and each symbol corresponds to z/nt. Some intermediate charge densities were obtained from 150 mM NH_4OAc solutions in presence of supercharging agent. This figure highlights that the CCS values measured for a duplex depend largely on the charge density. The trend lines corresponding to canonical B-helices obtained by X-ray crystallography and to unrestrained force field MD best match with the CCS of the duplexes at high charge density, but not to those of duplexes sprayed in the most physiological conditions, resulting in low charge density.

Porrini *et al.* tested several models to find what such compact structures may be.[701] A duplex (22 negative charges) was placed in an evaporating droplet, and upon water evaporation the 17 NH_4^+ ions (final charge state: 5-) spontaneously placed themselves between phosphate groups across the grooves (Figure 50F). The Consta group independently tested droplet evaporation for different charge states, and found similar compaction for a 11-bp duplex 5-, and elongated or dissociated states at higher charge states.[970] Then larger models of dual groove zipping were generated by restrained MD (Figure 50E), to generate the trendline of "zipped helix" in Figure 51. This illustrates how compact the low-charge state duplexes could be. However, this is not the only possibility. In particular, base hydrogen bonding is rather disrupted in those models, which contradicts gas-phase kinetic stability and ion spectroscopy findings. Thus, higher-level calculations such as DFT were attempted on the 10-bp duplex $[d(CG)_5]_2^{4-}$. Compaction is higher than in unrestrained MD, yet base pairing and base

stacking are perfectly conserved. Hydrogen bonds have formed between phosphate groups across the minor groove. The trend line generated by concatenating these models fits well with duplexes up to ~20-bp. For longer duplexes, however, further compaction occurs, which could not yet be modeled, but one can suspect additional formation of P–O–H···⁻O–P hydrogen bonds. This illustrates that, at low charge states, Coulomb repulsion can be low enough that it may be more energetically favorable to form new (hence, non-native) hydrogen bonds in the gas phase.

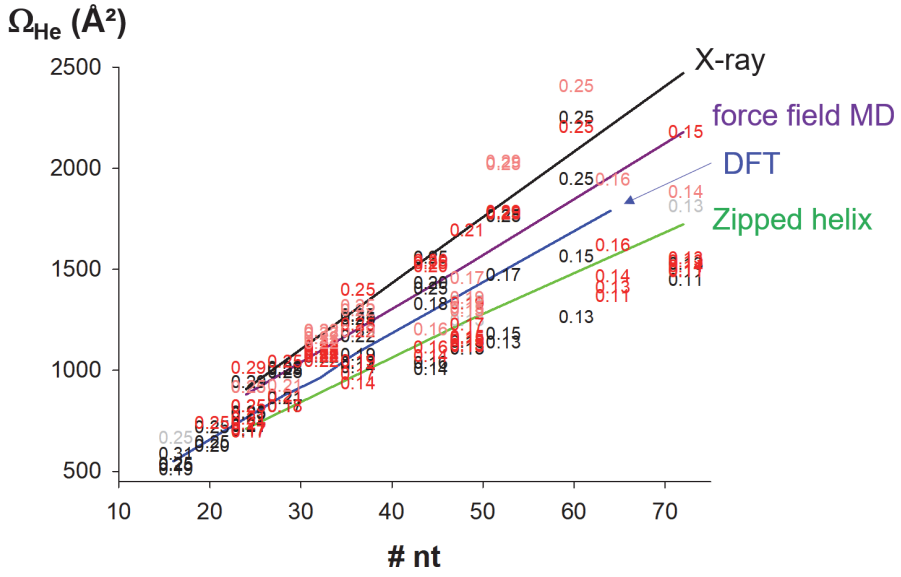

Figure 51. Collision cross sections in helium measured for duplex DNA and RNA, as a function of the number of nucleotides (compilation of data from references 145,698–702). The symbol is a number equal to the charge per nucleotide in the measured duplex. Black numbers are for sequences containing only CG base pairs and red symbols for mixed sequences. Lighter symbols are CCS of second minor peaks, if observed. The trendlines for X-ray canonical B-helix, unrestrained force field MD and zipped helix come from reference 701, and the DFT trendline comes from reference 145. See text and Figure 50 for further details.

4.3.2 Triplexes

In 2002, Rosu *et al.* reported the first study of a triplex DNA by ESI-MS.[926] The results showed, at pH 5.5, the detection of a 14-mer triplex at higher *m/z* values and under harsher source conditions than the duplex. The MS/MS of charge state 7- of the triplex revealed similar dissociation mechanism to solution folding, with separation between the Watson-Crick duplex and the third strand. Fragile TA-only triplex structures could be characterized by cold-spray ionization mass spectrometry.[527] CSI allowed to detect triplexes as short as 8-mers, although single strands predominate. When increasing the length of sequences up to 25-mers, only ion peaks of triplex were observed, suggesting higher stability for long forming triplex sequences. Later, Mariappan *et al.* studied the formation of short triplex (6-mers) by ESI-MS also in positive mode.[930]

Arcella *et al.* studied the formation of DNA triplexes in the gas phase using a combination of IMS-MS and long molecular dynamic simulations.[704] 12-mer and 18-mer triplexes were studied at neutral and acidic pH. The results suggest the preservation of triplex structure in the gas phase. In addition, the charge states distribution was shifted to high charge states at neutral pH and the CCS values decreased when the voltage was increased. The experimental and calculated CCS values were in good agreement.

Li *et al.* reported the formation of DNA-RNA triplexes by IMS-MS.[705] The results showed the formation of parallel DNA and RNA triplex from (GAA.TTC) 18-mers, 27mers and 36mers. The stability of triplex depends on the length of the oligonucleotides and the pH. In addition, the predominant charge states

of each sequence showed bimodal distributions with increase of CCS by increasing the length of the triplex.

The interaction of triplexes with ligands such as flavonoids,[596] cryptolepine,[606] neocryptolepine,[606] berenil,[930] netropsin,[930] distamycin,[930] acridine orange,[930] methylene blue[925] and mitoxantrone[928] was also studied by ESI-MS, as detailed in section 4.5.2.

4.3.3 G-quadruplexes

4.3.3.1 Bimolecular G-quadruplexes

Here the term "bimolecular" refers to the strand stoichiometry, while the term "G-quadruplex (G4)" refers to the core structure constituted of stacked G-quartets.[187,188] Bimolecular G-quadruplexes can be formed from sequences containing two G-tracks (four tracks being the minimum to form a G-quadruplex), as in the case of $dG_xT_yG_z$ sequence derivatives or two-repeat telomeric sequences $d(G_3TTA)_2$. Sequences with four G-tracks can, in addition to intramolecular G4, form higher-order stoichiometries such as bimolecular assemblies. Finally, sequences with one long G-tract (> 8 guanines) can, in addition to the expected tetramers, form lower-order stoichiometries.[904]

4.3.3.1.1 $[dG_xT_yG_z]_2$ and derivatives

The bimolecular G4 $(dG_4T_4G_4)_2$ is a good antiparallel G-quadruplex model for mass spectrometry studies because the folding is the same in NH_4^+, K^+ and Na^+.[92,971,972] It consists of a 4 G-quartets antiparallel-stranded structure with diagonal 'TTTT' loops.[972,973] It was studied early on, and used by our group in numerous ESI-MS ligand screening assays.[46,52,62–65] In ammonium, this bimolecular G-quadruplex is a very good test molecule for assessing the softness of instrumental tunings (see section 3.1.3). In very soft conditions, the complex with 5 ammonium (3 specific NH_4^+ between the G-tetrad and 2 extra ammonium ions presumably between the top quartets and the 2 loops) can be seen.[300]

Balthasart *et al.* discussed how faithfully the ammonium ion distribution matched with the known equilibrium binding constants of ammonium to the bimolecular G4 $(dG_4T_4G_4)_2$, $(dG_4T_3G_4)_2$, and $(dG_3T_4G_4)_2$ (Figure 52).[300] Extremely soft conditions (i.e., typically significantly lower voltages and temperatures than for other types of complexes) are required to conserve all the inner ammonium cations.[590] With some quadruplex sequences, not all inner cations can be preserved. ESI-MS of $(dG_4T_3G_4)_2$ revealed the 2-NH_4^+ stoichiometry (major peak) in all instrumental conditions, although the 3-NH_4^+ stoichiometry is expected based on solution data. For $(dG_3T_4G_4)_2$, the major population of two specific ammonium ion adducts matches well with the NH_4^+ binding sites postulated from solution.

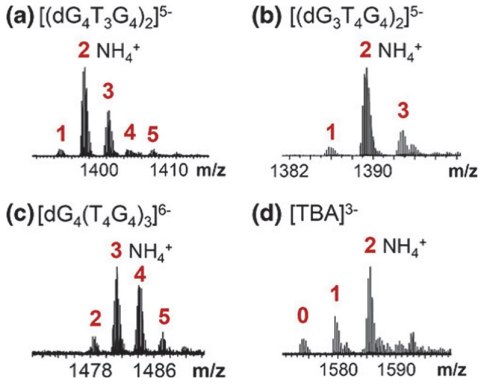

Figure 52. Ammonium ion distributions recorded using soft instrumental conditions on the Solarix ESI-FTICR instrument. Solution conditions: 100 % aqueous 150 mM NH4OAc with 10 µM DNA strand (a) $dG_4T_3G_4$, (b) $dG_3T_4G_4$ (Tdry gas: 150 °C), (c) $dG_4(T_4G_4)_3$ (Tdry gas: 220 °C), (d) $dG_2T_2G_2TGTG_2T_2G_2$=TBA. Adapted from Ammonium ion distributions recorded using soft instrumental conditions on the Solarix ESI-FTICR instrument. Solution conditions: 100 % aqueous 150 mM NH_4OAc with 10

µM DNA strand (a) $dG_4T_3G_4$, (b) $dG_3T_4G_4$ (Tdry gas: 150 °C), (c) $dG_4(T_4G_4)_3$ (Tdry gas: 220 °C), (d) $dG_2T_2G_2TGTG_2T_2G_2$=TBA. Figure adapted from Ref. 300. Copyright 2013 American Chemical Society.

The ease of ammonium loss depends on the charge state of the ion. Ion mobility spectrometry reveals that each ammonium ion loss is usually associated with a gas-phase rearrangement of the structure (Figure 53). Whatever the charge state, when three ammonium ions are present, the $^{TW}CCS_{N2\rightarrow He}$ is constant (~800 Å²). The three specific ammonium ions between the G-quartets thus stabilize the G-quadruplex structure in the gas phase. At low charge state (4-), upon activation, the structure of $(dG_4T_4G_4)_2$ with 2 ammoniums gets slightly more compact. At intermediate charge state (5-), the structure expands then contracts at high bias voltage. At high charge state (6-), the structure always expands.

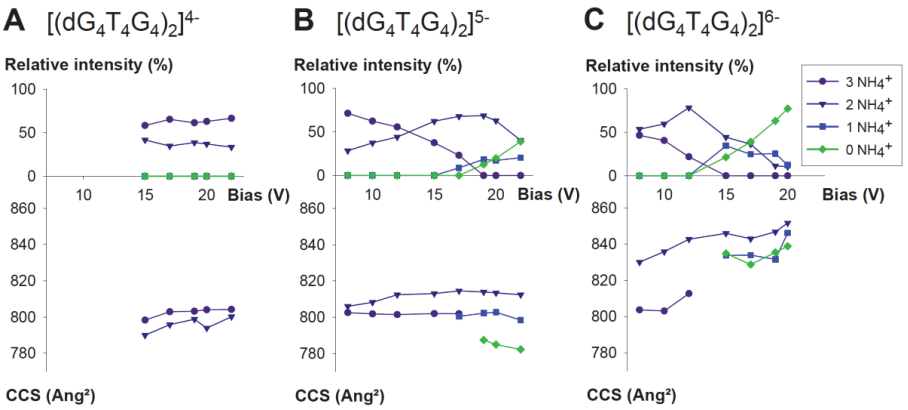

*Figure 53. Influence of the bias voltage on the number of preserved ammonium ions and on the collision cross sections (CCS) of the **bimolecular** G-quadruplexes at different charge states. The upper plots indicate the relative abundance of each species as a function of the bias. Figure adapted from Ref. 300. Copyright 2013 American Chemical Society.*

Finally, MS revealed that $dG_3T_4G_4$ and $dG_4T_4G_3$ can form trimolecular and tetramolecular assemblies in addition to the bimolecular assemblies.[901] ESI-MS is a key method to reveal unexpected strand stoichiometries.

4.3.3.1.2 Two-repeat human telomeric sequences

12-mer (2-repeat) telomeric sequences, forming bimolecular G-quadruplex in ammonium, were studied by ESI-MS and ion mobility spectrometry. The structures formed depend on the sequence variant (with different starting and ending bases). Solution-phase circular dichroism shows that $d(AGGGTT)_2$ and $d(GGGTTA)_2$ form hybrid or mixed dimers in the presence of ethanol, while $d(TAGGGT)_2$ and $d(TTAGGG)_2$ form parallel-stranded dimers.[514] The sequence $d(GGTTAG)_2$ forms a bimolecular G4 in ammonium as well.[975] In mass spectrometry, parallel-stranded structures always display more kinetically stable inner ammonium ions than antiparallel ones.[513,514] Note that $d(TAGGGT)_2$ was also studied in 1 mM KCl and 100 mM TMAA (no organic co-solvent), but in those conditions no bimolecular G-quadruplex did form.[976]

Organic co-solvents (methanol, ethanol, isopropanol, and acetonitrile) favor the folding of bimolecular G4s.[513] Quantitative analysis of the kinetic pathway showed that the presence of thymine at the 5'-end slows down the dissociation of parallel dimers.[514] Cosolvents accelerate the formation of bimolecular G4 up to ~200-fold at 60%, but have minimal influence on the dissociation rates. Methanol had a less strong G4 promoting effect than ethanol, propanol or acetonitrile.

Arrival time distributions (ATD) for $[d(TTAGGG)_2]_2^{5-}$ in aqueous ammonium acetate showed two peaks ($^{DT}CCS_{He}$ = 790 Å² and 838 Å²) at the lowest injection energy, which indicates the formation of two

distinct conformations (attributed to parallel and antiparallel conformations).[707] Based on molecular modeling, the extended conformation was associated to the parallel topology and the more compact one to antiparallel. Upon activation, the extended conformation disappears. A later study on $[d(TAGGGT)_2]_2^{5-}$ with the parallel/antiparallel proportions modulated by co-solvent showed three distinct mobility peaks: parallel ($^{TW}CCS_{N2\rightarrow He}$ = 850 Å²), antiparallel ($^{TW}CCS_{N2\rightarrow He}$ = 815 Å²) and collapsed ($^{TW}CCS_{N2\rightarrow He}$ = 775 Å²).[513] The compaction is associated with ammonium loss. The parallel structure is more resistant to ammonium loss and thus to collapse.

Telomeric RNA with two-repeat sequences can also form G-quadruplex structures. MALDI-MS detected several Na^+ clusters (n = 1 to 7) with the bimolecular complex of rUAGGGUUAGGGU.[914] In ESI-MS, the sequence $r(UUAGGG)_2$ was compared to its DNA counterpart in 100 mM NH_4OAc.[899] In addition to a bimolecular G-quadruplex, the RNA could also form a tetramolecular structure by stacking of two bimolecular subunits. The ammonium ions were more kinetically stable in the RNA than in the DNA bimolecular G4, again in line with a higher stability of ammoniums in parallel structures.

4.3.3.1.3 Fragmentation of bimolecular G-quadruplexes

The fragmentation pathways of bimolecular assemblies depend on the number of G-quartets. For G4s prepared in ammonium, the lowest-energy dissociation channel is ammonium loss.[300] The other CID pathways of $[(dG_4T_4G_4)_2]^{5-}$ and $[(d(T_2AG_3)_2)_2]^{5-}$ were guanine base losses from the parent ion as the major products, and strand separation as the minor products.[898] The lower relative abundance of single-strand products for $(dG_4T_4G_4)_2$ than for $(d(T_2AG_3)_2)_2$ was rationalized in terms of number of G-quartets, one additional G-tetrad giving extra stabilization.

4.3.3.1.4 Bimolecular complexes formed from 4-repeat sequences

The effect of loop length on the formation of multimeric assemblies have been tested with the G4 forming sequence ($dGGGW_iGGGW_jGGGW_kGGG$), (i, j, k = 1 to 3 or 4, W = A or T with equal probability) in 150 mM NH_4OAc.[710] The propensity for dimer and trimer formation is favored by short loops and these assemblies are most likely parallel. Dimerization was observed when the sequence contained single-nucleotide loops. Larger central loops restrict the stoichiometry to a monomer while 3' end loop has a larger impact than the 5'-end loop on the formation of higher-order G-quadruplex assemblies.

For the c-myc oncogene promoter sequence Pu22myc $dGAG_3TG_4AG_3TG_4AAG$, ion mobility experiment shows the formation of a parallel dimer structure *in vitro*.[710] Later studies showed that other c-myc G4 sequences such as $dG_4AG_3TG_4AG_3TG_3$ and $dTGAG_3TG_4AG_3TG_4AAG_2$ tend to dimerize in 100 mM NH_4OAc.[977] With unambiguous determination of the stoichiometries, ESI-MS highlights one of the caveats in using short oligonucleotides as models for *in vitro* biophysical studies. If the chosen model oligonucleotide is too short (e.g., when the G-quadruplex unit is starting and ending with a guanine), unexpected phenomena can occur *in vitro* (e.g., multimer formation).

Concentration-dependent dimerization by sequences T30923 $dG_3TG_3TG_3TG_3T$ and T30177 $dGTG_2TG_3TG_3TG_3T$ in presence of NH_4^+ have been studied by ESI-MS, with a determination of the amount of monomer and dimer formed with NH_4^+ (Figure 54).[978] For T30923 at 20 µM, the monomer dominates, while at 100 µM strand concentration the major peak corresponds to a stacked dimer with five NH_4^+ ions. These observations are supported by UV melting and previous solution NMR.[978,979] The 93del sequence $dG_4TG_3AG_2AG_3T$ exhibits a dimer peak with five NH_4^+ at all strand concentrations. Based on solution NMR studies an interlocked dimeric scaffold was proposed for 93del.[980] The elongation of loops by thymines can hamper the dimerization and favor the monomer conformation.

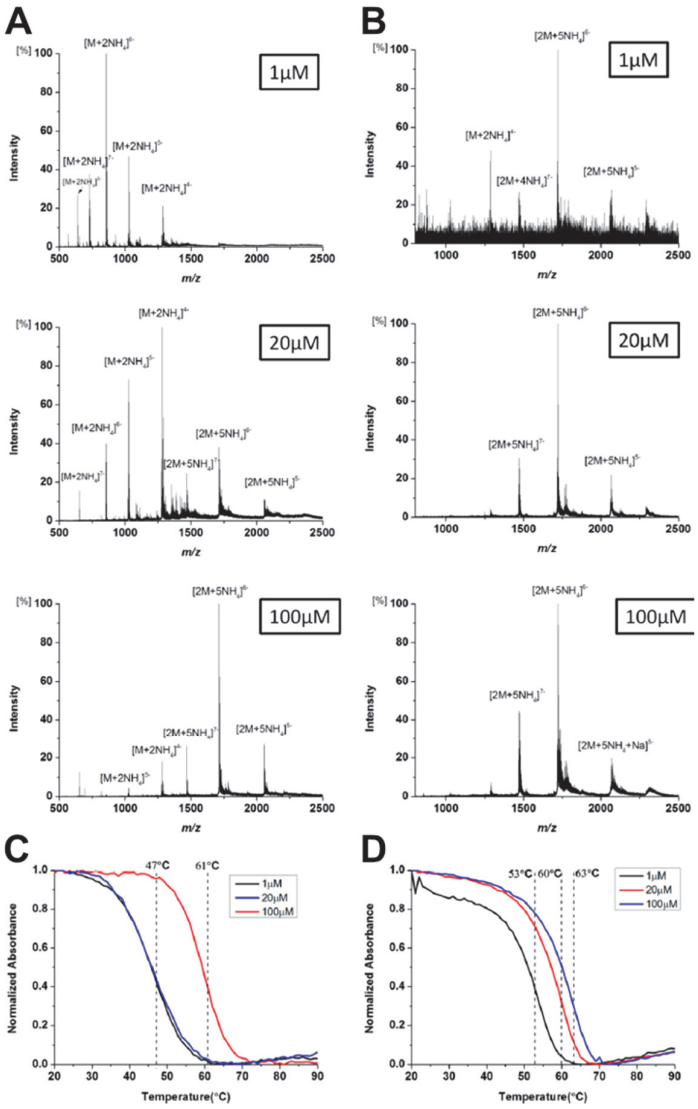

Figure 54. Mass spectra of A. T30923 and B. 93del obtained at oligonucleotide incubation concentrations of 1, 20, and 100 μM. UV melting curves of C. T30923 and D. 93del performed at the same strand concentrations as that in mass spectra. M in all mass spectra stands for monomer. Before the UV melting analysis, parts of the incubated samples were used for ESI-MS analysis. Figure adapted from Ref. 978. Copyright 2016 American Chemical Society.

Concentration-dependent dimerization of the bcl-2 oncogene $dG_3CGCG_3AG_2AAG_5CG_3$ was also studied by ESI-MS .[981] Apart from K^+ and NH_4^+, Na^+ and Pb^{2+} binding to dimeric quadruplexes has been observed by MALDI- MS.[913] For dTG_nT sequences with a long track of G (*n* = 12, 13) can form some dimer and it is favored at high NH_4OAc concentration.[904] Sequences with even longer G-track (*n* = 14-20) folded in dimeric structures in 150 mM NH_4OAc while at 10 mM NH_4OAc the monomeric species predominates.

The comparative ESI-MS study with 12-, 22- and 45-nt telomeric DNA (TTAGGG repeats) and their RNA counterparts (UUAGGG repeats) showed different self-assemblies in 150 mM NH_4OAc.[899] The shorter DNA sequences $d(TTAGGG)_2$ and $dAGGG(TTAGGG)_3$ predominantly formed monomeric species with a minor population of dimers, while the RNA counterparts formed dimeric and tetrameric assemblies. Longer sequences $dGGG(TTAGGG)_7$ and $rGGG(UUAGGG)_7$ form monomers. The number of trapped NH_4^+ ions (five) indicates a cation-induced stacking of two RNA G4 subunits. In a subsequent study, in NH_4OAc, ESI-MS identified monomers species for all 4 or 8-repeat telomeric DNA and 8-repeat RNA sequences, while for 4-repeat telomeric RNA the dimers predominate.[709] Tonomeric structure is

however always favored in TMAA+KCl.[899] Sr^{2+} stabilized a dimeric assembly from the telomeric sequence dAGGG(TTAGGG)$_3$.[923]

4.3.3.2 Tetramolecular G-quadruplexes

4.3.3.2.1 $[TG_nT]_4$ and analogues

The formation of a tetramolecular G-quadruplex depends on the length of guanine tracts and the number of the flanking bases in a given sequence. The first three G-quadruplexes reported by mass spectrometry were the tetramolecular assemblies $(dCGCG_5CG)_4$,[982] $(dT_2G_5T)_4$,[507] and $(dTG_4T)_4$.[926] The tendency of fifteen guanine-rich sequences to form tetramolecular G4 was studied by ESI-MS.[983] The impact of 9 different substitutions at each guanine of the sequence dTG_5T on the formation kinetics of the tetramolecular quadruplex $(dTG_5T)_4$ has also been studied by UV absorption and ESI-MS.[903] The number of bound NH_4^+ ions gives information about the number of effective G-quartets in the quadruplex. (*n*-1) ammonium ions are found in the $(dTG_nT)_4$ quadruplexes (Figure 55B). With the 8-oxoguanine mutation, four ammonium ions were detected in the tetramer $(dT\underline{8}GGGGT)_4$, suggesting that this modified tetrad forms a sufficiently stable architecture to keep the coordinated ammonium ion sandwiched between adjacent G4-tetrads. However, for all other modifications, an average of less than four ammonium ions is detected (Figure 55C).

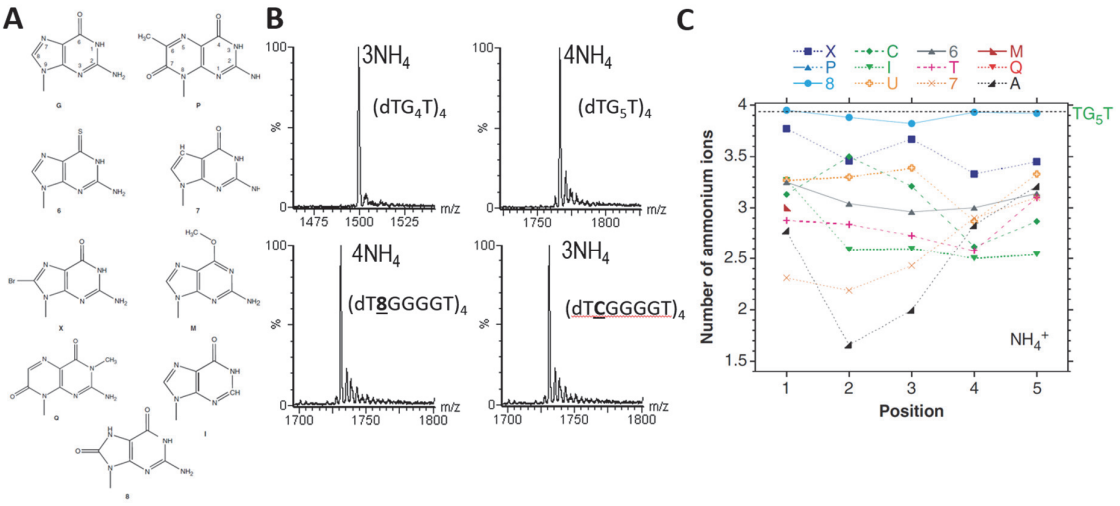

Figure 55. A) Chemical formulae of the bases tested here. I = Inosine; 6 = 6-thioguanine; 7 = 7-deazaguanine; 8 = 8-oxoguanine; P=6MI =6-methylisoxanthopterin; Q = 3MI = 3-methylisoxanthopterin; M = 6-methyl guanine; X = 8-bromo-guanine. Formula of the regular DNA and RNA bases (A, C, T, U) are not shown. B) Zoom on the 5- charge state of $(dTG_4T)_4$ quadruplex, $(dTG_5T)_4$, $(dT\underline{8}GGGGT)_4$ and $(dT\underline{C}GGGGT)_4$ quadruplex. 3 and 4 ammonium ions are detected with the model parallel quadruplexes $(dTG_4T)_4$ and $(dTG_5T)_4$ respectively. C) Effect of guanine substitution on the mean number of NH_4^+ ions present in the quadruplexes: MS analysis. ESI-MS spectra obtained in gentle condition help in understanding the formation of these tetramolecular structures, not only by providing the strand stoichiometry but also an unambiguous determination of the number of contributing structural cations. The position of each substitution is indicated on the x-axis. The mean number of ammonium ions (n_{NH4}) present in the complexes is obtained from equation: N_{NH4} = (4 x I($G4_{with\ 4NH4}$) + 3 x I($G4_{with\ 3NH4}$) + 2 x I($G4_{with\ 2NH4}$) + 1 x I($G4_{with\ 1NH4}$)) / Sum[I($G4_{all}$)] where I($G4_n$) are the relative intensities of the quadruplex with different number of ammonium ions. Figure adapted with permission from Ref. 903. Copyright 2007 Oxford Academic.

MS/MS on the tetramolecular quadruplexes show a sequential loss of the ammoniums as a function of the collision energy. Depending on the nature of the modification, different kinetics stabilities have been observed[903]. Substitution of deoxyguanosine with 8-aza-3-deaza-2'-deoxyguanosine interrupts the formation of quadruplex structures for the $(dTG_3AG)_4$ sequence as shown by the lower population of tetra-molecular species in ESI-MS.[984] Four contiguous guanines is not absolutely required to obtain a tetramer (see also section 4.3.3.2.2).

In NH_4OAc, sequences with longer G tracts (dTG_nT, n = 5—20) can form G-quadruplex trimers, dimers, and monomers in addition to the tetramers depending on n (Figure 56) and the concentration of NH_4OAc.[904] For n = 5—8, tetramers predominate; for n = 9—12 dimers and trimers were detected, for n = 13 or 14, monomers without ammonium (unfolded) are present in 10 mM NH_4OAc and dimers in 150 mM NH_4OAc. For n=15—20 only monomers with two ammonium ions are detected in 10 mM NH_4OAc, while dimers are detected in 150 mM NH_4OAc. Based on the stoichiometry unraveled by ESI-MS for $[(dTG_{15}T)_4 \cdot (NH_4^+)_2]$, a 3-quartet parallel-stranded model with three guanine loops was proposed,[904] a topology later confirmed by NMR spectroscopy.[985]

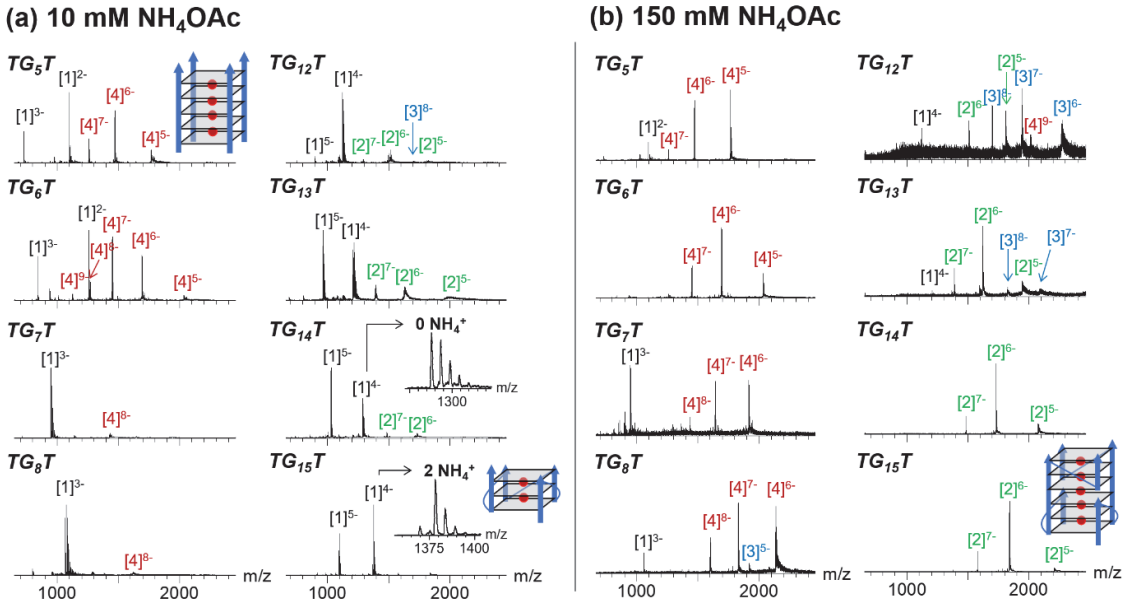

Figure 56. ESI-MS spectra of dTGnT sequences in a) 10 mM NH_4OAc or b) 150 mM NH_4OAc. Figure adapted with permission from Ref. 904. Copyright 2012 RSC Publishing.

Time-resolved ESI-MS revealed the pathways of NH_4^+-induced self-assembly of dTG_nT (n = 5—6) and the existence of kinetically trapped pentameric assemblies during the process,[512] such as tetrameric and pentameric assemblies detected with (n-2) and (n-1) bound NH_4^+, respectively. These stoichiometries experimentally confirm the existence of slipped-strand structures, which had been suggested by molecular modeling.[986,987] For dTG_4T, only tetrameric species with three bound NH_4^+ were observed. Methanol accelerates the formation of the G4s. Cao *et al.* could prepare mixed tetramolecular G-quadruplexes when mixing dTG_4T and dTG_5T and slowly annealing the preparation.[988]

Tetramolecular G-quadruplexes can also be formed in potassium and observed in ESI-MS. The first sample preparation is an annealing of the strands in potassium, followed by dilution in NH_4OAc. ESI-FTICR spectra showed a 3-quartet tetramolecular quadruplex formation with three bound cations for sequences $dT_4G_4T_3$ and $dT_4G_{10}T_3$.[989] A more robust preparation mixture with potassium for ESI-MS is 1 mM KCl in 100 mM trimethylammonium acetate.[198]

4.3.3.2.1 $[(dTG_4T)_4 \cdot (NH_4^+)_3]$: a model system to test gas-phase structural characterization methods.

The parallel-stranded tetramer formed by dTG_4T is easy to prepare and has a predictable structure. In ammonium, its detection with three specific NH_4^+ ion bound, i.e. $[(dTG_4T)_4 \cdot (NH_4^+)_3]$, ensures one deals with a preserved G-quadruplex, and molecular modeling confirms that the structures are very stable

in the gas phase, owing to the ionic interactions. Our group extensively used it as a benchmark for testing gas-phase methods on a known structure, for example molecule for gas-phase structural modeling,[706,724] gas-phase HDX-MS,[671] ion mobility spectrometry[700,706] (the CCS of the 5- charge state equals to 785 Å^2 in helium and 1000 Å^2 in nitrogen), gas-phase infrared action spectroscopy,[749] UV action spectroscopy,[693,753] and electronic circular dichroism ion spectroscopy.[190]

In contrast with the duplexes discussed above (section 4.3.1.6), the collision cross section of $[(dTG_4T)_4{\cdot}(NH_4^+)_3]$ is narrow and rather insensitive to the charge state, even in the presence of supercharging agents. This is a further proof of the rigidity of the complex in the gas phase. The IRMPD spectra of tetrameric quadruplex, $(dTG_4T)_4$ and its corresponding single strand showed a similar spectral signature in the PO_2^- vibrational region but the C=O stretching mode.[749] The redshift for the G-quadruplex is attributed to the H-bonding between guanine C=O and other bases and NH_4 ions.

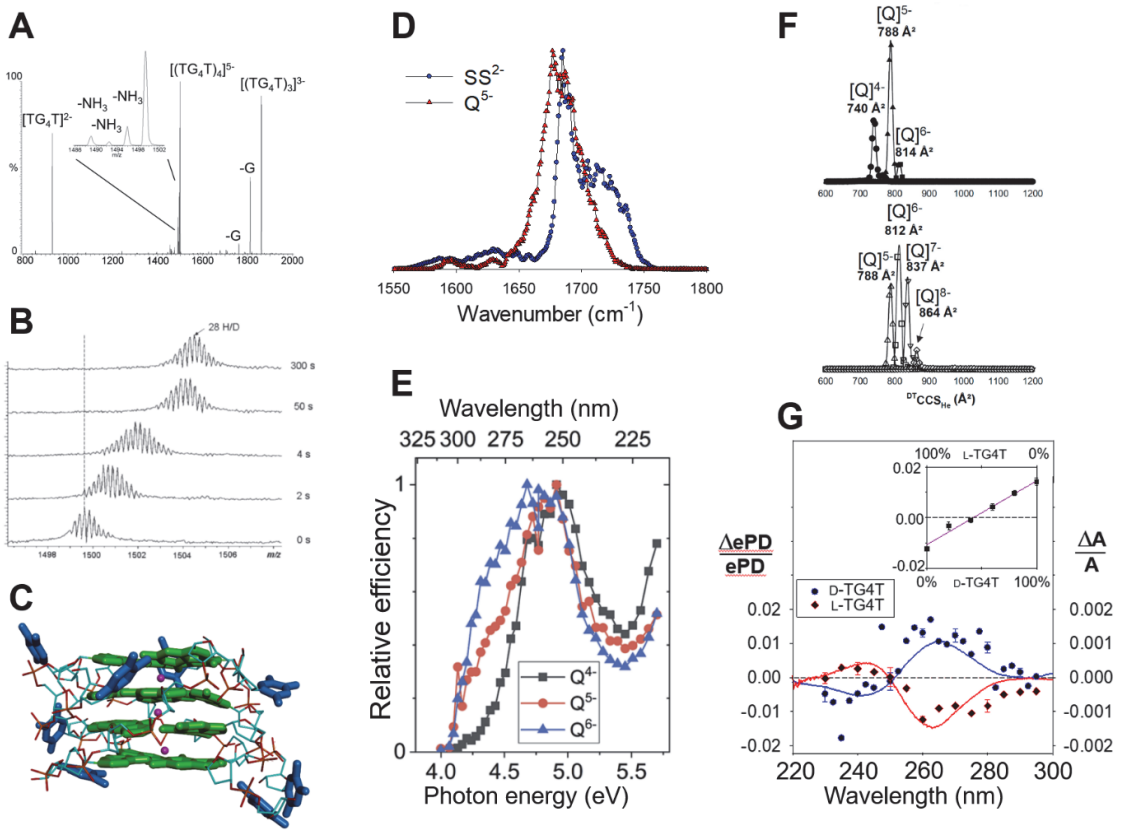

Figure 57. Gas-phase studies on $[(dTG_4T)_4{\cdot}(NH_4^+)_3]^{5-}$. A) slow activation CID MS/MS. Figure adapted with permission from Ref. 926. Copyright 2002 Wiley. B) Gas-phase HDX-MS in an FTICR-MS. Figure adapted with permission from Ref. 671. Copyright 2004 Wiley. C) Molecular modeling at the semi-empirical level (PM7). Figure adapted with permission from Ref. 190. Copyright 2020 AAAS. D) IRMPD spectroscopy compared to its single strand (unpublished data, higher resolution than those presented in reference 749). E) UV action spectroscopy at different charge states. Figure adapted with permission from Ref. 693. Copyright 2019 RSC Publishing. F) Drift tube ion mobility spectrometry in helium at different charge states (top) produced in 150 mM NH_4OAc and (bottom) in the same solution with addition of 0.75% sulfolane. Figure adapted from 701. Copyright 2017 American Chemical Society. G) Circular dichroism ion spectroscopy of the natural (D-) and enantiomer (L-) version of the quadruplex. The inset shows the CD signal measured at 260 nm with samples of varying proportions of D- and L- isomers. Figure adapted with permission from Ref. 190. Copyright 2020 AAAS.

4.3.3.2.2 Other tetrameric G-quadruplexes

NanoESI-MS detected tetramolecular assemblies with sodium adduct for the *tetrahymena thermophila* telomeric sequence dTG_4TTG_4T.[990] The parallel CD signature would support a model involving a stacked dimer of parallel-stranded bimolecular G4s. Another G4 sequence, the anti-HIV

aptamer dTG_3AG, can form a mixture of conformations including monomer, dimer, trimer, tetramer, and octamer (by stacking two tetramers) species as evident from the ESI-MS spectrum in 150 mM NH_4OAc.[630] The self-assembly kinetic pathways of dTG_3AG and its 5'-end conjugated analogs were studied by ESI-MS to understand higher-order quadruplex folding pathways. The rate of G4 tetramer and octamer formation was not affected by the derivatizations at the 5'-end. Similarly, $dTAG_3T$ can form monomeric, dimeric, and tetrameric assemblies revealed by nanoESI-MS.[991] It has been proposed that oligonucleotides with the $d(AG_nA)$ motif (*n* = 4 or 5) form slipped-strand tetramolecular G4s in acidic ammonium ions solutions.[992]

4.3.3.3 Other sequences & higher-order assemblies

Apart from the tetramolecular and bimolecular conformations, some G-rich sequences can produce higher-order assemblies by multimerization between several G-quadruplex units. NanoESI-MS showed the presence of tetramer and octamer species for the sequence dGGGT at two different strand concentrations, which were supported by solution-NMR and UV studies.[993] The ESI-MS spectra of dTGGTGGC showed the presence of tetrameric assembly, while dCGGTGGT and dCG_4T indicated tetrameric and octameric species in 150 mM NH_4OAc.[629] ESI-FTICRMS showed three and four NH_4^+ stoichiometries for $(dCGGTGGT)_4$ and $(dTGGTGGC)_4$, respectively, indicating a structural difference between the two tetrameric units. The incorporation of four NH_4^+ in the tetramer and eight NH_4^+ in the octamer for dCG_2TG_2T reflects the stacking of each tetrameric subunit within the octamer. Also, the dimerization of the tetramer to octamer was marked as the rate-limiting step during the interconversion process from monomer to the octamer.

Structural variations and preferences for self-organization among $r(AGG)_nX$, $r(CGG)_nX$, and $r(UGG)_nX$ trinucleotide repeat sequences (*n* = 2 or 4, X =A, C or U) have been studied by ESI-MS in conjugation with solution spectroscopic methods.[902] The ESI-MS spectrum of $r(AGG)_2A$ revealed monomeric and tetramolecular assemblies, while $r(AGG)_4A$ formed bimolecular assemblies with three NH_4^+. The NH_4^+ distribution suggested the cation-mediated stacking of four-quartet structures for both. $rG(CGG)_2C$ forms bimolecular (major) and tetramolecular (minor) assemblies. For bimolecular species, no ammonium ion adducts were detected which suggests the absence of G-quartet and thus the formation of mismatch-containing hairpins. For tetramolecular species the voltage-dependent study suggested the involvement of two NH_4^+ and thus the formation of three G-quartets. In contrast, $rG(CGG)_4C$ formed monomeric species (major) and bimolecular species (minor). The broad ammonium ion distribution at low bias voltage (soft condition) makes it difficult to interpret the G-quartet presence. $p(UGG)_2U$ (here "p" indicates that the RNA sequence starts with a phosphate group) showed monomeric and tetra-molecular assemblies in the ESI-MS spectrum. The progression of the ammonium ion distribution upon increasing bias voltage demonstrates the coordination of two ammonium ions in the structure for tetra-molecular species. For $p(UGG)_4U$ bimolecular assemblies detected with three NH_4^+ ions. This adduct distribution suggested the stacking of four G-quartets stabilized by NH_4^+ coordination. This comparative ESI-MS analysis proposed that $r(AGG)_4A$ and $p(UGG)_4U$ fold into bimolecular G4s while for $rG(CGG)_4A$ the results suggest the formation of hairpin conformations.

Modification of the phosphodiester backbone on the G-quadruplex formation has been studied by incorporation of an acyclic threoninol (aTNA); a sugar deficient backbone. As a function of the position of the aTNA on the sequence, the formation of a tetramolecular quadruplex is probed using ESI-MS.[994] Birrento *et al.* studied the formation of a bimolecular G4 and the hybrid duplex DNA/RNA by ESI-MS.[975] The results showed the detection of bimolecular G4 from telomeric DNA and hybrid DNA/RNA duplex in presence of RNA sequence. ESI-MS was able to show the loss of bimolecular structure signal and the increase of relative abundance of hybrid duplex. In addition, they studied the binding of both G4

and double strand with berberine that will be commented in the following section. Later, Tan *et al.* reported the dimerization of RNA G4 formed by miR-1587 by using ESI-MS and tandem MS.[995] The results showed that high concentration of NH_4^+ (100 mM) or molecular crowding environment such as methanol induced the formation of dimeric G4.

In summary, G-quadruplexes are most often observed as intramolecular, bimolecular, and tetramolecular species, and stacked subunits thereof. Mergny *et al.* had set the challenge to build a trimolecular G-quadruplex, which was successfully achieved by templating the self-assembly from three different subunits to form tri G-quadruplex, which was characterized by ESI-MS in 100 mM NH_4OAc solution.[996] Another intriguing construct consists of sequences with both a G-tract and a C-tract that, depending on the sample preparation method, form G-quadruplex and i-motif hybrids.[997]

4.3.4 i-motifs

Modi *et al.* studied the tetramolecular i-motif structure created from two DNA and two PNA strands by nanoESI-MS.[998] The mass spectra, together with CD and NMR spectroscopy, confirm the formation of tetrameric species. Later, the formation of tetrameric i-motif structures was reported by IRMPD spectroscopy and IM-MS.[711,999] Rosu *et al.* discussed the infrared spectroscopy of the dC_6 tetramer i-motif structure,[711] which is markedly different from the dC_6 single strand due to the broadening of the band at 1650 cm^{-1} related to the formation of the hemi-protonated C-H^+-C base pair. The modeling of IR spectra showed that this broadening is due to blue-shifts of the NH_2 scissoring modes and red shifts of C=O stretching modes.

Cao *et al.* reported interstrand i-motifs formed by several sequences containing a CCCC stretch, with different base residues located at the 5' and 3' termini.[988,1000] The results showed that a non-C base residue located at the 5'-end favored the formation of tetrameric structures with stabilizing effect of thymine bases. In addition, they observed the formation of hybrid i-motifs with penta- and hexa-strands (Figure 58), and detected trimeric ions when they applied collision-induced dissociation to tetramolecular ions. In another study, the impact of the length and position of a guanine repeat on the formation of tetrameric i-motif structures was studied by ESI-MS.[997] The results showed that sequences dTG_mAC_n ($m < n$) formed a stable tetra-stranded i-motif with relative long G-repeats at two ends. In addition, dTG_4AC_7 is able to form nanowire structures composed of antiparallel tetrameric i-motifs and parallel tetrameric G4s under acidic conditions in the presence of potassium cations.

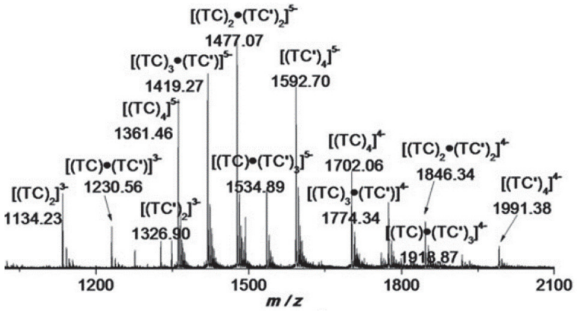

Figure 58. Mass spectra of 1:1 mixture of $d(TC_4T)(TC)$ and $d(TC_5T)(TC')$, incubated in ammonium acetate at 4 °C for 7 days. Figure adapted with permission from Ref. 988. Copyright 2016 Wiley.

Apart from tetrameric structures of i-motif, Garavis and co-authors reported the formation of dimeric small i-motif structures by NMR and ESI-MS.[1001,1002] The results confirmed a bimolecular i-motif stoichiometry formed by A and B boxes of human centromeric alpha-satellite DNA. PNA i-motifs also formed high-order assemblies such as dimeric, trimeric and tetrameric structures (see section 4.3.6).[211]

4.3.5 RNA kissing complexes

RNA kissing complexes are base pairs that can form especially in tertiary structures between two hairpin loops. The importance of this base paring on the stability of interstrand complexes was studied by Stephenson *et al.* by ESI-MS (Figure 60).[1003] The results showed the formation of kissing heterodimers stabilized by the stacked adenines in the GACG loop. The control sequence with mutated GUGG loop indicated only the formation of a monomeric hairpin and absence of dimeric structures. Later, Abi-Ghanem *et al.* reported the effect of wobble base pairs on the formation of RNA kissing complexes by native ESI-MS.[1004] The results revealed that the position and the nature of G·U wobble base pairs in the loop could influence the formation of kissing complexes due to the electrostatic phenomena of the entire loop region. Recently, the same authors investigated RNA hairpins and their kissing complexes by native ESI-IMS and molecular dynamics.[697] Both the RNA hairpin and kissing complexes showed more compaction in the gas-phase than in solution for low charge states at 150 mM ammonium acetate and in presence of Mg^{2+}. Then, high-level structure optimization was applied to understand the discrepancy between experimental and predicted CCS values. The results showed that base pairs are preserved but backbone rearrangements are responsible for this compaction.

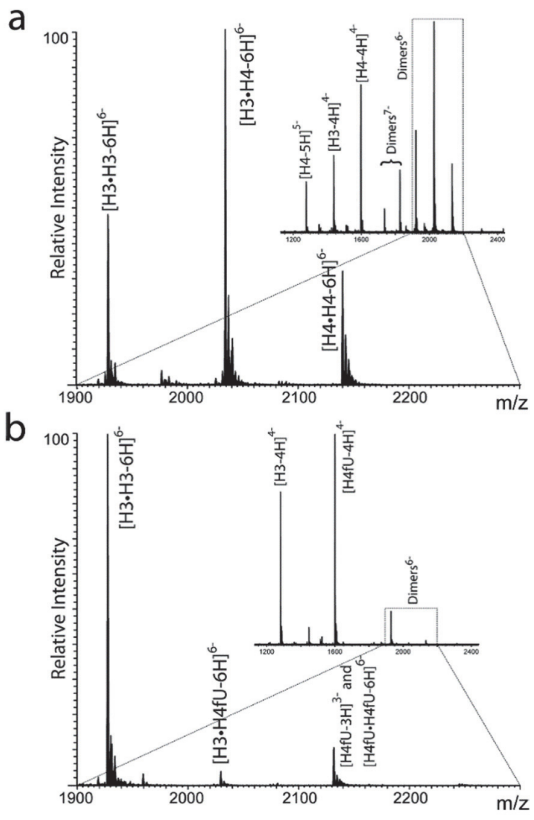

Figure 59. ESI-MS spectra of kissing interactions. Spectra obtained from samples containing (a) 1:1 GACG loops with light (H3) and heavy (H4) stems or (b) 1:1 GACG (H3) and GUCG (H4fU) loops in 150 mM ammonium acetate. Expanded views show the regions containing the 6− charge states of the dimeric species. Insets show full range spectra containing the corresponding monomeric species. Figure reproduced from Ref. 1003. Copyright 2013 American Chemical Society.

The interaction of a kissing-loop with proteins was also studied by nanoESI-FTICR (see section 4.6.3).[1005] Fabris *et al.* studied extensively the specific interaction between HIV-1 nucleocapsid protein and RNA involved in genome's packaging by nanoESI-FTICR.[1006–1008] The results showed two distinct binding sites on the apical loop and stem-bulge of the monomeric stemloop 1 (SL1) structure, which contains the dimerization initiation site. The stem-bulge provided feasible binding sites in both the

kissing-loop and the extended duplex forms of dimeric SL1. In the subsequent publications, SL3 and SL4 domains were also investigated. Binding to the apical loop competes directly with the annealing of self-complementary sequences to form a metastable kissing-loop (KL) dimer. In contrast, binding to the stem-bulge affects indirectly the monomer-dimer equilibrium by promoting the rearrangement of KL into the more stable extended duplex conformer.

4.3.6 PNA self-assemblies

Peptide nucleic acid (PNA) probes can self-assemble among themselves to form various multimeric construct which mimics G4 architecture. They can be used as a G-quadruplex ligand or they can hybridize to quadruplex in presence of a G4 template or GC-rich double helix DNA in addition to their self-assembling behavior.[1009,1010] In both scenarios, ESI-MS can be used to determine the stoichiometry of the noncovalent complex and the PNA-G4 hetero quadruplex. H/D-exchange MS can be further used to probe additional information about the H-bonding network in the complex.

The first G-quadruplex based only on PNA was studied by Krishnan-Ghosh *et al.* by nanoESI-MS.[189] The results indicate the formation of a G4 structure in both water and D_2O. The H/D exchange showed the deuteration of only 13 sites per monomer. The other six protons were protected and involved in the formation of the three tetrads of the G4. Later, Paul *et al.* reported the formation of hybrid PNA/DNA G4s from the interaction of G-rich PNA and three repeat guanines fragment of telomeric DNA by nanoESI-MS.[1011] They detected bimolecular complexes associated with NH_4^+ and K^+. PNAs having two G-tracts separated by an abasic linker can invade 3 quartets intramolecular G4s with long loops to form higher-order intermolecular hetero quadruplex with 5:1 and 6:1 PNA:DNA stoichiometries, which was confirmed by SPR.[1012] C-rich PNAs can bind to G4s to form an hetero DNA-PNA duplex.[1013]

Datta *et al.* reported the G4 formation between the PNA sequence H-$G_4T_4G_4$-Lys-NH_2 and homologous DNA strands by ESI-MS in positive mode.[1014] The results showed the formation of both dimeric and tetrameric G4 structures in presence of potassium, with a preference of dimeric quadruplex. NanoESI-MS identified the dimer ion peaks for self-templating PNA oligomer ($G_{SS}G$).[1015] The adduct distribution indicates the formation of a bimolecular PNA quadruplex which is further supported by the H/D exchange. Similar to DNA quadruplexes, G4-PNA was selective for K^+ over Cs^+.

The formation of PNA i-motifs was also studied by nanoESI-MS coupled with H/D exchange.[211] ESI-MS allowed to detect dimeric, trimeric and tetrameric structures. In order to study the non-covalent interaction in solution, hydrogen bonding of the dimeric species before and after H/D exchange showed that the five sites of hydrogen involved in N3 of the C-H^+-C base-pair formation were the strongest and less exposed to H/D exchange.

4.4 Probing intramolecular folding

In general, the mass measurement alone will not tell something about folding, with the exception of G-quadruplexes where specific cation binding indicates folding. For all other cases, one must use other mass spectrometry-based methods such as (1) observing the changes in charge state distribution, (2) solution or gas-phase reactivity, (3) ion mobility spectrometry, or (4) ion spectroscopy.

4.4.1 Hairpins, pseudoknots and cruciforms

Hairpins are a common secondary structure of RNA, and can also form in DNA. The interactions between hairpins (kissing complexes), between hairpins and ligands,[1016,1017] and between hairpins and proteins[763] have been studied by different MS techniques. These studies will be described in section 4.6.3.

In 2005, Guo *et al.* probed the intramolecular folding of DNA hairpins and single strands by ESI-MS.[1018] At high ammonium acetate concentrations, the charge state distribution was centered on lower charges for linear strands than hairpins of the same composition. Increasing the cone voltage and ammonium acetate concentration decreased the average charge state. By calculating the fraction of peak area of the most intense peaks and an internal standard, the authors found a higher response for the hairpins than for the linear strands.

Yu *et al.* reported different covalent probes and their cocktails to study the base pairing pattern in RNA hairpins.[763] They also characterized the complex formed by the RNA hairpin of HIV-1 and the nucleocapsid protein. The results showed that the loop bases of the hairpins were more exposed to modifying reagents in free RNA, but were effectively protected in protein-hairpin complexes.

Several fragmentation techniques (EDD, IRMPD, activated ion (AI) EDD, and EDD/IRMPD MS^3) were used to characterize three 15-mer DNA hairpins.[656] EDD, AIEDD and EDD/IRMPD generated different cleavage patterns, with less backbone fragmentation for the most stable structures in solution. EDD also provided additional structural information thanks to the preservation of non-covalent interactions. In contrast, IRMPD showed extensive backbone cleavage with no structural sensitivity.

Baker *et al.* studied the stability of various secondary structures such as hairpins, pseudoknots and cruciforms by ion mobility spectrometry.[696] The hairpins are more extended for high charge states than for low charge states at low ammonium acetate concentration (5 mM), presumably because they became single strands. The pseudoknot conformation is more stable than the hairpin because of the extra WC base pairs. In another ion mobility spectrometry study, molecular modeling showed that hairpins electrosprayed from 150 mM NH_4OAc (between 0.2 and 0.25 charges/phosphates) are more compact in the gas phase than in solution, because neutralized (protonated) and charged (deprotonated) phosphate groups form non-native hydrogen bonds in the gas phase.[697] Kissing complexes between hairpins undergo the same kind of compaction.

4.4.2 Intramolecular G-quadruplexes

As in intermolecular G-quadruplexes (section 4.3.3), specific cation binding observed by ESI-MS can directly inform on the folding, given that *n* specific cations bound indicates *n+1* stacked G-quartets. Most of the G-quadruplexes studied by ESI-MS are mentioned in Table 3 in section 4.5.3. Besides, the various monovalent and divalent cation-induced stabilization of G-quartets have been described in section 4.2. In this section, we will describe specific gas-phase experimental approaches, which can be coupled with native MS to provide structural information on G-quadruplex structures.

4.4.2.1 Choice of ESI electrolyte and validation of native solution folding in ESI condition

Native MS of quadruplexes was typically performed in NH_4OAc (10-150 mM, pH 7.0). In some reports, adding co-solvents (ethanol, methanol, hexafluoroisopropanol, isopropanol, acetonitrile) has been recommended to increase the signal-to-noise ratio, but the risk is to induce conformational changes (section 4.3.3.3).[505,513,514] Generally NH_4^+ adducts have a lower gas-phase kinetic stability for antiparallel conformations, but consequently the number of bound cations does sometimes not completely match with the number of G-quartets.[300,707] For studying intramolecular G-quadruplexes, NH_4OAc has also the disadvantage to enable bimolecular G-quadruplex formation from parallel-stranded topologies, alongside with the intramolecular ones. This was observed for example for some c-myc sequence variants[977] and for RNA telomeric G-quadruplexes (Figure 60B).[709,899]

Marchand *et al.* introduced the use of trimethylammonium acetate (TMAA) + up to 1 mM KCl to study quadruplex folding and ligand binding in K^+.[198] In TMAA/KCl, DNA and RNA sequences from four and eight repeats of telomeric DNA and RNA (TTAGGG and UUAGGG) were all (intramolecular) monomers (Figure 60).[709] In contrast to NH_4OAc, TMAA/KCl can does not favor multimer formation while probing intramolecular G-quadruplex sequences (compare Figure 60B and Figure 60D). A disadvantage of TMAA/KCl is the lower signal-to-noise ratio compared to NH_4OAc.

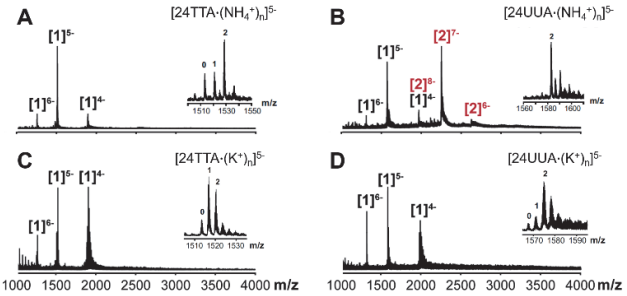

Figure 60. Negative mode ESI mass spectra of the telomeric DNA sequences 24TTA (d(TTAGGG)$_4$) and its RNA counterpart 24UUA (r(UUAGGG)$_4$), annealed in (A,B) 150 mM NH_4OAc or (C,D) 100 mM TMAA and 1 mM KCl. Final strand concentration is 10 µM. In peak annotations $[m]^{z-}$, m stands the number of strands and z− is the charge state; in the inset, n indicates the number of NH_4^+ or K^+ adducts. Figure adapted with permission from Ref. 709. Copyright 2019 RSC Publishing.

Another drawback is that, at 1 mM K^+, G-quadruplexes are less stable than in the usual high KCl buffer used in solution NMR and other biophysical experiments, or than in 150 mM NH_4OAc (in Figure 60, the 2-cation adduct is more prominent in NH_4OAc than in TMAA/KCl). As a result, the formation of misfolded and non-folded sub-states can occur to a significant extent. Moreover, since they are inherently polymorphic, there is a possibility of formation of an alternative fold in 1mM K^+. To clarify this issue, Ghosh *et al.* performed a systematic solution spectroscopic (CD, UV melting, and ^{1}H NMR) verification of the conformations of 28 intramolecular G-quadruplexes in native MS conditions (TMAA+KCl) and built an online database (https://ericlarg4.github.io/G4_database.html) of G4 sequences with sufficient stability and validated structures.[200] Parallel topologies are however over-represented in the database due to the lower stability of antiparallel and hybrid topologies in TMAA/KCl. In the future, this can be used to choose target sequences for MS-based ligand screening assay, and more sequences with unusual folding can be incorporated.

An excellent study by Su et al. investigated the folding of the human telomeric DNA sequences dA(GGGTTA)$_3$GGG in Na^+ and in K^+ using photocrosslinking of thymines into anti cyclobutene thymine dimers, and revelation with mass spectrometry.[1019] Such procedure did not require performing MS in native conditions. The study concluded that two hybrid structures and a basket-type antiparallel configuration coexist in potassium.

4.4.2.2 Folding thermodynamics inferred from temperature resolved ESI-MS

Thermal denaturation of intramolecular G-quadruplexes was studied by native mass spectrometry using a temperature-controlled nanoESI source (Figure 61).[638] Traditional UV and FRET-based melting experiments can only monitor the signal of population-averaged species and a two-state model is assumed during fitting.[1020–1022] However, the abundance of different sub-states (based on K^+ stoichiometry) can depend on the temperature during different enthalpy/entropy driving forces. For the sequence dTT(GGGTTA)$_3$GGGA, only two stoichiometries were observed: 2-K^+ (3-quartet) and 0-K^+ (unfolded single strand).[199] In contrast, for dTA(GGGTTA)$_3$GGG, a 2-quartet (1-K^+ complex) ensemble is observed and, upon temperature increase, its relative abundance first increases before total melting. This study used the cation binding stoichiometry states (0-K^+, 1-K^+, 2-K^+) to infer the abundances of three folding states (unfolded, 2-quartet and 3-quartet) and the G-quadruplex folding thermodynamics. Van't Hoff analysis shows that in all cases K^+-induced quartet formation is enthalpically favorable, but surprisingly the formation of the 2-quartet G-quadruplex is entropically favorable. This was rationalized in terms of predominant entropic contribution due to release of water molecules upon K^+ binding in the triplet and the less prominent rigidification of the system compared to ion binding in-between two G-quartets.

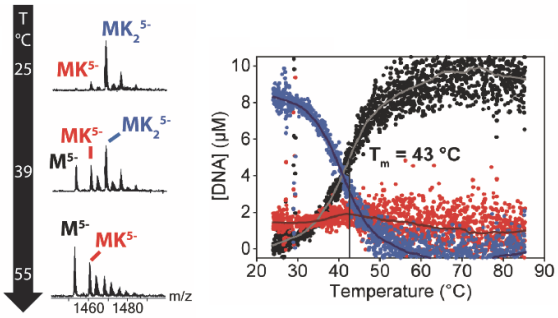

Figure 61. Thermal denaturation experiment of 10 μM dTA(GGGTTA)$_3$GGG in 100 mM TMAA and 1 mM KCl. Left: native mass spectra at different temperatures. Right: quantity of each stoichiometry as a function of temperature (after subtracting the nonspecific adducts contributions). Figure adapted from Ref. 638. Copyright 2018 American Chemical Society.

This approach was extended to multidomain (G-quadruplex/duplex hybrids and two-domain G-quadruplex homodimers) analytes, giving access to thermodynamics parameters of each unfolding step individually.[639] Unfolding events were detected by changes in mass caused by losses of potassium cations for G-quadruplex domains, or complementary strands for duplex domains. It was evidenced that duplex domains can be destabilized by quadruplexes at either their 5' or 3'-ends, but are conversely stabilized when both ends are G-quadruplexes. Stacking of consecutive G-quadruplex domains was also found to be energetically favorable, although the stacked interface melts at relatively low temperatures (< 40°C) compared to the G-quadruplex units themselves.

Using a T-jump electrospray source, one can also study the reincorporation of the K^+ as a function of time.[632] This allowed to determine the association and dissociation rate constants for the 1-K^+ binding to the sequence dA(GGGCTA)$_3$GGG, which was too fast to be characterized by manual mixing.[199]

4.4.2.3 Ion mobility spectrometry

Ion mobility measurements demonstrated the preservation of G-quadruplex structures in isolated deoxyguanosine clusters.[864] NanoESI-MS of d(T_2AG_3)$_4$ and d(T_2AG_3)$_6$ revealed the presence of single-stranded species, yet without NH_4^+ as dominant peaks.[707] Therefore, additional ion mobility in conjugation with molecular modeling was performed to understand whether quadruplex folding was retained in the ESI condition. The theoretical CCS values for the antiparallel chair and basket

topologies (with and without two NH_4^+) for $d(T_2AG_3)_4$ agree well with the experimental CCS values of the 5- charge state. Similarly, for $d(T_2AG_3)_6$, antiparallel chair or basket conformation was proposed with flanking G-rich segments in the 5'- or 3-end or one on each end. The shorter sequence $dGGG(TTAGGG)_3$ also adopts an antiparallel conformation based on ion mobility and molecular modeling analysis.[708] However, a clear distinction between chair and basket forms was not possible based on CCS values, and CCS values did not change significantly upon NH_4^+ loss. Two sequences from the c-myc oncogene d(GAGGGTGGGGAGGGTGGGGAAG) and d(TGGGGAGGGTGGGGAGGGTGGGGAAGG) have ion mobility data in line with a parallel-stranded conformation in solvent-free conditions.[708] For both telomeric and c-myc sequences, the conformations predicted from ion mobility and molecular modeling adopted the same fold as those of solution NMR derived topologies, which validates the hypothesis of preservation of solution memory in electrospray condition.[296,1023,1024]

The lowest charge states usually give a compact conformation while for higher charge states, extended and partially unfolded conformations were observed, presumably due to Coulomb repulsion. Ion mobility analysis in TMAA/KCl showed a marked difference between peak shape for 0-K^+ and 2-K^+ complexes, strongly suggesting a memory of the solution-phase conformation into the gas phase.[200] However, the longer the sequence, the broader the peaks and the lesser the difference between specifically folded and single-stranded compact conformations. Comparing the experimental CCS values with the theoretical model conformations from four and eight repeats of telomeric DNA and RNA (TTAGGG and UUAGGG) revealed that preservation of the folding of the solution structure in the gas phase is possible to some extent, but the structures may not be identical because of the charge state dependent rearrangement pathways in the gas phase.[709] In conclusion, structural validation based on ion mobility data alone is tricky. Higher-level quantum calculation methods might be essential to account for the rearrangements during desolvation and declustering processes. Yet, when the peaks are broad, many proposed structures can potentially be compatible with the results (Figure 62), and assigning a topology based on ion mobility spectrometry alone is challenging.

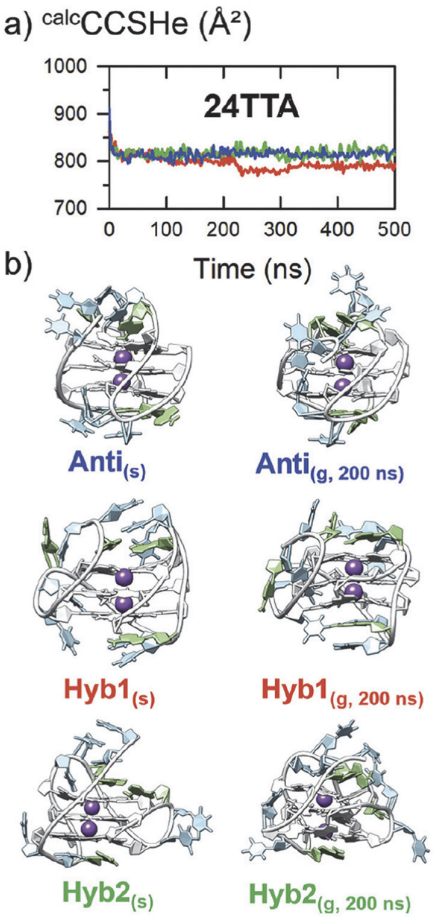

Figure 62. Evolution of the collision cross section as a function of gas-phase molecular dynamics for three models of d(TTAGGG)$_4$ (antiparallel, hybrid 1 and hybrid 2). Structures on the left are solution models extracted from solution MD, which served as starting points for gas-phase force field MD. Structures on the right are gas-phase structures extracted after 200 ns of gas-phase force field MD. Figure reproduced with permission from Ref. 709. Copyright 2019 RSC Publishing.

4.4.2.4 HDX/MS of G4

For intramolecular G-quadruplexes, adducts with monovalent and divalent cations may be due to nonspecific electrostatic interactions originating from the electrospray process. Gas-phase HDX reactivity may help distinguish secondary structures. Divalent metal ions (Sr^{2+} and Ba^{2+}) bind specifically to thrombin binding quadruplex aptamer d(GGTTGGTGTGGTTGG).[670] Gas-phase H/D exchange data revealed more protection of exchangeable sites in the presence of Sr^{2+} and K^+ due to metal ion-induced stabilization of quadruplex structures in the gas phase. However this is not necessarily general: for the (dTG$_4$T)$_4$ tetramer, gas-phase HDX was faster than for DNA duplexes or corresponding single-stranded species.[671] To date the general applicability of gas-phase HDX-MS has not been assessed.

In contrast, solution HDX integrated with nanoESI-MS showed a slow exchange of the (pTG$_3$)$_4$ tetrameric PNA quadruplex due to the formation of an H-bonded network by the guanines.[189] Largy and Gabelica established a robust workflow coupling native ESI-MS to solution HDX to probe the exchange rates of structured oligonucleotides over a wide time range (see section 3.3.1.4.1).[771] In TMAA/KCl solutions and "soft" conditions, the non-G4-forming control 24nonG4, whose sites are all available for exchange, is fully exchanged within a second. Conversely, the G4 24TTG exchanges much more slowly (several unexchanged sites after 5 minutes; Figure 63A), because some sites are H-

bonded in G-quartets. The exchange kinetics can highlight the influence of potassium concentration on G4 conformation dynamics: the 3-quartet conformation of the G4 222T (222T•2K$^+$) exchanges more rapidly at low K$^+$ concentration where it is destabilized (Figure 63B). Moreover, working under native MS conditions gives simultaneous access to the individual exchange rates of each binding stoichiometry. Hence, three conformers of 222T were mass-separated following their K$^+$ stoichiometry, showing that the 2-quartet conformation of 222T•1K$^+$ exchanges faster than 222T•2K$^+$, and 222T•0K$^+$ exchanges within a second owing to the absence of H-bonding (Figure 63B,C).

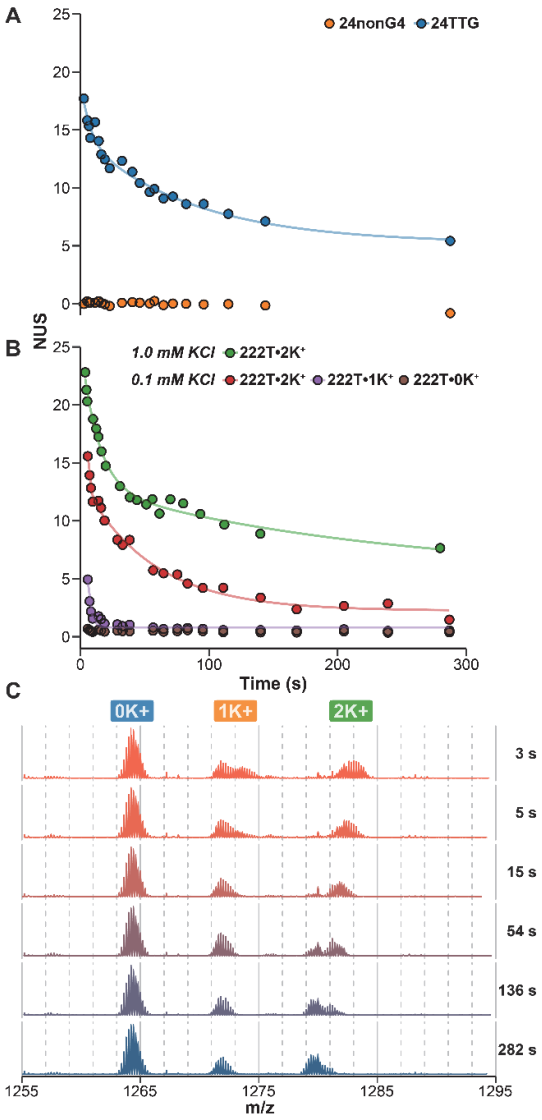

Figure 63. Hydrogen bonding status dependency of oligonucleotide native HDX/MS. Exchange kinetics acquired by continuous-flow HDX (90% to 9% D) of (A) unstructured (24nonG4; $dTG_3ATGCGACA(GA)_2G_2ACG_3A$) and structured (24TTG·2K$^+$; $TTG_3(TTAG_3)_3A$) oligonucleotides, and (B) the same oligonucleotide (222T; $T(G_3T)_4$) in the presence of 1.0 or 0.1 mM KCl, which leads to the formation of three distinct species (the G-quadruplexes 222T·2K$^+$ and 222T·1K$^+$, and the unfolded conformer 222T·0K$^+$). C. Corresponding spectra for 222T in 0.1 mM KCl solution, zoomed on the 5- charge state. The K$^+$-binding stoichiometry is indicated with labels. No exchange occurs in the explored time range for unfolded species (0 K$^+$), unlike the G-quadruplexes species (≥1 K$^+$). Figure reproduced from Ref. 771. Copyright 2020 American Chemical Society.

4.4.2.5 Ion spectroscopy

The hydrogen bonding status can be probed by vibrational spectroscopy. IRMPD spectra of the human telomeric DNA sequence,[749] dGGG(TTAGGG)$_3$ in the gas phase showed the distinct difference of C=O

stretching frequency compared to its single-stranded analog (0-K^+ adduct generated by activation in source) or the shorter single strand dTTAGGG (Figure 64). The redshift for the guanine C=O stretching frequency is explained based on cation induced H-bonding network present in the quartet conformation. Note that the carbonyl stretching frequency values match well with the solution IR data, which verifies the perseveration of the cation induced H-bonding network of the quartet in the gas phase, keeping in mind water does not interfere with the C=O stretching.

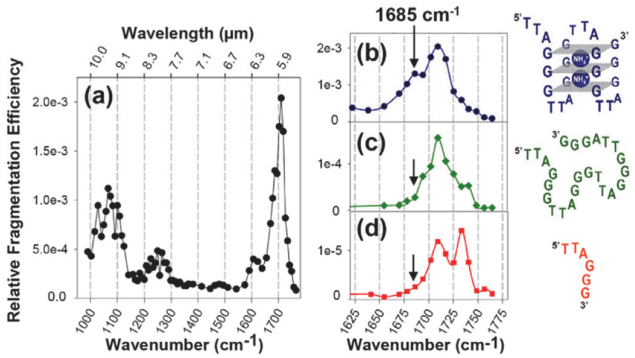

Figure 64. IRMPD spectra of telomeric DNA sequences. (a) Full-spectrum of $[d(TTAGGG)_4 \cdot (NH_4^+)_2]^{5-}$. (b-d) Zooms on the carbonyl stretch regions of (b) $[d(TTAGGG)_4 \cdot (NH_4^+)_2]^{5-}$, (c) $[d(TTAGGG)_4]^{5-}$, and (d) $[dTTAGGG]^{2-}$.

The base stacking pattern can be probed by electronic circular dichroism ion spectroscopy (see section 3.2.4.2 and Figure 34 therein).[190] This is especially valuable for G-quadruplexes, because parallel, antiparallel, hybrid and left-handed conformation have very distinct CD spectra.[758] The advantage of MS is the ability to obtain CD spectra for individual species that coexist in solution. For example, this was applied to the 1-K^+ (2-quartet) and 2-K^+ (3-quartet) stoichiometries formed by the sequence $dTAGGG(TTAGGG)_3$ (Figure 65).

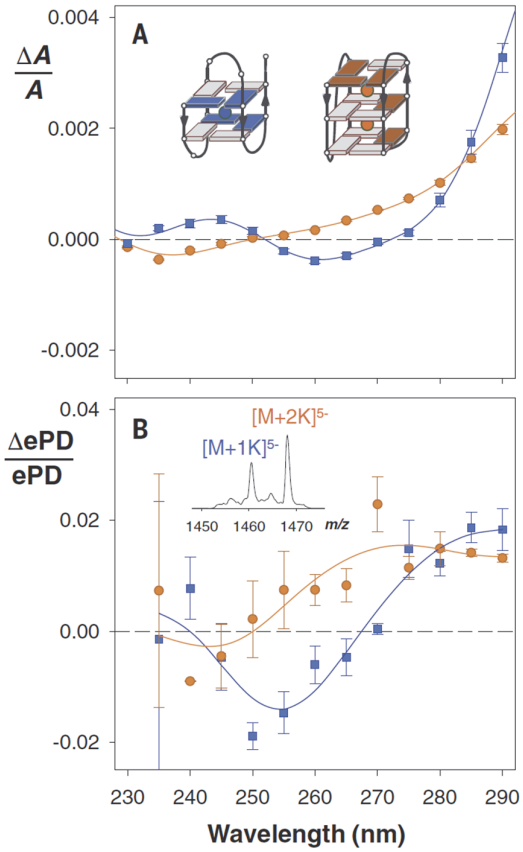

Figure 65. Application of mass-resolved circular dichroism to a mixture of conformations adopted by the human telomeric DNA sequence dTAGGG(TTAGGG)$_3$. (A) Deconvoluted solution-phase CD spectra for the three-quartet (2 K^+, orange circles) and two-quartet (1 K^+, blue squares) complexes coexisting at KCl concentrations between 0 and 1 mM.[199] The error bars are the standard uncertainties propagated from the original data; the lines were obtained by Savitzky-Golay smoothing. The insets show the stacking topologies deduced from the K^+ stoichiometry and the CD spectral shapes (light gray and colors denote anti and syn glycosidic bond angles, respectively). (B) Gas-phase CD spectra for the complexes $[M+1K]^{5-}$ (orange circles) and $[M+2K]^{5-}$ (blue squares) co-isolated from a solution containing 400 mM KCl. The error bars are the standard uncertainties from the replicates; the lines were obtained by Savitzky-Golay smoothing. The inset shows the two co-isolated parent ions. Figure reproduced with permission from Ref. 190. Copyright 2020 AAAS.

4.4.3 Intramolecular i-motifs

i-motif forming sequences have been studied by IMS.[490,1025] A study combining IRMPD spectroscopy and IMS proved that, for a model sequence of $(dC_6)_4$, the IR signature of the tetrameric i-motif structure contains a clear broadening of the band at 1650 cm^{-1} due to the formation of the hemi-protonated C-H^+-C base pair. Based on this signature, it was concluded for the intramolecular telomeric i-motif forming sequence d(CCCAAT)$_3$CCC that the compact structures observed by IMS had retained C-H^+-C base pairs, while the extended structures had not.[1025] For this 21-mer, the i-motif structure was well preserved for charge states 4- and 5-, while charge state 6- was sensitive to collisional unfolding.

Garabedian *et al.* have also observed, by nano-electrospray trapped ion mobility spectrometry-mass spectrometry (nanoESI-TIMS-MS), compact conformations for telomeric i-motif DNA at low pH values for low charge states, in both positive and negative ion modes, and partially folded i-motif structures for higher charge states. Later, the Gabelica group reported the behavior of the i-motif structure of human telomeric by IMS as a function of pH and ionic strength.[263] The surprising results were that, on single stranded structures (C-rich sequence at high pH or single-stranded control), the ionic strength

of the solution had a huge effect on the compactness of the gas-phase structures. This was ascribed to the charging process (CEM versus CRM) changing for intermediate charge states depending on the solution's ionic strength. This study highlights the importance of proper control experiments (with oligonucleotides of the same length and similar sequences), so that ion mobility mass spectrometry can be used to distinguish i-motifs folds from non-folded forms.

Native mass spectrometry has also been applied to study i-motif DNA sequences, for example to distinguish monomers from dimers,[1002,1026] or to study the binding of a small molecule ligand to the telomeric i-motif forming sequence.[1027] In a recent work, the interaction between the Bcl-2 oncogene promoter i-motif DNA and flavonoids has been studied by ESI-MS and pressure-assisted capillary electrophoresis frontal analysis (PACE-FA).[1028] The results showed that three natural flavonoids have clear affinity for i-motifs. The authors compared the determination of equilibrium association constants (K_A) by ESI-MS and PACE-FA, they found values agreeing within 25%. In addition, the collision induced dissociation (CID) was applied to the 1:1 complex to verify fragmentation pathway of i-motif/flavonoids complexes. MS/MS results indicated dissociation and loss of ligand at low collision energy (17%), suggesting a weak binding affinity for i-motif.

4.5 Nucleic acid complexes with small molecule ligands

4.5.1 Duplex ligands

4.5.1.1 Minor groove binders

4.5.1.1.1 Stoichiometries

Mass spectrometry has been used to characterize the interaction of duplexes with the common minor groove binders (see Chart 4 for the scheme of some ligands) DAPI,[13,489,506,525,609,655,1029–1031] netropsin,[489,506,521,525,609,655,1029–1034] berenil,[506,525,609,622,655,1035,1036] distamycin A,[12,13,506,955,1029–1031,1034–1040] pentamidine[1037] as well as the ligands Hoechst 33258,[489,506,531,595,624,655,1032,1035–1039,1041] Hoechst 33342[13,489,525,609,622,783,1029,1031,1035,1036,1042] and several other structures targeting the minor groove.[18,595,610,1033,1038,1042–1045]

ESI-MS revealed that minor groove binders form 1:1 and 2:1 complexes with DNA duplexes having a track of at least 4 A/T bases pairs (Figure 66).[12,13,489,506,521,595,609,610,622,955,1029,1034,1036,1038–1045] The ratio between these stoichiometries mostly depends on the localization of ligand charges and on the sequence of the binding site. Among all the classical minor groove binders, distamycin A has the highest propensity to cooperatively form 2:1 complexes (Figure 66),[1040,955,506] with ligands arranged head-to-tail. For the other minor groove binders, ligand dimer formation is hampered because terminal charges are present on both sides.[506,1029] One exception is the bisphenothiazine RP12274, which forms 2:1 complexes with duplexes containing an AATT binding site. Molecular modeling revealed how the four alkylammonium side chains can be placed to make this possible.[610] In general, higher stoichiometries become more abundant with increasing sequence length (as more independent binding sites become available) and decreasing ligand size.[506,609,1036] For example, netropsin 2:1 (ligand:duplex) complexes cannot be detected on a 12-mer dsDNA containing one binding site[489,506,609] but could be detected with a 20-mer dsDNA bearing two AT-rich binding sites.[521]

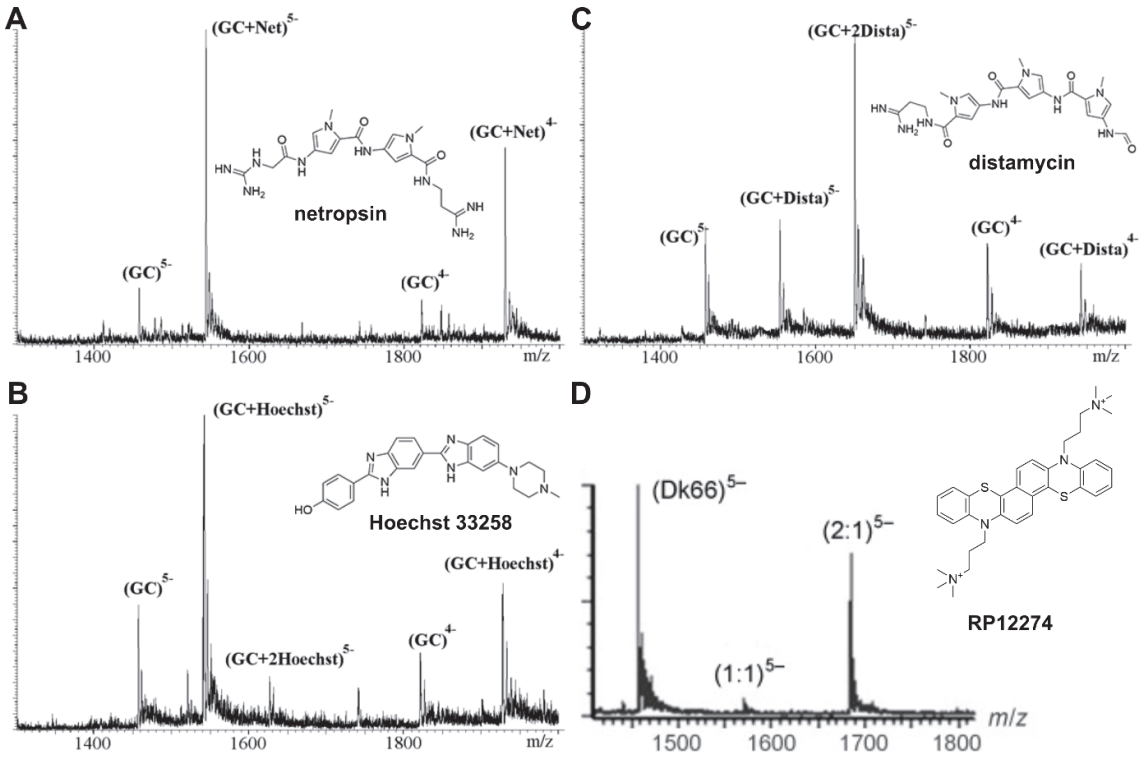

Figure 66. ESI-MS spectra of equimolar amounts of 12-mer duplex DNA with common minor groove binders (A) netropsin (10 µM), (B) Hoechst 33258 (10 µM), (C) distamycin A (10 µM), and (D) RP12274 (8 µM). Figures adapted with permission from Ref. 506, Copyright 1999 Wiley (A—C), and Ref. 610, Copyright 2008 Wiley (D).

4.5.1.1.2 Quantification and screening

Rapid ESI-MS screening of minor groove binders against dsDNA with varying fractions of GC base pairs gives information on sequence preference. Distamycin, berenil and other minor groove binders have a significantly lower affinity towards dsDNAs that contain only GC-pairs.[610,1036,1043,1045] This is in line with the known preference of minor groove binders for A/T base pairs (Figure 12), and testing duplexes of different base composition is thus a way to delineate the binding mode (groove binding vs. intercalation).

However, there are exceptions. Dicationic diamidines[349,357,1033,1034,1043,1046–1049] can recognize a target site with GC base pair in addition to flanking AT base pairs through minor groove binding. MW346 has a high affinity for ATGA sequences and dimerizes upon binding in the minor groove. The selective recognition of diamidides compounds was probed using a mixed set of DNA hairpins including ATATAT, AAATTT and ATGA binding sites (Figure 67). The compound MW346 binds with a 1:1 stoichiometry to the A/T tracks and with a 2:1 stoichiometry with the ATGA site.[1050] This example shows how ESI-MS can directly and unambiguously reveals the different stoichiometries.

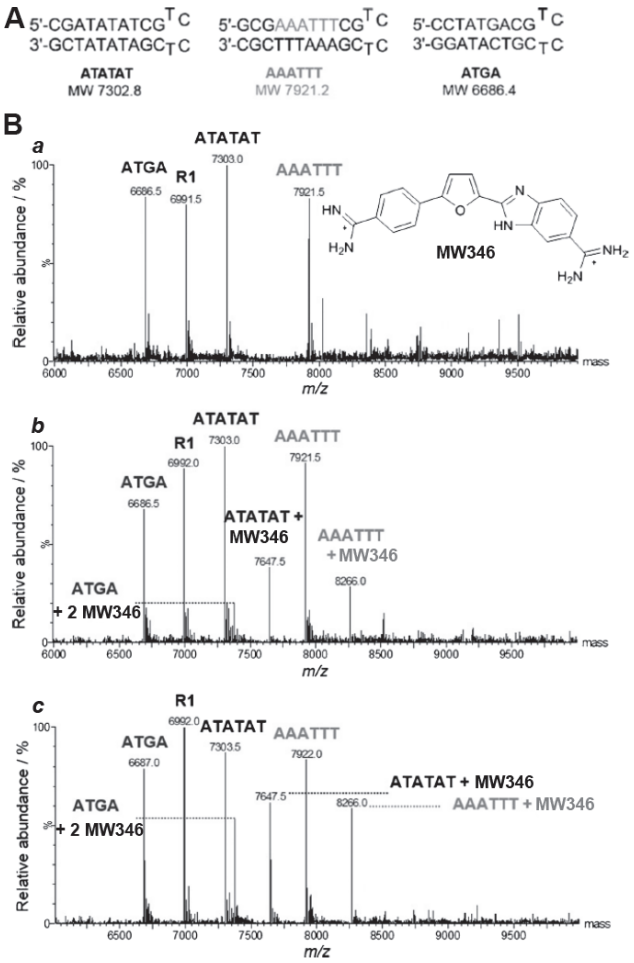

Figure 67. a) Mixed hairpin DNA sequences ATATAT, AAATTT, and ATGA used to screen interaction for monomer and dimer-forming diamidine. B) Deconvoluted ESI-MS spectra of MW346 titrated with multiple DNA sequences. Concentration in DNA is 5 µM in 150 mM NH_4Ac. Mole-to-mole ratio of MW346-to-DNA is 0:1 (a), 1:1 (b), and 2:1 (c). The cooperative nature of MW346 binding to ATGA is indicated by increasing peak for the dimer species and no detectable 1:1 species. Figure reproduced with permission from Ref. 1043. Copyright 2015 Wiley.

The equilibrium association constants of duplex-ligand complexes can be determined either by ESI-MS titration[489,609,622] or from a single ESI-MS spectrum (see section 3.1.4.2.1).[610,1042] While the exact values vary depending on the experimental setup conditions, the equilibrium association constants remain within the same order of magnitude and are as follows: $K_{A1} = 10^7$ M^{-1} for Hoechst ligands,[489,609,622,1042] $K_{A1} = 10^6$ M^{-1} for DAPI and Netropsin,[489,609] and $K_{A1} = 10^5$ M^{-1} for Berenil[609,622]. The K_A values of the 2:1 complexes are harder to obtain by other techniques than ESI-MS because the 2:1 complex is minor.[609] The determination of equilibrium association constants with several duplexes, each containing a different binding site (a different AT-rich central sequence) allowed to finely characterize the preferential ligand binding site.[609]

When assessing the merits of ESI-MS compared to classical solution spectroscopic methods (fluorescence or absorption titration), it is important to use the exact same solvent condition. Such studies demonstrated the merits of ESI-MS to quantitatively screen drug-nucleic acids interactions,[609,624] provided that the experiments are carried out in the negative ion mode.[489] K_A values determined in the positive mode are too low because the Coulomb repulsion between positively charged DNA and positively charged ligands destabilizes the complex in the gas phase,[489,1039] while negative ion mode analysis gives comparable results to classical solution methods.

The accurate determination of equilibrium association constants (K_A) by ESI-MS titration requires a determination of the relative response factors (see section 3.1.4.2.3). The response factors of the duplex-ligand complex can be lower than those of the free duplex, even with minor groove binders that cause little deformation of the Watson-Crick duplex structure.[622,624] This means that affinities can be underestimated by as much as 40% when assuming equal response factors. Nevertheless, when comparing ligands, one usually seeks for large (orders of magnitude) differences in K_A values, and using the assumption of equal response factors is in that case justified. Also, when ranking ligands, what matters is the ratio of response factors among complexes. These are less likely to change when comparing ligands having the same binding mode.

4.5.1.1.3 Gas-phase fragmentation of the complexes

The main CID fragmentation pathways of dsDNA complexes with minor groove binder involve strand separation and base loss, wherein the minor groove binder remains attached to a single strand. Ligand neutral loss from the duplex can also be observed for Hoechst ligands.[489,1029,1031,1035,1037,1041] The gas-phase kinetic stability of duplex-ligand complexes, assessed through collision-induced dissociation breakdown curves, is higher for netropsin than for Hoechst 33258.[1032] The kinetic stability is correlated to the number of H-bonds between the minor groove binder and the A/T base pairs. Netropsin and distamycin A can form 4 H-bonds, DAPI and berenil 3 H-bonds and the Hoechst ligands are limited to 2 H-bonds (Figure 68). However, despite their low gas-phase kinetic stability, the Hoechst complexes are the most stable in solution. This example underlines that gas-phase kinetic stabilities cannot be used as a proxy to rank solution equilibrium stabilities (see section 3.2.1.3 for further discussion), but rather indicate enthalpic stabilization due to the formation of specific non-covalent bonds, and are thus well correlated with crystallography data.[1051]

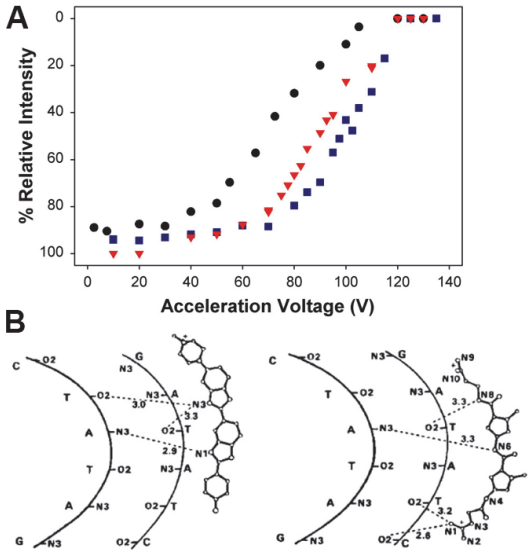

Figure 68. A. Breakdown curve of dsDNA [(dGGGGATATGGGG)/(dCCCCATATCCCC)]$^{5-}$ (circles) and the complex with Hoechst 33258 (triangle) and netrospin (squares). Figure adapted with permission from Ref. 1032. Copyright 2000 Wiley. B. Illustration of the interaction between Hoechst 33258 (left) and netrospin (right) with a double helix (dCGCGATATCGCG)$_2$. The hydrogen bonds formed between the drug and the duplex are shown by dotted lines. Figure adapted with permission from Ref. 506. Copyright 1999 Wiley. See also Figure 12.

IRMPD and CID were used to localize ligands on a duplex.[1031,1041] The main fragmentation pathway is strand separation. However, when using sustained off-resonance CID, base loss was less favored.[1031] It is hypothesized that the Hoechst ligands form salt bridges with the single strand, which increases the gas-phase stability. Fragmentation analysis of the ssDNA adducts confirm that minor groove binders are located at A/T rich regions.[1031,1041] Complexes between minor groove binders and dsDNA

were also studied by electron detachment dissociation (EDD, 18.5 V)[1041] or by laser irradiation at 355 nm (in the presumed in-vacuo ligand absorption band).[655] Both activation methods resulted in electron detachment from the intact complex, and no fragmentation. Photon irradiation produced electron detachment only in the case of fluorescent ligands, suggesting a role of long-lived excited states in the electron photodetachment mechanism.

4.5.1.2 Intercalators

4.5.1.2.1 ESI-MS probing of the complexes in solution

Mass spectrometry has been utilized to characterize the interaction of duplexes with simple intercalators (Chart 3) (ethidium bromide,[489,506,531,598,655,1038] amsacrine,[489,506,655] ascididemin,[506,1052] proflavine,[489,1038] (neo)cryptolepine,[13,489,606] thiazole orange[1053] and others[489,1038,1052,1054]), or intercalators that also bear functional groups interacting non-covalently in the grooves (actinomycin D,[783,960,1031,1035,1036,1055] echinomycin,[783,1031,1055] nogalamycin,[12,525,1016,1029,1031,1056] daunorubicin,[489,525,1029,1031,1056] doxorubicin,[489,598,655,1057,1058] mitoxantrone[489,593,928] and others[13,382,531,592,593,596,1057–1059]), bis-intercalators,[599,1055,1060–1063] alkylating intercalators (hedamycin,[12,18,1064,1065] psoralens,[18,597,794] acridine mustards,[18,1066] benzoacronycines[317]) and metallointercalators (ruthenium complexes,[1035,1036,1039,1067–1069] Pt and Pd complexes,[12,316,977] or complexes with other metals[508,934,940,1070]). The only complexes that can be detected in the positive ion mode are those with intercalators forming H-bonds.[489] Thus, for general purposes, native MS studies on these systems should be carried out in the negative ion mode.[489,598]

The stoichiometry of complexes between dsDNA and intercalators, assessed by ESI-MS, ranges from 1:1 to 8:1.[489,525,531,592,593,597,599,794,1038,1054–1056,1059,1066] One example of the diversity of stoichiometries is presented in Figure 69. The average number of intercalator ligands increases proportionally with the ligand-to-DNA ratio.[593,1029,1055,1056,1059] The fluorescence displacement of intercalators is a frequently used biophysical assay to probe duplex ligands,[1071] and ESI-MS helps to visualize the ligand displacement.[506]

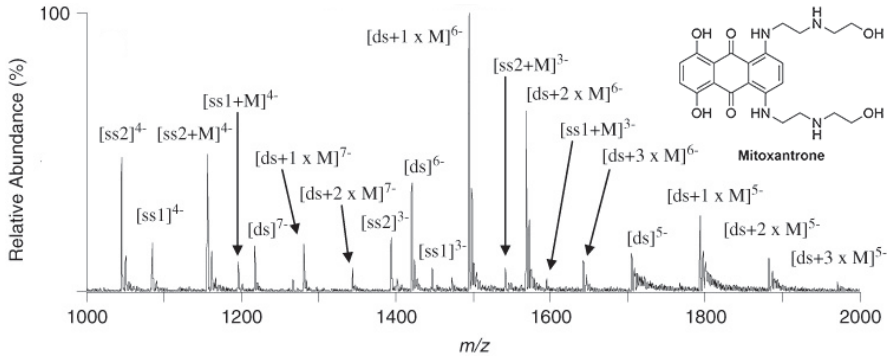

Figure 69. ESI-MS spectrum of equimolar amounts of Mitoxantrone (M) and a 14-mer duplex (ds = ss1 + ss2) with 85% GC base pairs. Multiples stoichiometries are detected both with the double helix and the single strand. Figure adapted with permission from Ref. 593. Copyright 2007 Wiley.

The presence of multiple stoichiometries deserves discussion. In the case of intercalators, this behavior is due to the multiplicity of intercalating sites on a given duplex, and thus does not necessarily reflect a non-specific aggregation during the ESI process. Yet, both would manifest themselves in the same kind of ligand binding distribution (see section 4.1.1). To test that the intercalator complexes are specific in the sense that they exist in solution, key experiments consist in comparing close ligand analogues for which the solution binding affinities were characterized separately (e.g., daunomycin, doxorubicin, and nogalamycin,[489,525,1029,1031,1056] or cryptolepine and neocryptolepine[13,489,606]). ESI-MS was found to faithfully reflect relative solution affinities.

The effect of intercalators on the DNA duplex structure in solution has been analyzed by chemical probing. Experiments with MnO_4^- revealed that intercalated duplexes are more susceptible to oxidation than regular dsDNA, indicating that intercalation deforms the canonical duplex into a less compact (i.e. exposed) structure.[783] This structural change may explain the difference in ESI-MS response factors as the number of bound intercalators increases (for 1 to 2 ethidium ligands bound to a 12-mer duplex, the response factor correction is less than 25%).[622]

Except for that study, the MS-derived equilibrium constants are typically not reported, as the focus was rather on comparing the ligand affinities for duplexes varying in GC-richness. Intercalators typically have a higher affinity for GC-rich sequences (Figure 70).[599,606,607,1036,1052,1055] Duplex intercalators have also often been studied by ESI-MS in the context of comparative screening against G-quadruplexes.[592,606,1052,1054,1057] Very few ligands designed as G-quadruplex binders do not interact with regular duplex DNA. Phen-DC6 is an example of a high structural specificity drug.[1053] Some duplex intercalators also target triplex DNA (section 4.5.2). Similar screening experiments revealed other ligands selectively targeting triplex DNA over duplex DNA.[13,382,596,599,606,928,1052,1072] Finally, Duskova et al. used ESI-MS to test the specificity of ligands for three-way junctions in comparison with regular duplex DNA.[1073]

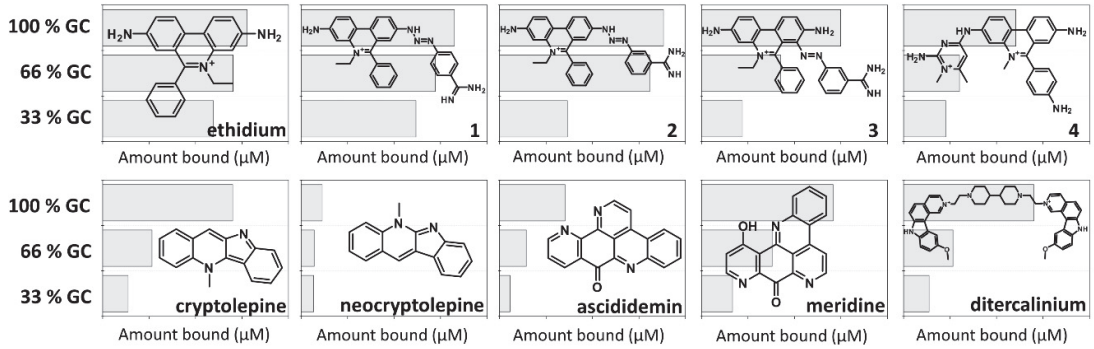

Figure 70. Sequence selectivity of some intercalators towards 12mer double helices. The amount of drug bound is shown as a function of the percentage of GC base pairs in the duplex DNA (5 μM): 100%GC = $(dCGCGGGCCCGCG)_2$, 66%GC = $(dCGCGAATTCGCG)_2$, 33%GC = $(dCGCAAATTTGCG)_2$. The data is compiled from references 599,606,607,1052.

4.5.1.2.2 Gas-phase fragmentation of the complexes

In an MS/MS experiment, the amount of intact complex for a given collision voltage depends on the fragmentation kinetics (see section 3.2.1.1.1). The correlation between the amount of fragment and the activation enthalpy (which is correlated with the interaction energy between the fragmenting partners) is valid only for fragmentation channels of similar activation entropy. A classification of the preferred dissociation pathway of the complexes is thus mandatory. The fragmentation of complexes between dsDNA and intercalators can mainly follow three paths: (1) ligand neutral loss (cryptolepine, neocryptolepine, daunomycin, doxorubicin, m-amsacrine, ellipticine, proflavine, mitoxantrone); (2) ligand anion ejection (actinomycin D) and (3) strand separation with the intercalator remaining attached to one (negatively charged) of the single strands (positively charged ligand such as ethidium).[382,489,1029,1031,1035,1054] For porphyrins with outer binding modes, Ramos et al. showed how this process depends on the number of cationic charges on the ligand.[1074]

The main fragmentation path depends more on ligand charge than on ligand structure or binding mode. The other main factor is the charge state of the precursor ion.[1029,1055] Neutral ligand ejection and base losses predominate at low charge states, whereas ligand anion ejection and strand separation prevail for higher charge states.[1029,1055] CID[18,382,525,592,598,794,960,1029,1035,1054,1055,1059,1066],

IRMPD[18,597,1031,1066] and EPD[655] were used to determine the main fragmentation paths of intercalators,[382,489,525,592,593,598,598,655,1029,1031,1054,1055,1059], bisintercalators[489,960,1031,1035,1055] and alkylating intercalators.[18,597,794,1066]

The CID experiment on positional isomers cryptolepine and neocryptolepine bound to a duplex DNA was key to demonstrate that the intercalation was preserved in the gas-phase complexes.[489] For both ligands, the fragmentation pathway is neutral ligand loss, and thus the collision voltage required for fragmentation is directly proportional to the activation energy. Figure *71* shows that, at a given hexapole collision voltage, the complex with cryptolepine is more kinetically stable than the complex with neocryptolepine. The activation enthalpy for dissociation is thus higher for the complex with cryptolepine, which is consistent with the solution-phase equilibrium association constants, and structurally explained by a higher stabilization of the cryptolepine complex due to a more favorable dipolar interaction between N-CH_3 group and the C=O of the base pair, while the N-CH_3 in neocryptolepine can also cause a steric hindrance with the base pair NH_2.[489]

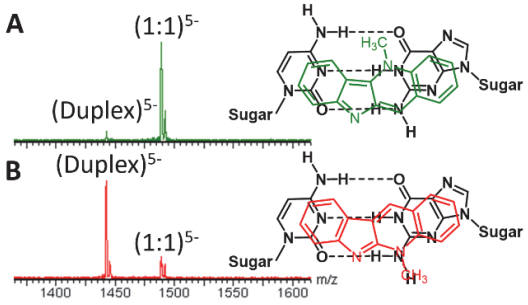

Figure 71. Negative ion mode MS/MS spectra of the complex $(1:1)^{5-}$ of duplex $(CGCGAATTCGCG)_2$ with A. cryptolepine and B. neocryptolepine at the same hexapole collision voltage (10 V): the resulting fragment is the $(duplex)^{5-}$. The complex with neocryptolepine (bottom) is more dissociated compared to the complex with cryptolepine (top)*. The opposite position of N-CH_3 group of neocryptolepine induced a destabilization of the complex. Right: Schematic overlap with a GC base pair and the drugs is showed. Figure adapted with permission from Ref. 489. Copyright 2006 Elsevier.*

4.5.1.3 Mismatch-targeting ligands

Macrocyclic bis-intercalators prefer mismatches because they intercalate more easily when offered a site of low thermodynamic stability.[1061–1063,1075] Another design principle, tested by ESI-MS, is the formation of hydrogen bonds with GG mismatched bases and adjacent bases (Figure 72A,B).[1076–1078] Coldspray ionization mass spectrometry revealed that the **NC** ligand binds cooperatively (2 ligands with 2 strands),[1076] forming a 2:1 complex with the duplex bearing the mismatches (Figure 72C).

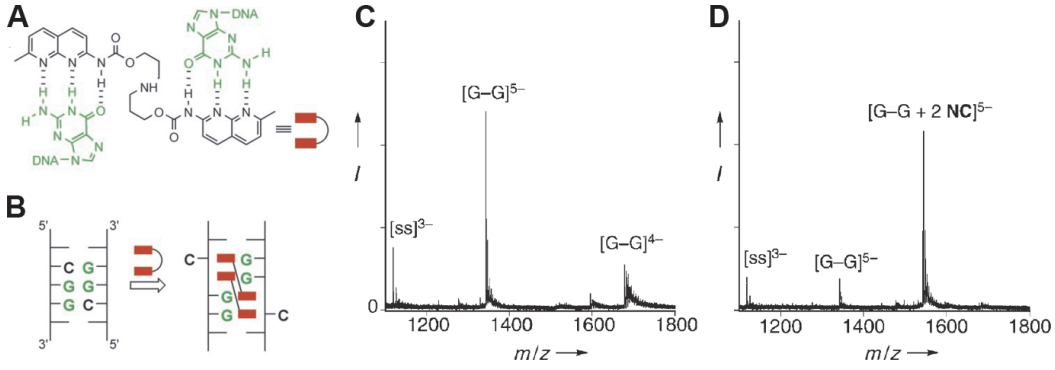

Figure 72. Hydrogen-bonding between A. NC and the G–G mismatch, B. Schematic illustrations of the proposed NC binding to the CGG/CGG triad (red rectangles: 2-amino-1,8-naphthyridine), C and D: CSI-TOF MS of the 11-mer self-complementary duplex dTCAACGGTTGA containing a CGG/CGG triad (20 μM), in absence (C) or presence (D, 20 μM) of NC, in 50% aqueous

methanol and 100 mM ammonium acetate. Samples were cooled at -10°C during injection at a flow rate of 0.5 mL h^{-1}. Figure adapted with permission from Ref. 1076. Copyright 2005 Wiley.

4.5.2 Triplex ligands

Native ESI-MS has been used as a screening method to probe the formation of triplex-ligand complexes and assess the complex stoichiometries. Most triplex ligands (shown in Chart 8) only form 1:1 complexes,[928,1072] while benzopyroindole (BPI) derivatives form 2:1 complexes[382] and flavonoid glucosides such as vitexin may form up to 4:1 complexes.[596]

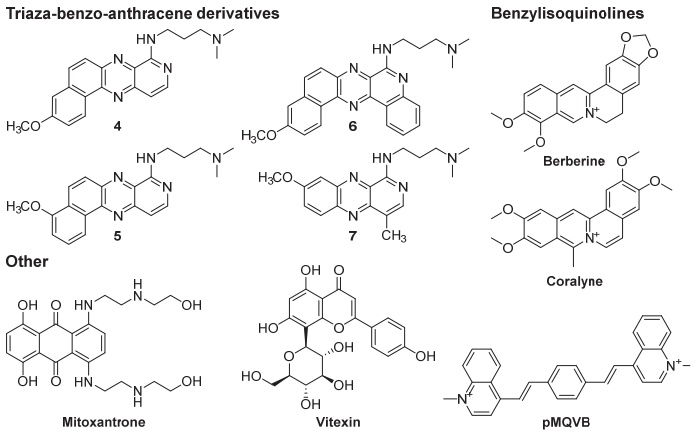

Chart 8. Some representative triplex ligands studied by mass spectrometry. The best triplex binders have a large heteroaromatic backbone.

Triplex ligands affinity and selectivity has been assessed by ESI-MS.[13,382,596,599,606,928,1052,1072] The majority of triplex ligand also bind to duplexes, therefore it is critical to assess the duplex/triplex selectivity when developing specific triplex ligands.[13,382,606] Strong duplex binders such as berenil, netropsin, distamycin and acridine disrupt the formation of triplexes by stabilizing the duplex.[930] In contrast, the ligand pMQVB induces the formation of a triplex, even when a standalone triplex was not observed.[1060]

The fragmentation pattern of triplex-ligand complexes has been analyzed in SORI-CID[596,928] and hexapole CID.[382] Two fragmentation channels are involved: (1) ligand loss (most often neutral loss),[382,596,928] leaving the triplex alone and (2) ejection of the triplex-forming oligonucleotide, leaving a duplex-ligand complex meaning that the ligand interacts mostly through the duplex part.[382] CID has been used in conjunction with molecular modeling to deduce the ligand binding modes (insertion through the minor or major groove) and binding sites (CGC-TAT or TAT-TAT base triplets). The ranking of the ligand interaction energies has been compared with the collision energies required to fragment 50% of the complexes. The results suggest that the ligands intercalate via the minor groove of the Watson-Crick duplex with TAT-TAT binding sites (Figure 73).[382]

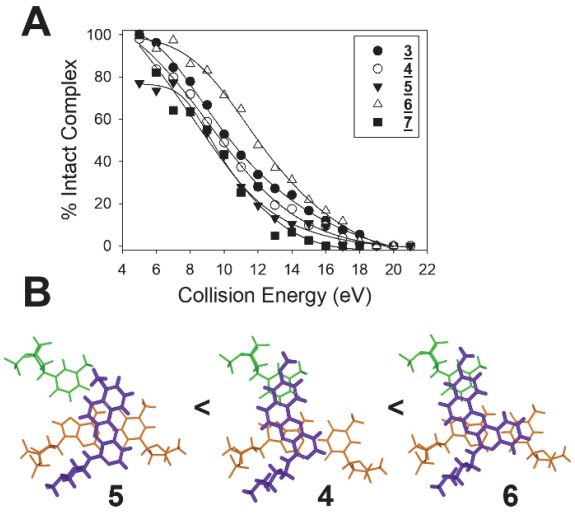

Figure 73. A) MS/MS breakdown curves of the complexes between ligands 4—7 (see Chart 8) and the triplex dCCTTTTCTCTTTCC and dGGAAAGAGAAAAGG which constitute a Watson-Crick duplex and dCCTTTCTCTTTTCCwich is the antigene strand. B) Models of three ligands intercalated in a TAT-TAT base triplet of the model triplex (dCTTTTCC•dGAAAAGG-dCTTTTCC), ranked by order of observed gas-phase kinetic stability, which matches with the order of calculated interaction energies. The planar ring system of the ligands (purple) is shown stacked with the base triplet (orange and green). Only the bottom triplet is shown for clarity. The Watson-Crick base pairs are in brown (at the bottom left and bottom right corners of each figure), the antigene base is green (at the top left corner of each figure), and the drug is stacked on top of the three bases. Adapted from Ref. 382. Copyright 2007 American Chemical Society.

4.5.3 G-quadruplex ligands

G-quadruplex(G4)-forming sequences are observed in all organisms including mammals, plants, bacteria, viruses, and parasites.[1079] They are involved in the regulation of several biological pathways.[192] Ligand binding to G4 structures can influence telomerase activity, helicase protein binding, replication, and transcription process.[192,900,1080] Therefore, to understand ligand binding to G4 structures, various low and high-resolution biophysical and biochemical techniques have been used during the past couple of decades.[1081] ESI-MS distinguishes itself by its capacity to detect all complexes formed in solution based on their stoichiometry (number of strands, ligands, and cations of each sort). Moreover, relative peak intensities give clues on relative binding affinities, and coupling with collision-induced dissociation (CID) or ion mobility (IM) spectrometry can potentially bring additional information about ligand binding modes. Table 3 lists the G-quadruplex-ligand complexes studied by native MS from 2002 to 2020. The ligand structures are shown in Chart 6 and Chart 9. We will discuss here the main lessons learned by native mass spectrometry.

Table 3. Overview of G-quadruplex (G4) ligand non-covalent interaction(s) studied by ESI-MS.

Ligands	Sequences	Ref.
Ditercalinium	$(dTG_4T)_4$ $(dG_4T_4G_4)_2$ $dG_3(T_2AG_3)_3$	599
Cryptolepine, Neocryptolepine	$(dTG_4T)_4$ $(dG_4T_4G_4)_2$ $dG_3(T_2AG_3)_3$	606
Ethidium derivatives	$(dTG_4T)_4$ $(dG_4T_4G_4)_2$ $dG_3(T_2AG_3)_3$	607
Ascididemin, Meridine	$d(G_3T_2A)_3G_3$ $(dTG_4T)_4$	1052
Nemorubicin, doxorubicin, PNU-159682	$(dT_2AG_3T)_4$	1057
Daidzin	$dA(G_3T_2A)_3G_3$	1082
Berberine and derivative (SS14) daunomycin	$(dT_2G_5T)_4$	1083
Berberine derivatives	$(dT_2G_5T)_4$ $(dG_4T_4G_4)_2$ $dG_3(T_2AG_3)_3$	1084
Natural products	$dTGAG_3TG_3TAG_3TG_3TA_2$	594
Natural products	$dAG_3CG_3AG_3AG_3A$	1085
Natural products	$dAG_3AG_3CGCTG_3AG_2AG_3$	1086
Alkaloids	$(dTG_4T)_4$	1087
Alkaloids	$dG_5C_2GUG_4UG_3AGCUG_4$	1088
Alkaloids	$dG_3(CTG_3)_2CG_4$	1089
Flavonoids	$dTA(G_3T_2A)_3G_3$	1090
Sanguinarine	$dAG_3(T_2AG_3)_3$	1091
Chelerythrine	$dAG_3(T_2AG_3)_3$ $r(U_2AG_3)_4U_2A$	1092
Pyrrolobenzodiazepine derivatives, TMPyP4	$d(T_2G_8)_4$	1093
Glucosaminoside derivatives	$d(T_2AG_3)_4T_2A$ $R(U_2AG_3)_4U_2A$	1094
Telomestatin	$d(G_3T_2A)_3G_3$	628
Telomestatin	$(dTG_4T)_4$ $(dT_2AG_3)_4$ $dGAG_3TG_4AG_3TG_4A_2G$	1095
Telomestatin derivatives, RHPS4	$dAG_3(T_2AG_3)_3$	1096
TRZ and RHPS4	$dAG_3(T_2AG_3)_3$ $dAG_3AG_3CGCTG_3AG_2AG_3$	1097
Cyclo[n]pyrroles (n=6-8)	$(dT_2AG_3)_4$	1098
Cyclic polyamide	$d(G_2A)_3G_2TCAC$ $r(G_2A)_4$ $d(G_2A)_4GA_2(G_2A)_4$ $d(G_2A)_3G_2TCACG_2A(G_2A)_3GA_2(G_2A)_4$	1099
LSA2-6OTD derivatives and dimer	$(dT_2AG_3)_4$	423
Mesoporphyrin IX	$(dTG_4T)_4$ $(dG_4T_4G_4)_2$ $dG_3(T_2AG_3)_3$	926
CuTMPyP4	$(dT_4G_nT_4)_4$ (n = 4, 10)	989

Cationic porphyrin derivatives	$(dTG_4T)_4$ $(dT_2G_5T)_4$	1100
Cationic porphyrin derivatives	$dG_3CGCG_3AG_2A_2G_5CG_3$	981
M-TMPyP4 (M = Ni, Cu, Zn)	$dAG_3(T_2AG_3)_3$	1101
TMPyP4 tetratosylate and tetrachloride	$d(T_2AG_3)_4T_2A$ $r(U_2AG_3)_4U_2A$	1102
M-Phen complexes M = Ni, Ru, Pt	$(dT_2G_5T)_4$	1069
M-ttpy, M-tMebip M = Pd, Pt	$(dTG_4T)_4$ $d(G_3T_2A)_3G_3$	316
Cu-tpy, Cu-ttpy, Cu-Clptp	$dG_3(T_2AG_3)_3T$ $(dG_4T_4G_4)_2$ $dTGAG_3TG_4AG_3TG_4A_2G_2$ $dTA(G_3T_2A)_3G_3$ $dA(G_3CTA)_3G_3$ $(dTG_4T)_4$	615
Pd(II) and Pt(II) metallo-assemblies	$(dTG_4T)_4$ $dAG_3(T_2AG_3)_3$ $dTGAG_3TG_4AG_3TG_4A_2G_2$	1099
Pt(II) & Ru(II) metallo-assemblies	$(dTG_4T_4)_4$ $dT_4(G_4T_4)_4$ $dT_2(G_4T_2)_3G4$ $d(TTAGGG)_4$	786
Ru(II) complexes	$dAG_3(T_2AG_3)_3$	1103
Ru(II) complex	$dAG_3(T_2AG_3)_3$	1104
[(ŋ6-biphenyl)Ru(en)Cl]	dT_2AG_3	1105
Pt(II)–phenanthroline	$(dT_2G_4T)_4$	1106
Pt(II)-tripod	$dA_3(G_3T_2A)_3G_3A_2$	410
Au(9-methyl caffein-8-ylidene)$_2BF_4$	$dTA(G_3T_2A)_3G_3$	1107
Bis carbene gold(I) complex	$dTA(G_3T_2A)_3G_3$	1108
Nickel Schiff base complexes	$(dT_2G_5T)_4$ $d(G_3T_2A)_3G_3$	1109
Perylene Diimide (PDI) derivatives	$(dT_2G_5T)_4$	592
PDI derivatives	$d(G_3T_2A)_3G_3$	1110
PDI derivative with oxirane	$d(G_3T_2A)_3G_3$	510
PIPER, TMPyP4, Quinacridines (MMQ1, MMQ3, BOQ1)	$(dT_2AG_3)_4$ $(dG_3T_2A)_3G_3$ $dGAG_3TG_3GAG_3TG_4A_2G$ (Pu22) $dTG_4AG_3TG_4AG_3TG_4A_2G_2$ (Pu27)	708
BOQ1	$dCAG_3T_2A_2G_3TATA_2CT_3AG_4T_2AG_3T_2$	1111
PIPER, TMPyP4, Distamycin A	$(dTG_4T)_4$ Tetra end-linked $(dTG_4T)_4$	1112
TmPyP4, PIPER derivatives, dehyocorydaline	$dG_3CGCG_3AG_2A_2G_5CG_3$	1113
DMAPP (PIPER derivative)	$dTGAG_3TG_4AG_3TG_4A$	1114
Perylene diimide derivatives K20 and PIPER	$dCG_3CG_3CGCGAG_3AG_4$ $dG_2CGAG_2AG_4CGT(G_2C_2)_2$	1115
BRACO-19, naphthalene diimides	$rAG_3(U_2AG_3)_3$ $dAG_3(T_2AG_3)_3$	608
Core-extended naphthalene diimide	$dTGAG_3TG_4AG_3TG_4A_2G_2$ $(dT_2AG_3)_4T_2$	413

PDI derivative, ImImImbDp, PyPyPybDp, macrocyclic phosphoramidates	$(dG_3TG_3TG_3TG_3T)_2$ $(dGTG_2TG_3TG_3TG_3T)_2$	1116
Tel01, distamycin A, DTC	$(dT_2G_5T)_4$	507
ImImImβDp, Tel01	$(dTG_4T)_4$ $(dAG_4A)_4$ $(dCG_4C)_4$	983
Tel01, ImImImbDp, PyPyPybDp,	$(dAG_3T_2)_4$	1117
ImImImbDp, PyPyPybDp,	$dG_3TG_3TG_3TG_3T)_2$ $dGTG_2TG_3TG_3TG_3T$	1113
pyrrole–inosine nucleoside	$(dTG_4T)_4$ $(dT_2G_4)_4$	1118
Dihydroindolizino indole derivatives	$(dT_2AG_3)_4$ $(d(T_2AG_3)_2)_2$	1119
Xanthone derivatives	$d(G_3T_2A)_3G_3$	1120
Trioxatriangulenium ion (TOTA)	$(dT_2G_5T)_4$ $(dT_2AG_3)_4$	1054
AZATRUX	$d(G_3T_2A)_3G_3$ $(dTG_4T)_4$	1121
Thioflavin T	$dA(G_3T_2A)_3G_3$ $d(G_3T_2A)_3G_3$ $d(G_3T_2A)_3G_3T$	625
Thiazole orange, MMQ derivatives, Phen-DC3, Phen-DC6	$dG_3(T_2AG_3)_3$ $d(G_2T_2G_2TGTG_2T_2G_2)$	1053
Phen-DC3, 360A, TrisQ, L2H2, TMPyP4, PDS	$d(T_2AG_3)_4T_2$ $dTT(G_3T_2A)_3G_3A$ $dTA(G_3T_2A)_3G_3$ $dGGG(T_2AG_3)_3T$ $dTGAG_3TG_4AG_3TG_4A_2G_2$	916
Phenanthroline derivatives	$dT_2(G_3T_2A)_3G_3A$	1122
Phenanthroline derivatives	$dT_2(G_3T_2A)_3G_3A$ $dG_3CGCG_3AG_2A_2G_5CG_3$ $dTGAG_3TG_3TAG_3TG_3TA_2$ $dAG_3CG_2TGTG_3A_2GAG_3A$	1123
360A, Phen-DC3, PDS	$dTG_3T_2G_3T_2G_3T_2G_3T$ $dTGAG_3TG_3GAG_3TG_4A_2G_2$ $dA_2G_3TG_3TGTA_2GTGTG_3TG_3T$ $(dG_3T_4G_4)_2$ $(dG_4T_4G_4)_2$ $(dG_4T_4G_3)_2$ $(dG_4T_3G_4)_2$ $(dTAG_3T_2AG_3T)_2$	976
Phen-DC3, Tris-Q, TMPyP4, Pt-ttpy, Cu-ttpy	$dT_2(G_3T)_4$ $dT_2(G_3T_2A)_3G_3A$ $d(G_3T_2A)_3G_3T$ $dA(G_3T_2A)_3G_3$	638
Phen-DC3, Phen-DC6, 360A, Tris-Q, TMPyP4, Pt-ttpy, Cu-ttpy, Thiazole orange	$dT_2(G_3T)_4$ $dT_2(G_3T_2A)_3G_3A$ $(dG_3T_2A)_3G_3T$	1124
Phen-DC3, 360A, PDS-C4-C	$dTA(G_3T_2A)_3G_3$ $dG_3(T_2AG_3)_3T$	660
Acylhydrazones derivatives	$dTA(G_3T_2A)_3G_3A_2$	1125

	$dTGAG_3TG_4AG_3TG_4AAG_2$ $dA(G_3T_2A)_3GGG$ $dTGAG_3TG_3TAG_3TG_3TA_2$	

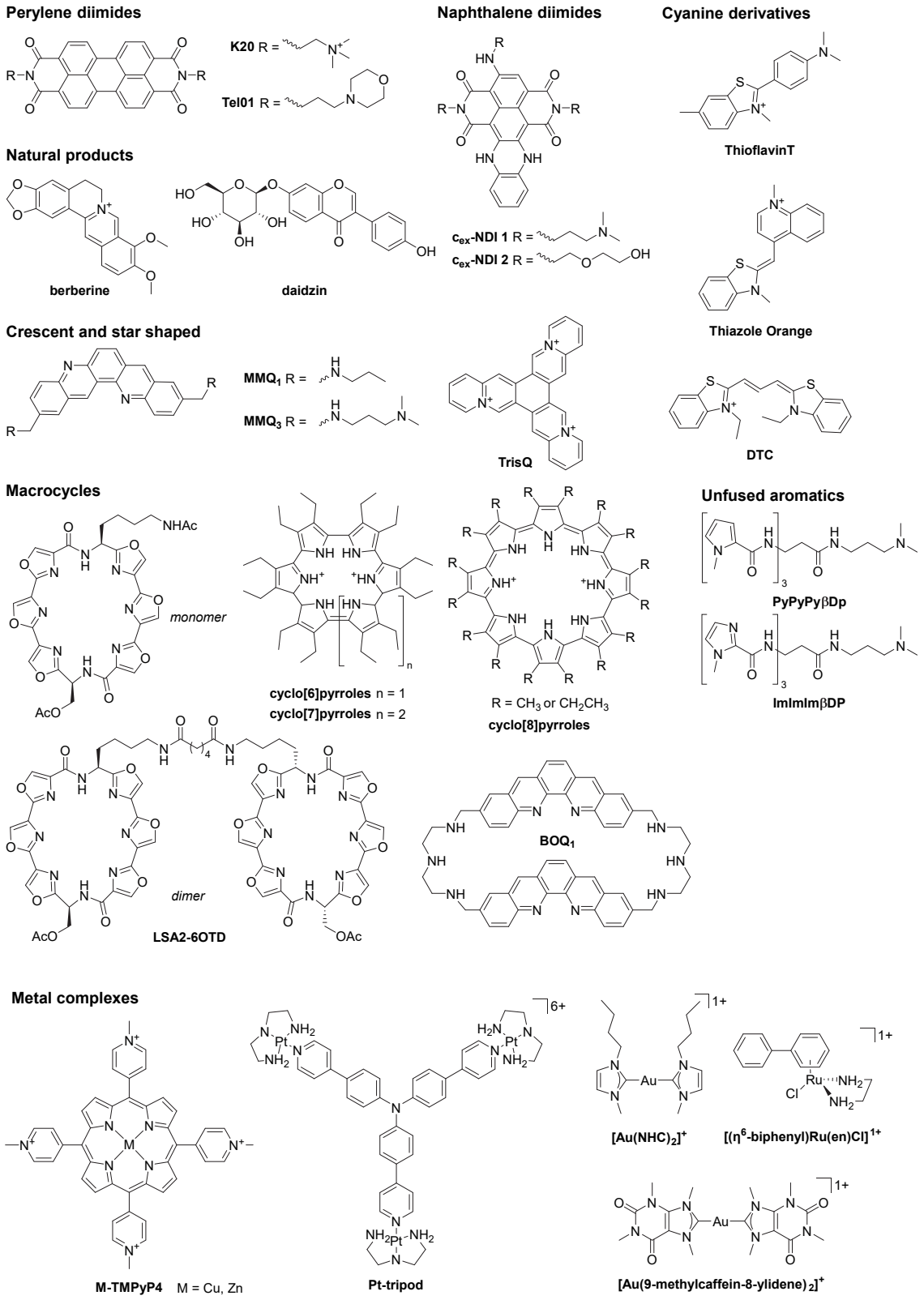

Chart 9. G-quadruplex ligands (continued).

4.5.3.1 Ligand binding stoichiometry

One of the most studied natural products is telomestatin, a macrocycle isolated from *streptomyces anulatus* bacteria. Telomestatin has the perfect size for stacking on a G-quartet plane.[1126] It binds to the human telomeric G4 d(GGGTTA)$_3$GGG with 1:1 and 2:1 stoichiometries (ligand:G4) with similar equilibrium association constants, suggesting equivalent binding sites.[628,1095] Several hexaoxazole analogs of telomestatin were further developed.[424,1127,1128] Their ESI-MS spectra in the presence of human telomeric quadruplex d(TTAGGG)$_4$ revealed a 1:1 stoichiometry for an 6OTD dimer and 1:1 to 2:1 stoichiometries for the 6OTD monomer (LSA2-6OTD).[423] Thanks to the proper size and flexibility of the linker the two 6OTD moieties of the dimer can target both terminal quartets of the quadruplex cooperatively. Therefore, an end-stacking binding mode is proposed for the parent ligand and its derivatives.

The isoflavone daidzin showed 1:1 and 2:1 complexation with the telomeric G4 dA(GGGTTA)$_3$GGG, and again the presence of two binding sites per quadruplex structure suggests end-stacking.[1082] This was observed for example with ethidium derivatives,[607] N-methyl-mesoporphyrin IX,[926] and metallated porphyrins CuTMPyP4 and ZnTMPyP4.[989] In contrast, several polyaromatic alkaloids (berberine derivatives, chelerythrine sanguinarine, cryptolepine, neocryptolepine, ascididemin, and meridine) bind sequences adopting different G4 topologies, for example d(GGGTTA)$_3$GGG, (dG$_4$T$_4$G$_4$)$_2$, (dTG$_4$T)$_4$, (dT$_2$G$_5$T)$_4$, with 1:1 to 8:1 stoichiometries.[606,1052,1083,1084,1091,1092] The preservation of two ammonium ions in the complex suggests an external stacking binding mode and the 1:1 and 2:1 stoichiometries are compatible with end-stacking, but the possibility of groove binding cannot be ruled out, especially when higher stoichiometries are observed. For example, distamycin A formed 1:1 and 2:1 complexes with the parallel G4 (dT$_2$G$_5$T)$_4$ at equimolar ratios,[507] although it is reportedly a G-quadruplex groove binder.[1129]

Ru and Pt-based mononuclear metal complexes bind to (dT$_2$G$_5$T)$_4$ to form 1:1 to 4:1 complexes.[1069,1106] The complex formation between Pt(II)-tripod ligand and human telomeric hybrid G4 dA$_3$(GGGTTA)$_3$GGGAA has been studied by NMR and ESI-MS. ESI-MS titration detected 1:1 complexation at equimolar ratio and higher stoichiometry at higher molar ratios. After adding 3 molar equiv. of Pt(II)-tripod, ligand-induced dimerization of G4 subunits occurred, as attested by the formation of 3:2 and 4:2 stoichiometries. NMR confirmed the monomer 1:1 and the interlocked dimer 4:2 structures and demonstrated the end-stacking with the G-quartet core (Figure 15C).[410] Other Pd and Pt metallo-rectangles complexes have been studied using ESI-MS. These studies confirm that the compounds interact with quadruplex DNA and, particularly in the case of the platinum(II) complex, a dimerization of G-quadruplex structures is observed.[977]

Dicarbene Au(I) planar complexes also bind to human telomeric G4 according to ESI-MS.[1107,1108] [Au(1-butyl-3-methyl-2-ylidene)$_2$]$^+$ binds to the human telomeric G4 dTA(GGGTTA)$_3$GGG with a 1:1 stoichiometry whereas (Au(9-methylcaffein-8-ylidene)$_2$) shows 1:1 to 3:1 stoichiometries at equimolar mixing ratio. Simultaneous binding of three ligands is confirmed by X-ray crystallography, showing two ligands at the 5'-end of the G4 and one ligand at the 3' end.[1107]

In summary, the binding stoichiometry inferred from ESI-MS can give clues about the ligand-binding mode (for example based on the number of known binding sites), and help formulate structural hypotheses that can be tested by NMR or X-ray crystallography. The preservation of specific cations along with ligands suggests the absence of intercalation binding mode of most ligands. However, it is not possible to distinguish between groove binding or end-stacking based solely on the stoichiometry. The detection of high ligand stoichiometries pinpoints additional binding sites, possibly nonspecific interactions with the grooves, loops or phosphate backbone of the quadruplex.

4.5.3.2 Ligand binding affinities and selectivities

From the relative intensities of the complexes and free target, the equilibrium association constants can be determined for each stoichiometry, or at least relative estimates of the binding affinities (section 3.1.4 for details). Comparing ligand affinities can be used to select the best ligand for a given target. For example, it was used to test different ligand substitutions on organometallic complexes.[786] NanoESI-MS spectra of the human telomeric G4 $d(T_2AG_3)_4$ with different cyclo[*n*]pyrroles (*n* = 6—8) showed 1:1 complex formation, and the relative binding affinity from ESI-MS was rationalized in terms of size and location of the positive charge in the macrocycle.[1098] The smaller size porphyrinoids binds strongly due to having a better superposition of the quartet with the ligand core. A positively charged ligand cyclo[6]pyrrole binds strongly compared to the neutral molecule octa-ethyl porphyrin.

One can also measure relative affinities to assess ligand selectivity among different targets (e.g. DNA vs RNA G4s, G4 vs dsDNA), or even different G4 topologies. Ascididemin and meridine display a slight preference for the intramolecular human telomeric G4 $d(GGGTTA)_3GGG$ over the tetramolecular parallel G4 $(dTGGGGT)_4$.[1052] BRACO-19 exhibited a two-fold higher binding affinity for telomeric DNA G4 $dAGGG(TTAGGG)_3$ vs its RNA counterpart $rAGGG(UUAGGG)_3$.[608] In contrast, chelerythrine, TMPyP4, and glucosaminoside derivatives showed stronger binding with human telomeric RNA G4 $r(UUAGGG)_4UUA$ in comparison to its DNA counterpart $d(TTAGGG)_4TTA$.[1092,1094,1102] However, as the same sequence adopts a different G-quadruplex topologies in DNA and RNA (RNA typically favoring parallel-stranded topologies), further studies would be required to parse the role of the backbone and the role of the topology.

The assessment of duplex versus quadruplex binding selectivity is important to design G4-specific molecular probes for biology. Since ESI-MS can monitor each species having different *m*/*z* in solution, a control ESI-MS experiment in presence of duplex DNA can give information about the target specificity of the ligands. Ditercalinium, ascididemin and meridine showed a higher binding affinity for quadruplexes in comparison to the Dickerson-Drew dodecamer duplex $(dCGCGAATTCGCG)_2$,[599,1052] while cryptolepine and neocryptolepine exhibited a higher affinity for triple helical DNA followed by GC-rich duplexes and then quadruplexes.[606] A 1,3-disubstituted indolyl berberine derivative (SS14) prefers quadruplex DNA over duplex DNA, although the binding affinity is modest.[1083] Tel01 demonstrated higher selectivity than distamycin A and DTC for G4 versus duplex DNA $(dGCGAATTCGC)_2$, as evidenced from ESI-MS titration.[507] Among perylene diimides derivatives, PIPER, Tel11, Tel19, and Tel32 have a poor selectivity while Tel01, Tel12, and Tel34 prefer G4s to duplex DNA. For some ethidium derivatives, preferential binding to G4 structure $d(GGGTTA)_3GGG$ in comparison to duplex DNA was observed.[607] Among all quadruplex binders, bisquinolinium dicarboxamide derivatives (Phen-DC3, Phen-DC6, 360A) showed the highest selectivity for quadruplex compared to DNA duplexes (Figure 74).[1053]

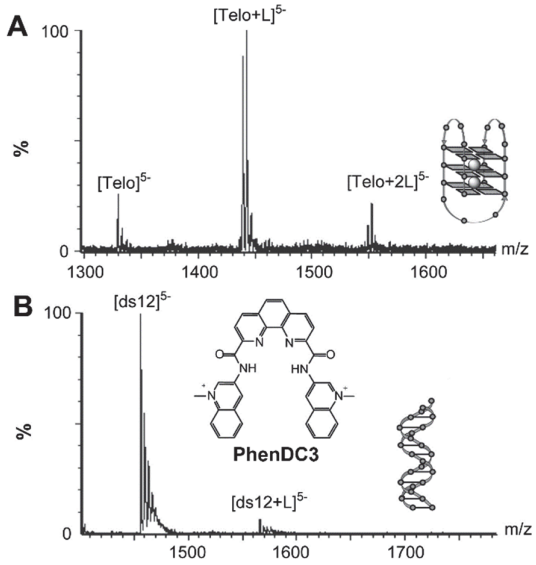

Figure 74. ESI-MS spectra of Phen-DC3 (L; 5 µM) with A. the telomeric G-quadruplex d(T_2AG_3)$_4$ (Telo; 5 µM) and B. the 12-mer duplex (dCGCGAATTCGCG)$_2$ (ds12; 5 µM), in 150 mM NH_4OAc and 15% MeOH. The amount of Phen-DC3 bound quadruplex is 4.9 µM and 0.1 µM, respectively. Figure adapted with permission from Ref. 1053. Copyright 2008 Elsevier.

The ligand specificity can in some instances induce equilibrium shifts.[1116] Dehydrocorydaline can shift the equilibrium from dsDNA toward G4, whereas TMPyP4 facilitates the transition of G4 to the dsDNA in a mixture of bcl-2 quadruplex and the complementary C-rich strand.[1097,1130] In a mixture of G4 and duplex DNA, ImImImβDp binds to both duplex and G4 while Tel01 and daidzin selectivity recognize the G4.[1082,1117]

In 2003, Rosu *et al.* revealed by ESI MS-based kinetics experiment that the binding of telomestatin to the human telomeric G4 d(GGGTTA)$_3$GGG delays the unwinding of the G4 structure and the formation of the duplex with its complementary strand (Figure 75).[628] This is primarily due to the selectivity of telomestatin for G-quadruplexes over duplexes. The free fraction of G4 is consumed at the same rate as without the ligand, but the fraction of G4 bound is consumed more slowly. Therefore, ESI-MS-based competition experiments can also be designed as kinetics experiments.

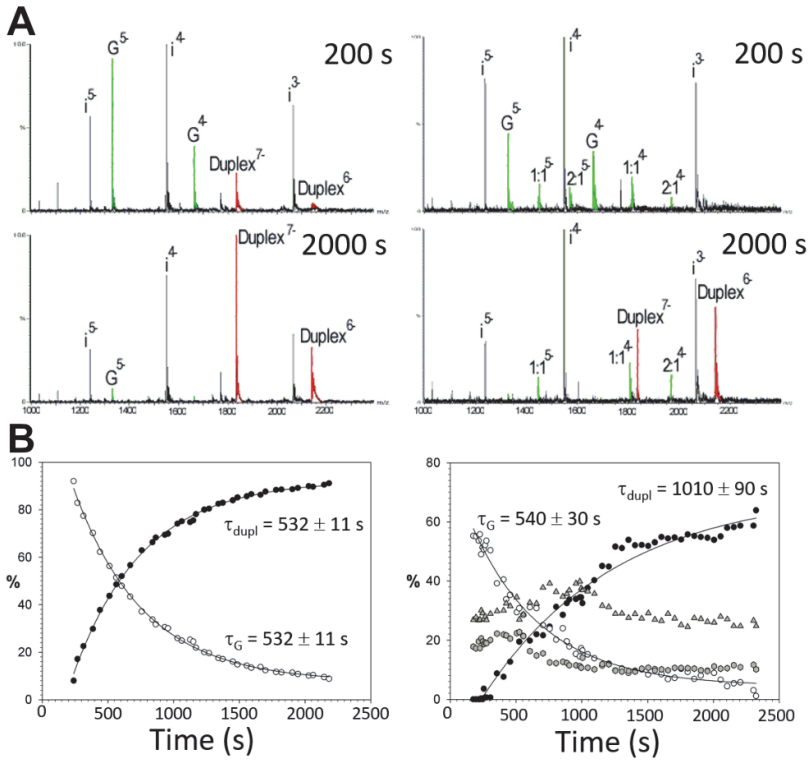

Figure 75. A) left: ESI-MS spectra of a mixture of 5 µM d(GGGTTA)$_3$GGG ("G") and 5 µM d(CCCAAT)$_3$CCC ("i") after 200 s (top) and 2000 s (bottom). Right: ESI-MS spectra of a mixture of 5 µM "G", 5µM telomestatin, and 5 µM "i" after 200 s (top) and 2000 s (bottom). "Duplex" stands for "G·i"; "1:1" stands for "telomestatin·G"; "2:1" stands for "2telomestatin·G". B) Relative abundances of the different forms of the G-strand as a function of time. The complementary strand (5 µM) is added to a solution (5 µM) of preformed d(GGGTTA)$_3$GGG quadruplex alone (left) or in the presence of 5 µM telomestatin (right). (black circle): duplex; (open circle): free G-strand; (triangle): 1:1 complex with telomestatin; (square): 2:1 complex with telomestatin. Figure adapted with permission from Ref. 628. Copyright 2003 RSC publishing.

4.5.3.3 Deduction of ligand binding mode and binding site(s)

4.5.3.3.1 Ligand-induced cation capture or release

In native ESI-MS, the binding of a ligand often preserves the number of specific cations (K^+, NH_4^+) coordinated between the G-quartets, which suggests no major rearrangement (in terms of number of quartets) upon ligand binding. This occurs for stable parallel-stranded G-quadruplexes, suggesting external ligand binding and not intercalation between the G-quartets. In this section, we will discuss the cases where ligand binding promotes cation addition or ejection from the target G4 sequence. Figure 76 summarizes some of the lessons learned using ESI-MS.

The geometry of the macrocycle ring of telomestatin facilitates monovalent cation coordination (K^+, NH_4^+) of telomestatin in its free form. A ternary complex (quadruplex:cation:ligand) was observed by ESI-MS for different G4 topologies i.e. $(dTG_4T)_4$ (parallel), $(dT_2AG_3)_4$ (hybrid), and $dGAG_3TG_4AG_3TG_4A_2G$ (parallel).[1095,1096] Cation-induced stabilization suggests an end-stacking binding mode, which is supported by molecular modeling studies.[1131] Later, high-resolution NMR derived conformation of telomestatin derivative L2H2-6M(2)OTD binding to the human telomeric hybrid quadruplex $dTT(GGGTTA)_3GGGA$ confirmed the end-stacking binding mode (Figure 15D).[1132] In those cases, the ligands did not cause a conformational change in the studied G-quadruplexes.

In another scenario, the ligand-induced cation capture can indicate a change of G-quadruplex conformation to a topology containing one more G-quartet. Circular dichroism spectroscopy is needed to distinguish the topology change. Cu-ttpy binds to the human telomeric G4, $dGGG(TTAGGG)_3T$ (this

structure has two quartets and contains one high-affinity K^+ binding site) with high affinity and cooperativity, and captures one additional K^+ in the (2:1) ligand:G4 complex.[615] Comparison of the Cu-ttpy selectivity for several antiparallel structures revealed a preference for a particular antiparallel fold (the so-called basket antiparallel, with a lateral-diagonal-lateral loop combination). With parallel G4 sequences, ligand binding cooperativity is absent. ESI-MS titration with other metal derivatives (Zn, Pt, and Pd) showed no ligand cooperative binding.

Ligand-induced cation capture can also occur upon G-quadruplex formation starting from unfolded strands. For example, a sequence such as $dTG_3ATGCGACAGAGAG_2ACG_3A$ cannot form a G4 in 1 mM K^+ and 100 mM TMAA because it has only two GGG repeats, one GG repeat and isolated Gs. However, in presence of Phen-DC3, a complex with two ligands and one K^+ is formed.[976] Such experimental design is a stringent test for finding ligands able to induce G4 formation. In our group's experience, every time we were asked to test a ligand that was found by other biophysical methods to induce G-quadruplex formation *in the absence of cation*, ESI-MS actually revealed cation uptake. Oftentimes supposedly "pure" water contained traces of alkali cations (Na^+, K^+,…) or oligonucleotide synthesis restudied contained NH_4^+ ions that cooperated with the ligand to induce G-quadruplex formation. When the experiments were repeated with purified samples, the results were different, reason for which such results ended up unpublished.

Phen-DC3,[916] 360A[916] and some analogues[1125] have such a strong preference for 2-quartet (1-K^+) antiparallel G-quadruplexes that they can induce a rearrangement from 3-quartets (2-K^+) human telomeric sequences to a 2-quartets topology. A conformational selection mechanism was proposed.[976] The noncovalent ligand binding site is close to the central loop and was pinpointed by electron photo-detachment (EPD) and CID on a Phen-DC3 derivative bearing a cross-linker.[660] A conformational selection mechanism is also established for the perylene derivative K20 binding to the c-KIT promoter G4 sequence. ESI-MS experiments showed that K20 preferentially binds to long-lived off-pathway 2-quartet conformation whereas the parent ligand PIPER binds more poorly.[1115]

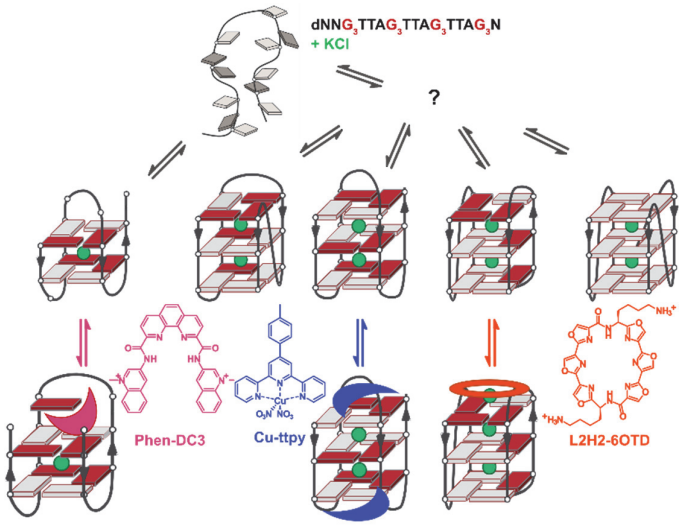

Figure 76. Summary of the polymorphism and folding pathways of telomeric G-quadruplexes,[199] and ligand preferences deduced from stoichiometries observed by ESI-MS (pink: Phen-DC3,[916] blue: Cu(II)-ttpy,[615] orange: L2H2-6OTD[916]).

4.5.3.3.1 Coordination vs. non-covalent binding of organometallic complexes

ESI-MS was used to distinguish and quantify noncovalent and coordination binding modes for Pt(II) and Pd(II) complexes containing a ttpy or tMebip tridentate ligand, and a chloride as the fourth ligand.[316] Upon dilution in water, the complexes are partially hydrolyzed (an aqua ligand replaces the

chloride) and both forms can bind non-covalently to G4s. ESI-MS allows the simultaneous detection of the non-covalently bound and the coordinated populations to the DNA targets (Figure 77). Pd(II) complexes show a larger amount of coordination to the nucleobases (loss of Cl^- or OH), which was further confirmed by shifts in the metal-to-ligand charge-transfer band by UV spectroscopy. Since all the specific ammonium cations are preserved, guanines of the quadruplex core are free from metalation. Relative quantification from ESI-MS indicated preferential noncovalent binding for platinum complexes and coordination for palladium complexes, but no structural selectivity was observed.

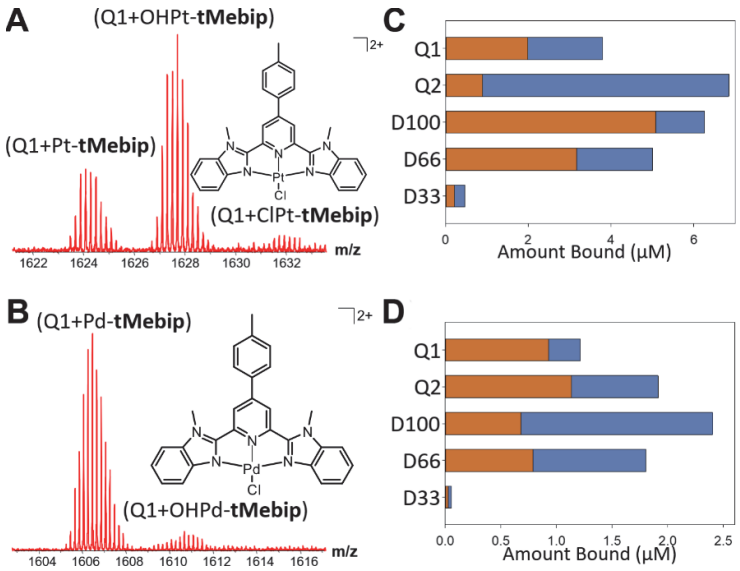

Figure 77. Left: ESI-MS mass spectra of Pt-tMebip (A) and Pd-tMebip (B) with the quadruplex $(dTGGGGT)_4$, 1 h after mixing (zoom on the 5- charge state). Right: amounts of Pt-tMebip (C) and Pd-tMebip (D) ligands (8 μM) bound to different DNA G-quadruplex (Q1 = $(dTGGGGT)_4$, Q2 = human telomeric sequence $d(GGGTTA)_3GGG$ and duplex (D100= $(dCGCGGGCCCGCG)_2$, D66 = $(dCGCGAATTCGCG)_2$, D33 = $(dCGCAAATTTCGC)_2$) structures (4.8 μM), 1h after mixing. The brown and blue bars correspond to the fractions of direct coordination and non-covalent binding (under the aqua or chloride forms), respectively. Figure adapted with permission from Ref. 316. Copyright 2011 Wiley.

4.5.3.3.2 Binding sites inferred from competition experiments

Fluorescent intercalator displacement (FID) is a widely used solution assay that probes the binding of small molecules to nucleic acids by displacement of a fluorescent probe that is quenched when free in solution. It was first introduced by Morgan *et al*. using ethidium bromide as a duplex probe[1071] and adapted to fast screening using 96 well plates.[1133] The assay was then adapted to G-quadruplex targets by Monchaud *et al.* using thiazole orange (TO) as the fluorescent probe.[1134] The relative affinity of a ligand for a given target is often evaluated with the DC_{50}, which is the concentration required to lower the fluorescence by half. Comparison between G-quadruplex targets is subject to the assumption of similar binding of TO (giving similar quantum yield) whatever the target.

The binding between TO and different duplex DNA target and quadruplexes (human telomeric sequence $dGGG(TTAGGG)_3$ and thrombin binding aptamer $dG_2T_2G_2TGTG_2T_2G_2$) has been evaluated by ESI-MS.[1053] For both G4s, ligand binding stoichiometries higher than (1:1) were observed (up to 3:1), suggesting several binding sites for TO. Fitting of fluorescence titrations was satisfactory with a (1:1) stoichiometry, so ESI-MS was key to reveal this point (see also section 3.1.4.3 on thioflavin T[625]). Mixed complexes between DNA target, TO and candidate ligand have also been observed. A consequence of the multiple binding sites is that ligand displacement is not always successful. ESI-MS for example helped to explain inconsistent FID results obtained for the Pu24 G-quadruplex

$dTGAG_3TG_3GAG_3TG_4A_2G_2$ with c_{ex}-NDI ligands and TO. Both individual complexes (TO:Pu24 and c_{ex}-NDI:Pu24) and the ternary complex TO:c_{ex}-NDI:Pu24 can be detected. This result explained the false-negative results in the G4-FID assay, as the two ligands can simultaneously bind different sites of G4-structure.[413]

In a competition experiment designed to account for other interacting macromolecules present in the cellular environment, Marchand *et al.* studied how ligand binding can influence interactions of a RHAU helicase peptide (Rhau18) with G4 sequences from gene promoters and human telomeres.[1124] In the orthosteric mechanism, ligands displace peptides from the same binding site depending upon their respective binding affinities. ESI-MS of the G4-ligand-peptide mixtures revealed that Phen-DC3 displaces the two bound peptides almost entirely from the parallel G4 $dTT(GGGT)_4$, forming Phen-$DC3)_2$:Rhau18 complexes and smaller amounts of the ternary complex Phen-DC3:Rhau18:G4 (Figure 78).TMPyP4 displaces one of the two peptides and forms mainly the complex TMPyP4:Rhau18:G4. Proflavin is barely able to displace Rhau18. The various displacement effects can be predicted from the relative binding affinity of different ligands and Rhau18 peptide. In contrast, in the allosteric mechanism, ligand binding induces a conformational change that influences the peptide binding affinity either positively or negatively. For example, Cu-ttpy induced a conformational change that increased the binding affinity of the peptide for human telomere G4, $dTT(GGGTTA)_3GGGA$. This result shows for the first time how ligand binding could influence the binding of other biomolecules.[1124]

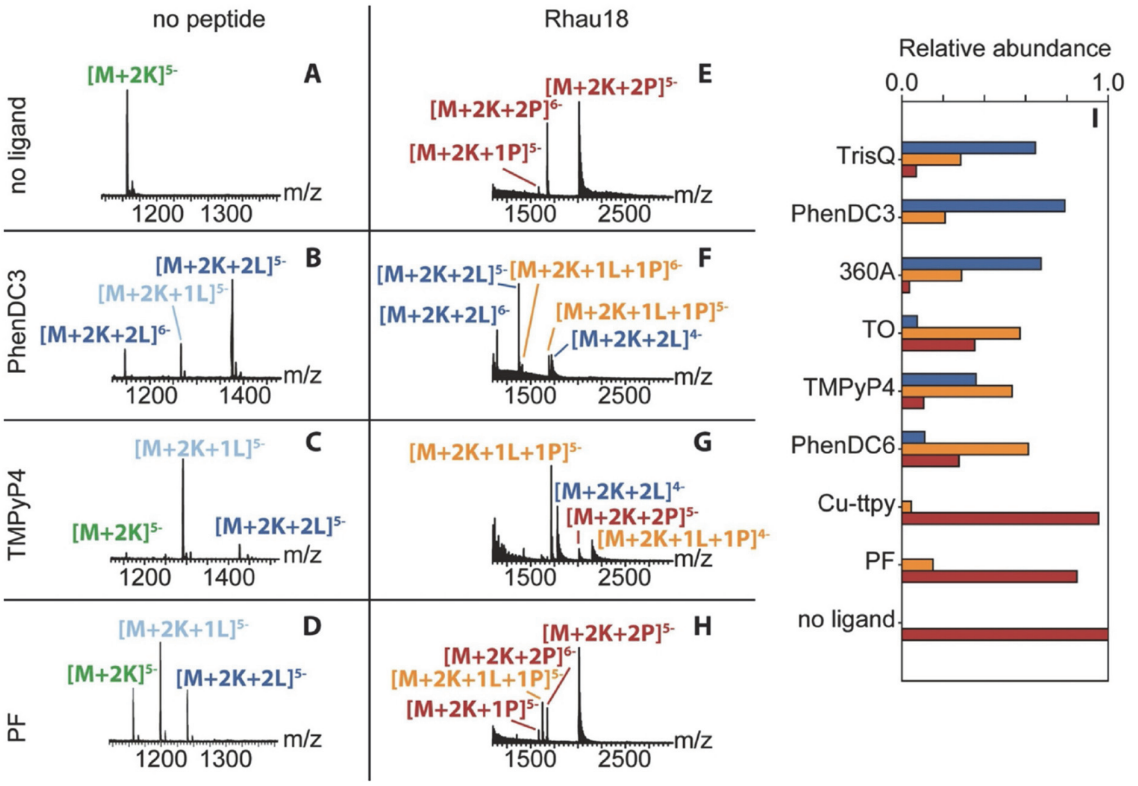

Figure 78. Mass spectra of 10 µM T95-2T ("M") without (A–D) and with 40 µM Rhau18 ("P") (E–H), and in the absence of ligand ("L") (A,E) and the presence of 20 µM Phen-DC3 (B,F), TMPyP4 (C,G), and proflavine (D,H). I. Relative abundance of DNA complexes containing only small-molecule ligands (blue), only Rhau18 (red), and both small-molecule ligands and Rhau18 (orange). Figure reproduced with permission from Ref. 1124. Copyright 2020 Wiley.

4.5.3.3.3 Gas-phase fragmentation

The CID profile of quadruplex-ligand complexes can help to assess ligand binding modes. In principle, a ligand that binds through end-stacking binding mode is expected to be lost before single-stranded fragments appear. For dsDNA minor groove binders, retention of ligands with the single-stranded fragments is anticipated due to the binding of the ligands in the groove.[489]

Mesoporphyrin IX binds to the tetramolecular parallel G4 $(dTG_4T)_4$ with the retention of the 3 specific ammoniums in the quadruplex. MS/MS experiments validate this hypothesis because upon collisional activation, the porphyrin is lost as neutral or with one negative charge, leaving behind the intact quadruplex with 3 specific cations.[926] Complexes between the perylene ligand tel01 and the tetramolecular quadruplex $(dT_2G_5T)_4$ undergo facile loss of the drug and dissociation into the constitutive single strand ions.[507] In contrast, complexes with distamycin A or diethylthiocarbocyanine dissociate into single strands onto which the drug molecule is retained. This led to a groove binding hypothesis for distamycin A and DTC and an end-stacking hypothesis for Tel01. The groove binding property of distamycin A towards quadruplex DNA has been postulated based on the previous 2D solution NMR.[1129] Note however that, depending on the instrument used, the time scale of the fragmentation can change and thus the CID fragmentation pathway can differ (see section 4.3.1.3 on duplex DNA). When performing CID on a bimolecular quadruplex $(dGGGTGGGTGGGTGGGT)_2$ using an ion trap, the sequential loss of inner NH_4^+ ions (as NH_3) is observed. Upon CID activation, the perylene ligand Tel03 leaves the quadruplex as a neutral. The complex with Tel03 has a higher gas-phase kinetic stability than linear pyrrole polyamide (PyPyPyβDp) and imidazole polyamide (ImImImβDp) derivatives.[1113] The end-stacking binding mode of perylene diimide derivatives is compatible with the fragmentation pathway and with the NMR-based end-stacking model of the perylene diimide derivative PIPER.[404] Upon CID, biphenyl ruthenium drug sticks to the fragments of negatively charged strands from the quadruplex $dA(G_3T_2A)_3G_3$.[1104] Analysis of the CID spectra identified coordination of thymines (T6, T17) and not guanines for a complex with human telomeric G4. This suggests the implication of flexible thymine loops (TTA) in the interaction of these Ru(II) complexes.

MS/MS has been used to localize ligands on a G-quadruplex. For non-covalent complexes, it is not a trivial experiment because of the possibility of losing the initial binding location during gas-phase rearrangements upon activation. Using radical-based fragmentation methods helps lowering the required activation energy because the covalent bonds are weaker (see section 3.2.1.1.2). Electron photodetachment (EPD) was used to locate the binding region of Phen-DC3 to telomeric G4s by native top-down sequencing of the drug-nucleic acids complex.[660] The radical cations were produced with a UV laser from the isolated complex of interest by electron photodetachment, then fragmented by CID. The fragmentation pattern indicates that the ligand is bound close to the central loop, thereby allowing to rule out some complex topologies.

In summary, straightforward interpretation of the binding mode from MS/MS spectra is difficult because of several limitations. As in the case of duplex ligands, the fragmentation channels (all studied in the negative ion mode) depend on the charge of the ligand: ligands with a permanent positive charge will stick to the strands, whereas neutral ligands or ligands that can become neutral by giving a proton to the nucleic acid can come off as neutral.[489] The charge state of the drug-nucleic acid complexes can also influence the dissociation pattern. For the determination of the binding site of non-covalent complexes, native top-down using radical-based dissociation methods however provide useful information.

4.5.3.3.4 Ion mobility spectrometry combined with molecular modeling

The combination of ESI-MS with ion mobility (IM-MS) and molecular modeling can help distinguish several conformations having the same *m*/*z*. This is beneficial to differentiate ligand-binding models for G4-ligand complexes. In 2006, Baker *et al.* studied the size-dependent binding of cyclo[*n*]pyrroles (*n* = 6—8) and porphyrins with human telomeric G4.[1098] The observation of one symmetrical peak in the ATD of all complexes suggested that either only one conformational ensemble is present or several conformation families having the same collision cross-section (CCS) values. Molecular modeling with several plausible binding modes as starting conformations showed that ligand end stacking to the antiparallel chair/basket forms of G4 was compatible with the observed CCS, while intercalation, groove biding, or non-specific adduct formation could be discarded. Note that, at the time, 3-quartet hybrid or 2-quartet antiparallel conformations were not considered. In 2007, Gabelica *et al.* demonstrated the end stacking binding models of G4 ligands (PIPER, TMPyP4, MMQ1, MMQ3, BOQ1) with the human telomeric quadruplex d(GGGTTA)$_3$GGG and the c-myc G4 dGAG$_3$TG$_3$GAG$_3$TG$_4$AAG, although intercalation could not be completely ruled out except for BOQ1.[708]

4.5.3.3.5 Ligand binding thermodynamics using temperature resolved ESI-MS

In 2018, Marchand *et al.* thermodynamically characterized individual stoichiometry sub-state G4:cation:ligand by monitoring the equilibria using a homemade temperature-controlled nanoESI source.[638] Only 1:1 complexes (ligand:G4) are observed at room temperature for several ligands (e.g. Phen-DC3, TMPyP4, Cu-ttpy, TrisQ), but 2:1 complexes are observed at high temperature. This unexpected observation might explain seemingly anomalous behaviors in the melting process monitored by solution UV-melting (e.g. for TrisQ; see Figure 79C) due to the release of water trapped in the system and conformational strain in end-stacked bases. In contrast, TMPyP4 binding to the human telomeric quadruplex dTT(GGGTTA)$_3$GGGA is enthalpically favorable, and this suggests a different binding mechanism.

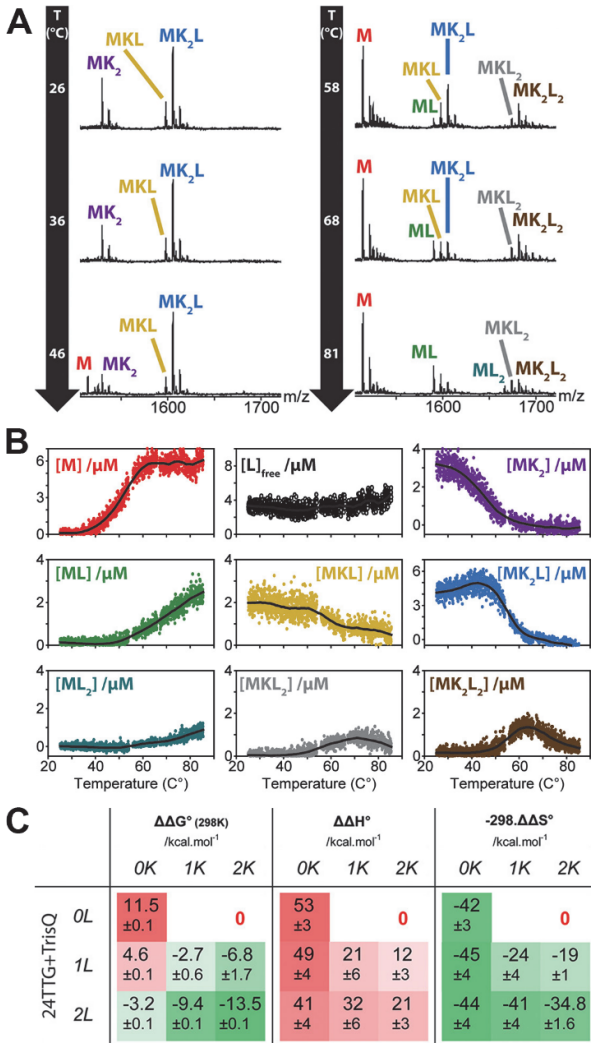

Figure 79. MS-melting of 10 µM 24TTG with 10 µM TrisQ in 100 mM TMAA and 1 mM KCl. A. Mass spectra obtained at various temperatures (zooms on the 5− charge state). B. Quantification of each state distinguished based on its stoichiometry. The concentration of free ligand is obtained by difference. C. Thermodynamic parameters for potassium cation and ligand binding to G-quadruplexes. ΔΔG°, ΔΔH°, and −298.ΔΔS° are relative to the folded G-quadruplex (MK_2). The values are color-coded, indicating how favorable (green) or unfavorable (red) is a given state compared to the free G-quadruplex, should the reaction be carried out at 1 M concentration of each partner. The reported uncertainties are the standard deviations from repeated experiments, considering uncertainty propagation when sequential reactions are used for the van't Hoff regressions. Figure adapted from Ref. 638. Copyright 2018 American Chemical Society.

4.5.4 Ligands targeting biologically relevant RNA

The use of ESI-MS to screen ligand libraries against RNA targets of pharmaceutical interest was pioneered in 1999 by Hofstadler, Sannes-Lowery and Griffey at Ibis Therapeutics. Figure 80 shows a typical ESI-FTICR-MS spectrum obtained from a mixture of two targets (the prokaryote 16S ribosomal RNA A-site, and the mass-tagged eukaryote variant) and several aminoglycoside ligands.[1135,1136] The goal was to find antibiotics specific of the prokaryote ribosome. Direct native MS binding assays were scaled up into high-throughput screening assays.[612,617,1137–1139] Moreover, direct ESI-MS titrations allow to determine the equilibrium dissociation constants. Earlier work used linearized Scatchard plots[611,1136] while later work used non-linear fitting of the fraction of RNA bound as a function of [L].[617] Besides the 16S rRNA A-site, other targets for Ibis Therapeutics were the 23S ribosomal RNA,[1140] or the hepatitis C virus internal ribosome entry site.[1139] ESI-MS is particularly well adapted to fragment-based drug discovery, because the technique is able to detect small amounts of complexes and thus weak

binders.[588,1140,1141] When two fragments are able to bind simultaneously to their target, they likely do so at different binding sites and can be combined to form a larger, higher-affinity molecule.

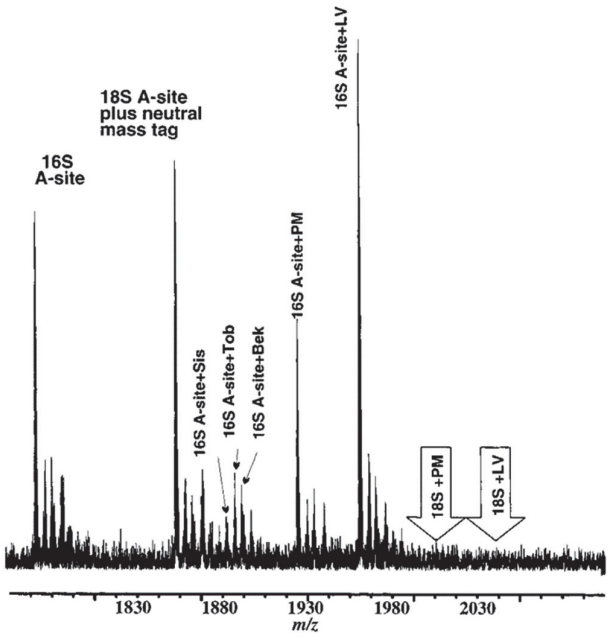

Figure 80. Multitarget affinity/specificity screening of 16S and 18S RNAs with a library of 5 aminoglycosides: sisomicin (Sis), tobramycin (Tob), bekanomycin (Bek), paromomycin (PM), and livodomycin (LV). Signals from the $(M - 5H)^{5-}$ charge states of free 16S and 18S RNAs are detected at m/z 1801.515 and 1868.338, respectively. Consistent with the higher binding affinity of these aminoglycosides for the 16S A-site relative to the 18S A-site, aminoglycoside complexes are observed only with the 16S rRNA target. Note the absence of 18S-paromomycin and 18S-lividomycin complexes, which would be observed at the m/z values indicated by the arrows. Figure adapted from Ref. 1135. Copyright 1999 American Chemical Society.

The Fabris group also studied ligand binding to the 16S rRNA A-site[1142], then devoted several papers to the stemloop (hairpin) domain of the HIV-1 packaging signal.[509,1005,1008,1143] Specific interactions between this Ψ-RNA and the nucleocapsid (NC) domain of the Gag polyprotein mediate the vital functions of genome recognition, dimerization and packaging, and therefore ligands that would disrupt this NC-RNA interaction were of prime interest. ESI-MS was used to determine the equilibrium dissociation constants of several aminoglycosides, as well as classical minor groove binders and intercalators, for three Ψ-RNA stemloops. The best binders were the aminoglycoside neomycin B and intercalators ethidium bromide and mitoxantrone. However, when tested on a stemloop·NC complex, only neomycin B was able to displace the NC by binding to the stemloop, while intercalators form ternary complexes. This type of competition experiment is key to test that binding has potentially the desired biological effect. The Fabris group also studied ligand binding to the kissing loop dimer or the extended duplex dimer forms of the considered stemloop, in the context of genome dimerization,[1005,1008] as well as ligand recognition by RNA:DNA hybrid duplexes from the HIV-1 polypurine tract.[1144,1145]

Collision-induced dissociation can be used to locate aminoglycoside binding sites on RNA. Griffey *et al.* reported that upon SORI-CID, the aminoglycoside binding sites were protected from fragmentation in 16S rRNA A-site.[1135,1146] Turner and Fabris exploited the approach to pinpoint the neomycin B (Chart 7) binding sites on stemloop RNAs (Figure 81).[509,1008] The salt bridge interactions between the protonated NH_2 groups of the aminoglycoside and the RNA make the complex more kinetically stable in the gas phase than the covalent phosphodiester bond cleavage, and thus native top-down approaches are appropriate.

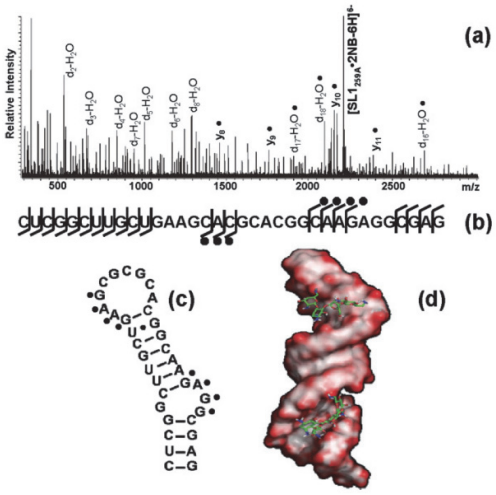

Figure 81. (a) Product ion spectrum and (b) fragmentation map of the $SL1_{G259A}$•2NB assembly. The fragmentation pattern obtained by SORI-CID displayed protection of G254:G257 and G270:G272, which are located in double-stranded regions near the internal bulge and immediately below the apical loop, as indicated on the hairpin secondary structure (c). These results were corroborated by docking the ligand molecule onto the electrostatic surfaces of SL1 (d). Figure reproduced with permission from Ref. 1008. Copyright 2008 Wiley.

The Chow group studied peptide binding to the 16S A-site[601] and 23S helix 69[602,605] ribosomal RNA using direct detection of the complexes and determination of the equilibrium dissociation constants. For both of these targets as well as helix 31 and TAR (transactivation response element) RNA, they also studied the underpinnings of fluorescence displacement experiments by ESI-MS.[1017] The Nakatani group developed ligands binding specifically to RNA CUG expansion repeats, and the binding was evaluated by ESI-MS.[1147]

A couple of methods papers on the direct detection of RNA-ligand interactions by ESI-MS are available,[604,1148] but despite its promises native mass spectrometry is still not widely adopted for the biophysical characterization of RNA-ligand complexes. A possible reason is the skill required to prepare salt-free RNA samples to obtain high-quality spectra. Affinity selection mass spectrometry methods alleviate this problem. In that method, the RNA targets are exposed to ligand libraries, separated by size-exclusion chromatography, then denatured so that the small molecule ligands can be identified and quantified by mass spectrometry.[1149–1151] This method is used for other targets as well, including G-quadruplex DNA.[1152]

4.5.5 Aptamer complexes with their targets

DNA or RNA aptamers can be raised against any kind of target, from small molecules to entire cells. Affinity capture on aptamers can be used to detect their targets, for example by MALDI-MS.[1153–1156] Such method did not rely the preservation of the intact complex. With carefully tuned sample preparation conditions, MALDI can be used to detect aptamer-protein complexes.[1157] This observation on the thrombin-TBA complex (the thrombin binding aptamer TBA is a G-quadruplex) is made possible by salt bridge interactions between the protein and RNA. Native ESI-MS studies on this complex showed that at low ionic strength, the complex is more stable and even 2 TBA can bind per thrombin.[1158] In the same study, native top-down sequencing of the protein by ECD allowed to pinpoint the aptamer binding sites. Native ESI-MS was used to determine peculiar stoichiometries of other aptamer-protein complexes, for example up to two aptamers bound per streptavidin,[1159] or one aptamer bound per NF-κB dimer.[1160]

The other native ESI-MS studies concern aptamers binding to small molecule ligands. The first aptamer-ligand complexes were reported by the Brodbelt group.[946] The amounts of detected complex between the tobramycin RNA aptamer and tobramycin and other aminoglycosides reflect the relative solution binding affinities. However, the complexes between the (DNA) ATP aptamer and (RNA) FMN aptamer and their respective negatively charged ligands required divalent cations (Mn^{2+} was used in this study). They were more fragile in the gas-phase, and the relative intensities did not reflect well the solution binding affinities.

Guo *et al.* studied the DNA argininamide binding aptamer (ABA) that binds up to two L-argininamide ligands,[1161] and studied the equilibrium affinity constants in detail. Salt-bridge interactions make this complex stable in the gas phase. Quinine binding to the (DNA) cocaine binding aptamer (CBA) was studied by several groups.[1162–1165] More complex is detected in both the negative and the positive mode (although there is less complex in that mode),[1165] and in high ammonium acetate concentrations.[1162] Based on the detection of the quinine-CBA and argininamide-ABA complexes, while the ampicillin complex with its aptamer could not be detected, Bottari *et al.* concluded that the ampicillin did not bind, and these results were confirmed by isothermal titration calorimetry.[1164] Hence ESI-MS helps revealing false positive obtained by indirect probing methods.

Aptamers raised to target small molecules often become more structured upon binding to their ligand. Hence, ion mobility spectrometry was used to investigate the effect of ligand binding on the aptamer collision cross sections.[1163] Figure 82 shows typical IM-MS results. The difference of CCS between the free and bound forms of the aptamer is smaller than expected. At the charge states typically produced by native MS, all structures are rather compact and have similar CCS values,[1162,1165] and in that sense an unstructured single strand can end up as compact as a folded aptamer.[263] The greatest difference between free and bound forms comes from charge state distributions, as observed in Figure 82A for the adenosine binding aptamer: the amount of complex greatly depends on the charge state, or in other words, the charge state distribution of the complex is very different from the charge state distribution of the free aptamer.[1163] According to the equilibrium partitioning model in ESI mechanisms (section 3.1.1.1.2), this indicates a conformational change.[621] One would thus expect significant differences of response factors between free and bound aptamers at a given charge state. Yet a careful study of several aptamers showed only up to a 2-fold change of response factors.[932]

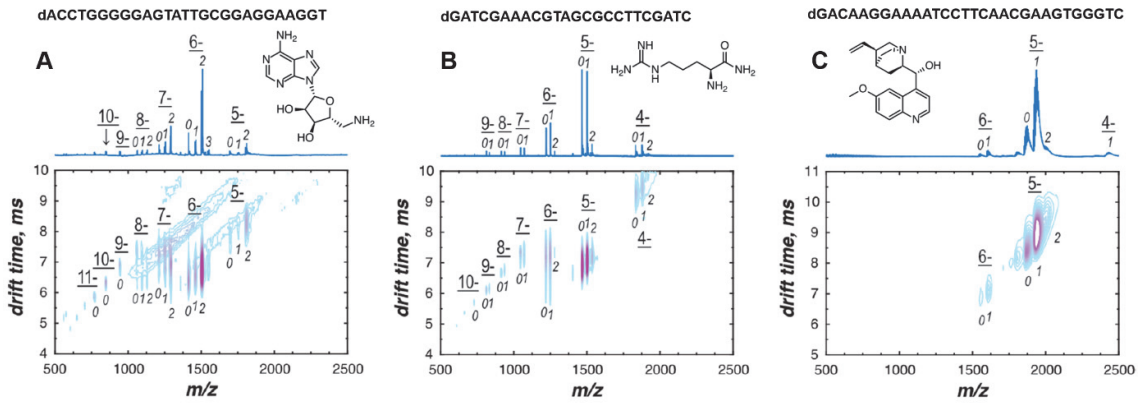

Figure 82. Native ion mobility-mass spectrometry (IM-MS) analysis of adenosine-binding (A), L-argininamide-binding (B), and cocaine-binding (C) aptamers in complexes with their specific ligands. Top traces represent mass spectra, and the contour plots below them show IM data (deeper color corresponds to higher signal intensity). Charge states of ions are indicated above the respective peaks. The number of bound ligands is indicated in smaller italic numbers. Samples (A-B) contained 10 µM aptamer, 100 µM ligand in 50 mM NH_4OAc and sample (C) contained 10 µM aptamer, 50 µM ligand in 300 mM NH_4OAc. Figure adapted from Ref. 1163. Copyright 2018 American Chemical Society.

4.6 Nucleic acid complexes with other biopolymers

4.6.1 Complexes with peptides

Negatively charged phosphate groups of nucleic acids form very stable complexes with positively charged basic side chains of the arginine and lysine residues of peptides.[537,539,658] Salt bridge formation between oppositely charged oligonucleotides and peptides stabilize the noncovalent complex,[537] as suggested by sequential MS^n experiments.[539] The relative strength of non-covalent interactions in RNA-peptide complexes and covalent RNA backbone bonds was studied by native top-down mass spectrometry.[658] MS/MS studies show that proton transfer from the peptide (protonated ligand) to the RNA (deprotonated) within salt bridges favors the ligand loss, but that proton transfer becomes energetically critical in presence of additional hydrogen bonds. Thus, salt-bridge non-covalent interactions remain in place while the nucleic acids backbone can fragment covalently.

Non covalent complexes of nucleic acids with peptides were also probed by MALDI-MS.[530,538] Strong electrostatic interactions favor the preservation of complexes between DNA and basic polypeptides (penta-L-arginine, penta-L-lysine) by MALDI-MS.[538] The relative intensity and stoichiometries of the complexes depends on the nature and size of the DNA and polybasic compounds. The observed complexes do not result from non-specific MALDI-MS aggregation but exist in solution.

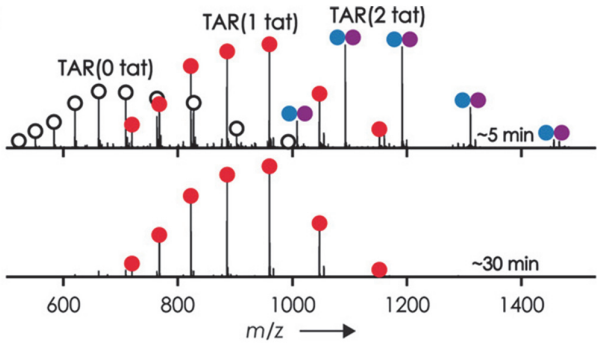

Figure 83. ESI-MS spectra of TAR and tat (2 µM each) in H_2O:MeOH (9:1) at pH 7.7 (adjusted by addition of piperidine, final concentration 1.125 mM) sprayed ca. 5 (top) and 30 min (bottom) after preparation of the solution. Empty circles corresponds to $(TAR\text{-}nH)^{n-}$; red circles are for $(TAR+tat\text{-}nH)^{n-}$; blue/purple circles are for $(TAR+2\ tat\text{-}nH)^{n-}$ ions. Figure adapted with permission from Ref. 659. Copyright 2016 Wiley.

As electrostatic interactions between the peptides and oligonucleotides are strong enough to survive in the gas phase,[659,1166] native top-down mass spectrometry of these complexes can be used to map the binding site. Complexes of HIV-1 TAR (transactivation responsive) RNA and a basic arginine-rich peptide (H_2N-GRKKRRQRRRPP-NH_2) were studied by CID.[659] This helped to probe the *tat* (transactivating) peptide binding sites in TAR RNA at the single residue level. Time-dependent MS data showed 1:2 and 1:1 stoichiometries of TAR-tat complexes, shown in Figure 83. Native mass spectrometry revealed the binding stoichiometry and binding mechanism of RRE stem IIB RNA with rev ARM peptides.[1166] ESI-MS showed that stem IIB RNA formed complexes with one or two ARM peptides and full length RRE stem IIB RNA binds with one or five rev ARM peptides. The binding site mapping was done by CID.

ESI-MS can be used to determine binding stoichiometries and ligand sequence selectivity of complexes between threading bis-intercalators and DNA.[1055] The ligand containing the -Gly_3-Lys-peptide scaffold binds to the specific site of duplex DNA containing 5'-GGTACC-3'. MS/MS data revealed information

about ligand binding interactions. Oligonucleotide-peptide cross-links can be identified by fractional mass measurements.[838] This process does not need isotope labelling or cross-linking reagents.

4.6.2 Complexes with PNA

In 2003, Sforza *et al.* published the first ESI-MS study of PNA complexes,[1167] and showed the detection of DNA-PNA duplex under soft conditions. When achiral PNA is mixed with parallel or antiparallel DNA, a stable duplex is formed. In contrast, chiral box PNA (with three adjacent D-lysine-based monomers in the middle of the strand) with parallel DNA sequence were unable to form duplex structure.

Baker *et al.* studied the formation of higher-order complexes between dye-labeled PNA and complementary dsDNA by FRET, nanoESI-MS and IM-MS.[1168] NanoESI detected the formation of hybrid PNA/DNA complexes with different stoichiometry such as PNA/DNA, PNA_2/DNA, PNA/DNA_2 and PNA_2/DNA_2. In addition, IM-MS combined with molecular dynamics showed all the possible conformations of each higher-order complex and sequence-specific binding in the complementary region for all complexes.

The binding of PNAs to G-quadruplexes was also studied by ESI-MS.[927,1009,1013] Amato *et al.* reported the formation of heteroduplexes and heterotriplexes between a short C-rich PNA and complementary DNA sequences at low ionic strength. The formation of heteroduplexes predominates over G4s in presence of high ammonium acetate and after heated and cooled at room temperature.[927] An external binding mode of C-rich PNA to G-rich DNA however preserves the G4 scaffold.[1013] Later, short PNAs sequences that can potentially bind and stabilize the c-kit87up G4 were studied using different spectroscopic techniques and ESI-MS.[1009] The shortest 5-mer PNA sequence (P1) complementary to the bases in the long loop of G4 is able to form a G4-P1 complex (the preservation of the two ammonium cations indicated the preservation of the G4 scaffold). The longer PNA sequences displayed different binding modes depending on the G4 stability: they acted as G4-binding agents in potassium while they formed hybrid PNA/DNA complexes in ammonium solution by acting as G4 openers.

4.6.3 Complexes with proteins

4.6.3.1 Detection, stoichiometry and affinity

The interactions of nucleic acids with proteins play important biological roles, for example in DNA repair and regulation, gene expression regulation, or transcription regulation. Mass spectrometry has been used to study these interactions at the molecular level.[11,1169] Here, we focus on native MS detection of protein-nucleic acid complexes and will highlight a few specific approaches to map protein-nucleic acid interfaces. Although protein-nucleic acid complexes can be studied by MALDI,[952,1157,1170,1171] the most conventional approach is nanoelectrospray.[522,1172,1173] Non-covalent DNA-protein complexes can be transferred to the gas-phase intact, where they retain the similar binding specificity and stoichiometry known in solution-phase.

Solution-phase binding stoichiometries of different non-covalent DNA-protein complexes were studied by ESI-MS early on.[1174,1175] In 1995, Greig and Griffey determined the K_D values for the complex between a 20-mer phosphorothioate oligonucleotide and bovine serum albumin (BSA).[1175] Binding of two oligonucleotides to BSA was observed. Size-specific and sequence-specific complexation was observed in protein-nucleic acid complexes.[1176,1177] For example, PU.1 interacts with a wild-type 17 base-pair sequence but not with a 19 base-pair mutant sequence.[1176] Binding of the trp apo-repressor protein under competitive conditions was observed only with dsDNA containing two specific CTAG motifs linked by a four base-pair spacer.[1177] CID experiments showed that this complex needs very high collision energy (same energy as required to break covalent bonds) to dissociate. The binding stoichiometry of the gene V protein of bacteriophage f1 with ssDNA (16 mers) was 4:1

(protein:oligonucleotide).[1178] MS results showed the presence of three protein Dicer, Ago2 and TRBP in 1:1:1 stoichiometry with an additional small RNA (11 kDa) bound to Ago2. The dynamic interactions of the E. coli RNA polymerase with σ^{70} and Rsd proteins was monitored by MS experiments.[1179] Results showed 1:1 stoichiometries for the Rsd:σ^{70} and core enzyme:RSD complexes. MS investigations revealed the stoichiometry of triple sieve tRNA editing complex.[1180] Two ProRS are complexed with one tRNA in both two- and three-component complexes. One YbaK protein binds to the 2:1 complex. Thus, the final stoichiometry for the triple sieve model ProRS:tRNA:YbaK is 2:1:1. Wild-type and mutant TRAP (trp RNA-binding attenuation protein) formed non-covalent complexes with RNA.[1181] NanoESI-MS showed that both proteins can bind a single-stranded RNA molecule at 1:1 molar ratio. The observed mass is 300 Da larger than the theoretical mass of the 1:1 complex of TRAP 11-mer with 11 Trp and RNA. Each TRAP monomer thus binds a Trp ligand in the TRAP-RNA complex. A similar trend was observed for the mutant 12-mer.

Large macromolecular protein-RNA complexes like ribosomes, spliceosomes and complexes of nucleosomes have masses in excess of 1 MDa, which are also amenable to MS studies.[1182] The study of ribosomal subunits and structural organization of the subcomplexes, small modification of intact particles can be done in the gas phase of mass spectrometers.[1173,1183–1187] MS of intact ribosomes from *E. coli* showed well resolved charge states for the small subunit 30S but for 50S and 70S charge states were not resolved. This problem was resolved in intact ribosomes from *Thermus thermophilus* by careful MS measurements,[1172] and more recently the use of higher-resolution high-mass orbitrap analyzers has improved the measurement capabilities (Figure 84).[1187]

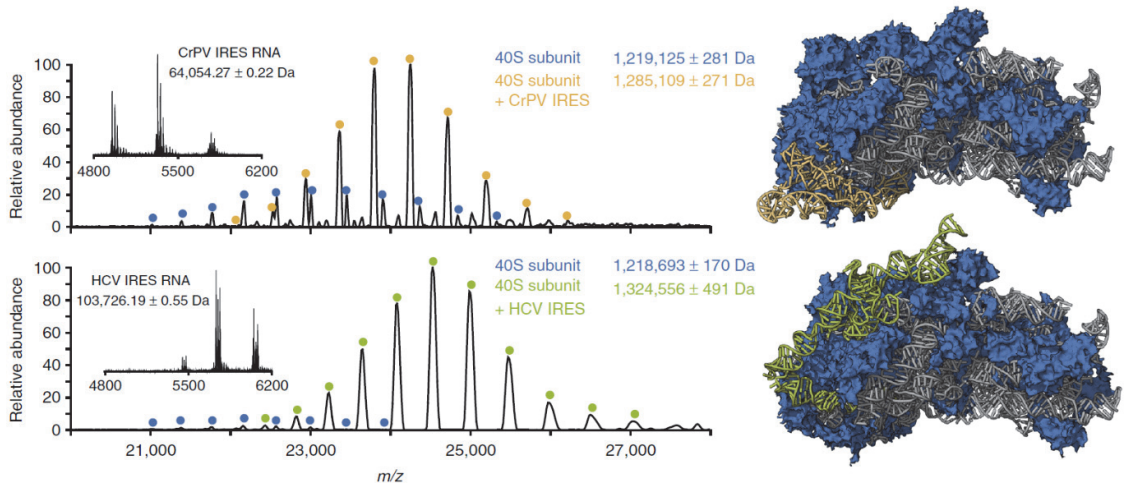

Figure 84. Monitoring of the formation of a complex containing human 40S ribosomes and Internal Ribosome Entry Site (IRES) RNA fragments of Cricket Paralysis Virus (CrPV) and Hepatits C virus (HCV). Mass spectra of the RNA fragments alone (insets) provide the accurate mass of the IRES elements. This mass corresponds well with the observed increase in mass of the 40S ribosome upon binding of the RNA indicating that the particles do not undergo a significant change in composition. Structures of the free 40S ribosomes (PDB 5A2Q) and particles bound by CrPV (PDB 4V91) and HCV IRES (PDB 5A2Q) are shown, with the ribosomal proteins in blue, the rRNA in gray and the IRES elements in yellow and green, respectively. Figure adapted with permission from Ref. 1187. Copyright 2018 Springer Nature.

4.6.3.2 Fragmentation

MS/MS helped to explore the interaction between the protein dimer BlaI (wild-type and mutant) and its double stranded DNA operator.[522] CID studies of the complexes between c-Myb DBD (DNA-binding domain) and dsDNA helped to determine the binding affinity of the complexes.[1188] MS of multiply protonated high-affinity complexes was observed. Complexes between the c-Myb DBD (DNA-binding domain) and 22-mer dsDNA exhibited different K_D values varying from 10^{-9} to 10^{-7} M. Later these complexes were studied by laser spray MS.[526] Unlike ESI-CID studies, the dissociations of the

complexes occur here in solution, not in the gas phase. Multiple reaction monitoring mass spectrometry helped to identify substrate-contacting sites in RNase P using chemical modification of lysines.[1189]

The ribosomal stalk complex plays a vital role in biology by delivering translational factors to the ribosome. However due to the dynamic nature of the stalk, it is difficult to characterize by X-ray crystallography or cryo-electron microscopy. They can be observed in the mass spectra of intact ribosomes. Tandem MS was done to separate the ions in the stalk complex.[1185] Protein-protein interactions were disrupted by increased internal energy in the gas phase. MS/MS results helped to establish the arrangement and the stoichiometry of the stalk complex in ten different species from bacteria, eukaryotes and archaea. MS/MS study confirmed the presence of heptameric organization of the stalk complex in *T. thermophilus*.[1184]

4.6.3.3 Ion mobility spectrometry

Nucleosome core protein (NCP) consists of histone protein octamers and DNA.[1190] IM-MS results resolved multiply charged ions of the hexasome (an important intermediate during the protein-DNA assembly and disassembly) by arrival times and *m/z* values in a 2D contour plot. Structural diversity of canonical NCP was shown by IM-MS.[1191] Histone tails play vital roles in many biological processes. Small CCS values suggested that the histone tails are compact for the ions with low charge states in the gas phase, but the large CCS values of higher charge states indicate that they became more extended.

The interaction and mechanism of DNA recognition of disordered proteins such as topoisomerase were determined by trapped ion mobility spectrometry.[1192] The Escherichia coli topoisomerase IA (EcTopIA) binds to single-stranded DNA with a 1:2 (protein:DNA) binding stoichiometry and with stem-loop DNA with a 1:1 stoichiometry. The *variola* virus topoisomerase IB (vTopIB) binds with stem-loop DNA with a 1:1 stoichiometry. A microstate is defined as a specific microscopic configuration of a thermodynamic system, which may occupy with a certain probability during its thermal fluctuations. Many microstates were reported for the unbound proteins but upon binding with DNA, the number of conformational states was reduced. A smaller CCS range and slightly narrower mobility bands were observed for the complexes with DNA than with the protein. These results indicate that DNA binding to topoisomerase reduces the flexibility of the proteins.

Structural analysis of the SgrAI-DNA complex was also performed using IM-MS.[1193] SgrAI, a type IIF restriction endonuclease, binds to and cleaves an 8-bp DNA sequence. IM-MS results showed that oligomers of different sizes formed with DNA-bound SgrAI dimer (DBD), where the SgrAI dimer attached to two precleaved DNA duplexes. Experimental CCS values of oligomers showed a linear relationship with the number of DBD in each oligomer. This suggests a regular repeating structure in the SgrAI-DNA oligomers. Psi RNA binding of wild-type HIV-1 Gag protein showed dimerization of the protein.[1194] Specific binding of Gag to Psi RNA favors the nucleation of Gag-Gag interaction at the early stage. It binds to control RNA, TpA, as a monomer.

4.6.3.4 Chemical probing

RNA-protein interactions in the complex formed by HIV-1 Ψ-RNA with the nucleocapsid protein (NC) was probed by ESI-FTMS.[763] Intact non-covalent complexes of RNA (each stem-loop SL2, SL3, SL4) and protein were observed thanks to the soft conditions of ESI-MS. Here, the solvent-accessible reagents were used as a complementary method to probe protein binding with RNA (see section 3.3.1.2.2). The low reactivity of β-ethoxy-α-ketobutyraldehyde (kethoxal) and 1-cyclohexyl-3-(2-morpholinoethyl)-carbodiimide metho-p-toluene sulfonate (CMCT) with SL2 is due to protection of the nucleobases by the complexed NC. Finally, experimental and computational workflows with photo-cross-linking

strategies were developed to map the interface of RNA-Protein complexes.[761,807,1195] RNA-binding sites were determined by high-resolution MS and automated database searching. With this methodology, 749 cross-links, that were mapped to 257 unique amino acids or protein regions in 124 different proteins, were identified for three biological systems of human and yeast origin.[1195] UV-induced cross-linking and MS of DNA-protein interactions in chromatin allowed to map the protein regions cross-linked to dsDNA.[824]

5. Conclusions and perspectives

Mass spectrometry has become an advanced biophysical method to study cation and ligand binding to nucleic acids, as well as nucleic acid self-assembly. In terms of impact on the nucleic acid research community, its use has nowadays mostly permeated in the G-quadruplex community, but after the research program on high-throughput native MS at Ibis Therapeutics was dropped, mass spectrometry as a biophysical method lost prominence in the RNA community. However, as RNA as druggable targets are gaining momentum again,[446,448,1196] both in academia and industry,[1197] there is a clear window of opportunity for native MS. To our opinion, it should become at least an indispensable control for the stoichiometry models on which other biophysical methods rely on. Moreover, to date only few contributions fully leveraged native MS for thermodynamic and kinetic studies, by performing quantitative measurements as a function of temperature[632,638] and/or time,[199,628,632] or by exploiting solution hydrogen-deuterium exchange in native conditions.[771] These information-rich measurements constitute a treasure trove that are worth exploiting more systematically to classify the ligand binding profiles.

Nucleic acid sample preparation for native MS is to our experience more delicate than for protein native MS, yet the compatibility with high-throughput screening has been demonstrated. There is however still room for improvement in terms of solution composition amenable to native MS. Progress has been made to analyze G-quadruplexes in potassium, and similar progress is necessary to analyze RNA complexes requiring the presence of magnesium. Small nanoelectrospray tips help diminish the nonspecific adducts, but their use is not high-throughput. Nowadays the best compounds have reported equilibrium dissociation constants in the nanomolar range, and the measurement sensitivity in native conditions must be improved to routinely analyze folded nucleic acids at nanomolar concentrations. There is further untapped potential in associating native MS with chromatography, as this will require an exchange of expertise between the communities.

In terms of mass spectrometry methods, nucleic acid duplexes and G-quadruplexes turned out to be fantastic models for developing and testing gas-phase methods. In particular, the stability of duplexes can be finely modulated by the sequence choice and allowed to test the effect of solution-phase and gas-phase dissociation equilibria and kinetics. In the case of G-quadruplexes, cations rigidify and stabilize the structures in the gas phase, which allowed to test advanced approaches to probe gas-phase ion structures such as ion mobility spectrometry and ion spectroscopy. These nucleic acid structures even inspired the development of a new method: circular dichroism spectroscopy is the most widely used solution method to determine the base stacking pattern, and the transposition of the technique into the gas phase led to the development of circular dichroism ion spectroscopy.[190] This illustrates the mutual fertilization between the fields of biochemistry/biophysics and analytical sciences.

Nucleic acid studies also led to question the generality of one of the most basic tenets of native mass spectrometry: the extent to which solution structures are preserved into the gas phase. In contrast to cation-rigidified structures, it was found that duplexes, hairpins and loop regions rearrange in the gas phase. The key player are the phosphates of the backbone. The electrospray process, usually viewed as a “charging process” is on nucleic acids rather a partial neutralization of the phosphate groups, and when the Coulomb repulsion is shielded enough, non-native hydrogen bonds between phosphate groups can form. Nucleic acids thus charge differently than proteins because of the nature and spatial distribution of their charge carriers. An open question is whether controlling the charge state could help devise conditions ensuring the preservation of the solution structure into the gas phase for all nucleic acid structures, not just cation-rigidified ones. These considerations are relevant to generalize native MS to all kinds of natural and artificial (supramolecular) complexes.

Focusing on the fundamental physical driving forces is key to such generalization. For example, in probing the strength of intermolecular interactions with fragmentation (collision-induced dissociation), we learned that it's only doable if the dissociation channel is the rupture of the bonds one aims to probe (for example, ligand neutral loss to probe ligand-nucleic acid intrinsic interactions). However, many strong binders are cationic, and thus remain attached to the negatively charged nucleic acids. Although this behavior is favorable to map binding sites (with radical-based fragmentation if necessary), it doesn't help to rank ligand-nucleic acid interactions. Collision-induced unfolding probed by ion mobility spectrometry could potentially probe the extent to which ligands bridge parts of the structure, but again this process will depend on initial charge state and internal energy control. Achieving this control and being able to quantitatively relate the outcomes to binding energies will require further fundamental work.

Acknowledgements

We acknowledge the European Research Council (grant ERC-2013-CoG-616551-DNAFOLDIMS to V.G.), the European Commission (grant H2020-MSCA-IF-2017-799695-CROWDASSAY to V.G. and A.G.), the ANR (grant ANR-18-CE29-0013-POLYnESI to V.G. and F.R.), the IdEX Bordeaux (project I-MOTIMS to S.B.), and the Ministère français de l'Enseignement supérieur, de la Recherche et de l'Innovation (PhD fellowship to A.K.), and funding over the years from the Inserm, CNRS and University of Bordeaux, which funding brought us together to write this review.

Author information

Corresponding Author

Valérie Gabelica -- Email: v.gabelica@iecb.u-bordeaux.fr

Author biographies

Eric Largy

Eric Largy obtained a PhD in chemistry in 2011 from the University of Paris XI (France) with Dr. Marie-Paule Teulade-Fichou at the Institut Curie, where he worked on ligand-G-quadruplex interactions. He then worked as a Banting postdoctoral fellow with Prof. David Perrin at the University of British Columbia (Canada). In 2013, he joined the groups of Drs. Jean-Louis Mergny and Valérie Gabelica as a postdoc at the Institut Européen de Chimie et Biologie (IECB, Bordeaux, France). He then worked as a research scientist in the pharmaceutical industry (Quality Assistance, Belgium) before rejoining the group of Dr. Gabelica at IECB as an assistant professor in 2017. He teaches analytical chemistry at the pharmacy department of the University of Bordeaux, and his research interests are centered on the characterization of nucleic acids structures and interactions by mass spectrometry and solution spectroscopy.

Alexander König

Alexander König graduated from the Freiberg University of Mining and Technology (Saxony, Germany) in 2020 with a Master of Science in Chemistry. In the same year, he joined the Gabelica group as a PhD student to research the cation-dependent folding of G-quadruplexes as well as the binding selectivity of G4-targeting ligands via native mass spectrometry.

Anirban Ghosh

Anirban Ghosh studied chemistry and obtained his PhD in 2017 at the University of Calcutta (India) with Prof. Anirban Bhunia (Bose Institute), where he gained expertise in NMR of amyloid aggregates. He then joined the Gabelica group as a postdoctoral researcher, where he obtained a Marie Skłodowska Curie individual fellowship. His research activity was focused on the characterization of ligands and co-solvent interactions effects on G-quadruplex DNA by ion mobility mass spectrometry and solution spectroscopy. He is currently postdoctoral researcher in the Trantírek group at the Central European Institute of Technology, Masaryk University, Czech Republic.

Debasmita Ghosh

Debasmita Ghosh studied chemistry and obtained her PhD in 2020 at the Indian Institute of Technology Madras with Prof. Thalappil Pradeep, where she studied conformational changes of proteins, and luminescent atomically precise noble metal clusters through ion mobility mass spectrometry and hydrogen/deuterium exchange. She is currently working with Dr. Valérie Gabelica as a postdoctoral fellow (INSERM, IECB). Her current research topic is fundamental aspects of mass spectrometry and ion mobility spectrometry for deducing polymer and biomolecule structure.

Sanae Benabou

Sanae Benabou obtained a PhD in Analytical Chemistry from the University of Barcelona (Spain) in 2018, specializing in biophysical studies of DNA (G-quadruplex and i-motif) and application of chemometric tools, under the joined supervision of Profs. Raimundo Gargallo and Anna de Juan. She is currently a post-doc in the Gabelica group and studies i-motif nucleic acids by native MS and ion mobility spectrometry.

Frédéric Rosu

Frédéric Rosu obtained his PhD in Science in 2005 at the University of Liège (Belgium) under the joined supervision of Profs. Edwin De Pauw and Pierre Colson. His doctoral studies focused on drug-nucleic

acids interactions using spectroscopic and mass spectrometric analysis. After post-doctoral research with Jean-Louis Mergny at Museum National d'Histoire Naturelle (France) on G-quadruplexes structures, he returned to Liège as an FNRs post-doctoral fellow. In 2012, he was visiting scientist in Thomas Rizzo's group at EPFL (Switzerland) and explored cold ion spectroscopy. In 2013, he joined the Institut Européen de Chimie et Biologie (IECB) in Bordeaux, France, and became research engineer at the CNRS. He is the head of the mass spectrometry platform of IECB. His major research interests are mass-spectrometry based approaches for structural chemistry, and he develops ion mobility and ion spectroscopy methods to study non-covalent complexes including nucleic acids.

Valérie Gabelica

Valérie Gabelica studied Chemistry and obtained her PhD in Sciences in 2002 at the University of Liège (Belgium) with Prof. Edwin De Pauw, with a thesis on mass spectrometry of non-covalent complexes. After a postdoc in Frankfurt (Germany) as Humboldt fellow in the group of Michael Karas, she rejoined the Mass Spectrometry Laboratory in Liège to study nucleic acid complexes by mass spectrometry, and she obtained a permanent position as FNRS research associate in October 2005. She joined the Institut Européen de Chimie et Biologie (IECB) in Bordeaux, France, in 2013 and became Research Director at the INSERM (French National Institute of Health and Medical Research). She is currently the director of IECB and associate editor of *Analytical Chemistry*. She was awarded and ERC consolidator grant in 2014, the prix du Dr. et de Mme Henri Labbé (in chemical biology) by the French Academy of Sciences in 2018, and the Liliane Bettencourt Prize for Life Sciences in 2021. Her main research interests are fundamental aspects of mass spectrometry and its application to non-covalent complexes in general and nucleic acid complexes in particular, with research themes spanning from physical chemistry to biophysics, structural chemistry and biology.

References

(1) Hurley, L. H. DNA and Its Associated Processes as Targets for Cancer Therapy. *Nat. Rev. Cancer* **2002**, *2*, 188–200. https://doi.org/10.1038/nrc749.

(2) Nitiss, J. L. Targeting DNA Topoisomerase II in Cancer Chemotherapy. *Nat. Rev. Cancer* **2009**, *9*, 338–350. https://doi.org/10.1038/nrc2607.

(3) Poehlsgaard, J.; Douthwaite, S. The Bacterial Ribosome as a Target for Antibiotics. *Nat. Rev. Microbiol.* **2005**, *3*, 870–881. https://doi.org/10.1038/nrmicro1265.

(4) Kohanski, M. A.; Dwyer, D. J.; Collins, J. J. How Antibiotics Kill Bacteria: From Targets to Networks. *Nat. Rev. Microbiol.* **2010**, *8*, 423–435. https://doi.org/10.1038/nrmicro2333.

(5) Hermann, T.; Patel, D. J. Adaptive Recognition by Nucleic Acid Aptamers. *Science* **2000**, *287*, 820–825. https://doi.org/10.1126/science.287.5454.820.

(6) Park, S.; Sugiyama, H. DNA-Based Hybrid Catalysts for Asymmetric Organic Synthesis. *Angew. Chem. Int. Ed.* **2010**, *49*, 3870–3878. https://doi.org/10.1002/anie.200905382.

(7) Wang, F.; Liu, X.; Willner, I. DNA Switches: From Principles to Applications. *Angew. Chem. Int. Ed.* **2015**, *54*, 1098–1129. https://doi.org/10.1002/anie.201404652.

(8) Panigaj, M.; Johnson, M. B.; Ke, W.; McMillan, J.; Goncharova, E. A.; Chandler, M.; Afonin, K. A. Aptamers as Modular Components of Therapeutic Nucleic Acid Nanotechnology. *ACS Nano* **2019**, *13*, 12301–12321. https://doi.org/10.1021/acsnano.9b06522.

(9) Hong, F.; Zhang, F.; Liu, Y.; Yan, H. DNA Origami: Scaffolds for Creating Higher Order Structures. *Chem. Rev.* **2017**, *117*, 12584–12640. https://doi.org/10.1021/acs.chemrev.6b00825.

(10) McLaughlin, C. K.; Hamblin, G. D.; Sleiman, H. F. Supramolecular DNA Assembly. *Chem. Soc. Rev.* **2011**, *40*, 5647–5656. https://doi.org/10.1039/c1cs15253j.

(11) Hofstadler, S. A.; Griffey, R. H. Analysis of Noncovalent Complexes of DNA and RNA by Mass Spectrometry. *Chem. Rev.* **2001**, *101*, 377–390. https://doi.org/10.1021/cr990105o.

(12) Beck, J.; Colgrave, M. L.; Ralph, S. F.; Sheil, M. M. Electrospray Ionization Mass Spectrometry of Oligonucleotide Complexes with Drugs, Metals, and Proteins. *Mass Spectrom. Rev.* **2001**, *20*, 61–87. https://doi.org/10.1002/mas.1003.

(13) Rosu, F.; De Pauw, E.; Gabelica, V. Electrospray Mass Spectrometry to Study Drug-Nucleic Acids Interactions. *Biochimie* **2008**, *90*, 1074–1087. https://doi.org/10.1016/j.biochi.2008.01.005.

(14) Brodbelt, J. S. Evaluation of DNA/Ligand Interactions by Electrospray Ionization Mass Spectrometry. *Annu. Rev. Anal. Chem.* **2010**, *3*, 67–87. https://doi.org/10.1146/annurev.anchem.111808.073627.

(15) Yuan, G.; Zhang, Q.; Zhou, J.; Li, H. Mass Spectrometry of G-Quadruplex DNA: Formation, Recognition, Property, Conversion, and Conformation. *Mass Spectrom. Rev.* **2011**, *30*, 1121–1142. https://doi.org/10.1002/mas.20315.

(16) Fabris, D. A Role for the MS Analysis of Nucleic Acids in the Post-Genomics Age. *J. Am. Soc. Mass Spectrom.* **2010**, *21*, 1–13. https://doi.org/10.1016/j.jasms.2009.09.006.

(17) Fabris, D. MS Analysis of Nucleic Acids in the Post-Genomic Era. *Anal. Chem.* **2011**, *83*, 5810–5816. https://doi.org/10.1021/ac200374y.

(18) Silvestri, C.; Brodbelt, J. S. Tandem Mass Spectrometry for Characterization of Covalent Adducts of DNA with Anticancer Therapeutics. *Mass Spectrom. Rev.* **2013**, *32*, 247–266. https://doi.org/10.1002/mas.21363.

(19) Abi-Ghanem, J.; Gabelica, V. Nucleic Acid Ion Structures in the Gas Phase. *Phys. Chem. Chem. Phys.* **2014**, *16*, 21204–21218. https://doi.org/10.1039/c4cp02362e.

(20) Schalley, C. A. Molecular Recognition and Supramolecular Chemistry in the Gas Phase. *Mass Spectrom. Rev.* **2001**, *20*, 253–309. https://doi.org/10.1002/mas.10009.

(21) Hofstadler, S. A.; Sannes-Lowery, K. A. Applications of ESI-MS in Drug Discovery: Interrogation of Noncovalent Complexes. *Nat. Rev. Drug Discov.* **2006**, *5*, 585–595. https://doi.org/10.1038/nrd2083.

(22) Hofstadler, S. A.; Sannes-Lowery, K. A.; Hannis, J. C. Analysis of Nucleic Acids by FTICR MS. *Mass Spectrom. Rev.* **2005**, *24*, 265–285. https://doi.org/10.1002/mas.20016.

(23) Banoub, J. H.; Newton, R. P.; Esmans, E.; Ewing, D. F.; Mackenzie, G. Recent Developments in Mass Spectrometry for the Characterization of Nucleosides, Nucleotides, Oligonucleotides, and Nucleic Acids. *Chem. Rev.* **2005**, *105*, 1869–1916. https://doi.org/10.1021/cr030040w.

(24) Neidle, S. Principles of Nucleic Acid Structure, First Edition.; Academic Press: Amsterdam, 2008; p 289.

(25) Tateishi-Karimata, H.; Sugimoto, N. Chemical Biology of Non-Canonical Structures of Nucleic Acids for Therapeutic Applications. *Chem. Commun.* **2020**, *56*, 2379–2390. https://doi.org/10.1039/c9cc09771f.

(26) Crooke, S. T.; Witztum, J. L.; Bennett, C. F.; Baker, B. F. RNA-Targeted Therapeutics. *Cell Metab.* **2018**, *27*, 714–739. https://doi.org/10.1016/j.cmet.2018.03.004.

(27) Duffy, K.; Arangundy-Franklin, S.; Holliger, P. Modified Nucleic Acids: Replication, Evolution, and next-Generation Therapeutics. *BMC Biol.* **2020**, *18*, 112. https://doi.org/10.1186/s12915-020-00803-6.

(28) Smith, C. I. E.; Zain, R. Therapeutic Oligonucleotides: State of the Art. *Annu. Rev. Pharmacol. Toxicol.* **2019**, *59*, 605–630. https://doi.org/10.1146/annurev-pharmtox-010818-021050.

(29) Ochoa, S.; Milam, V. T. Modified Nucleic Acids: Expanding the Capabilities of Functional Oligonucleotides. *Molecules* **2020**, *25*, 4659. https://doi.org/10.3390/molecules25204659.

(30) Gupta, A.; Mishra, A.; Puri, N. Peptide Nucleic Acids: Advanced Tools for Biomedical Applications. *J. Biotechnol.* **2017**, *259*, 148–159. https://doi.org/10.1016/j.jbiotec.2017.07.026.

(31) Hu, Y.; Cecconello, A.; Idili, A.; Ricci, F.; Willner, I. Triplex DNA Nanostructures: From Basic Properties to Applications. *Angew. Chem. Int. Ed Engl.* **2017**, *56*, 15210–15233. https://doi.org/10.1002/anie.201701868.

(32) Chandrasekaran, A. R.; Rusling, D. A. Triplex-Forming Oligonucleotides: A Third Strand for DNA Nanotechnology. *Nucleic Acids Res.* **2018**, *46*, 1021–1037. https://doi.org/10.1093/nar/gkx1230.

(33) Mergny, J.-L.; Sen, D. DNA Quadruple Helices in Nanotechnology. *Chem. Rev.* **2019**, *119*, 6290–6325. https://doi.org/10.1021/acs.chemrev.8b00629.

(34) Bilyard, M. K.; Becker, S.; Balasubramanian, S. Natural, Modified DNA Bases. *Curr. Opin. Chem. Biol.* **2020**, *57*, 1–7. https://doi.org/10.1016/j.cbpa.2020.01.014.

(35) Eremeeva, E.; Herdewijn, P. Non Canonical Genetic Material. *Curr. Opin. Biotechnol.* **2019**, *57*, 25–33. https://doi.org/10.1016/j.copbio.2018.12.001.

(36) Anosova, I.; Kowal, E. A.; Dunn, M. R.; Chaput, J. C.; Van Horn, W. D.; Egli, M. The Structural Diversity of Artificial Genetic Polymers. *Nucleic Acids Res.* **2016**, *44*, 1007–1021. https://doi.org/10.1093/nar/gkv1472.

(37) Lindahl, T. Instability and Decay of the Primary Structure of DNA. *Nature* **1993**, *362*, 709–715. https://doi.org/10.1038/362709a0.

(38) Meek, K. N.; Rangel, A. E.; Heemstra, J. M. Enhancing Aptamer Function and Stability via in Vitro Selection Using Modified Nucleic Acids. *Methods* **2016**, *106*, 29–36. https://doi.org/10.1016/j.ymeth.2016.03.008.

(39) Röthlisberger, P.; Hollenstein, M. Aptamer Chemistry. *Adv. Drug Deliv. Rev.* **2018**, *134*, 3–21. https://doi.org/10.1016/j.addr.2018.04.007.

(40) Gao, S.; Zheng, X.; Jiao, B.; Wang, L. Post-SELEX Optimization of Aptamers. *Anal. Bioanal. Chem.* **2016**, *408*, 4567–4573. https://doi.org/10.1007/s00216-016-9556-2.

(41) Adrian, M.; Heddi, B.; Phan, A. T. NMR Spectroscopy of G-Quadruplexes. *Methods* **2012**, *57*, 11–24. https://doi.org/10.1016/j.ymeth.2012.05.003.

(42) Ivancová, I.; Pohl, R.; Hubálek, M.; Hocek, M. Squaramate-Modified Nucleotides and DNA for Specific Cross-Linking with Lysine-Containing Peptides and Proteins. *Angew. Chem. Int. Ed.* **2019**, *58*, 13345–13348. https://doi.org/10.1002/anie.201906737.

(43) Nielsen, P. E. Targeting Double Stranded DNA with Peptide Nucleic Acid (PNA). *Curr. Med. Chem.* **2001**, *8*, 545–550. https://doi.org/10.2174/0929867003373373.

(44) Devi, G.; Zhou, Y.; Zhong, Z.; Toh, D.-F. K.; Chen, G. RNA Triplexes: From Structural Principles to Biological and Biotech Applications: RNA Triplexes. *Wiley Interdiscip. Rev. RNA* **2015**, *6*, 111–128. https://doi.org/10.1002/wrna.1261.

(45) Vasquez, K. M.; Glazer, P. M. Triplex-Forming Oligonucleotides: Principles and Applications. *Q. Rev. Biophys.* **2002**, *35*, 89–107. https://doi.org/10.1017/s0033583502003773.

(46) Kamiya, H.; Kasai, H. Formation of 2-Hydroxydeoxyadenosine Triphosphate, an Oxidatively Damaged Nucleotide, and Its Incorporation by DNA Polymerases. *J. Biol. Chem.* **1995**, *270*, 19446–19450. https://doi.org/10.1074/jbc.270.33.19446.

(47) Pierce, S. E.; Wang, J.; Jayawickramarajah, J.; Hamilton, A. D.; Brodbelt, J. S. Examination of the Effect of the Annealing Cation on Higher Order Structures Containing Guanine or Isoguanine Repeats. *Chem. - Eur. J.* **2009**, *15*, 11244–11255. https://doi.org/10.1002/chem.200901047.

(48) Kulikowska, E.; Kierdaszuk, B.; Shugar, D. Xanthine, Xanthosine and Its Nucleotides: Solution Structures of Neutral and Ionic Forms, and Relevance to Substrate Properties in Various Enzyme Systems and Metabolic Pathways. *Acta Biochim. Pol.* **2004**, *51*, 493–531.

(49) Wu, X.; Zhang, Y. TET-Mediated Active DNA Demethylation: Mechanism, Function and Beyond. *Nat. Rev. Genet.* **2017**, *18*, 517–534. https://doi.org/10.1038/nrg.2017.33.

(50) Anderson, D. J.; Reischer, R. J.; Taylor, A. J.; William J. Wechter. Preparation and Characterization of Oligonucleotides of D- and l-2' Deoxyuridine. *Nucleosides Nucleotides* **1984**, *3*, 499–512. https://doi.org/10.1080/07328318408081285.

(51) Fujimori, S.; Shudo, K.; Hashimoto, Y. Enantio-DNA Recognizes Complementary RNA but Not Complementary DNA. *J. Am. Chem. Soc.* **1990**, *112*, 7436–7438. https://doi.org/10.1021/ja00176a077.

(52) Garbesi, A.; Capobinanco, M. L.; Colonna, F. P.; Tondelli, L.; Arcamone, F.; Manzini, G.; hilbers, C. W.; Aelen, J. M. E.; Blommers, M. J. J. L-DNAs as Potenital Antimessenger Oligonucleotides: A Reassessment. *Nucleic Acids Res.* **1993**, *21*, 4159–4165. https://doi.org/10.1093/nar/21.18.4159.

(53) Vater, A.; Klussmann, S. Turning Mirror-Image Oligonucleotides into Drugs: The Evolution of

Spiegelmer® Therapeutics. *Drug Discov. Today* **2015**, *20*, 147–155. https://doi.org/10.1016/j.drudis.2014.09.004.

(54) Hayashi, G.; Hagihara, M.; Nakatani, K. Application of L-DNA as a Molecular Tag. *Nucleic Acids Symp. Ser.* **2005**, *49*, 261–262. https://doi.org/10.1093/nass/49.1.261.

(55) Ogata, M.; Hayashi, G.; Ichiu, A.; Okamoto, A. L-DNA-Tagged Fluorescence in Situ Hybridization for Highly Sensitive Imaging of RNAs in Single Cells. *Org. Biomol. Chem.* **2020**, *18*, 8084–8088. https://doi.org/10.1039/d0ob01635g.

(56) Ho, D.; Dose, C.; Albrecht, C. H.; Severin, P.; Falter, K.; Dervan, P. B.; Gaub, H. E. Quantitative Detection of Small Molecule/DNA Complexes Employing a Force-Based and Label-Free DNA-Microarray. *Biophys. J.* **2009**, *96*, 4661–4671. https://doi.org/10.1016/j.bpj.2009.02.059.

(57) Smith, J. D.; Dunn, D. B. An Additional Sugar Component of Ribonucleic Acids. *Biochim. Biophys. Acta* **1959**, *31*, 573–575. https://doi.org/10.1016/0006-3002(59)90045-9.

(58) Cummins, L. L.; Owens, S. R.; Risen, L. M.; Lesnik, E. A.; Freier, S. M.; McGee, D.; Guinosso, C. J.; Cook, P. D. Characterization of Fully 2'-Modified Oligoribonucleotide Hetero- and Homoduplex Hybridization and Nuclease Sensitivity. *Nucleic Acids Res.* **1995**, *23*, 2019–2024. https://doi.org/10.1093/nar/23.11.2019.

(59) Rottman, Fritz.; Heinlein, Karen. Polynucleotides Containing 2'-O-Methyladenosine. I. Synthesis by Polynucleotide Phosphorylase. *Biochemistry* **1968**, *7*, 2634–2641. https://doi.org/10.1021/bi00847a028.

(60) Inoue, H.; Hayase, Y.; Iwai, S.; Ohtsuka, E. Sequence-Dependent Hydrolysis of RNA Using Modified Oligonucleotide Splints and RNase H. *FEBS Lett.* **1987**, *215*, 327–330. https://doi.org/10.1016/0014-5793(87)80171-0.

(61) Inoue, H.; Hayase, Y.; Imura, A.; Iwai, S.; Miura, K.; Ohtsuka, E. Synthesis and Hybridization Studies on Two Complementary Nona(2'-O-Methyl)Ribonucleotides. *Nucleic Acids Res.* **1987**, *15*, 6131–6148. https://doi.org/10.1093/nar/15.15.6131.

(62) Lesnik, E. A.; Guinosso, C. J.; Kawasaki, A. M.; Sasmor, H.; Zounes, M.; Cummins, L. L.; Ecker, D. J.; Cook, P. D.; Freier, S. M. Oligodeoxynucleotides Containing 2'-O-Modified Adenosine: Synthesis and Effects on Stability of DNA:RNA Duplexes. *Biochemistry* **1993**, *32*, 7832–7838. https://doi.org/10.1021/bi00081a031.

(63) Eckstein, F. Phosphorothioate Oligodeoxynucleotides: What Is Their Origin and What Is Unique About Them? *Antisense Nucleic Acid Drug Dev.* **2000**, *10*, 117–121. https://doi.org/10.1089/oli.1.2000.10.117.

(64) Boczkowska, M.; Guga, P.; Stec, W. J. Stereodefined Phosphorothioate Analogues of DNA: Relative Thermodynamic Stability of the Model PS-DNA/DNA and PS-DNA/RNA Complexes. *Biochemistry* **2002**, *41*, 12483–12487. https://doi.org/10.1021/bi026225z.

(65) Nielsen, P.; Egholm, M.; Berg, R.; Buchardt, O. Sequence-Selective Recognition of DNA by Strand Displacement with a Thymine-Substituted Polyamide. *Science* **1991**, *254*, 1497–1500. https://doi.org/10.1126/science.1962210.

(66) Egholm, M.; Buchardt, O.; Christensen, L.; Behrens, C.; Freier, S. M.; Driver, D. A.; Berg, R. H.; Kim, S. K.; Norden, B.; Nielsen, P. E. PNA Hybridizes to Complementary Oligonucleotides Obeying the Watson–Crick Hydrogen-Bonding Rules. *Nature* **1993**, *365*, 566–568. https://doi.org/10.1038/365566a0.

(67) Nielsen, P. E. DNA Analogues with Nonphosphodiester Backbones. *Annu. Rev. Biophys. Biomol. Struct.* **1995**, *24*, 167–183. https://doi.org/10.1146/annurev.bb.24.060195.001123.

(68) Quijano, E.; Bahal, R.; Ricciardi, A.; Saltzman, W. M.; Glazer, P. M. Therapeutic Peptide Nucleic Acids: Principles, Limitations, and Opportunities. *Yale J. Biol. Med.* **2017**, *90*, 583–598.

(69) Ricciardi, A.; Quijano, E.; Putman, R.; Saltzman, W.; Glazer, P. Peptide Nucleic Acids as a Tool for Site-Specific Gene Editing. *Molecules* **2018**, *23*, 632. https://doi.org/10.3390/molecules23030632.

(70) Briones, C.; Moreno, M. Applications of Peptide Nucleic Acids (PNAs) and Locked Nucleic Acids (LNAs) in Biosensor Development. *Anal. Bioanal. Chem.* **2012**, *402*, 3071–3089. https://doi.org/10.1007/s00216-012-5742-z.

(71) Koshkin, A. A.; Singh, S. K.; Nielsen, P.; Rajwanshi, V. K.; Kumar, R.; Meldgaard, M.; Olsen, C. E.; Wengel, J. LNA (Locked Nucleic Acids): Synthesis of the Adenine, Cytosine, Guanine, 5-Methylcytosine, Thymine and Uracil Bicyclonucleoside Monomers, Oligomerisation, and Unprecedented Nucleic Acid Recognition. *Tetrahedron* **1998**, *54*, 3607–3630. https://doi.org/10.1016/s0040-4020(98)00094-5.

(72) Koshkin, A. A.; Nielsen, P.; Meldgaard, M.; Rajwanshi, V. K.; Singh, S. K.; Wengel, J. LNA (Locked Nucleic Acid): An RNA Mimic Forming Exceedingly Stable LNA:LNA Duplexes. *J. Am. Chem. Soc.* **1998**, *120*, 13252–13253. https://doi.org/10.1021/ja9822862.

(73) Obika, S.; Nanbu, D.; Hari, Y.; Andoh, J.; Morio, K.; Doi, T.; Imanishi, T. Stability and Structural Features of the Duplexes Containing Nucleoside Analogues with a Fixed N-Type Conformation, 2'-O,4'-C-Methyleneribonucleosides. *Tetrahedron Lett.* **1998**, *39*, 5401–5404.

https://doi.org/10.1016/s0040-4039(98)01084-3.

(74) Veedu, R. N.; Wengel, J. Locked Nucleic Acids: Promising Nucleic Acid Analogs for Therapeutic Applications. *Chem. Biodivers.* **2010**, *7*, 536–542. https://doi.org/10.1002/cbdv.200900343.

(75) Campbell, M. A.; Wengel, J. Locked vs. Unlocked Nucleic Acids (LNA vs. UNA): Contrasting Structures Work towards Common Therapeutic Goals. *Chem. Soc. Rev.* **2011**, *40*, 5680–5689. https://doi.org/10.1039/c1cs15048k.

(76) Zhang, L.; Peritz, A.; Meggers, E. A Simple Glycol Nucleic Acid. *J. Am. Chem. Soc.* **2005**, *127*, 4174–4175. https://doi.org/10.1021/ja042564z.

(77) Schlegel, M. K.; Peritz, A. E.; Kittigowittana, K.; Zhang, L.; Meggers, E. Duplex Formation of the Simplified Nucleic Acid GNA. *ChemBioChem* **2007**, *8*, 927–932. https://doi.org/10.1002/cbic.200600435.

(78) Schlegel, M. K.; Essen, L.-O.; Meggers, E. Duplex Structure of a Minimal Nucleic Acid. *J. Am. Chem. Soc.* **2008**, *130*, 8158–8159. https://doi.org/10.1021/ja802788g.

(79) Lescrinier, E.; Froeyen, M.; Herdewijn, P. Difference in Conformational Diversity between Nucleic Acids with a Six-Membered "sugar" Unit and Natural "Furanose" Nucleic Acids. *Nucleic Acids Res.* **2003**, *31*, 2975–2989. https://doi.org/10.1093/nar/gkg407.

(80) Lescrinier, E.; Esnouf, R.; Schraml, J.; Busson, R.; Heus, H.; Hilbers, C.; Herdewijn, P. Solution Structure of a HNA–RNA Hybrid. *Chem. Biol.* **2000**, *7*, 719–731. https://doi.org/10.1016/s1074-5521(00)00017-x.

(81) Hendrix, C.; Rosemeyer, H.; De Bouvere, B.; Van Aerschot, A.; Seela, F.; Herdewijn, P. 1′,5′-Anhydrohexitol Oligonucleotides: Hybridisation and Strand Displacement with Oligoribonucleotides, Interaction with RNase H and HIV Reverse Transcriptase. *Chem. - Eur. J.* **1997**, *3*, 1513–1520. https://doi.org/10.1002/chem.19970030920.

(82) Hendrix, C.; Rosemeyer, H.; Verheggen, I.; Van Aerschot, A.; Seela, F.; Herdewijn, P. 1′, 5′ - Anhydrohexitol Oligonucleotides: Synthesis, Base Pairing and Recognition by Regular Oligodeoxyribonucleotides and Oligoribonucleotides. *Chem. - Eur. J.* **1997**, *3*, 110–120. https://doi.org/10.1002/chem.19970030118.

(83) Sinden, R. R. DNA Structure and Function; Academic Press: San Diego, California, USA, 1994; p 398. https://doi.org/10.1016/C2009-0-02451-9.

(84) Bingman, C.; Jain, S.; Zon, G.; Sundaralingam, M. Crystal and Molecular Structure of the Alternating Dodecamer d(GCGTACGTACGC) in the A-DNA Form: Comparison with the Isomorphous Non-Alternating Dodecamer d(CCGTACGTACGG). *Nucleic Acids Res.* **1992**, *20*, 6637–6647. https://doi.org/10.1093/nar/20.24.6637.

(85) Westhof, E. Re-Refinement of the B-Dodecamer d(CGCGAATTCGCG) with a Comparative Analysis of the Solvent in It and in the Z-Hexamer d(5BrCG5BrCG5BrCG). *J. Biomol. Struct. Dyn.* **1987**, *5*, 581–600. https://doi.org/10.1080/07391102.1987.10506414.

(86) Luo, Z.; Dauter, M.; Dauter, Z. Phosphates in the Z-DNA Dodecamer Are Flexible, but Their P-SAD Signal Is Sufficient for Structure Solution. *Acta Crystallogr. D Biol. Crystallogr.* **2014**, *70*, 1790–1800. https://doi.org/10.1107/s1399004714004684.

(87) Asensio, J. L.; Brown, T.; Lane, A. N. Solution Conformation of a Parallel DNA Triple Helix with 5′ and 3′ Triplex–Duplex Junctions. *Structure* **1999**, *7*, 1–11. https://doi.org/10.1016/s0969-2126(99)80004-5.

(88) Esmaili, N.; Leroy, J. L. I-Motif Solution Structure and Dynamics of the d(AACCCC) and d(CCCCAA) Tetrahymena Telomeric Repeats. *Nucleic Acids Res.* **2005**, *33*, 213–224. https://doi.org/10.1093/nar/gki160.

(89) Creze, C.; Rinaldi, B.; Haser, R.; Bouvet, P.; Gouet, P. Structure of a d(TGGGGT) Quadruplex Crystallized in the Presence of Li+ Ions. *Acta Crystallogr. D Biol. Crystallogr.* **2007**, *63*, 682–688. https://doi.org/10.1107/s0907444907013315.

(90) Phan, A. T.; Kuryavyi, V.; Burge, S.; Neidle, S.; Patel, D. J. Structure of an Unprecedented G-Quadruplex Scaffold in the Human c-Kit Promoter. *J. Am. Chem. Soc.* **2007**, *129*, 4386–4392. https://doi.org/10.1021/ja068739h.

(91) Dai, J.; Carver, M.; Punchihewa, C.; Jones, R. A.; Yang, D. Structure of the Hybrid-2 Type Intramolecular Human Telomeric G-Quadruplex in K+ Solution: Insights into Structure Polymorphism of the Human Telomeric Sequence. *Nucleic Acids Res.* **2007**, *35*, 4927–4940. https://doi.org/10.1093/nar/gkm522.

(92) Haider, S.; Parkinson, G. N.; Neidle, S. Crystal Structure of the Potassium Form of an Oxytricha Nova G-Quadruplex. *J. Mol. Biol.* **2002**, *320*, 189–200. https://doi.org/10.1016/S0022-2836(02)00428-X.

(93) Wang, A. H.; Quigley, G. J.; Kolpak, F. J.; Crawford, J. L.; van Boom, J. H.; van der Marel, G.; Rich, A. Molecular Structure of a Left-Handed Double Helical DNA Fragment at Atomic Resolution. *Nature* **1979**, *282*, 680–686. https://doi.org/10.1038/282680a0.

(94) Fuller, W.; Wilkins, W. H. F.; Wilson, H. R.; Hamilton, L. D. The Molecular Configuration of Deoxyribonucleic Acid. *J. Mol. Biol.* **1965**, *12*, 60–76. https://doi.org/10.1016/s0022-2836(65)80282-0.

(95) Pohl, F. M.; Jovin, T. M. Salt-Induced Co-Operative Conformational Change of a Synthetic DNA: Equilibrium and Kinetic Studies with Poly(DG-DC). *J. Mol. Biol.* **1972**, *67*, 375–396. https://doi.org/10.1016/0022-2836(72)90457-3.

(96) Phan, A. T.; Kuryavyi, V.; Patel, D. J. DNA Architecture: From G to Z. *Curr. Opin. Struct. Biol.* **2006**, *16*, 288–298. https://doi.org/10.1016/j.sbi.2006.05.011.

(97) Iyer, R. R.; Pluciennik, A.; Burdett, V.; Modrich, P. L. DNA Mismatch Repair: Functions and Mechanisms. *Chem. Rev.* **2006**, *106*, 302–323. https://doi.org/10.1021/cr0404794.

(98) Young, L. C.; Hays, J. B.; Tron, V. A.; Andrew, S. E. DNA Mismatch Repair Proteins: Potential Guardians against Genomic Instability and Tumorigenesis Induced by Ultraviolet Photoproducts. *J. Invest. Dermatol.* **2003**, *121*, 435–440. https://doi.org/10.1046/j.1523-1747.2003.12450.x.

(99) Allawi, H. T.; SantaLucia, J. Thermodynamics and NMR of Internal G·T Mismatches in DNA. *Biochemistry* **1997**, *36*, 10581–10594. https://doi.org/10.1021/bi962590c.

(100) Allawi, H. T.; SantaLucia, J. Nearest-Neighbor Thermodynamics of Internal A·C Mismatches in DNA: Sequence Dependence and PH Effects. *Biochemistry* **1998**, *37*, 9435–9444. https://doi.org/10.1021/bi9803729.

(101) Allawi, H. T.; SantaLucia, J. Nearest Neighbor Thermodynamic Parameters for Internal G·A Mismatches in DNA. *Biochemistry* **1998**, *37*, 2170–2179. https://doi.org/10.1021/bi9724873.

(102) Allawi, H.; SantaLucia, J. Thermodynamics of Internal C.T Mismatches in DNA. *Nucleic Acids Res.* **1998**, *26*, 2694–2701. https://doi.org/10.1093/nar/26.11.2694.

(103) Peyret, N.; Seneviratne, P. A.; Allawi, H. T.; SantaLucia, J. Nearest-Neighbor Thermodynamics and NMR of DNA Sequences with Internal A.A, C.C, G.G, and T.T Mismatches. *Biochemistry* **1999**, *38*, 3468–3477. https://doi.org/10.1021/bi9825091.

(104) SantaLucia, J.; Hicks, D. The Thermodynamics of DNA Structural Motifs. *Annu. Rev. Biophys. Biomol. Struct.* **2004**, *33*, 415–440. https://doi.org/10.1146/annurev.biophys.32.110601.141800.

(105) Bhattacharya, P. K.; Cha, J.; Barton, J. K. 1H NMR Determination of Base-pair Lifetimes in Oligonucleotides Containing Single Base Mismatches. *Nucleic Acids Res.* **2002**, *30*, 4740–4750. https://doi.org/10.1093/nar/gkf601.

(106) Rossetti, G.; Dans, P. D.; Gomez-Pinto, I.; Ivani, I.; Gonzalez, C.; Orozco, M. The Structural Impact of DNA Mismatches. *Nucleic Acids Res.* **2015**, *43*, 4309–4321. https://doi.org/10.1093/nar/gkv254.

(107) Ghosh, A.; Kar, R. K.; Krishnamoorthy, J.; Chatterjee, S.; Bhunia, A. Double GC:GC Mismatch in DsDNA Enhances Local Dynamics Retaining the DNA Footprint: A High-Resolution NMR Study. *ChemMedChem* **2014**, *9*, 2059–2064. https://doi.org/10.1002/cmdc.201402238.

(108) Jourdan, M.; Granzhan, A.; Guillot, R.; Dumy, P.; Teulade-Fichou, M.-P. Double Threading through DNA: NMR Structural Study of a Bis-Naphthalene Macrocycle Bound to a Thymine–Thymine Mismatch. *Nucleic Acids Res.* **2012**, *40*, 5115–5128. https://doi.org/10.1093/nar/gks067.

(109) Trotta, E.; Paci, M. Solution Structure of DAPI Selectively Bound in the Minor Groove of a DNA T.T Mismatch-Containing Site: NMR and Molecular Dynamics Studies. *Nucleic Acids Res.* **1998**, *26*, 4706–4713. https://doi.org/10.1093/nar/26.20.4706.

(110) Hermann, T.; Patel, D. J. Stitching Together RNA Tertiary Architectures. *J. Mol. Biol.* **1999**, *294*, 829–849. https://doi.org/10.1006/jmbi.1999.3312.

(111) He, L.; Kierzek, R.; SantaLucia, J.; Walter, A. E.; Turner, D. H. Nearest-Neighbor Parameters for G.Cntdot.U Mismatches: 5'GU3'/3'UG5' Is Destabilizing in the Contexts CGUG/GUGC, UGUA/AUGU, and AGUU/UUGA but Stabilizing in GGUC/CUGG. *Biochemistry* **1991**, *30*, 11124–11132. https://doi.org/10.1021/bi00110a015.

(112) Varani, G.; McClain, W. H. The G·U Wobble Base Pair: A Fundamental Building Block of RNA Structure Crucial to RNA Function in Diverse Biological Systems. *EMBO Rep.* **2000**, *1*, 18–23. https://doi.org/10.1093/embo-reports/kvd001.

(113) Davis, A. R.; Kirkpatrick, C. C.; Znosko, B. M. Structural Characterization of Naturally Occurring RNA Single Mismatches. *Nucleic Acids Res.* **2011**, *39*, 1081–1094. https://doi.org/10.1093/nar/gkq793.

(114) Wincel, H. Gas-Phase Hydration Thermochemistry of Sodiated and Potassiated Nucleic Acid Bases. *J. Am. Soc. Mass Spectrom.* **2012**, *23*, 1479–1487. https://doi.org/10.1007/s13361-012-0436-5.

(115) Lhomme, J.; Constant, J. F.; Demeunynck, M. Abasic DNA Structure, Reactivity, and Recognition. *Biopolymers* **1999**, *52*, 65–83. https://doi.org/10.1002/1097-0282(1999)52:2<65::aid-bip1>3.0.co;2-u.

(116) Liu, Y.; Rodriguez, Y.; Ross, R. L.; Zhao, R.; Watts, J. A.; Grunseich, C.; Bruzel, A.; Li, D.; Burdick, J. T.; Prasad, R.; et al. RNA Abasic Sites in Yeast and Human Cells. *Proc. Natl. Acad. Sci.* **2020**, *117*, 20689–20695. https://doi.org/10.1073/pnas.2011511117.

(117) Gates, K. S. An Overview of Chemical Processes That Damage Cellular DNA: Spontaneous Hydrolysis, Alkylation, and Reactions with Radicals. *Chem. Res. Toxicol.* **2009**, *22*, 1747–1760. https://doi.org/10.1021/tx900242k.

(118) Fu, D.; Calvo, J. A.; Samson, L. D. Balancing Repair and Tolerance of DNA Damage Caused

by Alkylating Agents. *Nat. Rev. Cancer* **2012**, *12*, 104–120. https://doi.org/10.1038/nrc3185.

(119) Fortini, P.; Pascucci, B.; Parlanti, E.; D'Errico, M.; Simonelli, V.; Dogliotti, E. The Base Excision Repair: Mechanisms and Its Relevance for Cancer Susceptibility. *Biochimie* **2003**, *85*, 1053–1071. https://doi.org/10.1016/j.biochi.2003.11.003.

(120) Krokan, H. E.; Bjoras, M. Base Excision Repair. *Cold Spring Harb. Perspect. Biol.* **2013**, *5*, a012583. https://doi.org/10.1101/cshperspect.a012583.

(121) Beger, R. D.; Bolton, P. H. Structures of Apurinic and Apyrimidinic Sites in Duplex DNAs. *J. Biol. Chem.* **1998**, *273*, 15565–15573. https://doi.org/10.1074/jbc.273.25.15565.

(122) Marathias, V. M.; Jerkovic, B.; Bolton, P. H. Damage Increases the Flexibility of Duplex DNA. *Nucleic Acids Res.* **1999**, *27*, 1854–1858. https://doi.org/10.1093/nar/27.8.1854.

(123) Barsky, D.; Foloppe, N.; Ahmadia, S.; Wilson, D. M.; MacKerell, A. D. New Insights into the Structure of Abasic DNA from Molecular Dynamics Simulations. *Nucleic Acids Res.* **2000**, *28*, 2613–2626. https://doi.org/10.1093/nar/28.13.2613.

(124) Hoehn, S. T.; Turner, C. J.; Stubbe, J. Solution Structure of an Oligonucleotide Containing an Abasic Site: Evidence for an Unusual Deoxyribose Conformation. *Nucleic Acids Res.* **2001**, *29*, 3413–3423. https://doi.org/10.1093/nar/29.16.3413.

(125) Corbella, M.; Voityuk, A. A.; Curutchet, C. How Abasic Sites Impact Hole Transfer Dynamics in GC-Rich DNA Sequences. *Phys. Chem. Chem. Phys.* **2018**, *20*, 23123–23131. https://doi.org/10.1039/c8cp03572e.

(126) Cuniasse, Ph.; Fazakerley, G. V.; Guschlbauer, W.; Kaplan, B. E.; Sowers, L. C. The Abasic Site as a Challenge to DNA Polymerase. *J. Mol. Biol.* **1990**, *213*, 303–314. https://doi.org/10.1016/s0022-2836(05)80192-5.

(127) Huang, H.; Greenberg, M. M. Synthesis and Analysis of Oligonucleotides Containing Abasic Site Analogues. *J. Org. Chem.* **2008**, *73*, 2695–2703. https://doi.org/10.1021/jo702614p.

(128) Caron, C.; Duong, X. N. T.; Guillot, R.; Bombard, S.; Granzhan, A. Interaction of Functionalized Naphthalenophanes with Abasic Sites in DNA: DNA Cleavage, DNA Cleavage Inhibition, and Formation of Ligand–DNA Adducts. *Chem. – Eur. J.* **2019**, *25*, 1949–1962. https://doi.org/10.1002/chem.201805555.

(129) Lippert, B.; Gupta, D. Promotion of Rare Nucleobase Tautomers by Metal Binding. *Dalton Trans.* **2009**, No. 24, 4619–4634. https://doi.org/10.1039/b823087k.

(130) Elguero, J.; Katritzky, A. R.; Denisko, O. V. Prototropic Tautomerism of Heterocycles: Heteroaromatic Tautomerism—General Overview and Methodology. In *Advances in Heterocyclic Chemistry*; Academic Press: San Diego, California, USA, 2000; Vol. 76, p.1–84. https://doi.org/10.1016/S0065-2725(00)76003-X.

(131) Shahi, M. R.; Bagheri, S. The Effect of Metal Alkali Cations on the Properties of Hydrogen Bonds in Tautomeric Forms of Adenine – Guanine Mismatch. *J. Mol. Graph. Model.* **2020**, *100*, 107705. https://doi.org/10.1016/j.jmgm.2020.107705.

(132) Oomens, J.; Moehlig, A. R.; Morton, T. H. Infrared Multiple Photon Dissociation (IRMPD) Spectroscopy of the Proton-Bound Dimer of 1-Methylcytosine in the Gas Phase. *J. Phys. Chem. Lett.* **2010**, *1*, 2891–2897. https://doi.org/10.1021/jz101080x.

(133) Otto, C.; Thomas, G. A.; Rippe, K.; Jovin, T. M.; Peticolas, W. L. The Hydrogen-Bonding Structure in Parallel-Stranded Duplex DNA Is Reverse Watson-Crick. *Biochemistry* **1991**, *30*, 3062–3069. https://doi.org/10.1021/bi00226a012.

(134) Szabat, M.; Kierzek, R. Parallel-Stranded DNA and RNA Duplexes - Structural Features and Potential Applications. *FEBS J.* **2017**, *284*, 3986–3998. https://doi.org/10.1111/febs.14187.

(135) Hoogsteen, K. The Crystal and Molecular Structure of a Hydrogen-Bonded Complex between 1-Methylthymine and 9-Methyladenine. *Acta Crystallogr.* **1963**, *16*, 907–916. https://doi.org/10.1107/s0365110x63002437.

(136) Chan, P. P.; Glazer, P. M. Triplex DNA: Fundamentals, Advances, and Potential Applications for Gene Therapy. *J. Mol. Med.* **1997**, *75*, 267–282. https://doi.org/10.1007/s001090050112.

(137) Lee, J. S.; Johnson, D. A.; Morgan, A. R. Complexes Formed by (Pyrimidine)n ·(Purine)n DNAs on Lowering the PH Are Three-Stranded. *Nucleic Acids Res.* **1979**, *6*, 3073–3091. https://doi.org/10.1093/nar/6.9.3073.

(138) Müller, J. Nucleic Acid Duplexes with Metal-Mediated Base Pairs and Their Structures. *Coord. Chem. Rev.* **2019**, *393*, 37–47. https://doi.org/10.1016/j.ccr.2019.05.007.

(139) Takezawa, Y.; Müller, J.; Shionoya, M. Artificial DNA Base Pairing Mediated by Diverse Metal Ions. *Chem. Lett.* **2016**, *46*, 622–633. https://doi.org/10.1246/cl.160985.

(140) Katz, S. Reversible Reaction of Double-Stranded Polynucleotides and HgII : Separation of the Strands. *Nature* **1962**, *195*, 997–998. https://doi.org/10.1038/195997a0.

(141) Kondo, J.; Yamada, T.; Hirose, C.; Okamoto, I.; Tanaka, Y.; Ono, A. Crystal Structure of Metallo DNA Duplex Containing Consecutive Watson-Crick-like T-Hg(II)-T Base Pairs. *Angew. Chem. Int. Ed Engl.* **2014**, *53*, 2385–2388. https://doi.org/10.1002/anie.201309066.

(142) Ono, A.; Cao, S.; Togashi, H.; Tashiro, M.; Fujimoto, T.; Machinami, T.; Oda, S.; Miyake, Y.; Okamoto, I.; Tanaka, Y. Specific Interactions

between Silver(I) Ions and Cytosine-Cytosine Pairs in DNA Duplexes. *Chem. Commun.* **2008**, No. 39, 4825–4827. https://doi.org/10.1039/b808686a.

(143) Swasey, S. M.; Leal, L. E.; Lopez-Acevedo, O.; Pavlovich, J.; Gwinn, E. G. Silver (I) as DNA Glue: Ag + -Mediated Guanine Pairing Revealed by Removing Watson-Crick Constraints. *Sci. Rep.* **2015**, *5*, 10163. https://doi.org/10.1038/srep10163.

(144) Dairaku, T.; Furuita, K.; Sato, H.; Šebera, J.; Nakashima, K.; Kondo, J.; Yamanaka, D.; Kondo, Y.; Okamoto, I.; Ono, A.; et al. Structure Determination of an Ag(I) -Mediated Cytosine-Cytosine Base Pair within DNA Duplex in Solution with (1) H/(15) N/(109) Ag NMR Spectroscopy. *Chem. - Eur. J.* **2016**, *22*, 13028–13031. https://doi.org/10.1002/chem.201603048.

(145) Swasey, S. M.; Rosu, F.; Copp, S. M.; Gabelica, V.; Gwinn, E. G. Parallel Guanine Duplex and Cytosine Duplex DNA with Uninterrupted Spines of AgI -Mediated Base Pairs. *J. Phys. Chem. Lett.* **2018**, *9*, 6605–6610. https://doi.org/10.1021/acs.jpclett.8b02851.

(146) Johannsen, S.; Megger, N.; Bohme, D.; Sigel, R. K.; Muller, J. Solution Structure of a DNA Double Helix with Consecutive Metal-Mediated Base Pairs. *Nat. Chem.* **2010**, *2*, 229–234. https://doi.org/10.1038/nchem.512.

(147) Okamoto, I.; Ono, T.; Sameshima, R.; Ono, A. Metal Ion-Binding Properties of DNA Duplexes Containing Thiopyrimidine Base Pairs. *Chem. Commun.* **2012**, *48*, 4347–4349. https://doi.org/10.1039/c2cc15436f.

(148) Mei, H.; Röhl, I.; Seela, F. Ag+-Mediated DNA Base Pairing: Extraordinarily Stable Pyrrolo-DC–Pyrrolo-DC Pairs Binding Two Silver Ions. *J. Org. Chem.* **2013**, *78*, 9457–9463. https://doi.org/10.1021/jo401109w.

(149) Kuznetsov, S. V.; Ren, C.-C.; Woodson, S. A.; Ansari, A. Loop Dependence of the Stability and Dynamics of Nucleic Acid Hairpins. *Nucleic Acids Res.* **2007**, *36*, 1098–1112. https://doi.org/10.1093/nar/gkm1083.

(150) Svoboda, P.; Cara, A. Di. Hairpin RNA: A Secondary Structure of Primary Importance. *Cell. Mol. Life Sci.* **2006**, *63*, 901–908. https://doi.org/10.1007/s00018-005-5558-5.

(151) Draper, D. E. Themes in RNA-Protein Recognition. *J. Mol. Biol.* **1999**, *293*, 255–270. https://doi.org/10.1006/jmbi.1999.2991.

(152) Xodo, L. E.; Manzini, G.; Quadrifoglio, F.; van der Marel, G.; van Boom, J. H. Hairpin Structures in Synthetic Oligodeoxynucleotides: Sequence Effects on the Duplex-to-Hairpin Transition. *Biochimie* **1989**, *71*, 793–803. https://doi.org/10.1016/0300-9084(89)90042-4.

(153) Xodo, L. E.; Manzini, G.; Quadrifoglio, F.; Van der Marel, G. A.; Van Boom, J. H. Oligodeoxynucleotide Folding in Solution: Loop Size and Stability of B-Hairpins. *Biochemistry* **1988**, *27*, 6321–6326. https://doi.org/10.1021/bi00417a018.

(154) Varani, G. Exceptionally Stable Nucleic Acid Hairpins. *Annu. Rev. Biophys. Biomol. Struct.* **1995**, *24*, 379–404. https://doi.org/10.1146/annurev.bb.24.060195.002115.

(155) Groebe, D. R.; Uhlenbeck, O. C. Thermal Stability of RNA Hairpins Containing a Four-Membered Loop and a Bulge Nucleotide. *Biochemistry* **1989**, *28*, 742–747. https://doi.org/10.1021/bi00428a049.

(156) Zhao, C.; Zhang, D.; Jiang, Y.; Chen, S.-J. Modeling Loop Composition and Ion Concentration Effects in RNA Hairpin Folding Stability. *Biophys. J.* **2020**, *119*, 1439–1455. https://doi.org/10.1016/j.bpj.2020.07.042.

(157) Vallone, P. M.; Paner, T. M.; Hilario, J.; Lane, M. J.; Faldasz, B. D.; Benight, A. S. Melting Studies of Short DNA Hairpins: Influence of Loop Sequence and Adjoining Base Pair Identity on Hairpin Thermodynamic Stability. *Biopolymers* **1999**, *50*, 425–442. https://doi.org/10.1002/(sici)1097-0282(19991005)50:4<425::aid-bip8>3.0.co;2-b.

(158) Tinoco Jr, I.; Bustamante, C. How RNA Folds. *J. Mol. Biol.* **1999**, *293*, 271–281. https://doi.org/10.1006/jmbi.1999.3001.

(159) Chen, S.-J. RNA Folding: Conformational Statistics, Folding Kinetics, and Ion Electrostatics. *Annu. Rev. Biophys.* **2008**, *37*, 197–214. https://doi.org/10.1146/annurev.biophys.37.032807.125957.

(160) Tan, Z.-J.; Chen, S.-J. Salt Dependence of Nucleic Acid Hairpin Stability. *Biophys. J.* **2008**, *95*, 738–752. https://doi.org/10.1529/biophysj.108.131524.

(161) Largy, E.; Mergny, J.-L. Shape Matters: Size-Exclusion HPLC for the Study of Nucleic Acid Structural Polymorphism. *Nucleic Acids Res.* **2014**, *42*, e149. https://doi.org/10.1093/nar/gku751.

(162) Marky, L. A.; Blumenfeld, K. S.; Kozlowski, S.; Breslauer, K. J. Salt-Dependent Conformational Transitions in the Self-Complementary Deoxydodecanucleotide d(CGCAATTCGCG): Evidence for Hairpin Formation. *Biopolymers* **1983**, *22*, 1247–1257. https://doi.org/10.1002/bip.360220416.

(163) Hald, M.; Pedersen, J. B.; Stein, P. C.; Kirpekar, F.; Jacobsen, J. P. A Comparison of the Hairpin Stability of the Palindromic d(CGCG(A/T)4CGCG) Oligonucleotides. *Nucleic Acids Res.* **1995**, *23*, 4576–4582. https://doi.org/10.1093/nar/23.22.4576.

(164) Nakano, S.; Kirihata, T.; Fujii, S.; Sakai, H.; Kuwahara, M.; Sawai, H.; Sugimoto, N. Influence of Cationic Molecules on the Hairpin to Duplex Equilibria of Self-Complementary DNA and RNA Oligonucleotides. *Nucleic Acids*

Res. **2007**, *35*, 486–494. https://doi.org/10.1093/nar/gkl1073.

(165) Zuker, M. Mfold Web Server for Nucleic Acid Folding and Hybridization Prediction. *Nucleic Acids Res.* **2003**, *31*, 3406–3415. https://doi.org/10.1093/nar/gkg595.

(166) Markham, N. R.; Zuker, M. DINAMelt Web Server for Nucleic Acid Melting Prediction. *Nucleic Acids Res.* **2005**, *33*, W577-581. https://doi.org/10.1093/nar/gki591.

(167) Markham, N. R.; Zuker, M. UNAFold: Software for Nucleic Acid Folding and Hybridization. *Methods Mol. Biol. Clifton NJ* **2008**, *453*, 3–31. https://doi.org/10.1007/978-1-60327-429-6_1.

(168) Ramsing, Niels B.; Jovin, Thomas M. Parallel Stranded Duplex DNA. *Nucleic Acids Res.* **1988**, *16*, 6659–6676. https://doi.org/10.1093/nar/16.14.6659.

(169) van de Sande, J. H.; Ramsing, N. B.; Germann, M. W.; Elhorst, W.; Kalisch, B. W.; von Kitzing, E.; Pon, R. T.; Clegg, R. C.; Jovin, T. M. Parallel Stranded DNA. *Science* **1988**, *241*, 551–557. https://doi.org/10.1126/science.3399890.

(170) Parvathy, V. R.; Bhaumik, S. R.; Chary, K. V. R.; Govil, G.; Liu, K.; Howard, F. B.; Miles, H. T. NMR Structure of a Parallel-Stranded DNA Duplex at Atomic Resolution. *Nucleic Acids Res.* **2002**, *30*, 1500–1511. https://doi.org/10.1093/nar/30.7.1500.

(171) Germann, M. W.; Kalisch, B. W.; van de Sande, J. H. Relative Stability of Parallel- and Anti-Parallel-Stranded Duplex DNA. *Biochemistry* **1988**, *27*, 8302–8306. https://doi.org/10.1021/bi00422a002.

(172) Felsenfeld, G.; Davies, D. R.; Rich, A. Formation of A Three-Stranded Polynucleotide Molecule. *J. Am. Chem. Soc.* **1957**, *79*, 2023–2024. https://doi.org/10.1021/ja01565a074.

(173) Felsenfeld, G.; Rich, A. Studies on the Formation of Two- and Three-Stranded Polyribonucleotides. *Biochim. Biophys. Acta* **1957**, *26*, 457–468. https://doi.org/10.1016/0006-3002(57)90091-4.

(174) Mirkin, S. M.; Frank-Kamenetskii, M. D. H-DNA and Related Structures. *Annu. Rev. Biophys. Biomol. Struct.* **1994**, *23*, 541–576. https://doi.org/10.1146/annurev.bb.23.060194.002545.

(175) Bacolla, A.; Wang, G.; Vasquez, K. M. New Perspectives on DNA and RNA Triplexes As Effectors of Biological Activity. *PLOS Genet.* **2015**, *11*, e1005696. https://doi.org/10.1371/journal.pgen.1005696.

(176) Kinniburgh, A. J. A Cis-Acting Transcription Element of the c-Myc Gene Can Assume an H-DNA Conformation. *Nucleic Acids Res.* **1989**, *17*, 7771–7778. https://doi.org/10.1093/nar/17.19.7771.

(177) Frank-Kamenetskii, M. D.; Mirkin, S. M. Triplex DNA Structures. *Annu. Rev. Biochem.* **1995**, *64*, 65–95. https://doi.org/10.1146/annurev.bi.64.070195.000433.

(178) Li, Y.; Syed, J.; Sugiyama, H. RNA-DNA Triplex Formation by Long Noncoding RNAs. *Cell Chem. Biol.* **2016**, *23*, 1325–1333. https://doi.org/10.1016/j.chembiol.2016.09.011.

(179) Moser, H.; Dervan, P. Sequence-Specific Cleavage of Double Helical DNA by Triple Helix Formation. *Science* **1987**, *238*, 645–650. https://doi.org/10.1126/science.3118463.

(180) Beal, P. A.; Dervan, P. B. Second Structural Motif for Recognition of DNA by Oligonucleotide-Directed Triple-Helix Formation. *Science* **1991**, *251*, 1360–1363. https://doi.org/10.1126/science.2003222.

(181) Olivas, W. M.; Maher, L. J. I. Competitive Triplex/Quadruplex Equilibria Involving Guanine-Rich Oligonucleotides. *Biochemistry* **1995**, *34*, 278–284. https://doi.org/10.1021/bi00001a034.

(182) Noonberg, S. B.; François, J. C.; Garestier, T.; Hélène, C. Effect of Competing Self-Structure on Triplex Formation with Purine-Rich Oligodeoxynucleotides Containing GA Repeats. *Nucleic Acids Res.* **1995**, *23*, 1956–1963. https://doi.org/10.1093/nar/23.11.1956.

(183) Chandler, S. P.; Fox, K. R. Specificity of Antiparallel DNA Triple Helix Formation. *Biochemistry* **1996**, *35*, 15038–15048. https://doi.org/10.1021/bi9609679.

(184) Gowers, D. M.; Fox, K. R. DNA Triple Helix Formation at Oligopurine Sites Containing Multiple Contiguous Pyrimidines. *Nucleic Acids Res.* **1997**, *25*, 3787–3794. https://doi.org/10.1093/nar/25.19.3787.

(185) Cheng, A.-J.; Dyke, M. W. V. Oligodeoxyribonucleotide Length and Sequence Effects on Intermolecular Purine—Purine—Pyrimidine Triple-Helix Formation. *Nucleic Acids Res.* **1994**, *22*, 4742–4747. https://doi.org/10.1093/nar/22.22.4742.

(186) James, P. L.; Brown, T.; Fox, K. R. Thermodynamic and Kinetic Stability of Intermolecular Triple Helices Containing Different Proportions of C+*GC and T*AT Triplets. *Nucleic Acids Res.* **2003**, *31*, 5598–5606. https://doi.org/10.1093/nar/gkg782.

(187) Bedrat, A.; Lacroix, L.; Mergny, J.-L. Re-Evaluation of G-Quadruplex Propensity with G4Hunter. *Nucleic Acids Res.* **2016**, *44*, 1746–1759. https://doi.org/10.1093/nar/gkw006.

(188) Parkinson, G. N. Fundamentals of Quadruplex Structures. In *Quadruplex Nucleic Acids*; Neidle, S., Balasubramanian, S., Eds.; RSC Biomolecular Sciences; Royal Society of Chemistry: Cambridge, UK, 2006; p.1–30. https://doi.org/10.1039/9781847555298-00001.

(189) Krishnan-Ghosh, Y.; Stephens, E.; Balasubramanian, S. A PNA4 Quadruplex. *J.*

Am. Chem. Soc. **2004**, *126*, 5944–5945. https://doi.org/10.1021/ja031508f.

(190) Daly, S.; Rosu, F.; Gabelica, V. Mass-Resolved Electronic Circular Dichroism Ion Spectroscopy. *Science* **2020**, *368*, 1465–1468. https://doi.org/10.1126/science.abb1822.

(191) Bakalar, B.; Heddi, B.; Schmitt, E.; Mechulam, Y.; Phan, A. T. A Minimal Sequence for Left-Handed G-Quadruplex Formation. *Angew. Chem. Int. Ed.* **2019**, *58*, 2331–2335. https://doi.org/10.1002/anie.201812628.

(192) Rhodes, D.; Lipps, H. J. G-Quadruplexes and Their Regulatory Roles in Biology. *Nucleic Acids Res.* **2015**, *43*, 8627–8637. https://doi.org/10.1093/nar/gkv862.

(193) Varshney, D.; Spiegel, J.; Zyner, K.; Tannahill, D.; Balasubramanian, S. The Regulation and Functions of DNA and RNA G-Quadruplexes. *Nat. Rev. Mol. Cell Biol.* **2020**, *21*, 459–474. https://doi.org/10.1038/s41580-020-0236-x.

(194) Fay, M. M.; Lyons, S. M.; Ivanov, P. RNA G-Quadruplexes in Biology: Principles and Molecular Mechanisms. *J. Mol. Biol.* **2017**, *429*, 2127–2147. https://doi.org/10.1016/j.jmb.2017.05.017.

(195) Kharel, P.; Balaratnam, S.; Beals, N.; Basu, S. The Role of RNA G-quadruplexes in Human Diseases and Therapeutic Strategies. *WIREs RNA* **2020**, *11*, e1568. https://doi.org/10.1002/wrna.1568.

(196) Roxo, C.; Kotkowiak, W.; Pasternak, A. G-Quadruplex-Forming Aptamers—Characteristics, Applications, and Perspectives. *Molecules* **2019**, *24*, 3781. https://doi.org/10.3390/molecules24203781.

(197) Largy, E.; Mergny, J.-L.; Gabelica, V. Role of Alkali Metal Ions in G-Quadruplex Nucleic Acid Structure and Stability. In *The Alkali Metal Ions: Their Role for Life*; Sigel, A., Sigel, H., Sigel, R. K. O., Eds.; Metal Ions in Life Sciences; Springer Cham: Heidelberg, 2016; p.203–258. https://doi.org/10.1007/978-3-319-21756-7_7.

(198) Marchand, A.; Gabelica, V. Native Electrospray Mass Spectrometry of DNA G-Quadruplexes in Potassium Solution. *J. Am. Soc. Mass Spectrom.* **2014**, *25*, 1146–1154. https://doi.org/10.1007/s13361-014-0890-3.

(199) Marchand, A.; Gabelica, V. Folding and Misfolding Pathways of G-Quadruplex DNA. *Nucleic Acids Res.* **2016**, *44*, 10999–11012. https://doi.org/10.1093/nar/gkw970.

(200) Ghosh, A.; Largy, E.; Gabelica, V. DNA G-Quadruplexes for Native Mass Spectrometry in Potassium: A Database of Validated Structures in Electrospray-Compatible Conditions. *Nucleic Acids Res.* **2021**, *49*, 2333–2345. https://doi.org/10.1093/nar/gkab039.

(201) Dvorkin, S. A.; Karsisiotis, A. I.; Webba da Silva, M. Encoding Canonical DNA Quadruplex Structure. *Sci. Adv.* **2018**, *4*, eaat3007. https://doi.org/10.1126/sciadv.aat3007.

(202) Lightfoot, H. L.; Hagen, T.; Tatum, N. J.; Hall, J. The Diverse Structural Landscape of Quadruplexes. *FEBS Lett.* **2019**, *593*, 2083–2102. https://doi.org/10.1002/1873-3468.13547.

(203) Largy, E.; Marchand, A.; Amrane, S.; Gabelica, V.; Mergny, J.-L. Quadruplex Turncoats: Cation-Dependent Folding and Stability of Quadruplex-DNA Double Switches. *J. Am. Chem. Soc.* **2016**, *138*, 2780–2792. https://doi.org/10.1021/jacs.5b13130.

(204) Kuryavyi, V.; Majumdar, A.; Shallop, A.; Chernichenko, N.; Skripkin, E.; Jones, R.; Patel, D. J. A Double Chain Reversal Loop and Two Diagonal Loops Define the Architecture of a Unimolecular DNA Quadruplex Containing a Pair of Stacked G(Syn)-G(Syn)-G(Anti)-G(Anti) Tetrads Flanked by a G-(T-T) Triad and a T-T-T Triple. *J. Mol. Biol.* **2001**, *310*, 181–194. https://doi.org/10.1006/jmbi.2001.4759.

(205) Karg, B.; Mohr, S.; Weisz, K. Duplex-Guided Refolding into Novel G-Quadruplex (3+1) Hybrid Conformations. *Angew. Chem. Int. Ed Engl.* **2019**, *58*, 11068–11071. https://doi.org/10.1002/anie.201905372.

(206) Kotar, A.; Rigo, R.; Sissi, C.; Plavec, J. Two-Quartet Kit* G-Quadruplex Is Formed via Double-Stranded Pre-Folded Structure. *Nucleic Acids Res.* **2019**, *47*, 2641–2653. https://doi.org/10.1093/nar/gky1269.

(207) Guédin, A.; Gros, J.; Alberti, P.; Mergny, J.-L. How Long Is Too Long? Effects of Loop Size on G-Quadruplex Stability. *Nucleic Acids Res.* **2010**, *38*, 7858–7868. https://doi.org/10.1093/nar/gkq639.

(208) Ambrus, A.; Chen, D.; Dai, J.; Bialis, T.; Jones, R. A.; Yang, D. Human Telomeric Sequence Forms a Hybrid-Type Intramolecular G-Quadruplex Structure with Mixed Parallel/Antiparallel Strands in Potassium Solution. *Nucleic Acids Res.* **2006**, *34*, 2723–2735. https://doi.org/10.1093/nar/gkl348.

(209) Gehring, K.; Leroy, J.-L.; Guéron, M. A Tetrameric DNA Structure with Protonated Cytosine-Cytosine Base Pairs. *Nature* **1993**, *363*, 561–565. https://doi.org/10.1038/363561a0.

(210) Snoussi, K.; Nonin-Lecomte, S.; Leroy, J.-L. The RNA I-Motif. *J. Mol. Biol.* **2001**, *309*, 139–153. https://doi.org/10.1006/jmbi.2001.4618.

(211) Krishnan-Ghosh, Y.; Stephens, E.; Balasubramanian, S. PNA Forms an I-Motif. *Chem. Commun.* **2005**, No. 42, 5278–5280. https://doi.org/10.1039/b510405j.

(212) Wright, E. P.; Huppert, J. L.; Waller, Z. A. E. Identification of Multiple Genomic DNA Sequences Which Form I-Motif Structures at Neutral PH. *Nucleic Acids Res.* **2017**, *45*, 2951–2959. https://doi.org/10.1093/nar/gkx090.

(213) Rajendran, A.; Nakano, S.; Sugimoto, N. Molecular Crowding of the Cosolutes Induces an Intramolecular I-Motif Structure of Triplet Repeat DNA Oligomers at Neutral PH. *Chem.*

Commun. **2010**, *46*, 1299–1301. https://doi.org/10.1039/b922050j.

(214) Day, H. A.; Huguin, C.; Waller, Z. A. E. Silver Cations Fold I-Motif at Neutral PH. *Chem. Commun.* **2013**, *49*, 7696–7698. https://doi.org/10.1039/c3cc43495h.

(215) Zeraati, M.; Langley, D. B.; Schofield, P.; Moye, A. L.; Rouet, R.; Hughes, W. E.; Bryan, T. M.; Dinger, M. E.; Christ, D. I-Motif DNA Structures Are Formed in the Nuclei of Human Cells. *Nat. Chem.* **2018**, *10*, 631–637. https://doi.org/10.1038/s41557-018-0046-3.

(216) Dzatko, S.; Krafcikova, M.; Hänsel-Hertsch, R.; Fessl, T.; Fiala, R.; Loja, T.; Krafcik, D.; Mergny, J.-L.; Foldynova-Trantirkova, S.; Trantirek, L. Evaluation of the Stability of DNA I-Motifs in the Nuclei of Living Mammalian Cells. *Angew. Chem. Int. Ed.* **2018**, *57*, 2165–2169. https://doi.org/10.1002/anie.201712284.

(217) Abou Assi, H.; Garavís, M.; González, C.; Damha, M. J. I-Motif DNA: Structural Features and Significance to Cell Biology. *Nucleic Acids Res.* **2018**, *46*, 8038–8056. https://doi.org/10.1093/nar/gky735.

(218) Berger, I.; Egli, M.; Rich, A. Inter-Strand C-H...O Hydrogen Bonds Stabilizing Four-Stranded Intercalated Molecules: Stereoelectronic Effects of O4' in Cytosine-Rich DNA. *Proc. Natl. Acad. Sci.* **1996**, *93*, 12116–12121. https://doi.org/10.1073/pnas.93.22.12116.

(219) Han, X.; Leroy, J. L.; Guéron, M. An Intramolecular I-Motif: The Solution Structure and Base-Pair Opening Kinetics of d(5mCCT3CCT3ACCT3CC). *J. Mol. Biol.* **1998**, *278*, 949–965. https://doi.org/10.1006/jmbi.1998.1740.

(220) Phan, A. T.; Guéron, M.; Leroy, J.-L. The Solution Structure and Internal Motions of a Fragment of the Cytidine-Rich Strand of the Human Telomere 1 1Edited by I. Tinoco. *J. Mol. Biol.* **2000**, *299*, 123–144. https://doi.org/10.1006/jmbi.2000.3613.

(221) Leroy, J.-L.; Guéron, M.; Mergny, J.-L.; Hélène, C. Intramolecular Folding of a Fragment of the Cytosine-Rich Strand of Telomeric DNA into an i-Motif. *Nucleic Acids Res.* **1994**, *22*, 1600–1606. https://doi.org/10.1093/nar/22.9.1600.

(222) Nonin, S.; Phan, A. T.; Leroy, J.-L. Solution Structure and Base Pair Opening Kinetics of the I-Motif Dimer of d(5mCCTTTACC): A Noncanonical Structure with Possible Roles in Chromosome Stability. *Structure* **1997**, *5*, 1231–1247. https://doi.org/10.1016/s0969-2126(97)00273-6.

(223) Leroy, J.-L.; Guéron, M. Solution Structures of the I-Motif Tetramers of d(TCC), d(5methylCCT) and d(T5methylCC): Novel NOE Connections between Amino Protons and Sugar Protons. *Structure* **1995**, *3*, 101–120. https://doi.org/10.1016/s0969-2126(01)00138-1.

(224) Fojtík, P.; Vorlícková, M. The Fragile X Chromosome (GCC) Repeat Folds into a DNA Tetraplex at Neutral PH. *Nucleic Acids Res.* **2001**, *29*, 4684–4690. https://doi.org/10.1093/nar/29.22.4684.

(225) Lieblein, A. L.; Buck, J.; Schlepckow, K.; Fürtig, B.; Schwalbe, H. Time-Resolved NMR Spectroscopic Studies of DNA i-Motif Folding Reveal Kinetic Partitioning. *Angew. Chem. Int. Ed.* **2012**, *51*, 250–253. https://doi.org/10.1002/anie.201104938.

(226) Phan, A. T.; Mergny, J.-L. Human Telomeric DNA: G-Quadruplex, i-Motif and Watson-Crick Double Helix. *Nucleic Acids Res.* **2002**, *30*, 4618–4625. https://doi.org/10.1093/nar/gkf597.

(227) Mergny, J.-L.; Lacroix, L.; Han, X.; Leroy, J.-L.; Helene, C. Intramolecular Folding of Pyrimidine Oligodeoxynucleotides into an I-DNA Motif. *J. Am. Chem. Soc.* **1995**, *117*, 8887–8898. https://doi.org/10.1021/ja00140a001.

(228) Fleming, A. M.; Ding, Y.; Rogers, R. A.; Zhu, J.; Zhu, J.; Burton, A. D.; Carlisle, C. B.; Burrows, C. J. 4n–1 Is a "Sweet Spot" in DNA i-Motif Folding of 2'-Deoxycytidine Homopolymers. *J. Am. Chem. Soc.* **2017**, *139*, 4682–4689. https://doi.org/10.1021/jacs.6b10117.

(229) Fujii, T.; Sugimoto, N. Loop Nucleotides Impact the Stability of Intrastrand I-Motif Structures at Neutral PH. *Phys. Chem. Chem. Phys.* **2015**, *17*, 16719–16722. https://doi.org/10.1039/c5cp02794b.

(230) Lieblein, A. L.; Fürtig, B.; Schwalbe, H. Optimizing the Kinetics and Thermodynamics of DNA I-Motif Folding. *ChemBioChem* **2013**, *14*, 1226–1230. https://doi.org/10.1002/cbic.201300284.

(231) Gurung, S. P.; Schwarz, C.; Hall, J. P.; Cardin, C. J.; Brazier, J. A. The Importance of Loop Length on the Stability of I-Motif Structures. *Chem. Commun.* **2015**, *51*, 5630–5632. https://doi.org/10.1039/c4cc07279k.

(232) Reilly, S. M.; Morgan, R. K.; Brooks, T. A.; Wadkins, R. M. Effect of Interior Loop Length on the Thermal Stability and PK(a) of i-Motif DNA. *Biochemistry* **2015**, *54*, 1364–1370. https://doi.org/10.1021/bi5014722.

(233) Stofer, E.; Chipot, C.; Lavery, R. Free Energy Calculations of Watson−Crick Base Pairing in Aqueous Solution. *J. Am. Chem. Soc.* **1999**, *121*, 9503–9508. https://doi.org/10.1021/ja991092z.

(234) Malliavin, T. E.; Gau, J.; Snoussi, K.; Leroy, J.-L. Stability of the I-Motif Structure Is Related to the Interactions between Phosphodiester Backbones. *Biophys. J.* **2003**, *84*, 3838–3847. https://doi.org/10.1016/s0006-3495(03)75111-x.

(235) Šponer, J.; Jurečka, P.; Hobza, P. Accurate Interaction Energies of Hydrogen-Bonded Nucleic Acid Base Pairs. *J. Am. Chem. Soc.* **2004**, *126*, 10142–10151. https://doi.org/10.1021/ja048436s.

(236) Fonseca Guerra, C.; Bickelhaupt, F. M. Charge Transfer and Environment Effects Responsible

for Characteristics of DNA Base Pairing. *Angew. Chem. Int. Ed Engl.* **1999**, *38*, 2942–2945. https://doi.org/10.1002/(sici)1521-3773(19991004)38:19<2942::aid-anie2942>3.3.co;2-m.

(237) Stasyuk, O. A.; Solà, M.; Swart, M.; Fonseca Guerra, C.; Krygowski, T. M.; Szatylowicz, H. Effect of Alkali Metal Cations on Length and Strength of Hydrogen Bonds in DNA Base Pairs. *ChemPhysChem* **2020**, *21*, 2112–2126. https://doi.org/10.1002/cphc.202000434.

(238) Černý, J.; Hobza, P. Non-Covalent Interactions in Biomacromolecules. *Phys. Chem. Chem. Phys.* **2007**, *9*, 5291–5303. https://doi.org/10.1039/b704781a.

(239) Paragi, G.; Fonseca Guerra, C. Cooperativity in the Self-Assembly of the Guanine Nucleobase into Quartet and Ribbon Structures on Surfaces. *Chem. - Eur. J.* **2017**, *23*, 3042–3050. https://doi.org/10.1002/chem.201604830.

(240) Yang, B.; Rodgers, M. T. Base-Pairing Energies of Proton-Bound Heterodimers of Cytosine and Modified Cytosines: Implications for the Stability of DNA i-Motif Conformations. *J. Am. Chem. Soc.* **2014**, *136*, 282–290. https://doi.org/10.1021/ja409515v.

(241) Kool, E. T. Hydrogen Bonding, Base Stacking, and Steric Effects in DNA Replication. *Annu. Rev. Biophys. Biomol. Struct.* **2001**, *30*, 1–22. https://doi.org/10.1146/annurev.biophys.30.1.1.

(242) Dąbkowska, I.; Gonzalez, H. V.; Jurečka, P.; Hobza, P. Stabilization Energies of the Hydrogen-Bonded and Stacked Structures of Nucleic Acid Base Pairs in the Crystal Geometries of CG, AT, and AC DNA Steps and in the NMR Geometry of the 5‘-d(GCGAAGC)-3‘ Hairpin: Complete Basis Set Calculations at the MP2 and CCSD(T) Levels. *J. Phys. Chem. A* **2005**, *109*, 1131–1136. https://doi.org/10.1021/jp046738a.

(243) Kruse, H.; Banáš, P.; Šponer, J. Investigations of Stacked DNA Base-Pair Steps: Highly Accurate Stacking Interaction Energies, Energy Decomposition, and Many-Body Stacking Effects. *J. Chem. Theory Comput.* **2019**, *15*, 95–115. https://doi.org/10.1021/acs.jctc.8b00643.

(244) Friedman, R. A.; Honig, B. A Free Energy Analysis of Nucleic Acid Base Stacking in Aqueous Solution. *Biophys. J.* **1995**, *69*, 1528–1535. https://doi.org/10.1016/s0006-3495(95)80023-8.

(245) McDonald, A. R.; Denning, E. J.; MacKerell, A. D. Impact of Geometry Optimization on Base–Base Stacking Interaction Energies in the Canonical A- and B-Forms of DNA. *J. Phys. Chem. A* **2013**, *117*, 1560–1568. https://doi.org/10.1021/jp308364d.

(246) Poner, J.; Florián, J.; Ng, H.-L.; Poner, J. E.; Packová, N. Local Conformational Variations Observed in B-DNA Crystals Do Not Improve Base Stacking: Computational Analysis of Base Stacking in a d(CATGGGCCCATG)2 B↔A Intermediate Crystal Structure. *Nucleic Acids Res.* **2000**, *28*, 4893–4902. https://doi.org/10.1093/nar/28.24.4893.

(247) Auffinger, P.; D’Ascenzo, L.; Ennifar, E. Sodium and Potassium Interactions with Nucleic Acids. In *The Alkali Metal Ions: Their Role for Life*; Sigel, A., Sigel, H., Sigel, R. K. O., Eds.; Metal Ions in Life Sciences; Springer Cham: Heidelberg, 2016; Vol. 16, p.167–201. https://doi.org/10.1007/978-3-319-21756-7_6.

(248) Freund, J.; Kalbitzer, H. Physiological Buffers for NMR Spectroscopy. *J. Biomol. NMR* **1995**, *5*, 321–322. https://doi.org/10.1007/bf00211760.

(249) Lipfert, J.; Doniach, S.; Das, R.; Herschlag, D. Understanding Nucleic Acid–Ion Interactions. *Annu. Rev. Biochem.* **2014**, *83*, 813–841. https://doi.org/10.1146/annurev-biochem-060409-092720.

(250) Sharp, K. A.; Honig, B. Salt Effects on Nucleic Acids. *Curr. Opin. Struct. Biol.* **1995**, *5*, 323–328. https://doi.org/10.1016/0959-440x(95)80093-x.

(251) Anderson, C. F.; Record, M. T. Salt-Nucleic Acid Interactions. *Annu. Rev. Phys. Chem.* **1995**, *46*, 657–700. https://doi.org/10.1146/annurev.pc.46.100195.003301.

(252) Record, M. T.; Anderson, C. F.; Lohman, T. M. Thermodynamic Analysis of Ion Effects on the Binding and Conformational Equilibria of Proteins and Nucleic Acids: The Roles of Ion Association or Release, Screening, and Ion Effects on Water Activity. *Q. Rev. Biophys.* **1978**, *11*, 103–178. https://doi.org/10.1017/s003358350000202x.

(253) Bowman, J. C.; Lenz, T. K.; Hud, N. V.; Williams, L. D. Cations in Charge: Magnesium Ions in RNA Folding and Catalysis. *Curr. Opin. Struct. Biol.* **2012**, *22*, 262–272. https://doi.org/10.1016/j.sbi.2012.04.006.

(254) Owczarzy, R.; Moreira, B. G.; You, Y.; Behlke, M. A.; Walder, J. A. Predicting Stability of DNA Duplexes in Solutions Containing Magnesium and Monovalent Cations. *Biochemistry* **2008**, *47*, 5336–5353. https://doi.org/10.1021/bi702363u.

(255) Buckin, V. A.; Kankiya, B. I.; Rentzeperis, D.; Marky, L. A. Mg2+ Recognizes the Sequence of DNA through Its Hydration Shell. *J. Am. Chem. Soc.* **1994**, *116*, 9423–9429. https://doi.org/10.1021/ja00100a003.

(256) Baker, E. S.; Manard, M. J.; Gidden, J.; Bowers, M. T. Structural Analysis of Metal Interactions with the Dinucleotide Duplex, DCG·dCG, Using Ion Mobility Mass Spectrometry. *J. Phys. Chem. B* **2005**, *109*, 4808–4810. https://doi.org/10.1021/jp0501190.

(257) Juan, E. C. M.; Kondo, J.; Kurihara, T.; Ito, T.; Ueno, Y.; Matsuda, A.; Takénaka, A. Crystal Structures of DNA:DNA and DNA:RNA Duplexes

Containing 5-(N-Aminohexyl)Carbamoyl-Modified Uracils Reveal the Basis for Properties as Antigene and Antisense Molecules. *Nucleic Acids Res.* **2007**, *35*, 1969–1977. https://doi.org/10.1093/nar/gkl821.

(258) Anderson, M.; Schultz, E. P.; Martick, M.; Scott, W. G. Active-Site Monovalent Cations Revealed in a 1.55-Å-Resolution Hammerhead Ribozyme Structure. *J. Mol. Biol.* **2013**, *425*, 3790–3798. https://doi.org/10.1016/j.jmb.2013.05.017.

(259) Gruenwedel, D. W.; Hsu, C. H.; Lu, D. S. The Effects of Aqueous Neutral-Salt Solutions on the Melting Temperatures of Deoxyribonucleic Acids. *Biopolymers* **1971**, *10*, 47–68. https://doi.org/10.1002/bip.360100106.

(260) Gruenwedel, D. W. Salt Effects on the Denaturation of DNA. 3. A Calorimetric Investigation of the Transition Enthalpy of Calf Thymus DNA in Na2SO4 Solutions of Varying Ionic Strength. *Biochim. Biophys. Acta* **1974**, *340*, 16–30. https://doi.org/10.1016/0005-2787(74)90170-1.

(261) Stellwagen, E.; Muse, J. M.; Stellwagen, N. C. Monovalent Cation Size and DNA Conformational Stability. *Biochemistry* **2011**, *50*, 3084–3094. https://doi.org/10.1021/bi1015524.

(262) Tomac, S.; Sarkar, M.; Ratilainen, T.; Wittung, P.; Nielsen, P. E.; Nordén, B.; Gräslund, A. Ionic Effects on the Stability and Conformation of Peptide Nucleic Acid Complexes. *J. Am. Chem. Soc.* **1996**, *118*, 5544–5552. https://doi.org/10.1021/ja960495l.

(263) Khristenko, N.; Amato, J.; Livet, S.; Pagano, B.; Randazzo, A.; Gabelica, V. Native Ion Mobility Mass Spectrometry: When Gas-Phase Ion Structures Depend on the Electrospray Charging Process. *J. Am. Soc. Mass Spectrom.* **2019**, *30*, 1069–1081. https://doi.org/10.1007/s13361-019-02152-3.

(264) Bai, Y.; Greenfeld, M.; Travers, K. J.; Chu, V. B.; Lipfert, J.; Doniach, S.; Herschlag, D. Quantitative and Comprehensive Decomposition of the Ion Atmosphere around Nucleic Acids. *J. Am. Chem. Soc.* **2007**, *129*, 14981–14988. https://doi.org/10.1021/ja075020g.

(265) Tan, Z.-J.; Chen, S.-J. Salt Contribution to RNA Tertiary Structure Folding Stability. *Biophys. J.* **2011**, *101*, 176–187. https://doi.org/10.1016/j.bpj.2011.05.050.

(266) Hamaguchi, Kozo.; Geiduschek, E. Peter. The Effect of Electrolytes on the Stability of the Deoxyribonucleate Helix. *J. Am. Chem. Soc.* **1962**, *84*, 1329–1338. https://doi.org/10.1021/ja00867a001.

(267) Pegram, L. M.; Wendorff, T.; Erdmann, R.; Shkel, I.; Bellissimo, D.; Felitsky, D. J.; Record, M. T. Why Hofmeister Effects of Many Salts Favor Protein Folding but Not DNA Helix Formation. *Proc. Natl. Acad. Sci. U. S. A.* **2010**, *107*, 7716–7721. https://doi.org/10.1073/pnas.0913376107.

(268) Gruenwedel, D. W.; Hsu, C. H. Salt Effects on the Denaturation of DNA. *Biopolymers* **1969**, *7*, 557–570. https://doi.org/10.1002/bip.1969.360070412.

(269) Hilbers, C.; Haasnoot, C.; Debruin, S.; Joordens, J.; Vandermarel, G.; Vanboom, J. Hairpin Formation in Synthetic Oligonucleotides. *Biochimie* **1985**, *67*, 685–695. https://doi.org/10.1016/S0300-9084(85)80156-5.

(270) Najaf-Zadeh, R.; Wu, J. Q.; Macgregor, R. B. Effect of Cations on the Volume of the Helix-Coil Transition of Poly[d(A-T)]. *Biochim. Biophys. Acta BBA - Gene Struct. Expr.* **1995**, *1262*, 52–58. https://doi.org/10.1016/0167-4781(95)00047-k.

(271) Hud, N. V.; Sklenář, V.; Feigon, J. Localization of Ammonium Ions in the Minor Groove of DNA Duplexes in Solution and the Origin of DNA A-Tract Bending. *J. Mol. Biol.* **1999**, *286*, 651–660. https://doi.org/10.1006/jmbi.1998.2513.

(272) Stellwagen, N. C.; Stellwagen, E. DNA Thermal Stability Depends on Solvent Viscosity. *J. Phys. Chem. B* **2019**, *123*, 3649–3657. https://doi.org/10.1021/acs.jpcb.9b01217.

(273) Beebe, J. A.; Kurz, J. C.; Fierke, C. A. Magnesium Ions Are Required by Bacillus Subtilis Ribonuclease P RNA for Both Binding and Cleaving Precursor TRNA Asp. *Biochemistry* **1996**, *35*, 10493–10505. https://doi.org/10.1021/bi960870m.

(274) Dai, L.; Mu, Y.; Nordenskiöld, L.; Lapp, A.; van der Maarel, J. R. C. Charge Structure and Counterion Distribution in Hexagonal DNA Liquid Crystal. *Biophys. J.* **2007**, *92*, 947–958. https://doi.org/10.1529/biophysj.106.095745.

(275) Singleton, S. F.; Dervan, P. B. Equilibrium Association Constants for Oligonucleotide-Directed Triple Helix Formation at Single DNA Sites: Linkage to Cation Valence and Concentration. *Biochemistry* **1993**, *32*, 13171–13179. https://doi.org/10.1021/bi00211a028.

(276) Rougee, M.; Faucon, B.; Mergny, J. L.; Barcelo, F.; Giovannangeli, C.; Garestier, T.; Helene, C. Kinetics and Thermodynamics of Triple-Helix Formation: Effects of Ionic Strength and Mismatched. *Biochemistry* **1992**, *31*, 9269–9278. https://doi.org/10.1021/bi00153a021.

(277) Wu, P.; Kawamoto, Y.; Hara, H.; Sugimoto, N. Effect of Divalent Cations and Cytosine Protonation on Thermodynamic Properties of Intermolecular DNA Double and Triple Helices. *J. Inorg. Biochem.* **2002**, *91*, 277–285. https://doi.org/10.1016/s0162-0134(02)00444-0.

(278) Sugimoto, N.; Wu, P.; Hara, H.; Kawamoto, Y. PH and Cation Effects on the Properties of Parallel Pyrimidine Motif DNA Triplexes. *Biochemistry* **2001**, *40*, 9396–9405. https://doi.org/10.1021/bi010666l.

(279) Plum, G. E.; Park, Y. W.; Singleton, S. F.; Dervan, P. B.; Breslauer, K. J. Thermodynamic Characterization of the Stability and the

Melting Behavior of a DNA Triplex: A Spectroscopic and Calorimetric Study. *Proc. Natl. Acad. Sci.* **1990**, *87*, 9436–9440. https://doi.org/10.1073/pnas.87.23.9436.

(280) Lavelle, L.; Fresco, J. R. Stabilization of Nucleic Acid Triplexes by High Concentrations of Sodium and Ammonium Salts Follows the Hofmeister Series. *Biophys. Chem.* **2003**, *105*, 681–699. https://doi.org/10.1016/S0301-4622(03)00097-8.

(281) Hampel, K. J.; Crosson, P.; Lee, J. S. Polyamines Favor DNA Triplex Formation at Neutral PH. *Biochemistry* **1991**, *30*, 4455–4459. https://doi.org/10.1021/bi00232a012.

(282) Denisov, V. P.; Halle, B. Sequence-Specific Binding of Counterions to B-DNA. *Proc. Natl. Acad. Sci.* **2000**, *97*, 629–633. https://doi.org/10.1073/pnas.97.2.629.

(283) Ennifar, E.; Walter, P.; Ehresmann, B.; Ehresmann, C.; Dumas, P. Crystal Structures of Coaxially Stacked Kissing Complexes of the HIV-1 RNA Dimerization Initiation Site. *Nat. Struct. Biol.* **2001**, *8*, 1064–1068. https://doi.org/10.1038/nsb727.

(284) Leonarski, F.; D'Ascenzo, L.; Auffinger, P. Nucleobase Carbonyl Groups Are Poor Mg2+ Inner-Sphere Binders but Excellent Monovalent Ion Binders – A Critical PDB Survey. *RNA* **2018**, *25*, 173–192. https://doi.org/10.1261/rna.068437.118.

(285) Geng, Y.; Liu, C.; Zhou, B.; Cai, Q.; Miao, H.; Shi, X.; Xu, N.; You, Y.; Fung, C. P.; Din, R. U.; et al. The Crystal Structure of an Antiparallel Chair-Type G-Quadruplex Formed by Bromo-Substituted Human Telomeric DNA. *Nucleic Acids Res.* **2019**, *47*, 5395–5404. https://doi.org/10.1093/nar/gkz221.

(286) Pinnavaia, T. J.; Marshall, C. L.; Mettler, C. M.; Fisk, C. L.; Miles, H. T.; Becker, E. D. Alkali Metal Ion Specificity in the Solution Ordering of a Nucleotide, 5'-Guanosine Monophosphate. *J. Am. Chem. Soc.* **1978**, *100*, 3625–3627. https://doi.org/10.1021/ja00479a070.

(287) Seo, J.; Hong, E. S.; Yoon, H.-J.; Shin, S. K. Specific and Nonspecific Bindings of Alkaline-Earth Metal Ions to Guanine-Quadruplex Thrombin-Binding Aptamer DNA. *Int. J. Mass Spectrom.* **2012**, *330–332*, 262–270. https://doi.org/10.1016/j.ijms.2012.09.002.

(288) Venczel, E. A.; Sen, D. Parallel and Antiparallel G-DNA Structures from a Complex Telomeric Sequence. *Biochemistry* **1993**, *32*, 6220–6228. https://doi.org/10.1021/bi00075a015.

(289) Kankia, B. I.; Marky, L. A. Folding of the Thrombin Aptamer into a G-Quadruplex with Sr(2+): Stability, Heat, and Hydration. *J. Am. Chem. Soc.* **2001**, *123*, 10799–10804. https://doi.org/10.1021/ja010008o.

(290) Włodarczyk, A.; Grzybowski, P.; Patkowski, A.; Dobek, A. Effect of Ions on the Polymorphism, Effective Charge, and Stability of Human Telomeric DNA. Photon Correlation Spectroscopy and Circular Dichroism Studies. *J. Phys. Chem. B* **2005**, *109*, 3594–3605. https://doi.org/10.1021/jp045274d.

(291) Hardin, C. C.; Watson, T.; Corregan, M.; Bailey, C. Cation-Dependent Transition between the Quadruplex and Watson-Crick Hairpin Forms of d(CGCG3GCG). *Biochemistry* **1992**, *31*, 833–841. https://doi.org/10.1021/bi00118a028.

(292) Sidey, V. On the Effective Ionic Radii for Ammonium. *Acta Crystallogr. Sect. B Struct. Sci. Cryst. Eng. Mater.* **2016**, *72*, 626–633. https://doi.org/10.1107/S2052520616008064.

(293) Shannon, R. D. Revised Effective Ionic Radii and Systematic Studies of Interatomic Distances in Halides and Chalcogenides. *Acta Crystallogr. Sect. A* **1976**, *32*, 751–767. https://doi.org/10.1107/s0567739476001551.

(294) Phan, A. T. Human Telomeric G-Quadruplex: Structures of DNA and RNA Sequences: Human Telomeric G-Quadruplex Structures. *FEBS J.* **2010**, *277*, 1107–1117. https://doi.org/10.1111/j.1742-4658.2009.07464.x.

(295) Parkinson, G. N.; Lee, M. P. H.; Neidle, S. Crystal Structure of Parallel Quadruplexes from Human Telomeric DNA. *Nature* **2002**, *417*, 876–880. https://doi.org/10.1038/nature755.

(296) Wang, Y.; Patel, D. J. Solution Structure of the Human Telomeric Repeat d[AG3(T2AG3)3] G-Tetraplex. *Struct. Lond. Engl. 1993* **1993**, *1*, 263–282. https://doi.org/10.1016/0969-2126(93)90015-9.

(297) Luu, K. N.; Phan, A. T.; Kuryavyi, V.; Lacroix, L.; Patel, D. J. Structure of the Human Telomere in K+ Solution: An Intramolecular (3 + 1) G-Quadruplex Scaffold. *J. Am. Chem. Soc.* **2006**, *128*, 9963–9970. https://doi.org/10.1021/ja062791w.

(298) Hud, N. V.; Schultze, P.; Sklenár, V.; Feigon, J. Binding Sites and Dynamics of Ammonium Ions in a Telomere Repeat DNA Quadruplex. *J. Mol. Biol.* **1999**, *285*, 233–243. https://doi.org/10.1006/jmbi.1998.2327.

(299) Snoussi, K.; Halle, B. Internal Sodium Ions and Water Molecules in Guanine Quadruplexes: Magnetic Relaxation Dispersion Studies of [d(G3T4G3)]2 and [d(G4T4G4)]2. *Biochemistry* **2008**, *47*, 12219–12229. https://doi.org/10.1021/bi801657s.

(300) Balthasart, F.; Plavec, J.; Gabelica, V. Ammonium Ion Binding to DNA G-Quadruplexes: Do Electrospray Mass Spectra Faithfully Reflect the Solution-Phase Species? *J. Am. Soc. Mass Spectrom.* **2013**, *24*, 1–8. https://doi.org/10.1007/s13361-012-0499-3.

(301) Sket, P.; Crnugelj, M.; Plavec, J. Identification of Mixed Di-Cation Forms of G-Quadruplex in Solution. *Nucleic Acids Res.* **2005**, *33*, 3691–3697. https://doi.org/10.1093/nar/gki690.

(302) Rohs, R.; West, S. M.; Sosinsky, A.; Liu, P.; Mann, R. S.; Honig, B. The Role of DNA Shape in Protein-DNA Recognition. *Nature* **2009**, *461*, 1248–1253. https://doi.org/10.1038/nature08473.

(303) Tyagi, R.; Mathews, D. H. Predicting Helical Coaxial Stacking in RNA Multibranch Loops. *RNA* **2007**, *13*, 939–951. https://doi.org/10.1261/rna.305307.

(304) Zhuang, X.; Kim, H.; Pereira, M. J. B.; Babcock, H. P.; Walter, N. G.; Chu, S. Correlating Structural Dynamics and Function in Single Ribozyme Molecules. *Science* **2002**, *296*, 1473–1476. https://doi.org/10.1126/science.1069013.

(305) Duckett, D. R.; Lilley, D. M. The Three-Way DNA Junction Is a Y-Shaped Molecule in Which There Is No Helix-Helix Stacking. *EMBO J.* **1990**, *9*, 1659–1664. https://doi.org/10.1002/j.1460-2075.1990.tb08286.x.

(306) Guo, Q.; Lu, M.; Churchill, M. E. A.; Tullius, T. D.; Kallenbach, N. R. Asymmetric Structure of a Three-Arm DNA Junction. *Biochemistry* **1990**, *29*, 10927–10934. https://doi.org/10.1021/bi00501a010.

(307) Brázda, V.; Laister, R. C.; Jagelská, E. B.; Arrowsmith, C. Cruciform Structures Are a Common DNA Feature Important for Regulating Biological Processes. *BMC Mol. Biol.* **2011**, *12*, 33. https://doi.org/10.1186/1471-2199-12-33.

(308) Bikard, D.; Loot, C.; Baharoglu, Z.; Mazel, D. Folded DNA in Action: Hairpin Formation and Biological Functions in Prokaryotes. *Microbiol. Mol. Biol. Rev.* **2010**, *74*, 570–588. https://doi.org/10.1128/mmbr.00026-10.

(309) Gregorian, R. S.; Crothers, D. M. Determinants of RNA Hairpin Loop-Loop Complex Stability. *J. Mol. Biol.* **1995**, *248*, 968–984. https://doi.org/10.1006/jmbi.1995.0275.

(310) Deiman, B. A. L. M.; Pleij, C. W. A. Pseudoknots: A Vital Feature in Viral RNA. *Semin. Virol.* **1997**, *8*, 166–175. https://doi.org/10.1006/smvy.1997.0119.

(311) Brierley, I.; Pennell, S.; Gilbert, R. J. C. Viral RNA Pseudoknots: Versatile Motifs in Gene Expression and Replication. *Nat. Rev. Microbiol.* **2007**, *5*, 598–610. https://doi.org/10.1038/nrmicro1704.

(312) Neidle, S. Principles of Small Molecule-DNA Recognition. In *Principles of Nucleic Acid Structure*; Academic Press: Amsterdam, 2008; p.132–203. https://doi.org/10.1016/B978-012369507-9.50006-6.

(313) Pratviel, G. Porphyrins in Complex with DNA: Modes of Interaction and Oxidation Reactions. *Coord. Chem. Rev.* **2016**, *308*, 460–477. https://doi.org/10.1016/j.ccr.2015.07.003.

(314) Strekowski, L.; Wilson, B. Noncovalent Interactions with DNA: An Overview. *Mutat. Res.* **2007**, *623*, 3–13. https://doi.org/10.1016/j.mrfmmm.2007.03.008.

(315) Brodbelt, J. S.; Xu, Z. Ligand Binding to Nucleic Acids. In *Nucleic Acids in the Gas Phase*; Gabelica, V., Ed.; Physical Chemistry in Action; Springer: Berlin, Heidelberg, 2014; p.225–252. https://doi.org/10.1007/978-3-642-54842-0_9.

(316) Largy, E.; Hamon, F.; Rosu, F.; Gabelica, V.; De Pauw, E.; Guédin, A.; Mergny, J.-L.; Teulade-Fichou, M.-P. Tridentate N-Donor Palladium(II) Complexes as Efficient Coordinating Quadruplex DNA Binders. *Chem. - Eur. J.* **2011**, *17*, 13274–13283. https://doi.org/10.1002/chem.201102300.

(317) David-Cordonnier, M.-H.; Laine, W.; Lansiaux, A.; Rosu, F.; Colson, P.; De Pauw, E.; Michel, S.; Tillequin, F.; Koch, M.; Hickman, J. A.; et al. Covalent Binding of Antitumor Benzoacronycines to Double-Stranded DNA Induces Helix Opening and the Formation of Single-Stranded DNA: Unique Consequences of a Novel DNA-Bonding Mechanism. *Mol. Cancer Ther.* **2005**, *4*, 71–80.

(318) Chaires, J. B. Energetics of Drug-DNA Interactions. *Biopolymers* **1997**, *44*, 201–215. https://doi.org/10.1002/(SICI)1097-0282(1997)44:3<201::AID-BIP2>3.0.CO;2-Z.

(319) Liu, H.-K.; Sadler, P. J. Metal Complexes as DNA Intercalators. *Acc. Chem. Res.* **2011**, *44*, 349–359. https://doi.org/10.1021/ar100140e.

(320) Neidle, S.; Abraham, Z. Structural and Sequence-Dependent Aspects of Drug Intercalation into Nucleic Acids. *CRC Crit. Rev. Biochem.* **1984**, *17*, 73–121. https://doi.org/10.3109/10409238409110270.

(321) Manning, G. S. The Molecular Theory of Polyelectrolyte Solutions with Applications to the Electrostatic Properties of Polynucleotides. *Q. Rev. Biophys.* **1978**, *11*, 179–246. https://doi.org/10.1017/s0033583500002031.

(322) Li, S.; Cooper, V. R.; Thonhauser, T.; Lundqvist, B. I.; Langreth, D. C. Stacking Interactions and DNA Intercalation. *J. Phys. Chem. B* **2009**, *113*, 11166–11172. https://doi.org/10.1021/jp905765c.

(323) Rao, S. N.; Kollman, P. A. Molecular Mechanical Simulations on Double Intercalation of 9-Amino Acridine into d(CGCGCGC) X d(GCGCGCG): Analysis of the Physical Basis for the Neighbor-Exclusion Principle. *Proc. Natl. Acad. Sci. U. S. A.* **1987**, *84*, 5735–5739. https://doi.org/10.1073/pnas.84.16.5735.

(324) McGhee, J. D.; von Hippel, P. H. Theoretical Aspects of DNA-Protein Interactions: Co-Operative and Non-Co-Operative Binding of Large Ligands to a One-Dimensional Homogeneous Lattice. *J. Mol. Biol.* **1974**, *86*, 469–489. https://doi.org/10.1016/0022-2836(74)90031-x.

(325) Schellman, J. A. Cooperative Multisite Binding to DNA. *Isr. J. Chem.* **1974**, *12*, 219–238. https://doi.org/10.1002/ijch.197400021.

(326) Horowitz, E. D.; Lilavivat, S.; Holladay, B. W.; Germann, M. W.; Hud, N. V. Solution Structure and Thermodynamics of 2',5' RNA Intercalation. *J. Am. Chem. Soc.* **2009**, *131*, 5831–5838. https://doi.org/10.1021/ja810068e.

(327) Canals, A.; Purciolas, M.; Aymamí, J.; Coll, M. The Anticancer Agent Ellipticine Unwinds DNA by Intercalative Binding in an Orientation Parallel to Base Pairs. *Acta Crystallogr. D Biol. Crystallogr.* **2005**, *61*, 1009–1012. https://doi.org/10.1107/S0907444905015404.

(328) Howerton, S. B.; Nagpal, A.; Williams, L. D. Surprising Roles of Electrostatic Interactions in DNA-Ligand Complexes. *Biopolymers* **2003**, *69*, 87–99. https://doi.org/10.1002/bip.10319.

(329) Adams, A.; Guss, J. M.; Collyer, C. A.; Denny, W. A.; Wakelin, L. P. Crystal Structure of the Topoisomerase II Poison 9-Amino-[N-(2-Dimethylamino)Ethyl]Acridine-4-Carboxamide Bound to the DNA Hexanucleotide d(CGTACG)2. *Biochemistry* **1999**, *38*, 9221–9233. https://doi.org/10.1021/bi990352m.

(330) Gao, Q.; Williams, L. D.; Egli, M.; Rabinovich, D.; Chen, S. L.; Quigley, G. J.; Rich, A. Drug-Induced DNA Repair: X-Ray Structure of a DNA-Ditercalinium Complex. *Proc. Natl. Acad. Sci. U. S. A.* **1991**, *88*, 2422–2426. https://doi.org/10.1073/pnas.88.6.2422.

(331) Cuesta-Seijo, J. A.; Sheldrick, G. M. Structures of Complexes between Echinomycin and Duplex DNA. *Acta Crystallogr. D Biol. Crystallogr.* **2005**, *61*, 442–448. https://doi.org/10.1107/S090744490500137X.

(332) Niyazi, H.; Hall, J. P.; O'Sullivan, K.; Winter, G.; Sorensen, T.; Kelly, J. M.; Cardin, C. J. Crystal Structures of Λ-$[Ru(Phen)_2dppz]^{2+}$ with Oligonucleotides Containing TA/TA and AT/AT Steps Show Two Intercalation Modes. *Nat. Chem.* **2012**, *4*, 621–628. https://doi.org/10.1038/nchem.1397.

(333) Bailly, C.; OhUigin, C.; Rivalle, C.; Bisagni, E.; Hénichart, J. P.; Waring, M. J. Sequence-Selective Binding of an Ellipticine Derivative to DNA. *Nucleic Acids Res.* **1990**, *18*, 6283–6291. https://doi.org/10.1093/nar/18.21.6283.

(334) Hou, M.-H.; Robinson, H.; Gao, Y.-G.; Wang, A. H.-J. Crystal Structure of Actinomycin D Bound to the CTG Triplet Repeat Sequences Linked to Neurological Diseases. *Nucleic Acids Res.* **2002**, *30*, 4910–4917. https://doi.org/10.1093/nar/gkf619.

(335) Adams, A.; Guss, J. M.; Denny, W. A.; Wakelin, L. P. G. Crystal Structure of 9-Amino-N-[2-(4-Morpholinyl)Ethyl]-4-Acridinecarboxamide Bound to d(CGTACG)2: Implications for Structure-Activity Relationships of Acridinecarboxamide Topoisomerase Poisons. *Nucleic Acids Res.* **2002**, *30*, 719–725. https://doi.org/10.1093/nar/30.3.719.

(336) Todd, A. K.; Adams, A.; Thorpe, J. H.; Denny, W. A.; Wakelin, L. P.; Cardin, C. J. Major Groove Binding and "DNA-Induced" Fit in the Intercalation of a Derivative of the Mixed Topoisomerase I/II Poison N-(2-(Dimethylamino)Ethyl)Acridine-4-Carboxamide (DACA) into DNA: X-Ray Structure Complexed to d(CG(5-BrU)ACG)2 at 1.3-A Resolution. *J. Med. Chem.* **1999**, *42*, 536–540. https://doi.org/10.1021/jm980479u.

(337) Searle, M. S.; Maynard, A. J.; Williams, H. E. DNA Recognition by the Anthracycline Antibiotic Respinomycin D: NMR Structure of the Intercalation Complex with d(AGACGTCT)2. *Org. Biomol. Chem.* **2003**, *1*, 60–66. https://doi.org/10.1039/b208622k.

(338) Van Dyke, M. M.; Dervan, P. B. Echinomycin Binding Sites on DNA. *Science* **1984**, *225*, 1122–1127. https://doi.org/10.1126/science.6089341.

(339) Gao, X. L.; Patel, D. J. Antitumour Drug-DNA Interactions: NMR Studies of Echinomycin and Chromomycin Complexes. *Q. Rev. Biophys.* **1989**, *22*, 93–138. https://doi.org/10.1017/s0033583500003814.

(340) Wakelin, S. P.; Waring, M. J. The Binding of Echinomycin to Deoxyribonucleic Acid. *Biochem. J.* **1976**, *157*, 721–740. https://doi.org/10.1042/bj1570721.

(341) Kellett, A.; Molphy, Z.; Slator, C.; McKee, V.; Farrell, N. P. Molecular Methods for Assessment of Non-Covalent Metallodrug-DNA Interactions. *Chem. Soc. Rev.* **2019**, *48*, 971–988. https://doi.org/10.1039/c8cs00157j.

(342) Pages, B. J.; Ang, D. L.; Wright, E. P.; Aldrich-Wright, J. R. Metal Complex Interactions with DNA. *Dalton Trans.* **2015**, *44*, 3505–3526. https://doi.org/10.1039/c4dt02700k.

(343) Lippard, S. J.; Bond, P. J.; Wu, K. C.; Bauer, W. R. Stereochemical Requirements for Intercalation of Platinum Complexes into Double-Stranded DNA's. *Science* **1976**, *194*, 726–728. https://doi.org/10.1126/science.982037.

(344) Howe-Grant, M.; Lippard, S. J. Binding of Platinum(II) Intercalation Reagents to Deoxyribnonucleic Acid. Dependence on Base-Pair Composition, Nature of the Intercalator, and Ionic Strength. *Biochemistry* **1979**, *18*, 5762–5769. https://doi.org/10.1021/bi00593a003.

(345) Zeglis, B. M.; Pierre, V. C.; Barton, J. K. Metallo-Intercalators and Metallo-Insertors. *Chem. Commun.* **2007**, No. 44, 4565–4579. https://doi.org/10.1039/b710949k.

(346) Ishikawa, Y.; Yamakawa, N.; Uno, T. Binding of Cationic Bis-Porphyrins Linked with p- or m-Xylylenediamine and Their Zinc(II) Complexes to Duplex DNA. *Molecules* **2008**, *13*, 3117–3128. https://doi.org/10.3390/molecules13123117.

(347) Barkhudaryan, V. G.; Ananyan, G. V.; Dalyan, Y. B.; Haroutiunian, S. G. Development of Viscometric Methods for Studying the Interaction of Various Porphyrins with DNA. Part I: *Meso* -Tetra-(4N-Hydroxyethylpyridyl) Porphyrin and Its Ni -, Cu -, Co - and Zn - Containing Derivatives. *J. Porphyr. Phthalocyanines* **2014**, *18*, 594–599. https://doi.org/10.1142/S1088424614500357.

(348) Oguey, C.; Foloppe, N.; Hartmann, B. Understanding the Sequence-Dependence of DNA Groove Dimensions: Implications for DNA Interactions. *PloS One* **2010**, *5*, e15931. https://doi.org/10.1371/journal.pone.0015931.

(349) Nanjunda, R.; Wilson, W. D. Binding to the DNA Minor Groove by Heterocyclic Dications: From AT-Specific Monomers to GC Recognition with Dimers. *Curr. Protoc. Nucleic Acid Chem.* **2012**, *51*, 8.8.1-8.8.20. https://doi.org/10.1002/0471142700.nc0808s51.

(350) Kopka, M. L.; Yoon, C.; Goodsell, D.; Pjura, P.; Dickerson, R. E. Binding of an Antitumor Drug to DNA, Netropsin and C-G-C-G-A-A-T-T-BrC-G-C-G. *J. Mol. Biol.* **1985**, *183*, 553–563. https://doi.org/10.1016/0022-2836(85)90171-8.

(351) Haq, I.; Ladbury, J. E.; Chowdhry, B. Z.; Jenkins, T. C.; Chaires, J. B. Specific Binding of Hoechst 33258 to the d(CGCAAATTTGCG)2 Duplex: Calorimetric and Spectroscopic Studies. *J. Mol. Biol.* **1997**, *271*, 244–257. https://doi.org/10.1006/jmbi.1997.1170.

(352) Subramanian, P. S.; Ravishanker, G.; Beveridge, D. L. Theoretical Considerations on the "Spine of Hydration" in the Minor Groove of d(CGCGAATTCGCG).d(GCGCTTAAGCGC): Monte Carlo Computer Simulation. *Proc. Natl. Acad. Sci. U. S. A.* **1988**, *85*, 1836–1840. https://doi.org/10.1073/pnas.85.6.1836.

(353) Rentzeperis, D.; Marky, L. A.; Dwyer, T. J.; Geierstanger, B. H.; Pelton, J. G.; Wemmer, D. E. Interaction of Minor Groove Ligands to an AAATT/AATTT Site: Correlation of Thermodynamic Characterization and Solution Structure. *Biochemistry* **1995**, *34*, 2937–2945. https://doi.org/10.1021/bi00009a025.

(354) Dervan, P. B. Design of Sequence-Specific DNA-Binding Molecules. *Science* **1986**, *232*, 464–471. https://doi.org/10.1126/science.2421408.

(355) Bailly, C.; Waring, M. J. Transferring the Purine 2-Amino Group from Guanines to Adenines in DNA Changes the Sequence-Specific Binding of Antibiotics. *Nucleic Acids Res.* **1995**, *23*, 885–892. https://doi.org/10.1093/nar/23.6.885.

(356) Geierstanger, B. H.; Wemmer, D. E. Complexes of the Minor Groove of DNA. *Annu. Rev. Biophys. Biomol. Struct.* **1995**, *24*, 463–493. https://doi.org/10.1146/annurev.bb.24.060195.002335.

(357) Rahimian, M.; Kumar, A.; Say, M.; Bakunov, S. A.; Boykin, D. W.; Tidwell, R. R.; Wilson, W. D. Minor Groove Binding Compounds That Jump a Gc Base Pair and Bind to Adjacent AT Base Pair Sites. *Biochemistry* **2009**, *48*, 1573–1583. https://doi.org/10.1021/bi801944g.

(358) Kielkopf, C. L.; Baird, E. E.; Dervan, P. B.; Rees, D. C. Structural Basis for G.C Recognition in the DNA Minor Groove. *Nat. Struct. Biol.* **1998**, *5*, 104–109. https://doi.org/10.1038/nsb0298-104.

(359) Kelly, J. M.; Tossi, A. B.; McConnell, D. J.; OhUigin, C. A Study of the Interactions of Some Polypyridylruthenium (II) Complexes with DNA Using Fluorescence Spectroscopy, Topoisomerisation and Thermal Denaturation. *Nucleic Acids Res.* **1985**, *13*, 6017–6034. https://doi.org/10.1093/nar/13.17.6017.

(360) Molphy, Z.; Montagner, D.; Bhat, S. S.; Slator, C.; Long, C.; Erxleben, A.; Kellett, A. A Phosphate-Targeted Dinuclear Cu(II) Complex Combining Major Groove Binding and Oxidative DNA Cleavage. *Nucleic Acids Res.* **2018**, *46*, 9918–9931. https://doi.org/10.1093/nar/gky806.

(361) Hannon, M. J.; Moreno, V.; Prieto, M. J.; Moldrheim, E.; Sletten, E.; Meistermann, I.; Isaac, C. J.; Sanders, K. J.; Rodger, A. Intramolecular DNA Coiling Mediated by a Metallo-Supramolecular Cylinder. *Angew. Chem. Int. Ed Engl.* **2001**, *40*, 879–884. https://doi.org/10.1002/1521-3773(20010302)40:5<879::AID-ANIE879>3.0.CO;2-X.

(362) Grokhovsky, S. L.; Surovaya, A. N.; Burckhardt, G.; Pismensky, V. F.; Chernov, B. K.; Zimmer, C.; Gursky, G. V. DNA Sequence Recognition by Bis-Linked Netropsin and Distamycin Derivatives. *FEBS Lett.* **1998**, *439*, 346–350. https://doi.org/10.1016/s0014-5793(98)01379-9.

(363) Pindur, U.; Jansen, M.; Lemster, T. Advances in DNA-Ligands with Groove Binding, Intercalating and/or Alkylating Activity: Chemistry, DNA-Binding and Biology. *Curr. Med. Chem.* **2005**, *12*, 2805–2847. https://doi.org/10.2174/092986705774454698.

(364) Waring, M. J.; Bailly, C. DNA Recognition by Intercalators and Hybrid Molecules. *J. Mol. Recognit.* **1994**, *7*, 109–122. https://doi.org/10.1002/jmr.300070208.

(365) Bourdouxhe-Housiaux, C.; Colson, P.; Houssier, C.; Waring, M. J.; Bailly, C. Interaction of a DNA-Threading Netropsin-Amsacrine Combilexin with DNA and Chromatin. *Biochemistry* **1996**, *35*, 4251–4264. https://doi.org/10.1021/bi9528098.

(366) Kim, S. K.; Nordén, B. Methyl Green. A DNA Major-Groove Binding Drug. *FEBS Lett.* **1993**, *315*, 61–64. https://doi.org/10.1016/0014-5793(93)81133-k.

(367) Hamilton, P. L.; Arya, D. P. Natural Product DNA Major Groove Binders. *Nat. Prod. Rep.* **2012**, *29*, 134–143. https://doi.org/10.1039/c1np00054c.

(368) Robinson, H.; Wang, A. H. Neomycin, Spermine and Hexaamminecobalt (III) Share Common Structural Motifs in Converting B- to A-DNA. *Nucleic Acids Res.* **1996**, *24*, 676–682. https://doi.org/10.1093/nar/24.4.676.

(369) Etheve, L.; Martin, J.; Lavery, R. Decomposing Protein-DNA Binding and Recognition Using Simplified Protein Models. *Nucleic Acids Res.* **2017**, *45*, 10270–10283. https://doi.org/10.1093/nar/gkx627.

(370) Rohs, R.; Jin, X.; West, S. M.; Joshi, R.; Honig, B.; Mann, R. S. Origins of Specificity in Protein-DNA Recognition. *Annu. Rev. Biochem.* **2010**, *79*, 233–269. https://doi.org/10.1146/annurev-biochem-060408-091030.

(371) Seeman, N. C.; Rosenberg, J. M.; Rich, A. Sequence-Specific Recognition of Double Helical Nucleic Acids by Proteins. *Proc. Natl. Acad. Sci. U. S. A.* **1976**, *73*, 804–808. https://doi.org/10.1073/pnas.73.3.804.

(372) Patikoglou, G. A.; Kim, J. L.; Sun, L.; Yang, S. H.; Kodadek, T.; Burley, S. K. TATA Element Recognition by the TATA Box-Binding Protein Has Been Conserved throughout Evolution. *Genes Dev.* **1999**, *13*, 3217–3230. https://doi.org/10.1101/gad.13.24.3217.

(373) Paillard, G.; Lavery, R. Analyzing Protein-DNA Recognition Mechanisms. *Struct. Lond. Engl. 1993* **2004**, *12*, 113–122. https://doi.org/10.1016/j.str.2003.11.022.

(374) Koudelka, G. B.; Carlson, P. DNA Twisting and the Effects of Non-Contacted Bases on Affinity of 434 Operator for 434 Repressor. *Nature* **1992**, *355*, 89–91. https://doi.org/10.1038/355089a0.

(375) Frouws, T. D.; Duda, S. C.; Richmond, T. J. X-Ray Structure of the MMTV-A Nucleosome Core. *Proc. Natl. Acad. Sci. U. S. A.* **2016**, *113*, 1214–1219. https://doi.org/10.1073/pnas.1524607113.

(376) Zhou, H.-X.; Pang, X. Electrostatic Interactions in Protein Structure, Folding, Binding, and Condensation. *Chem. Rev.* **2018**, *118*, 1691–1741. https://doi.org/10.1021/acs.chemrev.7b00305.

(377) Hanaoka, S.; Nagadoi, A.; Nishimura, Y. Comparison between TRF2 and TRF1 of Their Telomeric DNA-Bound Structures and DNA-Binding Activities. *Protein Sci. Publ. Protein Soc.* **2005**, *14*, 119–130. https://doi.org/10.1110/ps.04983705.

(378) Wilson, W. D.; Mizan, S.; Tanious, F. A.; Yao, S.; Zon, G. The Interaction of Intercalators and Groove-Binding Agents with DNA Triple-Helical Structures: The Influence of Ligand Structure, DNA Backbone Modifications and Sequence. *J. Mol. Recognit.* **1994**, *7*, 89–98. https://doi.org/10.1002/jmr.300070206.

(379) Mergny, J. L.; Collier, D.; Rougée, M.; Montenay-Garestier, T.; Hélène, C. Intercalation of Ethidium Bromide into a Triple-Stranded Oligonucleotide. *Nucleic Acids Res.* **1991**, *19*, 1521–1526. https://doi.org/10.1093/nar/19.7.1521.

(380) Pilch, D. S.; Breslauer, K. J. Ligand-Induced Formation of Nucleic Acid Triple Helices. *Proc. Natl. Acad. Sci. U. S. A.* **1994**, *91*, 9332–9336. https://doi.org/10.1073/pnas.91.20.9332.

(381) Escude, C.; Nguyen, C. H.; Mergny, J.-L.; Sun, J.-S.; Bisagni, E.; Garestier, T.; Helene, C. Selective Stabilization of DNA Triple Helixes by Benzopyridoindole Derivatives. *J. Am. Chem. Soc.* **1995**, *117*, 10212–10219. https://doi.org/10.1021/ja00146a006.

(382) Rosu, F.; Nguyen, C.-H.; De Pauw, E.; Gabelica, V. Ligand Binding Mode to Duplex and Triplex Dna Assessed by Combining Electrospray Tandem Mass Spectrometry and Molecular Modeling. *J. Am. Soc. Mass Spectrom.* **2007**, *18*, 1052–1062. https://doi.org/10.1016/j.jasms.2007.03.010.

(383) Holt, P. A.; Ragazzon, P.; Strekowski, L.; Chaires, J. B.; Trent, J. O. Discovery of Novel Triple Helical DNA Intercalators by an Integrated Virtual and Actual Screening Platform. *Nucleic Acids Res.* **2009**, *37*, 1280–1287. https://doi.org/10.1093/nar/gkn1043.

(384) Strekowski, L.; Hojjat, M.; Wolinska, E.; Parker, A. N.; Paliakov, E.; Gorecki, T.; Tanious, F. A.; Wilson, W. D. New Triple-Helix DNA Stabilizing Agents. *Bioorg. Med. Chem. Lett.* **2005**, *15*, 1097–1100. https://doi.org/10.1016/j.bmcl.2004.12.019.

(385) Bergquist, H.; Nikravesh, A.; Fernández, R. D.; Larsson, V.; Nguyen, C.-H.; Good, L.; Zain, R. Structure-Specific Recognition of Friedreich's Ataxia (GAA)n Repeats by Benzoquinoquinoxaline Derivatives. *Chembiochem* **2009**, *10*, 2629–2637. https://doi.org/10.1002/cbic.200900263.

(386) Chaires, J. B.; Ren, J.; Henary, M.; Zegrocka, O.; Bishop, G. R.; Strekowski, L. Triplex Selective 2-(2-Naphthyl)Quinoline Compounds: Origins of Affinity and New Design Principles. *J. Am. Chem. Soc.* **2003**, *125*, 7272–7283. https://doi.org/10.1021/ja034181r.

(387) Zaid, A.; Sun, J.-S.; Nguyen, C.-H.; Bisagni, E.; Garestier, T.; Grierson, D. S.; Zain, R. Triple-Helix Directed Cleavage of Double-Stranded DNA by Benzoquinoquinoxaline-1,10-Phenanthroline Conjugates. *Chembiochem* **2004**, *5*, 1550–1557. https://doi.org/10.1002/cbic.200400074.

(388) Arya, D. P. New Approaches toward Recognition of Nucleic Acid Triple Helices. *Acc. Chem. Res.* **2011**, *44*, 134–146. https://doi.org/10.1021/ar100113q.

(389) Wilson, W. D.; Tanious, F. A.; Mizan, S.; Yao, S.; Kiselyov, A. S.; Zon, G.; Strekowski, L. DNA Triple-Helix Specific Intercalators as Antigene Enhancers: Unfused Aromatic Cations. *Biochemistry* **1993**, *32*, 10614–10621. https://doi.org/10.1021/bi00091a011.

(390) Strekowski, L.; Gulevich, Y.; Baranowski, T. C.; Parker, A. N.; Kiselyov, A. S.; Lin, S. Y.; Tanious, F. A.; Wilson, W. D. Synthesis and Structure-DNA Binding Relationship Analysis of DNA Triple-Helix Specific Intercalators. *J. Med.*

Chem. **1996**, *39*, 3980–3983. https://doi.org/10.1021/jm9603734.

(391) Escudé, C.; Nguyen, C. H.; Kukreti, S.; Janin, Y.; Sun, J. S.; Bisagni, E.; Garestier, T.; Hélène, C. Rational Design of a Triple Helix-Specific Intercalating Ligand. *Proc. Natl. Acad. Sci. U. S. A.* **1998**, *95*, 3591–3596. https://doi.org/10.1073/pnas.95.7.3591.

(392) Zain, R.; Marchand, C.; Sun, J.; Nguyen, C. H.; Bisagni, E.; Garestier, T.; Hélène, C. Design of a Triple-Helix-Specific Cleaving Reagent. *Chem. Biol.* **1999**, *6*, 771–777. https://doi.org/10.1016/s1074-5521(99)80124-0.

(393) Zain, R.; Polverari, D.; Nguyen, C.-H.; Blouquit, Y.; Bisagni, E.; Garestier, T.; Grierson, D. S.; Sun, J.-S. Optimization of Triple-Helix-Directed DNA Cleavage by Benzoquinoquinoxaline-Ethylenediaminetetraacetic Acid Conjugates. *Chembiochem* **2003**, *4*, 856–862. https://doi.org/10.1002/cbic.200300621.

(394) Durand, M.; Maurizot, J. C. Distamycin A Complexation with a Nucleic Acid Triple Helix. *Biochemistry* **1996**, *35*, 9133–9139. https://doi.org/10.1021/bi960023j.

(395) Durand, M.; Thuong, N. T.; Maurizot, J. C. Interaction of Hoechst 33258 with a DNA Triple Helix. *Biochimie* **1994**, *76*, 181–186. https://doi.org/10.1016/0300-9084(94)90011-6.

(396) Park, Y. W.; Breslauer, K. J. Drug Binding to Higher Ordered DNA Structures: Netropsin Complexation with a Nucleic Acid Triple Helix. *Proc. Natl. Acad. Sci. U. S. A.* **1992**, *89*, 6653–6657. https://doi.org/10.1073/pnas.89.14.6653.

(397) Durand, M.; Thuong, N. T.; Maurizot, J. C. Binding of Netropsin to a DNA Triple Helix. *J. Biol. Chem.* **1992**, *267*, 24394–24399. https://doi.org/10.1016/S0021-9258(18)35779-X.

(398) Arya, D. P.; Coffee, R. L.; Willis, B.; Abramovitch, A. I. Aminoglycoside-Nucleic Acid Interactions: Remarkable Stabilization of DNA and RNA Triple Helices by Neomycin. *J. Am. Chem. Soc.* **2001**, *123*, 5385–5395. https://doi.org/10.1021/ja003052x.

(399) Arya, D. P.; Micovic, L.; Charles, I.; Coffee, R. L.; Willis, B.; Xue, L. Neomycin Binding to Watson-Hoogsteen (W-H) DNA Triplex Groove: A Model. *J. Am. Chem. Soc.* **2003**, *125*, 3733–3744. https://doi.org/10.1021/ja027765m.

(400) Monchaud, D.; Teulade-Fichou, M.-P. A Hitchhiker's Guide to G-Quadruplex Ligands. *Org. Biomol. Chem.* **2008**, *6*, 627–636. https://doi.org/10.1039/b714772b.

(401) Monsen, R. C.; Trent, J. O. G-Quadruplex Virtual Drug Screening: A Review. *Biochimie* **2018**, *152*, 134–148. https://doi.org/10.1016/j.biochi.2018.06.024.

(402) Zhang, S.; Wu, Y.; Zhang, W. G-Quadruplex Structures and Their Interaction Diversity with Ligands. *ChemMedChem* **2014**, *9*, 899–911. https://doi.org/10.1002/cmdc.201300566.

(403) Read, M.; Harrison, R. J.; Romagnoli, B.; Tanious, F. A.; Gowan, S. H.; Reszka, A. P.; Wilson, W. D.; Kelland, L. R.; Neidle, S. Structure-Based Design of Selective and Potent G Quadruplex-Mediated Telomerase Inhibitors. *Proc. Natl. Acad. Sci. U. S. A.* **2001**, *98*, 4844–4849. https://doi.org/10.1073/pnas.081560598.

(404) Fedoroff, O. Y.; Salazar, M.; Han, H.; Chemeris, V. V.; Kerwin, S. M.; Hurley, L. H. NMR-Based Model of a Telomerase-Inhibiting Compound Bound to G-Quadruplex DNA. *Biochemistry* **1998**, *37*, 12367–12374. https://doi.org/10.1021/bi981330n.

(405) Koirala, D.; Dhakal, S.; Ashbridge, B.; Sannohe, Y.; Rodriguez, R.; Sugiyama, H.; Balasubramanian, S.; Mao, H. A Single-Molecule Platform for Investigation of Interactions between G-Quadruplexes and Small-Molecule Ligands. *Nat. Chem.* **2011**, *3*, 782–787. https://doi.org/10.1038/nchem.1126.

(406) De Cian, A.; Delemos, E.; Mergny, J.-L.; Teulade-Fichou, M.-P.; Monchaud, D. Highly Efficient G-Quadruplex Recognition by Bisquinolinium Compounds. *J. Am. Chem. Soc.* **2007**, *129*, 1856–1857. https://doi.org/10.1021/ja067352b.

(407) Vilar, R. Nucleic Acid Quadruplexes and Metallo-Drugs. In *Metallo-Drugs: Development and Action of Anticancer Agents*; Sigel, A., Sigel, H., Freisinger, E., Sigel, R. K. O., Eds.; Metal Ions in Life Sciences; De Gruyter: Berlin, 2018; p.325–349.

(408) Georgiades, S. N.; Abd Karim, N. H.; Suntharalingam, K.; Vilar, R. Interaction of Metal Complexes with G-Quadruplex DNA. *Angew. Chem. Int. Ed Engl.* **2010**, *49*, 4020–4034. https://doi.org/10.1002/anie.200906363.

(409) Cao, Q.; Li, Y.; Freisinger, E.; Qin, P. Z.; Sigel, R. K. O.; Mao, Z.-W. G-Quadruplex DNA Targeted Metal Complexes Acting as Potential Anticancer Drugs. *Inorg. Chem. Front.* **2017**, *4*, 10–32. https://doi.org/10.1039/C6QI00300A.

(410) Liu, W.; Zhong, Y.-F.; Liu, L.-Y.; Shen, C.-T.; Zeng, W.; Wang, F.; Yang, D.; Mao, Z.-W. Solution Structures of Multiple G-Quadruplex Complexes Induced by a Platinum(II)-Based Tripod Reveal Dynamic Binding. *Nat. Commun.* **2018**, *9*, 3496. https://doi.org/10.1038/s41467-018-05810-4.

(411) Chung, W. J.; Heddi, B.; Hamon, F.; Teulade-Fichou, M.-P.; Phan, A. T. Solution Structure of a G-Quadruplex Bound to the Bisquinolinium Compound Phen-DC(3). *Angew. Chem. Int. Ed Engl.* **2014**, *53*, 999–1002. https://doi.org/10.1002/anie.201308063.

(412) Moore, M. J. B.; Schultes, C. M.; Cuesta, J.; Cuenca, F.; Gunaratnam, M.; Tanious, F. A.; Wilson, W. D.; Neidle, S. Trisubstituted

Acridines as G-Quadruplex Telomere Targeting Agents. Effects of Extensions of the 3,6- and 9-Side Chains on Quadruplex Binding, Telomerase Activity, and Cell Proliferation. *J. Med. Chem.* **2006**, *49*, 582–599. https://doi.org/10.1021/jm050555a.

(413) Zuffo, M.; Guédin, A.; Leriche, E.-D.; Doria, F.; Pirota, V.; Gabelica, V.; Mergny, J.-L.; Freccero, M. More Is Not Always Better: Finding the Right Trade-off between Affinity and Selectivity of a G-Quadruplex Ligand. *Nucleic Acids Res.* **2018**, *46*, e115. https://doi.org/10.1093/nar/gky607.

(414) Funke, A.; Weisz, K. Thermodynamic Signature of Indoloquinolines Interacting with G-Quadruplexes: Impact of Ligand Side Chain. *Biochimie* **2019**, *157*, 142–148. https://doi.org/10.1016/j.biochi.2018.11.015.

(415) Bertrand, H.; Granzhan, A.; Monchaud, D.; Saettel, N.; Guillot, R.; Clifford, S.; Guédin, A.; Mergny, J.-L.; Teulade-Fichou, M.-P. Recognition of G-Quadruplex DNA by Triangular Star-Shaped Compounds: With or without Side Chains? *Chem. - Eur. J.* **2011**, *17*, 4529–4539. https://doi.org/10.1002/chem.201002810.

(416) Rossetti, L.; Franceschin, M.; Bianco, A.; Ortaggi, G.; Savino, M. Perylene Diimides with Different Side Chains Are Selective in Inducing Different G-Quadruplex DNA Structures and in Inhibiting Telomerase. *Bioorg. Med. Chem. Lett.* **2002**, *12*, 2527–2533. https://doi.org/10.1016/s0960-894x(02)00504-8.

(417) Micheli, E.; Lombardo, C. M.; D'Ambrosio, D.; Franceschin, M.; Neidle, S.; Savino, M. Selective G-Quadruplex Ligands: The Significant Role of Side Chain Charge Density in a Series of Perylene Derivatives. *Bioorg. Med. Chem. Lett.* **2009**, *19*, 3903–3908. https://doi.org/10.1016/j.bmcl.2009.03.106.

(418) Campbell, N. H.; Parkinson, G. N.; Reszka, A. P.; Neidle, S. Structural Basis of DNA Quadruplex Recognition by an Acridine Drug. *J. Am. Chem. Soc.* **2008**, *130*, 6722–6724. https://doi.org/10.1021/ja8016973.

(419) Largy, E.; Saettel, N.; Hamon, F.; Dubruille, S.; Teulade-Fichou, M.-P. Screening of a Chemical Library by HT-G4-FID for Discovery of Selective G-Quadruplex Binders. *Curr. Pharm. Des.* **2012**, *18*, 1992–2001. https://doi.org/10.2174/138161212799958350.

(420) Bertrand, H.; Monchaud, D.; De Cian, A.; Guillot, R.; Mergny, J.-L.; Teulade-Fichou, M.-P. The Importance of Metal Geometry in the Recognition of G-Quadruplex-DNA by Metal-Terpyridine Complexes. *Org. Biomol. Chem.* **2007**, *5*, 2555–2559. https://doi.org/10.1039/b708635k.

(421) Monchaud, D.; Granzhan, A.; Saettel, N.; Guédin, A.; Mergny, J.-L.; Teulade-Fichou, M.-P. "One Ring to Bind Them All"—Part I: The Efficiency of the Macrocyclic Scaffold for G-Quadruplex DNA Recognition. *J. Nucleic Acids* **2010**, *2010*, 525862. https://doi.org/10.4061/2010/525862.

(422) Chung, W. J.; Heddi, B.; Tera, M.; Iida, K.; Nagasawa, K.; Phan, A. T. Solution Structure of an Intramolecular (3 + 1) Human Telomeric G-Quadruplex Bound to a Telomestatin Derivative. *J. Am. Chem. Soc.* **2013**, *135*, 13495–13501. https://doi.org/10.1021/ja405843r.

(423) Iida, K.; Tera, M.; Hirokawa, T.; Shin-ya, K.; Nagasawa, K. G-Quadruplex Recognition by Macrocyclic Hexaoxazole (6OTD) Dimer: Greater Selectivity than Monomer. *Chem. Commun.* **2009**, No. 42, 6481–6483. https://doi.org/10.1039/b910242f.

(424) Tera, M.; Ishizuka, H.; Takagi, M.; Suganuma, M.; Shin-ya, K.; Nagasawa, K. Macrocyclic Hexaoxazoles as Sequence- and Mode-Selective G-Quadruplex Binders. *Angew. Chem. Int. Ed.* **2008**, *47*, 5557–5560. https://doi.org/10.1002/anie.200801235.

(425) Wheelhouse, R. T.; Sun, D.; Han, H.; Han, F. X.; Hurley, L. H. Cationic Porphyrins as Telomerase Inhibitors: The Interaction of Tetra-(*N* -Methyl-4-Pyridyl)Porphine with Quadruplex DNA. *J. Am. Chem. Soc.* **1998**, *120*, 3261–3262. https://doi.org/10.1021/ja973792e.

(426) Shi, D. F.; Wheelhouse, R. T.; Sun, D.; Hurley, L. H. Quadruplex-Interactive Agents as Telomerase Inhibitors: Synthesis of Porphyrins and Structure-Activity Relationship for the Inhibition of Telomerase. *J. Med. Chem.* **2001**, *44*, 4509–4523. https://doi.org/10.1021/jm010246u.

(427) Largy, E.; Hamon, F.; Teulade-Fichou, M.-P. Development of a High-Throughput G4-FID Assay for Screening and Evaluation of Small Molecules Binding Quadruplex Nucleic Acid Structures. *Anal. Bioanal. Chem.* **2011**, *400*, 3419–3427. https://doi.org/10.1007/s00216-011-5018-z.

(428) Largy, E.; Hamon, F.; Teulade-Fichou, M.-P. A Streptavidin Paramagnetic-Particle Based Competition Assay for the Evaluation of the Optical Selectivity of Quadruplex Nucleic Acid Fluorescent Probes. *Methods* **2012**, *57*, 129–137. https://doi.org/10.1016/j.ymeth.2012.02.008.

(429) Ren, J.; Chaires, J. B. Sequence and Structural Selectivity of Nucleic Acid Binding Ligands. *Biochemistry* **1999**, *38*, 16067–16075. https://doi.org/10.1021/bi992070s.

(430) Romera, C.; Bombarde, O.; Bonnet, R.; Gomez, D.; Dumy, P.; Calsou, P.; Gwan, J.-F.; Lin, J.-H.; Defrancq, E.; Pratviel, G. Improvement of Porphyrins for G-Quadruplex DNA Targeting. *Biochimie* **2011**, *93*, 1310–1317. https://doi.org/10.1016/j.biochi.2011.06.008.

(431) Martino, L.; Pagano, B.; Fotticchia, I.; Neidle, S.; Giancola, C. Shedding Light on the Interaction between TMPyP4 and Human Telomeric Quadruplexes. *J. Phys. Chem. B* **2009**, *113*,

14779–14786. https://doi.org/10.1021/jp9066394.

(432) Freyer, M. W.; Buscaglia, R.; Kaplan, K.; Cashman, D.; Hurley, L. H.; Lewis, E. A. Biophysical Studies of the C-MYC NHE III1 Promoter: Model Quadruplex Interactions with a Cationic Porphyrin. *Biophys. J.* **2007**, *92*, 2007–2015. https://doi.org/10.1529/biophysj.106.097246.

(433) Nicoludis, J. M.; Miller, S. T.; Jeffrey, P. D.; Barrett, S. P.; Rablen, P. R.; Lawton, T. J.; Yatsunyk, L. A. Optimized End-Stacking Provides Specificity of N-Methyl Mesoporphyrin IX for Human Telomeric G-Quadruplex DNA. *J. Am. Chem. Soc.* **2012**, *134*, 20446–20456. https://doi.org/10.1021/ja3088746.

(434) Nicoludis, J. M.; Barrett, S. P.; Mergny, J.-L.; Yatsunyk, L. A. Interaction of Human Telomeric DNA with N-Methyl Mesoporphyrin IX. *Nucleic Acids Res.* **2012**, *40*, 5432–5447. https://doi.org/10.1093/nar/gks152.

(435) Sabharwal, N. C.; Savikhin, V.; Turek-Herman, J. R.; Nicoludis, J. M.; Szalai, V. A.; Yatsunyk, L. A. N-Methylmesoporphyrin IX Fluorescence as a Reporter of Strand Orientation in Guanine Quadruplexes. *FEBS J.* **2014**, *281*, 1726–1737. https://doi.org/10.1111/febs.12734.

(436) Lin, L. Y.; McCarthy, S.; Powell, B. M.; Manurung, Y.; Xiang, I. M.; Dean, W. L.; Chaires, B.; Yatsunyk, L. A. Biophysical and X-Ray Structural Studies of the (GGGTT)3GGG G-Quadruplex in Complex with N-Methyl Mesoporphyrin IX. *PloS One* **2020**, *15*, e0241513. https://doi.org/10.1371/journal.pone.0241513.

(437) Hamon, F.; Largy, E.; Guédin-Beaurepaire, A.; Rouchon-Dagois, M.; Sidibe, A.; Monchaud, D.; Mergny, J.-L.; Riou, J.-F.; Nguyen, C.-H.; Teulade-Fichou, M.-P. An Acyclic Oligoheteroaryle That Discriminates Strongly between Diverse G-Quadruplex Topologies. *Angew. Chem. Int. Ed Engl.* **2011**, *50*, 8745–8749. https://doi.org/10.1002/anie.201103422.

(438) Petenzi, M.; Verga, D.; Largy, E.; Hamon, F.; Doria, F.; Teulade-Fichou, M.-P.; Guédin, A.; Mergny, J.-L.; Mella, M.; Freccero, M. Cationic Pentaheteroaryls as Selective G-Quadruplex Ligands by Solvent-Free Microwave-Assisted Synthesis. *Chem. - Eur. J.* **2012**, *18*, 14487–14496. https://doi.org/10.1002/chem.201202097.

(439) Martino, L.; Virno, A.; Pagano, B.; Virgilio, A.; Di Micco, S.; Galeone, A.; Giancola, C.; Bifulco, G.; Mayol, L.; Randazzo, A. Structural and Thermodynamic Studies of the Interaction of Distamycin A with the Parallel Quadruplex Structure [d(TGGGGT)]4. *J. Am. Chem. Soc.* **2007**, *129*, 16048–16056. https://doi.org/10.1021/ja075710k.

(440) Di Leva, F. S.; Novellino, E.; Cavalli, A.; Parrinello, M.; Limongelli, V. Mechanistic Insight into Ligand Binding to G-Quadruplex DNA. *Nucleic Acids Res.* **2014**, *42*, 5447–5455. https://doi.org/10.1093/nar/gku247.

(441) Sedghi Masoud, S.; Nagasawa, K. I-Motif-Binding Ligands and Their Effects on the Structure and Biological Functions of i-Motif. *Chem. Pharm. Bull. (Tokyo)* **2018**, *66*, 1091–1103. https://doi.org/10.1248/cpb.c18-00720.

(442) Day, H. A.; Pavlou, P.; Waller, Z. A. E. I-Motif DNA: Structure, Stability and Targeting with Ligands. *Bioorg. Med. Chem.* **2014**, *22*, 4407–4418. https://doi.org/10.1016/j.bmc.2014.05.047.

(443) Pagano, A.; Iaccarino, N.; Abdelhamid, M. A. S.; Brancaccio, D.; Garzarella, E. U.; Di Porzio, A.; Novellino, E.; Waller, Z. A. E.; Pagano, B.; Amato, J.; et al. Common G-Quadruplex Binding Agents Found to Interact With i-Motif-Forming DNA: Unexpected Multi-Target-Directed Compounds. *Front. Chem.* **2018**, *6*, 281. https://doi.org/10.3389/fchem.2018.00281.

(444) Abdelhamid, M. A. S.; Gates, A. J.; Waller, Z. A. E. Destabilization of I-Motif DNA at Neutral PH by G-Quadruplex Ligands. *Biochemistry* **2019**, *58*, 245–249. https://doi.org/10.1021/acs.biochem.8b00968.

(445) Satpathi, S.; Sappati, S.; Das, K.; Hazra, P. Structural Characteristics Requisite for the Ligand-Based Selective Detection of i-Motif DNA. *Org. Biomol. Chem.* **2019**, *17*, 5392–5399. https://doi.org/10.1039/c9ob01020c.

(446) Warner, K. D.; Hajdin, C. E.; Weeks, K. M. Principles for Targeting RNA with Drug-like Small Molecules. *Nat. Rev. Drug Discov.* **2018**, *17*, 547–558. https://doi.org/10.1038/nrd.2018.93.

(447) Howe, J. A.; Wang, H.; Fischmann, T. O.; Balibar, C. J.; Xiao, L.; Galgoci, A. M.; Malinverni, J. C.; Mayhood, T.; Villafania, A.; Nahvi, A.; et al. Selective Small-Molecule Inhibition of an RNA Structural Element. *Nature* **2015**, *526*, 672–677. https://doi.org/10.1038/nature15542.

(448) Meyer, S. M.; Williams, C. C.; Akahori, Y.; Tanaka, T.; Aikawa, H.; Tong, Y.; Childs-Disney, J. L.; Disney, M. D. Small Molecule Recognition of Disease-Relevant RNA Structures. *Chem. Soc. Rev.* **2020**, *49*, 7167–7199. https://doi.org/10.1039/d0cs00560f.

(449) Wallis, M. G.; Schroeder, R. The Binding of Antibiotics to RNA. *Prog. Biophys. Mol. Biol.* **1997**, *67*, 141–154. https://doi.org/10.1016/s0079-6107(97)00011-4.

(450) Yonath, A. ANTIBIOTICS TARGETING RIBOSOMES: Resistance, Selectivity, Synergism, and Cellular Regulation. *Annu. Rev. Biochem.* **2005**, *74*, 649–679. https://doi.org/10.1146/annurev.biochem.74.082803.133130.

(451) Magnet, S.; Blanchard, J. S. Molecular Insights into Aminoglycoside Action and Resistance. *Chem. Rev.* **2005**, *105*, 477–498. https://doi.org/10.1021/cr0301088.

(452) Guan, L.; Disney, M. D. Recent Advances in Developing Small Molecules Targeting RNA. *ACS Chem. Biol.* **2012**, *7*, 73–86. https://doi.org/10.1021/cb200447r.

(453) Aboul-ela, F. Strategies for the Design of RNA-Binding Small Molecules. *Future Med. Chem.* **2010**, *2*, 93–119. https://doi.org/10.4155/fmc.09.149.

(454) Hermann, T. Small Molecules Targeting Viral RNA. *Wiley Interdiscip. Rev. RNA* **2016**, *7*, 726–743. https://doi.org/10.1002/wrna.1373.

(455) Thomas, J. R.; Hergenrother, P. J. Targeting RNA with Small Molecules. *Chem. Rev.* **2008**, *108*, 1171–1224. https://doi.org/10.1021/cr0681546.

(456) Ursu, A.; Childs-Disney, J. L.; Andrews, R. J.; O'Leary, C. A.; Meyer, S. M.; Angelbello, A. J.; Moss, W. N.; Disney, M. D. Design of Small Molecules Targeting RNA Structure from Sequence. *Chem. Soc. Rev.* **2020**, *49*, 7252–7270. https://doi.org/10.1039/d0cs00455c.

(457) Yoshizawa, S.; Fourmy, D.; Puglisi, J. D. Recognition of the Codon-Anticodon Helix by Ribosomal RNA. *Science* **1999**, *285*, 1722–1725. https://doi.org/10.1126/science.285.5434.1722.

(458) François, B.; Russell, R. J. M.; Murray, J. B.; Aboul-ela, F.; Masquida, B.; Vicens, Q.; Westhof, E. Crystal Structures of Complexes between Aminoglycosides and Decoding A Site Oligonucleotides: Role of the Number of Rings and Positive Charges in the Specific Binding Leading to Miscoding. *Nucleic Acids Res.* **2005**, *33*, 5677–5690. https://doi.org/10.1093/nar/gki862.

(459) Purohit, P.; Stern, S. Interactions of a Small RNA with Antibiotic and RNA Ligands of the 30S Subunit. *Nature* **1994**, *370*, 659–662. https://doi.org/10.1038/370659a0.

(460) Miyaguchi, H.; Narita, H.; Sakamoto, K.; Yokoyama, S. An Antibiotic-Binding Motif of an RNA Fragment Derived from the A-Site-Related Region of Escherichia Coli 16S RRNA. *Nucleic Acids Res.* **1996**, *24*, 3700–3706. https://doi.org/10.1093/nar/24.19.3700.

(461) Corley, M.; Burns, M. C.; Yeo, G. W. How RNA-Binding Proteins Interact with RNA: Molecules and Mechanisms. *Mol. Cell* **2020**, *78*, 9–29. https://doi.org/10.1016/j.molcel.2020.03.011.

(462) Hu, W.; Qin, L.; Li, M.; Pu, X.; Guo, Y. A Structural Dissection of Protein–RNA Interactions Based on Different RNA Base Areas of Interfaces. *RSC Adv.* **2018**, *8*, 10582–10592. https://doi.org/10.1039/C8RA00598B.

(463) Zagrovic, B.; Bartonek, L.; Polyansky, A. A. RNA-Protein Interactions in an Unstructured Context. *FEBS Lett.* **2018**, *592*, 2901–2916. https://doi.org/10.1002/1873-3468.13116.

(464) Hentze, M. W.; Castello, A.; Schwarzl, T.; Preiss, T. A Brave New World of RNA-Binding Proteins. *Nat. Rev. Mol. Cell Biol.* **2018**, *19*, 327–341. https://doi.org/10.1038/nrm.2017.130.

(465) Treger, M.; Westhof, E. Statistical Analysis of Atomic Contacts at RNA-Protein Interfaces. *J. Mol. Recognit.* **2001**, *14*, 199–214. https://doi.org/10.1002/jmr.534.

(466) Han, K.; Nepal, C. PRI-Modeler: Extracting RNA Structural Elements from PDB Files of Protein-RNA Complexes. *FEBS Lett.* **2007**, *581*, 1881–1890. https://doi.org/10.1016/j.febslet.2007.03.085.

(467) Hoffman, M. M.; Khrapov, M. A.; Cox, J. C.; Yao, J.; Tong, L.; Ellington, A. D. AANT: The Amino Acid-Nucleotide Interaction Database. *Nucleic Acids Res.* **2004**, *32*, D174-181. https://doi.org/10.1093/nar/gkh128.

(468) Wilson, K. A.; Holland, D. J.; Wetmore, S. D. Topology of RNA-Protein Nucleobase-Amino Acid π-π Interactions and Comparison to Analogous DNA-Protein π-π Contacts. *RNA* **2016**, *22*, 696–708. https://doi.org/10.1261/rna.054924.115.

(469) Hudson, W. H.; Ortlund, E. A. The Structure, Function and Evolution of Proteins That Bind DNA and RNA. *Nat. Rev. Mol. Cell Biol.* **2014**, *15*, 749–760. https://doi.org/10.1038/nrm3884.

(470) Barraud, P.; Allain, F. H.-T. ADAR Proteins: Double-Stranded RNA and Z-DNA Binding Domains. *Curr. Top. Microbiol. Immunol.* **2012**, *353*, 35–60. https://doi.org/10.1007/82_2011_145.

(471) Allain, F. H.; Howe, P. W.; Neuhaus, D.; Varani, G. Structural Basis of the RNA-Binding Specificity of Human U1A Protein. *EMBO J.* **1997**, *16*, 5764–5772. https://doi.org/10.1093/emboj/16.18.5764.

(472) Yamashita, M.; Fenn, J. B. Electrospray Ion Source. Another Variation on the Free-Jet Theme. *J. Phys. Chem.* **1984**, *88*, 4451–4459. https://doi.org/10.1021/j150664a002.

(473) Kebarle, P.; Peschke, M. On the Mechanisms by Which the Charged Droplets Produced by Electrospray Lead to Gas Phase Ions. *Anal. Chim. Acta* **2000**, *406*, 11–35. https://doi.org/10.1016/s0003-2670(99)00598-x.

(474) Konermann, L.; Ahadi, E.; Rodriguez, A. D.; Vahidi, S. Unraveling the Mechanism of Electrospray Ionization. *Anal. Chem.* **2013**, *85*, 2–9. https://doi.org/10.1021/ac302789c.

(475) Kebarle, P. A Brief Overview of the Present Status of the Mechanisms Involved in Electrospray Mass Spectrometry. *J. Mass Spectrom.* **2000**, *35*, 804–817. https://doi.org/10.1002/1096-9888(200007)35:7<804::aid-jms22>3.0.co;2-q.

(476) Gomez, A.; Tang, K. Charge and Fission of Droplets in Electrostatic Sprays. *Phys. Fluids* **1994**, *6*, 404–414. https://doi.org/10.1063/1.868037.

(477) Juraschek, R.; Dülcks, T.; Karas, M. Nanoelectrospray—More than Just a Minimized-Flow Electrospray Ionization Source. *J. Am. Soc. Mass Spectrom.* **1999**, *10*, 300–308. https://doi.org/10.1016/S1044-0305(98)00157-3.

(478) Iribarne, J. V. On the Evaporation of Small Ions from Charged Droplets. *J. Chem. Phys.* **1976**, *64*, 2287–2294. https://doi.org/10.1063/1.432536.

(479) Kwan, V.; O'Dwyer, R.; Laur, D.; Tan, J.; Consta, S. Relation between Ejection Mechanism and Ion Abundance in the Electric Double Layer of Droplets. *J. Phys. Chem. A* **2021**, *125*, 2954–2966. https://doi.org/10.1021/acs.jpca.1c01522.

(480) Fernandez de la Mora, J. Electrospray Ionization of Large Multiply Charged Species Proceeds via Dole's Charged Residue Mechanism. *Anal. Chim. Acta* **2000**, *406*, 93–104. https://doi.org/10.1016/s0003-2670(99)00601-7.

(481) Hogan, C. J.; Carroll, J. A.; Rohrs, H. W.; Biswas, P.; Gross, M. L. Charge Carrier Field Emission Determines the Number of Charges on Native State Proteins in Electrospray Ionization. *J. Am. Chem. Soc.* **2008**, *130*, 6926–6927. https://doi.org/10.1021/ja801280c.

(482) Hogan, C. J.; Carroll, J. A.; Rohrs, H. W.; Biswas, P.; Gross, M. L. Combined Charged Residue-Field Emission Model of Macromolecular Electrospray Ionization. *Anal. Chem.* **2009**, *81*, 369–377. https://doi.org/10.1021/ac8016532.

(483) Larriba, C.; de la Mora, J. F.; Clemmer, D. E. Electrospray Ionization Mechanisms for Large Polyethylene Glycol Chains Studied Through Tandem Ion Mobility Spectrometry. *J. Am. Soc. Mass Spectrom.* **2014**, *25*, 1332–1345. https://doi.org/10.1007/s13361-014-0885-0.

(484) Tang, Liang.; Kebarle, Paul. Dependence of Ion Intensity in Electrospray Mass Spectrometry on the Concentration of the Analytes in the Electrosprayed Solution. *Anal. Chem.* **1993**, *65*, 3654–3668. https://doi.org/10.1021/ac00072a020.

(485) Enke, C. G. A Predictive Model for Matrix and Analyte Effects in Electrospray Ionization of Singly-Charged Ionic Analytes. *Anal Chem* **1997**, *69*, 4885–4893.

(486) Constantopoulos, T. L.; Jackson, G. S.; Enke, C. G. Challenges in Achieving a Fundamental Model for ESI. *Anal. Chim. Acta* **2000**, *406*, 37–52. https://doi.org/10.1016/s0003-2670(99)00600-5.

(487) Schmidt, A.; Karas, M.; Dülcks, T. Effect of Different Solution Flow Rates on Analyte Ion Signals in Nano-ESI MS, or: When Does ESI Turn into Nano-ESI? *J. Am. Soc. Mass Spectrom.* **2003**, *14*, 492–500. https://doi.org/10.1016/S1044-0305(03)00128-4.

(488) Chingin, K.; Xu, N.; Chen, H. Soft Supercharging of Biomolecular Ions in Electrospray Ionization Mass Spectrometry. *J. Am. Soc. Mass Spectrom.* **2014**, *25*, 928–934. https://doi.org/10.1007/s13361-014-0887-y.

(489) Rosu, F.; Pirotte, S.; Pauw, E. D.; Gabelica, V. Positive and Negative Ion Mode ESI-MS and MS/MS for Studying Drug–DNA Complexes. *Int. J. Mass Spectrom.* **2006**, *253*, 156–171. https://doi.org/10.1016/j.ijms.2005.11.027.

(490) Garabedian, A.; Butcher, D.; Lippens, J. L.; Miksovska, J.; Chapagain, P. P.; Fabris, D.; Ridgeway, M. E.; Park, M. A.; Fernandez-Lima, F. Structures of the Kinetically Trapped I-Motif DNA Intermediates. *Phys. Chem. Chem. Phys.* **2016**, *18*, 26691–26702. https://doi.org/10.1039/C6CP04418B.

(491) Robinson, C. V.; Radford, S. E. Weighing the Evidence for Structure: Electrospray Ionization Mass Spectrometry of Proteins. *Structure* **1995**, *3*, 861–865. https://doi.org/10.1016/S0969-2126(01)00221-0.

(492) Griffeycor, R. H.; Sasmor, H.; Greig, M. J. Oligonucleotide Charge States in Negative Ionization Electrospray-Mass Spectrometry Are a Function of Solution Ammonium Ion Concentration. *J. Am. Soc. Mass Spectrom.* **1997**, *8*, 155–160. https://doi.org/10.1016/S1044-0305(96)00200-0.

(493) Ganisl, B.; Taucher, M.; Riml, C.; Breuker, K. Charge as You Like! Efficient Manipulation of Negative Ion Net Charge in Electrospray Ionization of Proteins and Nucleic Acids. *Eur. J. Mass Spectrom.* **2011**, *17*, 333–343. https://doi.org/10.1255/ejms.1140.

(494) Iavarone, A. T.; Williams, E. R. Mechanism of Charging and Supercharging Molecules in Electrospray Ionization. *J. Am. Chem. Soc.* **2003**, *125*, 2319–2327. https://doi.org/10.1021/ja021202t.

(495) Loo, R. R. O.; Lakshmanan, R.; Loo, J. A. What Protein Charging (and Supercharging) Reveal about the Mechanism of Electrospray Ionization. *J. Am. Soc. Mass Spectrom.* **2014**, *25*, 1675–1693. https://doi.org/10.1007/s13361-014-0965-1.

(496) Xu, N.; Chingin, K.; Chen, H. Ionic Strength of Electrospray Droplets Affects Charging of DNA Oligonucleotides. *J Mass Spectrom* **2014**, *49*, 103–107. https://doi.org/10.1002/jms.3311.

(497) Brahim, B.; Alves, S.; Cole, R. B.; Tabet, J. C. Charge Enhancement of Single-Stranded DNA in Negative Electrospray Ionization Using the Supercharging Reagent Meta-Nitrobenzyl Alcohol. *J. Am. Soc. Mass Spectrom.* **2013**, *24*, 1988–1996. https://doi.org/10.1007/s13361-013-0732-8.

(498) Lodish, H.; Berk, A.; Zipursky, S. L.; Matsudaira, P.; Baltimore, D.; Darnell, J. Intracellular Ion Environment and Membrane Electric Potential. In *Molecular Cell Biology*; W. H. Freeman: New York, USA, 2000; p.1184.

(499) Konermann, L. Addressing a Common Misconception: Ammonium Acetate as Neutral

PH “Buffer” for Native Electrospray Mass Spectrometry. *J. Am. Soc. Mass Spectrom.* **2017**, *28*, 1827–1835. https://doi.org/10.1007/s13361-017-1739-3.

(500) Potier, N.; Van Dorsselaer, A.; Cordier, Y.; Roch, O.; Bischoff, R. Negative Electrospray Ionization Mass Spectrometry of Synthetic and Chemically Modified Oligonucleotides. *Nucleic Acids Res.* **1994**, *22*, 3895–3903. https://doi.org/10.1093/nar/22.19.3895.

(501) Deguchi, K.; Ishikawa, M.; Yokokura, T.; Ogata, I.; Ito, S.; Mimura, T.; Ostrander, C. Enhanced Mass Detection of Oligonucleotides Using Reverse-Phase High-Performance Liquid Chromatography/Electrospray Ionization Ion-Trap Mass Spectrometry. *Rapid Commun. Mass Spectrom.* **2002**, *16*, 2133–2141. https://doi.org/10.1002/rcm.840.

(502) Apffel, A.; Chakel, J. A.; Fischer, S.; Lichtenwalter, K.; Hancock, W. S. Analysis of Oligonucleotides by HPLC-Electrospray Ionization Mass Spectrometry. *Anal. Chem.* **1997**, *69*, 1320–1325. https://doi.org/10.1021/ac960916h.

(503) Basiri, B.; Murph, M. M.; Bartlett, M. G. Assessing the Interplay between the Physicochemical Parameters of Ion-Pairing Reagents and the Analyte Sequence on the Electrospray Desorption Process for Oligonucleotides. *J. Am. Soc. Mass Spectrom.* **2017**, *28*, 1647–1656. https://doi.org/10.1007/s13361-017-1671-6.

(504) Chen, B.; Mason, S. F.; Bartlett, M. G. The Effect of Organic Modifiers on Electrospray Ionization Charge-State Distribution and Desorption Efficiency for Oligonucleotides. *J. Am. Soc. Mass Spectrom.* **2013**, *24*, 257–264. https://doi.org/10.1007/s13361-012-0509-5.

(505) Scalabrin, M.; Palumbo, M.; Richter, S. N. Highly Improved Electrospray Ionization-Mass Spectrometry Detection of G-Quadruplex-Folded Oligonucleotides and Their Complexes with Small Molecules. *Anal. Chem.* **2017**, *89*, 8632–8637. https://doi.org/10.1021/acs.analchem.7b01282.

(506) Gabelica, V.; Pauw, E. D.; Rosu, F. Interaction between Antitumor Drugs and a Double-Stranded Oligonucleotide Studied by Electrospray Ionization Mass Spectrometry. *J. Mass Spectrom.* **1999**, *34*, 1328–1337. https://doi.org/10.1002/(sici)1096-9888(199912)34:12<1328::aid-jms889>3.0.co;2-f.

(507) David, W. M.; Brodbelt, J.; Kerwin, S. M.; Thomas, P. W. Investigation of Quadruplex Oligonucleotide-Drug Interactions by Electrospray Ionization Mass Spectrometry. *Anal Chem* **2002**, *74*, 2029–2033. https://doi.org/10.1021/ac011283w.

(508) Mazzitelli, C. L.; Rodriguez, M.; Kerwin, S. M.; Brodbelt, J. S. Evaluation of Metal-Mediated DNA Binding of Benzoxazole Ligands by Electrospray Ionization Mass Spectrometry. *J. Am. Soc. Mass Spectrom.* **2008**, *19*, 209–218. https://doi.org/10.1016/j.jasms.2007.05.009.

(509) Turner, K. B.; Hagan, N. A.; Kohlway, A. S.; Fabris, D. Mapping Noncovalent Ligand Binding to Stemloop Domains of the HIV-1 Packaging Signal by Tandem Mass Spectrometry. *J Am Soc Mass Spectrom* **2006**, *17*, 1401–1411. https://doi.org/10.1016/j.jasms.2006.06.009.

(510) Doria, F.; Nadai, M.; Folini, M.; Scalabrin, M.; Germani, L.; Sattin, G.; Mella, M.; Palumbo, M.; Zaffaroni, N.; Fabris, D.; et al. Targeting Loop Adenines in G-Quadruplex by a Selective Oxirane. *Chem. - Eur. J.* **2013**, *19*, 78–81. https://doi.org/10.1002/chem.201203097.

(511) Bleicher, K.; Bayer, E. Various Factors Influencing the Signal Intensity of Oligonucleotides in Electrospray Mass Spectrometry. *Biol. Mass Spectrom.* **1994**, *23*, 320–322. https://doi.org/10.1002/bms.1200230604.

(512) Rosu, F.; Gabelica, V.; Poncelet, H.; De Pauw, E. Tetramolecular G-Quadruplex Formation Pathways Studied by Electrospray Mass Spectrometry. *Nucleic Acids Res.* **2010**, *38*, 5217–5225. https://doi.org/10.1093/nar/gkq208.

(513) Ferreira, R.; Marchand, A.; Gabelica, V. Mass Spectrometry and Ion Mobility Spectrometry of G-Quadruplexes. A Study of Solvent Effects on Dimer Formation and Structural Transitions in the Telomeric DNA Sequence d(TAGGGTTAGGGT). *Methods* **2012**, *57*, 56–63. https://doi.org/10.1016/j.ymeth.2012.03.021.

(514) Marchand, A.; Ferreira, R.; Tateishi-Karimata, H.; Miyoshi, D.; Sugimoto, N.; Gabelica, V. Sequence and Solvent Effects on Telomeric DNA Bimolecular G-Quadruplex Folding Kinetics. *J. Phys. Chem. B* **2013**, *117*, 12391–12401. https://doi.org/10.1021/jp406857s.

(515) Nakano, S.; Miyoshi, D.; Sugimoto, N. Effects of Molecular Crowding on the Structures, Interactions, and Functions of Nucleic Acids. *Chem. Rev.* **2014**, *114*, 2733–2758. https://doi.org/10.1021/cr400113m.

(516) Vorlíčková, M.; Bednářová, K.; Kypr, J. Ethanol Is a Better Inducer of DNA Guanine Tetraplexes than Potassium Cations. *Biopolymers* **2006**, *82*, 253–260. https://doi.org/10.1002/bip.20488.

(517) Wilm, M.; Mann, M. Analytical Properties of the Nanoelectrospray Ion Source. *Anal. Chem.* **1996**, *68*, 1–8. https://doi.org/10.1021/ac9509519.

(518) Gibson, G. T. T.; Mugo, S. M.; Oleschuk, R. D. Nanoelectrospray Emitters: Trends and Perspective. *Mass Spectrom. Rev.* **2009**, *28*, 918–936. https://doi.org/10.1002/mas.20248.

(519) Kenderdine, T.; Xia, Z.; Williams, E. R.; Fabris, D. Submicrometer Nanospray Emitters Provide New Insights into the Mechanism of Cation Adduction to Anionic Oligonucleotides. *Anal. Chem.* **2018**, *90*, 13541–13548.

https://doi.org/10.1021/acs.analchem.8b03632.

(520) Sundqvist, G.; Benkestock, K.; Roeraade, J. Investigation of Multiple Binding Sites on Ribonuclease A Using Nano-Electrospray Ionization Mass Spectrometry. *Rapid Commun. Mass Spectrom.* **2005**, *19*, 1011–1016. https://doi.org/10.1002/rcm.1880.

(521) Nguyen, G. T. H.; Leung, W. Y.; Tran, T. N.; Wang, H.; Murray, V.; Donald, W. A. Mechanism for the Binding of Netropsin to Hairpin DNA Revealed Using Nanoscale Ion Emitters in Native Mass Spectrometry. *Anal. Chem.* **2020**, *92*, 1130–1137. https://doi.org/10.1021/acs.analchem.9b04209.

(522) Gabelica, V.; Vreuls, C.; Filée, P.; Duval, V.; Joris, B.; Pauw, E. D. Advantages and Drawbacks of Nanospray for Studying Noncovalent Protein–DNA Complexes by Mass Spectrometry. *Rapid Commun. Mass Spectrom.* **2002**, *16*, 1723–1728. https://doi.org/10.1002/rcm.776.

(523) Hiraoka, K.; Saito, S.; Katsuragawa, J.; Kudaka, I. A New Liquid Chromatography/Mass Spectrometry Interface: Laser Spray. *Rapid Commun. Mass Spectrom.* **1998**, *12*, 1170–1174. https://doi.org/10.1002/(sici)1097-0231(19980915)12:17<1170::aid-rcm297>3.0.co;2-o.

(524) Hiraoka, K. Laser Spray: Electric Field-Assisted Matrix-Assisted Laser Desorption/Ionization. *J. Mass Spectrom.* **2004**, *39*, 341–350. https://doi.org/10.1002/jms.621.

(525) Shi, X.; Takamizawa, A.; Nishimura, Y.; Hiraoka, K.; Akashi, S. Stability Analysis for Double-Stranded DNA Oligomers and Their Noncovalent Complexes with Drugs by Laser Spray. *J. Mass Spectrom.* **2006**, *41*, 1086–1095. https://doi.org/10.1002/jms.1069.

(526) Shi, X.; Nishimura, Y.; Akashi, S.; Takamizawa, A.; Hiraoka, K. Evaluation of Binding Affinity of Protein-Mutant Dna Complexes in Solution by Laser Spray Mass Spectrometry. *J. Am. Soc. Mass Spectrom.* **2006**, *17*, 611–620. https://doi.org/10.1016/j.jasms.2005.12.016.

(527) Sakamoto, S.; Yamaguchi, K. Hyperstranded DNA Architectures Observed by Cold-Spray Ionization Mass Spectrometry. *Angew. Chem. Int. Ed.* **2003**, *42*, 905–908. https://doi.org/10.1002/anie.200390239.

(528) Yamaguchi, K. Cold-Spray Ionization Mass Spectrometry: Principle and Applications. *J. Mass Spectrom.* **2003**, *38*, 473–490. https://doi.org/10.1002/jms.488.

(529) Hillenkamp, F.; Karas, M.; Beavis, R. C.; Chait, B. T. Matrix-Assisted Laser Desorption/Ionization Mass Spectrometry of Biopolymers. *Anal. Chem.* **1991**, *63*, 1193A-1203A. https://doi.org/10.1021/ac00024a716.

(530) Thiede, B.; von Janta-Lipinski, M. Noncovalent RNA-Peptide Complexes Detected by Matrix-Assisted Laser Desorption/Ionization Mass Spectrometry. *Rapid Commun. Mass Spectrom.* **1998**, *12*, 1889–1894. https://doi.org/10.1002/(sici)1097-0231(19981215)12:23<1889::aid-rcm411>3.0.co;2-0.

(531) Yamashita, K.; Sato, S.; Takamiya, H.; Takagi, M.; Takenaka, S. Analysis of the Complex of Oligonucleotide Duplexes with Ligands by MALDI-TOF Mass Spectroscopy. *Chem. Lett.* **2001**, *30*, 680–681. https://doi.org/10.1246/cl.2001.680.

(532) Karas, M.; Krüger, R. Ion Formation in MALDI: The Cluster Ionization Mechanism. *Chem. Rev.* **2003**, *103*, 427–440. https://doi.org/10.1021/cr010376a.

(533) Distler, A. M.; Allison, J. Additives for the Stabilization of Double-Stranded DNA in UV-MALDI. *J. Am. Soc. Mass Spectrom.* **2002**, *13*, 1129–1137. https://doi.org/10.1016/s1044-0305(02)00430-0.

(534) Zhu, Y. F.; Taranenko, N. I.; Allman, S. L.; Martin, S. A.; Haff, L.; Chen, C. H. The Effect of Ammonium Salt and Matrix in the Detection of DNA by Matrix-Assisted Laser Desorption/Ionization Time-of-Flight Mass Spectrometry. *Rapid Commun. Mass Spectrom.* **1996**, *10*, 1591–1596. https://doi.org/10.1002/(sici)1097-0231(199610)10:13<1591::aid-rcm715>3.0.co;2-w.

(535) Sudha, R.; Zenobi, R. The Detection and Stability of DNA Duplexes Probed by MALDI Mass Spectrometry. *Helv. Chim. Acta* **2002**, *85*, 3136–3143. https://doi.org/10.1002/1522-2675(200210)85:10<3136::aid-hlca3136>3.0.co;2-f.

(536) Bahr, U.; Aygun, H.; Karas, M. Detection and Relative Quantification of SiRNA Double Strands by MALDI Mass Spectrometry. *Anal. Chem.* **2008**, *80*, 6280–6285. https://doi.org/10.1021/ac800605z.

(537) Alves, S.; Woods, A.; Tabet, J. C. Charge State Effect on the Zwitterion Influence on Stability of Non-Covalent Interaction of Single-Stranded DNA with Peptides. *J. Mass Spectrom.* **2007**, *42*, 1613–1622. https://doi.org/10.1002/jms.1359.

(538) Terrier, P.; Tortajada, J.; Zin, G.; Buchmann, W. Noncovalent Complexes Between DNA and Basic Polypeptides or Polyamines by MALDI-TOF. *J. Am. Soc. Mass Spectrom.* **2007**, *18*, 1977–1989. https://doi.org/10.1016/j.jasms.2007.07.028.

(539) Alves, S.; Woods, A.; Delvolvé, A.; Tabet, J. C. Influence of Salt Bridge Interactions on the Gas-Phase Stability of DNA/Peptide Complexes. *Int. J. Mass Spectrom.* **2008**, *278*, 122–128. https://doi.org/10.1016/j.ijms.2008.04.023.

(540) Kleinekofort, W.; Avdiev, J.; Brutschy, B. A New Method of Laser Desorption Mass Spectrometry for the Study of Biological Macromolecules. *Int. J. Mass Spectrom. Ion Process.* **1996**, *152*, 135–142.

https://doi.org/10.1016/0168-1176(95)04330-6.

(541) Kleinekofort, W.; Pfenninger, A.; Plomer, T.; Griesinger, C.; Brutschy, B. Observation of Noncovalent Complexes Using Laser-Induced Liquid Beam Ionization/Desorption. *Int. J. Mass Spectrom. Ion Process.* **1996**, *156*, 195–202. https://doi.org/10.1016/S0168-1176(96)04507-7.

(542) Hoffmann, J.; Schmidt, T. L.; Heckel, A.; Brutschy, B. Probing the Limits of Liquid Droplet Laser Desorption Mass Spectrometry in the Analysis of Oligonucleotides and Nucleic Acids. *Rapid Commun. Mass Spectrom.* **2009**, *23*, 2176–2180. https://doi.org/10.1002/rcm.4129.

(543) Peetz, O.; Hellwig, N.; Henrich, E.; Mezhyrova, J.; Dötsch, V.; Bernhard, F.; Morgner, N. LILBID and NESI: Different Native Mass Spectrometry Techniques as Tools in Structural Biology. *J. Am. Soc. Mass Spectrom.* **2019**, *30*, 181–191. https://doi.org/10.1007/s13361-018-2061-4.

(544) Young, P.; Hense, G.; Immer, C.; Wöhnert, J.; Morgner, N. LILBID Laser Dissociation Curves: A Mass Spectrometry-Based Method for the Quantitative Assessment of DsDNA Binding Affinities. *Sci. Rep.* **2020**, *10*, 20398. https://doi.org/10.1038/s41598-020-76867-9.

(545) Morgner, N.; Barth, H. D.; Schmidt, T. L.; Heckel, A.; Scheffer, U.; Göbel, M.; Fucini, P.; Brutschy, B. Detecting Specific Ligand Binding to Nucleic Acids: A Test for Ultrasoft Laser Mass Spectrometry. *Z. Für Phys. Chem.* **2007**, *221*, 689–704. https://doi.org/10.1524/zpch.2007.221.5.689.

(546) Kleinekofort, W.; Schweitzer, M.; Engels, J. W.; Brutschy, B. Analysis of Double-Stranded Oligonucleotides by Laser-Induced Liquid Beam Mass Spectrometry. *Int. J. Mass Spectrom. Ion Process.* **1997**, *163*, L1–L4. https://doi.org/10.1016/S0168-1176(96)04533-8.

(547) Santos, I. C.; Brodbelt, J. S. Recent Developments in the Characterization of Nucleic Acids by Liquid Chromatography, Capillary Electrophoresis, Ion Mobility, and Mass Spectrometry (2010-2020). *J. Sep. Sci.* **2021**, *44*, 340–372. https://doi.org/10.1002/jssc.202000833.

(548) Schürch, S. Characterization of Nucleic Acids by Tandem Mass Spectrometry - The Second Decade (2004-2013): From DNA to RNA and Modified Sequences. *Mass Spectrom. Rev.* **2016**, *35*, 483–523. https://doi.org/10.1002/mas.21442.

(549) McGinnis, A. C.; Chen, B.; Bartlett, M. G. Chromatographic Methods for the Determination of Therapeutic Oligonucleotides. *J. Chromatogr. B Analyt. Technol. Biomed. Life. Sci.* **2012**, *883–884*, 76–94. https://doi.org/10.1016/j.jchromb.2011.09.007.

(550) El Zahar, N. M.; Magdy, N.; El-Kosasy, A. M.; Bartlett, M. G. Chromatographic Approaches for the Characterization and Quality Control of Therapeutic Oligonucleotide Impurities. *Biomed. Chromatogr.* **2018**, *32*, e4088. https://doi.org/10.1002/bmc.4088.

(551) Erb, R.; Oberacher, H. Comparison of Mobile-Phase Systems Commonly Applied in Liquid Chromatography-Mass Spectrometry of Nucleic Acids. *Electrophoresis* **2014**, *35*, 1226–1235. https://doi.org/10.1002/elps.201300269.

(552) McGinnis, A. C.; Grubb, E. C.; Bartlett, M. G. Systematic Optimization of Ion-Pairing Agents and Hexafluoroisopropanol for Enhanced Electrospray Ionization Mass Spectrometry of Oligonucleotides. *Rapid Commun. Mass Spectrom.* **2013**, *27*, 2655–2664. https://doi.org/10.1002/rcm.6733.

(553) Li, N.; El Zahar, N. M.; Saad, J. G.; van der Hage, E. R. E.; Bartlett, M. G. Alkylamine Ion-Pairing Reagents and the Chromatographic Separation of Oligonucleotides. *J. Chromatogr. A* **2018**, *1580*, 110–119. https://doi.org/10.1016/j.chroma.2018.10.040.

(554) Wu, Z.; Gao, W.; Phelps, M. A.; Wu, D.; Miller, D. D.; Dalton, J. T. Favorable Effects of Weak Acids on Negative-Ion Electrospray Ionization Mass Spectrometry. *Anal. Chem.* **2004**, *76*, 839–847. https://doi.org/10.1021/ac0351670.

(555) Liu, R.; Ruan, Y.; Liu, Z.; Gong, L. The Role of Fluoroalcohols as Counter Anions for Ion-Pairing Reversed-Phase Liquid Chromatography/High-Resolution Electrospray Ionization Mass Spectrometry Analysis of Oligonucleotides. *Rapid Commun. Mass Spectrom.* **2019**, *33*, 697–709. https://doi.org/10.1002/rcm.8386.

(556) Basiri, B.; van Hattum, H.; van Dongen, W. D.; Murph, M. M.; Bartlett, M. G. The Role of Fluorinated Alcohols as Mobile Phase Modifiers for LC-MS Analysis of Oligonucleotides. *J. Am. Soc. Mass Spectrom.* **2017**, *28*, 190–199. https://doi.org/10.1007/s13361-016-1500-3.

(557) Dickman, M. J. Effects of Sequence and Structure in the Separation of Nucleic Acids Using Ion Pair Reverse Phase Liquid Chromatography. *J. Chromatogr. A* **2005**, *1076*, 83–89. https://doi.org/10.1016/j.chroma.2005.04.018.

(558) Waghmare, S. P.; Pousinis, P.; Hornby, D. P.; Dickman, M. J. Studying the Mechanism of RNA Separations Using RNA Chromatography and Its Application in the Analysis of Ribosomal RNA and RNA:RNA Interactions. *J. Chromatogr. A* **2009**, *1216*, 1377–1382. https://doi.org/10.1016/j.chroma.2008.12.077.

(559) Yamauchi, Y.; Taoka, M.; Nobe, Y.; Izumikawa, K.; Takahashi, N.; Nakayama, H.; Isobe, T.

Denaturing Reversed Phase Liquid Chromatographic Separation of Non-Coding Ribonucleic Acids on Macro-Porous Polystyrene-Divinylbenzene Resins. *J. Chromatogr. A* **2013**, *1312*, 87–92. https://doi.org/10.1016/j.chroma.2013.09.021.

(560) Noll, B.; Seiffert, S.; Vornlocher, H.-P.; Roehl, I. Characterization of Small Interfering RNA by Non-Denaturing Ion-Pair Reversed-Phase Liquid Chromatography. *J. Chromatogr. A* **2011**, *1218*, 5609–5617. https://doi.org/10.1016/j.chroma.2011.06.057.

(561) Beverly, M.; Hartsough, K.; Machemer, L. Liquid Chromatography/Electrospray Mass Spectrometric Analysis of Metabolites from an Inhibitory RNA Duplex. *Rapid Commun. Mass Spectrom.* **2005**, *19*, 1675–1682. https://doi.org/10.1002/rcm.1972.

(562) Beverly, M.; Hartsough, K.; Machemer, L.; Pavco, P.; Lockridge, J. Liquid Chromatography Electrospray Ionization Mass Spectrometry Analysis of the Ocular Metabolites from a Short Interfering RNA Duplex. *J. Chromatogr. B* **2006**, *835*, 62–70. https://doi.org/10.1016/j.jchromb.2006.03.008.

(563) McCarthy, S. M.; Gilar, M.; Gebler, J. Reversed-Phase Ion-Pair Liquid Chromatography Analysis and Purification of Small Interfering RNA. *Anal. Biochem.* **2009**, *390*, 181–188. https://doi.org/10.1016/j.ab.2009.03.042.

(564) D'Alonzo, D.; Van Aerschot, A.; Guaragna, A.; Palumbo, G.; Schepers, G.; Capone, S.; Rozenski, J.; Herdewijn, P. Synthesis and Base Pairing Properties of 1',5'-Anhydro-L-Hexitol Nucleic Acids (L-HNA). *Chem. - Eur. J.* **2009**, *15*, 10121–10131. https://doi.org/10.1002/chem.200901847.

(565) Huang, M.; Xu, X.; Qiu, H.; Li, N. Analytical Characterization of DNA and RNA Oligonucleotides by Hydrophilic Interaction Liquid Chromatography-Tandem Mass Spectrometry. *J. Chromatogr. A* **2021**, *1648*, 462184. https://doi.org/10.1016/j.chroma.2021.462184.

(566) Kleparník, K.; Bocek, P. DNA Diagnostics by Capillary Electrophoresis. *Chem. Rev.* **2007**, *107*, 5279–5317. https://doi.org/10.1021/cr0101860.

(567) Voeten, R. L. C.; Ventouri, I. K.; Haselberg, R.; Somsen, G. W. Capillary Electrophoresis: Trends and Recent Advances. *Anal. Chem.* **2018**, *90*, 1464–1481. https://doi.org/10.1021/acs.analchem.8b00015.

(568) Galievsky, V. A.; Stasheuski, A. S.; Krylov, S. N. Capillary Electrophoresis for Quantitative Studies of Biomolecular Interactions. *Anal. Chem.* **2015**, *87*, 157–171. https://doi.org/10.1021/ac504219r.

(569) Harstad, R. K.; Johnson, A. C.; Weisenberger, M. M.; Bowser, M. T. Capillary Electrophoresis. *Anal. Chem.* **2016**, *88*, 299–319. https://doi.org/10.1021/acs.analchem.5b04125.

(570) Hernández-Borges, J.; Neusüß, C.; Cifuentes, A.; Pelzing, M. On-Line Capillary Electrophoresis-Mass Spectrometry for the Analysis of Biomolecules. *Electrophoresis* **2004**, *25*, 2257–2281. https://doi.org/10.1002/elps.200405954.

(571) Stolz, A.; Jooß, K.; Höcker, O.; Römer, J.; Schlecht, J.; Neusüß, C. Recent Advances in Capillary Electrophoresis-Mass Spectrometry: Instrumentation, Methodology and Applications. *Electrophoresis* **2019**, *40*, 79–112. https://doi.org/10.1002/elps.201800331.

(572) Durney, B. C.; Crihfield, C. L.; Holland, L. A. Capillary Electrophoresis Applied to DNA: Determining and Harnessing Sequence and Structure to Advance Bioanalyses (2009-2014). *Anal. Bioanal. Chem.* **2015**, *407*, 6923–6938. https://doi.org/10.1007/s00216-015-8703-5.

(573) Chen, B.; Bartlett, M. G. Determination of Therapeutic Oligonucleotides Using Capillary Gel Electrophoresis: Determination of Oligonucleotides Using CE. *Biomed. Chromatogr.* **2012**, *26*, 409–418. https://doi.org/10.1002/bmc.1696.

(574) van der Schans, M. J.; Kuypers, A. W. H. M.; Kloosterman, A. D.; Janssen, H. J. T.; Everaerts, F. M. Comparison of Resolution of Double-Stranded and Single-Stranded DNA in Capillary Electrophoresis. *J. Chromatogr. A* **1997**, *772*, 255–264. https://doi.org/10.1016/S0021-9673(97)00142-8.

(575) Wu, J.-F.; Chen, L.-X.; Luo, G.-A.; Liu, Y.-S.; Wang, Y.-M.; Jiang, Z.-H. Interaction Study between Double-Stranded DNA and Berberine Using Capillary Zone Electrophoresis. *J. Chromatogr. B Analyt. Technol. Biomed. Life. Sci.* **2006**, *833*, 158–164. https://doi.org/10.1016/j.jchromb.2006.01.028.

(576) Hamdan, I. I.; Skellern, G. G.; Waigh, R. D. Use of Capillary Electrophoresis in the Study of Ligand-DNA Interactions. *Nucleic Acids Res.* **1998**, *26*, 3053–3058. https://doi.org/10.1093/nar/26.12.3053.

(577) Růžička, M.; Čížková, M.; Jirásek, M.; Teplý, F.; Koval, D.; Kašička, V. Study of Deoxyribonucleic Acid-Ligand Interactions by Partial Filling Affinity Capillary Electrophoresis. *J. Chromatogr. A* **2014**, *1349*, 116–121. https://doi.org/10.1016/j.chroma.2014.04.061.

(578) Berezovski, M.; Krylov, S. N. Thermochemistry of Protein-DNA Interaction Studied with Temperature-Controlled Nonequilibrium Capillary Electrophoresis of Equilibrium Mixtures. *Anal. Chem.* **2005**, *77*, 1526–1529. https://doi.org/10.1021/ac048577c.

(579) Foteeva, L. S.; Matczuk, M.; Pawlak, K.; Aleksenko, S. S.; Nosenko, S. V.; Karandashev, V. K.; Jarosz, M.; Timerbaev, A. R. Combination of ICP-MS, Capillary Electrophoresis, and Their Hyphenation for Probing Ru(III) Metallodrug–DNA Interactions. *Anal. Bioanal. Chem.* **2017**, *409*, 2421–2427. https://doi.org/10.1007/s00216-017-0186-0.

(580) Artner, C.; Holtkamp, H. U.; Kandioller, W.; Hartinger, C. G.; Meier-Menches, S. M.; Keppler, B. K. DNA or Protein? Capillary Zone Electrophoresis–Mass Spectrometry Rapidly Elucidates Metallodrug Binding Selectivity. *Chem. Commun.* **2017**, *53*, 8002–8005. https://doi.org/10.1039/c7cc04582d.

(581) Bonvin, G.; Schappler, J.; Rudaz, S. Capillary Electrophoresis-Electrospray Ionization-Mass Spectrometry Interfaces: Fundamental Concepts and Technical Developments. *J. Chromatogr. A* **2012**, *1267*, 17–31. https://doi.org/10.1016/j.chroma.2012.07.019.

(582) Lindenburg, P. W.; Haselberg, R.; Rozing, G.; Ramautar, R. Developments in Interfacing Designs for CE–MS: Towards Enabling Tools for Proteomics and Metabolomics. *Chromatographia* **2015**, *78*, 367–377. https://doi.org/10.1007/s10337-014-2795-5.

(583) Przybylski, C.; Benito, J. M.; Bonnet, V.; Mellet, C. O.; García Fernández, J. M. Revealing Cooperative Binding of Polycationic Cyclodextrins with DNA Oligomers by Capillary Electrophoresis Coupled to Mass Spectrometry. *Anal. Chim. Acta* **2018**, *1002*, 70–81. https://doi.org/10.1016/j.aca.2017.11.034.

(584) Mironov, G. G.; Okhonin, V.; Khan, N.; Clouthier, C. M.; Berezovski, M. V. Conformational Dynamics of DNA G-Quadruplex in Solution Studied by Kinetic Capillary Electrophoresis Coupled On-Line with Mass Spectrometry. *ChemistryOpen* **2014**, *3*, 58–64. https://doi.org/10.1002/open.201400002.

(585) McLuckey, S. A. Principles of Collisional Activation in Analytical Mass Spectrometry. *J. Am. Soc. Mass Spectrom.* **1992**, *3*, 599–614. https://doi.org/10.1016/1044-0305(92)85001-Z.

(586) Vékey, K. Internal Energy Effects in Mass Spectrometry. *J. Mass Spectrom.* **1996**, *31*, 445–463. https://doi.org/10.1002/(sici)1096-9888(199605)31:5<445::aid-jms354>3.0.co;2-g.

(587) Gabelica, V.; Pauw, E. D. Internal Energy and Fragmentation of Ions Produced in Electrospray Sources. *Mass Spectrom. Rev.* **2005**, *24*, 566–587. https://doi.org/10.1002/mas.20027.

(588) Griffey, R. H.; Sannes-Lowery, K. A.; Drader, J. J.; Mohan, V.; Swayze, E. E.; Hofstadler, S. A. Characterization of Low-Affinity Complexes between RNA and Small Molecules Using Electrospray Ionization Mass Spectrometry. *J. Am. Chem. Soc.* **2000**, *122*, 9933–9938. https://doi.org/10.1021/ja0017108.

(589) Gabelica, V. Determination of Equilibrium Association Constants of Ligand–DNA Complexes by Electrospray Mass Spectrometry. In *Drug-DNA Interaction Protocols*; Fox, K. R., Ed.; Methods in Molecular Biology; Humana Press: Totowa, NJ, 2010; Vol. 613, p.89–101. https://doi.org/10.1007/978-1-60327-418-0_6.

(590) Gabelica, V.; Livet, S.; Rosu, F. Optimizing Native Ion Mobility Q-TOF in Helium and Nitrogen for Very Fragile Noncovalent Structures. *J. Am. Soc. Mass Spectrom.* **2018**, *29*, 2189–2198. https://doi.org/10.1007/s13361-018-2029-4.

(591) Casagrande, V.; Alvino, A.; Bianco, A.; Ortaggi, G.; Franceschin, M. Study of Binding Affinity and Selectivity of Perylene and Coronene Derivatives towards Duplex and Quadruplex DNA by ESI-MS. *J. Mass Spectrom.* **2009**, *44*, 530–540. https://doi.org/10.1002/jms.1529.

(592) Mazzitelli, C. L.; Brodbelt, J. S.; Kern, J. T.; Rodriguez, M.; Kerwin, S. M. Evaluation of Binding of Perylene Diimide and Benzannulated Perylene Diimide Ligands to Dna by Electrospray Ionization Mass Spectrometry. *J. Am. Soc. Mass Spectrom.* **2006**, *17*, 593–604. https://doi.org/10.1016/j.jasms.2005.12.011.

(593) Smith, S. I.; Guziec, L. J.; Guziec, F. S.; Hasinoff, B. B.; Brodbelt, J. S. Evaluation of Relative DNA Binding Affinities of Anthrapyrazoles by Electrospray Ionization Mass Spectrometry. *J. Mass Spectrom.* **2007**, *42*, 681–688. https://doi.org/10.1002/jms.1205.

(594) Liu, Y. Q.; Zheng, B.; Xu, X. J.; Yuan, G. Probing the Binding Affinity of Small-Molecule Natural Products to the G-Quadruplex in C-Myc Oncogene by Electrospray Ionization Mass Spectrometry. *Rapid Commun. Mass Spectrom.* **2010**, *24*, 3072–3075. https://doi.org/10.1002/rcm.4730.

(595) Chen, W.-H.; Qin, Y.; Cai, Z.; Chan, C.-L.; Luo, G.-A.; Jiang, Z.-H. Spectrometric Studies of Cytotoxic Protoberberine Alkaloids Binding to Double-Stranded DNA. *Bioorg. Med. Chem.* **2005**, *13*, 1859–1866. https://doi.org/10.1016/j.bmc.2004.10.049.

(596) Wan, C.; Cui, M.; Song, F.; Liu, Z.; Liu, S. A Study of the Non-Covalent Interaction between Flavonoids and DNA Triplexes by Electrospray Ionization Mass Spectrometry. *Int. J. Mass Spectrom.* **2009**, *283*, 48–55. https://doi.org/10.1016/j.ijms.2009.01.007.

(597) Smith, S. I.; Brodbelt, J. S. Rapid Characterization of Cross-Links, Mono-Adducts, and Non-Covalent Binding of Psoralens to Deoxyoligonucleotides by LC-UV/ESI-MS and IRMPD Mass Spectrometry. *Analyst* **2010**, *135*, 943–952. https://doi.org/10.1039/B924023C.

(598) Wang, Z.; Guo, X.; Liu, Z.; Cui, M.; Song, F.; Liu, S. Studies on Alkaloids Binding to GC-Rich Human Survivin Promoter DNA Using Positive and Negative Ion Electrospray Ionization Mass Spectrometry. *J. Mass Spectrom.* **2008**, *43*, 327–335. https://doi.org/10.1002/jms.1320.

(599) Carrasco, C.; Rosu, F.; Gabelica, V.; Houssier, C.; De Pauw, E.; Garbay-Jaureguiberry, C.; Roques, B.; Wilson, W. D.; Chaires, J. B.; Waring, M. J.; et al. Tight Binding of the Antitumor Drug Ditercalinium to Quadruplex DNA. *Chembiochem* **2002**, *3*, 1235–1241. https://doi.org/10.1002/1439-7633(20021202)3:12<1235::aid-cbic1235>3.0.co;2-i.

(600) Bligh, S. W. A.; Haley, T.; Lowe, P. N. Measurement of Dissociation Constants of Inhibitors Binding to Src SH2 Domain Protein by Non-Covalent Electrospray Ionization Mass Spectrometry. *J. Mol. Recognit.* **2003**, *16*, 139–148. https://doi.org/10.1002/jmr.622.

(601) Li, M.; E. Duc, A.-C.; Klosi, E.; Pattabiraman, S.; Spaller, M. R.; Chow, C. S. Selection of Peptides That Target the Aminoacyl-TRNA Site of Bacterial 16S Ribosomal RNA. *Biochemistry* **2009**, *48*, 8299–8311. https://doi.org/10.1021/bi900982t.

(602) Kaur, M.; Rupasinghe, C. N.; Klosi, E.; Spaller, M. R.; Chow, C. S. Selection of Heptapeptides That Bind Helix 69 of Bacterial 23S Ribosomal RNA. *Bioorg. Med. Chem.* **2013**, *21*, 1240–1247. https://doi.org/10.1016/j.bmc.2012.12.048.

(603) Sakakibara, Y.; Abeysirigunawardena, S. C.; Duc, A.-C. E.; Dremann, D. N.; Chow, C. S. Ligand- and PH-Induced Conformational Changes of RNA Domain Helix 69 Revealed by 2-Aminopurine Fluorescence. *Angew. Chem. Int. Ed.* **2012**, *51*, 12095–12098. https://doi.org/10.1002/anie.201206000.

(604) Dremann, D. N.; Chow, C. S. The Use of Electrospray Ionization Mass Spectrometry to Monitor RNA-Ligand Interactions. *Methods Enzym.* **2019**, *623*, 315–337. https://doi.org/10.1016/bs.mie.2019.05.013.

(605) Dremann, D. N.; Chow, C. S. The Development of Peptide Ligands That Target Helix 69 RRNA of Bacterial Ribosomes. *Bioorg. Med. Chem.* **2016**, *24*, 4486–4491. https://doi.org/10.1016/j.bmc.2016.07.050.

(606) Guittat, L.; Alberti, P.; Rosu, F.; Van Miert, S.; Thetiot, E.; Pieters, L.; Gabelica, V.; De Pauw, E.; Ottaviani, A.; Riou, J.-F.; et al. Interactions of Cryptolepine and Neocryptolepine with Unusual DNA Structures. *Biochimie* **2003**, *85*, 535–547. https://doi.org/10.1016/s0300-9084(03)00035-x.

(607) Rosu, F.; De Pauw, E.; Guittat, L.; Alberti, P.; Lacroix, L.; Mailliet, P.; Riou, J.-F.; Mergny, J.-L. Selective Interaction of Ethidium Derivatives with Quadruplexes: An Equilibrium Dialysis and Electrospray Ionization Mass Spectrometry Analysis. *Biochemistry* **2003**, *42*, 10361–10371. https://doi.org/10.1021/bi034531m.

(608) Collie, G.; Reszka, A. P.; Haider, S. M.; Gabelica, V.; Parkinson, G. N.; Neidle, S. Selectivity in Small Molecule Binding to Human Telomeric RNA and DNA Quadruplexes. *Chem. Commun.* **2009**, No. 48, 7482–7484. https://doi.org/10.1039/b901889a.

(609) Rosu, F.; Gabelica, V.; Houssier, C.; De Pauw, E. Determination of Affinity, Stoichiometry and Sequence Selectivity of Minor Groove Binder Complexes with Double-stranded Oligodeoxynucleotides by Electrospray Ionization Mass Spectrometry. *Nucleic Acids Res.* **2002**, *30*, e82. https://doi.org/10.1093/nar/gnf081.

(610) Rosu, F.; Gabelica, V.; Pauw, E. D.; Mailliet, P.; Mergny, J.-L. Cooperative 2:1 Binding of a Bisphenothiazine to Duplex DNA. *ChemBioChem* **2008**, *9*, 849–852. https://doi.org/10.1002/cbic.200700572.

(611) Sannes-Lowery, K. A.; Griffey, R. H.; Hofstadler, S. A. Measuring Dissociation Constants of RNA and Aminoglycoside Antibiotics by Electrospray Ionization Mass Spectrometry. *Anal Biochem* **2000**, *280*, 264–271. https://doi.org/10.1006/abio.2000.4550.

(612) Sannes-Lowery, K. A.; Drader, J. J.; Griffey, R. H.; Hofstadler, S. A. Fourier Transform Ion Cyclotron Resonance Mass Spectrometry as a High Throughput Affinity Screen to Identify RNA Binding Ligands. *TrAC Trends Anal. Chem.* **2000**, *19*, 481–491. https://doi.org/10.1016/s0165-9936(00)00029-7.

(613) Kuzmic, P. Program DYNAFIT for the Analysis of Enzyme Kinetic Data: Application to HIV Proteinase. *Anal Biochem* **1996**, *237*, 260–273.

(614) Kuzmič, P. DynaFit—A Software Package for Enzymology. In *Computer Methods Part B*; Johnson, M. L., Brand, L., Eds.; Methods in Enzymology; Academic Press: San Diego, California, USA, 2009; Vol. 467, p.247–280. https://doi.org/10.1016/S0076-6879(09)67010-5.

(615) Marchand, A.; Strzelecka, D.; Gabelica, V. Selective and Cooperative Ligand Binding to Antiparallel Human Telomeric DNA G-Quadruplexes. *Chem. - Eur. J.* **2016**, *22*, 9551–9555. https://doi.org/10.1002/chem.201601937.

(616) Hong, E. S.; Yoon, H.-J.; Kim, B.; Yim, Y.-H.; So, H.-Y.; Shin, S. K. Mass Spectrometric Studies of Alkali Metal Ion Binding on Thrombin-Binding Aptamer DNA. *J. Am. Soc. Mass Spectrom.* **2010**, *21*, 1245–1255. https://doi.org/10.1016/j.jasms.2010.03.035.

(617) Sannes-Lowery, K. A.; Cummins, L. L.; Chen, S.; Drader, J. J.; Hofstadler, S. A. High Throughput Drug Discovery with ESI-FTICR. *Drug Discov.* **2004**, *238*, 197–206. https://doi.org/10.1016/j.ijms.2004.04.018.

(618) Scatchard, G. The Attractions of Proteins for Small Molecules and Ions. *Ann. N. Y. Acad. Sci.* **1949**, *51*, 660–672.

https://doi.org/10.1111/j.1749-6632.1949.tb27297.x.

(619) Kapur, A.; Beck, J. L.; Brown, S. E.; Dixon, N. E.; Sheil, M. M. Use of Electrospray Ionization Mass Spectrometry to Study Binding Interactions between a Replication Terminator Protein and DNA. *Protein Sci.* **2002**, *11*, 147–157. https://doi.org/20101001074140772.

(620) Wilcox, J. M.; Rempel, D. L.; Gross, M. L. Method of Measuring Oligonucleotide−Metal Affinities: Interactions of the Thrombin Binding Aptamer with K+ and Sr2+. *Anal. Chem.* **2008**, *80*, 2365–2371. https://doi.org/10.1021/ac701903w.

(621) Chingin, K.; Barylyuk, K. Charge-State-Dependent Variation of Signal Intensity Ratio between Unbound Protein and Protein–Ligand Complex in Electrospray Ionization Mass Spectrometry: The Role of Solvent-Accessible Surface Area. *Anal. Chem.* **2018**, *90*, 5521–5528. https://doi.org/10.1021/acs.analchem.7b05349.

(622) Gabelica, V.; Galic, N.; Rosu, F.; Houssier, C.; Pauw, E. D. Influence of Response Factors on Determining Equilibrium Association Constants of Non-Covalent Complexes by Electrospray Ionization Mass Spectrometry. *J. Mass Spectrom.* **2003**, *38*, 491–501. https://doi.org/10.1002/jms.459.

(623) Barylyuk, K.; Gulbakan, B.; Xie, X.; Zenobi, R. DNA Oligonucleotides: A Model System with Tunable Binding Strength to Study Monomer-Dimer Equilibria with Electrospray Ionization-Mass Spectrometry. *Anal. Chem.* **2013**, *85*, 11902–11912. https://doi.org/10.1021/ac402669e.

(624) Gabelica, V.; Rosu, F.; De Pauw, E. A Simple Method to Determine Electrospray Response Factors of Noncovalent Complexes. *Anal. Chem.* **2009**, *81*, 6708–6715. https://doi.org/10.1021/ac900785m.

(625) Gabelica, V.; Maeda, R.; Fujimoto, T.; Yaku, H.; Murashima, T.; Sugimoto, N.; Miyoshi, D. Multiple and Cooperative Binding of Fluorescence Light-up Probe Thioflavin T with Human Telomere DNA G-Quadruplex. *Biochemistry* **2013**, *52*, 5620–5628. https://doi.org/10.1021/bi4006072.

(626) Shcherbakova, I.; Mitra, S.; Laederach, A.; Brenowitz, M. Energy Barriers, Pathways, and Dynamics during Folding of Large, Multidomain RNAs. *Curr. Opin. Chem. Biol.* **2008**, *12*, 655–666. https://doi.org/10.1016/j.cbpa.2008.09.017.

(627) Šponer, J.; Bussi, G.; Stadlbauer, P.; Kührová, P.; Banáš, P.; Islam, B.; Haider, S.; Neidle, S.; Otyepka, M. Folding of Guanine Quadruplex Molecules–Funnel-like Mechanism or Kinetic Partitioning? An Overview from MD Simulation Studies. *Biochim. Biophys. Acta BBA - Gen. Subj.* **2017**, *1861*, 1246–1263. https://doi.org/10.1016/j.bbagen.2016.12.008.

(628) Rosu, F.; Gabelica, V.; Shin-ya, K.; De Pauw, E. Telomestatin-Induced Stabilization of the Human Telomeric DNA Quadruplex Monitored by Electrospray Mass Spectrometry. *Chem. Commun.* **2003**, No. 21, 2702–2703. https://doi.org/10.1039/b309394h.

(629) Borbone, N.; Amato, J.; Oliviero, G.; D'Atri, V.; Gabelica, V.; De Pauw, E.; Piccialli, G.; Mayol, L. D(CGGTGGT) Forms an Octameric Parallel G-Quadruplex via Stacking of Unusual G(:C):G(:C):G(:C):G(:C) Octads. *Nucleic Acids Res.* **2011**, *39*, 7848–7857. https://doi.org/10.1093/nar/gkr489.

(630) Romanucci, V.; Marchand, A.; Mendoza, O.; D'Alonzo, D.; Zarrelli, A.; Gabelica, V.; Di Fabio, G. Kinetic ESI-MS Studies of Potent Anti-HIV Aptamers Based on the G-Quadruplex Forming Sequence d(TGGGAG). *ACS Med. Chem. Lett.* **2016**, *7*, 256–260. https://doi.org/10.1021/acsmedchemlett.5b00408.

(631) Lento, C.; Wilson, D. J. Unravelling the Mysteries of Sub-Second Biochemical Processes Using Time-Resolved Mass Spectrometry. *Analyst* **2017**, *142*, 1640–1653. https://doi.org/10.1039/C7AN00338B.

(632) Marchand, A.; Czar, M. F.; Eggel, E. N.; Kaeslin, J.; Zenobi, R. Studying Biomolecular Folding and Binding Using Temperature-Jump Mass Spectrometry. *Nat. Commun.* **2020**, *11*, 566. https://doi.org/10.1038/s41467-019-14179-x.

(633) Benesch, J. L. P.; Sobott, F.; Robinson, C. V. Thermal Dissociation of Multimeric Protein Complexes by Using Nanoelectrospray Mass Spectrometry. *Anal. Chem.* **2003**, *75*, 2208–2214. https://doi.org/10.1021/ac034132x.

(634) Wang, G.; Abzalimov, R. R.; Kaltashov, I. A. Direct Monitoring of Heat-Stressed Biopolymers with Temperature-Controlled Electrospray Ionization Mass Spectrometry. *Anal. Chem.* **2011**, *83*, 2870–2876. https://doi.org/10.1021/ac200441a.

(635) El-Baba, T. J.; Woodall, D. W.; Raab, S. A.; Fuller, D. R.; Laganowsky, A.; Russell, D. H.; Clemmer, D. E. Melting Proteins: Evidence for Multiple Stable Structures upon Thermal Denaturation of Native Ubiquitin from Ion Mobility Spectrometry-Mass Spectrometry Measurements. *J. Am. Chem. Soc.* **2017**, *139*, 6306–6309. https://doi.org/10.1021/jacs.7b02774.

(636) Lippens, J. L.; Mangrum, J. B.; McIntyre, W.; Redick, B.; Fabris, D. A Simple Heated-Capillary Modification Improves the Analysis of Non-Covalent Complexes by Z-Spray Electrospray Ionization. *Rapid Commun Mass Spectrom* **2016**, *30*, 773–783. https://doi.org/10.1002/rcm.7490.

(637) Hommersom, B.; Porta, T.; Heeren, R. M. A. Ion Mobility Spectrometry Reveals Intermediate States in Temperature-Resolved DNA

Unfolding. *Int. J. Mass Spectrom.* **2017**, *419*, 52–55. https://doi.org/10.1016/j.ijms.2017.03.008.

(638) Marchand, A.; Rosu, F.; Zenobi, R.; Gabelica, V. Thermal Denaturation of DNA G-Quadruplexes and Their Complexes with Ligands: Thermodynamic Analysis of the Multiple States Revealed by Mass Spectrometry. *J. Am. Chem. Soc.* **2018**, *140*, 12553–12565. https://doi.org/10.1021/jacs.8b07302.

(639) Pruška, A.; Marchand, A.; Zenobi, R. Novel Insight into Proximal DNA Domain Interactions from Temperature-Controlled Electrospray Ionization Mass Spectrometry. *Angew. Chem. Int. Ed Engl.* **2021**, *60*, 15390–15398. https://doi.org/10.1002/anie.202016757.

(640) McLuckey, S. A.; Habibi-Goudarzi, S. Decompositions of Multiply Charged Oligonucleotide Anions. *J. Am. Chem. Soc.* **1993**, *115*, 12085–12095. https://doi.org/10.1021/ja00078a054.

(641) Wu, J.; McLuckey, S. A. Gas-Phase Fragmentation of Oligonucleotide Ions. *Int. J. Mass Spectrom.* **2004**, *237*, 197–241. https://doi.org/10.1016/j.ijms.2004.06.014.

(642) Griffey, R. H.; Greig, M. J. Detection of Base Pair Mismatches in Duplex DNA and RNA Oligonucleotides Using Electrospray Mass Spectrometry. *ProcSPIE-IntSocOptEng* **1997**, *2985*, 82–86.

(643) Baer, T.; Mayer, P. M. Statistical Rice-Ramsperger-Kassel-Marcus Quasiequilibrium Theory Calculations in Mass Spectrometry. *J. Am. Soc. Mass Spectrom.* **1997**, *8*, 103–115. https://doi.org/10.1016/S1044-0305(96)00212-7.

(644) Eyler, J. R. Infrared Multiple Photon Dissociation Spectroscopy of Ions in Penning Traps. *Mass Spectrom. Rev.* **2009**, *28*, 448–467. https://doi.org/10.1002/mas.20217.

(645) Dunbar, R. C. BIRD (Blackbody Infrared Radiative Dissociation): Evolution, Principles, and Applications. *Mass Spectrom. Rev.* **2004**, *23*, 127–158. https://doi.org/10.1002/mas.10074.

(646) Klassen, J. S.; Schnier, P. D.; Williams, E. R. Blackbody Infrared Radiative Dissociation of Oligonucleotide Anions. *J. Am. Soc. Mass Spectrom.* **1998**, *9*, 1117–1124. https://doi.org/10.1016/S1044-0305(98)00098-1.

(647) Schnier, P. D.; Klassen, J. S.; Strittmatter, E. F.; Williams, E. R. Activation Energies for Dissociation of Double Strand Oligonucleotide Anions: Evidence for Watson−Crick Base Pairing in Vacuo. *J. Am. Chem. Soc.* **1998**, *120*, 9605–9613. https://doi.org/10.1021/ja973534h.

(648) Hakansson, K.; Hudgins, R. R.; Marshall, A. G.; O'Hair, R. A. Electron Capture Dissociation and Infrared Multiphoton Dissociation of Oligodeoxynucleotide Dications. *J. Am. Soc. Mass Spectrom.* **2003**, *14*, 23–41. https://doi.org/10.1016/s1044-0305(02)00708-0.

(649) Schultz, K. N.; Hakansson, K. Rapid Electron Capture Dissociation of Mass-Selectively Accumulated Oligodeoxynucleotide Dications. *Int. J. Mass Spectrom.* **2004**, *234*, 123–130. https://doi.org/10.1016/j.ijms.2004.02.019.

(650) Smith, S. I.; Brodbelt, J. S. Electron Transfer Dissociation of Oligonucleotide Cations. *Int. J. Mass Spectrom.* **2009**, *283*, 85–93. https://doi.org/10.1016/j.ijms.2009.02.012.

(651) Yang, J.; Hakansson, K. Fragmentation of Oligoribonucleotides from Gas-Phase Ion-Electron Reactions. *J. Am. Soc. Mass Spectrom.* **2006**, *17*, 1369–1375. https://doi.org/10.1016/j.jasms.2006.05.006.

(652) Kinet, C.; Gabelica, V.; Balbeur, D.; De Pauw, E. Electron Detachment Dissociation (EDD) Pathways in Oligonucleotides. *Int. J. Mass Spectrom.* **2009**, *283*, 206–213. https://doi.org/10.1016/j.ijms.2009.03.012.

(653) Gao, Y.; McLuckey, S. A. Electron Transfer Followed by Collision-Induced Dissociation (NET-CID) for Generating Sequence Information from Backbone-Modified Oligonucleotide Anions. *Rapid Commun. Mass Spectrom.* **2013**, *27*, 249–257. https://doi.org/10.1002/rcm.6428.

(654) Peters-Clarke, T. M.; Quan, Q.; Brademan, D. R.; Hebert, A. S.; Westphall, M. S.; Coon, J. J. Ribonucleic Acid Sequence Characterization by Negative Electron Transfer Dissociation Mass Spectrometry. *Anal. Chem.* **2020**, *92*, 4436–4444. https://doi.org/10.1021/acs.analchem.9b05388.

(655) Gabelica, V.; Rosu, F.; Pauw, E.; Antoine, R.; Tabarin, T.; Broyer, M.; Dugourd, P. Electron Photodetachment Dissociation of DNA Anions with Covalently or Noncovalently Bound Chromophores. *J. Am. Soc. Mass Spectrom.* **2007**, *18*, 1990–2000. https://doi.org/10.1016/j.jasms.2007.08.007.

(656) Mo, J.; Hakansson, K. Characterization of Nucleic Acid Higher Order Structure by High-Resolution Tandem Mass Spectrometry. *Anal. Bioanal. Chem.* **2006**, *386*, 675–681. https://doi.org/10.1007/s00216-006-0614-z.

(657) Cuervo, A.; Dans, P. D.; Carrascosa, J. L.; Orozco, M.; Gomila, G.; Fumagalli, L. Direct Measurement of the Dielectric Polarization Properties of DNA. *Proc. Natl. Acad. Sci.* **2014**, *111*, E3624–E3630. https://doi.org/10.1073/pnas.1405702111.

(658) Vusurovic, J.; Breuker, K. Relative Strength of Noncovalent Interactions and Covalent Backbone Bonds in RNA-Peptide Complexes. *Anal Chem* **2019**, *91*, 1659–1664. https://doi.org/10.1021/acs.analchem.8b05387.

(659) Schneeberger, E.-M.; Breuker, K. Native Top-Down Mass Spectrometry of TAR RNA in Complexes with a Wild-Type Tat Peptide for

Binding Site Mapping. *Angew. Chem. Int. Ed.* **2017**, *56*, 1254–1258. https://doi.org/10.1002/anie.201610836.

(660) Paul, D.; Marchand, A.; Verga, D.; Teulade-Fichou, M.-P.; Bombard, S.; Rosu, F.; Gabelica, V. Probing Ligand and Cation Binding Sites in G-Quadruplex Nucleic Acids by Mass Spectrometry and Electron Photodetachment Dissociation Sequencing. *The Analyst* **2019**, *144*, 3518–3524. https://doi.org/10.1039/c9an00398c.

(661) Janin, J. Ångströms and Calories. *Structure* **1997**, *5*, 473–479. https://doi.org/10.1016/S0969-2126(97)00204-9.

(662) Campbell, S.; Rodgers, M. T.; Marzluff, E. M.; Beauchamp, J. L. Deuterium Exchange Reactions as a Probe of Biomolecule Structure. Fundamental Studies of Gas Phase H/D Exchange Reactions of Protonated Glycine Oligomers with D2O, CD3OD, CD3CO2D, and ND3. *J. Am. Chem. Soc.* **1995**, *117*, 12840–12854. https://doi.org/10.1021/ja00156a023.

(663) Hofstadler, S. A.; Sannes-Lowery, K. A.; Griffey, R. H. Enhanced Gas-Phase Hydrogen–Deuterium Exchange of Oligonucleotide and Protein Ions Stored in an External Multipole Ion Reservoir. *J. Mass Spectrom.* **2000**, *35*, 62–70. https://doi.org/10.1002/(sici)1096-9888(200001)35:1<62::aid-jms913>3.0.co;2-9.

(664) Wyttenbach, T.; Bowers, M. T. Gas Phase Conformations of Biological Molecules: The Hydrogen/Deuterium Exchange Mechanism. *J. Am. Soc. Mass Spectrom.* **1999**, *10*, 9–14. https://doi.org/10.1016/S1044-0305(98)00121-4.

(665) Robinson, E. W.; Williams, E. R. Multidimensional Separations of Ubiquitin Conformers in the Gas Phase: Relating Ion Cross Sections to H/D Exchange Measurements. *J. Am. Soc. Mass Spectrom.* **2005**, *16*, 1427–1437. https://doi.org/10.1016/j.jasms.2005.04.007.

(666) Balbeur, D.; Dehareng, D.; De Pauw, E. Conformationally Driven Gas-Phase H/D Exchange of Dinucleotide Negative Ions. *J. Am. Soc. Mass Spectrom.* **2007**, *18*, 1827–1834. https://doi.org/10.1016/j.jasms.2007.07.014.

(667) Chipuk, J. E.; Brodbelt, J. S. Gas-Phase Hydrogen/Deuterium Exchange of Dinucleotides and 5′-Monophosphate Dinucleotides in a Quadrupole Ion Trap. *Int. J. Mass Spectrom.* **2009**, *287*, 87–95. https://doi.org/10.1016/j.ijms.2008.09.011.

(668) Mo, J.; Håkansson, K. Oligonucleotide Gas-Phase Hydrogen/Deuterium Exchange with D2S in the Collision Cell of a Quadrupole-Fourier Transform Ion Cyclotron Resonance Mass Spectrometer. *Anal. Chem.* **2007**, *79*, 7893–7898. https://doi.org/10.1021/ac0713095.

(669) Mo, J.; Todd, G. C.; Håkansson, K. Characterization of Nucleic Acid Higher Order Structure by Gas-Phase H/D Exchange in a Quadrupole-FT-ICR Mass Spectrometer. *Biopolymers* **2009**, *91*, 256–264. https://doi.org/10.1002/bip.21134.

(670) Vairamani, M.; Gross, M. L. G-Quadruplex Formation of Thrombin-Binding Aptamer Detected by Electrospray Ionization Mass Spectrometry. *J. Am. Chem. Soc.* **2003**, *125*, 42–43. https://doi.org/10.1021/ja0284299.

(671) Gabelica, V.; Rosu, F.; Witt, M.; Baykut, G.; Pauw, E. D. Fast Gas-Phase Hydrogen/Deuterium Exchange Observed for a DNA G-Quadruplex. *Rapid Commun. Mass Spectrom.* **2005**, *19*, 201–208. https://doi.org/10.1002/rcm.1772.

(672) Williams, E. R. Proton Transfer Reactivity of Large Multiply Charged Ions. *J. Mass Spectrom.* **1996**, *31*, 831–842. https://doi.org/10.1002/(sici)1096-9888(199608)31:8<831::aid-jms392>3.0.co;2-7.

(673) Kharlamova, A.; Prentice, B. M.; Huang, T.-Y.; McLuckey, S. A. Electrospray Droplet Exposure to Gaseous Acids for the Manipulation of Protein Charge State Distributions. *Anal. Chem.* **2010**, *82*, 7422–7429. https://doi.org/10.1021/ac101578q.

(674) Kharlamova, A.; McLuckey, S. A. Negative Electrospray Droplet Exposure to Gaseous Bases for the Manipulation of Protein Charge State Distributions. *Anal. Chem.* **2011**, *83*, 431–437. https://doi.org/10.1021/ac1027319.

(675) Czar, M. F.; Marchand, A.; Zenobi, R. A Modified Traveling Wave Ion Mobility Mass Spectrometer as a Versatile Platform for Gas-Phase Ion–Molecule Reactions. *Anal. Chem.* **2019**, *91*, 6624–6631. https://doi.org/10.1021/acs.analchem.9b00541.

(676) Nonose, S.; Yamashita, K.; Okamura, T.; Fukase, S.; Kawashima, M.; Sudo, A.; Isono, H. Conformations of Disulfide-Intact and -Reduced Lysozyme Ions Probed by Proton-Transfer Reactions at Various Temperatures. *J. Phys. Chem. B* **2014**, *118*, 9651–9661. https://doi.org/10.1021/jp505621f.

(677) Danell, A. S.; Parks, J. H. Fraying and Electron Autodetachment Dynamics of Trapped Gas Phase Oligonucleotides. *J. Am. Soc. Mass Spectrom.* **2003**, *14*, 1330–1339. https://doi.org/10.1016/s1044-0305(03)00578-6.

(678) McLuckey, S. A.; Stephenson, J. L. Ion/Ion Chemistry of High-Mass Multiply Charged Ions. *Mass Spectrom. Rev.* **1998**, *17*, 369–407. https://doi.org/10.1002/(sici)1098-2787(1998)17:6<369::aid-mas1>3.0.co;2-j.

(679) Herron, W. J.; Goeringer, D. E.; McLuckey, S. A. Ion-Ion Reactions in the Gas Phase: Proton Transfer Reactions of Protonated Pyridine with Multiply Charged Oligonucleotide Anions. *J. Am. Soc. Mass Spectrom.* **1995**, *6*, 529–532.

https://doi.org/10.1016/1044-0305(95)00199-N.

(680) McLuckey, S. A.; Wu, J.; Bundy, J. L.; Stephenson, J. L.; Hurst, G. B. Oligonucleotide Mixture Analysis via Electrospray and Ion/Ion Reactions in a Quadrupole Ion Trap. *Anal. Chem.* **2002**, *74*, 976–984. https://doi.org/10.1021/ac011015y.

(681) Huang, T.-Y.; Liu, J.; McLuckey, S. A. Top-down Tandem Mass Spectrometry of TRNA via Ion Trap Collision-Induced Dissociation. *J. Am. Soc. Mass Spectrom.* **2010**, *21*, 890–898. https://doi.org/10.1016/j.jasms.2009.12.007.

(682) Turner, K. B.; Monti, S. A.; Fabris, D. Like Polarity Ion/Ion Reactions Enable the Investigation of Specific Metal Interactions in Nucleic Acids and Their Noncovalent Assemblies. *J. Am. Chem. Soc.* **2008**, *130*, 13353–13363. https://doi.org/10.1021/ja8045734.

(683) Clemmer, D. E.; Jarrold, M. F. Ion Mobility Measurements and Their Applications to Clusters and Biomolecules. *J. Mass Spectrom.* **1997**, *32*, 577–592. https://doi.org/10.1002/(sici)1096-9888(199706)32:6<577::aid-jms530>3.0.co;2-4.

(684) Bohrer, B. C.; Merenbloom, S. I.; Koeniger, S. L.; Hilderbrand, A. E.; Clemmer, D. E. Biomolecule Analysis by Ion Mobility Spectrometry. *Annu. Rev. Anal. Chem. Palo Alto Calif* **2008**, *1*, 293–327. https://doi.org/10.1146/annurev.anchem.1.031207.113001.

(685) Wyttenbach, T.; Pierson, N. A.; Clemmer, D. E.; Bowers, M. T. Ion Mobility Analysis of Molecular Dynamics. *Annu. Rev. Phys. Chem.* **2014**, *65*, 175–196. https://doi.org/10.1146/annurev-physchem-040513-103644.

(686) Gabelica, V.; Shvartsburg, A. A.; Afonso, C.; Barran, P.; Benesch, J. L. P.; Bleiholder, C.; Bowers, M. T.; Bilbao, A.; Bush, M. F.; Campbell, J. L.; et al. Recommendations for Reporting Ion Mobility Mass Spectrometry Measurements. *Mass Spectrom. Rev.* **2019**, *38*, 291–320. https://doi.org/10.1002/mas.21585.

(687) Giles, K.; Pringle, S. D.; Worthington, K. R.; Little, D.; Wildgoose, J. L.; Bateman, R. H. Applications of a Travelling Wave-Based Radio-Frequency-Only Stacked Ring Ion Guide. *Rapid Commun. Mass Spectrom.* **2004**, *18*, 2401–2414. https://doi.org/10.1002/rcm.1641.

(688) Fernandez-Lima, F.; Kaplan, D. A.; Suetering, J.; Park, M. A. Gas-Phase Separation Using a Trapped Ion Mobility Spectrometer. *Int. J. Ion Mobil. Spectrom.* **2011**, *14*, 93–98. https://doi.org/10.1007/s12127-011-0067-8.

(689) Ruotolo, B. T.; Benesch, J. L. P.; Sandercock, A. M.; Hyung, S.-J.; Robinson, C. V. Ion Mobility-Mass Spectrometry Analysis of Large Protein Complexes. *Nat. Protoc.* **2008**, *3*, 1139–1152. https://doi.org/10.1038/nprot.2008.78.

(690) Marchand, A.; Livet, S.; Rosu, F.; Gabelica, V. Drift Tube Ion Mobility: How to Reconstruct Collision Cross Section Distributions from Arrival Time Distributions? *Anal. Chem.* **2017**, *89*, 12674–12681. https://doi.org/10.1021/acs.analchem.7b01736.

(691) Poyer, S.; Comby-Zerbino, C.; Choi, C. M.; MacAleese, L.; Deo, C.; Bogliotti, N.; Xie, J.; Salpin, J.-Y.; Dugourd, P.; Chirot, F. Conformational Dynamics in Ion Mobility Data. *Anal. Chem.* **2017**, *89*, 4230–4237. https://doi.org/10.1021/acs.analchem.7b00281.

(692) Gidden, J.; Bowers, M. T. Gas-Phase Conformations of Deprotonated Trinucleotides (DGTT - , DTGT - , and DTTG -): The Question of Zwitterion Formation. *J. Am. Soc. Mass Spectrom.* **2003**, *14*, 161–170. https://doi.org/10.1016/s1044-0305(02)00866-8.

(693) Daly, S.; Porrini, M.; Rosu, F.; Gabelica, V. Electronic Spectroscopy of Isolated DNA Polyanions. *Faraday Discuss.* **2019**, *217*, 361–382. https://doi.org/10.1039/c8fd00207j.

(694) Hoaglund, C. S.; Liu, Y.; Ellington, A. D.; Pagel, M.; Clemmer, D. E. Gas-Phase DNA: Oligothymidine Ion Conformers. *J. Am. Chem. Soc.* **1997**, *119*, 9051–9052. https://doi.org/10.1021/ja970652w.

(695) Arcella, A.; Dreyer, J.; Ippoliti, E.; Ivani, I.; Portella, G.; Gabelica, V.; Carloni, P.; Orozco, M. Structure and Dynamics of Oligonucleotides in the Gas Phase. *Angew. Chem. Int. Ed.* **2015**, *54*, 467–471. https://doi.org/10.1002/anie.201406910.

(696) Baker, E. S.; Dupuis, N. F.; Bowers, M. T. DNA Hairpin, Pseudoknot, and Cruciform Stability in a Solvent-Free Environment. *J. Phys. Chem. B* **2009**, *113*, 1722–1727. https://doi.org/10.1021/jp807529m.

(697) Abi-Ghanem, J.; Rabin, C.; Porrini, M.; Rosu, F.; Gabelica, V. Compaction of RNA Hairpins and Their Kissing Complexes in Native Electrospray Mass Spectrometry. *J. Am. Soc. Mass Spectrom.* **2020**, *31*, 2035–2043. https://doi.org/10.1021/jasms.0c00060.

(698) Gidden, J.; Ferzoco, A.; Baker, E. S.; Bowers, M. T. Duplex Formation and the Onset of Helicity in Poly d(CG)n Oligonucleotides in a Solvent-Free Environment. *J. Am. Chem. Soc.* **2004**, *126*, 15132–15140. https://doi.org/10.1021/ja046433+.

(699) Baker, E. S.; Bowers, M. T. B-DNA Helix Stability in a Solvent-Free Environment. *J. Am. Soc. Mass Spectrom.* **2007**, *18*, 1188–1195. https://doi.org/10.1016/j.jasms.2007.03.001.

(700) Gidden, J.; Baker, E. S.; Ferzoco, A.; Bowers, M. T. Structural Motifs of DNA Complexes in the Gas Phase. *Int. J. Mass Spectrom.* **2005**, *240*, 183–193. https://doi.org/10.1016/j.ijms.2004.09.011.

(701) Porrini, M.; Rosu, F.; Rabin, C.; Darré, L.; Gómez, H.; Orozco, M.; Gabelica, V. Compaction of Duplex Nucleic Acids upon Native Electrospray Mass Spectrometry. *ACS Cent. Sci.* **2017**, *3*, 454–461. https://doi.org/10.1021/acscentsci.7b00084.

(702) Burmistrova, A.; Gabelica, V.; Duwez, A.-S.; De Pauw, E. Ion Mobility Spectrometry Reveals Duplex DNA Dissociation Intermediates. *J. Am. Soc. Mass Spectrom.* **2013**, *24*, 1777–1786. https://doi.org/10.1007/s13361-013-0721-y.

(703) Butcher, D.; Chapagain, P.; Leng, F.; Fernandez-Lima, F. Differentiating Parallel and Antiparallel DNA Duplexes in the Gas Phase Using Trapped Ion Mobility Spectrometry. *J. Phys. Chem. B* **2018**, *122*, 6855–6861. https://doi.org/10.1021/acs.jpcb.7b12544.

(704) Arcella, A.; Portella, G.; Ruiz, M. L.; Eritja, R.; Vilaseca, M.; Gabelica, V.; Orozco, M. Structure of Triplex DNA in the Gas Phase. *J. Am. Chem. Soc.* **2012**, *134*, 6596–6606. https://doi.org/10.1021/ja209786t.

(705) Li, J.; Begbie, A.; Boehm, B. J.; Button, A.; Whidborne, C.; Pouferis, Y.; Huang, D. M.; Pukala, T. L. Ion Mobility-Mass Spectrometry Reveals Details of Formation and Structure for GAA·TCC DNA and RNA Triplexes. *J. Am. Soc. Mass Spectrom.* **2019**, *30*, 103–112. https://doi.org/10.1007/s13361-018-2077-9.

(706) D'Atri, V.; Porrini, M.; Rosu, F.; Gabelica, V. Linking Molecular Models with Ion Mobility Experiments. Illustration with a Rigid Nucleic Acid Structure: Ion Mobility Calculations and Experiments. *J. Mass Spectrom.* **2015**, *50*, 711–726. https://doi.org/10.1002/jms.3590.

(707) Baker, E. S.; Bernstein, S. L.; Gabelica, V.; De Pauw, E.; Bowers, M. T. G-Quadruplexes in Telomeric Repeats Are Conserved in a Solvent-Free Environment. *Int. J. Mass Spectrom.* **2006**, *253*, 225–237. https://doi.org/10.1016/j.ijms.2006.03.016.

(708) Gabelica, V.; Shammel Baker, E.; Teulade-Fichou, M.-P.; De Pauw, E.; Bowers, M. T. Stabilization and Structure of Telomeric and C-Myc Region Intramolecular G-Quadruplexes: The Role of Central Cations and Small Planar Ligands. *J. Am. Chem. Soc.* **2007**, *129*, 895–904. https://doi.org/10.1021/ja065989p.

(709) D'Atri, V.; Gabelica, V. DNA and RNA Telomeric G-Quadruplexes: What Topology Features Can Be Inferred from Ion Mobility Mass Spectrometry? *The Analyst* **2019**, *144*, 6074–6088. https://doi.org/10.1039/c9an01216h.

(710) Smargiasso, N.; Rosu, F.; Hsia, W.; Colson, P.; Baker, E. S.; Bowers, M. T.; De Pauw, E.; Gabelica, V. G-Quadruplex DNA Assemblies: Loop Length, Cation Identity, and Multimer Formation. *J. Am. Chem. Soc.* **2008**, *130*, 10208–10216. https://doi.org/10.1021/ja801535e.

(711) Rosu, F.; Gabelica, V.; Joly, L.; Grégoire, G.; Pauw, E. D. Zwitterionic I-Motif Structures Are Preserved in DNA Negatively Charged Ions Produced by Electrospray Mass Spectrometry. *Phys. Chem. Chem. Phys.* **2010**, *12*, 13448–13454. https://doi.org/10.1039/c0cp00782j.

(712) Zhong, Y.; Han, L.; Ruotolo, B. T. Collisional and Coulombic Unfolding of Gas-Phase Proteins: High Correlation to Their Domain Structures in Solution. *Angew. Chem. Int. Ed Engl.* **2014**, *53*, 9209–9212. https://doi.org/10.1002/anie.201403784.

(713) Hoaglund-Hyzer, C. S.; Counterman, A. E.; Clemmer, D. E. Anhydrous Protein Ions. *Chem. Rev.* **1999**, *99*, 3037–3080. https://doi.org/10.1021/cr980139g.

(714) Bleiholder, C.; Dupuis, N. F.; Wyttenbach, T.; Bowers, M. T. Ion Mobility–Mass Spectrometry Reveals a Conformational Conversion from Random Assembly to β-Sheet in Amyloid Fibril Formation. *Nat. Chem.* **2011**, *3*, 172–177. https://doi.org/10.1038/nchem.945.

(715) Haler, J. R. N.; Morsa, D.; Lecomte, P.; Jérôme, C.; Far, J.; De Pauw, E. Predicting Ion Mobility-Mass Spectrometry Trends of Polymers Using the Concept of Apparent Densities. *Methods* **2018**, *144*, 125–133. https://doi.org/10.1016/j.ymeth.2018.03.010.

(716) Haler, J. R. N.; Béchet, E.; Far, J.; De Pauw, E. Geometric Analysis of Shapes in Ion Mobility-Mass Spectrometry, *ChemRxiv*, *Physical chemistry*, September 4, 2019. https://doi.org/10.26434/chemrxiv.9758057.v1.

(717) Gan, Q.; Wang, X.; Kauffmann, B.; Rosu, F.; Ferrand, Y.; Huc, I. Translation of Rod-like Template Sequences into Homochiral Assemblies of Stacked Helical Oligomers. *Nat. Nanotechnol.* **2017**, *12*, 447–452. https://doi.org/10.1038/nnano.2017.15.

(718) Berman, H. M.; Olson, W. K.; Beveridge, D. L.; Westbrook, J.; Gelbin, A.; Demeny, T.; Hsieh, S. H.; Srinivasan, A. R.; Schneider, B. The Nucleic Acid Database. A Comprehensive Relational Database of Three-Dimensional Structures of Nucleic Acids. *Biophys. J.* **1992**, *63*, 751–759. https://doi.org/10.1016/S0006-3495(92)81649-1.

(719) Coimbatore Narayanan, B.; Westbrook, J.; Ghosh, S.; Petrov, A. I.; Sweeney, B.; Zirbel, C. L.; Leontis, N. B.; Berman, H. M. The Nucleic Acid Database: New Features and Capabilities. *Nucleic Acids Res.* **2014**, *42*, D114-122. https://doi.org/10.1093/nar/gkt980.

(720) Gidden, J.; Bowers, M. T. Gas-Phase Conformational and Energetic Properties of Deprotonated Dinucleotides. *Eur. Phys. J. - At. Mol. Opt. Plasma Phys.* **2002**, *20*, 409–419. https://doi.org/10.1140/epjd/e2002-00170-7.

(721) Vangaveti, S.; D'Esposito, R. J.; Lippens, J. L.; Fabris, D.; Ranganathan, S. V. A Coarse-Grained Model for Assisting the Investigation of Structure and Dynamics of Large Nucleic Acids by Ion Mobility Spectrometry-Mass Spectrometry. *Phys. Chem. Chem. Phys.* **2017**,

19, 14937–14946. https://doi.org/10.1039/c7cp00717e.

(722) Rueda, M.; Kalko, S. G.; Luque, F. J.; Orozco, M. The Structure and Dynamics of DNA in the Gas Phase. *J. Am. Chem. Soc.* **2003**, *125*, 8007–8014. https://doi.org/10.1021/ja0300564.

(723) Rueda, M.; Luque, F. J.; Orozco, M. Nature of Minor-Groove Binders-DNA Complexes in the Gas Phase. *J. Am. Chem. Soc.* **2005**, *127*, 11690–11698. https://doi.org/10.1021/ja0422110.

(724) Rueda, M.; Luque, F. J.; Orozco, M. G-Quadruplexes Can Maintain Their Structure in the Gas Phase. *J. Am. Chem. Soc.* **2006**, *128*, 3608–3619. https://doi.org/10.1021/ja055936s.

(725) Zhao, Y.; Truhlar, D. G. The M06 Suite of Density Functionals for Main Group Thermochemistry, Thermochemical Kinetics, Noncovalent Interactions, Excited States, and Transition Elements: Two New Functionals and Systematic Testing of Four M06-Class Functionals and 12 Other Functionals. *Theor. Chem. Acc.* **2008**, *120*, 215–241. https://doi.org/10.1007/s00214-007-0310-x.

(726) Stewart, J. J. P. Optimization of Parameters for Semiempirical Methods VI: More Modifications to the NDDO Approximations and Re-Optimization of Parameters. *J. Mol. Model.* **2013**, *19*, 1–32. https://doi.org/10.1007/s00894-012-1667-x.

(727) Winnerdy, F. R.; Bakalar, B.; Das, P.; Heddi, B.; Marchand, A.; Rosu, F.; Gabelica, V.; Phan, A. T. Unprecedented Hour-Long Residence Time of a Cation in the Left-Handed G-Quadruplex. *Chem Sci* **2021**, *12*, 7151–7157. https://doi.org/10.1039/d1sc00515d.

(728) Gabelica, V.; Marklund, E. Fundamentals of Ion Mobility Spectrometry. *Curr. Opin. Chem. Biol.* **2018**, *42*, 51–59. https://doi.org/10.1016/j.cbpa.2017.10.022.

(729) Shvartsburg, A. A.; Jarrold, M. F. An Exact Hard-Spheres Scattering Model for the Mobilities of Polyatomic Ions. *Chem. Phys. Lett.* **1996**, *261*, 86–91. https://doi.org/10.1016/0009-2614(96)00941-4.

(730) Mesleh, M. F.; Hunter, J. M.; Shvartsburg, A. A.; Schatz, G. C.; Jarrold, M. F. Structural Information from Ion Mobility Measurements: Effects of the Long-Range Potential. *J. Phys. Chem.* **1996**, *100*, 16082–16086. https://doi.org/10.1021/jp961623v.

(731) Bleiholder, C.; Wyttenbach, T.; Bowers, M. T. A Novel Projection Approximation Algorithm for the Fast and Accurate Computation of Molecular Collision Cross Sections (I). Method. *Int. J. Mass Spectrom.* **2011**, *308*, 1–10. https://doi.org/10.1016/j.ijms.2011.06.014.

(732) Siu, C.-K.; Guo, Y.; Saminathan, I. S.; Hopkinson, A. C.; Siu, K. W. M. Optimization of Parameters Used in Algorithms of Ion-Mobility Calculation for Conformational Analyses. *J. Phys. Chem. B* **2010**, *114*, 1204–1212. https://doi.org/10.1021/jp910858z.

(733) Larriba, C.; Hogan, C. J. Ion Mobilities in Diatomic Gases: Measurement versus Prediction with Non-Specular Scattering Models. *J. Phys. Chem. A* **2013**, *117*, 3887–3901. https://doi.org/10.1021/jp312432z.

(734) Larriba, C.; Hogan, C. J. Free Molecular Collision Cross Section Calculation Methods for Nanoparticles and Complex Ions with Energy Accommodation. *J. Comput. Phys.* **2013**, *251*, 344–363. https://doi.org/10.1016/j.jcp.2013.05.038.

(735) Laser Photodissociation and Spectroscopy of Mass-Separated Biomolecular Ions; Polfer, N. C., Dugourd, P., Eds.; Lecture Notes in Chemistry; Springer Cham: Heidelberg, 2013; p 119.

(736) Iavarone, A. T.; Patriksson, A.; van der Spoel, D.; Parks, J. H. Fluorescence Probe of Trp-Cage Protein Conformation in Solution and in Gas Phase. *J. Am. Chem. Soc.* **2007**, *129*, 6726–6735. https://doi.org/10.1021/ja065092s.

(737) Czar, M. F.; Zosel, F.; König, I.; Nettels, D.; Wunderlich, B.; Schuler, B.; Zarrine-Afsar, A.; Jockusch, R. A. Gas-Phase FRET Efficiency Measurements To Probe the Conformation of Mass-Selected Proteins. *Anal. Chem.* **2015**, *87*, 7559–7565. https://doi.org/10.1021/acs.analchem.5b01591.

(738) Danell, A. S.; Parks, J. H. FRET Measurements of Trapped Oligonucleotide Duplexes. *Int. J. Mass Spectrom.* **2003**, *229*, 35–45. https://doi.org/10.1016/s1387-3806(03)00253-7.

(739) Sciuto, S. V.; Jockusch, R. A. The Intrinsic Photophysics of Gaseous Ethidium Ions. *J. Photochem. Photobiol. Chem.* **2015**, *311*, 186–192. https://doi.org/10.1016/j.jphotochem.2015.06.020.

(740) Chen, J. C.; Jockusch, R. A. Protomers of DNA-Binding Dye Fluoresce Different Colours: Intrinsic Photophysics of Hoechst 33258. *Phys. Chem. Chem. Phys.* **2019**, *21*, 16848–16858. https://doi.org/10.1039/c9cp02421b.

(741) Kung, J. C. K.; Vurgun, N.; Chen, J. C.; Nitz, M.; Jockusch, R. A. Intrinsic Turn-On Response of Thioflavin T in Complexes. *Chem. – Eur. J.* **2020**, *26*, 3479–3483. https://doi.org/10.1002/chem.201905100.

(742) Daly, S.; Poussigue, F.; Simon, A.-L.; MacAleese, L.; Bertorelle, F.; Chirot, F.; Antoine, R.; Dugourd, P. Action-FRET: Probing the Molecular Conformation of Mass-Selected Gas-Phase Peptides with Förster Resonance Energy Transfer Detected by Acceptor-Specific Fragmentation. *Anal. Chem.* **2014**, *86*, 8798–8804. https://doi.org/10.1021/ac502027y.

(743) Daly, S.; Knight, G.; Halim, M. A.; Kulesza, A.; Choi, C. M.; Chirot, F.; MacAleese, L.; Antoine, R.; Dugourd, P. Action-FRET of a Gaseous Protein. *J. Am. Soc. Mass Spectrom.* **2017**, *28*,

38–49. https://doi.org/10.1007/s13361-016-1449-2.

(744) Fridgen, T. D. Infrared Consequence Spectroscopy of Gaseous Protonated and Metal Ion Cationized Complexes. *Mass Spectrom. Rev.* **2009**, *28*, 586–607. https://doi.org/10.1002/mas.20224.

(745) Polfer, N. C. Infrared Multiple Photon Dissociation Spectroscopy of Trapped Ions. *Chem. Soc. Rev.* **2011**, *40*, 2211–2221. https://doi.org/10.1039/C0CS00171F.

(746) Nei, Y. -w.; Crampton, K. T.; Berden, G.; Oomens, J.; Rodgers, M. T. Infrared Multiple Photon Dissociation Action Spectroscopy of Deprotonated RNA Mononucleotides: Gas-Phase Conformations and Energetics. *J. Phys. Chem. A* **2013**, *117*, 10634–10649. https://doi.org/10.1021/jp4039495.

(747) Gabelica, V.; Rosu, F. Gas-Phase Spectroscopy of Nucleic Acids. In *Nucleic Acids in the Gas Phase*; Gabelica, V., Ed.; Physical Chemistry in Action; Springer-Verlag: Berlin, Heidelberg, 2014; p.103–130. https://doi.org/10.1007/978-3-642-54842-0_5.

(748) Azargun, M.; Fridgen, T. D. Guanine Tetrads: An IRMPD Spectroscopy, Energy Resolved SORI-CID, and Computational Study of M(9-Ethylguanine)4+ (M = Li, Na, K, Rb, Cs) in the Gas Phase. *Phys. Chem. Chem. Phys.* **2015**, *17*, 25778–25785. https://doi.org/10.1039/c5cp00580a.

(749) Gabelica, V.; Rosu, F.; De Pauw, E.; Lemaire, J.; Gillet, J.-C.; Poully, J.-C.; Lecomte, F.; Grégoire, G.; Schermann, J.-P.; Desfrançois, C. Infrared Signature of DNA G-Quadruplexes in the Gas Phase. *J. Am. Chem. Soc.* **2008**, *130*, 1810–1811. https://doi.org/10.1021/ja077321w.

(750) Couprie, M.-E.; Ortéga, J.-M. Free-Electron Lasers Sources for Scientific Applications. *Analusis* **2000**, *28*, 725–736. https://doi.org/10.1051/analusis:2000143.

(751) Gabelica, V.; Rosu, F.; Tabarin, T.; Kinet, C.; Antoine, R.; Broyer, M.; De Pauw, E.; Dugourd, P. Base-Dependent Electron Photodetachment from Negatively Charged DNA Strands upon 260-Nm Laser Irradiation. *J. Am. Chem. Soc.* **2007**, *129*, 4706–4713. https://doi.org/10.1021/ja068440z.

(752) Antoine, R.; Dugourd, P. Visible and Ultraviolet Spectroscopy of Gas Phase Protein Ions. *Phys. Chem. Chem. Phys.* **2011**, *13*, 16494–16509. https://doi.org/10.1039/C1CP21531K.

(753) Rosu, F.; Gabelica, V.; De Pauw, E.; Antoine, R.; Broyer, M.; Dugourd, P. UV Spectroscopy of DNA Duplex and Quadruplex Structures in the Gas Phase. *J. Phys. Chem. A* **2012**, *116*, 5383–5391. https://doi.org/10.1021/jp302468x.

(754) Vonderach, M.; Ehrler, O. T.; Weis, P.; Kappes, M. M. Combining Ion Mobility Spectrometry, Mass Spectrometry, and Photoelectron Spectroscopy in a High-Transmission Instrument. *Anal. Chem.* **2011**, *83*, 1108–1115. https://doi.org/10.1021/ac1029677.

(755) Vonderach, M.; Ehrler, O. T.; Matheis, K.; Weis, P.; Kappes, M. M. Isomer-Selected Photoelectron Spectroscopy of Isolated DNA Oligonucleotides: Phosphate and Nucleobase Deprotonation at High Negative Charge States. *J. Am. Chem. Soc.* **2012**, *134*, 7830–7841. https://doi.org/10.1021/ja300619j.

(756) Emanuele, E.; Markovitsi, D.; Millié, P.; Zakrzewska, K. UV Spectra and Excitation Delocalization in DNA: Influence of the Spectral Width. *ChemPhysChem* **2005**, *6*, 1387–1392. https://doi.org/10.1002/cphc.200500014.

(757) D'Abramo, M.; Castellazzi, C. L.; Orozco, M.; Amadei, A. On the Nature of DNA Hyperchromic Effect. *J. Phys. Chem. B* **2013**, *117*, 8697–8704. https://doi.org/10.1021/jp403369k.

(758) Kypr, J.; Kejnovská, I.; Renciuk, D.; Vorlícková, M. Circular Dichroism and Conformational Polymorphism of DNA. *Nucleic Acids Res.* **2009**, *37*, 1713–1725. https://doi.org/10.1093/nar/gkp026.

(759) Nechay, M.; Kleiner, R. E. High-Throughput Approaches to Profile RNA-Protein Interactions. *Curr. Opin. Chem. Biol.* **2020**, *54*, 37–44. https://doi.org/10.1016/j.cbpa.2019.11.002.

(760) Ramanathan, M.; Porter, D. F.; Khavari, P. A. Methods to Study RNA-Protein Interactions. *Nat. Methods* **2019**, *16*, 225–234. https://doi.org/10.1038/s41592-019-0330-1.

(761) Schmidt, C.; Kramer, K.; Urlaub, H. Investigation of Protein–RNA Interactions by Mass Spectrometry—Techniques and Applications. *J. Proteomics* **2012**, *75*, 3478–3494. https://doi.org/10.1016/j.jprot.2012.04.030.

(762) Fabris, D.; Yu, E. T. Elucidating the Higher-Order Structure of Biopolymers by Structural Probing and Mass Spectrometry: MS3D. *J. Mass Spectrom.* **2010**, *45*, 841–860. https://doi.org/10.1002/jms.1762.

(763) Yu, E.; Fabris, D. Direct Probing of RNA Structures and RNA-Protein Interactions in the HIV-1 Packaging Signal by Chemical Modification and Electrospray Ionization Fourier Transform Mass Spectrometry. *J. Mol. Biol.* **2003**, *330*, 211–223. https://doi.org/10.1016/s0022-2836(03)00589-8.

(764) Kellersberger, K. A.; Yu, E.; Kruppa, G. H.; Young, M. M.; Fabris, D. Top-down Characterization of Nucleic Acids Modified by Structural Probes Using High-Resolution Tandem Mass Spectrometry and Automated Data Interpretation. *Anal. Chem.* **2004**, *76*, 2438–2445. https://doi.org/10.1021/ac0355045.

(765) Yu, E.; Fabris, D. Toward Multiplexing the Application of Solvent Accessibility Probes for the Investigation of RNA Three-Dimensional

Structures by Electrospray Ionization-Fourier Transform Mass Spectrometry. *Anal. Biochem.* **2004**, *334*, 356–366. https://doi.org/10.1016/j.ab.2004.07.034.

(766) Yu, E. T.; Zhang, Q.; Fabris, D. Untying the FIV Frameshifting Pseudoknot Structure by MS3D. *J. Mol. Biol.* **2005**, *345*, 69–80. https://doi.org/10.1016/j.jmb.2004.10.014.

(767) Zhang, Q.; Yu, E. T.; Kellersberger, K. A.; Crosland, E.; Fabris, D. Toward Building a Database of Bifunctional Probes for the MS3D Investigation of Nucleic Acids Structures. *J. Am. Soc. Mass Spectrom.* **2006**, *17*, 1570–1581. https://doi.org/10.1016/j.jasms.2006.06.002.

(768) Yu, E. T.; Hawkins, A.; Eaton, J.; Fabris, D. MS3D Structural Elucidation of the HIV-1 Packaging Signal. *Proc. Natl. Acad. Sci. U. S. A.* **2008**, *105*, 12248–12253. https://doi.org/10.1073/pnas.0800509105.

(769) Parr, C.; Pierce, S. E.; Smith, S. I.; Brodbelt, J. S. Investigation of the Reactivity of Oligodeoxynucleotides with Glyoxal and KMnO(4) Chemical Probes by Electrospray Ionization Mass Spectrometry. *Int. J. Mass Spectrom.* **2011**, *304*, 115–123. https://doi.org/10.1016/j.ijms.2010.06.007.

(770) Turner, K. B.; Yi-Brunozzi, H. Y.; Brinson, R. G.; Marino, J. P.; Fabris, D.; Le Grice, S. F. J. SHAMS: Combining Chemical Modification of RNA with Mass Spectrometry to Examine Polypurine Tract-Containing RNA/DNA Hybrids. *RNA* **2009**, *15*, 1605–1613. https://doi.org/10.1261/rna.1615409.

(771) Largy, E.; Gabelica, V. Native Hydrogen/Deuterium Exchange Mass Spectrometry of Structured DNA Oligonucleotides. *Anal. Chem.* **2020**, *92*, 4402–4410. https://doi.org/10.1021/acs.analchem.9b05298.

(772) Weeks, K. M. Advances in RNA Structure Analysis by Chemical Probing. *Curr. Opin. Struct. Biol.* **2010**, *20*, 295–304. https://doi.org/10.1016/j.sbi.2010.04.001.

(773) Anichina, J.; Dobrusin, Z.; Bohme, D. K. Detection of T-T Mismatches Using Mass Spectrometry: Specific Interactions of Hg(II) with Oligonucleotides Rich in Thymine (T). *J. Phys. Chem. B* **2010**, *114*, 15106–15112. https://doi.org/10.1021/jp1022373.

(774) Tullius, T. D.; Greenbaum, J. A. Mapping Nucleic Acid Structure by Hydroxyl Radical Cleavage. *Curr. Opin. Chem. Biol.* **2005**, *9*, 127–134. https://doi.org/10.1016/j.cbpa.2005.02.009.

(775) Brenowitz, M.; Chance, M. R.; Dhavan, G.; Takamoto, K. Probing the Structural Dynamics of Nucleic Acids by Quantitative Time-Resolved and Equilibrium Hydroxyl Radical "Footprinting." *Curr. Opin. Struct. Biol.* **2002**, *12*, 648–653. https://doi.org/10.1016/s0959-440x(02)00366-4.

(776) Shcherbakova, I.; Mitra, S. Hydroxyl-Radical Footprinting to Probe Equilibrium Changes in RNA Tertiary Structure. *Methods Enzymol.* **2009**, *468*, 31–46. https://doi.org/10.1016/S0076-6879(09)68002-2.

(777) Hertzberg, R. P.; Dervan, P. B. Cleavage of DNA with Methidiumpropyl-EDTA-Iron(II): Reaction Conditions and Product Analyses. *Biochemistry* **1984**, *23*, 3934–3945. https://doi.org/10.1021/bi00312a022.

(778) Liu, X. R.; Zhang, M. M.; Gross, M. L. Mass Spectrometry-Based Protein Footprinting for Higher-Order Structure Analysis: Fundamentals and Applications. *Chem. Rev.* **2020**, *120*, 4355–4454. https://doi.org/10.1021/acs.chemrev.9b00815.

(779) Kiselar, J. G.; Chance, M. R. Future Directions of Structural Mass Spectrometry Using Hydroxyl Radical Footprinting. *J. Mass Spectrom.* **2010**, *45*, 1373–1382. https://doi.org/10.1002/jms.1808.

(780) Nielsen, P. E. Chemical and Photochemical Probing of DNA Complexes. *J. Mol. Recognit.* **1990**, *3*, 1–25. https://doi.org/10.1002/jmr.300030102.

(781) Benn, M. H.; Chatamra, B.; Jones, A. S. The Permanganate Oxidation of Thymine and Some 1-Substituted Thymines. *J. Chem. Soc.* **1960**, No. 0, 1014–1020. https://doi.org/10.1039/jr9600001014.

(782) Bui, C. T.; Rees, K.; Cotton, R. G. H. Permanganate Oxidation Reactions of DNA: Perspective in Biological Studies. *Nucleosides Nucleotides Nucleic Acids* **2003**, *22*, 1835–1855. https://doi.org/10.1081/NCN-120023276.

(783) Mazzitelli, C. L.; Brodbelt, J. S. Probing Ligand Binding to Duplex DNA Using KMnO4 Reactions and Electrospray Ionization Tandem Mass Spectrometry. *Anal. Chem.* **2007**, *79*, 4636–4647. https://doi.org/10.1021/ac070145p.

(784) Bailly, C.; Gentle, D.; Hamy, F.; Purcell, M.; Waring, M. J. Localized Chemical Reactivity in DNA Associated with the Sequence-Specific Bisintercalation of Echinomycin. *Biochem. J.* **1994**, *300*, 165–173. https://doi.org/10.1042/bj3000165.

(785) Farah, J. A.; Smith, G. R. The RecBCD Enzyme Initiation Complex for DNA Unwinding: Enzyme Positioning and DNA Opening. *J. Mol. Biol.* **1997**, *272*, 699–715. https://doi.org/10.1006/jmbi.1997.1259.

(786) Pierce, S. E.; Kieltyka, R.; Sleiman, H. F.; Brodbelt, J. S. Evaluation of Binding Selectivities and Affinities of Platinum-Based Quadruplex Interactive Complexes by Electrospray Ionization Mass Spectrometry. *Biopolymers* **2009**, *91*, 233–243. https://doi.org/10.1002/bip.21130.

(787) Pluskota-Karwatka, D.; Pawłowicz, A. J.; Tomas, M.; Kronberg, L. Formation of Adducts in the Reaction of Glyoxal with 2'-Deoxyguanosine and with Calf Thymus DNA. *Bioorganic Chem.*

2008, *36*, 57–64. https://doi.org/10.1016/j.bioorg.2007.10.004.

(788) Shapiro, R.; Hachmann, J. The Reaction of Guanine Derivatives with 1,2-Dicarbonyl Compounds. *Biochemistry* **1966**, *5*, 2799–2807. https://doi.org/10.1021/bi00873a004.

(789) Shapiro, R.; Cohen, B. I.; Shiuey, S. J.; Maurer, H. On the Reaction of Guanine with Glyoxal, Pyruvaldehyde, and Kethoxal, and the Structure of the Acylguanines. A New Synthesis of N2-Alkylguanines. *Biochemistry* **1969**, *8*, 238–245. https://doi.org/10.1021/bi00829a034.

(790) Krol, A.; Carbon, P. A Guide for Probing Native Small Nuclear RNA and Ribonucleoprotein Structures. *Methods Enzymol.* **1989**, *180*, 212–227. https://doi.org/10.1016/0076-6879(89)80103-x.

(791) Christiansen, J.; Garrett, R. Enzymatic and Chemical Probing of Ribosomal RNA-Protein Interactions. *Methods Enzymol.* **1988**, *164*, 456–468. https://doi.org/10.1016/s0076-6879(88)64061-4.

(792) Bakin, A.; Ofengand, J. Four Newly Located Pseudouridylate Residues in Escherichia Coli 23S Ribosomal RNA Are All at the Peptidyltransferase Center: Analysis by the Application of a New Sequencing Technique. *Biochemistry* **1993**, *32*, 9754–9762. https://doi.org/10.1021/bi00088a030.

(793) Noble, E.; Mathews, D. H.; Chen, J. L.; Turner, D. H.; Takimoto, T.; Kim, B. Biophysical Analysis of Influenza A Virus RNA Promoter at Physiological Temperatures. *J. Biol. Chem.* **2011**, *286*, 22965–22970. https://doi.org/10.1074/jbc.M111.239509.

(794) Scalabrin, M.; Dixit, S. M.; Makshood, M. M.; Krzemien, C. E.; Fabris, D. Bifunctional Cross-Linking Approaches for Mass Spectrometry-Based Investigation of Nucleic Acids and Protein-Nucleic Acid Assemblies. *Methods* **2018**, *144*, 64–78. https://doi.org/10.1016/j.ymeth.2018.05.001.

(795) Leitner, A.; Dorn, G.; Allain, F. H.-T. Combining Mass Spectrometry (MS) and Nuclear Magnetic Resonance (NMR) Spectroscopy for Integrative Structural Biology of Protein-RNA Complexes. *Cold Spring Harb. Perspect. Biol.* **2019**, *11*, a032359. https://doi.org/10.1101/cshperspect.a032359.

(796) Harris, M. E.; Christian, E. L. RNA Crosslinking Methods. *Methods Enzymol.* **2009**, *468*, 127–146. https://doi.org/10.1016/S0076-6879(09)68007-1.

(797) Shetlar, M. D.; Carbone, J.; Steady, E.; Hom, K. Photochemical Addition of Amino Acids and Peptides to Polyuridylic Acid. *Photochem. Photobiol.* **1984**, *39*, 141–144. https://doi.org/10.1111/j.1751-1097.1984.tb03419.x.

(798) Shetlar, M. D.; Christensen, J.; Hom, K. Photochemical Addition of Amino Acids and Peptides to DNA. *Photochem. Photobiol.* **1984**, *39*, 125–133. https://doi.org/10.1111/j.1751-1097.1984.tb03417.x.

(799) Shetlar, M. D.; Home, K.; Carbone, J.; Moy, D.; Steady, E.; Watanabe, M. Photochemical Addition of Amino Acids and Peptides to Homopolyribonucleotides of the Major DNA Bases. *Photochem. Photobiol.* **1984**, *39*, 135–140. https://doi.org/10.1111/j.1751-1097.1984.tb03418.x.

(800) Sinz, A. Chemical Cross-Linking and Mass Spectrometry to Map Three-Dimensional Protein Structures and Protein-Protein Interactions. *Mass Spectrom. Rev.* **2006**, *25*, 663–682. https://doi.org/10.1002/mas.20082.

(801) Sinz, A. Investigation of Protein-Protein Interactions in Living Cells by Chemical Crosslinking and Mass Spectrometry. *Anal. Bioanal. Chem.* **2010**, *397*, 3433–3440. https://doi.org/10.1007/s00216-009-3405-5.

(802) Sinz, A.; Arlt, C.; Chorev, D.; Sharon, M. Chemical Cross-Linking and Native Mass Spectrometry: A Fruitful Combination for Structural Biology. *Protein Sci. Publ. Protein Soc.* **2015**, *24*, 1193–1209. https://doi.org/10.1002/pro.2696.

(803) O'Reilly, F. J.; Rappsilber, J. Cross-Linking Mass Spectrometry: Methods and Applications in Structural, Molecular and Systems Biology. *Nat. Struct. Mol. Biol.* **2018**, *25*, 1000–1008. https://doi.org/10.1038/s41594-018-0147-0.

(804) Iacobucci, C.; Götze, M.; Sinz, A. Cross-Linking/Mass Spectrometry to Get a Closer View on Protein Interaction Networks. *Curr. Opin. Biotechnol.* **2020**, *63*, 48–53. https://doi.org/10.1016/j.copbio.2019.12.009.

(805) Sinz, A. Cross-Linking/Mass Spectrometry for Studying Protein Structures and Protein-Protein Interactions: Where Are We Now and Where Should We Go from Here? *Angew. Chem. Int. Ed Engl.* **2018**, *57*, 6390–6396. https://doi.org/10.1002/anie.201709559.

(806) Chavez, J. D.; Bruce, J. E. Chemical Cross-Linking with Mass Spectrometry: A Tool for Systems Structural Biology. *Curr. Opin. Chem. Biol.* **2019**, *48*, 8–18. https://doi.org/10.1016/j.cbpa.2018.08.006.

(807) Kuhn-Holsken, E.; Dybkov, O.; Sander, B.; Luhrmann, R.; Urlaub, H. Improved Identification of Enriched Peptide RNA Cross-Links from Ribonucleoprotein Particles (RNPs) by Mass Spectrometry. *Nucleic Acids Res.* **2007**, *35*, e95. https://doi.org/10.1093/nar/gkm540.

(808) Thiede, B.; Urlaub, H.; Neubauer, H.; Grelle, G.; Wittmann-Liebold, B. Precise Determination of RNA-Protein Contact Sites in the 50 S Ribosomal Subunit of Escherichia Coli. *Biochem. J.* **1998**, *334*, 39–42. https://doi.org/10.1042/bj3340039.

(809) Thiede, B.; Urlaub, H.; Neubauer, H.; Wittmann-Liebold, B. Identification and Sequence Analysis of RNA-Protein Contact Sites by N-Terminal Sequencing and MALDI-MS. *Methods Mol. Biol. Clifton NJ* **1999**, *118*,

63–72. https://doi.org/10.1385/1-59259-676-2:63.

(810) Richter, F. M.; Hsiao, H.-H.; Plessmann, U.; Urlaub, H. Enrichment of Protein-RNA Crosslinks from Crude UV-Irradiated Mixtures for MS Analysis by on-Line Chromatography Using Titanium Dioxide Columns. *Biopolymers* **2009**, *91*, 297–309. https://doi.org/10.1002/bip.21139.

(811) Nottrott, S.; Urlaub, H.; Lührmann, R. Hierarchical, Clustered Protein Interactions with U4/U6 SnRNA: A Biochemical Role for U4/U6 Proteins. *EMBO J.* **2002**, *21*, 5527–5538. https://doi.org/10.1093/emboj/cdf544.

(812) Kramer, K.; Hummel, P.; Hsiao, H.-H.; Luo, X.; Wahl, M.; Urlaub, H. Mass-Spectrometric Analysis of Proteins Cross-Linked to 4-Thio-Uracil- and 5-Bromo-Uracil-Substituted RNA. *Int. J. Mass Spectrom.* **2011**, *304*, 184–194. https://doi.org/10.1016/j.ijms.2010.10.009.

(813) Müller, M.; Heym, R. G.; Mayer, A.; Kramer, K.; Schmid, M.; Cramer, P.; Urlaub, H.; Jansen, R.-P.; Niessing, D. A Cytoplasmic Complex Mediates Specific MRNA Recognition and Localization in Yeast. *PLoS Biol.* **2011**, *9*, e1000611. https://doi.org/10.1371/journal.pbio.1000611.

(814) Ghalei, H.; Hsiao, H.-H.; Urlaub, H.; Wahl, M. C.; Watkins, N. J. A Novel Nop5-SRNA Interaction That Is Required for Efficient Archaeal Box C/D SRNP Formation. *RNA* **2010**, *16*, 2341–2348. https://doi.org/10.1261/rna.2380410.

(815) Luo, X.; Hsiao, H.-H.; Bubunenko, M.; Weber, G.; Court, D. L.; Gottesman, M. E.; Urlaub, H.; Wahl, M. C. Structural and Functional Analysis of the E. Coli NusB-S10 Transcription Antitermination Complex. *Mol. Cell* **2008**, *32*, 791–802. https://doi.org/10.1016/j.molcel.2008.10.028.

(816) Kühn-Hölsken, E.; Lenz, C.; Dickmanns, A.; Hsiao, H.-H.; Richter, F. M.; Kastner, B.; Ficner, R.; Urlaub, H. Mapping the Binding Site of Snurportin 1 on Native U1 SnRNP by Cross-Linking and Mass Spectrometry. *Nucleic Acids Res.* **2010**, *38*, 5581–5593. https://doi.org/10.1093/nar/gkq272.

(817) Lenz, C.; Kühn-Hölsken, E.; Urlaub, H. Detection of Protein-RNA Crosslinks by NanoLC-ESI-MS/MS Using Precursor Ion Scanning and Multiple Reaction Monitoring (MRM) Experiments. *J. Am. Soc. Mass Spectrom.* **2007**, *18*, 869–881. https://doi.org/10.1016/j.jasms.2007.01.013.

(818) Kühn-Hölsken, E.; Lenz, C.; Sander, B.; Lührmann, R.; Urlaub, H. Complete MALDI-ToF MS Analysis of Cross-Linked Peptide-RNA Oligonucleotides Derived from Nonlabeled UV-Irradiated Ribonucleoprotein Particles. *RNA* **2005**, *11*, 1915–1930. https://doi.org/10.1261/rna.2176605.

(819) Urlaub, H. A Two-Tracked Approach to Analyze RNA–Protein Crosslinking Sites in Native, Nonlabeled Small Nuclear Ribonucleoprotein Particles. *Methods* **2002**, *26*, 170–181. https://doi.org/10.1016/s1046-2023(02)00020-8.

(820) Dorn, G.; Leitner, A.; Boudet, J.; Campagne, S.; von Schroetter, C.; Moursy, A.; Aebersold, R.; Allain, F. H.-T. Structural Modeling of Protein-RNA Complexes Using Crosslinking of Segmentally Isotope-Labeled RNA and MS/MS. *Nat. Methods* **2017**, *14*, 487–490. https://doi.org/10.1038/nmeth.4235.

(821) Qamar, S.; Kramer, K.; Urlaub, H. Studying RNA-Protein Interactions of Pre-MRNA Complexes by Mass Spectrometry. *Methods Enzymol.* **2015**, *558*, 417–463. https://doi.org/10.1016/bs.mie.2015.02.010.

(822) Sharma, K.; Hrle, A.; Kramer, K.; Sachsenberg, T.; Staals, R. H. J.; Randau, L.; Marchfelder, A.; van der Oost, J.; Kohlbacher, O.; Conti, E.; et al. Analysis of Protein-RNA Interactions in CRISPR Proteins and Effector Complexes by UV-Induced Cross-Linking and Mass Spectrometry. *Methods* **2015**, *89*, 138–148. https://doi.org/10.1016/j.ymeth.2015.06.005.

(823) Zaman, U.; Richter, F. M.; Hofele, R.; Kramer, K.; Sachsenberg, T.; Kohlbacher, O.; Lenz, C.; Urlaub, H. Dithiothreitol (DTT) Acts as a Specific, UV-Inducible Cross-Linker in Elucidation of Protein-RNA Interactions. *Mol. Cell. Proteomics MCP* **2015**, *14*, 3196–3210. https://doi.org/10.1074/mcp.M115.052795.

(824) Stützer, A.; Welp, L. M.; Raabe, M.; Sachsenberg, T.; Kappert, C.; Wulf, A.; Lau, A. M.; David, S.-S.; Chernev, A.; Kramer, K.; et al. Analysis of Protein-DNA Interactions in Chromatin by UV Induced Cross-Linking and Mass Spectrometry. *Nat. Commun.* **2020**, *11*, 5250. https://doi.org/10.1038/s41467-020-19047-7.

(825) Tiss, A.; Barre, O.; Michaud-Soret, I.; Forest, E. Characterization of the DNA-Binding Site in the Ferric Uptake Regulator Protein from Escherichia Coli by UV Crosslinking and Mass Spectrometry. *FEBS Lett.* **2005**, *579*, 5454–5460. https://doi.org/10.1016/j.febslet.2005.08.067.

(826) Geyer, H.; Geyer, R.; Pingoud, V. A Novel Strategy for the Identification of Protein-DNA Contacts by Photocrosslinking and Mass Spectrometry. *Nucleic Acids Res.* **2004**, *32*, e132. https://doi.org/10.1093/nar/gnh131.

(827) Farrow, M. A.; Aboul-ela, F.; Owen, D.; Karpeisky, A.; Beigelman, L.; Gait, M. J. Site-Specific Cross-Linking of Amino Acids in the Basic Region of Human Immunodeficiency Virus Type 1 Tat Peptide to Chemically Modified TAR RNA Duplexes. *Biochemistry* **1998**, *37*, 3096–3108. https://doi.org/10.1021/bi972695v.

(828) Lelyveld, V. S.; Björkbom, A.; Ransey, E. M.; Sliz, P.; Szostak, J. W. Pinpointing RNA-Protein Cross-Links with Site-Specific Stable Isotope-Labeled Oligonucleotides. *J. Am. Chem. Soc.*

2015, *137*, 15378–15381. https://doi.org/10.1021/jacs.5b10596.

(829) Rosenfeld, K. K.; Ziv, T.; Goldin, S.; Glaser, F.; Manor, H. Mapping of DNA Binding Sites in the Tetrahymena Telomerase Holoenzyme Proteins by UV Cross-Linking and Mass Spectrometry. *J. Mol. Biol.* **2011**, *410*, 77–92. https://doi.org/10.1016/j.jmb.2011.04.040.

(830) Johannsson, S.; Neumann, P.; Wulf, A.; Welp, L. M.; Gerber, H.-D.; Krull, M.; Diederichsen, U.; Urlaub, H.; Ficner, R. Structural Insights into the Stimulation of S. Pombe Dnmt2 Catalytic Efficiency by the TRNA Nucleoside Queuosine. *Sci. Rep.* **2018**, *8*, 8880. https://doi.org/10.1038/s41598-018-27118-5.

(831) Steen, H.; Petersen, J.; Mann, M.; Jensen, O. N. Mass Spectrometric Analysis of a UV-Cross-Linked Protein-DNA Complex: Tryptophans 54 and 88 of E. Coli SSB Cross-Link to DNA. *Protein Sci. Publ. Protein Soc.* **2001**, *10*, 1989–2001. https://doi.org/10.1110/ps.07601.

(832) Urlaub, H.; Hartmuth, K.; Kostka, S.; Grelle, G.; Lührmann, R. A General Approach for Identification of RNA-Protein Cross-Linking Sites within Native Human Spliceosomal Small Nuclear Ribonucleoproteins (SnRNPs). Analysis of RNA-Protein Contacts in Native U1 and U4/U6.U5 SnRNPs. *J. Biol. Chem.* **2000**, *275*, 41458–41468. https://doi.org/10.1074/jbc.m007434200.

(833) Bennett, S. E.; Jensen, O. N.; Barofsky, D. F.; Mosbaugh, D. W. UV-Catalyzed Cross-Linking of Escherichia Coli Uracil-DNA Glycosylase to DNA. Identification of Amino Acid Residues in the Single-Stranded DNA Binding Site. *J. Biol. Chem.* **1994**, *269*, 21870–21879.

(834) Urlaub, H.; Thiede, B.; Müller, E. C.; Brimacombe, R.; Wittmann-Liebold, B. Identification and Sequence Analysis of Contact Sites between Ribosomal Proteins and RRNA in Escherichia Coli 30 S Subunits by a New Approach Using Matrix-Assisted Laser Desorption/Ionization-Mass Spectrometry Combined with N-Terminal Microsequencing. *J. Biol. Chem.* **1997**, *272*, 14547–14555. https://doi.org/10.1074/jbc.272.23.14547.

(835) Schilling, B.; Row, R. H.; Gibson, B. W.; Guo, X.; Young, M. M. MS2Assign, Automated Assignment and Nomenclature of Tandem Mass Spectra of Chemically Crosslinked Peptides. *J. Am. Soc. Mass Spectrom.* **2003**, *14*, 834–850. https://doi.org/10.1016/S1044-0305(03)00327-1.

(836) Slavata, L.; Chmelík, J.; Kavan, D.; Filandrová, R.; Fiala, J.; Rosůlek, M.; Mrázek, H.; Kukačka, Z.; Vališ, K.; Man, P.; et al. MS-Based Approaches Enable the Structural Characterization of Transcription Factor/DNA Response Element Complex. *Biomolecules* **2019**, *9*, 535. https://doi.org/10.3390/biom9100535.

(837) Baik, M.-H.; Friesner, R. A.; Lippard, S. J. Theoretical Study of Cisplatin Binding to Purine Bases: Why Does Cisplatin Prefer Guanine over Adenine? *J. Am. Chem. Soc.* **2003**, *125*, 14082–14092. https://doi.org/10.1021/ja036960d.

(838) Pourshahian, S.; Limbach, P. A. Application of Fractional Mass for the Identification of Peptide-Oligonucleotide Cross-Links by Mass Spectrometry. *J. Mass Spectrom.* **2008**, *43*, 1081–1088. https://doi.org/10.1002/jms.1391.

(839) Rojsitthisak, P.; Jongaroonngamsang, N.; Romero, R. M.; Haworth, I. S. HPLC-UV, MALDI-TOF-MS and ESI-MS/MS Analysis of the Mechlorethamine DNA Crosslink at a Cytosine-Cytosine Mismatch Pair. *PloS One* **2011**, *6*, e20745. https://doi.org/10.1371/journal.pone.0020745.

(840) Velema, W. A.; Kool, E. T. The Chemistry and Applications of RNA 2'-OH Acylation. *Nat. Rev. Chem.* **2020**, *4*, 22–37. https://doi.org/10.1038/s41570-019-0147-6.

(841) Kutchko, K. M.; Laederach, A. Transcending the Prediction Paradigm: Novel Applications of SHAPE to RNA Function and Evolution. *Wiley Interdiscip. Rev. RNA* **2017**, *8*, e1374. https://doi.org/10.1002/wrna.1374.

(842) Spitale, R. C.; Flynn, R. A.; Torre, E. A.; Kool, E. T.; Chang, H. Y. RNA Structural Analysis by Evolving SHAPE Chemistry. *Wiley Interdiscip. Rev. RNA* **2014**, *5*, 867–881. https://doi.org/10.1002/wrna.1253.

(843) Merino, E. J.; Wilkinson, K. A.; Coughlan, J. L.; Weeks, K. M. RNA Structure Analysis at Single Nucleotide Resolution by Selective 2'-Hydroxyl Acylation and Primer Extension (SHAPE). *J. Am. Chem. Soc.* **2005**, *127*, 4223–4231. https://doi.org/10.1021/ja043822v.

(844) McGinnis, J. L.; Dunkle, J. A.; Cate, J. H. D.; Weeks, K. M. The Mechanisms of RNA SHAPE Chemistry. *J. Am. Chem. Soc.* **2012**, *134*, 6617–6624. https://doi.org/10.1021/ja2104075.

(845) Gherghe, C. M.; Shajani, Z.; Wilkinson, K. A.; Varani, G.; Weeks, K. M. Strong Correlation between SHAPE Chemistry and the Generalized NMR Order Parameter (S2) in RNA. *J. Am. Chem. Soc.* **2008**, *130*, 12244–12245. https://doi.org/10.1021/ja804541s.

(846) Wilkinson, K. A.; Vasa, S. M.; Deigan, K. E.; Mortimer, S. A.; Giddings, M. C.; Weeks, K. M. Influence of Nucleotide Identity on Ribose 2'-Hydroxyl Reactivity in RNA. *RNA* **2009**, *15*, 1314–1321. https://doi.org/10.1261/rna.1536209.

(847) Benhaim, M.; Lee, K. K.; Guttman, M. Tracking Higher Order Protein Structure by Hydrogen-Deuterium Exchange Mass Spectrometry. *Protein Pept. Lett.* **2019**, *26*, 16–26. https://doi.org/10.2174/0929866526666181212165037.

(848) Hodge, E. A.; Benhaim, M. A.; Lee, K. K. Bridging Protein Structure, Dynamics, and Function Using Hydrogen/Deuterium-Exchange Mass Spectrometry. *Protein Sci. Publ. Protein Soc.*

2020, *29*, 843–855. https://doi.org/10.1002/pro.3790.

(849) Oganesyan, I.; Lento, C.; Wilson, D. J. Contemporary Hydrogen Deuterium Exchange Mass Spectrometry. *Methods* **2018**, *144*, 27–42. https://doi.org/10.1016/j.ymeth.2018.04.023.

(850) Engen, J. R.; Botzanowski, T.; Peterle, D.; Georgescauld, F.; Wales, T. E. Developments in Hydrogen/Deuterium Exchange Mass Spectrometry. *Anal. Chem.* **2021**, *93*, 567–582. https://doi.org/10.1021/acs.analchem.0c04281.

(851) Zheng, J.; Strutzenberg, T.; Pascal, B. D.; Griffin, P. R. Protein Dynamics and Conformational Changes Explored by Hydrogen/Deuterium Exchange Mass Spectrometry. *Curr. Opin. Struct. Biol.* **2019**, *58*, 305–313. https://doi.org/10.1016/j.sbi.2019.06.007.

(852) Lee, J.-H.; Pardi, A. Thermodynamics and Kinetics for Base-Pair Opening in the P1 Duplex of the Tetrahymena Group I Ribozyme. *Nucleic Acids Res.* **2007**, *35*, 2965–2974. https://doi.org/10.1093/nar/gkm184.

(853) Scalabrin, M.; Siu, Y.; Asare-Okai, P. N.; Fabris, D. Structure-Specific Ribonucleases for MS-Based Elucidation of Higher-Order RNA Structure. *J. Am. Soc. Mass Spectrom.* **2014**, *25*, 1136–1145. https://doi.org/10.1007/s13361-014-0911-2.

(854) van den Heuvel, R. H. H.; Gato, S.; Versluis, C.; Gerbaux, P.; Kleanthous, C.; Heck, A. J. R. Real-Time Monitoring of Enzymatic DNA Hydrolysis by Electrospray Ionization Mass Spectrometry. *Nucleic Acids Res.* **2005**, *33*, e96. https://doi.org/10.1093/nar/gni099.

(855) Zins, E.-L.; Rochut, S.; Pepe, C. Formation of Complexes between Uracil and Calcium Ions: An ESI/MS/MS Study in Combination with Theoretical Calculations. *J. Mass Spectrom.* **2009**, *44*, 813–820. https://doi.org/10.1002/jms.1561.

(856) Zins, E. Large Mixed Complexes Involving Uracil, Cytosine, Thymine and/or 1-Methyl Uracil around Ca2+ Ions: An Electrospray Ionization/MS Study. *J. Mass Spectrom.* **2013**, *48*, 438–447. https://doi.org/10.1002/jms.3175.

(857) Zhang, D.; Cooks, R. G. Doubly Charged Cluster Ions [(NaCl)m(Na)2]2+: Magic Numbers, Dissociation, and Structure11A Tribute to the Memory of Robert R. Squires. *Int. J. Mass Spectrom.* **2000**, *195–196*, 667–684. https://doi.org/10.1016/s1387-3806(99)00184-0.

(858) Fraschetti, C.; Montagna, M.; Guarcini, L.; Guidoni, L.; Filippi, A. Spectroscopic Evidence for a Gas-Phase Librating G-Quartet–Na+ Complex. *Chem. Commun.* **2014**, *50*, 14767–14770. https://doi.org/10.1039/c4cc05149a.

(859) Mezzache, S.; Alves, S.; Paumard, J.-P.; Pepe, C.; Tabet, J.-C. Theoretical and Gas-Phase Studies of Specific Cationized Purine Base Quartet. *Rapid Commun. Mass Spectrom.* **2007**, *21*, 1075–1082. https://doi.org/10.1002/rcm.2934.

(860) Moriwaki, H. Complexes of Cadmium Ion with Guanine Bases Detected by Electrospray Ionization Mass Spectrometry. *J. Mass Spectrom.* **2003**, *38*, 321–327. https://doi.org/10.1002/jms.444.

(861) Qiu, B.; Luo, H. Desorption Electrospray Ionization Mass Spectrometry of DNA Nucleobases: Implications for a Liquid Film Model. *J. Mass Spectrom.* **2009**, *44*, 772–779. https://doi.org/10.1002/jms.1554.

(862) Koch, K. J.; Aggerholm, T.; Nanita, S. C.; Cooks, R. G. Clustering of Nucleobases with Alkali Metals Studied by Electrospray Ionization Tandem Mass Spectrometry: Implications for Mechanisms of Multistrand DNA Stabilization. *J. Mass Spectrom.* **2002**, *37*, 676–686. https://doi.org/10.1002/jms.326.

(863) Aggerholm, T.; Nanita, S. C.; Koch, K. J.; Cooks, R. G. Clustering of Nucleosides in the Presence of Alkali Metals: Biologically Relevant Quartets of Guanosine, Deoxyguanosine and Uridine Observed by ESI-MS/MS. *J. Mass Spectrom.* **2003**, *38*, 87–97. https://doi.org/10.1002/jms.405.

(864) Baker, E. S.; Bernstein, S. L.; Bowers, M. T. Structural Characterization of G-Quadruplexes in Deoxyguanosine Clusters Using Ion Mobility Mass Spectrometry. *J. Am. Soc. Mass Spectrom.* **2005**, *16*, 989–997. https://doi.org/10.1016/j.jasms.2005.03.012.

(865) Sakamoto, S.; Nakatani, K.; Saito, I.; Yamaguchi, K. Formation and Destruction of the Guanine Quartet in Solution Observed by Cold-Spray Ionization Mass Spectrometry. *Chem. Commun.* **2003**, No. 6, 788–789. https://doi.org/10.1039/b212432g.

(866) Sravani, M.; Nagaveni, V.; Prabhakar, S.; Vairamani, M. G-Quadruplex Formation of Deoxyguanosine in the Presence of Alkaline Earth Metal Ions Studied by Electrospray Ionization Mass Spectrometry. *Rapid Commun. Mass Spectrom.* **2011**, *25*, 2095–2098. https://doi.org/10.1002/rcm.5082.

(867) Frańska, M. New Tetrads Formed by Deprotonated Guanosine Molecules and Stabilized by Alkali Earth Metal Cations, as Studied by Electrospray Ionization Mass Spectrometry. *Rapid Commun. Mass Spectrom.* **2013**, *27*, 2823–2827. https://doi.org/10.1002/rcm.6740.

(868) Fukushima, K.; Iwahashi, H. 1∶1 Complex of Guanine Quartet with Alkali Metal Cations Detected by Electrospray Ionization Mass Spectrometry. *Chem. Commun.* **2000**, No. 11, 895–896. https://doi.org/10.1039/b002235g.

(869) Manet, I.; Francini, L.; Masiero, S.; Pieraccini, S.; Spada, G. P.; Gottarelli, G. An ESI-MS and NMR Study of the Self-Assembly of Guanosine Derivates. *Helv. Chim. Acta* **2001**, *84*, 2096–2107. https://doi.org/10.1002/1522-

2675(20010711)84:7<2096::aid-hlca2096>3.0.co;2-g.

(870) Cai, M.; Shi, X.; Sidorov, V.; Fabris, D.; Lam, Y.; Davis, J. T. Cation-Directed Self-Assembly of Lipophilic Nucleosides: The Cation's Central Role in the Structure and Dynamics of a Hydrogen-Bonded Assembly. *Tetrahedron* **2002**, *58*, 661–671. https://doi.org/10.1016/s0040-4020(01)01101-2.

(871) Kwan, I. C. M.; She, Y.-M.; Wu, G. Trivalent Lanthanide Metal Ions Promote Formation of Stacking G-Quartets. *Chem. Commun.* **2007**, No. 41, 4286–4288. https://doi.org/10.1039/b710299b.

(872) Kwan, I. C. M.; She, Y.-M.; Wu, G. Nuclear Magnetic Resonance and Mass Spectrometry Studies of 2′,3′,5′-O-Triacetylguanosine Self-Assembly in the Presence of Alkaline Earth Metal Ions (Ca2+, Sr2+, Ba2+). *Can. J. Chem.* **2011**, *89*, 835–844. https://doi.org/10.1139/v10-179.

(873) Liu, X.; Kwan, I. C. M.; Wang, S.; Wu, G. G-Quartet Formation from an N2-Modified Guanosine Derivative. *Org. Lett.* **2006**, *8*, 3685–3688. https://doi.org/10.1021/ol061236w.

(874) Kaucher, M. S.; Davis, J. T. N2, C8-Disubstituted Guanosine Derivatives Can Form G-Quartets. *Tetrahedron Lett.* **2006**, *47*, 6381–6384. https://doi.org/10.1016/j.tetlet.2006.06.175.

(875) Ma, L.; Iezzi, M.; Kaucher, M. S.; Lam, Y.-F.; Davis, J. T. Cation Exchange in Lipophilic G-Quadruplexes: Not All Ion Binding Sites Are Equal. *J. Am. Chem. Soc.* **2006**, *128*, 15269–15277. https://doi.org/10.1021/ja064878n.

(876) Rivera, J. M.; Silva-Brenes, D. A Photoresponsive Supramolecular G-Quadruplex. *Org. Lett.* **2013**, *15*, 2350–2353. https://doi.org/10.1021/ol400610x.

(877) Martín-Hidalgo, M.; García-Arriaga, M.; González, F.; Rivera, J. M. Tuning Supramolecular G-Quadruplexes with Mono- and Divalent Cations. *Supramol. Chem.* **2015**, *27*, 174–180. https://doi.org/10.1080/10610278.2014.924626.

(878) Frańska, M. Interactions of Nucleobases with Alkali Earth Metal Cations—Electrospray Ionization Mass Spectrometric Study. *Eur. J. Mass Spectrom.* **2007**, *13*, 339–346. https://doi.org/10.1255/ejms.890.

(879) Frańska, M.; Łabędzka, M. Detection of 9-Methylhypoxanthine Tetrad by Electrospray Ionization Mass Spectrometry. *Int. J. Mass Spectrom.* **2012**, *323–324*, 41–44. https://doi.org/10.1016/j.ijms.2012.06.022.

(880) Davis, J. T. G-Quartets 40 Years Later: From 5′-GMP to Molecular Biology and Supramolecular Chemistry. *Angew. Chem. Int. Ed.* **2004**, *43*, 668–698. https://doi.org/10.1002/anie.200300589.

(881) Qiu, B.; Qin, Z.; Liu, J.; Luo, H. Thymine Quintets and Their Higher Order Assemblies Studied by Electrospray Ionization Mass Spectrometry and Theoretical Calculation. *J. Mass Spectrom.* **2011**, *46*, 587–594. https://doi.org/10.1002/jms.1928.

(882) Zins, E.-L.; Rochut, S.; Pepe, C. Theoretical and Experimental Studies of Cationized Uracil Complexes in the Gas Phase. *J. Mass Spectrom.* **2008**, *44*, 40–49. https://doi.org/10.1002/jms.1468.

(883) Na, N.; Shi, R.; Long, Z.; Lu, X.; Jiang, F.; Ouyang, J. Real-Time Analysis of Self-Assembled Nucleobases by Venturi Easy Ambient Sonic-Spray Ionization Mass Spectrometry. *Talanta* **2014**, *128*, 366–372. https://doi.org/10.1016/j.talanta.2014.04.080.

(884) Qin, Z.; Qiu, B.; Sun, J.; Zhao, W.; Luo, H. Protonated Primary Amines Induced Thymine Quintets Studied by Electrospray Ionization Mass Spectrometry and Density Functional Theory Calculations. *J. Mass Spectrom.* **2014**, *49*, 266–273. https://doi.org/10.1002/jms.3334.

(885) Qiu, B.; Liu, J.; Qin, Z.; Wang, G.; Luo, H. Quintets of Uracil and Thymine: A Novel Structure of Nucleobase Self-Assembly Studied by Electrospray Ionization Mass Spectrometry. *Chem. Commun.* **2009**, No. 20, 2863–2865. https://doi.org/10.1039/b903857d.

(886) Zins, E.-L.; Pepe, C.; Schröder, D. Decameric Uracil Complexes around Li+. *J. Mass Spectrom.* **2010**, *45*, 740–749. https://doi.org/10.1002/jms.1764.

(887) Trujillo, C.; Lamsabhi, A. M.; Mó, O.; Yáñez, M.; Salpin, J.-Y. Unimolecular Reactivity upon Collision of Uracil–Ca2+ Complexes in the Gas Phase: Comparison with Uracil–M+ (M=H, Alkali Metals) and Uracil–M2+ (M=Cu, Pb) Systems. *Int. J. Mass Spectrom.* **2011**, *306*, 27–36. https://doi.org/10.1016/j.ijms.2011.05.018.

(888) Guillaumont, S.; Tortajada, J.; Salpin, J.-Y.; Lamsabhi, A. M. Experimental and Computational Study of the Gas-Phase Interactions between Lead(II) Ions and Two Pyrimidic Nucleobases: Uracil and Thymine. *Int. J. Mass Spectrom.* **2005**, *243*, 279–293. https://doi.org/10.1016/j.ijms.2005.03.011.

(889) Gutlé, C.; Salpin, J.-Y.; Cartailler, T.; Tortajada, J.; Gaigeot, M.-P. Proton Transfers Induced by Lead(II) in a Uracil Nucleobase: A Study Based on Quantum Chemistry Calculations. *J. Phys. Chem. A* **2006**, *110*, 11684–11694. https://doi.org/10.1021/jp0621528.

(890) Salpin, J.-Y.; Haldys, V.; Guillaumont, S.; Tortajada, J.; Hurtado, M.; Lamsabhi, A. M. Gas-Phase Interactions between Lead(II) Ions and Cytosine: Tandem Mass Spectrometry and Infrared Multiple-Photon Dissociation Spectroscopy Study. *ChemPhysChem* **2014**, *15*, 2959–2971. https://doi.org/10.1002/cphc.201402369.

(891) Lamsabhi, A. M.; Alcamí, M.; Mó, O.; Yáñez, M.; Tortajada, J.; Salpin, J.-Y. Unimolecular Reactivity of Uracil–Cu2+ Complexes in the Gas Phase. *ChemPhysChem* **2007**, *8*, 181–187. https://doi.org/10.1002/cphc.200600399.

(892) Paston, S. V.; Nikolaev, A. I.; Ushkov, P. A. EDTA, Thymidine, and Cu2+ Ion Complexes from Mass Spectrometry Data. *J. Struct. Chem.* **2017**, *58*, 392–398. https://doi.org/10.1134/s0022476617020251.

(893) Mochizuki, S.; Wakisaka, A. Interactions of a Nucleoside Cytidine with Metal Ions in Water Observed through Mass Spectrometry: Clustering Controlled by Electrostatic Interaction and Coordinating Interaction. *J. Phys. Chem. B* **2003**, *107*, 5612–5616. https://doi.org/10.1021/jp030105z.

(894) Nakagawa, T.; Wakui, M.; Hayashida, T.; Nishime, C.; Murata, M. Intensive Optimization and Evaluation of Global DNA Methylation Quantification Using LC-MS/MS. *Anal. Bioanal. Chem.* **2019**, *411*, 7221–7231. https://doi.org/10.1007/s00216-019-02115-3.

(895) Yang, B.; Rodgers, M. T. Base-Pairing Energies of Protonated Nucleoside Base Pairs of DCyd and M5dCyd: Implications for the Stability of DNA i-Motif Conformations. *J. Am. Soc. Mass Spectrom.* **2015**, *26*, 1394–1403. https://doi.org/10.1007/s13361-015-1144-8.

(896) Ung, H. U.; Huynh, K. T.; Poutsma, J. C.; Oomens, J.; Berden, G.; Morton, T. H. Investigation of Proton Affinities and Gas Phase Vibrational Spectra of Protonated Nucleosides, Deoxynucleosides, and Their Analogs. *Int. J. Mass Spectrom.* **2015**, *378*, 294–302. https://doi.org/10.1016/j.ijms.2014.09.017.

(897) Fu, H.; Yang, P.; Hai, J.; Li, H. Utilization of Circular Dichroism and Electrospray Ionization Mass Spectrometry to Understand the Formation and Conversion of G-Quadruplex DNA at the Human c-Myb Proto-Oncogene. *Spectrochim. Acta. A. Mol. Biomol. Spectrosc.* **2018**, *203*, 70–76. https://doi.org/10.1016/j.saa.2018.05.079.

(898) Mazzitelli, C. L.; Wang, J.; Smith, S. I.; Brodbelt, J. S. Gas-Phase Stability of G-Quadruplex DNA Determined by Electrospray Ionization Tandem Mass Spectrometry and Molecular Dynamics Simulations. *J. Am. Soc. Mass Spectrom.* **2007**, *18*, 1760–1773. https://doi.org/10.1016/j.jasms.2007.07.008.

(899) Collie, G. W.; Parkinson, G. N.; Neidle, S.; Rosu, F.; De Pauw, E.; Gabelica, V. Electrospray Mass Spectrometry of Telomeric RNA (TERRA) Reveals the Formation of Stable Multimeric G-Quadruplex Structures. *J. Am. Chem. Soc.* **2010**, *132*, 9328–9334. https://doi.org/10.1021/ja100345z.

(900) Collie, G. W.; Parkinson, G. N. The Application of DNA and RNA G-Quadruplexes to Therapeutic Medicines. *Chem. Soc. Rev.* **2011**, *40*, 5867–5892. https://doi.org/10.1039/c1cs15067g.

(901) Guo, X.; Liu, S.; Yu, Z. Bimolecular Quadruplexes and Their Transitions to Higher-Order Molecular Structures Detected by ESI-FTICR-MS. *J. Am. Soc. Mass Spectrom.* **2007**, *18*, 1467–1476. https://doi.org/10.1016/j.jasms.2007.05.003.

(902) Malgowska, M.; Gudanis, D.; Kierzek, R.; Wyszko, E.; Gabelica, V.; Gdaniec, Z. Distinctive Structural Motifs of RNA G-Quadruplexes Composed of AGG, CGG and UGG Trinucleotide Repeats. *Nucleic Acids Res.* **2014**, *42*, 10196–10207. https://doi.org/10.1093/nar/gku710.

(903) Gros, J.; Rosu, F.; Amrane, S.; De Cian, A.; Gabelica, V.; Lacroix, L.; Mergny, J.-L. Guanines Are a Quartet's Best Friend: Impact of Base Substitutions on the Kinetics and Stability of Tetramolecular Quadruplexes. *Nucleic Acids Res.* **2007**, *35*, 3064–3075. https://doi.org/10.1093/nar/gkm111.

(904) Joly, L.; Rosu, F.; Gabelica, V. D(TGnT) DNA Sequences Do Not Necessarily Form Tetramolecular G-Quadruplexes. *Chem. Commun.* **2012**, *48*, 8386–8388. https://doi.org/10.1039/c2cc33316c.

(905) Sutton, J. M.; Bartlett, M. G. Modeling Cationic Adduction of Oligonucleotides Using Electrospray Desorption Ionization. *Rapid Commun. Mass Spectrom.* **2020**, *34*, e8696. https://doi.org/10.1002/rcm.8696.

(906) Piekarczyk, A.; Bald, I.; Flosadóttir, H. D.; Ómarsson, B.; Lafosse, A.; Ingólfsson, O. Influence of Metal Ion Complexation on the Metastable Fragmentation of DNA Hexamers. *Eur. Phys. J. D* **2014**, *68*, 146. https://doi.org/10.1140/epjd/e2014-40838-7.

(907) Favre, A.; Gonnet, F.; Tabet, J.-C. Location of the Na+ Cation in Negative Ions of DNA Evidenced by Using MS2 Experiments in Ion Trap Mass Spectrometry11Dedicated to J.F.J. Todd and R.E. March in Recognition of Their Original Contributions to Quadrupole Ion Trap Mass Spectrometry. *Int. J. Mass Spectrom.* **1999**, *190–191*, 303–312. https://doi.org/10.1016/s1387-3806(99)00049-4.

(908) Wu, Q.; Cheng, X.; Hofstadler, S. A.; Smith, R. D. Specific Metal-Oligonucleotide Binding Studied by High Resolution Tandem Mass Spectrometry. *J. Mass Spectrom.* **1996**, *31*, 669–675. https://doi.org/10.1002/(sici)1096-9888(199606)31:6<669::aid-jms340>3.0.co;2-5.

(909) Wang, Y.; Taylor, J.-S.; Gross, M. L. Fragmentation of Electrospray-Produced Oligodeoxynucleotide Ions Adducted to Metal Ions. *J. Am. Soc. Mass Spectrom.* **2001**, *12*, 550–556. https://doi.org/10.1016/S1044-0305(01)00231-8.

(910) Mass Spectrometry of Nucleosides and Nucleic Acids; Banoub, J. H., Limbach, P. A., Eds.; CRC Press: Boca Raton, FL, USA, 2009. https://doi.org/10.1201/9781420044034.

(911) Ma, G.; Yu, Z.; Zhou, W.; Li, Y.; Fan, L.; Li, X. Investigation of Na+ and K+ Competitively Binding with a G-Quadruplex and Discovery of a Stable K+–Na+-Quadruplex. *J. Phys. Chem. B* **2019**, *123*, 5405–5411. https://doi.org/10.1021/acs.jpcb.9b02823.

(912) Baker, E. S.; Gidden, J.; Ferzoco, A.; Bowers, M. T. Sodium Stabilization of Dinucleotide Multiplexes in the Gas Phase. *Phys. Chem. Chem. Phys.* **2004**, *6*, 2786–2795. https://doi.org/10.1039/B315727J.

(913) Yu, Z.; Zhou, W.; Han, J.; Li, Y.; Fan, L.; Li, X. Na+-Induced Conformational Change of Pb2+-Stabilized G-Quadruplex and Its Influence on Pb2+ Detection. *Anal. Chem.* **2016**, *88*, 9375–9380. https://doi.org/10.1021/acs.analchem.6b02466.

(914) Xu, Y.; Kaminaga, K.; Komiyama, M. G-Quadruplex Formation by Human Telomeric Repeats-Containing RNA in Na+ Solution. *J. Am. Chem. Soc.* **2008**, *130*, 11179–11184. https://doi.org/10.1021/ja8031532.

(915) Christian, N. P.; Colby, S. M.; Giver, L.; Houston, C. T.; Arnold, R. J.; Ellington, A. D.; Reiily, J. P. High Resolution Matrix-Assisted Laser Desorption/Ionization Time-of-Flight Analysis of Single-Stranded DNA of 27 to 68 Nucleotides in Length. *Rapid Commun. Mass Spectrom.* **1995**, *9*, 1061–1066. https://doi.org/10.1002/rcm.1290091118.

(916) Marchand, A.; Granzhan, A.; Iida, K.; Tsushima, Y.; Ma, Y.; Nagasawa, K.; Teulade-Fichou, M.-P.; Gabelica, V. Ligand-Induced Conformational Changes with Cation Ejection upon Binding to Human Telomeric DNA G-Quadruplexes. *J. Am. Chem. Soc.* **2015**, *137*, 750–756. https://doi.org/10.1021/ja5099403.

(917) Yu, Z.; Zhou, W.; Ma, G.; Li, Y.; Fan, L.; Li, X.; Lu, Y. Insights into the Competition between K^+ and Pb^{2+} Binding to a G-Quadruplex and Discovery of a Novel K^+–Pb^{2+}–Quadruplex Intermediate. *J. Phys. Chem. B* **2018**, *122*, 9382–9388. https://doi.org/10.1021/acs.jpcb.8b08161.

(918) Zhang, D.; Han, J.; Li, Y.; Fan, L.; Li, X. Aptamer-Based K+ Sensor: Process of Aptamer Transforming into G-Quadruplex. *J. Phys. Chem. B* **2016**, *120*, 6606–6611. https://doi.org/10.1021/acs.jpcb.6b05002.

(919) Keller, K. M.; Brodbelt, J. S. Charge State-Dependent Fragmentation of Oligonucleotide/Metal Complexes. *J. Am. Soc. Mass Spectrom.* **2005**, *16*, 28–37. https://doi.org/10.1016/j.jasms.2004.09.016.

(920) Torigoe, H.; Okamoto, I.; Dairaku, T.; Tanaka, Y.; Ono, A.; Kozasa, T. Thermodynamic and Structural Properties of the Specific Binding between Ag+ Ion and C:C Mismatched Base Pair in Duplex DNA to Form C–Ag–C Metal-Mediated Base Pair. *Biochimie* **2012**, *94*, 2431–2440. https://doi.org/10.1016/j.biochi.2012.06.024.

(921) Swasey, S. M.; Gwinn, E. G. Silver-Mediated Base Pairings: Towards Dynamic DNA Nanostructures with Enhanced Chemical and Thermal Stability. *New J. Phys.* **2016**, *18*, 045008. https://doi.org/10.1088/1367-2630/18/4/045008.

(922) Schultz, D.; Gwinn, E. G. Silver Atom and Strand Numbers in Fluorescent and Dark Ag:DNAs. *Chem. Commun.* **2012**, *48*, 5748–5750. https://doi.org/10.1039/c2cc17675k.

(923) Moye, A. L.; Porter, K. C.; Cohen, S. B.; Phan, T.; Zyner, K. G.; Sasaki, N.; Lovrecz, G. O.; Beck, J. L.; Bryan, T. M. Telomeric G-Quadruplexes Are a Substrate and Site of Localization for Human Telomerase. *Nat. Commun.* **2015**, *6*, 7643. https://doi.org/10.1038/ncomms8643.

(924) Wan, C.; Cui, M.; Song, F.; Liu, Z.; Liu, S. Evaluation of Effects of Bivalent Cations on the Formation of Purine-Rich Triple-Helix DNA by ESI-FT-MS. *J. Am. Soc. Mass Spectrom.* **2009**, *20*, 1281–1286. https://doi.org/10.1016/j.jasms.2009.02.026.

(925) Zhao, L. L.; Cao, T.; Zhou, Q. Y.; Zhang, X. H.; Zhou, Y. L.; Yang, L.; Zhang, X. X. The Exploration of a New Stable G-Triplex DNA and Its Novel Function in Electrochemical Biosensing. *Anal. Chem.* **2019**, *91*, 10731–10737. https://doi.org/10.1021/acs.analchem.9b02161.

(926) Rosu, F.; Gabelica, V.; Houssier, C.; Colson, P.; Pauw, E. D. Triplex and Quadruplex DNA Structures Studied by Electrospray Mass Spectrometry. *Rapid Commun. Mass Spectrom.* **2002**, *16*, 1729–1736. https://doi.org/10.1002/rcm.778.

(927) Amato, J.; Oliviero, G.; De Pauw, E.; Gabelica, V. Hybridization of Short Complementary PNAs to G-Quadruplex Forming Oligonucleotides: An Electrospray Mass Spectrometry Study. *Biopolymers* **2009**, *91*, 244–255. https://doi.org/10.1002/bip.21124.

(928) Wan, C.; Guo, X.; Song, F.; Liu, Z.; Liu, S. Interactions of Mitoxantrone with Duplex and Triplex DNA Studied by Electrospray Ionization Mass Spectrometry. *Rapid Commun. Mass Spectrom.* **2008**, *22*, 4043–4048. https://doi.org/10.1002/rcm.3793.

(929) Wan, C.; Guo, X.; Liu, Z.; Liu, S. Studies of the Intermolecular DNA Triplexes of C+·GC and T·AT Triplets by Electrospray Ionization Fourier-Transform Ion Cyclotron Resonance Mass Spectrometry. *J. Mass Spectrom.* **2008**, *43*, 164–172. https://doi.org/10.1002/jms.1277.

(930) Mariappan, S. V. S.; Cheng, X.; van Breemen, R. B.; Silks, L. A.; Gupta, G. Analysis of GAA/TTC DNA Triplexes Using Nuclear Magnetic Resonance and Electrospray Ionization Mass Spectrometry. *Anal. Biochem.* **2004**, *334*, 216–226. https://doi.org/10.1016/j.ab.2004.07.036.

(931) Rabin, C. Investigation of RNA Kissing Complexes by Native Electrospray Mass

Spectrometry: Magnesium Binding and Ion Mobility, Université de Bordeaux, Bordeaux, 2018.

(932) Piccolo, S. Biophysical Characterization of Aptamer-Ligand Interactions by Native Mass Spectrometry, Université de Bordeaux, Bordeaux, 2020.

(933) Pan, J.; Zhang, S. Interaction between Cationic Zinc Porphyrin and Lead Ion Induced Telomeric Guanine Quadruplexes: Evidence for End-Stacking. *JBIC J. Biol. Inorg. Chem.* **2009**, *14*, 401–407. https://doi.org/10.1007/s00775-008-0457-5.

(934) Anichina, J.; Bohme, D. K. Mass-Spectrometric Studies of the Interactions of Selected Metalloantibiotics and Drugs with Deprotonated Hexadeoxynucleotide GCATGC. *J. Phys. Chem. B* **2009**, *113*, 328–335. https://doi.org/10.1021/jp807034v.

(935) Monn, S. T. M.; Schürch, S. Investigation of Metal-Oligonucleotide Complexes by Nanoelectrospray Tandem Mass Spectrometry in the Positive Mode. *J. Am. Soc. Mass Spectrom.* **2005**, *16*, 370–378. https://doi.org/10.1016/j.jasms.2004.11.019.

(936) Hettich, R. L. Formation and Characterization of Iron–Oligonucleotide Complexes with Matrix-Assisted Laser Desorption/Ionization Fourier Transform Ion Cyclotron Resonance Mass Spectrometry11Dedicated to the Memory of Professor Ben Sherman Freiser, a Mentor Who Contributed Much to the Understanding of the Gas Phase Chemistry of Metal Ions and Their Complexes. *J. Am. Soc. Mass Spectrom.* **1999**, *10*, 941–949. https://doi.org/10.1016/S1044-0305(99)00073-2.

(937) Hettich, R. L. Investigating the Effect of Transition Metal Ion Oxidation State on Oligodeoxyribonucleotide Binding by Matrix-Assisted Laser Desorption/Ionization Fourier Transform Ion Cyclotron Resonance Mass Spectrometry. *Int. J. Mass Spectrom.* **2001**, *204*, 55–75. https://doi.org/10.1016/S1387-3806(00)00338-9.

(938) Christian, N. P.; Giver, L.; Ellington, A. D.; Reilly, J. P. Effects of Matrix Variations and the Presence of Iron on Matrix-Assisted Laser Desorption/Ionization Mass Spectra of DNA. *Rapid Commun. Mass Spectrom.* **1996**, *10*, 1980–1986. https://doi.org/10.1002/(sici)1097-0231(199612)10:15<1980::aid-rcm787>3.0.co;2-7.

(939) Punt, P. M.; Clever, G. H. Imidazole-Modified G-Quadruplex DNA as Metal-Triggered Peroxidase. *Chem. Sci.* **2019**, *10*, 2513–2518. https://doi.org/10.1039/c8sc05020a.

(940) Oehlers, L.; Mazzitelli, C. L.; Brodbelt, J. S.; Rodriguez, M.; Kerwin, S. Evaluation of Complexes of DNA Duplexes and Novel Benzoxazoles or Benzimidazoles by Electrospray Ionization Mass Spectrometry. *J. Am. Soc. Mass Spectrom.* **2004**, *15*, 1593–1603. https://doi.org/10.1016/j.jasms.2004.07.015.

(941) Sugiyama, K.; Kageyama, Y.; Okamoto, I.; Ono, A. Preparation and Metal Ion-Binding of 4-N-Substituted Cytosine Pairs in DNA Duplexes. *Nucleic Acids Symp. Ser.* **2007**, *51*, 177–178. https://doi.org/10.1093/nass/nrm089.

(942) Tanaka, K.; Clever, G. H.; Takezawa, Y.; Yamada, Y.; Kaul, C.; Shionoya, M.; Carell, T. Programmable Self-Assembly of Metal Ions inside Artificial DNA Duplexes. *Nat. Nanotechnol.* **2006**, *1*, 190–194. https://doi.org/10.1038/nnano.2006.141.

(943) Chiang, C.-K.; Lin, Y.-W.; Hu, C.-C.; Chang, H.-T. Using Electrospray Ionization Mass Spectrometry to Explore the Interactions among Polythymine Oligonucleotides, Ethidium Bromide, and Mercury Ions. *J. Am. Soc. Mass Spectrom.* **2009**, *20*, 1834–1840. https://doi.org/10.1016/j.jasms.2009.06.009.

(944) Miyake, Y.; Togashi, H.; Tashiro, M.; Yamaguchi, H.; Oda, S.; Kudo, M.; Tanaka, Y.; Kondo, Y.; Sawa, R.; Fujimoto, T.; et al. MercuryII-Mediated Formation of Thymine−HgII−Thymine Base Pairs in DNA Duplexes. *J. Am. Chem. Soc.* **2006**, *128*, 2172–2173. https://doi.org/10.1021/ja056354d.

(945) Smith, N. M.; Amrane, S.; Rosu, F.; Gabelica, V.; Mergny, J.-L. Mercury–Thymine Interaction with a Chair Type G-Quadruplex Architecture. *Chem. Commun.* **2012**, *48*, 11464–11466. https://doi.org/10.1039/c2cc36481f.

(946) Keller, K. M.; Breeden, M. M.; Zhang, J. M.; Ellington, A. D.; Brodbelt, J. S. Electrospray Ionization of Nucleic Acid Aptamer/Small Molecule Complexes for Screening Aptamer Selectivity. *J. Mass Spectrom.* **2005**, *40*, 1327–1337. https://doi.org/10.1002/jms.915.

(947) Puipaiboon, U.; Jai-nhukan, J.; Cowan, J. A. Rapid and Direct Seuencing of Double-Stranded DNA Using Exonulcease III and MALDI-TOF. *Anal. Chem.* **2000**, *72*, 3338–3341. https://doi.org/10.1021/ac000181n.

(948) Ross, P.; Hall, L.; Smirnov, I.; Haff, L. High Level Multiplex Genotyping by MALDI-TOF Mass Spectrometry. *Nat. Biotechnol.* **1998**, *16*, 1347–1351. https://doi.org/10.1038/4328.

(949) Haff, L. A.; Smirnov, I. P. Single-Nucleotide Polymorphism Identification Assays Using a Thermostable DNA Polymerase and Delayed Extraction MALDI-TOF Mass Spectrometry. *Genome Res.* **1997**, *7*, 378–388. https://doi.org/10.1101/gr.7.4.378.

(950) Su, K.-Y.; Goodman, S. D.; Lai, H.-M.; Yen, R.-S.; Hu, W.-Y.; Cheng, W.-C.; Lin, L.-I.; Yang, Y.-C.; Fang, W.-H. Proofreading and DNA Repair Assay Using Single Nucleotide Extension and MALDI-TOF Mass Spectrometry Analysis. *JoVE J. Vis. Exp.* **2018**, No. 136, e57862. https://doi.org/10.3791/57862.

(951) Johnson, K. M.; Price, N. E.; Wang, J.; Fekry, M. I.; Dutta, S.; Seiner, D. R.; Wang, Y.; Gates, K. S. On the Formation and Properties of Interstrand

DNA–DNA Cross-Links Forged by Reaction of an Abasic Site with the Opposing Guanine Residue of 5′-CAp Sequences in Duplex DNA. *J. Am. Chem. Soc.* **2013**, *135*, 1015–1025. https://doi.org/10.1021/ja308119q.

(952) Chang, H.-L.; Su, K.-Y.; Goodman, S. D.; Yen, R.-S.; Cheng, W.-C.; Yang, Y.-C.; Lin, L.-I.; Chang, S.-Y.; Fang, W. Measurement of Uracil-DNA Glycosylase Activity by Matrix Assisted Laser Desorption/Ionization Time-of-Flight Mass Spectrometry Technique. *DNA Repair* **2021**, *97*, 103028. https://doi.org/10.1016/j.dnarep.2020.103028.

(953) Ketterer, T.; Stadler, H.; Rickert, J.; Bayer, E.; Göpel, W. Detection of Oligonucleotide Sequences with Quartz Crystal Oscillators. *Sens. Actuators B Chem.* **2000**, *65*, 73–75. https://doi.org/10.1016/S0925-4005(99)00345-7.

(954) Ganem, B.; Li, Y.-T.; Henion, J. D. Detection of Oligonucleotide Duplex Forms by Ion-Spray Mass Spectrometry. *Tetrahedron Lett.* **1993**, *34*, 1445–1448. https://doi.org/10.1016/s0040-4039(00)60314-3.

(955) Gale, D. C.; Goodlett, D. R.; Light-Wahl, K. J.; Smith, R. D. Observation of Duplex DNA-Drug Noncovalent Complexes by Electrospray Ionization Mass Spectrometry. *J. Am. Chem. Soc.* **1994**, *116*, 6027–6028. https://doi.org/10.1021/ja00092a087.

(956) Bayer, Ernst.; Bauer, Tatjana.; Schmeer, Karl.; Bleicher, Konrad.; Maier, Martin.; Gaus, H.-Joachim. Analysis of Double-Stranded Oligonucleotides by Electrospray Mass Spectrometry. *Anal. Chem.* **1994**, *66*, 3858–3863. https://doi.org/10.1021/ac00094a004.

(957) Light-Wahl, K. J.; Springer, D. L.; Winger, B. E.; Edmonds, C. G.; Camp, D. G.; Thrall, B. D.; Smith, R. D. Observation of a Small Oligonucleotide Duplex by Electrospray Ionization Mass Spectrometry. *J. Am. Chem. Soc.* **1993**, *115*, 803–804. https://doi.org/10.1021/ja00055a070.

(958) Jianmei Ding, R. J. A. Specific and Nonspecific Dimer Formation in the Electrospray Ionization Mass Spectrometry of Oligonucleotides. *J. Am. Soc. Mass Spectrom.* **1995**, *6*, 159–164. https://doi.org/10.1016/1044-0305(94)00102-6.

(959) Hoyne, P. R.; Benson, L. M.; Veenstra, T. D.; Maher, L. J.; Naylor, S. RNA-RNA Noncovalent Interactions Investigated by Microspray Ionization Mass Spectrometry. *Rapid Commun. Mass Spectrom.* **2001**, *15*, 1539–1547. https://doi.org/10.1002/rcm.404.

(960) Gabelica, V.; De Pauw, E. Comparison of the Collision-Induced Dissociation of Duplex DNA at Different Collision Regimes: Evidence for a Multistep Dissociation Mechanism. *J. Am. Soc. Mass Spectrom.* **2002**, *13*, 91–98. https://doi.org/10.1016/S1044-0305(01)00335-X.

(961) Madsen, J. A.; Brodbelt, J. S. Asymmetric Charge Partitioning upon Dissociation of DNA Duplexes. *J. Am. Soc. Mass Spectrom.* **2010**, *21*, 1144–1150. https://doi.org/10.1016/j.jasms.2010.03.003.

(962) Ickert, S.; Schwaar, T.; Springer, A.; Grabarics, M.; Riedel, J.; Beck, S.; Pagel, K.; Linscheid, M. W. Comparison of the Fragmentation Behavior of DNA and LNA Single Strands and Duplexes. *J Mass Spectrom* **2019**, *54*, 402–411. https://doi.org/10.1002/jms.4344.

(963) Hari, Y.; Dugovic, B.; Istrate, A.; Fignole, A.; Leumann, C. J.; Schurch, S. The Contribution of the Activation Entropy to the Gas-Phase Stability of Modified Nucleic Acid Duplexes. *J. Am. Soc. Mass Spectrom.* **2016**, *27*, 1186–1196. https://doi.org/10.1007/s13361-016-1391-3.

(964) Gabelica, V.; Tabarin, T.; Antoine, R.; Rosu, F.; Compagnon, I.; Broyer, M.; De Pauw, E.; Dugourd, P. Electron Photodetachment Dissociation of DNA Polyanions in a Quadrupole Ion Trap Mass Spectrometer. *Anal. Chem.* **2006**, *78*, 6564–6572. https://doi.org/10.1021/ac060753p.

(965) Gabelica, V.; Pauw, E. D. Comparison between Solution-Phase Stability and Gas-Phase Kinetic Stability of Oligodeoxynucleotide Duplexes. *J. Mass Spectrom.* **2001**, *36*, 397–402. https://doi.org/10.1002/jms.141.

(966) Gabelica, V.; De Pauw, E. Collision-Induced Dissociation of 16-Mer DNA Duplexes with Various Sequences: Evidence for Conservation of the Double Helix Conformation in the Gas Phase. *Int. J. Mass Spectrom.* **2002**, *219*, 151–159. https://doi.org/10.1016/s1387-3806(01)00580-2.

(967) Yang, M.; Thompson, R.; Hall, G. Comparative Stability Determination of Oligonucleotide Duplexes in Gas and Solution Phase. *J. Am. Soc. Mass Spectrom.* **2004**, *15*, 1354–1359. https://doi.org/10.1016/j.jasms.2004.06.008.

(968) Pan, S.; Sun, X.; Lee, J. K. Stability of Complementary and Mismatched DNA Duplexes: Comparison and Contrast in Gas versus Solution Phases. *Int. J. Mass Spectrom.* **2006**, *253*, 238–248. https://doi.org/10.1016/j.ijms.2006.03.014.

(969) Lippens, J. L.; Ranganathan, S. V.; D'Esposito, R. J.; Fabris, D. Modular Calibrant Sets for the Structural Analysis of Nucleic Acids by Ion Mobility Spectrometry Mass Spectrometry. *Analyst* **2016**, *141*, 4084–4099. https://doi.org/10.1039/c6an00453a.

(970) Sharawy, M.; Consta, S. How Do Non-Covalent Complexes Dissociate in Droplets? A Case Study of the Desolvation of DsDNA from a Charged Aqueous Nanodrop. *Phys. Chem. Chem. Phys.* **2015**, *17*, 25550–25562. https://doi.org/10.1039/c5cp04331j.

(971) Schultze, P.; Hud, N. V.; Smith, F. W.; Feigon, J. The Effect of Sodium, Potassium and

Ammonium Ions on the Conformation of the Dimeric Quadruplex Formed by the Oxytricha Nova Telomere Repeat Oligonucleotide d(G(4)T(4)G(4)). *Nucleic Acids Res.* **1999**, *27*, 3018–3028. https://doi.org/10.1093/nar/27.15.3018.

(972) Schultze, P.; Smith, F. W.; Feigon, J. Refined Solution Structure of the Dimeric Quadruplex Formed from the Oxytricha Telomeric Oligonucleotide d(GGGGTTTTGGGG). *Structure* **1994**, *2*, 221–233. https://doi.org/10.1016/S0969-2126(00)00023-X.

(973) Hazel, P.; Parkinson, G. N.; Neidle, S. Topology Variation and Loop Structural Homology in Crystal and Simulated Structures of a Bimolecular DNA Quadruplex. *J. Am. Chem. Soc.* **2006**, *128*, 5480–5487. https://doi.org/10.1021/ja058577+.

(974) Arévalo-Ruiz, M.; Amrane, S.; Rosu, F.; Belmonte-Reche, E.; Peñalver, P.; Mergny, J.-L.; Morales, J. C. Symmetric and Dissymmetric Carbohydrate-Phenyl Ditriazole Derivatives as DNA G-Quadruplex Ligands: Synthesis, Biophysical Studies and Antiproliferative Activity. *Bioorganic Chem.* **2020**, *99*, 103786. https://doi.org/10.1016/j.bioorg.2020.103786.

(975) Birrento, M. L.; Bryan, T. M.; Samosorn, S.; Beck, J. L. ESI-MS Investigation of an Equilibrium between a Bimolecular Quadruplex DNA and a Duplex DNA/RNA Hybrid. *J. Am. Soc. Mass Spectrom.* **2015**, *26*, 1165–1173. https://doi.org/10.1007/s13361-015-1121-2.

(976) Lecours, M. J.; Marchand, A.; Anwar, A.; Guetta, C.; Hopkins, W. S.; Gabelica, V. What Stoichiometries Determined by Mass Spectrometry Reveal about the Ligand Binding Mode to G-Quadruplex Nucleic Acids. *Biochim. Biophys. Acta BBA - Gen. Subj.* **2017**, *1861*, 1353–1361. https://doi.org/10.1016/j.bbagen.2017.01.010.

(977) Ghosh, S.; Mendoza, O.; Cubo, L.; Rosu, F.; Gabelica, V.; White, A. J. P.; Vilar, R. Assembly of Palladium(II) and Platinum(II) Metallo-Rectangles with a Guanosine-Substituted Terpyridine and Study of Their Interactions with Quadruplex DNA. *Chem. – Eur. J.* **2014**, *20*, 4772–4779. https://doi.org/10.1002/chem.201304905.

(978) Gao, S.; Cao, Y.; Yan, Y.; Guo, X. Sequence Effect on the Topology of 3 + 1 Interlocked Bimolecular DNA G-Quadruplexes. *Biochemistry* **2016**, *55*, 2694–2703. https://doi.org/10.1021/acs.biochem.5b01190.

(979) Do, N. Q.; Lim, K. W.; Teo, M. H.; Heddi, B.; Phan, A. T. Stacking of G-Quadruplexes: NMR Structure of a G-Rich Oligonucleotide with Potential Anti-HIV and Anticancer Activity. *Nucleic Acids Res.* **2011**, *39*, 9448–9457. https://doi.org/10.1093/nar/gkr539.

(980) Phan, A. T.; Kuryavyi, V.; Ma, J.-B.; Faure, A.; Andréola, M.-L.; Patel, D. J. An Interlocked Dimeric Parallel-Stranded DNA Quadruplex: A Potent Inhibitor of HIV-1 Integrase. *Proc. Natl. Acad. Sci. U. S. A.* **2005**, *102*, 634–639. https://doi.org/10.1073/pnas.0406278102.

(981) Li, H.; Zhang, Q.; Yuan, G. Investigation of the Formation and Recognition of a Dimeric G-Quadruplex in the Promoter of Bcl-2 Proto-Oncogene by Electrospray Ionization Mass Spectrometry. *Rapid Commun. Mass Spectrom.* **2010**, *24*, 393–395. https://doi.org/10.1002/rcm.4397.

(982) Goodlett, D. R.; Camp, D. G.; Hardin, C. C.; Corregan, M.; Smith, R. D. Direct Observation of a DNA Quadruplex by Electrospray Ionization Mass Spectrometry. *Biol. Mass Spectrom.* **1993**, *22*, 181–183. https://doi.org/10.1002/bms.1200220307.

(983) Zhou, J.; Yuan, G.; Liu, J.; Zhan, C.-G. Formation and Stability of G-Quadruplexes Self-Assembled from Guanine-Rich Strands. *Chem. - Eur. J.* **2007**, *13*, 945–949. https://doi.org/10.1002/chem.200600424.

(984) Jaksa, S.; Kralj, B.; Pannecouque, C.; Balzarini, J.; De Clercq, E.; Kobe, J. How a Modification (8-Aza-3-Deaza-2'-Deoxyguanosine) Influences the Quadruplex Structure of Hotoda's 6-Mer TGGGAG with 5'- and 3'-End Modifications. *Nucleosides Nucleotides Nucleic Acids* **2004**, *23*, 77–88. https://doi.org/10.1081/ncn-120027819.

(985) Sengar, A.; Heddi, B.; Phan, A. T. Formation of G-Quadruplexes in Poly-G Sequences: Structure of a Propeller-Type Parallel-Stranded G-Quadruplex Formed by a G15 Stretch | Biochemistry. *Biochemistry* **2014**, *53*, 7718–7723. https://doi.org/10.1021/bi500990v.

(986) Štefl, R.; Cheatham, T. E.; Špačková, N.; Fadrná, E.; Berger, I.; Koča, J.; Šponer, J. Formation Pathways of a Guanine-Quadruplex DNA Revealed by Molecular Dynamics and Thermodynamic Analysis of the Substates. *Biophys. J.* **2003**, *85*, 1787–1804.

(987) Šponer, J.; Špačková, N. Molecular Dynamics Simulations and Their Application to Four-Stranded DNA. *Methods* **2007**, *43*, 278–290. https://doi.org/10.1016/j.ymeth.2007.02.004.

(988) Cao, Y.; Gao, S.; Li, C.; Yan, Y.; Wang, B.; Guo, X. Structural Varieties of Selectively Mixed G- and C-Rich Short DNA Sequences Studied with Electrospray Ionization Mass Spectrometry. *J. Mass Spectrom.* **2016**, *51*, 931–937. https://doi.org/10.1002/jms.3804.

(989) Evans, S. E.; Mendez, M. A.; Turner, K. B.; Keating, L. R.; Grimes, R. T.; Melchoir, S.; Szalai, V. A. End-Stacking of Copper Cationic Porphyrins on Parallel-Stranded Guanine Quadruplexes. *J. Biol. Inorg. Chem.* **2007**, *12*, 1235–1249. https://doi.org/10.1007/s00775-007-0292-0.

(990) Oganesian, L.; Graham, M. E.; Robinson, P. J.; Bryan, T. M. Telomerase Recognizes G-

Quadruplex and Linear DNA as Distinct Substrates. *Biochemistry* **2007**, *46*, 11279–11290. https://doi.org/10.1021/bi700993q.

(991) Porter, J. E.; Chapagain, P.; Fernandez-Lima, F. Single-Stranded DNA Structural Diversity: TAGGGT from Monomers to Dimers to Tetramer Formation. *Rapid Commun. Mass Spectrom.* **2019**, *33*, 60–65. https://doi.org/10.1002/rcm.8367.

(992) Xiang, X.; Bao, Y.; Sun, L.; Zhang, Y.; Guo, X. A Stable Uncompleted Tetramolecular G-Quadruplex Formed by d(AGnA) under Acidic Condition. *Int. J. Biol. Macromol.* **2021**, *176*, 66–71. https://doi.org/10.1016/j.ijbiomac.2021.02.059.

(993) Krishnan-Ghosh, Y.; Liu, D. S.; Balasubramanian, S. Formation of an Interlocked Quadruplex Dimer by d(GGGT). *J. Am. Chem. Soc.* **2004**, *126*, 11009–11016. https://doi.org/10.1021/ja049259y.

(994) Zhou, J.; Murayama, K.; Amrane, S.; Rosu, F.; Kashida, H.; Bourdoncle, A.; Asanuma, H.; Mergny, J.-L. A "Sugar-Deficient" G-Quadruplex: Incorporation of ATNA in G4 Structures. *Chem. Sci.* **1392**, *4*, 3693–3698. https://doi.org/10.1039/C3SC50474C.

(995) Tan, W.; Yi, L.; Zhu, Z.; Zhang, L.; Zhou, J.; Yuan, G. Hsa-miR-1587 G-quadruplex Formation and Dimerization Induced by NH4+, Molecular Crowding Environment and Jatrorrhizine Derivatives. *Talanta* **2018**, *179*, 337–343. https://doi.org/10.1016/j.talanta.2017.11.041.

(996) Zhou, J.; Bourdoncle, A.; Rosu, F.; Gabelica, V.; Mergny, J.-L. Tri-G-Quadruplex: Controlled Assembly of a G-Quadruplex Structure from Three G-Rich Strands. *Angew. Chem. Int. Ed.* **2012**, *51*, 11002–11005. https://doi.org/10.1002/anie.201205390.

(997) Cao, Y.; Gao, S.; Yan, Y.; Bruist, M. F.; Wang, B.; Guo, X. Assembly of Supramolecular DNA Complexes Containing Both G-Quadruplexes and i-Motifs by Enhancing the G-Repeat-Bearing Capacity of i-Motifs. *Nucleic Acids Res.* **2017**, *45*, 26–38. https://doi.org/10.1093/nar/gkw1049.

(998) Modi, S.; Wani, A. H.; Krishnan, Y. The PNA-DNA Hybrid I-Motif: Implications for Sugar-Sugar Contacts in i-Motif Tetramerization. *Nucleic Acids Res.* **2006**, *34*, 4354–4363. https://doi.org/10.1093/nar/gkl443.

(999) Yang, B.; Wu, R. R.; Berden, G.; Oomens, J.; Rodgers, M. T. Infrared Multiple Photon Dissociation Action Spectroscopy of Proton-Bound Dimers of Cytosine and Modified Cytosines: Effects of Modifications on Gas-Phase Conformations. *J. Phys. Chem. B* **2013**, *117*, 14191–14201. https://doi.org/10.1021/jp405105w.

(1000) Cao, Y.; Qin, Y.; Bruist, M.; Gao, S.; Wang, B.; Wang, H.; Guo, X. Formation and Dissociation of the Interstrand I-Motif by the Sequences d(XnC4Ym) Monitored with Electrospray Ionization Mass Spectrometry. *J. Am. Soc. Mass Spectrom.* **2015**, *26*, 994–1003. https://doi.org/10.1007/s13361-015-1093-2.

(1001) Garavís, M.; Escaja, N.; Gabelica, V.; Villasante, A.; González, C. Centromeric Alpha-Satellite DNA Adopts Dimeric i-Motif Structures Capped by AT Hoogsteen Base Pairs. *Chem. – Eur. J.* **2015**, *21*, 9816–9824. https://doi.org/10.1002/chem.201500448.

(1002) Garavís, M.; Méndez-Lago, M.; Gabelica, V.; Whitehead, S. L.; González, C.; Villasante, A. The Structure of an Endogenous Drosophila Centromere Reveals the Prevalence of Tandemly Repeated Sequences Able to Form I-Motifs. *Sci. Rep.* **2015**, *5*, 13307. https://doi.org/10.1038/srep13307.

(1003) Stephenson, W.; Asare-Okai, P. N.; Chen, A. A.; Keller, S.; Santiago, R.; Tenenbaum, S. A.; Garcia, A. E.; Fabris, D.; Li, P. T. The Essential Role of Stacking Adenines in a Two-Base-Pair RNA Kissing Complex. *J. Am. Chem. Soc.* **2013**, *135*, 5602–5611. https://doi.org/10.1021/ja310820h.

(1004) Abi-Ghanem, J.; Rabin, C.; Porrini, M.; Dausse, E.; Toulmé, J.; Gabelica, V. Electrostatics Explains the Position-Dependent Effect of G·U Wobble Base Pairs on the Affinity of RNA Kissing Complexes. *ChemPhysChem* **2017**, *18*, 2782–2790. https://doi.org/10.1002/cphc.201700337.

(1005) Turner, K. B.; Hagan, N. A.; Fabris, D. Understanding the Isomerization of the HIV-1 Dimerization Initiation Domain by the Nucleocapsid Protein. *J. Mol. Biol.* **2007**, *369*, 812–828. https://doi.org/10.1016/j.jmb.2007.03.065.

(1006) Fabris, D.; Chaudhari, P.; Hagan, N.; Turner, K. Functional Investigations of Retroviral Protein—Ribonucleic Acid Complexes by Nanospray Fourier Transform Ion Cyclotron Resonance Mass Spectrometry. *Eur. J. Mass Spectrom.* **2007**, *13*, 29–33. https://doi.org/10.1255/ejms.839.

(1007) Hagan, N. A.; Fabris, D. Dissecting the Protein–RNA and RNA–RNA Interactions in the Nucleocapsid-Mediated Dimerization and Isomerization of HIV-1 Stemloop 1. *J. Mol. Biol.* **2007**, *365*, 396–410. https://doi.org/10.1016/j.jmb.2006.09.081.

(1008) Turner, K. B.; Kohlway, A. S.; Hagan, N. A.; Fabris, D. Noncovalent Probes for the Investigation of Structure and Dynamics of Protein-Nucleic Acid Assemblies: The Case of NC-Mediated Dimerization of Genomic RNA in HIV-1. *Biopolymers* **2009**, *91*, 283–296. https://doi.org/10.1002/bip.21107.

(1009) Amato, J.; Pagano, B.; Borbone, N.; Oliviero, G.; Gabelica, V.; Pauw, E. D.; D'Errico, S.; Piccialli, V.; Varra, M.; Giancola, C.; et al. Targeting G-Quadruplex Structure in the Human c-Kit Promoter with Short PNA Sequences.

Bioconjug. Chem. **2011**, *22*, 654–663. https://doi.org/10.1021/bc100444v.

(1010) Onyshchenko, M. I.; Gaynutdinov, T. I.; Englund, E. A.; Appella, D. H.; Neumann, R. D.; Panyutin, I. G. Stabilization of G-Quadruplex in the BCL2 Promoter Region in Double-Stranded DNA by Invading Short PNAs. *Nucleic Acids Res.* **2009**, *37*, 7570–7580. https://doi.org/10.1093/nar/gkp840.

(1011) Paul, A.; Sengupta, P.; Krishnan, Y.; Ladame, S. Combining G-Quadruplex Targeting Motifs on a Single Peptide Nucleic Acid Scaffold: A Hybrid (3+1) PNA–DNA Bimolecular Quadruplex. *Chem. – Eur. J.* **2008**, *14*, 8682–8689. https://doi.org/10.1002/chem.200800605.

(1012) Kormuth, K. A.; Woolford, J. L.; Armitage, B. A. Homologous PNA Hybridization to Noncanonical DNA G-Quadruplexes. *Biochemistry* **2016**, *55*, 1749–1757. https://doi.org/10.1021/acs.biochem.6b00026.

(1013) Amato, J.; Gabelica, V.; Borbone, N.; Rosu, F.; Pauw, E. D.; Oliviero, G.; Piccialli, G.; Mayol, L. A Short C-Rich PNA Fragment Capable to Form Novel G-Quadruplex-PNA Complexes. *Nucleic Acids Symp. Ser.* **2008**, *52*, 167–168. https://doi.org/10.1093/nass/nrn085.

(1014) Datta, B.; Bier, M. E.; Roy, S.; Armitage, B. A. Quadruplex Formation by a Guanine-Rich PNA Oligomer. *J. Am. Chem. Soc.* **2005**, *127*, 4199–4207. https://doi.org/10.1021/ja0446202.

(1015) Krishnan-Ghosh, Y.; Whitney, A. M.; Balasubramanian, S. Dynamic Covalent Chemistry on Self-Templating PNA Oligomers: Formation of a Bimolecular PNA Quadruplex. *Chem. Commun.* **2005**, No. 24, 3068–3070. https://doi.org/10.1039/b503578c.

(1016) Colgrave, M. L.; Beck, J. L.; Sheil, M. M.; Searle, M. S. Electrospray Ionisation Mass Spectrometric Detection of Weak Non-Covalent Interactions in Nogalamycin–DNA Complexes. *Chem. Commun.* **2002**, No. 6, 556–557. https://doi.org/10.1039/b200235n.

(1017) Asare-Okai, P. N.; Chow, C. S. A Modified Fluorescent Intercalator Displacement Assay for RNA Ligand Discovery. *Anal. Biochem.* **2011**, *408*, 269–276. https://doi.org/10.1016/j.ab.2010.09.020.

(1018) Guo, X. H.; Bruist, M. F.; Davis, D. L.; Bentzley, C. M. Secondary Structural Characterization of Oligonucleotide Strands Using Electrospray Ionization Mass Spectrometry. *Nucleic Acids Res.* **2005**, *33*, 3659–3666. https://doi.org/10.1093/nar/gki671.

(1019) Su, D. G. T.; Fang, H.; Gross, M. L.; Taylor, J.-S. A. Photocrosslinking of Human Telomeric G-Quadruplex Loops by Anti Cyclobutane Thymine Dimer Formation. *Proc. Natl. Acad. Sci. U. S. A.* **2009**, *106*, 12861–12866. https://doi.org/10.1073/pnas.0902386106.

(1020) Mergny, J. L.; Phan, A. T.; Lacroix, L. Following G-Quartet Formation by UV-Spectroscopy. *FEBS Lett.* **1998**, *435*, 74–78. https://doi.org/10.1016/s0014-5793(98)01043-6.

(1021) Rachwal, P. A.; Fox, K. R. Quadruplex Melting. *Methods* **2007**, *43*, 291–301. https://doi.org/10.1016/j.ymeth.2007.05.004.

(1022) Mergny, J.-L.; Lacroix, L. Analysis of Thermal Melting Curves. *Oligonucleotides* **2003**, *13*, 515–537. https://doi.org/10.1089/154545703322860825.

(1023) Ambrus, A.; Chen, D.; Dai, J.; Jones, R. A.; Yang, D. Solution Structure of the Biologically Relevant G-Quadruplex Element in the Human c-MYC Promoter. Implications for G-Quadruplex Stabilization. *Biochemistry* **2005**, *44*, 2048–2058. https://doi.org/10.1021/bi048242p.

(1024) Seenisamy, J.; Rezler, E. M.; Powell, T. J.; Tye, D.; Gokhale, V.; Joshi, C. S.; Siddiqui-Jain, A.; Hurley, L. H. The Dynamic Character of the G-Quadruplex Element in the c-MYC Promoter and Modification by TMPyP4. *J. Am. Chem. Soc.* **2004**, *126*, 8702–8709. https://doi.org/10.1021/ja040022b.

(1025) Rosu, F.; Gabelica, V.; Joly, L.; Grégoire, G.; De Pauw, E. Zwitterionic I-Motif Structures Are Preserved in DNA Negatively Charged Ions Produced by Electrospray Mass Spectrometry. *Phys. Chem. Chem. Phys.* **2010**, *12*, 13448–13454.

(1026) Garavís, M.; Escaja, N.; Gabelica, V.; Villasante, A.; González, C. Centromeric Alpha-Satellite DNA Adopts Dimeric i-Motif Structures Capped by at Hoogsteen Base Pairs. *Chem. - Eur. J.* **2015**, *21*, 9816–9824. https://doi.org/10.1002/chem.201500448.

(1027) Sedghi, M. S.; Yamaoki, Y.; Ma, Y.; Marchand, A. Analysis of Interactions between Telomeric I-Motif DNA and a Cyclic Tetraoxazole Compound. *ChemBioChem* **2018**, *19*, 2268–2272. https://doi.org/10.1002/cbic.201800425.

(1028) Yang, Y.; Fu, H.; Qian, C.; Li, H.; Chen, D. D. Y. Characterization of Interaction between Bcl-2 Oncogene Promoter I-Motif DNA and Flavonoids Using Electrospray Ionization Mass Spectrometry and Pressure-Assisted Capillary Electrophoresis Frontal Analysis. *Talanta* **2020**, *215*, 120885. https://doi.org/10.1016/j.talanta.2020.120885.

(1029) Keller, K. M.; Zhang, J. M.; Oehlers, L.; Brodbelt, J. S. Influence of Initial Charge State on Fragmentation Patterns for Noncovalent Drug/DNA Duplex Complexes. *J. Mass Spectrom.* **2005**, *40*, 1362–1371. https://doi.org/10.1002/jms.927.

(1030) Schlosser, G.; Vekey, K.; Malorni, A.; Pocsfalvi, G. Combination of Solid-Phase Affinity Capture on Magnetic Beads and Mass Spectrometry to Study Non-Covalent Interactions: Example of Minor Groove Binding Drugs. *Rapid Commun.*

Mass Spectrom. **2005**, *19*, 3307–3314. https://doi.org/10.1002/rcm.2193.

(1031) Wilson, J. J.; Brodbelt, J. S. Infrared Multiphoton Dissociation of Duplex DNA/Drug Complexes in a Quadrupole Ion Trap. *Anal. Chem.* **2007**, *79*, 2067–2077. https://doi.org/10.1021/ac061946f.

(1032) Gabelica, V.; Rosu, F.; Houssier, C.; De Pauw, E. Gas Phase Thermal Denaturation of an Oligonucleotide Duplex and Its Complexes with Minor Groove Binders. *Rapid Commun. Mass Spectrom.* **2000**, *14*, 464–467. https://doi.org/10.1002/(SICI)1097-0231(20000331)14:6<464::AID-RCM895>3.0.CO;2-M.

(1033) Laughlin, S.; Wilson, W. D. May the Best Molecule Win: Competition ESI Mass Spectrometry. *Int. J. Mol. Sci.* **2015**, *16*, 24506–24531. https://doi.org/10.3390/ijms161024506.

(1034) Wang, S.; Munde, M.; Wang, S.; Wilson, W. D. Minor Groove to Major Groove, an Unusual DNA Sequence-Dependent Change in Bend Directionality by a Distamycin Dimer. *Biochemistry* **2011**, *50*, 7674–7683. https://doi.org/10.1021/bi201010g.

(1035) Wan, K. X.; Gross, M. L.; Shibue, T. Gas-Phase Stability of Double-Stranded Oligodeoxynucleotides and Their Noncovalent Complexes with DNA-Binding Drugs as Revealed by Collisional Activation in an Ion Trap. *J. Am. Soc. Mass Spectrom.* **2000**, *11*, 450–457. https://doi.org/10.1016/s1044-0305(00)00095-7.

(1036) Wan, K. X.; Shibue, T.; Gross, M. L. Non-Covalent Complexes between DNA-Binding Drugs and Double-Stranded Oligodeoxynucleotides: A Study by ESI Ion-Trap Mass Spectrometry. *J. Am. Chem. Soc.* **2000**, *122*, 300–307. https://doi.org/10.1021/ja990684e.

(1037) Gale, D. C.; Smith, R. D. Characterization of Noncovalent Complexes Formed between Minor Groove Binding Molecules and Duplex DNA by Electrospray Ionization-Mass Spectrometry. *J. Am. Soc. Mass Spectrom.* **1995**, *6*, 1154–1164. https://doi.org/10.1016/1044-0305(95)00530-7.

(1038) Greig, M. J.; Robinson, J. M. Detection of Oligonucleotide-Ligand Complexes by ESI-MS (DOLCE-MS) as a Component of High Throughput Screening. *J. Biomol. Screen.* **2000**, *5*, 441–454. https://doi.org/10.1177/108705710000500607.

(1039) Gupta, R.; Beck, J. L.; Ralph, S. F.; Sheil, M. M.; Aldrich-Wright, J. R. Comparison of the Binding Stoichiometries of Positively Charged DNA-Binding Drugs Using Positive and Negative Ion Electrospray Ionization Mass Spectrometry. *J. Am. Soc. Mass Spectrom.* **2004**, *15*, 1382–1391. https://doi.org/10.1016/j.jasms.2004.07.005.

(1040) Triolo, A.; Arcamone, F. M.; Raffaelli, A.; Salvadori, P. Non-Covalent Complexes between DNA-Binding Drugs and Double-Stranded Deoxyoligonucleotides: A Study by Ionspray Mass Spectrometry. *J. Mass Spectrom.* **1997**, *32*, 1186–1194. https://doi.org/10.1002/(sici)1096-9888(199711)32:11<1186::aid-jms575>3.0.co;2-g.

(1041) Xu, Y.; Afonso, C.; Wen, R.; Tabet, J.-C. Investigation of Double-Stranded DNA/Drug Interaction by ESI/FT ICR: Orientation of Dissociations Relates to Stabilizing Salt Bridges. *J. Mass Spectrom.* **2008**, *43*, 1531–1544. https://doi.org/10.1002/jms.1430.

(1042) Jain, A. K.; Gupta, S. K.; Tandon, V. Evaluation of Electronic Effect of Phenyl Ring Substituents on the DNA Minor Groove Binding Properties of Novel Bis and Terbenzimidazoles: Synthesis and Spectroscopic Studies of Ligand-DNA Interaction. *Oligonucleotides* **2009**, *19*, 329–340. https://doi.org/10.1089/oli.2009.0190.

(1043) Laughlin, S.; Wang, S.; Kumar, A.; Farahat, A. A.; Boykin, D. W.; Wilson, W. D. Resolution of Mixed Site DNA Complexes with Dimer-Forming Minor-Groove Binders by Using Electrospray Ionization Mass Spectrometry: Compound Structure and DNA Sequence Effects. *Chem. – Eur. J.* **2015**, *21*, 5528–5539. https://doi.org/10.1002/chem.201406322.

(1044) Zhou, J.; Yuan, G.; Tang, F. L. Estimation of Binding Constants for Complexes of Polyamides and Human Telomeric DNA Sequences by Electrospray Ionization Mass Spectrometry. *Rapid Commun. Mass Spectrom.* **2006**, *20*, 2365–2367. https://doi.org/10.1002/rcm.2597.

(1045) Li, H.; Yuan, G. Evaluation of Binding Selectivity of a Polyamide Probe to Single Base-Pair Different Dna in A·T-Rich Region by Electrospray Ionization Mass Spectrometry. *J. Am. Soc. Mass Spectrom.* **2006**, *17*, 1742–1748. https://doi.org/10.1016/j.jasms.2006.07.028.

(1046) Laughlin, S.; Wang, S.; Kumar, A.; Boykin, D. W.; Wilson, W. D. A Novel Approach Using Electrospray Ionization Mass Spectrometry to Study Competitive Binding of Small Molecules with Mixed DNA Sequences. *Anal. Bioanal. Chem.* **2014**, *406*, 6441–6445. https://doi.org/10.1007/s00216-014-8044-9.

(1047) Liu, Y.; Chai, Y.; Kumar, A.; Tidwell, R. R.; Boykin, D. W.; Wilson, W. D. Designed Compounds for Recognition of 10 Base Pairs of DNA with Two AT Binding Sites. *J. Am. Chem. Soc.* **2012**, *134*, 5290–5299. https://doi.org/10.1021/ja211628j.

(1048) Paul, A.; Nanjunda, R.; Kumar, A.; Laughlin, S.; Nhili, R.; Depauw, S.; Deuser, S. S.; Chai, Y.; Chaudhary, A. S.; David-Cordonnier, M.-H.; et al. Mixed up Minor Groove Binders: Convincing A·T Specific Compounds to Recognize a G·C Base Pair. *Bioorg. Med. Chem. Lett.* **2015**, *25*,

4927–4932. https://doi.org/10.1016/j.bmcl.2015.05.005.

(1049) Paul, A.; Chai, Y.; Boykin, D. W.; Wilson, W. D. Understanding Mixed Sequence DNA Recognition by Novel Designed Compounds: The Kinetic and Thermodynamic Behavior of Azabenzimidazole Diamidines. *Biochemistry* **2015**, *54*, 577–587. https://doi.org/10.1021/bi500989r.

(1050) Guo, P.; Paul, A.; Kumar, A.; Farahat, A. A.; Kumar, D.; Wang, S.; Boykin, D. W.; Wilson, W. D. The Thiophene "Sigma-Hole" as a Concept for Preorganized, Specific Recognition of G·C Base Pairs in the DNA Minor Groove. *Chem. – Eur. J.* **2016**, *22*, 15404–15412. https://doi.org/10.1002/chem.201603422.

(1051) Rogniaux, H.; Van Dorsselaer, A.; Barth, P.; Biellmann, J. F.; Barbanton, J.; van Zandt, M.; Chevrier, B.; Howard, E.; Mitschler, A.; Potier, N.; et al. Binding of Aldose Reductase Inhibitors: Correlation of Crystallographic and Mass Spectrometric Studies. *J. Am. Soc. Mass Spectrom.* **1999**, *10*, 635–647. https://doi.org/10.1016/S1044-0305(99)00030-6.

(1052) Guittat, L.; De Cian, A.; Rosu, F.; Gabelica, V.; De Pauw, E.; Delfourne, E.; Mergny, J.-L. Ascididemin and Meridine Stabilise G-Quadruplexes and Inhibit Telomerase in Vitro. *Biochim. Biophys. Acta BBA - Gen. Subj.* **2005**, *1724*, 375–384. https://doi.org/10.1016/j.bbagen.2005.04.023.

(1053) Monchaud, D.; Allain, C.; Bertrand, H.; Smargiasso, N.; Rosu, F.; Gabelica, V.; De Cian, A.; Mergny, J.-L.; Teulade-Fichou, M.-P. Ligands Playing Musical Chairs with G-Quadruplex DNA: A Rapid and Simple Displacement Assay for Identifying Selective G-Quadruplex Binders. *Biochimie* **2008**, *90*, 1207–1223. https://doi.org/10.1016/j.biochi.2008.02.019.

(1054) Pothukuchy, A.; Mazzitelli, C. L.; Rodriguez, M. L.; Tuesuwan, B.; Salazar, M.; Brodbelt, J. S.; Kerwin, S. M. Duplex and Quadruplex DNA Binding and Photocleavage by Trioxatriangulenium Lone. *Biochemistry* **2005**, *44*, 2163–2172. https://doi.org/10.1021/bi0485981.

(1055) Mazzitelli, C. L.; Chu, Y.; Reczek, J. J.; Iverson, B. L.; Brodbelt, J. S. Screening of Threading Bis-Intercalators Binding to Duplex DNA by Electrospray Ionization Tandem Mass Spectrometry. *J. Am. Soc. Mass Spectrom.* **2007**, *18*, 311–321. https://doi.org/10.1016/j.jasms.2006.09.021.

(1056) Kapur, A.; Beck, J. L.; Sheil, M. M. Observation of Daunomycin and Nogalamycin Complexes with Duplex DNA Using Electrospray Ionization Mass Spectrometry. *Rapid Commun. Mass Spectrom.* **1999**, *13*, 2489–2497. https://doi.org/10.1002/(sici)1097-0231(19991230)13:24<2489::aid-rcm816>3.0.co;2-f.

(1057) Scaglioni, L.; Mondelli, R.; Artali, R.; Sirtori, F. R.; Mazzini, S. Nemorubicin and Doxorubicin Bind the G-Quadruplex Sequences of the Human Telomeres and of the c-MYC Promoter Element Pu22. *Biochim. Biophys. Acta BBA - Gen. Subj.* **2016**, *1860*, 1129–1138. https://doi.org/10.1016/j.bbagen.2016.02.011.

(1058) Scalabrin, M.; Quintieri, L.; Palumbo, M.; Riccardi Sirtori, F.; Gatto, B. Virtual Cross-Linking of the Active Nemorubicin Metabolite PNU-159682 to Double-Stranded DNA. *Chem. Res. Toxicol.* **2017**, *30*, 614–624. https://doi.org/10.1021/acs.chemrestox.6b00362.

(1059) Wang, Z.; Cui, M.; Song, F.; Lu, L.; Liu, Z.; Liu, S. Evaluation of Flavonoids Binding to DNA Duplexes by Electrospray Ionization Mass Spectrometry. *J. Am. Soc. Mass Spectrom.* **2008**, *19*, 914–922. https://doi.org/10.1016/j.jasms.2008.04.018.

(1060) Juskowiak, B.; Gałęzowska, E.; Takenaka, S. Spectral Properties and Binding Study of DNA Complexes with a Rigid Bisintercalator 1,4-Bis((N-Methylquinolinium-4-Yl)Vinyl)Benzene. *Spectrochim. Acta. A. Mol. Biomol. Spectrosc.* **2003**, *59*, 1083–1094. https://doi.org/10.1016/S1386-1425(02)00276-7.

(1061) Bahr, M.; Gabélica, V.; Granzhan, A.; Weinhold, E.; Teulade-Fichou, M.-P. Recognition of Homopyrimidine Mismatches by Distance-Constrained Macrocyclic Bisintercalators. *Nucleic Acids Symp. Ser.* **2008**, *52*, 109–110. https://doi.org/10.1093/nass/nrn056.

(1062) Bahr, M.; Gabelica, V.; Granzhan, A.; Teulade-Fichou, M.-P.; Weinhold, E. Selective Recognition of Pyrimidine-Pyrimidine DNA Mismatches by Distance-Constrained Macrocyclic Bis-Intercalators. *Nucleic Acids Res.* **2008**, *36*, 5000–5012. https://doi.org/10.1093/nar/gkn392.

(1063) Granzhan, A.; Kotera, N.; Teulade-Fichou, M.-P. Finding Needles in a Basestack: Recognition of Mismatched Base Pairs in DNA by Small Molecules. *Chem. Soc. Rev.* **2014**, *43*, 3630–3665. https://doi.org/10.1039/c3cs60455a.

(1064) Iannitti, P.; Sheil, M. M.; Wickham, G. High Sensitivity and Fragmentation Specificity in the Analysis of Drug−DNA Adducts by Electrospray Tandem Mass Spectrometry. *J. Am. Chem. Soc.* **1997**, *119*, 1490–1491. https://doi.org/10.1021/ja962439q.

(1065) Wickham, G.; Iannitti, P.; Boschenok, J.; Sheil, M.-M. The Observation of a Hedamycin-d(CACGTG)2 Covalent Adduct by Electrospray Mass Spectrometry. *FEBS Lett.* **1995**, *360*, 231–234. https://doi.org/10.1016/0014-5793(95)00110-u.

(1066) Smith, S. I.; Jr, F. S. G.; Guziec, L.; Brodbelt, J. S. Interactions of Sulfur-Containing Acridine Ligands with DNA by ESI-MS. *Analyst* **2009**, *134*,

2058–2066. https://doi.org/10.1039/B905071J.

(1067) Beck, J.; Gupta, G.; Urathamakul, T.; Williamson, N. L.; Sheil, M. M.; Aldrich-Wright, J. R.; Ralph, S. F. Probing DNA Selectivity of Ruthenium Metallointercalators Using ESI Mass Spectrometry. *Chem. Commun.* **2003**, No. 5, 626–627. https://doi.org/10.1039/b212132h.

(1068) Urathamakul, T.; Beck, J. L.; Sheil, M. M.; Aldrich-Wright, J. R.; Ralph, S. F. A Mass Spectrometric Investigation of Non-Covalent Interactions between Ruthenium Complexes and DNA. *Dalton Trans.* **2004**, No. 17, 2683–2690. https://doi.org/10.1039/b406889k.

(1069) Talib, J.; Green, C.; Davis, K. J.; Urathamakul, T.; Beck, J. L.; Aldrich-Wright, J. R.; Ralph, S. F. A Comparison of the Binding of Metal Complexes to Duplex and Quadruplex DNA. *Dalton Trans.* **2008**, No. 8, 1018–1026. https://doi.org/10.1039/B715458E.

(1070) Reyzer, M.; Brodbelt, J. S.; Kerwin, S. M.; Kumar, D. Evaluation of Complexation of Metal-Mediated DNA-Binding Drugs to Oligonucleotides via Electrospray Ionization Mass Spectrometry. *Nucleic Acids Res.* **2001**, *29*, e103. https://doi.org/10.1093/nar/29.21.e103.

(1071) Morgan, A. R.; Lee, J. S.; Pulleyblank, D. E.; Murray, N. L.; Evans, D. H. Review: Ethidium Fluorescence Assays. Part 1. Physicochemical Studies. *Nucleic Acids Res.* **1979**, *7*, 547–569. https://doi.org/10.1093/nar/7.3.547.

(1072) Xu, N.; Yang, H.; Cui, M.; Wan, C.; Liu, S. High-Performance Liquid Chromatography-Electrospray Ionization-Mass Spectrometry Ligand Fishing Assay: A Method for Screening Triplex DNA Binders from Natural Plant Extracts. *Anal. Chem.* **2012**, *84*, 2562–2568. https://doi.org/10.1021/ac202796v.

(1073) Duskova, K.; Lamarche, J.; Amor, S.; Caron, C.; Queyriaux, N.; Gaschard, M.; Penouilh, M. J.; de Robillard, G.; Delmas, D.; Devillers, C. H.; et al. Identification of Three-Way DNA Junction Ligands through Screening of Chemical Libraries and Validation by Complementary in Vitro Assays. *J. Med. Chem.* **2019**, *62*, 4456–4466. https://doi.org/10.1021/acs.jmedchem.8b01978.

(1074) Ramos, C. I. V.; Barros, C. M.; Fernandes, A. M.; Santana-Marques, M. G.; Correia, A. J. F.; Tomé, J. P. C.; Carrilho, M. do C. T.; Faustino, M. A. F.; Tomé, A. C.; Neves, M. G. P. M. S.; et al. Interactions of Cationic Porphyrins with Double-Stranded Oligodeoxynucleotides: A Study by Electrospray Ionisation Mass Spectrometry. *J. Mass Spectrom.* **2005**, *40*, 1439–1447. https://doi.org/10.1002/jms.936.

(1075) Amrane, S.; Cian, A. D.; Rosu, F.; Kaiser, M.; Pauw, E. D.; Teulade-Fichou, M.-P.; Mergny, J.-L. Identification of Trinucleotide Repeat Ligands with a FRET Melting Assay. *ChemBioChem* **2008**, *9*, 1229–1234. https://doi.org/10.1002/cbic.200800062.

(1076) Peng, T.; Nakatani, K. Binding of Naphthyridine Carbamate Dimer to the (CGG)n Repeat Results in the Disruption of the G-C Base Pairing. *Angew. Chem. Int. Ed Engl.* **2005**, *44*, 7280–7283. https://doi.org/10.1002/anie.200502282.

(1077) Nakatani, K.; Kobori, A.; Kumasawa, H.; Goto, Y.; Saito, I. The Binding of Guanine-Guanine Mismatched DNA to Naphthyridine Dimer Immobilized Sensor Surfaces: Kinetic Aspects. *Bioorg. Med. Chem.* **2004**, *12*, 3117–3123. https://doi.org/10.1016/j.bmc.2004.04.005.

(1078) Nakatani, K.; Sando, S.; Saito, I. Scanning of Guanine-Guanine Mismatches in DNA by Synthetic Ligands Using Surface Plasmon Resonance. *Nat. Biotechnol.* **2001**, *19*, 51–55. https://doi.org/10.1038/83505.

(1079) Ruggiero, E.; Richter, S. N. G-Quadruplexes and G-Quadruplex Ligands: Targets and Tools in Antiviral Therapy. *Nucleic Acids Res.* **2018**, *46*, 3270–3283. https://doi.org/10.1093/nar/gky187.

(1080) Balasubramanian, S.; Neidle, S. G-Quadruplex Nucleic Acids as Therapeutic Targets. *Curr. Opin. Chem. Biol.* **2009**, *13*, 345–353. https://doi.org/10.1016/j.cbpa.2009.04.637.

(1081) Murat, P.; Singh, Y.; Defrancq, E. Methods for Investigating G-Quadruplex DNA/Ligand Interactions. *Chem. Soc. Rev.* **2011**, *40*, 5293–5307. https://doi.org/10.1039/c1cs15117g.

(1082) Li, W.; Zhang, M.; Zhang, J.; Li, H.; Zhang, X.; Sun, Q.; Qiu, C. Interactions of Daidzin with Intramolecular G-Quadruplex. *FEBS Lett.* **2006**, *580*, 4905–4910. https://doi.org/10.1016/j.febslet.2006.08.007.

(1083) Gornall, K. C.; Samosorn, S.; Talib, J.; Bremner, J. B.; Beck, J. L. Selectivity of an Indolyl Berberine Derivative for Tetrameric G-Quadruplex DNA. *Rapid Commun. Mass Spectrom.* **2007**, *21*, 1759–1766. https://doi.org/10.1002/rcm.3019.

(1084) Gornall, K. C.; Samosorn, S.; Tanwirat, B.; Suksamrarn, A.; Bremner, J. B.; Kelso, M. J.; Beck, J. L. A Mass Spectrometric Investigation of Novel Quadruplex DNA-Selective Berberine Derivatives. *Chem. Commun.* **2010**, *46*, 6602–6604. https://doi.org/10.1039/c0cc01933j.

(1085) Li, F.; Chen, H.; Zhou, J.; Yuan, G. Exploration of the Selective Recognition of the G-Quadruplex in the N-Myc Oncogene by Electrospray Ionization Mass Spectrometry. *Rapid Commun. Mass Spectrom.* **2015**, *29*, 247–252. https://doi.org/10.1002/rcm.7101.

(1086) Wang, S.; Yang, Y.; Yang, Y.; Li, H.; Chen, D. D. Y. Quantitative Characterization of Human Oncogene Promoter G-Quadruplex DNA-Ligand Interactions Using a Combination of Mass Spectrometry and Capillary Electrophoresis. *Electrophoresis* **2021**, in press. https://doi.org/10.1002/elps.202100077.

(1087) Xu, N.; Yang, H.; Cui, M.; Song, F.; Liu, Z.; Liu, S. Evaluation of Alkaloids Binding to the Parallel Quadruplex Structure [d(TGGGGT)]4 by Electrospray Ionization Mass Spectrometry. *J. Mass Spectrom.* **2012**, *47*, 694–700. https://doi.org/10.1002/jms.2997.

(1088) Tan, W.; Yuan, G. Electrospray Ionization Mass Spectrometric Exploration of the High-Affinity Binding of Three Natural Alkaloids with the MRNA G-Quadruplex in the BCL2 5'-Untranslated Region. *Rapid Commun. Mass Spectrom.* **2013**, *27*, 560–564. https://doi.org/10.1002/rcm.6484.

(1089) Li, H.; Hai, J.; Zhou, J.; Yuan, G. Exploration of Binding Affinity and Selectivity of Brucine with G-Quadruplex in the c-Myb Proto-Oncogene by Electrospray Ionization Mass Spectrometry: Binding of Brucine with G-Quadruplex in the c-Myb Oncogene by ESI-MS. *Rapid Commun. Mass Spectrom.* **2016**, *30*, 407–414. https://doi.org/10.1002/rcm.7454.

(1090) Ribaudo, G.; Oselladore, E.; Ongaro, A.; Zagotto, G.; Memo, M.; Gianoncelli, A. Enhanced G-Quadruplex Selectivity of Flavonoid Glycoside Rutin over Quercetin. *Nat. Prod. Res.* **2020**, 1–5. https://doi.org/10.1080/14786419.2020.1859505.

(1091) Bai, L.-P.; Hagihara, M.; Jiang, Z.-H.; Nakatani, K. Ligand Binding to Tandem G Quadruplexes from Human Telomeric DNA. *ChemBioChem* **2008**, *9*, 2583–2587. https://doi.org/10.1002/cbic.200800256.

(1092) Bai, L.-P.; Hagihara, M.; Nakatani, K.; Jiang, Z.-H. Recognition of Chelerythrine to Human Telomeric DNA and RNA G-Quadruplexes. *Sci. Rep.* **2014**, *4*, 6767. https://doi.org/10.1038/srep06767.

(1093) Raju, G.; Srinivas, R.; Reddy, V. S.; Idris, M. M.; Kamal, A.; Nagesh, N. Interaction of Pyrrolobenzodiazepine (PBD) Ligands with Parallel Intermolecular G-Quadruplex Complex Using Spectroscopy and ESI-MS. *PloS One* **2012**, *7*, e35920. https://doi.org/10.1371/journal.pone.0035920.

(1094) Bai, L.-P.; Ho, H.-M.; Ma, D.-L.; Yang, H.; Fu, W.-C.; Jiang, Z.-H. Aminoglycosylation Can Enhance the G-Quadruplex Binding Activity of Epigallocatechin. *PLoS ONE* **2013**, *8*, e53962. https://doi.org/10.1371/journal.pone.0053962.

(1095) Rosu, F.; Gabelica, V.; Smargiasso, N.; Mazzucchelli, G.; Shin-Ya, K.; De Pauw, E. Cation Involvement in Telomestatin Binding to G-Quadruplex DNA. *J. Nucleic Acids* **2010**, *2010*, 121259. https://doi.org/10.4061/2010/121259.

(1096) Linder, J.; Garner, T. P.; Williams, H. E. L.; Searle, M. S.; Moody, C. J. Telomestatin: Formal Total Synthesis and Cation-Mediated Interaction of Its *Seco* -Derivatives with G-Quadruplexes. *J. Am. Chem. Soc.* **2011**, *133*, 1044–1051. https://doi.org/10.1021/ja109158k.

(1097) Garner, T. P.; Williams, H. E. L.; Gluszyk, K. I.; Roe, S.; Oldham, N. J.; Stevens, M. F. G.; Moses, J. E.; Searle, M. S. Selectivity of Small Molecule Ligands for Parallel and Anti-Parallel DNA G-Quadruplex Structures. *Org. Biomol. Chem.* **2009**, *7*, 4194–4200. https://doi.org/10.1039/b910505k.

(1098) Baker, E. S.; Lee, J. T.; Sessler, J. L.; Bowers, M. T. Cyclo[n]Pyrroles: Size and Site-Specific Binding to G-Quadruplexes. *J. Am. Chem. Soc.* **2006**, *128*, 2641–2648. https://doi.org/10.1021/ja0564968.

(1099) Cui, X.; Zhang, Q.; Chen, H.; Zhou, J.; Yuan, G. ESI Mass Spectrometric Exploration of Selective Recognition of G-Quadruplex in c-Myb Oncogene Promoter Using a Novel Flexible Cyclic Polyamide. *J. Am. Soc. Mass Spectrom.* **2014**, *25*, 684–691. https://doi.org/10.1007/s13361-013-0802-y.

(1100) Ramos, C. I. V.; Tomé, J. P. C.; Santana-Marques, M. G. Charge and Substituent Effects on the Stability of Porphyrin/G-Quadruplex Adducts. *J. Mass Spectrom.* **2012**, *47*, 173–179. https://doi.org/10.1002/jms.2048.

(1101) DuPont, J. I.; Henderson, K. L.; Metz, A.; Le, V. H.; Emerson, J. P.; Lewis, E. A. Calorimetric and Spectroscopic Investigations of the Binding of Metallated Porphyrins to G-Quadruplex DNA. *Biochim. Biophys. Acta BBA - Gen. Subj.* **2016**, *1860*, 902–909. https://doi.org/10.1016/j.bbagen.2015.09.004.

(1102) Bai, L.-P.; Liu, J.; Han, L.; Ho, H.-M.; Wang, R.; Jiang, Z.-H. Mass Spectrometric Studies on Effects of Counter Ions of TMPyP4 on Binding to Human Telomeric DNA and RNA G-Quadruplexes. *Anal. Bioanal. Chem.* **2014**, *406*, 5455–5463. https://doi.org/10.1007/s00216-014-7943-0.

(1103) Wu, K.; Liu, S.; Luo, Q.; Hu, W.; Li, X.; Wang, F.; Zheng, R.; Cui, J.; Sadler, P. J.; Xiang, J.; et al. Thymines in Single-Stranded Oligonucleotides and G-Quadruplex DNA Are Competitive with Guanines for Binding to an Organoruthenium Anticancer Complex. *Inorg. Chem.* **2013**, *52*, 11332–11342. https://doi.org/10.1021/ic401606v.

(1104) Huang, C.; Ma, Z.; Lin, J.; Gong, X.; Zhang, F.; Wu, X.; Wang, F.; Zheng, W.; Zhao, Y.; Wu, K. Tandem Mass Spectrometry Reveals Preferential Ruthenation of Thymines in Human Telomeric G-Quadruplex DNA by an Organometallic Ruthenium Anticancer Complex. *Organometallics* **2020**, *39*, 3315–3322. https://doi.org/10.1021/acs.organomet.0c00399.

(1105) Cheng, Y.; Zeng, W.; Cheng, Y.; Zhang, J.; Zou, T.; Wu, K.; Wang, F. Selective Binding of an Organoruthenium Complex to G-Rich Human Telomeric Sequence by Tandem Mass

Spectrometry. *Rapid Commun. Mass Spectrom.* **2018**, *32*, 2152–2158. https://doi.org/10.1002/rcm.8292.

(1106) Ang, D. L.; Kelso, C.; Beck, J. L.; Ralph, S. F.; Harman, D. G.; Aldrich-Wright, J. R. A Study of Pt(II)–Phenanthroline Complex Interactions with Double-Stranded and G-Quadruplex DNA by ESI–MS, Circular Dichroism, and Computational Docking. *JBIC J. Biol. Inorg. Chem.* **2020**, *25*, 429–440. https://doi.org/10.1007/s00775-020-01773-4.

(1107) Bazzicalupi, C.; Ferraroni, M.; Papi, F.; Massai, L.; Bertrand, B.; Messori, L.; Gratteri, P.; Casini, A. Determinants for Tight and Selective Binding of a Medicinal Dicarbene Gold(I) Complex to a Telomeric DNA G-Quadruplex: A Joint ESI MS and XRD Investigation. *Angew. Chem. Int. Ed Engl.* **2016**, *55*, 4256–4259. https://doi.org/10.1002/anie.201511999.

(1108) Guarra, F.; Marzo, T.; Ferraroni, M.; Papi, F.; Bazzicalupi, C.; Gratteri, P.; Pescitelli, G.; Messori, L.; Biver, T.; Gabbiani, C. Interaction of a Gold(I) Dicarbene Anticancer Drug with Human Telomeric DNA G-Quadruplex: Solution and Computationally Aided X-Ray Diffraction Analysis. *Dalton Trans.* **2018**, *47*, 16132–16138. https://doi.org/10.1039/c8dt03607a.

(1109) Davis, K. J.; Assadawi, N. M. O.; Pham, S. Q. T.; Birrento, M. L.; Richardson, C.; Beck, J. L.; Willis, A. C.; Ralph, S. F. Effect of Structure Variations on the Quadruplex DNA Binding Ability of Nickel Schiff Base Complexes. *Dalton Trans.* **2018**, *47*, 13573–13591. https://doi.org/10.1039/c8dt02727g.

(1110) D'Ambrosio, D.; Reichenbach, P.; Micheli, E.; Alvino, A.; Franceschin, M.; Savino, M.; Lingner, J. Specific Binding of Telomeric G-Quadruplexes by Hydrosoluble Perylene Derivatives Inhibits Repeat Addition Processivity of Human Telomerase. *Biochimie* **2012**, *94*, 854–863. https://doi.org/10.1016/j.biochi.2011.12.004.

(1111) Smargiasso, N.; Gabelica, V.; Damblon, C.; Rosu, F.; De Pauw, E.; Teulade-Fichou, M.-P.; Rowe, J.; Claessens, A. Putative DNA G-Quadruplex Formation within the Promoters of Plasmodium Falciparum Var Genes. *BMC Genomics* **2009**, *10*, 362. https://doi.org/10.1186/1471-2164-10-362.

(1112) Amato, J.; Oliviero, G.; Borbone, N.; D'Errico, S.; Piccialli, G.; Mailliet, P.; Rosu, F.; Pauw, E. D.; Gabelica, V. Ligand Binding to Tetra-End-Linked (TGGGGT)4 G-Quadruplexes: An Electrospray Mass Spectroscopy Study. *Nucleic Acids Symp. Ser.* **2008**, *52*, 165–166. https://doi.org/10.1093/nass/nrn084.

(1113) Li, H.; Yuan, G. Collision-Induced Dissociation of Dimeric G-Quadruplexes of HIV-1 Integrase Inhibitors and Their Complexes by Tandem-in-Time Mass Spectrometry. *Eur. J. Mass Spectrom.* **2009**, *15*, 731–737. https://doi.org/10.1255/ejms.1033.

(1114) Zhang, Z.; He, X.; Yuan, G. Regulation of the Equilibrium between G-Quadruplex and Duplex DNA in Promoter of Human c-Myc Oncogene by a Pyrene Derivative. *Int. J. Biol. Macromol.* **2011**, *49*, 1173–1176. https://doi.org/10.1016/j.ijbiomac.2011.05.024.

(1115) Ceschi, S.; Largy, E.; Gabelica, V.; Sissi, C. A Two-Quartet G-Quadruplex Topology of Human KIT2 Is Conformationally Selected by a Perylene Derivative. *Biochimie* **2020**, *179*, 77–84. https://doi.org/10.1016/j.biochi.2020.09.015.

(1116) Li, H.; Yuan, G.; Du, D. Investigation of Formation, Recognition, Stabilization, and Conversion of Dimeric G-Quadruplexes of HIV-1 Integrase Inhibitors by Electrospray Ionization Mass Spectrometry. *J. Am. Soc. Mass Spectrom.* **2008**, *19*, 550–559. https://doi.org/10.1016/j.jasms.2008.01.012.

(1117) Zhou, J.; Yuan, G. Specific Recognition of Human Telomeric G-Quadruplex DNA with Small Molecules and the Conformational Analysis by ESI Mass Spectrometry and Circular Dichroism Spectropolarimetry. *Chem. - Eur. J.* **2007**, *13*, 5018–5023. https://doi.org/10.1002/chem.200601605.

(1118) Pierce, S. E.; Sherman, C. L.; Jayawickramarajah, J.; Lawrence, C. M.; Sessler, J. L.; Brodbelt, J. S. ESI-MS Characterization of a Novel Pyrrole–Inosine Nucleoside That Interacts with Guanine Bases. *Anal. Chim. Acta* **2008**, *627*, 129–135. https://doi.org/10.1016/j.aca.2008.04.018.

(1119) Nagesh, N.; Raju, G.; Srinivas, R.; Ramesh, P.; Reddy, M. D.; Reddy, Ch. R. A Dihydroindolizino Indole Derivative Selectively Stabilizes G-Quadruplex DNA and down-Regulates c-MYC Expression in Human Cancer Cells. *Biochim. Biophys. Acta BBA - Gen. Subj.* **2015**, *1850*, 129–140. https://doi.org/10.1016/j.bbagen.2014.10.004.

(1120) Altieri, A.; Alvino, A.; Ohnmacht, S.; Ortaggi, G.; Neidle, S.; Nocioni, D.; Franceschin, M.; Bianco, A. Xanthene and Xanthone Derivatives as G-Quadruplex Stabilizing Ligands. *Molecules* **2013**, *18*, 13446–13470. https://doi.org/10.3390/molecules181113446.

(1121) Ginnari-Satriani, L.; Casagrande, V.; Bianco, A.; Ortaggi, G.; Franceschin, M. A Hydrophilic Three Side-Chained Triazatruxene as a New Strong and Selective G-Quadruplex Ligand. *Org. Biomol. Chem.* **2009**, *7*, 2513–2516. https://doi.org/10.1039/b904723a.

(1122) Gueddouda, N. M.; Hurtado, M. R.; Moreau, S.; Ronga, L.; Das, R. N.; Savrimoutou, S.; Rubio, S.; Marchand, A.; Mendoza, O.; Marchivie, M.; et al. Design, Synthesis, and Evaluation of 2,9-Bis[(Substituted-Aminomethyl)Phenyl]-1,10-Phenanthroline Derivatives as G-Quadruplex Ligands. *ChemMedChem* **2017**, *12*, 146–160. https://doi.org/10.1002/cmdc.201600511.

(1123) Guillon, J.; Denevault-Sabourin, C.; Chevret, E.; Brachet-Botineau, M.; Milano, V.; Guédin-Beaurepaire, A.; Moreau, S.; Ronga, L.; Savrimoutou, S.; Rubio, S.; et al. Design, Synthesis, and Antiproliferative Effect of 2,9-Bis[4-(Pyridinylalkylaminomethyl)Phenyl]-1,10-Phenanthroline Derivatives on Human Leukemic Cells by Targeting G-Quadruplex. *Arch. Pharm. (Weinheim)* **2021**, *354*, e2000450. https://doi.org/10.1002/ardp.202000450.

(1124) Marchand, A.; Beauvineau, C.; Teulade-Fichou, M.; Zenobi, R. Competition of Ligands and the 18-mer Binding Domain of the RHAU Helicase for G-Quadruplexes: Orthosteric or Allosteric Binding Mechanism? *Chem. – Eur. J.* **2020**, *27*, 1113–1121. https://doi.org/10.1002/chem.202004040.

(1125) Reznichenko, O.; Cucchiarini, A.; Gabelica, V.; Granzhan, A. Quadruplex DNA-Guided Ligand Selection from Dynamic Combinatorial Libraries of Acylhydrazones. *Org. Biomol. Chem.* **2021**, *19*, 379–386. https://doi.org/10.1039/D0OB01908A.

(1126) Shin-ya, K.; Wierzba, K.; Matsuo, K.; Ohtani, T.; Yamada, Y.; Furihata, K.; Hayakawa, Y.; Seto, H. Telomestatin, a Novel Telomerase Inhibitor from *Streptomyces Anulatus*. *J. Am. Chem. Soc.* **2001**, *123*, 1262–1263. https://doi.org/10.1021/ja005780q.

(1127) Iida, K.; Majima, S.; Nakamura, T.; Seimiya, H.; Nagasawa, K. Evaluation of the Interaction between Long Telomeric DNA and Macrocyclic Hexaoxazole (6OTD) Dimer of a G-Quadruplex Ligand. *Molecules* **2013**, *18*, 4328–4341. https://doi.org/10.3390/molecules18044328.

(1128) Kim, M.-Y.; Vankayalapati, H.; Shin-ya, K.; Wierzba, K.; Hurley, L. H. Telomestatin, a Potent Telomerase Inhibitor That Interacts Quite Specifically with the Human Telomeric Intramolecular G-Quadruplex. *J. Am. Chem. Soc.* **2002**, *124*, 2098–2099. https://doi.org/10.1021/ja017308q.

(1129) Randazzo, A.; Galeone, A.; Mayol, L. 1H-NMR Study of the Interaction of Distamycin A and Netropsin with the Parallel Stranded Tetraplex [d(TGGGGT)]4. *Chem. Commun.* **2001**, No. 11, 1030–1031. https://doi.org/10.1039/b100460n.

(1130) Li, H.; Liu, Y.; Lin, S.; Yuan, G. Spectroscopy Probing of the Formation, Recognition, and Conversion of a G-Quadruplex in the Promoter Region of the Bcl-2 Oncogene. *Chemistry* **2009**, *15*, 2445–2452. https://doi.org/10.1002/chem.200801922.

(1131) Agrawal, S.; Ojha, R. P.; Maiti, S. Energetics of the Human Tel-22 Quadruplex−Telomestatin Interaction: A Molecular Dynamics Study. *J. Phys. Chem. B* **2008**, *112*, 6828–6836. https://doi.org/10.1021/jp7102676.

(1132) Chung, W. J.; Heddi, B.; Tera, M.; Iida, K.; Nagasawa, K.; Phan, A. T. Solution Structure of an Intramolecular (3 + 1) Human Telomeric G-Quadruplex Bound to a Telomestatin Derivative. *J. Am. Chem. Soc.* **2013**, *135*, 13495–13501. https://doi.org/10.1021/ja405843r.

(1133) Boger, D. L.; Fink, B. E.; Brunette, S. R.; Tse, W. C.; Hedrick, M. P. A Simple, High-Resolution Method for Establishing DNA Binding Affinity and Sequence Selectivity. *J. Am. Chem. Soc.* **2001**, *123*, 5878–5891. https://doi.org/10.1021/ja010041a.

(1134) Monchaud, D.; Allain, C.; Teulade-Fichou, M.-P. Development of a Fluorescent Intercalator Displacement Assay (G4-FID) for Establishing Quadruplex-DNA Affinity and Selectivity of Putative Ligands. *Bioorg. Med. Chem. Lett.* **2006**, *16*, 4842–4845. https://doi.org/10.1016/j.bmcl.2006.06.067.

(1135) Hofstadler, S. A.; Sannes-Lowery, K. A.; Crooke, S. T.; Ecker, D. J.; Sasmor, H.; Manalili, S.; Griffey, R. H. Multiplexed Screening of Neutral Mass-Tagged RNA Targets against Ligand Libraries with Electrospray Ionization FTICR MS: A Paradigm for High-Throughput Affinity Screening. *Anal. Chem.* **1999**, *71*, 3436–3440. https://doi.org/10.1021/ac990262n.

(1136) Griffey, R. H.; Hofstadler, S. A.; Sannes-Lowery, K. A.; Ecker, D. J.; Crooke, S. T. Determinants of Aminoglycoside-Binding Specificity for RRNA by Using Mass Spectrometry. *Proc. Natl. Acad. Sci. U. S. A.* **1999**, *96*, 10129–10133. https://doi.org/10.1073/pnas.96.18.10129.

(1137) Ding, Y.; Hofstadler, S. A.; Swayze, E. E.; Risen, L.; Griffey, R. H. Design and Synthesis of Paromomycin-Related Heterocycle-Substituted Aminoglycoside Mimetics Based on a Mass Spectrometry RNA-Binding Assay. *Angew. Chem. Int. Ed Engl.* **2003**, *42*, 3409–3412. https://doi.org/10.1002/anie.200351354.

(1138) Cummins, L. L.; Chen, S.; Blyn, L. B.; Sannes-Lowery, K. A.; Drader, J. J.; Griffey, R. H.; Hofstadler, S. A. Multitarget Affinity/Specificity Screening of Natural Products: Finding and Characterizing High-Affinity Ligands from Complex Mixtures by Using High-Performance Mass Spectrometry. *J.Nat.Prod.* **2003**, *66*, 1186–1190. https://doi.org/10.1021/np0301137.

(1139) Seth, P. P.; Miyaji, A.; Jefferson, E. A.; Sannes-Lowery, K. A.; Osgood, S. A.; Propp, S. S.; Ranken, R.; Massire, C.; Sampath, R.; Ecker, D. J.; et al. SAR by MS: Discovery of a New Class of RNA-Binding Small Molecules for the Hepatitis C Virus: Internal Ribosome Entry Site IIA Subdomain. *J. Med. Chem.* **2005**, *48*, 7099–7102. https://doi.org/10.1021/jm050815o.

(1140) Swayze, E. E.; Jefferson, E. A.; Sannes-Lowery, K. A.; Blyn, L. B.; Risen, L. M.; Arakawa, S.; Osgood, S. A.; Hofstadler, S. A.; Griffey, R. H. SAR by MS: A Ligand Based Technique for Drug Lead Discovery Against Structured RNA Targets. *J. Med. Chem.* **2002**, *45*, 3816–3819. https://doi.org/10.1021/jm0255466.

(1141) Wu, B.; Yang, J.; Robinsin, D.; Hofstadler, S. A.; Griffey, R. H.; Swayze, E. E.; He, Y. Synthesis of Linked Carbohydrates and Evaluation of Their Binding for 16S RNA by Mass Spectrometry. *Bioorg.Med.Chem.Lett.* **2003**, *13*, 3915–3918. https://doi.org/10.1016/j.bmcl.2003.09.005.

(1142) Maddaford, S. P.; Motamed, M.; Turner, K. B.; Choi, M. S. K.; Ramnauth, J.; Rakhit, S.; Hudgins, R. R.; Fabris, D.; Johnson, P. E. Identification of a Novel Non-Carbohydrate Molecule That Binds to the Ribosomal A-Site RNA. *Bioorg. Med. Chem. Lett.* **2004**, *14*, 5987–5990. https://doi.org/10.1016/j.bmcl.2004.09.088.

(1143) Turner, K. B.; Hagan, N. A.; Fabris, D. Inhibitory Effects of Archetypical Nucleic Acid Ligands on the Interactions of HIV-1 Nucleocapsid Protein with Elements of Psi-RNA. *Nucleic Acids Res.* **2006**, *34*, 1305–1316. https://doi.org/10.1093/nar/gkl004.

(1144) Turner, K. B.; Brinson, R. G.; Yi-Brunozzi, H. Y.; Rausch, J. W.; Miller, J. T.; Le Grice, S. F. J.; Marino, J. P.; Fabris, D. Structural Probing of the HIV-1 Polypurine Tract RNA:DNA Hybrid Using Classic Nucleic Acid Ligands. *Nucleic Acids Res.* **2008**, *36*, 2799–2810. https://doi.org/10.1093/nar/gkn129.

(1145) Brinson, R. G.; Turner, K. B.; Yi-Brunozzi, H. Y.; Le Grice, S. F. J.; Fabris, D.; Marino, J. P. Probing Anomalous Structural Features in Polypurine Tract-Containing RNA-DNA Hybrids with Neomycin B. *Biochemistry* **2009**, *48*, 6988–6997. https://doi.org/10.1021/bi900357j.

(1146) Griffey, R. H.; Greig, M. J.; An, H.; Sasmor, H.; Manalili, S. Targeted Site-Specific Gas-Phase Cleavage of Oligoribonucleotides. Application in Mass Spectrometry-Based Identification of Ligand Binding Sites. *J. Am. Chem. Soc.* **1999**, *121*, 474–475. https://doi.org/10.1021/ja983131x.

(1147) Li, J.; Matsumoto, J.; Bai, L.-P.; Murata, A.; Dohno, C.; Nakatani, K. A Ligand That Targets CUG Trinucleotide Repeats. *Chem. – Eur. J.* **2016**, *22*, 14881–14889. https://doi.org/10.1002/chem.201602741.

(1148) Wolff, P.; Ennifar, E. Native Electrospray Ionization Mass Spectrometry of RNA-Ligand Complexes. In *RNA Spectroscopy: Methods and Protocols*; Arluison, V., Wien, F., Eds.; Methods in Molecular Biology; Springer US: New York, NY, 2020; p.111–118. https://doi.org/10.1007/978-1-0716-0278-2_9.

(1149) Rizvi, N. F.; Howe, J. A.; Nahvi, A.; Klein, D. J.; Fischmann, T. O.; Kim, H.-Y.; McCoy, M. A.; Walker, S. S.; Hruza, A.; Richards, M. P.; et al. Discovery of Selective RNA-Binding Small Molecules by Affinity-Selection Mass Spectrometry. *ACS Chem. Biol.* **2018**, *13*, 820–831. https://doi.org/10.1021/acschembio.7b01013.

(1150) Rizvi, N. F.; Nickbarg, E. B. RNA-ALIS: Methodology for Screening Soluble RNAs as Small Molecule Targets Using ALIS Affinity-Selection Mass Spectrometry. *Methods* **2019**, *167*, 28–38. https://doi.org/10.1016/j.ymeth.2019.04.024.

(1151) Rizvi, N. F.; John P. Santa Maria, J.; Nahvi, A.; Klappenbach, J.; Klein, D. J.; Curran, P. J.; Richards, M. P.; Chamberlin, C.; Saradjian, P.; Burchard, J.; et al. Targeting RNA with Small Molecules: Identification of Selective, RNA-Binding Small Molecules Occupying Drug-Like Chemical Space: *SLAS Discov. Adv. Sci. Drug Discov.* **2019**, *25*, 384–396. https://doi.org/10.1177/2472555219885373.

(1152) Flusberg, D. A.; Rizvi, N. F.; Kutilek, V.; Andrews, C.; Saradjian, P.; Chamberlin, C.; Curran, P.; Swalm, B.; Kattar, S.; Smith, G. F.; et al. Identification of G-Quadruplex-Binding Inhibitors of Myc Expression through Affinity Selection–Mass Spectrometry. *SLAS Discov. Adv. Sci. Drug Discov.* **2019**, *24*, 142–157. https://doi.org/10.1177/2472555218796656.

(1153) Dick, L. W.; McGown, L. B. Aptamer-Enhanced Laser Desorption/Ionization for Affinity Mass Spectrometry. *Anal. Chem.* **2004**, *76*, 3037–3041. https://doi.org/10.1021/ac049860e.

(1154) Connor, A. C.; Frederick, K. A.; Morgan, E. J.; McGown, L. B. Insulin Capture by an Insulin-Linked Polymorphic Region G-Quadruplex DNA Oligonucleotide. *J. Am. Chem. Soc.* **2006**, *128*, 4986–4991. https://doi.org/10.1021/ja056097c.

(1155) Cole, J. R.; Dick, Lawrence W.; Morgan, E. J.; McGown, L. B. Affinity Capture and Detection of Immunoglobulin E in Human Serum Using an Aptamer-Modified Surface in Matrix-Assisted Laser Desorption/Ionization Mass Spectrometry. *Anal. Chem.* **2007**, *79*, 273–279. https://doi.org/10.1021/ac061256b.

(1156) Xiao, J.; McGown, L. B. Mass Spectrometric Determination of ILPR G-Quadruplex Binding Sites in Insulin and IGF-2. *J. Am. Soc. Mass Spectrom.* **2009**, *20*, 1974–1982. https://doi.org/10.1016/j.jasms.2009.08.002.

(1157) Chen, F.; Gülbakan, B.; Zenobi, R. Direct Access to Aptamer–Protein Complexes via MALDI-MS. *Chem. Sci.* **2013**, *4*, 4071–4078. https://doi.org/10.1039/c3sc51410b.

(1158) Zhang, J.; Loo, R. R. O.; Loo, J. A. Structural Characterization of a Thrombin-Aptamer Complex by High Resolution Native Top-Down Mass Spectrometry. *J. Am. Soc. Mass Spectrom.* **2017**, *28*, 1815–1822. https://doi.org/10.1007/s13361-017-1751-7.

(1159) Ruigrok, V. J. B.; Duijn, E. van; Barendregt, A.; Dyer, K.; Tainer, J. A.; Stoltenburg, R.; Strehlitz, B.; Levisson, M.; Smidt, H.; Oost, J. van der. Kinetic and Stoichiometric Characterisation of Streptavidin-Binding Aptamers. *ChemBioChem* **2012**, *13*, 829–836. https://doi.org/10.1002/cbic.201100774.

(1160) Cassiday, L. A.; Lebruska, L. L.; Benson, L. M.; Naylor, S.; Owen, W. G.; Maher, L. J. Binding Stoichiometry of an RNA Aptamer and Its Transcription Factor Target. *Anal. Biochem.*

2002, *306*, 290–297. https://doi.org/10.1006/abio.2002.5710.

(1161) Guo, X. H.; Liu, Z. Q.; Liu, S. Y.; Bentzley, C. M.; Bruist, M. F. Structural Features of the L-Argininamide-Binding DNA Aptamer Studied with ESI-FTMS. *Anal. Chem.* **2006**, *78*, 7259–7266. https://doi.org/10.1021/ac060606r.

(1162) Gavriilidou, A. F. M.; Gülbakan, B.; Zenobi, R. Influence of Ammonium Acetate Concentration on Receptor-Ligand Binding Affinities Measured by Native Nano ESI-MS: A Systematic Study. *Anal. Chem.* **2015**, *87*, 10378–10384. https://doi.org/10.1021/acs.analchem.5b02478.

(1163) Gülbakan, B.; Barylyuk, K.; Schneider, P.; Pillong, M.; Schneider, G.; Zenobi, R. Native Electrospray Ionization Mass Spectrometry Reveals Multiple Facets of Aptamer–Ligand Interactions: From Mechanism to Binding Constants. *J. Am. Chem. Soc.* **2018**, *140*, 7486–7497. https://doi.org/10.1021/jacs.7b13044.

(1164) Bottari, F.; Daems, E.; de Vries, A.-M.; Van Wielendaele, P.; Trashin, S.; Blust, R.; Sobott, F.; Madder, A.; Martins, J. C.; De Wael, K. Do Aptamers Always Bind? The Need for a Multifaceted Analytical Approach When Demonstrating Binding Affinity between Aptamer and Low Molecular Weight Compounds. *J. Am. Chem. Soc.* **2020**, *142*, 19622–19630. https://doi.org/10.1021/jacs.0c08691.

(1165) Daems, E.; Dewaele, D.; Barylyuk, K.; De Wael, K.; Sobott, F. Aptamer-Ligand Recognition Studied by Native Ion Mobility-Mass Spectrometry. *Talanta* **2021**, *224*, 121917. https://doi.org/10.1016/j.talanta.2020.121917.

(1166) Schneeberger, E.-M.; Halper, M.; Palasser, M.; Heel, S. V.; Vušurović, J.; Plangger, R.; Juen, M.; Kreutz, C.; Breuker, K. Native Mass Spectrometry Reveals the Initial Binding Events of HIV-1 Rev to RRE Stem II RNA. *Nat. Commun.* **2020**, *11*, 5750. https://doi.org/10.1038/s41467-020-19144-7.

(1167) Sforza, S.; Tedeschi, T.; Corradini, R.; Dossena, A.; Marchelli, R. Direction Control in DNA Binding of Chiral D-Lysine-Based Peptide Nucleic Acid (PNA) Probed by Electrospray Mass Spectrometry. *Chem. Commun.* **2003**, No. 9, 1102–1103. https://doi.org/10.1039/b212718k.

(1168) Baker, E. S.; Hong, J. W.; Gaylord, B. S.; Bazan, G. C.; Bowers, M. T. PNA/DsDNA Complexes: Site Specific Binding and DsDNA Biosensor Applications. *J. Am. Chem. Soc.* **2006**, *128*, 8484–8492. https://doi.org/10.1021/ja060069s.

(1169) Hanson, C. L.; Robinson, C. V. Protein-Nucleic Acid Interactions and the Expanding Role of Mass Spectrometry. *J. Biol. Chem.* **2004**, *279*, 24907–24910. https://doi.org/10.1074/jbc.R300037200.

(1170) Chen, F.; Mädler, S.; Weidmann, S.; Zenobi, R. MALDI-MS Detection of Noncovalent Interactions of Single Stranded DNA with Escherichia Coli Single-Stranded DNA-Binding Protein: MALDI-MS of Protein-DNA Complexes. *J. Mass Spectrom.* **2012**, *47*, 560–566. https://doi.org/10.1002/jms.2989.

(1171) Suh, M.-J.; Pourshahian, S.; Limbach, P. A. Developing Limited Proteolysis and Mass Spectrometry for the Characterization of Ribosome Topography. *J. Am. Soc. Mass Spectrom.* **2007**, *18*, 1304–1317. https://doi.org/10.1016/j.jasms.2007.03.028.

(1172) McKay, A. R.; Ruotolo, B. T.; Ilag, L. L.; Robinson, C. V. Mass Measurements of Increased Accuracy Resolve Heterogeneous Populations of Intact Ribosomes. *J. Am. Chem. Soc.* **2006**, *128*, 11433–11442. https://doi.org/10.1021/ja061468q.

(1173) Rostom, A. A.; Fucini, P.; Benjamin, D. R.; Juenemann, R.; Nierhaus, K. H.; Hartl, F. U.; Dobson, C. M.; Robinson, C. V. Detection and Selective Dissociation of Intact Ribosomes in a Mass Spectrometer. *Proc. Natl. Acad. Sci.* **2000**, *97*, 5185–5190. https://doi.org/10.1073/pnas.97.10.5185.

(1174) New Methods for the Study of Biomolecular Complexes; Ens, W., Standing, K. G., Chernushevich, I. V., Eds.; NATO ASI Series; Sringer Science+Business Media: Dordrecht, 1998; Vol. 510, p 354. https://doi.org/10.1007/978-94-015-9046-4.

(1175) Greig, M. J.; Gaus, H.; Cummins, L. L.; Sasmor, H.; Griffey, R. H. Measurement of Macromolecular Binding Using Electrospray Mass Spectrometry. Determination of Dissociation Constants for Oligonucleotide: Serum Albumin Complexes. *J. Am. Chem. Soc.* **1995**, *117*, 10765–10766. https://doi.org/10.1021/ja00148a028.

(1176) Cheng, X.; Morin, P. E.; Harms, A. C.; Bruce, J. E.; Ben-David, Y.; Smith, R. D. Mass Spectrometric Characterization of Sequence-Specific Complexes of DNA and Transcription Factor PU.1 DNA Binding Domain. *Anal. Biochem.* **1996**, *239*, 35–40. https://doi.org/10.1006/abio.1996.0287.

(1177) Potter, N.; Chernushevich, I.; Ens, W.; Standing, K. G.; Donald, L. J.; Ayed, A.; Duckworth, H. W.; Arrowsmith, C. H. Study of a Noncovalent Trp Repressor: DNA Operator Complex by Electrospray Ionization Time-of-Flight Mass Spectrometry. *Protein Sci.* **1998**, *7*, 1388–1395. https://doi.org/10.1002/pro.5560070615.

(1178) Cheng, X.; Harms, A. C.; Goudreau, P. N.; Terwilliger, T. C.; Smith, R. D. Direct Measurement of Oligonucleotide Binding Stoichiometry of Gene V Protein by Mass Spectrometry. *Proc. Natl. Acad. Sci.* **1996**, *93*, 7022–7027. https://doi.org/10.1073/pnas.93.14.7022.

(1179) Ilag, L. L.; Westblade, L. F.; Deshayes, C.; Kolb, A.; Busby, S. J. W.; Robinson, C. V. Mass

Spectrometry of Escherichia Coli RNA Polymerase: Interactions of the Core Enzyme with Σ70 and Rsd Protein. *Structure* **2004**, *12*, 269–275. https://doi.org/10.1016/j.str.2004.01.007.

(1180) Chen, L.; Tanimoto, A.; So, B. R.; Bakhtina, M.; Magliery, T. J.; Wysocki, V. H.; Musier-Forsyth, K. Stoichiometry of Triple-Sieve TRNA Editing Complex Ensures Fidelity of Aminoacyl-TRNA Formation. *Nucleic Acids Res.* **2019**, *47*, 929–940. https://doi.org/10.1093/nar/gky1153.

(1181) Akashi, S.; Watanabe, M.; Heddle, J. G.; Unzai, S.; Park, S.-Y.; Tame, J. R. H. RNA and Protein Complexes of Trp RNA-Binding Attenuation Protein Characterized by Mass Spectrometry. *Anal. Chem.* **2009**, *81*, 2218–2226. https://doi.org/10.1021/ac802354j.

(1182) Gordiyenko, Y.; Robinson, C. V. The Emerging Role of MS in Structure Elucidation of Protein–Nucleic Acid Complexes. *Biochem. Soc. Trans.* **2008**, *36*, 723–731. https://doi.org/10.1042/BST0360723.

(1183) Videler, H.; Ilag, L. L.; McKay, A. R. C.; Hanson, C. L.; Robinson, C. V. Mass Spectrometry of Intact Ribosomes. *FEBS Lett.* **2005**, *579*, 943–947. https://doi.org/10.1016/j.febslet.2004.12.003.

(1184) Ilag, L. L.; Videler, H.; McKay, A. R.; Sobott, F.; Fucini, P.; Nierhaus, K. H.; Robinson, C. V. Heptameric (L12)6/L10 Rather than Canonical Pentameric Complexes Are Found by Tandem MS of Intact Ribosomes from Thermophilic Bacteria. *Proc. Natl. Acad. Sci.* **2005**, *102*, 8192–8197. https://doi.org/10.1073/pnas.0502193102.

(1185) Gordiyenko, Y.; Deroo, S.; Zhou, M.; Videler, H.; Robinson, C. V. Acetylation of L12 Increases Interactions in the Escherichia Coli Ribosomal Stalk Complex. *J. Mol. Biol.* **2008**, *380*, 404–414. https://doi.org/10.1016/j.jmb.2008.04.067.

(1186) van de Waterbeemd, M.; Fort, K. L.; Boll, D.; Reinhardt-Szyba, M.; Routh, A.; Makarov, A.; Heck, A. J. R. High-Fidelity Mass Analysis Unveils Heterogeneity in Intact Ribosomal Particles. *Nat. Methods* **2017**, *14*, 283–286. https://doi.org/10.1038/nmeth.4147.

(1187) van de Waterbeemd, M.; Tamara, S.; Fort, K. L.; Damoc, E.; Franc, V.; Bieri, P.; Itten, M.; Makarov, A.; Ban, N.; Heck, A. J. R. Dissecting Ribosomal Particles throughout the Kingdoms of Life Using Advanced Hybrid Mass Spectrometry Methods. *Nat. Commun.* **2018**, *9*, 2493. https://doi.org/10.1038/s41467-018-04853-x.

(1188) Akashi, S.; Osawa, R.; Nishimura, Y. Evaluation of Protein-DNA Binding Affinity by Electrospray Ionization Mass Spectrometry. *J. Am. Soc. Mass Spectrom.* **2005**, *16*, 116–125. https://doi.org/10.1016/j.jasms.2004.09.021.

(1189) Chen, T.-H.; Tanimoto, A.; Shkriabai, N.; Kvaratskhelia, M.; Wysocki, V.; Gopalan, V. Use of Chemical Modification and Mass Spectrometry to Identify Substrate-Contacting Sites in Proteinaceous RNase P, a TRNA Processing Enzyme. *Nucleic Acids Res.* **2016**, *44*, 5344–5355. https://doi.org/10.1093/nar/gkw391.

(1190) Azegami, N.; Saikusa, K.; Todokoro, Y.; Nagadoi, A.; Kurumizaka, H.; Nishimura, Y.; Akashi, S. Conclusive Evidence of the Reconstituted Hexasome Proven by Native Mass Spectrometry. *Biochemistry* **2013**, *52*, 5155–5157. https://doi.org/10.1021/bi4005655.

(1191) Saikusa, K.; Osakabe, A.; Kato, D.; Fuchigami, S.; Nagadoi, A.; Nishimura, Y.; Kurumizaka, H.; Akashi, S. Structural Diversity of Nucleosomes Characterized by Native Mass Spectrometry. *Anal. Chem.* **2018**, *90*, 8217–8226. https://doi.org/10.1021/acs.analchem.8b01649.

(1192) Jeanne Dit Fouque, K.; Garabedian, A.; Leng, F.; Tse-Dinh, Y.-C.; Fernandez-Lima, F. Microheterogeneity of Topoisomerase IA/IB and Their DNA-Bound States. *ACS Omega* **2019**, *4*, 3619–3626. https://doi.org/10.1021/acsomega.8b02887.

(1193) Ma, X.; Shah, S.; Zhou, M.; Park, C. K.; Wysocki, V. H.; Horton, N. C. Structural Analysis of Activated SgrAI–DNA Oligomers Using Ion Mobility Mass Spectrometry. *Biochemistry* **2013**, *52*, 4373–4381. https://doi.org/10.1021/bi3013214.

(1194) Sarni, S.; Biswas, B.; Liu, S.; Olson, E. D.; Kitzrow, J. P.; Rein, A.; Wysocki, V. H.; Musier-Forsyth, K. HIV-1 Gag Protein with or without P6 Specifically Dimerizes on the Viral RNA Packaging Signal. *J. Biol. Chem.* **2020**, *295*, 14391–14401. https://doi.org/10.1074/jbc.RA120.014835.

(1195) Kramer, K.; Sachsenberg, T.; Beckmann, B. M.; Qamar, S.; Boon, K.-L.; Hentze, M. W.; Kohlbacher, O.; Urlaub, H. Photo-Cross-Linking and High-Resolution Mass Spectrometry for Assignment of RNA-Binding Sites in RNA-Binding Proteins. *Nat. Methods* **2014**, *11*, 1064–1070. https://doi.org/10.1038/nmeth.3092.

(1196) Falese, J. P.; Donlic, A.; Hargrove, A. E. Targeting RNA with Small Molecules: From Fundamental Principles towards the Clinic. *Chem. Soc. Rev.* **2021**, *50*, 2224–2243. https://doi.org/10.1039/D0CS01261K.

(1197) Cross, R. The RNA Drug Hunters. *CEN News* **2017**, *95*, 16–18.

TOC Graphics